Investigating the sustained impact of the physical cellular microenvironment on the structure and function of a hepatocellular carcinoma cell line.

ALLCOCK, BENJAMIN,PHILIP

Department of Biosciences

Investigating the sustained impact of the physical cellular microenvironment on the structure and function of a hepatocellular carcinoma cell line.

Benjamin Philip Allcock

March 2021

A thesis submitted for the degree of Doctor of Philosophy

Abstract

Mechanotransduction defines the functional activity of cells by altering gene expression in accordance with cellular structure. With this in mind, a novel *in vitro* model has been developed where cells are 'primed' to a three-dimensional (3D) phenotype through growth on a biologically inert 3D substrate before liberation and reseeding into a secondary culture. To characterise this protocol, the structural and functional effects of 3D priming were evaluated on the HepG2 hepatocellular carcinoma cell line, frequently used for *in vitro* liver research on drug discovery and pathology.

It was found that through using a 3D priming model, cells adopted a mechanical and functional memory based on the historical physical microenvironment. HepG2 cells primed in 3D demonstrated altered cytoskeletal organisation and cell morphology after reseeding, with cell populations more readily forming 3D structures compared to cells reseeded from conventional two-dimensional (2D) substrates. Global gene expression was significantly altered in the priming model, with enrichment of mechanical and structural genes occurring in 2D HepG2 cells compared to enrichment in key genes involved in hepatic metabolism and biosynthesis in the 3D primed HepG2 cells. 3D priming also resulted in enhanced production of the liver specific biomarkers albumin and urea; even within secondary 3D spheroid cultures. Metabolic activity was significantly altered through priming, with the 3D priming model showing decreased sensitivity to xenobiotic toxicity, though this difference balanced out in the secondary models.

Overall, this study has shown that changing the substrate geometry impacts directly on cell structure and results in an altered transcriptional state in HepG2 cells that gives rise to a more physiologically relevant phenotype that is sustained even after enzymatic and mechanical disruption. This holds potential for improving the functionality of *in vitro* models and further elucidates the role of mechanotransduction in directing cell biology.

Acknowledgements

I would like to acknowledge the BBSRC for funding this project. I would also like to thank ECACC and Jim Cooper for their partnership and backing. I sincerely thank Professor Stefan Przyborski for his support, guidance and encouragement throughout this PhD. I would also like to thank Dr. Mathilde Roger who helped a clueless younger me to find my feet in the lab.

The list of people I could (and should) thank is inordinately large, but I will start by thanking Dr Wenbin Wei for his support on the RNAseq bioinformatics work. I also thank Vicky Kelly, Gillian Summerill and Beccy Manning in the sequencing department; Dr Tim Hawkins and Joanne Robson in microscopy and Christine Richardson in electron microscopy.

This has been a fantastic lab to work in and I thank all my friends and colleagues who have made this a truly memorable four years. I thank Henry (for his friendship, tall tales, beer appreciation and musicality), Melissa (for top notch food, deep chats and being genuine), Claire (for being a funny, inspiring and truly amazing desk-mate), Nicole (for being supportive, kind and funny), Steve (for being fun loving, kind, and hilariously observational), Lucy (for her support, and great taste in films), Matt (for his acerbic wit and willingness to teach), Hugh (for keeping it real), Amy (for great discussions about music, gaming and films), Lydia (for her unflappable optimism and kindness), Steven (for his long standing friendship and generosity), Bek (for her early guidance and support), Kirsty (for her humour and a shared love of horror films). I also thank Ra'ad, Ian, Kleo, Eve, Nicola, Alejandro, Paola, Vikki, Charlie, Peter, Ed, Alex, Kelly, Peter, Matthew and many others.

Thanks to Tim and Stuart and Sophie for being legends, and of course, I thank Aaaadam, potatoes and Guinness for their holy powers. Shout out to ultimate synergy too for great chat and instant friendship in my twilight PhD days.

Finally, I've got to thank God and my family – Mum, Dad and Lauren, you're all amazing and thank you for always being there. And Liv, thanks for being amazing.

I will say it though… I should have been on the high council…

Declaration

The work described herein was carried out in the Department of Biosciences, University of Durham between October 2016 and March 2021. All of the work is my own, except where specifically stated otherwise. No part has previously been submitted for a degree at this or any other university.

Statement of Copyright

Table of Contents

List of figures

List of abbreviations

ABC	ATP-binding cassette transporter
ACTN	Actinin
ADMET	Absorption, distribution, metabolism and excretion and toxicity
ADP	Adenosine diphosphate
AFP	Alpha fetoprotein
AJ	Adherens junctions
ALB	Albumin
ANOVA	Analysis of variance
APS	Ammonium persulfate
ATP	Adenosine triposphate
AU	Arbitrary units
AZA	5-azacytidine
BC	Bile canaliculi
BRB	Blot rinse buffer
BSA	Bovine serum albumin
CAMERA	Correlation Adjusted Mean Rank gene set test
CAR	Constitutive androstane receptor
CDH	Cadherin
CLDN	Claudin
CPD	Critical point dryer

CYP450	Cytochrome P450
DILI	Drug induced liver injury
DMEM	Dulbecco's Modified Eagle Media
DMSO	Dimethyl sulfoxide
DNA	Deoxyribonucleic acid
DS	Desmosome
DTT	Dithiothreitol
DVL	Dishevelled
ECACC	European Collection of Authenticated Cell Cultures
ECM	Extracellular matrix
EDTA	Versene
ELISA	Enzyme-linked immunosorbent assay
EMT	Epithelial mesenchymal transition
ENA	Enabled
ETOH	Ethanol
FA	Focal adhesion
FAK	Focal adhesion kinase
FBS	Fetal bovine serum
FDR	False discovery rate
FGA	Fibrinogen alpha
FGB	Fibrinogen beta
FGG	Fibrinogen gamma

FPGS	Folylpolyglutamate synthase
FRET	Fluorescent resonance energy transfer
GDI	Guanine nucleotide-dissociation inhibitors
GEF	Guanine nucleotide-exchange factors
GO	Gene ontology
GSEA	Gene set enrichment analysis
GSK-3	Glycogen synthase kinase 3
GST	Glutathione S-transferase
HAMP	Hepcidin antimicrobial peptide
HCC	Hepatocellular carcinoma cells
HL	Human liver
HMG CoA reductase	3-hydroxy-3-methylglutaryl CoA reductase
HNF	Hepatocyte nuclear factor
HRP	Horse radish peroxidase
HTA	Human tissue act
IF	Intermediate filament
INM	Inner nuclear membrane
ITG	Integrin
KEGG	Kyoto Encyclopedia of Genes and Genomes
LDH	Lactase dehydrogenase
LINC	Linker of nucleoskeleton and cytoskeleton
LMN	Lamin

MAPK	Mitogen activated protein kinase
MDR1	Multi-drug resistance protein 1
MEM	Minimal essential medium
Mk11	Megakaryoblastic Leukemia 1
MLC	Myosin light chain
MRP2	Multi-drug resistance protein 2
MSC	Mesenchymal stem cells
MTHFR	Methylenetetrahydrofolate reducta
MTT	Thiazolyl Blue Tetrazolium Bromide
NAFLD	Non-alcoholic fatty liver disease
NAT	N-acetyltransferase
NGS	Next generation sequencing
NPC	Nuclear pore complex
NSAID	Non-steroidal anti-inflammatory drug
OCT	Optimal cutting temperature
ONM	Outer nuclear membrane
ORA	Over-represenation analysis
PALLD	Palladin
PAS	Periodic acid schiff
PAX	Paxillin
PBS	Phosphate buffered saline
PCA	Principal component analysis

PCDH	Proto-cadherins
PCR	Polymerase chain reaction
M-PER	Mammalian protein extraction reagent
PFA	Paraformaldehyde
PHH	Primary hepatocyte
PI	Propidium iodide
PROC	Protein C
PROS	Protein S
PXR	Pregnane X receptor
RIN	RNA integrity number
RNA	Ribonucleic acid
ROCK	Rho-associated protein kinases
RTqPCR	Reverse transcriptase quantitative polymerase chain reaction
SDS	sodium dodecyl sulfate
SEM	Scannning electron microscopy
SEM	Standard error of the mean
SLC	Solute carrier family
SRF	Serum Response Factor
STD	Standard
SULT	Sulfotransferase
TAZ	WW Domain-Containing Transcription Regulator Protein 1
TEM	Transmission electron microscopy

TGF	Transforming growth factor
THPO	Thrombopoietin
TJ	Tight junction
TTR	Transthyretin
UGT	UDP-glucuronosyltransferase
UV	Ultra violet
VASP	Vasodilator-stimulated phosphoprotein
VBS	Vinculin binding site
VCL	Vinculin
YAP	Yes-associated protein 1
ZO	Zonula occludens
ZYX	Zyxin
2D	Two dimensional
3D	Three dimensional

Chapter 1: Introduction

1.1 Introduction

1.1.1 Thesis overview

In this first chapter, the literature review will outline the key factors involved in mechanotransduction which will demonstrate how cells can transduce extracellular mechanical signals to affect their structure, and how this consequently affects their function. This will help identify why two-dimensional cell culture is not adequate for creating accurate physiological models and will provide a biological rationale behind this project. Following on from this, the advantages of 3D culture over conventional 2D culture will be discussed with relation to the concept of mechanotransduction. Next, the research landscape of *in vitro* liver models will be covered, revealing some of the shortfalls in current techniques used, and how through understanding mechanotransduction better, an improved liver model may be possible.

This thesis will then describe the methods and materials used throughout the course of the project in **Chapter 2**. Following on from this, the first data chapter of the thesis (**Chapter 3**) will look at optimisation of a novel *in vitro* model that is able to support 8-day long culture of HepG2 cells on a three-dimensional topography. This will involve testing a range of different variables in 3D cell-culture to see how growth of the HepG2 cell line is affected, with the ultimate aim of creating a reproducible model that has a thick cell layer with *in vivo*-like morphology that can be easily dissociated and reseeded onto a secondary substrate. Various liberation techniques will also be explored here to ascertain the best method of removing cells from a 3D substrate while maintaining viability. Once this is optimised, **Chapter 4** will detail the structural characterisation of the model. This will include testing for whether the structure of cells grown in a three-dimensional substrate remains altered after liberation and reseeding. This chapter will also detail the optimisation of the secondary model; a second and different 3D culture format in which cells previously grown either in 2D in 3D can be reseeded. Structural characterisation will also look at specific structural markers of interest, visualising these through immunofluorescence to compare the organisation and expression of these markers between 2D and 3D models. **Chapter 5** will consist primarily of a thorough genome wide gene expression analysis experiment, using next generation RNA sequencing to gain a snapshot of the global transcriptome of cells in 2D and 3D at the end point of the primary model stage. This gene expression data from the HepG2 models will also be compared to *in vivo* human liver and primary human hepatocytes to examine how similar or dissimilar both the 2D and 3D priming models are to primary cell sources. This

transcriptomic analysis will provide both a structural and functional insight into the biological changes occurring as a result of 3D culture which should back up the previous structural characterisation as well as providing a basis for functional characterisation and validation of the enriched processes. **Chapter 6** will provide a range of functional tests to characterise what biologically meaningful alterations 3D culture elicits, as well as testing for altered function in the secondary models after reseeding from previous culture in either 2D or 3D.

1.1.2 The role of the extracellular matrix in the human body.

The human body possesses an inherently three dimensional internal environment, with cells growing in the extracellular matrix, a structural support network made up of multiple components including proteins and sugars (Kular et al., 2014). The ECM is especially important in connective tissue (McKee et al., 2019), but can be found in a multitude of tissues, and it also plays a significant role in the wound healing response (Olczyk et al., 2014). The components of the ECM are functionally very important due to both providing active biological cues to the residing cells, and providing a mechanical support network for cell growth, through which the structure and function of cells can be affected.

The mechanical and biological cues imposed by the ECM ultimately direct the functional properties of cells (Martino et al., 2018) and because of this, the properties of the ECM differ significantly throughout areas in the body. For example, in musculoskeletal tissues, growth plate tissue ECM was found to contain proteins that promoted matrix regulation, angiogenesis promotion and osteogenesis promotion. These components were significantly more abundant than in articular cartilage, which contained chondrogenesis promoting factors (Cunniffe et al., 2019). It has also been shown that cells exhibit increased proliferation and differentiation in culture dishes coated in ECM solutions that were tissue matched with the cell types, compared to non-tissue matched ECM-cell pairings (Zhang et al., 2009). Thus, the ECM is clearly adapted to promote the growth and function of the cell types specific to their respective tissues. It is clear that the composition of active biological factors in the ECM are a driving force of cellular function, however the structural make-up of the matrix is equally as important. The stiffness and structure of the ECM varies throughout the body, with the higher concentrations of structural proteins (collagen and elastin) promoting stiffer ECM environments (Bonnans et al., 2014). Different cell types in the body exhibit vast diversity in terms of their morphologies which is often closely related to their specialised functions – and it is the ECM that determines what morphology a cell will adopt. As will become clear in this literature review, the shape of a cell is inextricably linked to the

function, and thus recreating this mechanical environment becomes an essential consideration for *in vitro* cell culture.

When it comes to *in vitro* cell culture, especially on the traditional two-dimensional substrate of a flask, cells are at risk of losing the high-level biological properties seen in physiological conditions, and this is largely due to the effect of a process called mechanotransduction. Changes in the mechanical make-up of the growth matrix can elicit signalling cascades that result in functional changes in the cells, and this concept is key to understanding how the microenvironment affects cells (and consequently the considerations one must make when culturing cells for biological analysis).

1.2 Mechanotransduction

1.2.1 Mechanical Cues Affect Cell Structure and Gene Expression

Mina Bissell was central to introducing the concept of 'mechanotransduction', suggesting that mechanical cues may affect the genetic profile of the cells, and that structure as a whole defines function. It was proposed by Bissell's group that extracellular matrix induced functional differentiation is exerted through alterations in the cell shape that affect gene transcription. This was suggested to be due to interactions between the ECM and transmembrane proteins in the cell and cytoskeletal elements (M. J. Bissell and Barcellos-Hoff, 1987). 'Dynamic reciprocity' was a concept developed in this paper; the interplay between the ECM and the residing cells, which was demonstrated via functional indicators such as milk protein production being dependent on morphological differentiation. Despite this early breakthrough, only recently have the effects and mechanisms of mechanotransduction been investigated in depth. There is now a wealth of research into the consequences of altering the mechanical properties of the growth substrate: its effects on differentiation of stem cells (Engler et al., 2007), gene expression changes due to morphological changes (Birgersdotter et al., 2005), and differences in histone acetylation with cell shape (Le Beyec et al., 2007) to name just a few studies. These known effects of morphological changes will be discussed in more depth later, in relation to cells grown on 2D and 3D substrates.

Mechanotransduction is an important factor that needs to be considered in cell culture, with the actin cytoskeleton in particular acting as an essential signal transducer and 'middle man' between external mechanical cues and the subsequent nuclear changes that affect gene expression (Paluch et al., 2015). It is important to note that mechanotransduction is a two

way process; as well as cells responding to the external environment, cells are able to dynamically alter the composition of the ECM (Humphrey et al., 2014) and generate forces internally which is known as 'inside-out' signalling. For this project however the focus is more weighted towards the effect of the external environment on the cells rather than vice versa.

The signalling events in mechanotransduction are very complex in nature but our understanding of how everything interacts is gradually becoming clearer (Martino et al., 2018a). Investigating different mechanical properties of the cell growth matrix has often involved the use of 3D cell culture techniques and has proved vital in elucidating the underlying mechanisms involved in mechanosensing and mechanotransduction. One significant breakthrough in was the understanding of durotaxis, the migration of cells according to stiffness gradients. This was discovered through the observation that mesenchymal stem cells (MSCs) migrated towards stiffer areas when grown on polyacrylamide surfaces displaying a stiffness gradient (Vincent et al., 2013). This has direct implications for *in vivo* biology as it appears that this could be the homing mechanism through which MSC cells are recruited to fibrotic sites which are significantly stiffer regions than their healthy tissue counterparts.

The evidence indicating the mechanical sensitivity of cells is compelling, with studies showing that stiffer substrates lead to increased adhesion, proliferation and potentially differentiation of osteogenic mesenchymal stem cells (Sun et al., 2018), periodontal ligament stem cells (Liu et al., 2018), epidermal cells (Wang et al., 2012) and more. Mechanosensation has been demonstrated in experimental literature multiple times, with traction force microscopy capable of indicating levels of force exerted on the ECM due to the cell driven displacement of sub-surface beads (Ingber, 2003). A more precise method to measure force exerted by cells was also established using microfabricated postarray detectors to measure the deflection of microneedles on the substrate surface (Tan et al., 2003). This technique demonstrated that cells could exert as much as 75 nN of force on the individual post (needles), with the actin cytoskeleton shown to be the driver. This added to a body of research indicating that cells respond to local ECM alterations by increasing adhesive stress through focal adhesion formation (Ingber, 2003). Later research showed that the cytoskeletal architecture of cells could adapt precisely to the geometry of the microenvironment (Théry, 2010). This was achieved through micro-patterning cell-culture substrates to impose restrictions on cell shape during growth. Additionally, using micropatterning to change the size of culture islets for myofibroblast growth resulted in a

redistribution of matrix adhesion components such as tensin, β1 integrin and vinculin (Goffin et al., 2006). With the addition of data showing that substrate stiffness directs migration of cells (Jo et al., 2020), such as how anisotropic rigidity can direct epithelial cells towards stiffer regions (Saez et al., 2007), there is clear experimental evidence that cells can sense and respond to their external environment. The profound effect of substrate stiffness on differentiation means that there is a large focus on mechanotransduction regarding stem cells due to this concept having great potential in clinical applications. Nevertheless, this principle is applicable across all cell types; the mechanical properties of a substrate can significantly alter cell behaviour.

There is usually a distinction drawn between the terms mechanotransduction and mechanosensation, with the latter being more commonly associated with the ability of cells to respond to changes in the mechanical properties of their surrounding environment (D.-H. Kim et al., 2013). Mechanotransduction as a term tends to encompass the mechanisms through which the cell biology changes as a result of the mechanosensory apparatus inducing structural changes. Specifically, mechanotransduction can be defined as the conversion of physical signals to biochemical responses (Ingber, 2006). Importantly though, these terms directly feed into one another, and for the purposes of this review mechanosensation will be considered as an aspect of the broader biological process of mechanotransduction.

There are multiple elements in the cell at play regarding the biological changes as a result of mechanical pressure, with changes in gene expression being the shared outcome (Uhler and Shivashankar, 2017). The exact mechanisms through which gene expression is altered from mechanotransduction are still being investigated and form a relatively new area of research given the increased recent interest in mechanotransduction. Cytoskeletal machinery changes that affect the nucleoskeleton, and direct activation and shuttling of message delivering proteins (mechano-actuators) from the mechanosensitive sites have been identified as prominent factors (Hieda, 2019). These two mechanisms of action are key to the outside-in signalling events of mechanotransduction and they provide the nucleus with biochemical and physical cues that result in the cell altering its gene expression accordingly. To allow these two different mechanisms occur, the cells require mechanosensitive apparatus – primarily at the membrane surface – which allows them to identify and respond to the physical nature of the surrounding environment. The primary mechanically sensitive elements of cells are found in the form of adhesion molecules and junctional complexes, both between cells and the matrix, and between cells themselves.

1.3 Junctional complexes and their role in mechanical regulation

Junctional complexes are found at the cell membranes, occurring at the points of contact between cell-cell and cell-matrix in all tissues (Alberts et al., 2002a). Mechanotransduction is largely dependent on cell adhesion and junctions (both between cells and between cells and the matrix) which are critical for directing the function of cells, affecting aspects such as metabolism, protein synthesis and cellular architecture (Goldmann, 2012). Of the different types of junctions present in the cell, there are two categories that are mechanically important to the cells; anchoring junctions and occluding junctions. Anchoring junctions mechanically link cells and their cytoskeletons to the external environment, whether that is a neighbouring cell, or the ECM (Alberts et al., 2002a). The two types of anchoring junctions particularly involved in mechanical signalling are adherens junctions (cell-cell adhesion) and focal adhesions (cell-ECM adhesion). These link actin to the external environment which allows the cells to respond to mechanical cues and alter their structure and function accordingly. Occluding junctions act as selective permeability barriers, sealing cells tightly together in epithelia, and these can also bind to the cytoskeleton (Hatte et al., 2018) therefore playing a role in mechanical integrity.

1.3.1 Focal adhesions

Focal adhesions (FAs) are one such type of cellular adhesion that are essential in the interplay between cells and the ECM. FAs provide an adhesion site between the two and they directly link to the actin cytoskeleton through cytoplasmic proteins that anchor it to integrin clusters (Hirata et al., 2008a). Various experiments have tested the effects of mechanically stimulating cells, and many of these have demonstrated that focal adhesion associated proteins are primarily altered (in relation to their binding and activation) as a result of this stimulation (Goldmann, 2012), suggesting that FAs are a key adhesion complex where involved in mechanosensing.

Focal adhesions are complex structures consisting of transmembrane and intracellular layers (see **Figure 1.1**), with scaffolding, docking and signalling proteins forming the intracellular layers and ECM and cytoskeleton binding proteins forming the transmembrane layers (Martino et al., 2018a). When mature, the focal adhesion complexes can be divided into distinct nanodomains, with the integrin signalling layer being closest to the plasma membrane (0-30 nm into the cell), the force transduction layer (30-60 nm), and the actin regulatory layer (>60 nm) (Giannone, 2015). The ECM binding proteins in the focal adhesions

are the integrin family cell adhesion receptors which are required for cell migration and the activation of various intracellular signalling pathways, accomplished through their links to prominent cytoskeletal binding and signalling molecules (Alberts et al., 2002b; Zhao and Guan, 2011). The links to the actin cytoskeleton and to the intermediate filaments are mediated by specialised integrins in addition to adaptor proteins in the focal adhesions (Delon and Brown, 2007). Some of the key components of the FAs include focal adhesion kinase, talin, vinculin, paxillin and zyxin and these will be discussed in detail below.

1.3.1.1 Integrins

In large, the direct relationship between the ECM and the focal adhesion sites of attached cells is due to integrins expressed on the cell surface. These anchor to proteins in the ECM such as collagen, fibrinogen and laminin (Humphries et al., 2006) and act as signal transducers to the cell. The link between integrins and the cytoskeleton is incredibly complex, involving over 50 proteins which form an intricate network of interactions (Zamir and Geiger, 2001). These 'docking' proteins form the FA core, and many are involved in mediating cytoskeletal reorganisation. Some of these docking proteins also possess the ability to shuttle between the cytoplasm and the nucleus to act as transcription factors and directly influence gene expression (Martino et al., 2018a).

Integrins require the ability to alter their specificity for various extracellular ligands to enable them to bind with the heterogeneous environment of the ECM. Collagens, laminins and fibronectins are some of the essential structural components of the ECM and many of these (fibronectin, fibrinogen and more) possess an integrin binding motif – Arg-Gly-Asp (RGD). Other ligands may use different recognition sites, but proteolytic cleavage may also reveal cryptic RGD sites (Danen, 2013). The integrin receptor is formed from two subunits, α- and β- integrin, which are type I transmembrane glycoproteins (Danen, 2013). Alternative splicing of mRNA gives rise to multiple forms of these subunits, with different pairs of subunits subsequently affecting the ligand specificity. The pairing of $\alpha_5\beta_1$ for example is the classical fibronectin receptor, whereas $\alpha_6\beta_1$ and $\alpha_7\beta_1$ are laminin receptors. A demonstration of this is that in adult skeletal muscle, the only ubiquitously expressed form of integrin is $\alpha_7\beta_1$, reflecting the need for strong laminin binding to support contraction (Mayer, 2003). As well as differing compositions of subunits, the affinity for integrin's ligands can be regulated through conformational changes that are a result of either external ligands exerting force (Chen et al., 2012) or brought about by inside-out signalling (Martino et al., 2018b). Activation of the integrins is also induced through both outside-in and inside-out signalling;

the integrins are usually maintained at the cell membrane in a bent conformation that renders them with a low affinity for ligands, but upon activation from either direction, this affinity is increased through conformational changes which leads to stable adhesions. Inside-out signalling induces this conformational change through the binding of talin to the cytoplasmic tail of β subunits. With outside-in signalling, this conformational change is induced through the binding of ECM proteins and external forces (Seetharaman and Etienne-Manneville, 2018).

1.3.1.2 Integrins and the ECM

The composition of the extracellular matrix determines the expression of the specific integrin subunits, and this considerably affects the biological behaviour of the cell (Seetharaman and Etienne-Manneville, 2018). These changes in behaviour are partly due to the differences in the bond strengths between integrins and various ligands, with the bonds between $\alpha_V\beta_3$ and its ligand vitronectin being weaker than the bond between $\alpha_5\beta_1$ and fibronectin for example. This difference in bond strength then affects the actin connections, with the weaker bonds resulting in increased cytoskeletal flexibility and creating short actin fibres mediated through GEFH1-Rho-mDia, whereas the stronger bonds lead to long range force generation and long actin fibre creation/recruitment through Rho-ROCK-myosin II mediated contractility (Seetharaman and Etienne-Manneville, 2018).

The signalling of the integrins to the actin cytoskeleton due to ECM adhesion works via numerous pathways, including Rho family GTPases and cAMP-dependent protein kinase (DeMali et al., 2003). Consequent remodelling of the actin cytoskeleton works largely through affecting the formation of actin structures through altered nucleation via Arp2/3 or formins (DeMali et al., 2002). This demonstrates an integrin dependent mechanism showing that mechanical changes in the ECM, or the mechanical properties of the cell growth substrate will result in remodelling of the cytoskeleton, and this cytoskeletal remodelling subsequently leads to changes in the gene expression and thus changes in the function of the cell (see **Figure 1.1**). Integrin may also affect gene expression through signalling molecules. For example, strain exerted on smooth muscle cells via stretching them elicited a conversion of integrin to a high affinity state (Katsumi et al., 2005), and this resulted in increased integrin binding and integrin mediated activation of JNK, which is important in regulating many cellular processes including apoptosis (Liu and Lin, 2005), proliferation (Zhang and Liu, 2002a) and differentiation (Xu and Davis, 2010).

1.3.1.3 Focal Adhesion Kinase

Focal adhesion kinase (FAK) is one of the earliest identified signalling molecules involved in focal adhesions (Parsons, 2003). FAK is a 120kDa sized non-receptor tyrosine kinase, with a critical role in migration and angiogenesis through various signalling pathways. These molecules are recruited early on in the formation of FAs, due to changes in the morphology and distribution of integrin clusters (Martino et al., 2018a). Integrin mediated cell-ECM adhesion results in the N-terminal FERM domain of FAK being displaced by an activating protein which induces a conformational change, allowing autophosphorylation at the phosphorylation site Y397. Src family kinases can now bind, leading to phosphorylation of other sites on FAK, fully activating the protein. The activated FAK can subsequently initiate phosphorylation mediated signalling cascades that have profound effects on multiple cellular functions (Zhao and Guan, 2011). FAK therefore responds to mechanical signals via recruitment to developing focal adhesions where it activates through autophosphorylation which triggers mechanotransduction pathways (Martino et al., 2018a) including the stabilisation (Fabry et al., 2011) and polymerisation (Roa-Espitia et al., 2016) of the cytoskeleton. Contractile activity of the actin cytoskeleton is driven by RhoA activity which may also promote the recruitment of FAK to the cell adhesions through creating a positive feedback loop encouraging more FAK activation (Tang, 2015).

This protein appears particularly responsive to stretch and mechanical signalling (Sawada and Sheetz, 2002; Wang et al., 2001). Therefore it is unsurprisingly closely related to mechanotransduction, with its presence (both in the inactive and active form) being essential for durotaxis and the localisation of YAP – an important mechanotransducer – to the nucleus (Lachowski et al., 2018). It also plays a role in regulating integrin activation with FAK expression being linked to increased adhesion strengthening and higher rate of integrin binding during early stages of adhesion. Then, as adhesive forces reach equilibrium, FAK expression leads to a weaker steady state of adhesion when compared to FAK null cells, which shows that FAK has a time dependent role in the regulation and generation of adhesive forces (Michael et al., 2009).

1.3.1.4 Paxillin

Paxillin is another key protein involved in focal adhesions, with a role in scaffolding through recruitment of structural and signalling molecules that drive cell migration. Like FAK, Paxillin is involved in the transduction of extracellular mechanical cues into the cell. Integrin binding to the ECM promotes tyrosine phosphorylation of paxillin which as a result provides a scaffold for the recruitment of the tyrosine kinases FAK and Src as well as several other

enzymes and structural molecules (López-Colomé et al., 2017). Paxillin is necessary both for the assembly of focal adhesion complexes at the front of the cell, but also for the disassembly at the rear of the cell. Localisation of this protein is primarily at the focal adhesions, however it has been found to shuttle between the cytoplasm and the nucleus where it potentially acts as a transcription factor, and has been shown to stimulate DNA synthesis and cell proliferation (Dong et al., 2009). This localisation of paxillin has been shown to be modulated by phosphorylation which is in large undertaken by the FAK-Src complex, meaning there is a close interplay between paxillin and FAK activity (Stutchbury et al., 2017). Phosphorylation of paxillin, FAKs and vinculin increase with stiffer substrates, demonstrating the mechanosensitive nature of the protein (Bae et al., 2014) and the tension dependent phosphorylation of paxillin may aid in the recruitment of vinculin to focal adhesions, but this may also work through mechanisms unrelated to FAK (Bae et al., 2014). The turnover of paxillin and FAK – which function as signalling module proteins – does not appear to change in response to ECM stiffness suggesting these might not be direct cellular mechanosensors, instead being involved in mechanosensation through phosphorylation by other mechanically sensitive proteins. The turnover of *other* structural proteins such as talin, vinculin and tensin does alter in response to stiffness though, which indicates that it is these particular structural proteins – linking integrins with the cytoskeleton – that are the direct mechanosensors (Stutchbury et al., 2017).

1.3.1.5 Vinculin/Talin

Vinculin and talin are structural proteins involved in focal adhesions and mechanosensing which provide a physical link between the integrins and the actin cytoskeleton (Stutchbury et al., 2017). These two proteins work closely together, with vinculin's presence at focal adhesions being dependent upon the presence of talin (Zhang et al., 2008). It is believed that vinculin is recruited to the integrin signalling layer of focal adhesions whereupon activation, it 'climbs' talin to reach and bind to the actin cytoskeleton. These two proteins are activated through tension dependent conformational changes, with stretching of talin rods exposing cryptic binding sites for vinculin (del Rio et al., 2009). Talin acts a mechanosensor both indirectly through the outside-in signalling activation of integrin, and directly through unfolding under force loading to expose cryptic vinculin binding sites (VBS) (Martino et al., 2018b). Under low mechanical strain, talin reveals one VBS which activates and binds one vinculin molecule (Haining et al., 2016). This binding of vinculin to the exposed talin sites increases the connections to actin which consequently stretches talin further and exposes more vinculin binding sites (Giannone, 2015), functioning as a form of positive feedback loop

linked to mechanotransduction. Thus, talin's extended conformation requires vinculin binding, and talin binding is a requirement of vinculin activation (Giannone, 2015).

The talins are essential for linking integrins to the cytoskeleton, and for subsequently directing the organisation and formation of the actin filaments. There are two talin genes expressed in humans (talin-1 and talin-2) that both contribute differently towards mechanotransduction. Talin-2 seems to be more sensitive to tension, and cells with individually expressed talin-2 spread out more than talin-1 cells (Austen et al., 2015). Distinct integrin subtypes and talin isoforms possess different binding affinities, for example integrin β_3 has a higher affinity for talin-1 than talin-2, and talin-1 has a higher affinity for integrin β_3 than integrin β_{1A} (Seetharaman and Etienne-Manneville, 2018), so the composition of integrin subunits is an important factor for the binding of talins.

Vinculin is a mechanosensory protein like talin and is interestingly also present in cadherin adhesions as well integrin-based ones. Vinculin binding to talin helps reinforce the talin-actin link by recruiting further actin filaments to the focal adhesions, and this is a tension mediated process with higher forces upon vinculin encouraging FA assembly, and low forces resulting in disassembly (Grashoff et al., 2010). Interestingly, vinculin recruitment is only tension dependent for talin-1, whereas vinculin recruitment occurs even without the presence of force bearing C-terminal F-actin binding on talin-2 (Austen et al., 2015). This further demonstrates how the different affinities of integrin β subunits to the talin isoforms may lead to downstream differences in cell mechanotransduction and it indicates how ECM composition may alter the activity of vinculin and talin.

The phosphorylation of vinculin is also essential for mechanotransduction, with constitutively inactivated vinculin resulting in cells that are lacking in adhesion strength and exhibiting reduced cytoskeletal stiffness; whilst rescuing vinculin phosphorylation restores these mechanical properties (Auernheimer et al., 2015). Vinculin also demonstrates a dependency on actomyosin contraction for localisation to the focal adhesions. The actin binding tail region of vinculin is essential in providing the cells with the ability to repolarise (Humphries et al., 2007), and the clear effects of vinculin on cellular mechanical integrity (Auernheimer et al., 2015) coupled with the dependence on talin's mechanically driven extension highlights the importance of these two proteins in transmitting extracellular mechanical stimuli.

1.3.1.6 Zyxin

Another protein involved in focal adhesions and mechanotransduction is zyxin which also affects actin polymerisation and is known to shuttle to the nucleus. Application of force is known to alter the localisation of zyxin which is predominantly based at focal adhesions; stretching cells results in the mobilisation of zyxin to actin filaments (Yoshigi et al., 2005), particularly at force bearing sites in the leading edge of cells (Uemura et al., 2011) where it influences the organisation of the cytoskeleton. Zyxin alters actin through both affecting contractility with its ability to bind the crosslinking protein α-actinin (Crawford et al., 1992) and altering polymerisation through its activity with Ena/VASP. There is evidence showing that Zyxin recruits VASP to the barbed ends of actin filaments where it helps protect the filaments from capping activity, promoting polymerisation (Hoffman et al., 2006). The protein contains a LIM domain which has been shown to be essential in the force dependent accumulation of the protein, with zyxin proteins that lack the LIM domain showing no localisation to force bearing sites (Uemura et al., 2011). LIM domains are also important in the activity of paxillin with its binding to various cytoskeletal signalling proteins being dependent on four C-terminal LIM domains (Kadrmas and Beckerle, 2004).

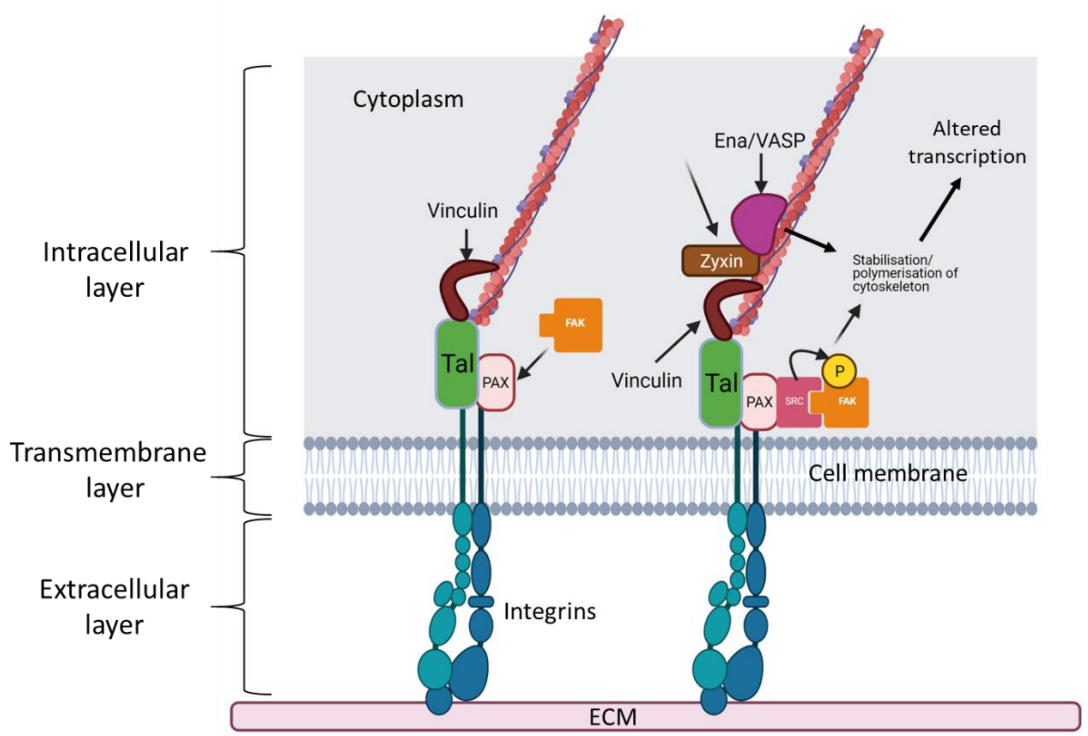

Figure 1.1: Focal adhesions drive structural remodelling of the cytoskeleton.

Figure adapted from (steve, n.d.; Tsimbouri, 2015). Integrins recruit actin filaments through Talin (Tal) and vinculin and paxillin (PAX) provides a scaffold through which focal adhesion kinase (FAK) and SRC are recruited. SRC family kinases phosphorylate FAK, encouraging actin polymerisation. Zyxin is recruited to the actin filaments and further encourages crosslinking through α-actinin and polymerisation through Ena/VASP. Altered actin structure causes changes in gene transcription through signalling pathways and mechanical changes in the nucleus. Created with BioRender.com.

1.3.2 Adherens junctions

Focal adhesions are evidently very critical in linking the cytoskeleton to the ECM surrounding the cells (Roca-Cusachs et al., 2013), and integrin plays a central role in this and the transduction of the mechanical signals to the cytoskeleton. Cells do not just exist as individual entities on a matrix however, they are in contact with multiple other cells either of the same or different types when *in vivo,* and contact with other cells is another significant driver of structure and function. Therefore, cell to cell adhesion complexes also play a role in mechanotransduction and should not be overlooked.

Adherens junctions (AJs) consist of cadherins and their binding partners catenins (Pinheiro and Bellaïche, 2018). This group of cell-to-cell adhesion molecules - transmembrane proteins essential for cell to cell adhesion – could be considered analogous to integrins but are less extensively studied regarding their capacity for mechanotransduction. Cadherins are transmembrane proteins essential for cell to cell adhesion which works via Ca^{+2} dependent homophilic interaction of their ecto-domains (Ayollo et al., 2009). This extracellular domain involves five beta-barrel domains, with the three calcium binding sites residing in the interdomain junctions (Cailliez and Lavery, 2005). The binding of calcium is essential for the correct functioning of cadherin, with the molecules being vulnerable to protease attack in the absence of calcium (Takeichi, 1990). There is a transmembrane and cytoplasmic domain of the cadherins too, and these domains are important for binding proteins that link the junctions to the cytoskeleton consisting primarily α, β, γ and P120 catenin (Leckband and Rooij, 2014). Various cadherins exist (N-cadherin, P-cadherin, E-cadherin), with E-cadherin perhaps being the most extensively characterised of the group. Calcium binding is known to be majorly important in the junction between the top two domains in E-cadherin (EC1 and EC2), affecting the function of the molecule through altering its conformation (Cailliez and Lavery, 2005).

Cadherins may aid in defining structure and function similar to integrins, due to the link between the actin cytoskeleton and cadherins via the cadherin-catenin complex (Desai et al., 2013). Contrary to initial thoughts that cadherins were just passive, there is significant evidence that they possess mechanosensing abilities that can result in appropriate signalling cascades to alter cellular function. The nature of cadherins in mediating cell to cell contacts means they are subject to tensile and mechanical forces transmitted through the cells, and therefore they have a role to play in deformation of cytoskeletal elements (Leckband and Rooij, 2014). Rigid surfaces appeared more conducive to the formation of cadherin

adhesions, with more spread out cells and increased cytoskeletal organisation compared to softer substrates (Ladoux et al., 2010). Force on cells increases the development of cadherin adhesions, and the altered morphology indicates that the actin machinery is an active component in the regulation of cadherins.

The mechanosensory abilities of E-cadherin were demonstrated through showing that applying force to cells through magnetic twisting cytometry, there was up to a 70 % force dependent increase in stiffness of the junctions. This was shown to be dependent on the mechanical linkage to and presence of an organised cytoskeleton, as cytoskeletal disruption agents severely impacted the response (le Duc et al., 2010). This is coupled with the observation that vinculin accumulates at the actin anchored cadherin adhesions in a force dependent manner and helps potentiate the mechanosensory nature of E-cadherin. Mechanically stretching cells has also been shown to alter the size of adherens junctions, with myosin independent application of force triggering the growth of AJs, and myosin activity also affecting AJ size (Liu et al., 2010). AJ remodelling and polarisation is a vital process *in vivo* with many examples of mechanically induced changes of this being seen in physiological situations (Pinheiro and Bellaïche, 2018). The mechanosensory response of adherens junctions is particularly critical in the morphogenesis of epithelia tissues and the remodelling of epithelial architecture (Pinheiro and Bellaïche, 2018).

1.3.2.1 Adherens junctions and the cytoskeleton

The cytoskeleton is reactive to changes in intercellular force due to the presence of vinculin which reinforces binding of the AJs to the actin cytoskeleton, as well as promoting the nucleation of F-actin through Arp2/3 and Ena/VASP (Pinheiro and Bellaïche, 2018). It is suggested that one of vinculin's potential roles in AJs is to protect the junctions from opening during the remodelling process, however it is not needed for initial formation of the junctions (Huveneers et al., 2012).

Zyxin is another protein involved in actin polymerisation and implicated in mechanotransduction that has been known to act at cadherin junctions. Zyxin, VASP and testin (a zyxin related LIM-domain protein) have all been found to be localised to AJs where they may aid in the regulation of the actin cytoskeleton (Oldenburg et al., 2015). Thrombin is an endothelial permeability factor that is known to induce actomyosin contraction that puts tension on cell-cell junctions. During application of this factor to human umbilical veins endothelial cells, it was seen that VASP, zyxin and testin were increased at the AJs, with VASP and zyxin complexing together. Conversely, when F-actin stress fibres were disrupted using

the Rock inhibitor Y-27632, the localisation of these proteins significantly decreased, indicating a tension dependent recruitment of these to AJs (Oldenburg et al., 2015). Dominant-negative mutants for zyxin and LPP (a close relative of zyxin) result in an accumulation of capping protein at the cell junctions which prevents the polymerisation of actin filaments (Hansen and Beckerle, 2006). The localisation of these molecules is independent of the presence of vinculin and the conformation of α-catenin (which can be modulated through mechanical tension). This may in part explain a mechanism through which AJs transduce mechanical signals through the cytoskeleton; through the help of vinculin and zyxin which allow the elongation of actin filaments. The actin cytoskeleton is also intrinsically able to respond to mechanical loads, and this will be discussed later. The signalling of the AJs to the actin cytoskeleton may help give rise to transcriptional differences and genetic changes known to arise downstream of actin remodelling due to the link between the cytoskeleton and the nucleus.

Cadherins are bound to actomyosin principally through the catenins, and α-catenin is a particularly critical protein in mechanotransduction through AJs. The F-actin associated α-catenin is linked to the specific cadherin= E-cadherin via β-catenin (Desai et al., 2013). This protein is able to change its conformation when under tension, where the unfurling of the D3a domain provides a binding site with vinculin as a potential ligand. It is likely then that tension is a mediator of the vinculin binding to α-catenin, reinforcing the link to the actin cytoskeleton at cell-cell junctions (Leckband and Rooij, 2014). Besides vinculin, α-actinin is also capable of binding to the same domain of α-catenin as vinculin (Nieset et al., 1997), and while certain proteins binding to this D3a domain may attenuate the activity of vinculin, α-actinin could provide another link between the cadherins and mechanotransduction. For example, α-actinin-4 associates with the cadherin-catenin complex and aids in the assembly of actin at cadherin junctions by binding and bundling the F-actin. The capture and recruitment of actin to the junctions by α-actinin may be further facilitated through Arp2/3 with its nucleation activity being a requirement for α-actinin dependent actin assembly (Tang and Brieher, 2012, p.). Arp2/3 was also shown to be localised at the cadherin-catenin complexes during junctional assembly, showing that these complexes are essential for actin incorporation.

While less studied than their cell-matrix counterparts (FAs/integrins), it is clear that cadherins should not be overlooked when considering mechanotransduction and the potential mechanisms through which the cytoskeleton may rearrange itself as a result of

extracellular mechanical cues. Interestingly, integrins are also important in mediating cell-cell adhesions (Zhang and Wang, 2012), affecting multiple aspects of cell behaviour including migration, homeostasis and activation (Hynes, 2002), so it is possible that both focal adhesions and adherens junctions interact with each other.

1.3.3 Tight Junctions

In cells such as epithelial cells, where the passage of solutes and ions in between cells is important, tight junctions are required for correct functioning (Hartsock and Nelson, 2008). Tight junctions are also essential for the prevention of protein mixing between apical and basolateral membranes, and the sealing of cells with tight junctions is the key to forming polarity and creating an apical and basal surface (Anderson and Van Itallie, 2009). The functional importance of tight junctions *in vivo* means that the number and proximity of cells in *in vitro* culture are an important consideration due to the potential formation of tight junctions that that have such functional implications for the cells. Tight junctions consist of various transmembrane proteins (claudins, occludin), which bind to the actin cytoskeleton through the intracellular ZO proteins (Hatte et al., 2018). ZO proteins are not the only TJ associated proteins that bind actin however, with cingulin also being an important protein recruited to tight junctions by ZO-1 that interacts with actin filaments, myosin and microtubules (Citi, 2019). Afadin is another protein present in tight junctions (and AJs) that binds actin, increases under tension and works with ZO-1 to help maintain junctional architecture (Choi et al., 2016).

While tight junctions mechanically couple cells together, there is less research on these in relation to mechanotransduction. One study indicates a potential role of tight junctions in regulating the mechanical tension applied to the adherens junctions, with depletion of ZO-1 resulting in cytokinesis defects in *Xenopus laevis* embryos (Hatte et al., 2018). Interestingly this protection from excessive tension goes both ways, with one study showing that vinculin dependent reinforcement of AJs under tension allows TJs to maintain barrier function in *Xenopus* epithelia (Higashi et al., 2016). Tight junctions also directly associate with adherens junctions, with ZO proteins being seen to localise to AJs in multiple situations (Citi, 2019). This mechanical link to adherens junctions suggests that the tight junctions have an indirect role in mechanotransduction, but there is also evidence to suggest a more straightforward link to mechanotransduction.

One more direct effect of mechanical force may come from the ability of the ZO proteins to bind important ligands. The N-terminal region of ZO-1 that contains the PDZ3, SH3, U5 and GUK domains (the ZPSG-1 region) is essential for interaction with occludin and for the ZO-1 / ZO-2 dependent sequestration of DbpA/ZONAB (Spadaro et al., 2017). DbpA is a transcription factor that regulates gene expression and cell proliferation. In confluent epithelial cell layers, ZO-2 inhibits the nuclear activity of DbpA with ZO-1's regulation being shown to be redundant (Balda and Matter, 2000; Spadaro et al., 2014). This binding of the ZPSG-1 region to occludin and DbpA is inhibited by the C terminal of ZO-1 which also interacts with the ZPSG region, yet it was observed that application of force stretches the ZO proteins and is able to disrupt the C-terminal-ZPSG interaction *in vitro*. This suggests that force directed modulation of the C-terminal-ZPSG interaction is one mechanism through which the cell can modulate the ligand binding activity of ZO-1 and ZO-2 and consequently alter its function (Spadaro et al., 2017). From this, it was suggested that ZO proteins are active whilst in their stretched conformation, and inactive when folded due to autoinhibition of ZPSG-1. It appears that actomyosin contractility and organisation has a direct effect on the stretching and therefore activation of the ZO proteins, due to the direct connection through the C terminal ends of ZO-1 and ZO-2 to the actin filaments (Spadaro et al., 2017). One group of proteins essential in the organisation of the actin cytoskeleton are the Rho family GTPases which are also known to interact with multiple tight junction proteins such as ZO-1, cingulin and paracingulin (Citi, 2019). It is unclear the exact effect that these interactions elicit on the Rho GTPases, however it does indicate that the tight junctions possess the ability to reorganise the cytoskeleton. ZO-2 has also been shown to regulate the nuclear shuttling of an important transcription factor/mechanotransducer – YAP, further implicating tight junctions in mechanotransduction (Spadaro et al., 2014).

Multiple ZO-1 protein knockout experiments have shown that depletion of these proteins significantly affects cellular architecture, actin localisation and monolayer mechanics in epithelial cells (Bazellières et al., 2015; Odenwald et al., 2018; Tokuda et al., 2014). Despite this, the mechanical integrity of cells however was found to be largely unaffected in ZO-1 knockout epithelial cells, whereas AJ disruption with Dithiothreitol (DTT) significantly affected the cellular mechanics (Brückner and Janshoff, 2018). The effect of knocking out ZO-1 on cell structure is significantly more pronounced when ZO-2 is simultaneously depleted, with elevated epithelial tension (Choi et al., 2016), expansion and delayed formation of the actomyosin ring associated with the AJs (Fanning et al., 2012; Yamazaki et al., 2008) being some of the observed outcomes. It is evident that the ZO proteins (and by extension, tight

junctions) are closely involved in the organisation of the actin cytoskeleton and therefore they should not be overlooked when investigating altered cell function due to changes in morphology.

1.3.4 Desmosomes

Little is known about the link between desmosomes and the cytoskeleton, however it is known that they help mammalian tissues to resist mechanical stress (Price et al., 2018). Desmosomes do not appear sensitive to intracellular mechanical forces arising from actin contractility, unlike cadherin-based junctions which are directly linked to actin. Desmosomes are the only epithelial junctions that are associated with intermediate filaments (IFs) (Sluysmans et al., 2017), and they are linked to the Ifs through desmoplakin. The stress absorbing properties of desmosomes may be partly attributed to desmoplakin – a protein that may have isoform specific roles in its sensitivity to mechanical stress. Due to the unclear nature of these junctions regarding mechanotransduction, they will not be focused on here.

It is clear that some of the critical points of origin for outside-in mechanotransduction are the junctional complexes both at the cell-cell and cell-matrix interface. The profound effect of structure on cellular function means that considering the arrangement and morphology of cells *in vitro* is essential if the aim is to recapitulate the *in vivo* phenotype as closely as possible.

1.4 The cytoskeleton and mechanotransduction

The first of the two mechanisms through which mechanical signals at the membrane of the cell are transduced to the nucleus is through reorganisation of the actin cytoskeleton. This results in physical changes in the nucleoskeleton exerted through the cytoskeletal connections to the LINC complex. The cytoskeleton consists of 3 elements, the actin fibres, microtubules and intermediate filaments, with the actin cytoskeleton primarily having a well-known and critical role in mechanotransduction. Extracellular mechanical cues are transduced via the remodelling of the actin cytoskeleton – a process dependent on adherens junctions and the focal adhesions that form at the cell-matrix interface.

The actin cytoskeleton is a dynamic structural component of the cell that consists of filamentous actin fibres (F-actin), globular actin molecules (G-actin), and actin binding proteins (Ohashi et al., 2017). This has three primary functions: spatial organisation of the cell and its components, physical and biochemical interaction with the microenvironment

surrounding the cell, and cell motility/morphology. The actin cytoskeleton is in constant flux, with the regulation of tension acting as a second messenger for mechanical signals (Martino et al., 2018a).

1.4.1 Actomyosin contractility

One of the core attributes of the actin cytoskeleton is its contractility, carried out through the association of F-actin filaments with the motor protein myosin II to form stress fibres. These stress fibres, along with the polymerisation and depolymerisation of actin filaments are central to the cell's ability to migrate and remain responsive to its external environment. Myosin II is bound to the actin filaments through crosslinking proteins such as α-actinin and palladin and is essential for the contractile nature of cells due to its ability to 'walk' along the actin filaments (Naumanen et al., 2008). Stress fibres link the cytoskeleton to focal adhesions, with three main types of stress fibre existing, each with different functions: dorsal, ventral and transverse arcs. Ventral fibres and transverse arcs demonstrate periodic distribution of α-actinin–myosin (Hotulainen and Lappalainen, 2006), however dorsal stress fibres do not exhibit this distribution and they are not bound to myosin. Ventral stress fibres are important for the contractility of the cytoskeleton, anchored to focal adhesions at both ends which makes them responsible for changes in cell shape and tail retraction (Naumanen et al., 2008). Dorsal stress fibres only associate with focal adhesions at one end, and are not contractile but act as stabilisers, and a platform for linking the other stress fibres to the focal adhesions (Tojkander et al., 2012). Transverse arcs are not directly linked to any focal adhesions, but carry out their contractile activity through indirect connections to the FAs via the dorsal stress fibres (Naumanen et al., 2008).

A fourth stress fibre sub-type with an important role in mechanotransduction has been recently identified – perinuclear actin caps (Tojkander et al., 2012). These consist of actin-myosin filaments that are directly connected to the nuclear lamina through LINC complexes, and they directly connect the nuclear envelope to focal adhesions, making them essential in transducing external mechanical signals directly to the nucleus (D.-H. Kim et al., 2013; Shiu et al., 2018). One of the first identified features of the perinuclear cap was regulating the shape of the nucleus (Khatau et al., 2009), and the discovery of this stress fibre type highlighted the direct relationship between nucleus shape and cell shape as directed by the external environment. Stress fibres are known to contribute to cell adhesion (Parsons et al., 2010), but evidence is more ambiguous regarding their role on cell migration. They have the ability to alter the conformation of mechanosensitive focal adhesion proteins such as β-

integrin (Puklin-Faucher et al., 2006) and talin (Gingras et al., 2006), and they are able to regulate the assembly and dynamics of focal adhesions through contractile forces (Tojkander et al., 2012). Regarding migration however, stress fibres are not always present in migratory cells, suggesting that they are not essential for migration – but perhaps they aid migration on stiffer matrices due to their ability to deform the surrounding substrate through generation of tensile forces (Castella et al., 2010).

1.4.1.1 The Rho/ROCK pathway is a mechanically sensitive driver of cytoskeletal reorganisation.

One of the central pathways involved in cytoskeletal mechanosensation is the activation of Rho GTPases, particularly RhoA which has a distinct effect on the cytoskeleton with its regulatory action on myosin II activity (Chrzanowska-Wodnicka and Burridge, 1996; Lessey et al., 2012). RhoA is a G-protein whose activity is regulated by three different proteins; guanine nucleotide-dissociation inhibitors (GDIs), guanine nucleotide-exchange factors (GEFs) and GTPase-activating proteins (GAPs). These proteins regulate the cycle between an inactive GDP state of RhoA and an active GTP state. GDI binds to the inactive RhoA to maintain an inactive pool of it in the cytosol, with GEFs activating the protein by catalysing the exchange of GDP for GTP. GAPs return the proteins to their inactive state by stimulating GTPase activity (Lessey et al., 2012).

RhoA activates Rho-associated protein kinases (ROCK) which play an important role in the propagation of mechanical signals. There are two ROCK proteins: ROCK1 and ROCK2 with ubiquitous expression in most tissues, and both appearing to have similar functions – stress fibre formation with ROCK1 and cell contraction/phagocytosis for ROCK2 (Amano et al., 2010). These work through phosphorylation of specific substrates, of which there are many with a significant involvement in cytoskeletal morphology (MLC, Adducin, CPI-17, MYPT1 and many more) (Amano et al., 2010). Myosin II activity is induced by (ROCK) activation which directly phosphorylates myosin regulatory light chain (MLC), increasing the contractile activity of myosin II with the actin filaments due to it promoting the assembly of myosin II into bipolar filaments, inducing actin-myosin interaction and myosin II ATPase activation (Lessey et al., 2012). MLC phosphatase is a regulatory enzyme that dephosphorylates MLC and therefore reduces the contractility of stress fibres. As well as directly activating MLC, the Rho/ROCK pathway also suppresses the activity of MLC phosphatase through phosphorylating the subunit myosin phosphatase targeting subunit 1 (MYPT1), decreasing

its activity and thereby leading to an increase in phosphorylated MLC (Kimura et al., 1996). See **Figure 1.2** for a summary of how Rho/ROCK affects the actin machinery.

Actin cytoskeleton stabilisation is largely mediated by cofilin a protein that severs F-actin, allowing depolymerisation from the now exposed barbed end and reducing tension in the cell (Martino et al., 2018b). Cofilin is active when dephosphorylated, and mechanical stimulation encourages the deactivation of cofilin through its phosphorylation by the kinase LIMK which is activated by the Rho/ROCK pathway (Mizuno, 2013). It has been observed that ROCK inhibition results in the loss of actin stress fibres due to the lack of cofilin inhibition, which further demonstrates the role of ROCK in preventing depolymerisation of actin filaments (Driscoll et al., 2015). Mechanical forces upon the cell also directly inhibit the activity of cofilin; by both reducing the affinity of cofilin and increasing the affinity of Myosin II to the actin filaments (Ohashi et al., 2017). A potential explanation for the reduced affinity of cofilin is due to changes in the helical structure of actin fibres when under tension. This is due to cofilin's preference in binding to actin filaments that are more twisted, a property that decreases the more an actin filament is stretched (Hayakawa et al., 2011). The extended nature of stretched actin filaments also favours myosin II binding, promoting contractility (Ohashi et al., 2017).

Externally generated forces that either stretch or compress cells are known to activate RhoA (Lessey et al., 2012), which leads to stabilisation of the actin cytoskeleton through the activity of ROCK which promotes myosin II activity and inhibits cofilin mediated actin severing as discussed above. RhoA activity is linked to mechanical signals through the association of its regulatory proteins to the cytoskeleton and cell adhesion molecules. It was demonstrated for example, that two GEF proteins, GEF-H1 and LARG were recruited to adhesion sites upon application of mechanical force (Guilluy et al., 2011). RhoA expression is regulated by a number of transcription factors, including NF-κB (Kim et al., 2018), the nuclear transport of which is known to be modulated by mechanical disruption in endothelial cells (Mammoto et al., 2012).

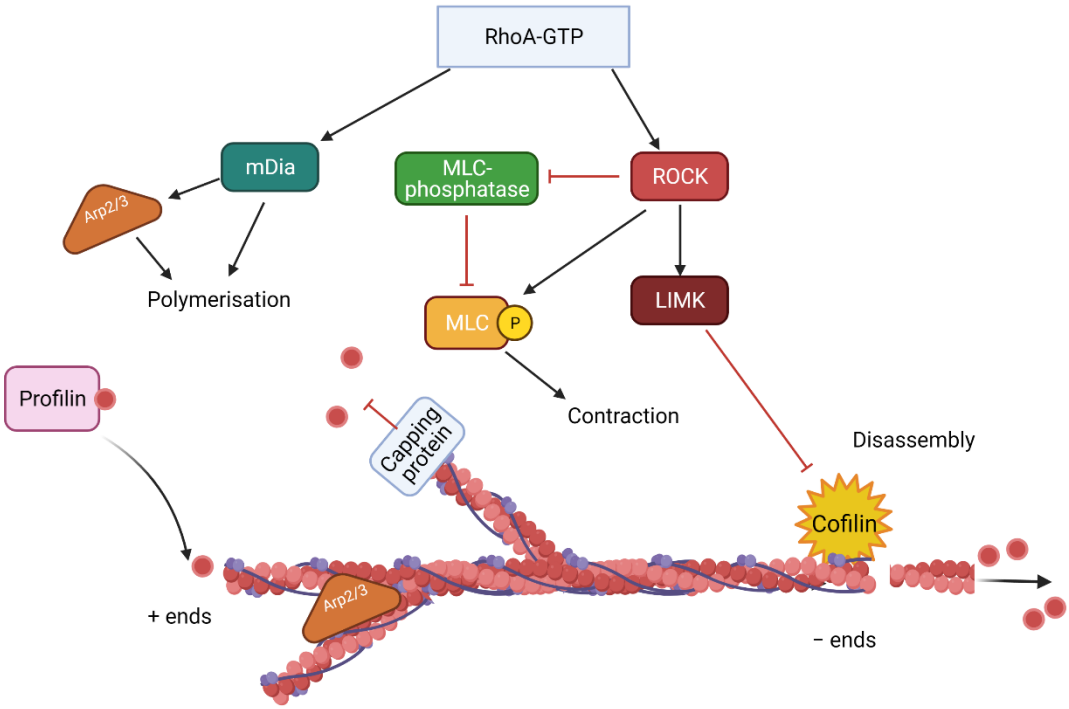

Figure 1.2: Actin polymerisation is regulated through RhoA-GTP

Figure adapted from (Disanza et al., 2004; Martino et al., 2018b). Profilin refreshes the pool of ATP bound monomers for actin assembly at the barbed end (+ end) and Arp2/3 facilitates branching of the filaments. Cofilin severs actin filaments from the ADP bound pointed end (- end) by destabilising the filament structure resulting in filament disassembly. RhoA-GTP promotes actin elongation through activation of mDia1, which promotes polymerisation (Lessey et al., 2012). RhoA-GTP stabilises actin through ROCK activating LIMK which phosphorylates cofilin, thereby inhibiting its actin severing activity. RhoA-GTP can also induce contractile force through direct phosphorylation of myosin light chain (MLC) which increases the contractile activity of myosin II, and also through inhibition of MLC phosphatase. Created with BioRender.com.

1.4.2 Actin assembly/disassembly

Actin disassembly and nucleation/elongation is the other essential aspect of the actin cytoskeleton in ensuring cell motility and shape alteration. To respond to external cues, actin filaments must assemble rapidly at specific locations, however the formation of *de novo* actin filaments is limited due to the unfavourable nature of actin nucleation. Nucleation is very inefficient owing to the highly unstable actin dimers and trimers (polymerisation intermediates) involved in the process which rapidly dissociate (Chesarone and Goode, 2009). While nucleation is the rate limiting step, elongation of existing actin filaments can occur rapidly due to the large reservoir of actin monomers available. Elongation occurs at the barbed ends of filaments after nucleation has taken place, but this is limited through the activity of actin capping protein, which binds to the barbed ends of actin filaments and regulates their polymerisation (Cooper and Sept, 2008). The rate of elongation is directly proportional to the concentration of actin monomers available in the cytosol (Pollard, 1986). One particular characteristic of actin filaments is a 'treadmilling' like activity, where actin monomers bound to Mg-ATP associate at the barbed end of the filaments, and ADP-actin (a product of ATP hydrolysis and phosphate dissociation) dissociates from the pointed end, which results in the motor like activity of actin filaments. The dissociation of the γ-phosphate after ATP hydrolysis occurs slowly compared to the hydrolysis itself, but once complete it induces debranching and binding of actin depolymerizing factor and cofilin which severs the actin subunits (Pollard and Borisy, 2003). This equilibrium between association and dissociation of actin monomers results in directional movement of the actin filaments, however this process is naturally very slow and it is only through the activity of regulatory proteins that this becomes a mechanism for cell migration.

1.4.2.1 Actin nucleation factors

To overcome the unfavourable nature of nucleation, certain proteins are expressed that promote actin assembly: actin nucleators and elongation factors, and these play key roles in regulating the polymerisation of actin. Actin nucleators work through either structurally mimicking the polymerisation intermediates required, stabilising the spontaneously formed intermediates or through forming a basis for polymerisation via recruitment and alignment of actin monomers (Chesarone and Goode, 2009). Amongst the important nucleation factors is the Arp2/3 complex, which works via mimicry of the polymerisation intermediates, thus encouraging nucleation. Arp2/3 is activated by WASP proteins – a group of nucleation promoting factors (NPFs) – which induce conformational changes in Arp2/3 and deliver the

first actin monomer to the complex (Padrick et al., 2011). This complex then catalyses the formation of 'daughter' filaments which branch off 'mother' filaments at 70^{o} angles. Arp2/3 depends on membrane bound nucleation promoting factors, and this ensures the creation of anisotropic actin filaments (Bieling et al., 2016). Formins are also important nucleation proteins that bind to the barbed end of spontaneously formed actin dimers/trimers with their donut-shaped FH2 domains, where they help stabilise the otherwise unstable dimers/trimers (Chesarone and Goode, 2009). One particular formin protein that promotes actin nucleation is the formin mdia1 which is interestingly activated through RhoA binding (Lessey et al., 2012), revealing that RhoA signalling mediates both contractility and polymerisation. A further essential protein involved in actin polymerisation is profilin which catalyses the exchange of ADP for ATP in the actin monomers, refreshing the pool of ATP bound monomers ready for assembly (Pollard and Borisy, 2003). When bound to actin monomers however, profilin strongly inhibits the nucleation and elongation of actin filaments at the pointed end (Pollard and Cooper, 1984).

1.4.2.2 Actin elongation factors

The other category of actin regulatory proteins is the actin elongation factors which help control the rate of elongation through moving with the barbed ends of actin filaments and shielding them from capping proteins which significantly limit filament length and typically have a high association rate (Chesarone and Goode, 2009). Formins – already characterised as a nucleation factor, also act as elongation factors through a similar mechanism to their nucleation enhancing process. They influence the rate of elongation via the processive binding to filament barbed ends via their dimeric FH2 domains, preventing filament annealing and blocking the binding of capping proteins (Courtemanche, 2018). Profilin has a high affinity for polyproline and formins encourage recruitment of profilin-actin monomers through polyproline tracts contained within the FH1 domains of formins. After binding to the FH1 domain (increasing the local concentration at the barbed ends), the profilin-actin is delivered to the FH2 domain of formin, whereupon the profilin dissociates due to a weak affinity with the barbed end, allowing incorporation of the actin monomer into the filament (Courtemanche, 2018). Enabled/vasodilator-stimulated phosphoprotein (Ena/VASP) is another elongation factor known to prevent association of capping proteins, whilst promoting recruitment of profilin-actin to the barbed ends (Barzik et al., 2005). Ena/VASP works as a tetramer with distinct polyproline rich regions that form regulatory, recruiting and loading modules. Through the action of these regions, Ena/VASP acts through processing

profilin-actin and directing its transition to the GAB domain where it can then join the barbed end of the actin filament (Ferron et al., 2007).

1.4.2.3 Mechanical signals affect actin polymerisation

Actin polymerisation is a mechanically sensitive event, with tensile forces regulating the polymerisation activity of various actin nucleators. Tension dependent changes in the rate of formin mediated elongation of actin filaments for example have been observed in multiple experiments (Courtemanche, 2018), with an isoform specific response but a general increase in elongation rate when under tension. This is due to conformational changes induced in the formins, with applied force encouraging the FH2 dimer to adopt an open conformation which favours polymerisation (Courtemanche, 2018). The end-to-end length of the FH1 region can also influence the rate of polymerisation, with increased distances resulting in a lower probability of collision with the barbed end, and therefore slower polymerisation. This can be altered mechanically, with force application to the highly disordered FH1 domain revealing the binding site, and thus promoting the capture and binding of profilin-actin (Bryant et al., 2017). The mechano-sensitivity of formin mediated elongation appears dependent on the presence of profilin, with polymerisation slowing down in the absence of profilin, but elongation rates increasing when profilin is present (Harris et al., 2018). The network structure of actin can be significantly affected when polymerisation is directed against force, with filament density increasing with forces that stall network growth (Bieling et al., 2016). Remarkably, actin networks appear to respond to and 'remember' their loading history with newly formed networks being stronger after having been historically subjected to increasing loads (Bieling et al., 2016). Actin networks typically assume dendritic geometry, with 70^{o} branch points generated by Arp2/3, however under increased tension, this network becomes denser, exhibiting a broader range of angles (Mueller et al., 2017). When force was applied to cells subjected to the myosin II inhibitor blebbistatin which stops contractility, actin polymerisation was induced at focal adhesions but was dependent on the presence of the actin regulatory protein zyxin (Hirata et al., 2008b). Zyxin accumulation at focal adhesions was induced by stretching the cells, suggesting zyxin has a role in mechanosensation and altering the polymerisation of the cytoskeleton in response to the exogenous environment.

As well as linking with focal adhesions, the actin filaments also link with adherens junctions (cell – cell) contacts, another important aspect of mechano-sensing discussed earlier. There are indications that actin actively and directly involved in sensing mechanical triggers, with the cofilin mediated action of severing actin filaments displaying tension dependence when

force was applied to single actin filaments (Hayakawa et al., 2011). Recapitulating actin network formation *in vitro* also demonstrated how direct force application resulted in a denser structure of filaments, more free ends for branching, increased stiffness, yet decreased incorporation of actin monomers (Bieling et al., 2016). This study highlighted how the energy efficiency of actin acting as a motor increased under tension, but its approach did not investigate the *mechanisms* through which force alters the network formation. Further direct evidence for actin acting as a tension sensing cellular component is sparse (Harris et al., 2018), but evidently external forces lead to altered actin organisation, be it through direct mechanosensing or through regulatory proteins.

1.4.3 Microtubules

Microtubules are involved in mechanotransduction to an extent. These comprise the stiffest aspect of the cytoskeleton (Martino et al., 2018b) and are essential for multiple cellular processes including intracellular organelle transport, polarisation and chromosome separation (Cooper, 2000). Microtubules are composed of tubulin, a globular protein which is a dimer composed of α- and β- tubulin. Tubulin forms microtubules through polymerisation where they form head to tail arrays of the tubulin dimers that are assembled around a hollow core. These arrays are called protofilaments and usually there are 13 of these gathered around the core, where they create the polarised microtubule (Cooper, 2000).

Microtubules have been shown to exhibit a responsiveness to mechanical stress, though are less directly involved in mechanotransduction than the actin cytoskeleton. This mechano-sensitivity been evidenced by the alignment of mitotic spindles parallel to the direction of force applied to stretched mitotic cells (Fink et al., 2011). Importantly, the microtubules bind to certain proteins involved in transducing mechanical signals directly to the nuclear envelope (Graham and Burridge, 2016) (see **Chapter 1.6**). These proteins include Sun2, Nesprin-1 and Nesprin-2 which are all components of the LINC complex, an essential mediator of nuclear structure and chromatin organisation. When microtubules and SUN2 were perturbed in human adipose derived stem cells *in vitro*, differentiation and adipogenesis was significantly modulated (Y. Yang et al., 2018). This study proposed that the microtubules form a high-density cobweb-like structure around the nucleus where it may help regulate nuclear shape and thus direct cell fate. The demonstration of durotaxis in MSCs (Vincent et al., 2013) highlighted the importance of microtubules for directed migration due to their role in MSC polarisation. Actin was shown as essential for non-directional migration

and cell spreading, but seems to work synergistically with the microtubules to permit directed migration.

1.5 Shuttling proteins involved in mechanotransduction.

The second method of mechanotransduction other than the role of physical changes in the cytoskeleton is the shuttling of proteins to deliver messages from the cell membrane to the nucleus upon reception of mechanical information. There are multiple proteins involved in these signalling cascades, many with important roles as transcriptional regulators.

1.5.1 Zyxin

The aforementioned protein zyxin is one such messenger of mechanical signals. Zyxin is known as a focal adhesion protein that is involved in integrin dependent cell motility through its cooperation with α-actinin and Ena/VASP, affecting actin polymerisation and contractility (Crawford et al., 1992; Hoffman et al., 2006). This protein has been observed to shuttle between the focal adhesions and the nucleus – which raised the idea that it may be involved in regulating gene transcription following mechanical stimuli (Nix and Beckerle, 1997; Sun et al., 2012). The LIM domains of zyxin are particularly important regarding its activity at focal adhesions and in the nucleus. LIM domains have diverse biological functions, with certain cytoplasmic LIM proteins displaying the ability to regulate actin dynamics, and others acting as transcription factors and providing a regulatory role (Kadrmas and Beckerle, 2004). LIM domains share a similar structural organisation with zinc-finger DNA-binding sequences however it is likely that the LIM domains do not directly bind DNA; instead, LIM proteins may interact with transcriptional complexes and possible modulate the spatial distribution and therefore activity of transcription factors (Petit et al., 2000). A high percentage of LIM proteins are found at focal adhesions, as is the case for zyxin, with the LIM domains enabling the binding of important focal adhesion proteins. Overexpression of the LIM region of zyxin results in mislocalisation of endogenous zyxin from focal adhesions as well as alterations in the actin cytoskeleton (Nix et al., 2001). Zyxin is only observed transiently in the nucleus, and its shuttling between the cytoplasm and nucleus is driven by altered binding kinetics (Wang et al., 2019). This shuttling is at least partly controlled by a nuclear export region in the protein, and deletion of this signal induces a nuclear build-up of zyxin (Nix et al., 2001). Despite knowledge of its presence in the nucleus, the regulatory activity of zyxin on gene expression has not been fully investigated.

1.5.2 β-catenin

B-catenin was one of the first proteins involved at junctions discovered to have a shuttling ability. This protein is closely associated with E-cadherin, with an essential role in linking it to the actin cytoskeleton, but it has another important role in signalling – specifically in the canonical Wnt signalling cascade (Valenta et al., 2012). Wnt signalling is vastly important for cellular processes, regulating aspects such as cell fate determination, motility, polarity and more (Komiya and Habas, 2008). Originally, β-catenin was discovered through two independent instances, one on the basis of it as a structural protein (Ozawa et al., 1989), and the other through discovering it as a signalling molecule in drosophila (Wieschaus et al., 1984), thus it is clear that its functions are wide ranging.

Newly synthesised β-catenin is first recruited to E-cadherin where it is immobilised. Here at the AJs it interacts with α-catenin where it can assist in regulating the organisation of the actin cytoskeleton (see **Chapter 1.3.2**). Downregulation of E-cadherin and the activity of protein kinases allow the of release β-catenin into the cytoplasm (Valenta et al., 2012). In the absence of Wnt signalling, cytoplasmic β-catenin is degraded by the proteasome after phosphorylation and subsequent ubiquitination by the destruction complex (Stamos and Weis, 2013). The degradation of β-catenin by the destruction complex is preventable through Wnt signalling which results in increase of cytoplasmic β-catenin. Upon this build-up, β-catenin is able to translocate to the nucleus where it associates with TCF/Lef proteins and converts them into TCF/β-catenin transcriptional activators, promoting the transcription of target genes downstream of the Wnt pathway (Valenta et al., 2012).

An important part of the destruction complex is the glycogen synthase kinase 3 (GSK-3) which phosphorylates the β-catenin, thus targeting it for degradation (Stamos and Weis, 2013). GSK-3β can be inactivated itself through phosphorylation, and this prevents the degradation of β-catenin. Mechanically stretching osteoblastic cells causes an increase in GSK-3β phosphorylation, and elevated levels of nuclear β-catenin (Li et al., 2018). Accordingly, the activity of the transcription factor TCF was also enhanced, along with increased expression of Wnt target genes. The binding level of β-catenin to E-cadherin was also significantly reduced under tensile stress, potentially due to the structural deformation of the cytoskeleton and cell membrane disrupting the β-catenin – E-cadherin complex (Li et al., 2018).

Wnt/β-catenin signalling is also increased in lymphatic endothelial cells undergoing oscillatory shear stress, with increased levels of active β-catenin found in the cells under stress (Cha et al., 2016). One suggested mechanism through which this occurs is due to

receptor tyrosine kinases which inhibit catenin-cadherin binding at the junctions and promote nuclear translocation of β-catenin (Cha et al., 2016). Certain receptor tyrosine kinases (Ret, VEGFR2 and VEGFR3) are mechanoresponsive and can be activated through mechanical strain (Cha et al., 2016; Coon et al., 2015; Fernández-Sánchez et al., 2015). It was shown that β-catenin binding to VE-cadherin could be reduced through stretching, however this study curiously saw no reduction in β-catenin to E-cadherin binding under stress (Adkison et al., 2006). There is evidently a significant role of β-catenin in mechanotransduction, with mechanical forces playing a role in increased activation of canonical Wnt signalling due to increasing the nuclear shuttling of β-catenin. The exact means and conditions through which it is activated still require further elucidation.

B-catenin is also closely linked to the epithelial to mesenchymal transition (EMT), a process with strong relevance to *in vitro* cell culture, particularly when using cancer cell lines (Fontana et al., 2019; Pal et al., 2019). A common feature of cancer, cells undergoing EMT lose their epithelial characteristics and adopt a highly motile and invasive mesenchymal stem cell phenotype. Wnt signalling is a key pathway involved in EMT (Mylavarapu et al., 2019) and one of the downstream targets of this pathway is the transcription factor Twist which downregulates E-cadherin, and induces N-cadherin.(Yang et al., 2004). Loss of E-cadherin at the cell membrane and increased N-cadherin is a hallmark of EMT (Mylavarapu et al., 2019; Valenta et al., 2012), and this loss of E-cadherin is linked to more free cytoplasmic β-catenin, potentially further increasing the transcription of genes that promote EMT.

1.5.3 YAP/TAZ

In recent years, yes-associated protein (YAP) and WW Domain-Containing Transcription Regulator Protein 1 (WWTR1/TAZ) have emerged as critical shuttling proteins involved in mechanotransduction that are not associated with the focal adhesions (Martino et al., 2018a). These proteins are transcriptional co-activators that are regulated downstream of the Hippo pathway. The TEAD family of transcription factors have a major role in mediating the transcriptional activity of YAP/TAZ, forming a transcriptional module with nuclear YAP/TAZ to transcribe downstream target genes (Hansen et al., 2015). The Hippo pathway affects the cell in multiple ways, regulating organ size, cell fate, tissue homeostasis and tumour progression (Chang et al., 2020). Hippo signalling inhibits YAP through Lats mediated phosphorylation, which results in cytoplasmic retention and degradation of YAP (Zhao et al., 2010). The Hippo pathway is also involved in Wnt signalling, with cytoplasmic TAZ possessing the ability to inhibit phosphorylation of dishevelled (DVL) a protein in the Wnt pathway

whose phosphorylation precedes β-catenin activation (Varelas et al., 2010). Loss of TAZ results in increased accumulation of cytoplasmic and nuclear β-catenin in *TAZ*-null mice, demonstrating the link between the two pathways (Varelas et al., 2010).

The Hippo pathway and YAP/TAZ are substantially involved in mechanotransduction (see **Figure 1.3**), Yap is sensitive to contact inhibition with the expression of E-cadherin preventing the localisation of Yap in the nucleus of MDA-MB-231 cells (Kim et al., 2011). Yap is inactivated through phosphorylation by the Lats tumour suppressive kinase which shows increased activity in high density cultures. Phosphorylation of Yap at specific serine sites by Lats helps retain cytoplasmic Yap through creating a binding site for the scaffolding protein 14-3-3 which sequesters it in the cytoplasm (Zhao et al., 2007). Increased phosphorylation of Yap and exclusion from the nucleus in high density cultures correlates with this (Zhao et al., 2007). The wound edge of scratched cultures resulted in the induction of YAP nuclear localisation, and YAP overexpression results in the expression of genes that promote proliferation, with an opposite expression profile to that of confluent cells (Zhao et al., 2007). A set of the core proteins in the Hippo pathways – the Hpo/mammalian Ste20-like kinases 1/2 (MST1/2) – were found to be colocalised with F-actin and were activated upon disruption of the actin cytoskeleton (Densham et al., 2009).

Morphology and the formation of stress fibres appears to significantly affect the Hippo pathway as well, with rounder more compact cells containing more cytoplasmic Yap and flatter cells exhibiting more nuclear Yap (Wada et al., 2011). Phosphorylation (inactivation) of Yap is also affected, with stress fibre disruption by CytoD treatment resulting in a rounder cell morphology and increased Yap phosphorylation. Consistent with this, highly phosphorylated Yap was present in higher cell densities which gives rise to a rounded morphology, and vice-versa in low densities where the Yap was more localised to the nucleus (Wada et al., 2011). It appears then that actin stress fibres inhibit the Hippo pathway via interference directly with or upstream of Lats, which results in reduced phosphorylation of Yap and higher nuclear localisation (Wada et al., 2011). This is strong evidence for the mechanosensitive nature of Yap which corroborates with its sensitive nature to cell to cell contacts (Zhao et al., 2007).

Actin polymerisation appears to positively regulate Yap activity too, with the actin severing proteins Cofilin and Gelsolin appearing to antagonise Yap functioning in cells with low mechanical stress (Aragona et al., 2013). On the other hand, a formin-related actin polymerisation driver protein called Diaphanous promotes Yap nuclear translocation (Gaspar

and Tapon, 2014). Interestingly, the Hippo pathway may also regulate the assembly of actin filaments, with reduction of Hippo pathway activity resulting in abnormal F-actin accumulation (Fernández et al., 2011). There is evidently signalling in both directions between the Hippo pathway and the cytoskeleton which is key for the mechanosensitive nature of Yap activity/nuclear shuttling.

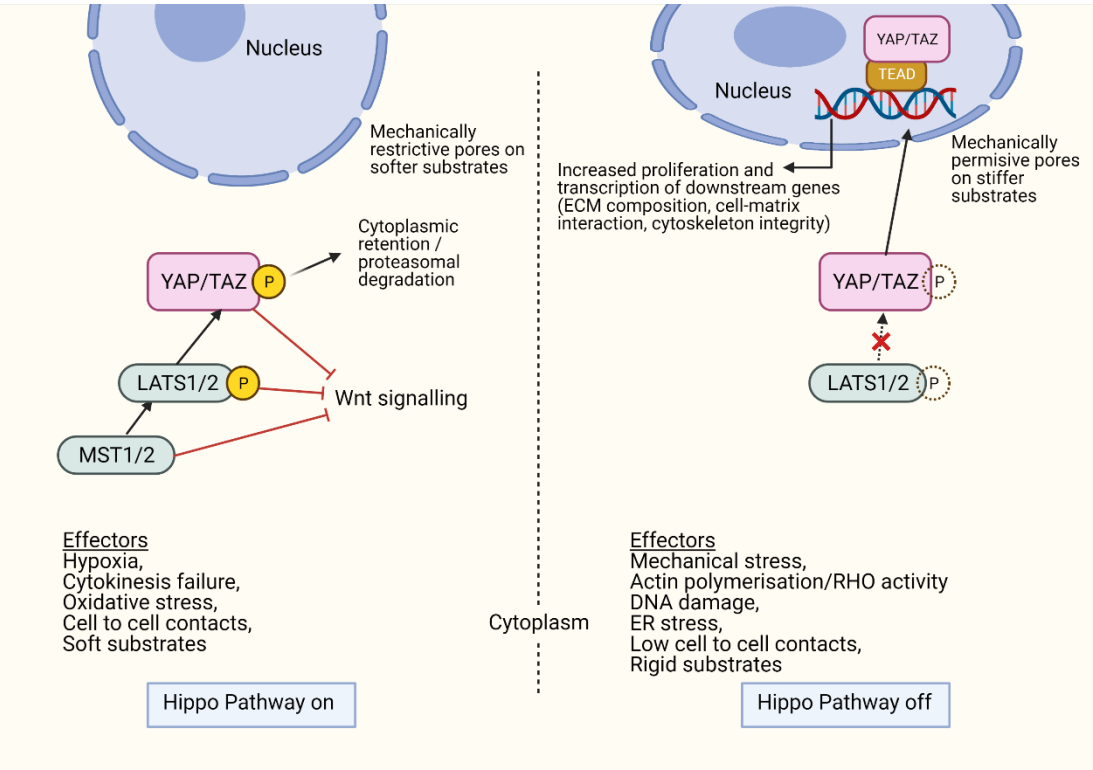

Figure 1.3: Softer substrates with increased cell to cell contacts inhibit YAP/TAZ activity through LATS mediated phosphorylation.

Figure adapted from (Hansen et al., 2015). A number of effectors regulate YAP either directly through the Hippo pathway or through interacting signalling pathways. When the Hippo pathway is active, YAP/TAZ is inactivated through LATS1/2 mediated phosphorylation, increasing cytoplasmic retention and proteasomal degradation of YAP/TAZ, and this inhibits wnt signalling. When the HIPPO pathway is inactive, hypophosphorylated YAP/TAZ nuclear translocation is increased allowing TEAD mediated transcription of downstream genes and increased proliferation. Stiff substrates positively regulate YAP/TAZ activity through RHO signalling. In softer substrates, nuclear membrane pores are more mechanically resistant to entry of transcription factors compared to more permissive pores in stiffer substrates which also contributes to increased YAP/TAZ nuclear translocation (Alisafaei et al., 2019). Created with BioRender.com.

Finally, one more mechanism through which Yap activity may be altered is the mechanical link between the cytoskeleton and the nucleus. The LINC complex will be discussed in more depth below, but this consists of multiple proteins and provides a physical link between the nucleus and cytoskeleton. Tensile forces produced from the cytoskeleton and transferred to the nucleus were shown to be essential for stretch based YAP/TAZ activation (Driscoll et al., 2015). One protein in the complex – Nesprin 1 – seemed particularly key in enabling the transfer of cytoskeletal strain to the nucleus, with said transfer being compromised upon reduced Nesprin-1 giant levels, leading to a reduced YAP response to dynamic stress (Driscoll et al., 2015). While YAP is known to promote proliferation, its role in mechanotransduction is potentially more related to promoting the transcription of genes involved in cell-matrix interaction, ECM composition and cytoskeleton integrity (Martino et al., 2018a).

1.6 The Nuclear Envelope and the LINC complex

Changes in the morphology of the cell and the organisation of the actin cytoskeleton have been shown to have marked effects on the expression of genes and on the biological functions of the cell. These changes arise through the linker of nucleoskeleton and cytoskeleton (LINC) protein complex that couples the actin cytoskeleton to the nuclear lamina (see **Figure 1.4**). This is found in the inner (INM) and outer nuclear membrane (ONM) of the nuclear envelope and contains multiple components; SUN and nesprin proteins (Martino et al., 2018b). The nuclear envelope is considered a regulator of both physical connections between the cytoskeleton and the nucleus, but also a biochemical regulator (Uzer et al., 2016). Underneath the nuclear envelope lies the nuclear lamina; a network consisting of lamins and lamin associated proteins, with a role of providing mechanical support to the nucleus. Pertinently it also regulates chromatin organisation (Gruenbaum et al., 2003), amongst other nuclear related functions such as DNA replication and RNA transcription. The nuclear envelope lamina spanning complexes (NELSCs) bind chromatin and affect its structure due to force transmission, and the consequent change in the 3D arrangement of genes in the chromosomal territories affects the expression of genes (Gieni and Hendzel, 2008). Nuclear integrity is vital in protecting the components of chromatin from the cytoplasm, with nuclear envelope ruptures making DNA susceptible to damage from nucleases for example. This manipulability of the nucleus is dependent on the expression of lamin A/C, with deficiency of this resulting in irreversible nuclear deformation (Cao et al., 2016).

In addition to the importance of lamins in the mechanical behaviour of the nucleus, they are closely implicated in severe disease when mutated (laminopathies). At least 15 diseases are attributed to mutations in LMNA, ranging from muscular dystrophies to progerias (Schreiber and Kennedy, 2013). These diseases affect a diverse range of tissues and functions, indicating the essential role that lamins have in maintaining healthy physiological function. LMNB1 and LMNB2 mutations are also linked to rare diseases such as adult-onset leukodystrophy (LMNB1 autosomal dominant mutations). Mechanistically, there is evidence that LMNA mutations lead to altered signal transduction pathways including β-catenin / Wnt and mechanical stress signalling, which can be linked to gain-of-function toxicity and/or loss of function (Schreiber and Kennedy, 2013).

1.6.1 Nesprins

The nesprin proteins in the LINC complex are located at the ONM and interact with SUN proteins through a C-terminal KASH domain conserved across the five mammalian Nesprin genes (SYNE 1-4, KASH5) (Graham and Burridge, 2016). The different nesprins are responsible for binding separate cytoskeletons. Nesprin-1 and -2 are actin binding, but can also connect with microtubules, nesprin-3 binds to intermediate filaments, and nesprin-4 and KASH5 indirectly bind to microtubules albeit through separate mechanisms (Graham and Burridge, 2016). KASH5 is specific to cells undergoing meiosis and is important for telomere localisation (Morimoto et al., 2012). The giant nesprins (nesprin-1 and -2) bind F-actin through their N-terminal domains (Mellad et al., 2011) and nesprin-3 binds to the intermediate filaments via the IF linker protein plectin (Bouzid et al., 2019).

These proteins are essential for transduction of cytoskeletal tension to the LINC complex; nesprin-2 giant for example is subject to actomyosin dependent mechanical tension in fibroblasts (Arsenovic et al., 2016), demonstrated through a fluorescent resonance energy transfer (FRET) biosensor. This is purported to be one of the primary ways through which the nuclear shape is altered as a result of myosin dependent cellular shape changes. This deformation of the nuclear shape as a result of cellular tension has been demonstrated multiple times (Hu et al., 2004; Lombardi et al., 2011; Lovett et al., 2013) and these studies further consolidate the role of the LINC complex in directing nuclear morphology through its cytoskeletal links. One such study highlighted this through disruption of the LINC complex which resulted in disturbance to the perinuclear actin, along with impaired nuclear positioning, cell polarity and disrupted intracellular force transmission (Lombardi et al., 2011). This study also investigated alterations in mechanosensitive gene expression of Egr-

1, Iex-1, Pai-I, Tenascin C, Talin and Vinculin upon LINC disruption; but these curiously did not exhibit the expected reduced expression suggesting that nuclear deformation is not necessarily a modulator of the expression of at least this set of mechanosensitive genes. The organisation and shape of the nucleus is important biologically due to the connection of the LINC complexes to nuclear chromatin (Rashmi et al., 2012). It is believed that nesprins and nuclear structure may act a transcriptional regulator through bringing the chromatin 'into a surrounding favourable or unfavourable for activity' (Rashmi et al., 2012).

1.6.2 SUN proteins

The SUN proteins are the second main component of the LINC complex, and these lie in the perinuclear space between the two membranes in the nucleus. The KASH domain proteins (nesprins) have various complimentary SUN proteins, meaning there are multiple LINC complex isoforms (Bouzid et al., 2019). The SUN proteins consist of nucleoplasmic N-terminal domain, a transmembrane helix that crosses through the INM with a SUN domain at the C-terminal tail (Cain and Starr, 2014) in the perinuclear space which binds with the C-terminal domain of the nesprins (Bouzid et al., 2019). The balance of Sun1 and Sun2 proteins in the LINC complexes can directly affect gene expression through the Serum Response Factor/Megakaryoblastic Leukemia 1 (SRF/Mk11) transcription factor/co-activator complex. Sun2 promotes a positive feedback loop comprising of this complex, whereas Sun1 inhibits it (May and Carroll, 2018). Sun1 is more efficiently incorporated into the LINC complex than Sun2, however SRF/Mk11 signalling increases Sun2 incorporation, revealing a dynamic interplay between the SUN proteins and SRF mediated gene expression (May and Carroll, 2018). The SUN proteins form trimers with the helixes spanning to the transmembrane domain and potentially act as 'molecular rulers' to ensure that the nuclear envelope is evenly spaced when cells are under high mechanical strain (Cain and Starr, 2014), suggesting that these proteins are key for maintaining mechanical integrity of the nucleus. SUN proteins interact indirectly with the nucleus through interacting with lamin A (Martino et al., 2018a) where it may indirectly interact with chromatin.

1.6.3 The nucleoskeleton

The nucleoskeleton encompasses multiple mechanical structures within the nucleus – the lamina, actin, multi-subunit proteins and chromatin (Dahl and Kalinowski, 2011). This multi-faceted structure has a significant role in the organisation of chromatin, with tension both inside and outside of the nucleoskeleton markedly altering how chromatin interfaces with

the INM which influences differentiation, division and wide ranging aspects of cell biology (Ungricht and Kutay, 2017).

The nuclear lamina is able to cope with various mechanical insults due to its unique structure which consists of A- and B- type lamins that assemble into tetrameric filaments (Turgay et al., 2017). The nuclear lamina is capable of interacting both directly and indirectly with chromatin (Burke and Stewart, 2013; Butin-Israeli et al., 2012; Link et al., 2015). Lamins are able to adapt the nuclear structure according to cellular morphology through changes in their mechanical folding and phosphorylation (Cho et al., 2017). The transcription and expression of lamins is sensitive to substrate stiffness and the presence of retinoic acid, and is upregulated in cells grown stiffer substrates with RARγ, resulting in a stiffer nucleus (Swift et al., 2013). Knockout of lamin B1 (LB1) revealed a mechanism through with the lamins are able to control transcription and chromatin organisation; LB1 deficient nuclei exhibited the formation of nuclear blebs that contained gene rich euchromatin. Therefore, this study proposed that LB1 is essential for the organisation of lamin A/C and LB2 microdomains which have various functions in chromatin organisation and gene regulation (Shimi et al., 2008). RNA polymerase II transcription was also reduced in LB1 deficient cells indicating a direct role of LB1 in affecting the transcriptional machinery. The transcription of certain genes is also dependent on being tethered to nuclear pore complexes (NPCs) (which were absent in the blebs) suggesting that genes linked to the B-type lamin microdomains might not be activated unless in the presence of NPCs (Shimi et al., 2008). Nuclear pore complexes are associated with the expression of Sun1, as depletion of Sun1 resulted in NPC clustering suggesting it plays a role in their distribution (Liu et al., 2007).

Nuclear actin is also closely linked to chromatin dynamics; short filamentous actin for example has been observed in the nucleus where it may associate with lamins and potentially act as a scaffold/matrix to help organise various nuclear components, including the altering of intranuclear transport of RNA (Belin et al., 2013). Non polymeric actin acts as a co-factor to many gene transcription factors too, demonstrating further importance of actin in regulating gene expression (Virtanen and Vartiainen, 2017). Nuclear actin has also been shown to directly modify chromatin organisation (Le et al., 2016; Miroshnikova et al., 2017), with mechanical signals being transduced into the nucleus through the perinuclear actin ring formed with the help of myosin IIA and emerin. Emerin helps anchor SUN proteins to lamin A and also is a direct interactor with chromatin (Martino et al., 2018b). The perinuclear ring facilitates F-actin polymerisation around the nucleus upon mechanical strain, whereupon

emerin also dissociates from lamin A/C, highlighting an actin dependent mechanosensory aspect to the nucleus. These alterations in the perinuclear cap are correlated with a decrease of non-polymeric actin in the nucleus, which resulted in a reduction of transcriptional activity revealing a clear link between the organisation of the actin cytoskeleton and gene expression (Le et al., 2016).

The interplay between the nuclear envelope and the nucleoplasm is important in the mechano-sensitivity of cells. Differentiated stem cells for example exhibit increased nuclear stiffness over their pluripotent counterparts; a result of lamin and chromatin reorganisation that then alters the cell's ability to respond to external mechanical cues (Heo et al., 2016a). This allows the cell to prime itself in relation to how it responds to mechanical cues, with sensitisation of the transduction apparatus arising from increased nuclear stiffness (Heo et al., 2016a). The nucleoskeleton may compensate for stiffer nuclei by increasing stress and deformation at the LINC complexes, and the ECM through focal adhesions. In the transition from pluripotent to differentiated cells, the nucleus is reconfigured to behave as a stress concentrator, with an increase in calcium mobilisation which may impact lamin processing (Heo et al., 2016a). Indeed, in human adipose derived stem cells, LINC complex density was seen to increase after 4 days of adipogenesis, indicating that nuclear reinforcement was occurring to maintain stability under mechanical strain (Y. Yang et al., 2018). In tandem with this, the cytoskeleton decreased in density, which highlights the balance and interplay between the nucleoskeleton and cytoskeleton. These two cellular components may act like a molecular 'seesaw' to maintain mechanical integrity of the cell; upon the strengthening of one, the other weakens. The fact that the nucleus is a dynamic mechanical element of the cell means that it is able to constantly adjust to the demands of the surrounding environment and can modulate the mechano-sensitivity of the cell accordingly. Differences in nuclear stiffness are also lineage specific, and lamin A levels appear to aid in guiding cells towards specific fates, potentially due to their ability to affect gene expression through alterations of nuclear structure (Shin et al., 2013).

1.6.4 Chromatin organisation

Chromatin is found in the nuclear interior and is essential in packing the vast amount of DNA into the nucleus through forming a tightly wound complex consisting of DNA wound around histone proteins (Tsompana and Buck, 2014). The structure and location of chromatin are correlated with the function of the cell, with densely packed chromatin (heterochromatin) mainly being transcriptionally inactive, and the more openly structured euchromatin being

much more transcriptionally active (Dahl et al., 2008). Heterochromatin is often found near the periphery of the nucleus whereas euchromatin is more commonly found at the interior. One main driver for epigenetic regulation of cell function is remodelling of chromatin through post-transcriptional modifications such as methylation and acetylation, which permits the chromatin to shift between hetero- and euchromatin (Miroshnikova et al., 2017). However heterochromatin – being mainly located at the periphery – is physically linked via lamin-associated chromatin domains (LADs) to the nuclear envelope, and is structurally dynamic (Miroshnikova et al., 2017). Changes in chromatin dynamics generate mechanical forces which are also transduced to the nuclear envelope through the associations between lamin and chromatin (Kumar et al., 2014).

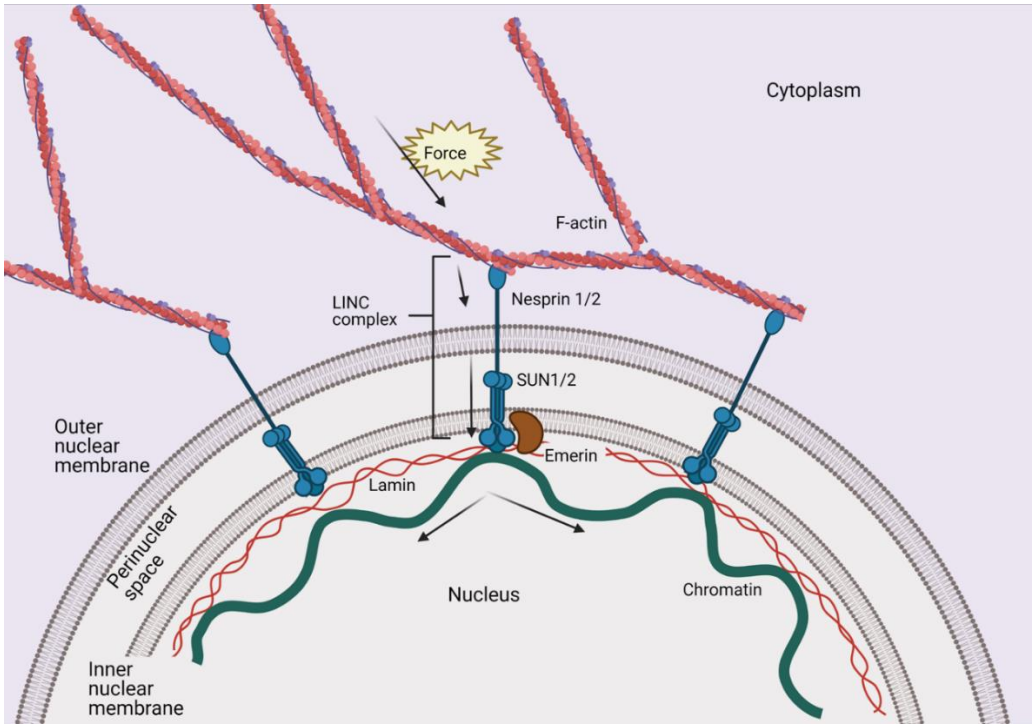

Figure 1.4: The actin cytoskeleton transmits force to the nucleus through the LINC complex.

Figure adapted from (Martino et al., 2018b). The LINC complex is primarily formed from SUN1/2 proteins and nesprins. SUN proteins span the inner nuclear membrane, and closely associate with the nuclear lamina through interactions with the lamin proteins, emerin and small INM nesprin isoforms (Rajgor and Shanahan, 2013). SUN proteins bind to the C-terminal KASH domain on nesprins in the perinuclear space (Martino et al., 2018b). Nesprin-1/2 directly links to the actin cytoskeleton through an actin binding domain (Taranum et al., 2012). Force can be transmitted to the nucleus from the ECM due to the close nuclear-cytoskeletal coupling. Created with BioRender.com.

Chromatin is a highly deformable component of the nucleus, possessing viscous and elastic properties (Bouck and Bloom, 2007) whilst also playing an important role in defining the mechanical properties of the nucleus as a whole. Only through the liquid-like properties of chromatin are cells able to maintain genetic integrity and remain damage free when existing on or moving through matrices that demand cellular deformation (Cao et al., 2016). As mentioned, external mechanical forces are capable of altering the mobility and positioning of chromatin (Booth-Gauthier et al., 2012) which has profound consequences on the cell. The chromatin can be considered a rheological element of the nucleus that is able to adapt mechanically to changes in cellular and nuclear structure. The arrangement of chromatin directly affects its mechanical properties with the tightly packed heterochromatin and the loosely packed euchromatin exhibiting differential viscosity measurements (Spagnol and Dahl, 2016). This also impacts the properties of the nuclear interior, with a more viscous environment being evident after de-condensation of the tightly packed heterochromatin (Spagnol and Dahl, 2016), and it is hypothesised that the ability of chromatin to stiffen upon condensation means that chromatin itself plays a role in stress absorption (Miroshnikova et al., 2017). The condensation of chromatin restricts the access of transcription machinery but is still selective by allowing the expression of certain constitutively expressed genes. One study showed that when cells are subjected to mechanical stress, the immediate response (within seconds) is that the chromatin alters its conformation to an open state, and this increases transcription. The sustained response however (after 10 minutes) results in an increase of heterochromatin due to ATP mediated chromatin condensation, and this results in reduced expression of genes residing in those regions (Heo et al., 2016b), though other studies have shown that on stiffer substrates, chromatin is more permanently decondensed (Alisafaei et al., 2019). Chromatin dynamics are evidently a complex aspect of mechanobiology and there is still more to be done to fully clarify the mechanics involved.

There is large body of evidence pointing towards the bi-directional relationship between the nucleus and the cytoskeleton (Burridge et al., 2019), with the nucleus showing a clear sensitivity to mechanical forces exerted through alterations in mechanical properties of the ECM (Haase et al., 2016). To some degree, nuclear stiffening as a result of cytoskeletal forces might be an inherent mechanism to protect and preserve chromatin structure and organisation from excessive strain (Guilluy and Burridge, 2015). However, it would appear that chromatin organisation is altered between different substrate geometries (Alisafaei et al., 2019), meaning that the tight linkage between the cytoskeleton and the nucleus *does* appear to have profound impacts on the epigenetic profile of the cell. Indeed, this study by

Alisafaei et al. provided a thorough mechanical insight into how the shape of a cell – as guided by substrate mechanics – has a direct effect on the nucleus. Longer elongated cells resulted in increased stress fibres, nuclear lamina stiffening and chromatin loosening compared to more spherical cells where actomyosin contractility was disrupted and chromatin condensation occurred.

It is very clear that from the cell surface, right down to the nucleus and chromatin itself, that the mechanical microenvironment has profound implications on cell biology. While this has not provided an exhaustive list of all involved aspects of mechanotransduction, it has shown a set of key factors that influence this process and demonstrated the inherent complexity that guides gene expression as a result of cell morphology. This demonstrates the importance of considering the microenvironment when creating an *in vitro* model, and indicates why 3D cultures often exhibit more physiologically relevant properties over 2D; because they more closely mimic the structural properties of the native tissue.

1.7 Issues with 2D Cell Culture: Is 3D Cell Culture the Solution?

As previously described, there is a very strong rationale for trying to more closely mimic physiological structures when developing *in vitro* models. However, this is not necessarily a simple ask, and to truly invoke a change in research, there needs to be a paradigm shift towards deeper consideration of matching the cell-based models to their native tissue architecture. This will largely involve evolution in the cell culture techniques used; 2D cell culture (commonly on a flat polystyrene surface) is currently the most popular way to maintain cells, either primary or immortalised, for the purpose of drug tests, model production and more (Edmondson et al., 2014a). 2D cell culture is however inherently non-physiological as the flat surface of culture flasks lack the complex 3D interactions present in the body. As described, a 2D substrate is often stiffer than a 3D counterpart, and this mechanical property results in altered cell morphology and, as a consequence of mechanotransduction, altered cell biology. These changes result in a phenotype that differs from the phenotype of the cells *in vivo*, and therefore this raises an issue with biological validity, with 2D cells showing a range of poorer physiological properties including poorer differentiation , and vastly different gene expression to 3D cultures (Langhans, 2018).

The issues with poor physiological relevance have wide ranging impacts. In the clinical trial pipeline, drugs are commonly tested on *in vitro* cultures before being moved to animal and eventually human trials. In these later, and more expensive stages of the clinical trial pipeline

there is a extraordinarily high number of failed candidates, with data from 2013 highlighting that less than half of drugs pass Phase II and Phase III clinical trials. Over 50 % of these failures are attributable to a lack of efficacy, and over 25 % are due to an inaccurate therapeutic (safety) index (Arrowsmith and Miller, 2013). These numbers are a stark reminder that there is a drastic need for improved *in vitro* models to filter out unsuccessful candidates at an earlier stage to save both a significant amount of time and money. With the vastly improved metabolic profiles of 3D cells over 2D, they are often more accurate in predicting efficacy of drugs and preventing false positives (Jensen and Teng, 2020). Furthermore, stem cells cultured in 2D have been shown to be inappropriate for large scale randomized clinical trials due to the decrease in replicative ability (Jensen and Teng, 2020). 2D cells are also only partially polarised with significant differences observes in viability, morphology, proliferation and differentiation (Chaicharoenaudomrung et al., 2019), with the often higher proliferative rates in 2D leading to difficulties in facilitating long term cultures due to over-confluence.

The current and promising solution to this issue is 3D cell culture; growing cells in a 3D microenvironment that more closely mimics the structure of the ECM. This is a rapidly growing area of research with the number of papers focussing on 3D culture having drastically increased since the late 1990s (Jensen and Teng, 2020). The various techniques of 3D cell culture are wide ranging, with many different applications and in many cases, they provide enhanced functional properties in the models. This provides a significant leap towards resolving the issues that arise with 2D cell culture, however using a consistent cell type between different models yields largely varied structural and functional phenotypes and a complete recapitulation of the *in vivo* phenotype of any cell line is yet to be seen. **Table 1** highlights some of the key differences between 2D and 3D culture, and this demonstrates the advantages of culturing cells in 3D. Strangely, there has been a notable lack of research that investigates the connection between mechanotransduction and improved 3D *in vitro* models, with most mechanotransduction research being focussed on the molecular pathways that arise from altered mechanical properties in the microenvironment. This project attempts to start bringing the two research areas of mechanobiology and applied *in vitro* research together to help further bridge the gap between structure and function. Despite the generally improved functional and physiological properties of 3D cultures, standard 2D cultures do have advantages in some areas, such as generally high reproducibility, which is lost to some extent in certain 3D cultures due to the more variable qualities of certain 3D technologies (Chaicharoenaudomrung et al., 2019). Additionally 2D cultures are often significantly cheaper to produce due to lower manufacturing costs

Table 1.1: Cellular differences between 2D and 3D culture. Adapted from (Edmondson et al., 2014a)

Cellular aspect changing	2D	3D
Morphology	Flat and spread out to maximise contacts with the flask surface. (Baker and Chen, 2012).	Closer shape to *in vivo* cells, more complex morphology due to existence in 3D microenvironment. (Kim, 2005).
Architecture	Monolayer cultures mean that there is unlimited access to nutrients and any biological factors added to the culture (Chaicharoenaudomrung et al., 2019).	Denser layers of cells mean concentration gradients are possible, differential access to nutrients and biological factors throughout the model and hypoxic cores (Langhans, 2018).
Cell Contacts	Cells are in less contact with each other due to monolayer nature, however adherens junctions may increase on stiffer surfaces (Ladoux et al., 2010). Localised cell to ECM contacts on surface in contact with substrate (Astashkina and Grainger, 2014).	More stable adhesions, increased cell-cell contact and more natural spread of cell to ECM adhesions. (Doyle et al., 2015; Doyle and Yamada, 2016).
Drug Sensitivity	Highly sensitive, potential for false positives, poor expression of drug metabolising enzymes. (Luckert et al., 2016).	Higher resistance, potential for false negatives, increased enzyme expression and activity. (Hongisto et al., 2013; Imamura et al., 2015; Ramaiahgari et al., 2014a).
Function	Different gene expression to *in vivo,* decreased functionality (Szot et al., 2011). Poor differentiation (Jensen and Teng, 2020).	Closer gene expression to *in vivo* and improved function (Luckert et al., 2016; Price et al., 2012). Good differentiation (Jensen and Teng, 2020)

(Friedrich et al., 2009), and are easier to use due to more complex preparations and training required to grow cells in certain 3D technologies. Despite this, 3D culture is becoming more commonplace and this brings with it new 3D culture techniques that are more practical and cheaper.

1.7.1 3D Cell Culture Technologies

This literature review has made it clear that the structure of the cell defines function and has highlighted that as a consequence of this central paradigm, 2D *in vitro* cultures elicit non-physiological responses in cells. 3D culture is therefore the first step in eliminating the issue of poor cell function in culture, though there are many techniques to choose from in 3D cell culture, each with different properties that may benefit specific cell types when matching them to native tissues. **Table 1.2** shows the main 3D culture methods that are available and highlights some known advantages and disadvantages of each. Some of the key aspects to consider in deciding on an optimum model are the structural and mechanical properties of the 3D model, the presence of any biological factors, and the reproducibility. With these in mind, in a project such as this one, aiming to study purely mechanical effects of a substrate on the growth of cells, the key aim would be to use a 3D culture method that is highly reproducible that limits any additional variables so that a change in the mechanical microenvironment is the only effector on the models. The other factor to consider when deciding on a model is the end goal; does the model need to be high throughput for broad and rapid screening of drug toxicity for example, or is the model focussed on a more bespoke purpose such as tissue engineering for pathology research?

The PolyHIPE scaffold Alvetex® will be the substrate primarily focused on in this project. Alvetex® is a polystyrene scaffold providing a biologically inert substrate which currently offers 2 commercial and 1 non-commercially available products with varying void sizes to allow control over whether the cells invade fully, or rest on top of the 3D structure. **Table 1.3** lists the three types of Alvetex® available, providing more detail about their respective properties. This is a form of a scaffold-based 3D technology which provides physical support to cells to support their growth in a three-dimensional microenvironment. The structure and chemical make-up of scaffold based substrates can vary between different technologies, however the key aspect of scaffold technologies is that cells are grown on/in a matrix where physical and potentially chemical factors can influence the biology of the cells residing in the models (Langhans, 2018). These scaffolds can be synthetically made or biologically derived, with each having potential advantages. Synthetic scaffolds tend to be produced in tightly

controlled environments that can closely tune the mechanical properties such as porosity and stiffness to create a reproducible structure within the substrate, however these may lack additional chemical components that could also influence and support cell growth and function. On the other hands, biologically derived scaffolds may be more inherently ECM-like in some cases, however the nature of these means that inclusion of biological factors can increase variability and uncertainty in the precise composition of the substrate (O'Brien, 2011).

Table 1.2: 3D culture techniques and related advantages and disadvantages.

Type of 3D Cuture	Example	Pros	Cons
Scaffold	Alvetex®, Speritech (polymer foams), Novamatrix 3D	Can mimic ECM, stable and low variability, wide variety of materials available, high level of control over variables such as porosity. (Gurski, 2010).	Potential difficulty in harvesting or visualising cells (Carletti et al., 2011). Biological variability in natural scaffolds creates issues with reproducibility (Tibbitt and Anseth, 2009a).
Hydrogel	Advanced biomatrix (collagen), Nova-matrix 3D (alginate), Sigma (polyacrylamide)	Provide a specific set of desired cues (mechanical, compositional and structural), can be tailored to suit needs, mimics ECM and soft tissue (Caliari and Burdick, 2016).	Certain gels can be difficult to harvest cells from (this is being improved), can be difficult to sterilise, biological variability (Caliari and Burdick, 2016).
Aggregate	Scivax (Nanoculture plates), 3D biomatrix (hanging drop plates)	Do not require scaffolds, easily characterised – readily imaged by microscopy, high throughput (Haycock, 2011).	Can form non-uniform cell masses, disorganised structure, and variable success in forming spheroids (also being improved) (Edmondson et al., 2014a).

Table 1.3: Table listing the three types of Alvetex® available along with their key properties.

Alvetex® Type	SEM Micrograph	Properties
Scaffold	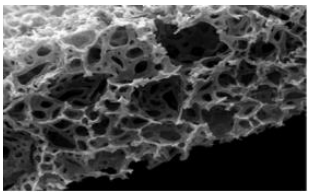	Voids: 40 µm Interconnects: 13 µm Deep penetration and spread of cells, less hypoxic and better availability of media. Commercially available.
Strata	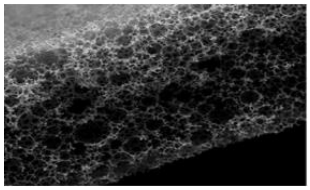	Voids: 20 µm Interconnects: 5 µm Some penetration still permitted, but cells may form a layer on top, invasive cells may penetrate further. Commercially available.
Polaris	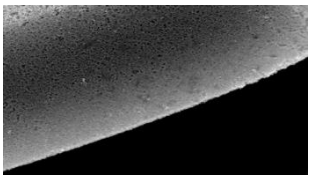	Voids: 3 µm Interconnects: 1 µm Almost no penetration, provides a porous surface for cells to grow on top of. Very little media availability between sides. Commercially unavailable.

1.7.2 3D models in liver research.

This project is focussing on the effects of 3D culture on cell biology, and liver models have been chosen as a medium to explore this through. The liver is an organ that has a role in a number of key biological functions; it is responsible for drug detoxification and metabolism, protein and amino acid biosynthesis and metabolism, lipid and cholesterol homeostasis and blood volume regulation (Trefts et al., 2017). The parenchymal epithelial cell population in the liver is hepatocytes, responsible for performing a large number of the liver specific functions and make up the majority of the volume (Trefts et al., 2017). Hepatocytes exhibit a unique polarity, with distinctive apical regions adjacent to small lumen structures forming between the cells called bile canaliculi which function in draining bile towards the gallbladder (Boyer, 2013). The basal membrane of the cells is adjacent to the blood sinusoids (Boyer, 2013) which are small capillaries flanked by hepatocytes than running throughout the liver creating a highly vascularised environment. The structure of the liver can be microscopically divided into the anatomic unit of the liver, the lobule. The liver lobule adopts an irregular polygonal organisation as seen in **Figure 1.5**, which is composed of dense populations of hepatocytes radiating outwards from a central vain to portal triads (Rogers and Dintzis, 2018; Washabau and Day, 2013, p. 61).

1.7.3 HepG2 cells; a well-characterised hepatocyte cell line as a model system to improve cell growth.

Given the vast number of biological functions carried out within the liver, it is no surprise that there is a large area of research devoted to creating liver models that can accurately reflect these functions *in vitro*. Liver models form a significant part of *in vitro* research, with potential applications ranging from drug screening to disease modelling, response to injury and precision medicine (Collins et al., 2019). Given the highly specific, considerably three-dimensional structure, it makes sense that in order to recapitulate the function of the liver *in vitro,* there is a requirement for more bespoke 3D technologies that can more accurately reflect the physiological structure and function of the liver. The burgeoning field of 3D liver models sees researchers using a range of different technologies and cell types and some of these will be explored in more depth in later chapters. A highly popular cell type for liver research is the HepG2 cell line; an immortalised cell line derived from human hepatocellular carcinoma ("Hep G2 [HEPG2] ATCC® HB-8065™," n.d., p. 2) that have an unlimited lifespan, exhibit a stable phenotype and are easily handled (Donato et al., 2015). A significant limitation within this cell line is the lacking metabolic activity compared with primary

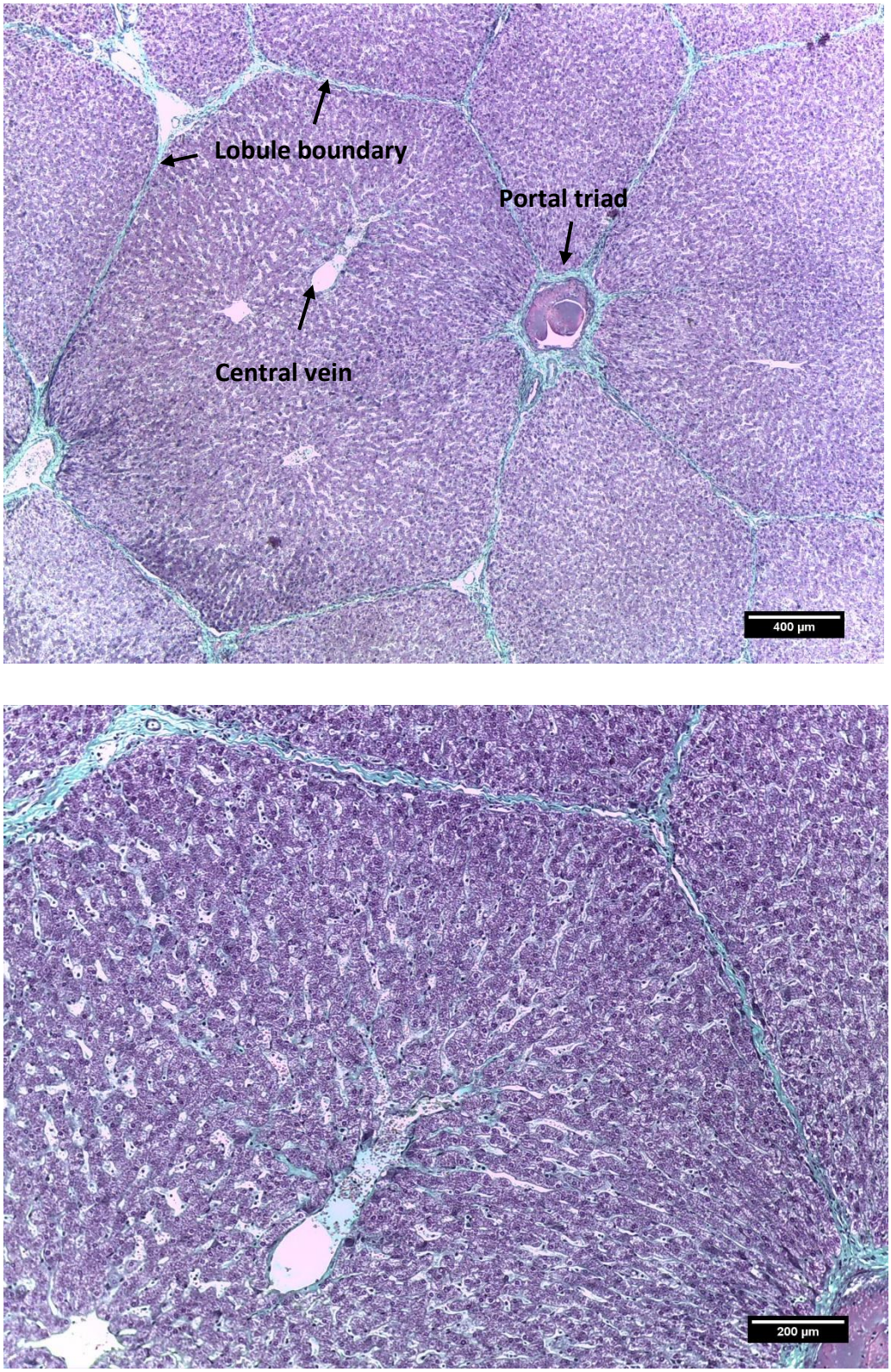

Figure 1.5: The liver consists of lobules that are highly vascularised and contain tightly packed hepatocytes.

Masson's trichrome stained pig liver section provided by Professor Stefan Przyborski's lab. Scale: 400 µm and 200 µm respectively.

hepatocytes. Improving this, and the expression of biomarkers has been a major focus of various *in vitro* models.

Although this cell line is immortalised, it can be used as a model for the in-vitro study of human hepatocytes due to being highly functionally and morphological differentiated (Sassa et al., 1987) and being capable of expressing multiple liver specific functions (Dehn et al., 2004), similar to primary hepatocytes. Due to being immortalised and having a technically indefinite lifespan, HepG2 cells are more flexible and easier to work with compared to primary hepatocytes. A large portion of clinical *in vitro* research on drug metabolism and drug induced liver injury therefore uses the HepG2 cell line (Godoy et al., 2013), so it is important to ensure that HepG2 hepatocyte models are as accurate to *in vivo* physiology as possible. Due to the relatively large choice of functional assays (albumin, urea, lactic acid production, CYP expression and activity), and structural tests for liver specific structures (bile canaliculi, bile transporters, multipolarity), they are also ideal for comparing different culture formats and the consequent effects on the structure and function of the cells. There are however significant considerations to make when using an immortalised cell line; there are inherently fundamental biological differences when compared to primary healthy cells. These differences can be seen right down to the transcriptomic level in HepG2 cells, with 30 % of the HepG2 transcriptome being identified as unique to the immortalised cell line (Harris et al., 2004).

HepG2 cells are incredibly well characterised regarding their use in *in vitro* research, however there are still a number of areas to explore. *In vitro* liver research requires accurate and consistent liver models to replicate effects such as drug induced liver injury and to mimic the biomarker expression as seen *in vivo*. HepG2 cells tend to show enhanced functional profiles when cultured in 3D compared to 2D cultured cells; with elevated albumin production, CYP450 expression and activity shown when comparing simple spheroid cultures to monolayer HepG2 cultures (Mueller et al., 2011). Issues may exist however in terms of drug sensitivity, with certain HepG2 spheroid cultures showing a decreased sensitivity to toxicity (Bokhari et al., 2007; Mueller et al., 2011) which may be an issue if trying to screen for drug induced liver injury, as many *in vitro* models have shown poor prediction of hepatotoxicity (Xu et al., 2004). On the other hand however, the 3D HepG2 models may be better at predicting genotoxicity (Shah et al., 2018) and may be more physiological as a cancer cell line in responding to anti-cancer drugs (Mueller et al., 2011; Oshikata et al., 2011). Alongside the lack of clarity with drug testing, there is also a clear absence of an individual 3D culture

format that universally improves structure and function, and while this is an idealistic notion, the array of different results between different HepG2 cell models makes this lack of a one-size-fits-all solution particularly obvious. There is a high level of variability between the diverse types of 3D culture and the subsequent effects on the structural and functional profile of these cells, with some studies even directly contradicting others. For example, while the majority of studies shows that 3D liver culture does improve expression of biomarkers such as albumin and urea (Milner et al., 2020), one study showed that 3D spheroids actually decreased albumin synthesis after 8 days (Elje et al., 2019).

Additionally, three-dimensional culture might not be the only influencer on biological properties; one study suggested that the time spent in a culture system, even if just in a monolayer may be sufficient to enhance hepatic function to a similar level to 3D models (Luckert et al., 2017). This may be in part due to 2D cultures forming quasi-3D cultures after reaching 100 % confluency, and time indeed may be a factor in increasing biological function, however there is still a wealth of work that demonstrates the more immediate benefits of 3D culture at least. This same study performed a comparison of three different 3D culture methods; a collagen sandwich, Matrigel (which promoted spheroid formation) and Alvetex® (Luckert et al., 2016) and demonstrated largely different results in the expression of liver specific biomarkers. There was a relatively low expression of CYP450 enzymes (essential for drug metabolism) across the board – a known characteristic of HepG2 cells (Westerink and Schoonen, 2007a). Yet albumin production was distinctively higher in Matrigel models when compared to compared to collagen and Alvetex® Scaffold cultures. While this study showed poor expression of CYP450 enzymes in 3D cultures, a different study showed significantly higher levels of induction of CYP450 enzymes through the use Matrigel spheroids (Ramaiahgari et al., 2014b), and despite overall changes in the same direction, this highlights the poor reproducibility of results between different 3D culture methods.

As discussed, hepatocytes are epithelial cells that exhibit a unique multipolarity, with multiple basal surfaces in contact with the endothelial domain (Treyer and Müsch, 2013). This allows for the formation of the bile canaliculi which means that the multipolar organisation of hepatocytes and the overall tissue architecture has a key role to play in liver function. With HepG2 cells, the importance of maintaining this architecture has been highlighted multiple times, with one particular example showing that when cultured in monolayers, only 20 – 40 % of HepG2 cells formed canalicular like structures (van IJzendoorn et al., 2004). However, when multi-layered HepG2 cells were cultured on pre-deposited ECM,

the canaliculi-like structures were more elongated and spanned multiple cells (Herrema et al., 2006) (using HepG2 monolayers on glass coverslips as a comparison). The current shortcomings in consistency highlight there is still more work to be done in 3D HepG2 models to understand the mechanisms driving these functional changes, and how these can be harnessed to create more relevant *in vitro* models. This will be one of the primary focal points of this project, which will aim to more thoroughly investigate the underlying mechanisms that link structural changes to functional changes in a novel HepG2 model.

The potential financial implications of failed drug tests due to inaccurate *in vitro* models (Breslin and O'Driscoll, 2013a) could be averted if cell culture could more accurately predict the *in vivo* response, and this is why the selection of an appropriate 3D cell culture method is important. Additionally, creating more physiologically relevant *in vitro* cultures is essential to better understanding *in vivo* biology, and how various factors influence cell behaviour. The idea behind this project is that with all the aforementioned considerations it may be possible to enhance the structure of cells via maintained growth on a substrate, using a 3D microenvironment (Alvetex®), and that through the mechanisms of mechanotransduction, this altered structure will result in altered function. Cells grown on Alvetex® are referred to as 3D for this thesis, but in reality, the chosen substrate (Alvetex® Strata), is more akin to a 2.5D surface. The cells are not grown within a 3D synthetic matrix, rather they reside on top of a rough 2D surface that provides unique topography allowing the cells to organise themselves into multi-layered 3D structures. The expectation is that these epigenetic changes will occur at a transcriptional level, and that due to this, it will effectively precondition or 'prime' the 3D cells to the more physiological microenvironment. Therefore, the function of these 3D primed cells is hypothesised to improve over 2D grown cells for moving into secondary 3D cultures or for analysis and assays such as drug testing.

1.8 The sustained impact of the physical cellular microenvironment on the structure and function of a hepatocarcinoma cell line.

1.8.1 Project Introduction

The aim of this project is to investigate the effects of the physical microenvironment on the structure and function of a HepG2 based liver model, whilst simultaneously investigating whether the underlying mechanisms driving these effects can be exploited to create an improved hepatic model. The notion of exploiting mechanotransduction arises from the idea of preconditioning or 'priming' of cells in a 3D microenvironment to prepare them for an end

stage model. Our process of priming is described in **Figure 1.6**; it provides an extra primary culture stage on a 3D scaffold (Alvetex®) to allow for the adaption of cells to the 3D microenvironment over a period of time, whereupon it is expected that the structural and functional properties will be enhanced for reseeding into a secondary 3D model. It hypothesised in this project that the maintenance of cells in an initial 3D microenvironment will prime the cells through altered gene expression as a result of the unique mechanical microenvironment that a three-dimensional structure provides. This altered gene expression as a result of differential cell mechanics and structure in 3D is expected to manifest in functional differences, with biological properties of 3D primed cells being closer to the physiology of *in vivo* hepatocytes.

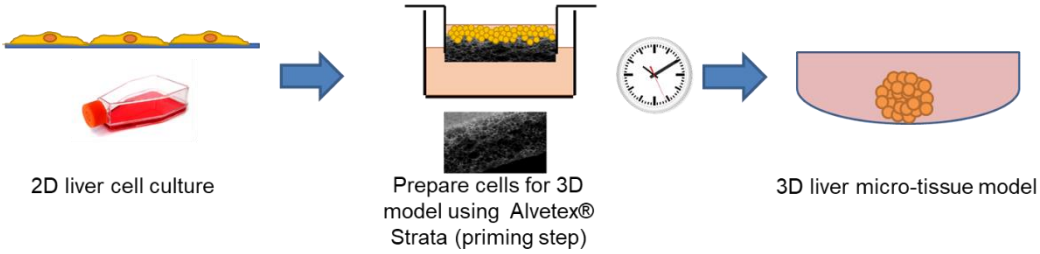

Figure 1.6: Priming cells in a 3D microenvironment to prepare them for a final 3D model.

Instead of placing cells straight into a 3D model for testing after initial cell bulking in 2D, it is hypothesised that by giving cells time to adapt to a 3D environment, that the structure and function will be enhanced, better preparing cells for a final 3D model after liberation.

The 3D primed cells will be compared to 2D grown cells by investigating a multitude of factors including morphological changes both during the priming stage and after reseeding onto secondary substrates. These structural changes will be investigated both globally in confluent cell populations and in single cells that have been liberated from the primary culture step and reseeded onto coverslips. Particular attention will be given to the actin cytoskeleton due to its close link with the cell and nuclear structure. After structural characterisation of cells both during and after priming, functional changes will be interrogated through deep global gene expression analysis, production of key liver biomarkers and response to drug toxicity. The transcriptomic analysis will be carried out on cells at the very end point of the priming stage compared to cells in 2D as it is expected that the structural and functional differential gene expression will be the most prominent at this point, and the wider functional studies

will be performed on HepG2 cells both during the primary and secondary stages of cell culture.

1.8.3 Previous Work

There is a rich background of work in 3D culture in this research group, including some specific work on 'priming' cells to a 3D microenvironment. This work includes a PhD undertaken by Dr Rebecca Quelch which involved priming stem cells for 10 days on a 3D microenvironment. This priming resulted in enhanced differentiation both *in vitro* and *in vivo* and the 3D geometry of the substrate was posited to decrease the nucleation of actin and this showed a correlative link with the enhanced differentiation in 3D (QUELCH, 2018). Another study by Alisha Chhatwal showed that continuous propagation of HepG2 cells in 3D culture for varying passage numbers was able improve their functional phenotype and bring them closer to an *in vivo* profile (Chhatwal, 2016). However due to the labour intensive and time-consuming nature of 3D propagation, we aim to refine and simplify this process to just one extra step with the HepG2 cells and to further investigate the mechanisms underpinning this biological response.

1.8.4 Project Aims

The first aim of this project was to create and characterise a novel *in vitro* model on which HepG2 cells could be grown in a robust and reproducible manner. This model should use a unique three-dimensional topography to host the cells and should permit easy liberation of cells from the substrate for reseeding into secondary cultures. This will involve a significant optimisation step where the effects of changing a range of different variables will be explored in relation to the cell growth and global architecture of the model. Additionally, a secondary 3D model will be optimised to allow a simple and high throughput technique to reproducibly grow reseeded HepG2 cells. Both the primary and secondary models will be thoroughly characterised structurally and functionally in comparison to HepG2 cells that have been grown in 2D. These experiments should reveal unique insights into the mechanisms through which enhanced function arises from altered substrate geometry and will help to unpick how mechanotransduction can be used to beneficial effect in order to tune the properties of *in vitro* models through priming.

1.8.5 Project Objectives

- To create a novel, robust and reproducible in vitro model for growing HepG2 cells in 3D, with an easily retrievable cell layer where hepatic function is enhanced over standard 2D monolayers.
- To create a secondary model for growing cells either from 2D or cells liberated from the 3D priming model in a consistent manner, where functional properties can be tested.
- To characterise models at both these stages structurally by examining single cell morphology, global tissue architecture and presence of important structural markers.
- To examine the global gene expression of 3D primed cells compared to cells grown in 2D, and to compare this against the transcriptome of native human liver tissue and primary human hepatocytes.
- To contextualise these transcriptomic results by looking at differential expression of selected genes and by using enrichment analysis to determine what biological processes and pathways are altered.
- To functionally characterise the models by looking at expression and synthesis of key hepatic biomarkers and exploring sensitivity to drug toxicity.

Chapter 2: Methods and Materials

2.1 Cell culture

2.1.1 2D culture of HepG2 cells

HepG2 (human hepatocellular carcinoma cells) cells (ECACC, Porton Down UK) were grown in minimal essential media with non-essential amino acids (Thermo Fisher Scientific, Massachusetts USA), with 2 mM glutamine (Thermo Fisher Scientific) and 10 % FBS (Thermo Fisher Scientific) added. Cells were seeded onto T75 flasks (Sarstedt, Nümbrecht Germany) at $2x10^6$ cells per flask and grown to 80 % confluency before passaging. Upon reaching confluency, media was aspirated or stored as appropriate and cells were washed twice with sterile phosphate buffered saline (PBS, 8 g NaCl, 0.2 g KCl, 1.15 g Na_2HPO_4, 0.2 g KH_2PO_4) before incubating the flasks with 2 ml of 0.25 % Trypsin EDTA (Thermo Fisher Scientific) for 10 minutes. The suspension was neutralised with 4 ml of serum containing minimal essential medium (MEM) and then centrifuged at 1000 rpm for 3 minutes. Supernatant was subsequently removed, and the cell pellet was resuspended in 5 ml of MEM where the cells could be counted. Once seeded at the appropriate densities, cells were incubated at 37 ^oC and 5 % CO_2.

2.1.2 2D culture of Sk-Hep-1 cells

Sk-Hep-1 (liver endothelial adenocarcinoma cells) cells (ECACC) were grown in minimal essential media with non-essential amino acids (Thermo Fisher Scientific), with 2 mM glutamine (Thermo Fisher Scientific) and 10 % FBS (Thermo Fisher Scientific) added. Cells were seeded onto T75 flasks (Sarstedt) at $1x10^6$ cells per flask. At 80 % confluency, media was aspirated, and the cells were washed twice with sterile PBS (formulated in lab) before incubation with 2 ml of 0.25 % Trypsin EDTA (Thermo Fisher Scientific) for 5 minutes. This suspension was then neutralised with 4 ml of serum containing MEM and centrifuged at 1000 rpm for 3 minutes, after which the supernatant was removed and the pellet resuspended in 5 ml of MEM. Once seeded at the appropriate densities, cells were incubated at 37 ^oC and 5 % CO_2. Media was changed after 4 days of growth.

2.1.3 Pre-treatment of Alvetex® substrates for cell culture

To allow the growth of cells on the Alvetex® surface, it needed to be rendered hydrophilic through soaking the membrane in 70 % ethanol for 10 minutes. The membranes were then washed twice with sterile PBS (lab formulated) and soaked in the appropriate media before applying cells.

2.1.4 3D culture of HepG2 cells on Alvetex®

The Alvetex® (ReproCELL Europe Ltd., Sedgefield UK) substrates were left to soak in media while preparing cells from flasks. Inserts were placed into either 6 well or 12 well plates (Sarstedt). After resuspension of the cell pellet, the HepG2 cells were counted and cells were added onto Alvetex® membranes at $1x10^6$ cells per 6 well insert, or $5x10^5$ cells per 12 well insert. In early experiments using 6 well inserts, two different methods of media application were used: submerged and contact. With submerged cultures, the cells were made up to the required seeding density in 100 µL of media and applied to the membrane. This was incubated for an hour to allow cells to attach and to avoid disturbance from adding media. After this incubation, 10 ml of media was added to the well, fully submerging the inserts. With contact cultures, 5 ml of media was applied underneath the insert which made contact with the bottom of the membrane. HepG2 cells were made up to the appropriate density in 500 µL of media which was then applied to the membrane. In 12 well cultures, contact was the only method used, and in this case 2.5 µL of media was added underneath the inserts, and the suspension was adjusted to seed the required density in 250 µL of media. Media was changed on the inserts every 2 days, and after 8 days models were stopped for analysis.

For comparison to 3D cultures, HepG2 cells were also seeded directly onto the 2D surface of the wells. These were seeded at half the density to their 3D counterparts to account for the differences in population doubling time.

2.1.5 3D priming culture of Sk-Hep-1 cells on Alvetex®

Whilst soaking Alvetex® Strata membranes in media, a suspension of Sk-Hep-1 cells was prepared from 2D flasks. These cells were then seeded directly onto membranes at a density of $1x10^6$ cells per insert. This cell suspension was made up in 500 µL of media which was applied to the membrane, with 5 ml of media having been added underneath the insert prior. Media was changed every 2 days, and after 8 days of growth the models were stopped for analysis.

2.1.6 3D co-culture of HepG2 cells and Sk-Hep-1 cells on Alvetex®

HepG2 cells were grown on Alvetex® Strata in combination with Sk-Hep-1 cells, and various formats of co-culture were tested. All of these formats used the 'contact' media application method, with a layer of 500 µL of media sitting on top of the insert membrane, and 5 ml of media underneath. The first seeding technique involved application of $7.5x10^5$ HepG2 cells

to the membrane first, incubation for half an hour, then applying $2.5x10^5$ Sk-Hep-1 cells to the membrane. For the second seeding method, Sk-Hep-1 cells were applied to the insert at $2.5x10^5$ cells per insert first and incubated for half an hour. HepG2 cells were then applied at $7.5x10^5$ cells per insert. The third method – simultaneous seeding – used a mixed suspension of HepG2 and Sk-Hep-1 cells and applied this to the membrane. This suspension contained the appropriate densities of cells to be seeded at $7.5x10^5$ cells per insert for HepG2 cells and $2.5x10^5$ cells per insert for the Sk-Hep-1 cells, in a 500 µL volume of media. Finally, paracrine cultures were tested, with HepG2 cells seeded onto Alvetex® Strata at a density of $1x10^6$ cells per insert as described above, and Sk-Hep-1 cells seeded underneath the insert onto the base of the well at $1x10^6$ cells per well. Regardless of format, media was changed every 2 days, and the models were stopped at 8 days or earlier.

2.1.7 Liberation of HepG2 cells from Alvetex® for reseeding into secondary models

At the 8-day time point, HepG2 cells were ready to liberate from the substrate. After optimisation (discussed in **Chapter 3**), the final liberation technique first required the unclipping of the Alvetex® membranes from the plastic inserts holding them in place. The membranes were then placed into individual wells of a fresh 6 well plate and submerged in sterile PBS (lab formulated) twice, with gentle agitation. The PBS was then aspirated, and 2 ml of 0.25 % trypsin (Thermo Fisher Scientific) was added to each well, which was incubated for 15 minutes at 37 ^oC and 5 % CO_2. After this period, soft cell scrapers (Sarstedt) were used to gently scrape the membranes, ensuring that the cell layer was fully removed, but being careful not to damage the substrate and release debris. This suspension was neutralised with the addition of 2 ml of media, and then centrifuged at 1000 rpm for 3 minutes, where the cells could then be counted and re-seeded.

2.1.8 Re-seeding of HepG2 cells onto coverslips for single cell or population analysis.

After liberation of HepG2 cells from either 2D wells or on Alvetex®, cells could be re-seeded onto coverslips for either single cell analysis at low seeding densities, or for analysis of larger cell populations at higher seeding densities. Coverslips were placed into 12 well plates where they were cell culture treated by using a plasma treater with an ashing time of 5 minutes at 40 W, then sterilised in 70 % EtOH before washing twice in sterile PBS. 5 ml of media was then added to the coverslip containing wells, and HepG2 cells were seeded at varying densities depending on the experiment, though most commonly a density of either $1x10^4$

cells per well for single cell analysis, or $2.5x10^5$ cells per well for more confluent cultures in a 100 µL volume of media. These were grown for either 1,4 or 8 days depending on the experiment, and were stopped by fixation.

2.1.9 Re-seeding of HepG2 cells into low adherence Petri dishes for self-assembled aggregates.

Liberated HepG2 cells from 2D and 3D could also be re-seeded into low adherence Petri dishes (Thermo Fisher Scientific) which allowed for the self-assembly of aggregates. For this, 25 ml of minimal essential media was added to the dishes, before $1x10^6$ cells were seeded into the petri dish, in a 100 µL volume of media. These aggregates were grown for up to 10 days, with imaging at different time points being carried out on a phase contrast microscope.

2.1.10 Re-seeding of HepG2 cells into hanging drops for spheroid cultures.

HepG2 cells were re-seeded into hanging drops after 3D priming or growing in 2D. This was performed using a technique adapted from (Shah et al., 2018). HepG2 cell suspensions were adjusted to create a density of $1x10^3$ cells per 20 µL drop of minimal essential media (after optimisation). These drops were then applied to the inside of the lid of a 9.6 cm Petri dish. Normally, 30 drops were made per Petri dish. 5 ml of sterile PBS was added to the base of the petri dish to humidify the dishes and prevent drying out of drops. Another 20 µL of media was added on day 4 of growth, and models were grown up to 10 days for visualisation but stopped at 7 days for analysis.

2.1.11 Collection and application of conditioned media from HepG2 and Sk-Hep-1 cultures for migration assay.

12 well plates were seeded with $2.5x10^5$ of either Sk-Hep-1 cells or HepG2 cells, which were then grown in 2D for 7 days with media changed on day 4. Simultaneously, Sk-Hep-1 cells and HepG2 cells were grown in T75 flasks, from which media was stored for use as conditioned media. This media was taken from the cultures at the 4-day time point and sterile filtered using a 50 ml syringe (Greiner Bio-one, Kremsmünster, Austria) and 0.2 micron filter (Thermo Fisher Scientific), stored at 4 ^oC and then applied to the 12 well cultures. Cells were then imaged over the period of 4 days on the Zeiss Cell Observer (Zeiss, Oberkochen, Germany), with temperature set to 37^oC with 5 % CO_2.

2.1.12 Addition of xenobiotic compounds to cultures for toxicity testing

Stocks solutions containing different xenobiotic compounds were made using dimethyl sulfoxide (DMSO) or EtOH as a vehicle, or in fresh media for isoniazid, and these were serially diluted in media to make a range of concentrations. Drug concentrations were based on prior literature, or on 100x the Cmax reported in human plasma (Jj et al., 2008; Maiuri et al., 2017). When dissolved in media, vehicle concentrations did not exceed 0.5 % and vehicle controls were included each time. Data for these was not shown, but vehicles alone had no effect on toxicity. For 2D and Alvetex® cultures, media was aspirated at day 7 of growth and replaced with the appropriate dilutions of compounds in fresh media which was left on the cells for 24 hours. For hanging drops, 20 µL of media was added to the drop on day 6 of culture with the appropriate dilution to reach the desired final concentration range, and this was left for 24 hours. After 24 hours, media was collected for immediate LDH assays, and in the case of cells grown in 2D and on Alvetex®, MTT assays were also performed instantly.

Table 2.1: Xenobiotic compounds with their respective vehicles and dilutions.

Compound name	Vehicle used	Reference for concentration	Final concentration range
Gemfibrozil (Sigma Aldrich, G9518)	EtOH	Previous group work (unpublished)	8, 4, 2, 1, 0.5, 0 (mM)
Isoniazid (Fisher Scientific, 10225120)	Media	>100x Cmax of 76.6 µM (Ramaiahgari et al., 2014a)	20, 10, 5, 2.5, 1.25, 0 (µM)
Amiodarone (Fisher Scientific, 15502233)	DMSO	>100x Cmax of 0.85 µM (Shah et al., 2015)	300, 150, 75, 37.5, 18.75, 0 (µM)
Ibuprofen (Sigma Aldrich, I4883)	ETOH	Previous group work (unpublished)	5, 2.5, 1.25, 0.625, 0.3125, 0 (µM)
Tamoxifen (Fisher Scientific, 11445161)	DMSO	LD50 seen in literature: 56.8 µM in spheroids, 13.9 µM in monolayers (Mueller et al., 2011)	150, 75, 37.5, 18.75, 9.375 (µM)

Methotrexate (Sigma Aldrich, M9929)	DMSO	Toxicity at 125 µM seen in literature (Bokhari et al., 2007, p. 2)	150, 75, 37.5, 18.75, 9.375 (µM)

2.1.13 Human Tissue Acquisition and Use.

Fixed human liver tissue was collected by Biopta (Glasgow, United Kingdom) under appropriate ethical protocols in compliance with local laws and regulations. Tissue was received at Durham University under a formal MTA agreement and were processed following relevant UK HTA rules and guidelines at the time of publication. The liver sample acquired was from a middle-aged healthy female donor.

2.2 Storage and collection of samples for analysis

2.2.1 Collection and storage of media

Media was collected from cells grown in 2D, 3D on Alvetex® and from hanging drop cultures for later analysis. In 2D cultures, media was taken from the cultures at the required time point and stored at -20 ^{o}C until needed for further use. In cultures on Alvetex®, membranes were first unclipped from the plastic insert holders and submerged in the media underneath to ensure that media from the top and bottom compartments were suitably mixed. After this, media was collected, taking care not to disturb the inserts, and stored at -20 ^{o}C until required. With hanging drops, 1 mL of fresh media was flushed over the inside of the lid multiple times, ensuring that all hanging drops were collected in the liquid. The spheroids were left to settle and the media was collected and stored at -20 ^{o}C, making sure no hanging drops were collected in the process.

2.2.2 Lysing cells for use in Western blots and Bradford assays

Cells were lysed using the lysis buffer Mammalian Protein Extraction Reagent (M-PER™, Thermo Fisher Scientific), supplemented with 1x Halt™ Protease and Phosphatase Inhibitor Cocktail (Thermo Fisher Scientific). For cells in 2D 6 well cultures, media was aspirated or stored as appropriate, and 500 µL of lysis buffer was added. Cells were left for 1 hour on ice and vortexed every 10 minutes. For cells grown on Alvetex®, membranes were first unclipped from the plastic insert holders, before washing them twice in sterile PBS in a fresh 6 well

plate (Greiner Bio-one). The membranes were cut into 8 pieces with a scalpel and placed into a microcentrifuge tube (Greiner Bio-one) where 500 µL of lysis buffer was added. These tubes were left on ice for 1 hour and vortexed every 10 minutes. For hanging drop cultures, 1 mL of media was flushed over the inside of the lid multiple times to ensure the collection of all spheroids. This was transferred to a microcentrifuge tube where the spheroids were left to settle. Media was then aspirated, and the cells were washed in sterile PBS twice, allowing the spheroids to settle between each wash. The PBS was aspirated and 100 µL of lysis buffer was added. The tubes were transferred to ice for 1 hour and vortexed every 10 minutes. In all cases, after vortexing while on ice, the lysis mix was transferred to microcentrifuge tubes and spun for 30 minutes at 12,000 rpm. Supernatant was collected without disturbing the pellet and stored at -20 ^{o}C until needed.

2.3 Assessment of cell growth

2.3.1 Living and dead cell counts through trypan blue exclusion

Cell suspensions were added to trypan blue (Sigma-Aldrich, Missouri USA) in a ratio of 1:4 and transferred to a haemocytometer. Cell counts were taken from 3 quadrants of the haemocytometer and averaged, and viability could be determined as a percentage from the ratio of live cells (light colour) and dead cells (dark blue colour).

2.3.2 Assessment of metabolic activity through MTT assay

At the desired timepoints where metabolic activity was to be measured, cells in 2D were washed twice with PBS, whereas with cells grown on Alvetex®, the membranes were unclipped from the inserts and placed into a fresh plate before washing twice with PBS. Subsequently, Thiazolyl Blue Tetrazolium Bromide solution (MTT, Sigma-Aldrich) (1 mg/ml in phenol free Dulbecco's Modified Eagle Media (DMEM Thermo Fisher Scientific)) was added to each well at 0.5 ml for 12 well plates, or 1 ml for 6 well plates. These were incubated for 1 hour at 37 ^{o}C and 5 % CO_2 away from light. The MTT solution was then aspirated, and acidified isopropanol was added to the wells at the same quantities as the MTT solution and the plates were left on an orbital shaker for 20 minutes whilst protected from light. Finally, 20 µL of each acidified isopropanol well was diluted in 180 µL of isopropanol in a flat bottomed 96 well plate, and absorbance was measured at 570 nm using a Bio-Tek ELx800 plate reader (Bio-Tek, Vermont USA).

2.3.3 Determination of total protein concentration with Bradford assay.

The total protein concentration of cell lysates was determined through the Bradford assay, to allow normalisation to protein levels, and equal loading in western blotting. A kit of BSA standards (Bio-Rad, Hertfordshire, UK) was used to create a standard curve. Lysates were thawed on ice, then 5 µL of sample/standard were added to individual wells of a 96 well plate, and mixed with 250 µL of Quick Start™ Bradford 1x Dye Reagent (Bio-Rad). This was incubated for 5 minutes before reading absorbance at 590 nm using a Bio-Tek ELx800 plate reader (Bio-Tek). Protein concentration was determined through plotting the standard curve in GraphPad Prism software, where plotting the linear regression allowed extrapolation of unknown y values (the sample readings).

2.4 Structural characterisation of models.

2.4.1 Neutral red staining

To visualise the macrostructure of the cells whilst growing in 2D or Alvetex, neutral red staining was used. At the desired timepoint, 2D cells were washed in PBS twice, and Alvetex® membranes were unclipped and transferred to a new plate and washed twice in PBS. 500 µL of neutral red solution was applied to 6 well cultures, and plates were left on an orbital shaker for 10 minutes. Wells were washed 5 times with PBS and images were taken on both a Samsung galaxy S9 camera and using a brightfield microscope.

2.4.2 Processing of 2D samples and whole mount spheroids for visualisation

Cells grown in 2D on coverslips were prepared for immunofluorescence by fixing with 4 % paraformaldehyde (PFA, Thermo Fisher Scientific). Firstly, coverslips were gently washed twice with PBS, before submerging them in 4 % PFA either overnight or for 30 minutes at room temperature. After fixation, coverslips were washed three times with PBS and were stored submerged in PBS at 4 ^{o}C until further processing. For whole mount imaging of spheroids, this process was also followed using 15 ml centrifuge tubes, making sure that the spheroids settled at the bottom of the centrifuge tube between each wash.

2.4.3 Processing for paraffin wax embedding

For histology and particular immunofluorescent antibodies, 3D samples were embedded in paraffin wax. For this, samples in Alvetex® were unclipped and washed in PBS twice, before 4 % paraformaldehyde was added. For spheroids, aggregates were collected by washing the inside of the Petri dish lid with PBS, transferring them to a 15 ml centrifuge tube, and washing

the aggregates twice in PBS (letting them settle each time) and finally adding 4 % PFA. Human liver was also processed for histology, and was processed in a similar manner to aggregates, with the liver being cut into chunks of roughly 2x2x2 mm size.

Samples were left in PFA for either 30 minutes at room temperature or 4 °C overnight to fix them. After fixation, the samples were washed twice in PBS and taken through a series of EtOH dehydrations, using 30 %, 50 %, 70 %, 80 %, 90 %, 95 % and 100 % EtOH solutions, leaving them for 15 minutes at each step and 30 minutes in 100 % EtOH. For spheroids, the 70 % solution was replaced with crystal violet (Sigma Aldrich) diluted in 70 % ethanol to make it easier to see the aggregates once embedded. Ethanol was drained off and samples were soaked in Histo-Clear (National Diagnostics, Lichfield UK) for 30 minutes, a 1:1 mix of Histo-Clear and paraffin wax (Thermo Fisher Scientific) for 30 minutes at 60 °C, and 100 % paraffin wax for 60 minutes at 60 °C. At this stage, Alvetex® membranes were cut in half and embedded in semi-set 100 % wax in dispomoulds (Thermo Fisher Scientific), whereas spheroids were collected with a plastic Pasteur pipette and gently released into the setting wax moulds. Wax blocks were set at room temperature and cut on a Leica EG1120 Microtome (Leica Microsystems, Wetzlar DE) to a thickness of 7 µm per section. Sections were transferred to a mounting bath at 45 °C to flatten out and were mounted on microscope slides then left on a drying bench for at least 2 hours.

2.4.4 Processing for OCT embedding

Certain antibodies were inappropriate for use in paraffin embedded samples, and embedding in optimal cutting temperature compound (OCT, Thermo Fisher Scientific) provided better images. For this, samples were washed in PBS as described above, then fixed in a 1:1 mix of ice-cold methanol and acetone (M/A) for 5 minutes at -20 °C. Samples were then placed in OCT (Alvetex® membranes were cut in half) and left to equilibrate for 20 minutes. OCT was frozen using dry ice, and samples could be stored at -80 °C until cutting at 10 µm thickness using a Cryostat Bright OTF5000 (Bright Instruments, Luton, UK).

2.4.5 Histological analysis through haematoxylin and eosin (H&E) staining

H&E stains enable visualisation of the cytoplasm and nuclei through differential staining – haematoxylin stains nucleic acids in a dark purple colour whereas eosin stains nonspecific proteins a pink colour (Fischer et al., 2008). H&E stains were performed on aggregates and on cross sections of cells grown on Alvetex®, both of which were processed through paraffin wax embedding. Slides with wax sections on were first deparaffinised in Histo-Clear for 5

minutes, then rehydrated through immersing in 100 % EtOH for 2 minutes, 95 % EtOH for 1 minute and 70 % EtOH for 1 minute. Samples were then immersed in distilled water (dH_2O) for 1 minute to wash them, then stained through submerging in Mayer's Haematoxylin (Sigma-Aldrich) for 5 minutes and subsequently washed in dH_2O for 30 seconds. Cell nuclei were blued through immersion in alkaline alcohol for 30 seconds, and samples were then dehydrated with 70 % EtOH and 95 % EtOH for 30 seconds each. Samples were left in eosin for 1 minute to stain the cytoplasm, and they were then submerged in 95 % EtOH twice for 10 seconds, and absolute EtOH twice for 10 seconds, then 15 seconds. Finally, samples were cleared in Histo-Clear twice for 3 minutes each before drying off and mounting a coverslip using omni-mount (National Diagnostics).

2.4.6 Immunofluorescent staining

2.4.6.1 Staining cross sections of 3D models

Wax or OCT sections of Alvetex or spheroids could be probed with specific antibodies to detect and visualise the presence of specific biomarkers. For paraffin embedded sections, slides were deparaffinised in Histo-Clear for 15 minutes before rehydration in 100 % EtOH, 70 % EtOH and PBS for 5 minutes each. Antigen retrieval was carried out through incubating samples in citrate buffer at 95 ^{o}C for 20 minutes. After cooling the slides, they were blocked and permeabilised in a solution of 20 % normal goat serum (NGS, Sigma-Aldrich) with 0.4 % Triton X-100 (Sigma-Aldrich) for 1 hour at room temperature. OCT embedded samples were simply immersed in PBS and washed a further 3 times for 10 minutes each in PBS to clear the OCT, and no antigen retrieval or permeabilisation was needed due to methanol acetone fixation already permeabilising the samples. Blocking for OCT embedded samples was performed using 20 % NGS in PBS for 1 hour at room temperature.

Primary antibody was then added to the slides at the required dilution (diluted in blocking buffer), and these were incubated in a humidified chamber overnight at 4 ^{o}C. Samples were subsequently washed 3 times in PBS for 10 minutes each time, before incubation with the secondary antibody diluted in PBS for an hour. Finally, slides were washed three times in PBS for 10 minutes each and were incubated with a 1:10000 dilution of Hoescht-33342 (Thermo Fisher Scientific) in PBS for 30 seconds before mounting in VECTASHIELD® (Vector Laboratories, Peterborough, UK) and sealing with nail varnish.

2.4.6.2 Staining whole mount spheroids

An appropriate number of aggregates was collected from the centrifuge tube and transferred to a 1.5 ml microcentrifuge tube for subsequent processing. Firstly, excess PBS was aspirated, before permeabilisation in 0.4 % Triton X-100 for 20 minutes at room temperature. The spheroids were blocked in a solution of 10 % NGS for 1 hour, after which primary antibodies diluted in blocking buffer were added for 1 hour at room temperature. The samples were washed 3 times in PBS for 10 minutes each time, and the appropriate secondary antibodies diluted in PBS were added for 1 hour at room temperature. After washing 3 more times in PBS for 10 minutes each time, the spheroids were incubated for 10 minutes in a 1:10000 dilution of Hoescht-33342 in PBS. Finally, spheroids were gently pipetted onto slides, trying to minimise excess liquid which could be dabbed away, VECTASHIELD® was added and a coverslip was gently pressed onto the slide, sealing with nail varnish.

2.4.6.3 Preparation of 2D coverslips for immunostaining

2D coverslips were transferred into a fresh 12 well plate and then were blocked and permeabilised with 0.4 % Triton X-100 for 1 hour at room temperature. Coverslips were incubated with primary antibodies diluted in blocking buffer for 1 hour at room temperature. Samples were then washed 3 times in PBS for 10 minutes each, before incubation with secondary antibodies diluted in PBS, for 1 hour at room temperature. Again, samples were washed 3 times with PBS, with a final 30 second incubation with Hoescht-33342 diluted in PBS. Coverslips were then mounted on slides using VECTASHIELD® and nail varnish for sealing.

2.4.6.4 Visualising the cytoskeleton through phalloidin staining

To visualise the F-actin cytoskeleton, a phalloidin stain (acti-stain 488 phalloidin, Cytoskeleton, Inc., Denver, Colorado, USA) was used which only worked on PFA fixed cells. This stain could be added in the last set of PBS washes after the secondary antibody, by incubating the samples in phalloidin diluted in PBS for 30 minutes during the first wash. If only staining for phalloidin, sections were deparaffinised, rehydrated and washed in PBS as described above, and whole mount or 2D cells were washed 3 times in PBS for 10 minutes each. Samples were permeabilised in 0.4 % Triton X-100 for 5 minutes at room temperature and washed once in PBS for 30 seconds at room temperature. Samples were then incubated with phalloidin diluted in PBS for 30 minutes in the dark at room temperature. Samples were next washed 3 times in PBS for 10 minutes each, with a final 30 second incubation with Hoescht-33342 diluted in PBS before mounting on microscope slides with VECTASHIELD® and nail varnish to seal.

2.4.6.5 Antibodies used in immunofluorescence

Table 2.2: Primary antibodies used in immunofluorescence

Target	Dilution	Host species	Supplier	Product code
E-cadherin	1:100	Mouse	Abcam	ab1416
N-cadherin	1:200	Rabbit	Abcam	ab18203
MDR1	1:100	Mouse	Santa Cruz Biotechnologies	sc-13131
Claudin-1	1:200	Rabbit	Abcam	ab15098
SUN-1	1:200	Rabbit	Abcam	ab124770
SUN-2	1:200	Rabbit	Abcam	ab124916

Table 2.3: Secondary antibodies and dyes used in immunofluorescence

Target	Dilution	Supplier	Product code
Alexa-fluor anti-rabbit 488	1:600	Thermo Fisher Scientific	A-11034
Alexa-fluor anti-rabbit 594	1:600	Thermo Fisher Scientific	A32740
Alexa-fluor anti-mouse 488	1:600	Thermo Fisher Scientific	A-11001
Alexa-fluor anti-mouse 594	1:600	Thermo Fisher Scientific	A-21203
Hoechst 33342	1:10000	Thermo Fisher Scientific	H3570
Acti-stain 488 phalloidin	1:200	Cytoskeleton, Inc.	PHDG1

2.4.7 Propidium iodide staining

To visualise dead cells in aggregates, propidium iodide (Sigma Aldrich) was used which is excluded from live cells with in-tact membranes. This stain had to be applied before fixation to ensure exclusion from living cell membranes. At the desired time point of culture, aggregates were collected in a 15 ml centrifuge tube and rinsed 2 times with PBS. Aggregates

were submerged in PI at a concentration of 500 nM diluted in PBS and left for 30 minutes, after which they could be fixed and processed as required for microscopy.

2.4.8 Detecting apoptotic cells with the TUNEL Assay

To visualise and detect the presence of apoptotic cells on Alvetex®, the DeadEnd™ Fluorometric TUNEL System (Promega, Southampton, UK) was used. Sections of Alvetex® were deparaffinised and rehydrated as listed above, before permeabilisation in 0.4 % Triton X-100 in PBS, followed by 2 washes in PBS for 5 minutes each. Positive controls were created through incubating samples for 10 minutes with 100 µL of DNase I buffer, which contained 5 UmL^{-1} of DNase I. Samples were then all incubated with 100 µL of equilibration buffer for 10 minutes at room temperature and were subsequently incubated with the reaction mixture (45 µL of equilibration buffer, 5 µL nucleotide mix and 1 µL rTdT enzyme) for 60 minutes at 37 ^{o}C for 60 minutes in the dark. The reaction was stopped by incubating the samples with 2X SSC (87.7g NaCl, 44.1g sodium citrate) for 15 minutes at room temperature, and the samples were then washed 2 times in PBS for 5 minutes before mounting using Hardset Vectasheild with DAPI (Vector Laboratories).

2.4.9 Brightfield microscopy

Brightfield microscopy was used to image the histological stains of models as well as for viewing the hanging drop spheroids whilst in culture. For this, a Leica ICC50 high-definition camera mounted to a Leica microscope was used, with images taken using the objectives x5, x10, x20 and x40. Leica EZ software was used for the image capture.

2.4.10 Phase contrast microscopy

Phase contrast images were taken to visualise 2D cells and low adherence aggregates in culture. These images were obtained on a Nikon ECLIPSE TS100 microscope with an attached Nikon digital camera DXM1200, using x5, x10, x20 objectives.

2.4.11 Fluorescence imaging

Fluorescent images were obtained through either conventional fluorescence microscopy or through confocal microscopy. For conventional microscopy, a Zeiss Axioskop 40 microscope (Zeiss) was used. The x5, x10, x20 and x40 objectives were used, with DAPI, 488 nm and 594 nm filters.

For confocal microscopy, the Zeiss 880 confocal laser scanning microscope with airy scan (Zeiss) was used, which provided higher resolution images. The objectives used were x10 EC Plan Neo DC I, x20 Plan Apochromat DIC II, x40 EC Plan Neo DIC II and x63 Plan Aprochromat DIC II. Zeiss Zen software was used for image capture, with Z-stacks being taken to produce 3D images of the samples.

2.4.12 Live cell imaging

Time lapse movies of cells in culture were created using the Zeiss Cell Observer (Zeiss). For this microscope the temperature was set to 37 °C and CO_2 to 5 %, and images were taken using the phase contrast setting, with the x10 objective. Images were taken every 30 minutes from each well, for different durations depending on the experiment. Zeiss Axiovision software was used for image capture and microscope control.

2.5 Western Blotting

2.5.1 Gel electrophoresis and transfer

After measuring total protein concentration, lysates were diluted in lysis buffer to equalise the concentrations so that the same amount of protein was contained within a given volume between samples. Samples were diluted 3:1 with 4 x Laemmli sample buffer (Bio-Rad) and in 10 % 2-mercaptoethanol (Sigma-Aldrich) at 95 °C for 5 minutes to denature proteins. Samples were then run on a polyacrylamide gel (percentage depended on proteins of interest) (recipes in table 2.4), at 120 V for roughly 90 minutes in 1 x tank buffer (3.028 g Tris, 14.41 g Glycine, 1 g sodium dodecyl sulfate (SDS), in 1 L dH_2O).

Table 2.4 Resolving gel recipes

N.B Prosieve is a 50 % acrylamide solution, other commercial acrylamide solutions have different acrylamide contents and gel recipes must be adjusted accordingly.

Components	8 % Gel	10 % Gel	12 % Gel
Deionized water	5.7 mL	5.7 mL	4.9 mL
Prosieve® 50 acrylamide gel solution	1.6 mL	2 mL	2.4 mL
1.5 M Tris-HCL pH 8.8	2.5 mL	2.5 mL	2.5 mL

10 % SDS	100 µL	100 µL	100 µL
10 % Ammonium persulfate (APS)	100 µL	100 µL	100 µL
TEMED	5 µL	5 µL	5 µL

After running samples, the gel was placed onto a nitrocellulose membrane (GE Healthcare, Buckinghamshire, UK), with blotting paper and sponges sandwiching the membrane and gel. This was gently massaged to ensure no bubbles were present and was held in a cassette which was placed into a transfer tank with an ice block and ice-cold transfer buffer (3.03 g tris, 14.41 g glycine, 200 mL methanol, 800 mL H_2O). Transfer was carried out overnight for 20 hours at 15 V in 4 °C, with the voltage turned up to 30 V for 2 hours the next day. Membranes were subsequently stained with Ponceau before blocking for 1 hour at room temperature in 5 % milk in blot rinse buffer (BRB, 1.21 g Tris, 8.8 g NaCl, 0.327 g EDTA, 1 mL Tween20, in 1 L dH_2O). Membranes were then incubated with a primary antibody overnight at 4 °C and were later washed 3 times in BRB for 10 minutes each. Secondary antibody was added for 1 hour at room temperature, followed by 3 more 10-minute washes in BRB. Finally, Clarity™ ECL detection kit (Bio-Rad) was applied for 5 minutes, with the two solutions mixed at a 1:1 ratio, before exposure with photographic film (Thermo Fisher Scientific).

Table 2.5: Antibodies used in western blotting

Target	Dilution	Host species	Supplier	Product code
SUN-1	1:1000	Rabbit	Abcam	ab124770
SUN-2	1:1000	Rabbit	Abcam	ab124916
Albumin	1:500	Mouse	Santa Cruz Biotechnologies	sc-271605
α-Fibrinogen	1:500	Mouse	Santa Cruz Biotechnologies	sc-398806
Vinculin	1:1000	Mouse	Abcam	ab18058

β-catenin	1:1000	Mouse	BD Biosciences	610153
PCNA	1:1000	Rabbit	Abcam	ab18197
GAPDH	1:5000	Rabbit	Abcam	ab9485
β-actin	1:1000	Mouse	Abcam	ab8224
Anti-rabbit-HRP	1:5000	Donkey	Millipore	AP182P
Anti-mouse-HRP	1:5000	Goat	Sigma-Aldrich	A4416

2.5.2 Densitometry measurements

Densitometry was performed in Image J using the protocol provided at the following website: https://lukemiller.org/index.php/2010/11/analyzing-gels-and-western-blots-with-image-j/. Relative expression between samples was calculated and normalised to loading controls.

2.6 Image analysis

2.6.1 Quantification of penetration into Alvetex® and thickness of cell layer

To measure how far the cells penetrated into the Alvetex® substrate, ImageJ software was used. After setting the scale, 5 equidistant lines were drawn across the image perpendicular to the orientation of the substrate. To measure penetration, lines were drawn from the surface of the substrate (figure 2.1 white dashed line) to where the bottom cells lie (figure 2.1 blue arrow) and measured using the software. To measure thickness of the cell layer on top of the substrate, lines were drawn from the substrate surface to the top cells in the layer (figure 2.1 red arrow). To measure total thickness, lines were drawn from the bottom cells to the top cells (figure 2.1 white arrow). To account for variability, this was done across multiple images from multiple sections of multiple model replicates.

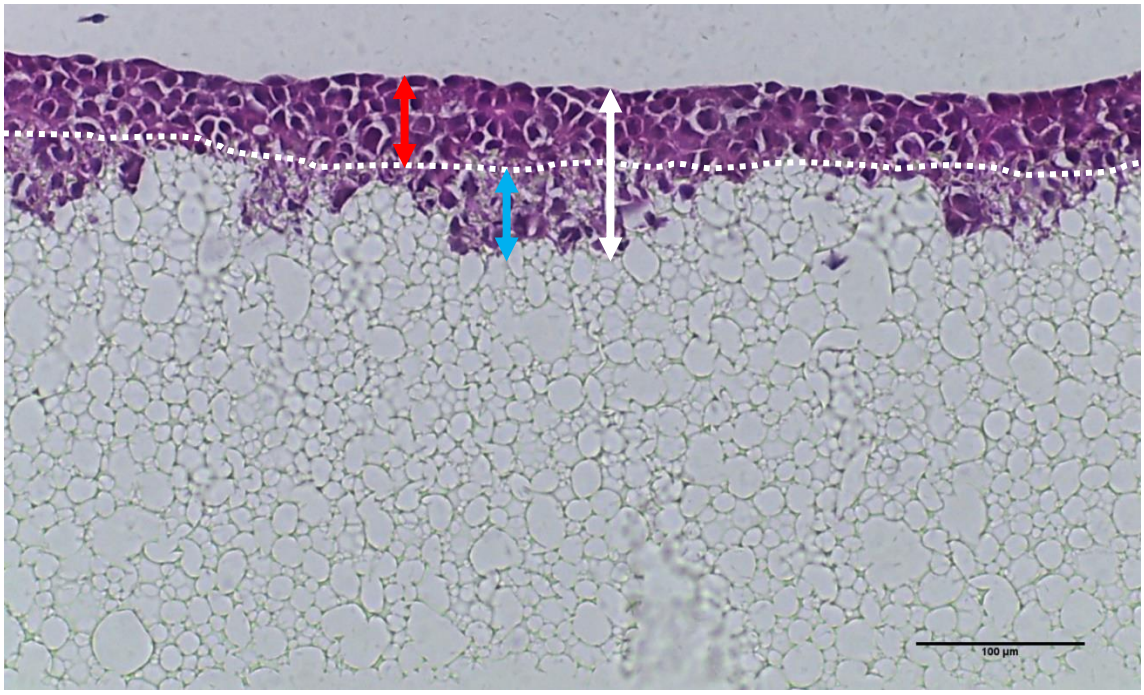

Figure 2.1: Measurement of cell layer depth from H&E images

Representative H&E image of HepG2 cells grown on Alvetex® Strata. Dashed line indicates the top surface of the substrate from which measurements can be taken. Red line: Residing cell layer thickness, Blue line: Cell penetration, White line: Total cell layer depth. Scale: 100 µm

2.6.2 Quantification of cytoskeleton area and height

The actin cytoskeleton was visualised through phalloidin stains on the Zeiss 880 microscope which created high resolution images that could be measured precisely. Measurements were made in Zen Blue software, with the area of the cytoskeleton being measured through outlining the phalloidin staining and measuring the area within. Height was measured through measuring how many Z-stacks were required to measure from the bottom to the top of the cell and multiplying this by the Z-stack section thickness. This was limited by the Z stack section size, however the typical thickness of Z stacks was in the range of 0.1 – 0.2 µm, which provided suitable precision.

2.6.3 Quantification of aggregate size, circularity and density.

Aggregates were measured using ImageJ software. After scaling the images, outlines were drawn around intact aggregates and the measure tool was used to provide measurements

for both area and circularity of the outline drawn. Density was measured by outlining the aggregates and measuring a histogram in ImageJ which displayed average grey value (bins), with a higher value indicating a lighter colour which indicated lower density.

2.6.4 Quantification of cell migration

For live cell imaging videos, ImageJ software was used to analyse the migration of cells, with the TrackMate plugin being used for automatic tracking of the cells. The settings used were 25 pixels for cell size and 0.2 for thresholding.

2.7 Assessment of functional properties

2.7.1 Albumin Assay

Albumin produced in the models was secreted into the media, which could be stored as described in section 2.2.1. This production of albumin was quantifiable through a commercial enzyme-linked immunosorbent assay (ELISA) plate (AssayPro, EA3201-1, Missouri, USA) and manufacturer's instructions were followed for the kit. To accurately quantify the albumin in media, it was measured against a standard curve created from serial dilutions of an albumin standard of known concentration. This assay was carried out at room temperature. Firstly, 50 µL of standard or sample was incubated in individual wells for an hour, with the plate sealed using the provided sealing tape. Wash buffer was used to thoroughly rinse the plate 5 times, before 50 µL of biotinylated antibody was added to each well, with a subsequent 30-minute incubation. The plate was washed another 5 times with wash buffer before 50 µL of SP conjugate was added to each well, with another 30 minute incubation. The plate was then washed again as before, with 50 µL of chromogen substrate being added per well followed by a 20-minute incubation, the end of which 50 µL of stop solution was added to each well. The plate was read immediately on a BioTek™ ELx800 plate reader at a wavelength of 450 nm. Albumin levels were calculated through the standard curve using Graphpad Prism software and were normalised to total protein concentration as determined by Bradford assay.

2.7.2 Urea Assay

Urea secretion into the media was measurable through a commercial QuantiChrom™ Urea Assay Kit (DIUR-100, BioAssay Systems, California, USA), where manufacturers instructions were followed. In brief, 5 µL of water (as a blank), 5 µL of 50 mg/dL standard, and 5 µL of

each sample were placed in individual wells. 200 µL of working reagent (made from a 1:1 ratio mix of reagent A and reagent B) was next added to each well which was incubated for 20 minutes at room temperature. The plate was then read at 520 nm on a BioTek™ Synergy™ H4 Hybrid Multi-Mode Microplate Reader, and urea concentration (mg/dL) was calculated through this equation=

$$[\text{Urea}] = \frac{OD_{sample} - OD_{blank}}{OD_{standard} - OD_{blank}} x\ n\ x\ [STD]\ (\frac{mg}{dL})$$

OD_{sample}, OD_{blank} and $OD_{standard}$ are optical density values of sample, water and standard respectively. n is the dilution factor. [STD] is 50 for the urea standard concentration (mg/dL).

2.7.3 Measuring cell death with LDH assay

For testing the toxicity of xenobiotic compounds, the lactase dehydrogenase (LDH) assay was used to provide an orthologous technique to MTT assays to provide a more direct measure of toxicity. LDH is released into cell culture media when the plasma membranes of cells are damaged, indicating the cytotoxicity of test compounds. For this assay, the commercial Pierce™ LDH Cytotoxicity Assay Kit (Thermo Fisher Scientific) was used, with the protocol adapted to suit 3D culture. Briefly, the assay was immediately performed on media taken from models exposed to xenobiotic compounds for 24 hours. A maximum LDH activity control was created by adding a 1:10 dilution of 10 x Lysis Buffer provided in the kit to selected models on the day of harvesting and incubated for 45 minutes at 37 ^{o}C, 5 % CO_2. Spontaneous LDH activity was measured from control wells with no xenobiotic compound added. For the assay, 50 µL of each sample (including controls) was pipetted into wells of a 96 well plate. 50 µL of reaction mixture was then added to each sample well and mixed well. The plate was incubated for 30 minutes at room temperature and in the dark, before 50 µL of stop solution was added to each well and mixed by tapping. Absorbance was measured at 490 nm and 680 nm using a BioTek™ Synergy™ H4 Hybrid Multi-Mode Microplate Reader. The 680 nm background reading was subtracted from the 490 nm reading before working out cytotoxicity from the following equation=

$$\%\ \text{cytotoxicity} = \frac{Compound-treated\ LDH\ activity - Spontaneous\ LDH\ activity}{Maximum\ LDH\ activity - Spontaneous\ LDH\ activity}\ x100$$

2.8 Gene Expression experiments

2.8.1 RNA collection from cultured HepG2 cells

HepG2 cells were primed on 6 well Alvetex® Strata or the 2D surface of 6 well plates for 8 days, and cells were lysed and counted as standard, but were spun down a second time to produce a cell pellet. To ensure no debris was released from Alvetex®, when lysing the 3D primed cells, trypsin was flushed over the membrane repeatedly rather than using a cell scraper as this minimised debris that could clog the RNA collection column. The kit used for RNA extraction was Qiagen RNeasy® mini plus (Qiagen, Hilden, Germany), with manufacturer's instructions followed. Briefly, 350 µL Buffer RLT Plus (with 1 % of 2-mercaptoethanol) was added to each tube of pelleted cells, with the pellet loosened by thoroughly flicking the tube. The lysate was homogenised through passing it through a 20-gauge needle fitted to an RNase-free syringe (BD, New Jersey, USA). The homogenised lysate was transferred to a gDNA Eliminator spin column which was placed in a 2 mL collection tube and centrifuged for 30 seconds at ≥8000 x g, and the column was discarded, with the flow through retained. 350 µL of 70 % ethanol was then added to the flow through from each sample and mixed with pipetting. The sample was then transferred to an RNeasy spin column, which was again placed in a 2 mL collection tube and centrifuged for 15 seconds at ≥800 x g, and the flow through was discarded. 700 µL of Buffer RW1 was added to the RNeasy spin columns and these were centrifuged at ≥800 x g for 15 seconds, and the flow through was discarded. The RNeasy spin column was washed twice with 500 µL of Buffer RPE each time, the first time for 15 seconds at ≥8000 x g, and the second time for 2 minutes at ≥8000 x g. The RNeasy spin columns were placed in new 2 mL collection tubes and centrifuged at full speed for 1 minute. Finally, 50 µL of RNase-free water was added to the spin column membrane which was placed in a fresh 1.5 ml collection tube and centrifuged for 1 minute at ≥8000 x g to elute the RNA. RNA was quantified using a NanoDrop™ spectrophotometer. At this point, the samples were ready for quality testing.

2.8.2 RNA collection from human liver tissue.

A sample of healthy human liver from a middle-aged female was snap frozen in small chunks prior to RNA processing and stored at -80 °C. For processing, a scalpel was used to cut samples of less than 20 mg of liver from different areas off the main section. The RNeasy® mini plus kit was used again here for RNA extraction. Because of the high RNase content present in the liver, homogenisation was carried out in liquid nitrogen and over dry ice, and the rest of the extraction over ice to prevent RNase activity. Liver samples were homogenised by thoroughly grinding with a pestle and mortar, before decanting the powder into an RNase free liquid nitrogen cooled 2 mL centrifuge tube. After evaporation of liquid nitrogen, 350 µL

of Buffer RLT Plus was added to the samples, followed by passing the sample through a 20-gauge needle (BD) fitted to an RNase-free syringe at least 5 times. The lysate was centrifuged for 3 minutes at maximum speed, with the supernatant being transferred to a gDNA Eliminator spin column in a 2 mL collection tube. This was centrifuged for 30 seconds at ≥8000 x g, and the flow through was kept but the spin column discarded. 350 µL of 50 % ethanol was added to each sample and mixed in with pipetting. The sample was transferred to an RNeasy spin column placed in a 2 mL collection tube and centrifuged for 15 seconds at ≥8000 x g, with the flow-through discarded. Next, 700µL of Buffer RW1 was added to the RNeasy spin columns, and they were centrifuged for 15 seconds at ≥8000 x g. The spin column membranes were then washed twice with 500 µL of Buffer RPE, with a 15 second centrifugation at ≥8000 x g after the first wash, and 2 minutes at ≥8000 x g after the second with the flow through discarded after each wash. Columns were then placed in fresh 2 mL collection tubes and centrifuged at full speed for 1 minute, before moving the columns to a 1.5 mL collection tube where 50 µL of RNase free water was added directly to the spin column membrane. This was centrifuged at ≥8000 x g, eluting the RNA. The samples were now ready for quality control steps. RNA was quantified using a NanoDrop™ spectrophotometer.

2.8.3 RNA quality control

Quality control was carried out on samples for next generation RNA sequencing (RNAseq), ensuring that the best quality samples would be submitted.

2.8.3.1 Agarose gel electrophoresis

As a preliminary measure of RNA quality, the samples were run on non-denaturing agarose gels. Gels were made from 1 % agarose in TAE buffer with 0.5 µg ethidium bromide, and 5 µL of sample loaded. Tanks were filled with TAE buffer containing 0.5 µg of ethidium bromide, and gels were run at 100 V for roughly 70 minutes and imaged using a UV gel imager.

2.8.3.2 TapeStation

Samples were loaded onto an Agilent TapeStation (Agilent, California, USA) by the Sequencing department in the Department of Biosciences at Durham University (Durham University, Durham, UK). This was able to quantify the integrity of RNA and provide a score which determined whether sequencing the samples was a viable option. A score of 8 or over was accepted as suitable for sequencing. At this point, the four best quality replicates of each sample were kept and used for sequencing, resulting in 4 x 2D, 4 x 3D primed, and 4 x human liver samples.

2.8.4 RNA library preparation

The RNA libraries were assembled by the sequencing department within the Department of Biosciences at Durham University. NEBNext Poly(A) mRNA Magnetic Isolation Module and NEBNext Ultra II Directional Library Prep Kit for Illumina (New England Biolabs, Massachusetts, USA) were used to create the libraries.

2.8.5 Sequencing

Samples were sequenced using 125bp paired end sequencing on HiSeq 2500 using v4 chemistry in High Output mode, providing up to 60M paired end reads. This was carried out by the sequencing department within the department of Biosciences at Durham University. The adaptors used were NEBNext® Multiplex Oligos for Illumina® and the raw data was returned as FastQ files.

2.8.6 Data processing

For processing the raw data, Dr Wenbin Wei in the Department of Biosciences at Durham University helped with the use of Linux and in using a pipeline to map the raw data to the human genome and produce read counts from these. Data was processed using the BCBio toolkit, which provided a pipeline through which Salmon was used for quasi-alignment to the human genome with Homo_sapiens.GRCh38.cdna.all.fa.gz of ensembl release 98. This produced gene counts which were imported into R for gene level analysis, and genes with counts of ≥10 in 2 or more samples were kept. Count data was transformed using regularised-logarithm transformation method and principle component analysis was performed on this (and on untransformed data). Clustering analysis was performed using both rlog transformed data, and untransformed data with Poisson Distance, and differentially expressed genes were identified using DESeq2 which provided excel

spreadsheets that included normalised expression values, fold change between the selected conditions and associated statistics. Additionally, gene expression data from 1-day cultured 2D primary hepatocytes was obtained from https://www.ebi.ac.uk/gxa/experiments/E-MTAB-5984/Downloads and differential expression against our samples was run in order to provide an additional point of comparison. From this point, further data analysis and interpretation was performed in RStudio by myself. See **Appendix 1** for information about supplementary DESEQ2 data supplied as an Excel spreadsheet.

2.8.7 Data analysis

RStudio software was used to analyse the differential expression data, with gplots being used to produce many of the figures from the data. The heatmap.2 package was utilised to produce gene expression heatmaps, venndiagram used for the Venn diagrams and EnhancedVolcano used for the volcano plots.

Further in-depth interpretation was achieved through investigating the differentially expressed genes in terms of their ontological groupings. Comparing a test gene set (for example upregulated genes in 3D) against a reference library (for example, the human genome), means that one can compare the genes in reference to particular annotations (such as gene ontology), and search for over-representation in our test set compared to the reference set. This provides a more meaningful insight into biological changes occurring as it puts genes into context rather than looking at differences in individual genes which may have wide reaching interactions in pathways that are obscured through isolated analysis. The software used for this form of analysis was available online, and figures were produced using the following: EnrichR (Chen et al., 2013), WebGestalt (Liao et al., 2019) and Reactome (Fabregat et al., 2017).

2.8.8 RTqPCR

To validate the RNAseq results, and to investigate gene expression changes in hanging drop models, RTqPCR was used with separately grown models. For validation of sequencing, 4 new biological repeats were grown of both hepG2 cells grown in 2D and on Alvetex® Strata, with RNA extraction being carried out as aforementioned.

2.8.8.1 Reverse transcription

After quantifying on a nanodrop, the RNA samples were converted to cDNA using the high capacity cDNA reverse transcription kit (Thermo Fisher Scientific). A 20 µL reaction mix was used consisting of the following:

- 2 µL 10X RT buffer
- 0.8 µL 25X dNTP
- 2 µL RT random primers
- 1 µL Reverse Transcriptase
- 14.2 µL of sample diluted with nuclease free water to make a final concentration of 1 µg.

The Thermocycler was used with the following parameters:

- Step 1: Temperature 25 ^{o}C, Time 10 min
- Step 2: Temperature 37 ^{o}C, Time 120 min
- Step 3: Temperature 85 ^{o}C, Time 5 min
- Step 4: Temperature 4 ^{o}C, Time indefinite

Samples were then diluted with 80 µL of nuclease free water to make a final concentration of 10 ng/µL.

2.8.8.1 Primers

Predesigned KiCqStart® SYBR® Green Primers primers were bought from Sigma Aldrich for the following genes:

Table 2.6: Primers used in RTqPCR

Common Name	Gene ID	Forward Sequence
Antithrombin	SERPINC1	CTTGAGGTAAATGAAGAAGGC
N-cadherin	CDH2	CTGGAACATATGTGATGACC
Fibrinogen gamma chain	FGG	CTGGGACAATGACAATGATAAG
Vasodilator-stimulated phosphoprotein	VASP	GGAATTGCAGAAAGTGAAAG
Transforming growth factor β1	TGFB1	AACCCACAACGAAATCTATG
Zyxin	ZYX	ACTACCACAAGCAGTACG
SUN1	SUN1	GTGTTTCTTCTTACCAGGTG
SUN2	SUN2	AGCCTTCAGATTCTCTTCAG
Hepcidin	HAMP	GTTTTCCCACAACAGACG
Sulfotransferase 1A1	SULT1A1	CTTCTATGAAGACATGAAGGAG
Glutathione S-transferase A1	GSTA1	AGGTATAGCAGATTTGGGTG
Albumin	ALB	AGCCTACCATGAGAATAAGAG
Hypoxanthine-guanine phosphoribosyltransferase	HPRT1	ATAAGCCAGACTTTGTTGG
DNA topoisomerase 1	TOP1	CAAAGACGAAGAAGGTAGTAG
Ubiquitin C	UBC	CGTCACTTGACAATGCAG

The final three genes (HPRT1, TOP1 and UBC) were used as housekeeping genes based on the stable expression in the RNAseq data, and from identification of stable housekeeping genes between 2D and 3D culture conditions in previous papers (Adeola, 2018; Rauh et al., 2015).

Forward and revers primers were reconstituted to a concentration of 100 µM with Tris-EDTA, and a 10 µM stock was made with 10 µL of both reverse and forward primers in 80 µL of nuclease free water. A working 2.5 µM solution of primers was used when running PCR by diluting the stock 1 in 4 with nuclease free water. For each reaction, 20 ng of cDNA for each sample was used. For the PCR, a 10 µL reaction was used which required the following components for each reaction=

Table 2.7: Components required for 10 µL PCR reaction

Reagent/component	Quantity
2x SYBR dye	5 µL
Forward/reverse Primer	1 µL
Sample	2 µL
Nuclease free water	2 µL
Total volume	10 µL

Once everything was pipetted into 96 well PCR plates (Bio-rad), they were centrifuged at 1000 rpm for 3 minutes before being ran on the Bio-Rad CFX connect™ Real-Time System (Bio-rad) using the following conditions:

Table 2.8: Settings for RTqPCR

Stage	Temperature (°C)	Time
cDNA synthesis	50	2 minutes
Initial denaturation	95	10 minutes
Denaturation	95	15 seconds
Annealing and extension	60	1 minute (x40 cycles)

Data was analysed through normalisation to the three reference genes (HPRT1, TOP1, UBC) using the ΔΔCt method, and averaging the fold change after this normalisation.

2.9 Electron microscopy

2.9.1 Scanning electron microscopy

To visualise HepG2 cells in high detail, scanning electron microscopy was used. Three conditions were visualised: cells grown on 6 well Alvetex® Strata for 8 days, cells grown for 8 days in 2D then liberated and grown on 2D silicon chips for 1 day, and cells grown for 8 days Alvetex® Strata then liberated and grown on 2D silicon chips for 1 day.

Alvetex® samples were cut into small sections and fixed in Karnovsky's fixative (2 % paraformaldehyde (PFA) (Sigma Aldrich) and 2.5 % glutaraldehyde (Agar Scientific, Standsted, UK) in 0.1 M cacodylate buffer pH 7.4 (Agar Scientific) with distilled water) for 1 hour at room temperature before washing for 5 minutes in 0.1 M cacodylate buffer pH 7.6. Samples were then incubated in 1 % Osmium tetroxide (Agar Scientific) made up in 0.1 M cacodylate buffer for 1 hour followed by dehydrations in 50 %, 70 %, 95 % and 100 % ethanol for 3x 5 minutes in each dilution. Samples were then dried using a Bal-tec CPD 030 critical point dryer followed by sticking the Alvetex® onto silicon chips using double sided sticky tape. Samples were then platinum coated using a Cressington 328UHR and were imaged on the Hitachi S-5200 at 15 kV.

For cells grown on the silicon chips, they were fixed in Karnovsky fixative for 10 minutes before washing for 5 minutes in a 0.1 M phosphate buffer. Samples were treated with 1 % Osmium tetroxide made up in 0.1 M phosphate buffer for 10 minutes followed by dehydrations in 50 %, 70 %, 95 % and 100 % ethanol for 2 minutes in each dilution with two incubations in 100 % ethanol. Samples were then dried using a Bal-tec CPD 030 critical point dryer and were then platinum coated using a Cressington 328UHR and imaged on the Hitachi S-5200 at 15 kV.

2.9.2 Transmission Electron Microscopy

HepG2 cells grown on Alvetex® Strata for 8 days were analysed using transmission electron microscopy (TEM) to examine structural properties. Small sections of the Alvetex® were fixed in Karnovsky's fixative for 1 hour at room temperature and were then washed three times in 0.1 M cacodylate buffer pH 7.6 for 5 minutes each. These samples were treated in 1 % osmium tetroxide for 1 hour, washed in 0.1 M cacodylate buffer, then dehydrated through 50 %, 70 %, 95 % and 100 % ethanol for 3x 5 minutes in each dilution. Following this, samples were embedded in resin by first immersing them for 15 minutes in a 1:1 ratio mix of 100 %

ethanol and propylene oxide (Agar Scientific) before being moved into a solution of pure propylene oxide for another 15 minutes. Next, samples were immersed in a 1:1 mix of propylene oxide and Agar 100 Epon resin (24 g Agar 100 Epon Resin, 9 g dodecenylsuccinic anhydride, 15 g methyl nadic anhydride and 1.4 g benzyldimethylamine (Agar Scientific)) for 15 minutes, then were taken through three sets of 1-hour incubations in pure Agar 100 Epon resin. Fresh resin was used to embed the samples in rubber moulds, and these were left to polymerise at 60 ^{o}C for 24 hours. Sections of 1 µm thickness were initially taken from samples for toluidine blue staining. These were cut using a glass knife and a water boat on a Leica UC6 microtome. Finally, for the TEM, ultra-thin sections (50 – 80 nm) were cut using a diamond knife (Agar Scientific) on the Leica UC6 microtome and placed onto 200 mesh copper formvar coated grids (Agar Scientific). These sections were stained with 1 % uranyl acetate in 70 % ethanol for 10 minutes followed by washing in water and staining in Reynold's lead citrate for 10 minutes. Visualisation was carried out on the Hitachi H7600 TEM.

2.9.3 Toluidine Blue O Staining

Toluidine blue staining solution was made using 0.8 g sodium tetraborate, 100 mL distilled water, 0.8 g toluidine blue and 0.2 g Pyronine and was filtered before use. Samples were stained in toluidine blue by submerging them in the solution for 2 minutes followed by washing in dH_2O and imaging on the Leica ICC50 microscope.

2.11 Diagram generation.

Diagrams were made either using Microsoft PowerPoint or created with BioRender.com.

2.11 Statistical analysis.

For analysis of quantitative data, GraphPad Prism 5 software was used. For comparison of 2 samples, the two tailed t-test was used (unpaired or paired depending on the data type), and for more than 2 samples, the one-way analysis of variance (ANOVA) test was used, with Tukey's post-test being employed to compare each sample. All error bars on data (unless otherwise specified) indicate standard error of the mean (SEM) as worked out in GraphPad Prism 5. Throughout the data, independent biological repeats are denoted by using a capital N, and technical replicates are denoted by using a lower-cased n. The following indicates levels of significance denoted by stars:

Symbol	Meaning
ns	$P > 0.05$
*	$P \leq 0.05$
**	$P \leq 0.01$
***	$P \leq 0.001$

Chapter 3 – Protocol to maintain the 3D structure of cells through priming on a three-dimensional substrate.

3.1 Introduction

As discussed in the introduction, the liver plays an essential role in many biological processes – namely glucose and fat metabolism, protein synthesis, hormone synthesis, urea production, detoxification and storage (Silverthorn, 2013). The parenchymal and key functional cell type in the liver is the hepatocytes, making up 70 % of the liver mass (Manco et al., 2018), and therefore hepatocytes often remain the focus of liver research. Many *in vitro* models of the human liver exist, with 2D cell culture having been long utilised to provide a first point of contact for testing the toxicity of compounds and researching liver biology.

With research (especially in drug discovery) being particularly under the pressure of time and money, simple yet functionally competent models are highly desirable, and as a result many areas of liver research utilise the robust immortalised hepatocarcinoma cell line: HepG2. Other cell types are also sometimes utilised in liver research, such as primary hepatocytes, or terminally differentiated immortalised hepatic cell lines (HepaRG) – but ultimately the methodology when 2D culture stays largely the same.

When cultured in 2D, the biological properties of hepatic cells deviate significantly from *in vivo* hepatocytes, with de-differentiation posing a significant problem in primary hepatocytes (Catherine C. Bell et al., 2018), resulting in cells losing hepatic function even within the first 24 hours of culture due to an increased expression of microRNAs (Lauschke et al., 2016). HepG2 cells lack expression of many key Phase I enzymes and liver specific genes, resulting in poor predictions of toxicity and a lack of physiological relevance (Gerets et al., 2012; Westerink and Schoonen, 2007a). HepaRG cells exhibit enhanced hepatic function over HepG2 cells, but are expensive and still are not as predictive as terminally differentiated primary hepatocytes (Gerets et al., 2012).

Culturing hepatic cells using 3D technologies has proven advantageous in preventing de-differentiation in primary hepatocytes (Lauschke et al., 2019), and in partially bridging the functional gap seen in hepatic cell lines (Luckert et al., 2017). However, shortfalls still exist in the most easily utilised cell line – HepG2 cells, with highly variable differences in albumin and urea production (key liver functional biomarkers) between HepG2 cells cultured in different 3D technologies (Luckert et al., 2017). Many of the current three dimensional liver models use spheroid technologies to grow their cells (Ramaiahgari et al., 2014a; Shah et al., 2018; Takahashi et al., 2015; Zhou et al., 2019) due to the relative ease with which these can be grown, and the high throughput capabilities of such models. Hepatic function is also elevated

in these models (Ramaiahgari et al., 2014a), with albumin and urea synthesis increasing, and an increased tolerance for repeated doses of xenobiotic compounds being seen over the 2D alternative. The spheroid models are evidently beneficial in terms of biological function, however scaffold/hydrogel based models have also shown promising results in terms of enhancing both the structure and function of HepG2 cells (Bokhari et al., 2007; Luckert et al., 2017), and these technologies are able to support much larger cell numbers per model than aggregates, whose size (and therefore cell number) are restricted by the fact that nutrients cannot diffuse past a certain distance (~200 µm) (Rouwkema et al., 2010). Spheroids may also present challenges in imaging, due to their small size, whereas hydrogels and scaffolds provide an easier medium for manual handling and processing. Therefore, in certain applications where high cell numbers, or manipulation/handling of the model are desired, scaffold-based technologies may be preferable.

One aspect that is often overlooked in creating physiologically relevant models is the influence of time on the ability to form mature *in vivo* like structures. Culture of breast epithelial cells for example involves formation of clonal acini from single cells which is a time dependent process (Ow et al., 1992). The length of culture time in 3D has been shown to affect the heterogeneity of tumours (Jain et al., 2020), and long term cultures of human brain organoids allowed the establishment of mature features (Quadrato et al., 2017). Interestingly, time is sometimes a problem in the opposite sense, particularly in 2D cultures – primary hepatocytes, for example, dedifferentiate over time, with 272 differentially expressed proteins being detected after 168 hours of culture on a collagen coated plate when compared with freshly isolated cells, whereas only 40 proteins were differentially expressed at 24 hours of culture (Heslop et al., 2017). This demonstrates the importance of considering temporal variables when developing a new model. With HepG2 cells, elevated expression and activity of the cytochrome P450 enzymes has been attributed more to the influence of prolonged culture time than to the effect of 3D culture, with 2D cells after 21 days exhibiting similar metabolic functionality to 3D cells cultured for the same time (Luckert et al., 2017). It is unknown whether this is due to a progressive differentiation related to cell ageing, or due to a transition of the 2D monolayer into a third dimension from cells piling up on each other once passing full confluency. Some differences were still noticed between 3D and 2D culture at earlier time points (7 and 14 days) indicating that perhaps 3D culture helps encourage faster progression into a mature functional model, but this highlights the drastic influence of time. In this study, spheroids only fully matured at 7 days, and this is a time point often used at minimum for 3D cultures.

There is clearly a delicate balance between time, simplicity and the culture technique of the model. Long term maintenance of cultures can be costly and inefficient; the potential impact of infections or failed models becomes increasingly severe when more time has been invested into the model. However it is suggested that models should not force the rapid formation of 3D structures, as this would prevent full maturation of models, and limit proper tissue architecture from forming (Lelièvre et al., 2017). Mechanotransduction is also a time dependent process with temporal signalling events taking place, and the mechanical properties of cells being time-dependent (M et al., 1997; Shuaib et al., 2019; Tee et al., 2009), and thus it is critical to give ample time for the cells to adapt mechanically to their environment. Therefore, this project aims to strike a balance between culture time and simplicity through creation of a unique culture method for HepG2 cells that allows time for the appropriate mechanical changes to take place, while keeping in mind the practicality of the model. By priming cells in a 3D microenvironment before reseeding into a secondary 3D culture format, it is expected that the ability to form mature three-dimensional structures with enhanced functional properties will be increased when compared to 2D cells seeded straight into a 3D model. This could further build on the work of Luckert et al. in 2017 too, as it is expected that adding a priming step in 3D may have clear beneficial effects even after liberating and reseeding cells. This would help clarify the role of both temporal and mechanical responses in cells changing their biological profiles in line with their culture conditions.

Previous research in our lab has indicated that maintaining HepG2 cells in a 3D microenvironment over continued passages results in enhanced functional properties compared to 2D cells and cells grown for one passage in 3D. Cells *maintained* on a 3D scaffold displayed structural features more reminiscent of the liver, a significant increase in albumin production and phase I enzyme expression and a differential response to xenobiotic compounds (Chhatwal, 2016). Despite the benefits of this method, it proved to be labour intensive and time consuming. Therefore, the idea was simplified and utilised in this project through creating a novel and easy to utilise technique for growing cells that provides one additional stage in 3D culture to allow the cells chance to adapt structurally and functionally, preparing them for placement into a 3D *in vitro* model for testing. The biological rationale behind this is that mechanotransduction is a time-dependent process, and that this can be harnessed through 'priming' cells in an initial 3D priming model which will provide chance for mechanically induced changes to occur. Cells can then be liberated from this 'priming' model, before seeding into a final 3D model where we hypothesise that they will carry over

their enhanced hepatic functionality compared to cells taken straight from 2D and placed into the final model. This priming model will utilise the biologically inert three-dimensional polystyrene substrate - Alvetex®, which comes in three different formats with different void sizes depending on cell culture requirements as outlined in **Chapter 1.7** of the introduction. Alvetex® provides a suitable three dimensional topography on which to grow HepG2 cells, with a capability of maintaining viability in large cell populations, and the fact that this is a biologically inert substrate restricts any effect on the cells from extraneous variables outside of the mechanical changes. All experiments in this chapter were carried out using 6 well sized Alvetex® membranes.

3.2 Hypothesis and aims

The aim of this chapter is to create a reproducible 3D priming model for growing cells on, to prime them structurally and functionally for subsequent reseeding into a final 3D model. This model should create a thick layer of HepG2 cells that are able to form multiple cell-cell contacts as well as cell-substrate contacts in order to mimic the tight, multipolar packing of hepatocytes seen in the human liver. This layer of cells needs to be accessible and easy to liberate due to the desired purpose of reseeding them into a final 3D model. Finally, this model needs to be simple, time effective, and provide enough cells to make it a viable technique for subsequent seeding into high throughput assays.

It was expected that through testing different formats of Alvetex®, different ways of applying media, and different growth conditions, that we could create an optimised technique for growing HepG2 cells on Alvetex®. This optimised technique should result in enhanced structural properties of the HepG2 cells, bringing them closer to the morphology of *in vivo* hepatocytes, and that due to mechanotransduction, the function would also be improved (these aspects will be tested for in later chapters). These enhanced qualities should carry over and be retained in the final 3D model, where the primed HepG2 cells would display more biologically relevant properties over HepG2 cells placed into a 3D model straight from 2D.

3.3 Objectives

The objectives of this section were as follows:

- Test which format of Alvetex® allows for optimum growth of HepG2 cells aligning with the aims.

- Test how the Alvetex® placement in the well (i.e. in inserts, or unclipped at the bottom of the well) affects the growth of HepG2 cells.
- Test how media application and availability affects the growth of the HepG2 cells.
- Test how long to culture the HepG2 cells for in the priming model, in order to make a thick and viable cellular layer whilst avoiding apoptosis and necrosis.
- Investigate different liberation techniques, and how best to preserve cell viability when removing cells from the priming model.

3.4 Results

3.4.1 The placement and format of Alvetex® impacts cell growth on the membranes

In order to achieve a substantial layer of HepG2 cells growing on the 3D substrate, optimisation was needed to investigate which format of Alvetex® (Scaffold, Strata or Polaris) facilitated this the best. Consideration was also given as to how the membranes should be placed within the wells. If the membranes were clipped into the inserts (**Figure 3.1** – 'insert'), then media would be available from both above and below the membrane, ensuring that essential nutrients were readily available to the growing cells. Unclipping the Alvetex® membrane and placing it at the bottom of the well (**Figure 3.1** – 'well base') was also considered a potential method as well, due to the possibility that restricting media availability to only above the cells could lead to a thicker layer of cells growing on top of the membrane because of chemotaxis towards the nutrient gradient. Therefore H&E images were taken of HepG2 cells being grown on each format of Alvetex® for 7 and 14 days with the Alvetex® either in the well base or in an insert (**Figure 3.2)**.

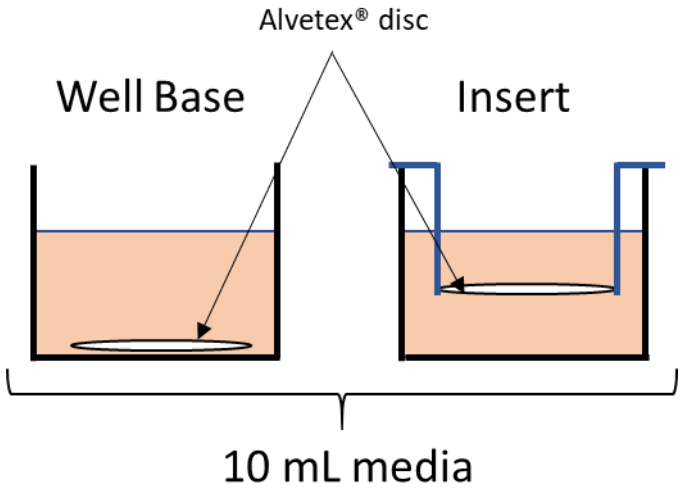

Figure 3.1: Alvetex discs can be placed at the bottom of a well (well base) or in an insert.

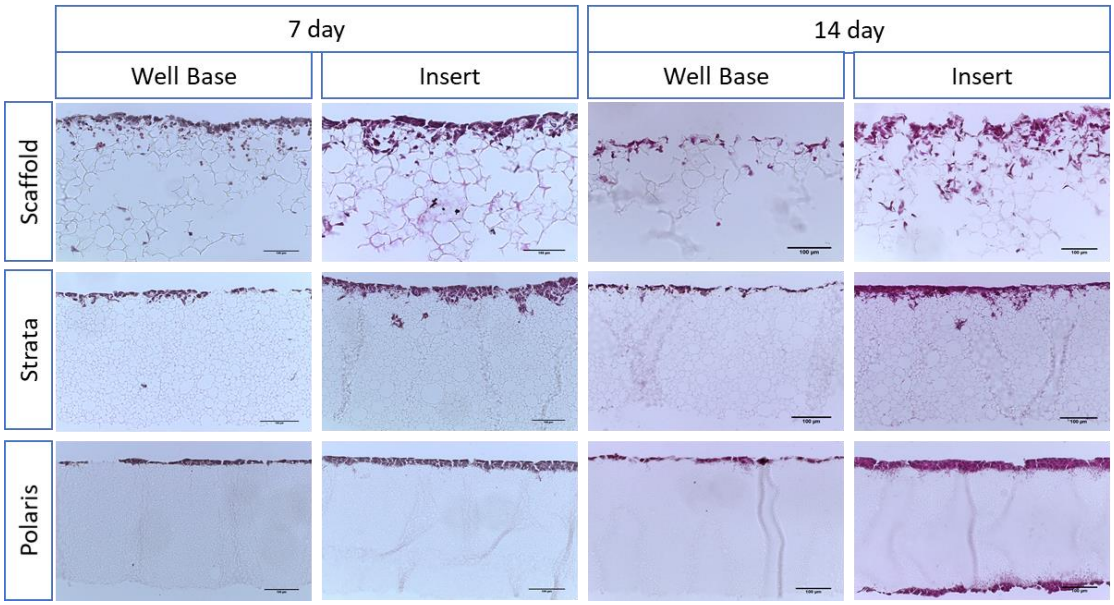

Figure 3.2: Growing cells in an Alvetex® insert showed better morphologies than growing on an Alvetex® disc at the bottom of the well.

H&E stain of 7 day and 14 day grown HepG2s seeded at 1 x 10^6 cells per well on 3 different formats of Alvetex®, with the substrate either clipped into an insert or placed at the bottom of a well (well base). Scale bar = 50 µm.

Figure 3.2 clearly demonstrates that cells grown on Alvetex® in the inserts were able to form thicker multilayers compared to the very thin and sparse populations of cells seen in the 'well base' format. The thickness did not appear to increase significantly in most formats of Alvetex® after 14 days, apart from in the 'insert' placement of Alvetex Scaffold where the thickness more than doubled after 14 days (**Figure 3.3**). This experiment indicated that restricting the media availability to just above the substrate did not benefit the growth of the cells. From the quantification data (**Figure 3.3**) it would appear that Alvetex® Scaffold was able to facilitate growth of the thickest layers of HepG2 cells, but upon examining the histology, the cells grown in Alvetex® Scaffold were clearly more spread out within the substrate – especially after 14 days. This does not align with the aim of creating a thick, compact and easily accessible layer of HepG2 cells which are able to form multiple cell to cell contacts.

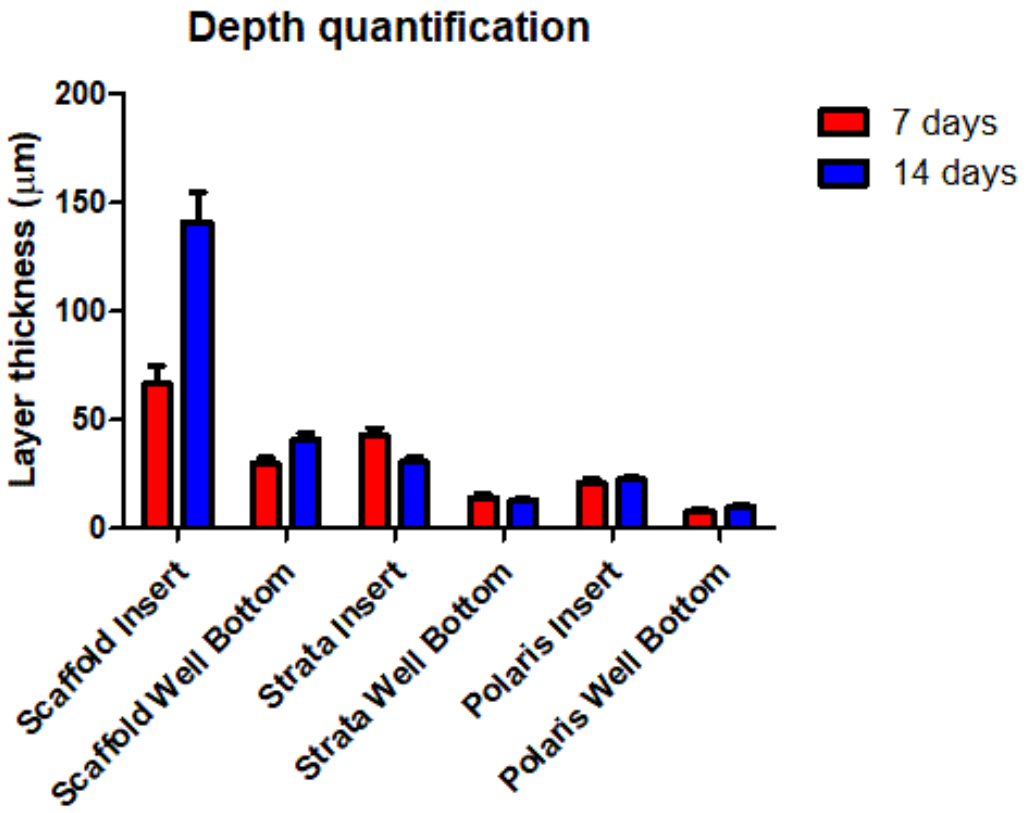

Figure 3.3: Cells formed thicker layers in inserts compared to at the bottom of a well.

Total cell layer thickness quantification of cells grown in the 3 types of Alvetex® either in an insert or at the well base (well bottom) for either 7 or 14 days. N= 3 n= 3, Error bars = SEM.

Further evidence that the 'well base' placement of the Alvetex® disc was sub-optimum is provided with fluorescent microscopy images of 7 day grown HepG2 cells. HepG2 cells were stained with Hoescht 33342 in **Figure 3.4** to stain the cell nuclei allowing for easy visualisation of their positions, and of HepG2 cells stained with Hoescht 33342 and probed for E-cadherin in **Figure 3.5**, to indicate the presence of cell-to-cell contacts. E-cadherin was chosen for a preliminary structural marker due to its high expression in epithelial cell types (of which hepatocytes are one) (Pećina-Šlaus, 2003). The Hoescht 33342 stain clearly shows the same pattern as the H&E stains, with poor growth of HepG2 cells displayed in the well base Alvetex®, and thicker layers displayed in Alvetex® within the inserts. Again, there are thicker but more spread-out layers of HepG2 cells in Alvetex® Scaffold, but Strata and Polaris appear to show multi-layered growth with more opportunity for cell to cell contacts. Indeed, this was confirmed with the E-cadherin probe seen in **Figure 3.5**, where the presence of E-

cadherin is clearly elevated in the Alvetex® placed in an insert. The presence of E-cadherin is not consistent across the cell layers even in the inserts but appears to be more steadily expressed across the HepG2 cells grown on Strata and Polaris compared to Scaffold. With these data combined, it was clear that the well base placement of Alvetex® did not provide the conditions necessary to facilitate growth of the HepG2 cells to a suitable level, and therefore this was ruled out as a condition. All data going forward was gathered from cells grown in Alvetex® discs placed in inserts.

3.4.2 The media application technique significantly altered the thickness of the cell layers.

Moving forward, the next consideration in optimisation of the model was how the media was applied. Previous lab data suggested that a thinner layer of media on top of the membrane resulted in thicker cell sheets forming, so this was tested using the 'contact' method (**Figure 3.6**). This method used 5 mL of media underneath the Alvetex insert, and 0.5 mL containing the cells on top, meaning media was in contact with the cells but not overly flooding them. The growth of cells using the contact method was compared to using submerged cultures with either 8 mL or 10 mL of media (**Figure 3.6**). An added point of comparison was whether applying media inside or outside the insert first would make a difference due to possible effect of flushing freshly seeded cells out of the insert when fully submerged.

These conditions were visualised first by using a neutral red stain to macroscopically visualise HepG2 cell growth after 3 days (**Figure 3.7**). Neutral red was applied to both the Alvetex® substrates and to the bottom of the wells to detect if any cells were being washed off and were growing on the plastic well surface.

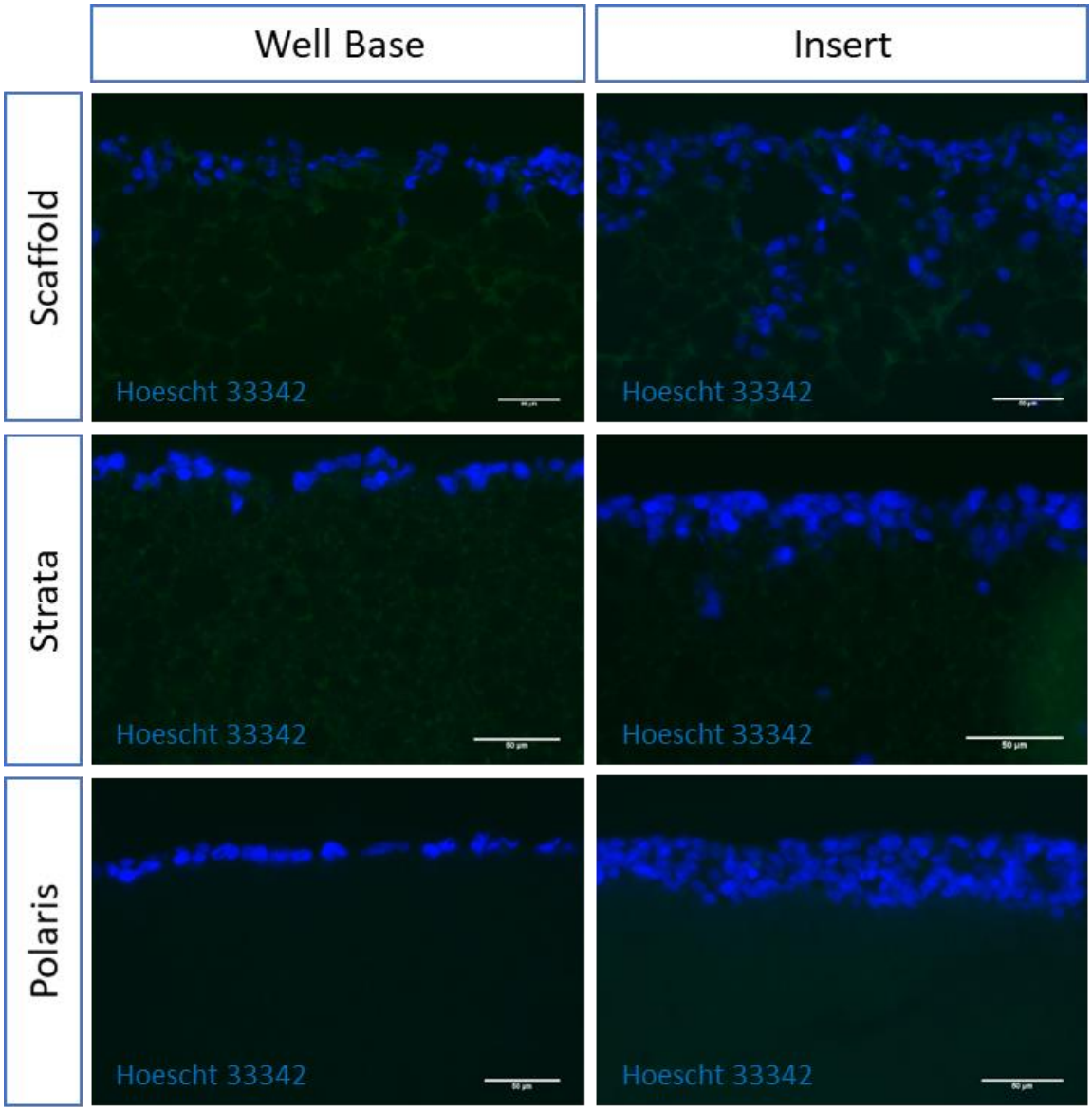

Figure 3.4: Hoescht 33342 staining further highlights the benefits of growing cells on Alvetex® kept in the insert rather than at the well base.

Images taken of paraffin embedded HepG2 cells stained with Hoescht 33342. HepG2 cells were seeded at a density of 2 x 10^6 cells onto the three formats of Alvetex® either in inserts or at the well base and were stopped after 7 days of growth. Scale bar = 50 µm.

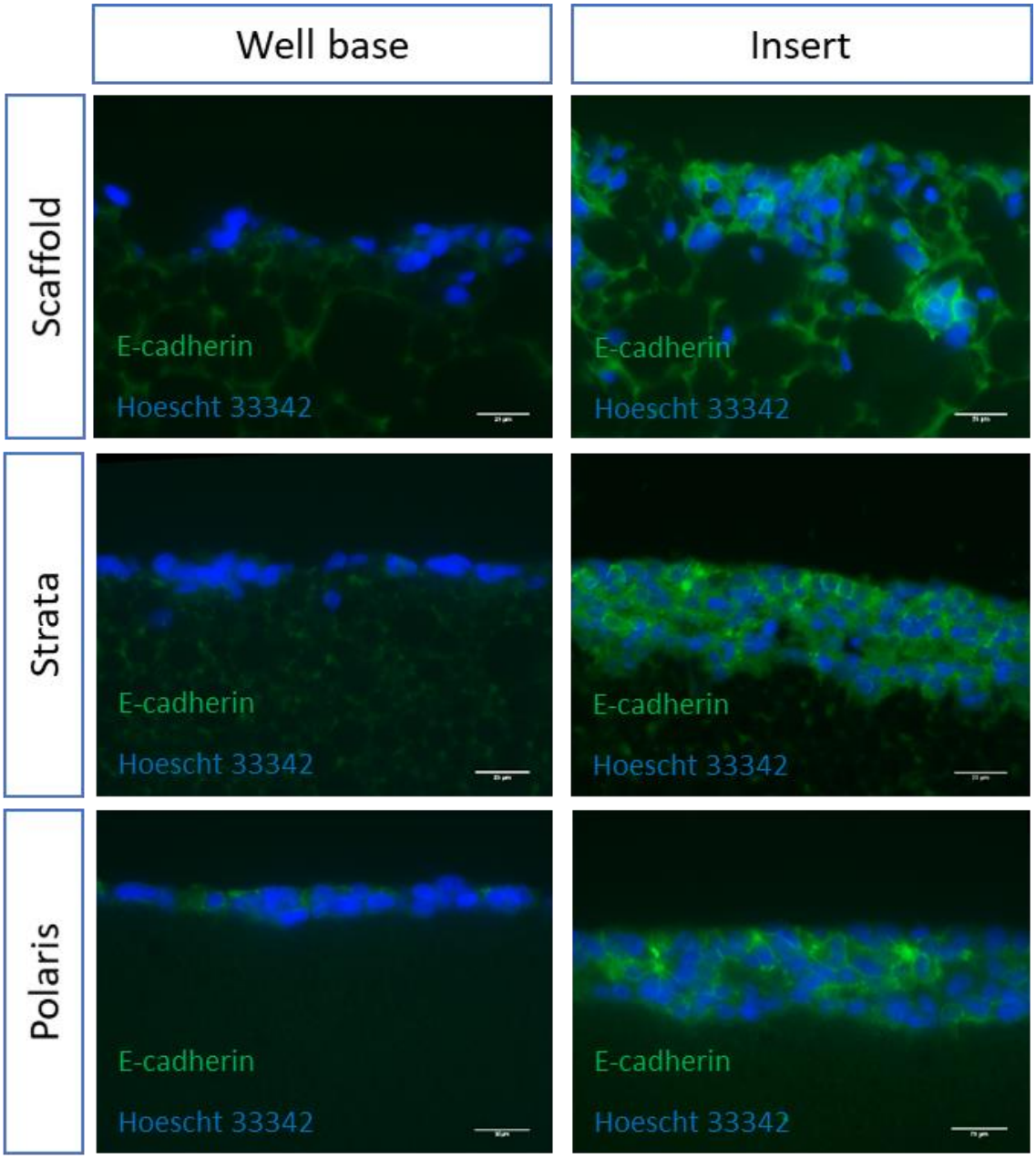

Figure 3.5: E-cadherin immunofluorescence indicates more cell to cell contact formation in the insert format as opposed to the well base format.

Images taken of paraffin embedded HepG2 cells probed with anti-E-cadherin using immunofluorescence. HepG2 cells were seeded at a density of 2 x 10^6 cells onto the three formats of Alvetex® either in inserts or at the well base and were stopped after 7 days of growth. Scale bar = 50 µm.

The neutral red stains do not reveal many differences between the different methods of applying media when completely submerged. However, there is a clear increase in neutral red stain intensity with the contact method. This indicates a thicker cell layer present, and this is likely due to less disruption to the cells during media changes, meaning less instances where cells might be flushed out of the insert. This format also potentially allows for a greater oxygen gradient, which is important in the liver for zonation and the function of the hepatocytes (Kietzmann, 2017). The oxygen concentration will be higher for cells at the top in the contact method due to them being closer to the air-liquid interface. Interestingly, in the Polaris contact condition, cells seem to be growing at the bottom of the well (**Figure 3.7**). This may be due to a limited ability for the cells to anchor themselves in this format of Alvetex® which has very small void sizes, meaning the cell layers can be washed off more easily. The neutral red stains indicate that the cells are growing across the whole membrane of the Alvetex®, but in the submerged methods, the layers seem to be the thickest around the outside edges which may indicate that the submerged method pushes cells to the outer boundaries of the membrane more than the contact method.

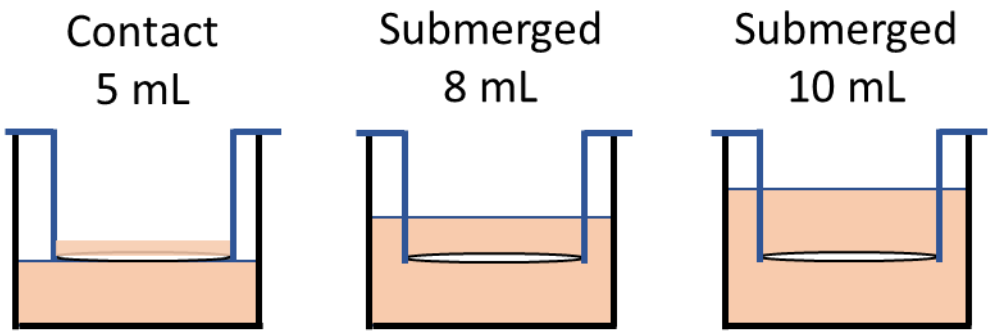

Figure 3.6: Media was applied at three different volumes to test cell growth.

Due to the lack of difference seen within the submerged conditions, using 10 mL of media with media applied inside then outside the insert, was picked to be used as a comparison against the contact method. Growth of the HepG2 cells was assessed through histological staining with H&E to investigate the difference between submerged and contact growth over 7 days (**Figure 3.8**). These images made it very apparent that cells were able to grow much thicker layers using the contact method, particularly within Alvetex® Scaffold which had evidently more cells growing within it than Strata and Polaris. Importantly, the cells growing in Scaffold were located within the substrate rather than residing on the surface.

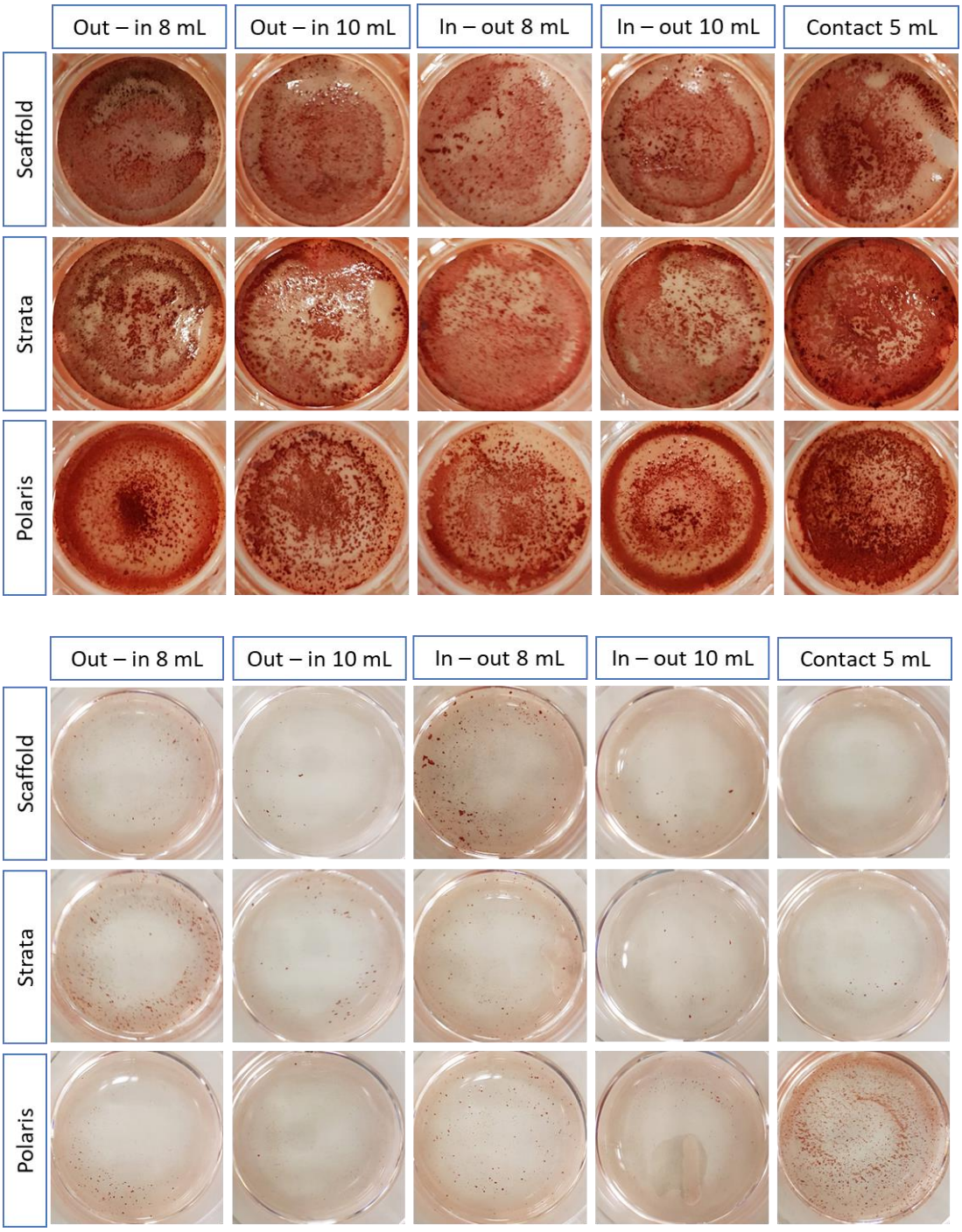

Figure 3.7: Neutral red images highlight how using a 'contact' media application method results in thicker cell layers.

Images taken of neutral red stained Alvetex® membranes and well surfaces from cultures of HepG2 cells seeded at 5 x 10^5 cells onto the three formats of Alvetex® in varying presentations after 3 days of growth. The order of Out and In refers to the order in which the media was applied to the insert (outside the insert then inside, or vice versa), or contact where a thin layer was applied on top. The volume refers to how much media in total was applied.

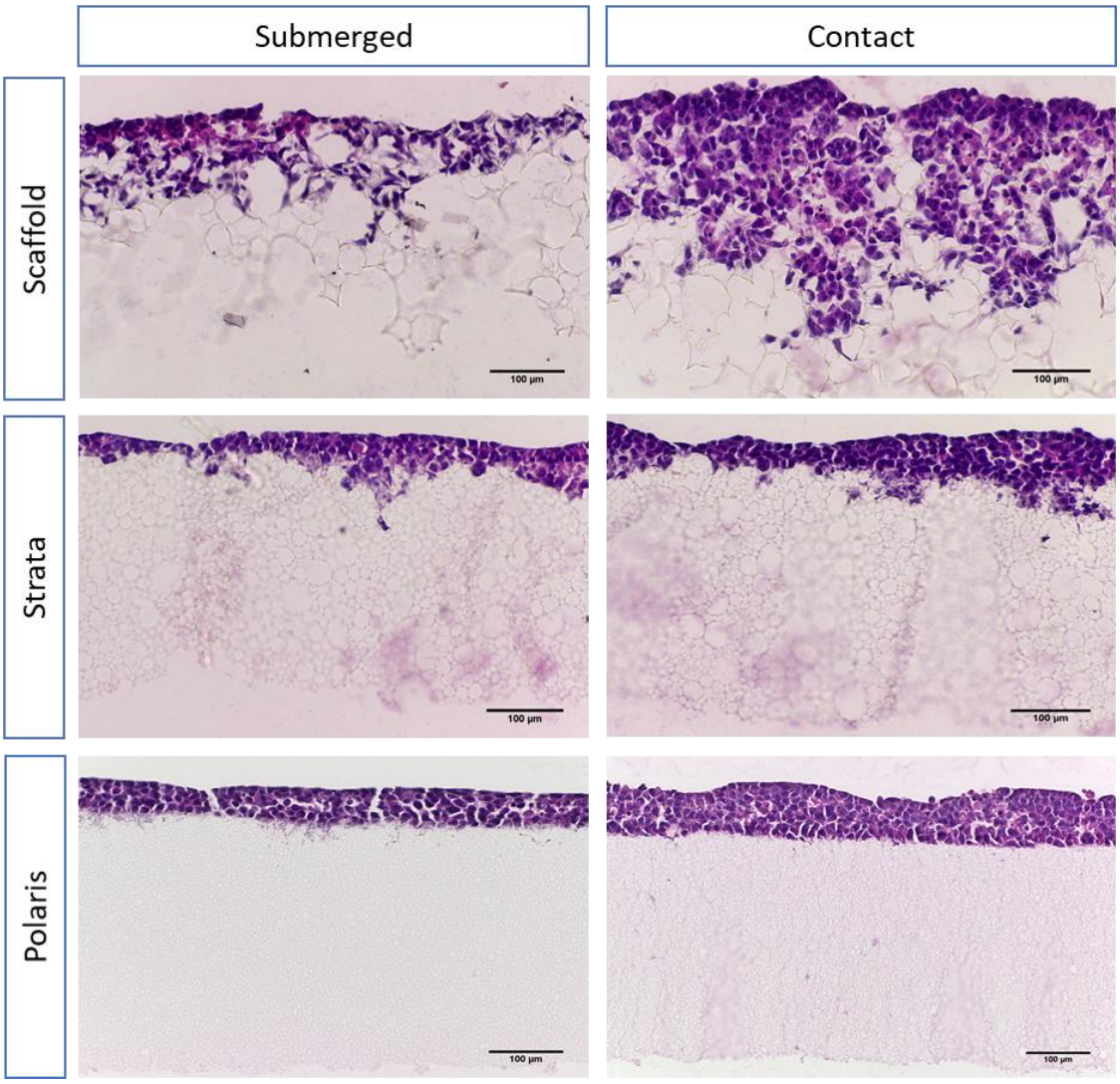

Figure 3.8: H&E stains of 7 day grown HepG2 cells shows thicker cell layer growth with the contact method compared to submerged.

Images taken of paraffin embedded H&E stained HepG2 cells seeded at 5 x 10^5 cells onto the three formats of Alvetex® in using two different media application techniques, grown for 7 days. Scale = 100 µm.

This presented potential issues for liberation and also restricted the amount of cell-cell contact possible. The cells growing on Strata and Polaris displayed desirable qualities for the priming model – they grew on a 3D topography, exhibiting a multi-layered cell sheet, yet were not penetrating the substrate significantly meaning that cell-to-cell contacts can form, and easy liberation was possible.

It was also noticed that in certain regions of growth in Scaffold that the cells near the top were exhibiting unusual morphology (**Figure 3.9 top panel**) with features suggesting apoptosis: cell shrinkage, nuclear shrinkage, and hypereosinophilic cytoplasms (Maronpot, 2016). Therefore, to test for this, a TUNEL assay was performed which tests for apoptosis by detecting double stranded DNA breaks. Indeed, HepG2 cells grown in Scaffold showed positive staining in the upper layers (**Figure 3.9**) showing that apoptosis was occurring. This was likely due to nutrient starvation occurring in Scaffold, considering that nutrient diffusion is reported to be limited to distances of up to 200 μm in engineered tissues (Rouwkema et al., 2010), and the cell layer thickness were growing close to that on Scaffold. Therefore, Scaffold was ruled out as a format of Alvetex® format for use in the priming model.

3.4.3 Seeding density did not significantly affect the growth of HepG2 cells on Alvetex®.

The number of cells seeded onto Alvetex® was altered to see if it would affect the cell layer thickness (**Figure 3.10**). This experiment also compared the contact and submerged media application again, but this time only with Strata and Polaris. H&E images revealed that there was little visual difference in cell growth between three different seeding densities (0.5 $x10^6$, 1 $x10^6$ and 1.5$x10^6$), aside from a slightly thinner layer present in contact Strata at 1.5$x10^6$ cells compared to the other two densities. The quantification of cell layer thickness indicated the same trend, with the thickest layers present in the lower two seeding densities of contact Strata. A stark contrast in the layer thickness was present between submerged and contact cultures, with contact cultures having distinctively deeper layers. Using the contact method of applying media is clearly beneficial in terms of producing a thick cell sheet that is healthy in appearance. The cells appeared to be more anchored within the substrate in Strata compared to Polaris, where the cells were purely sitting on top of the membrane. Moving forward, a seeding density of **1x10^6 cells** per 6 well Alvetex® membrane was selected due to the consistent cell layers observed.

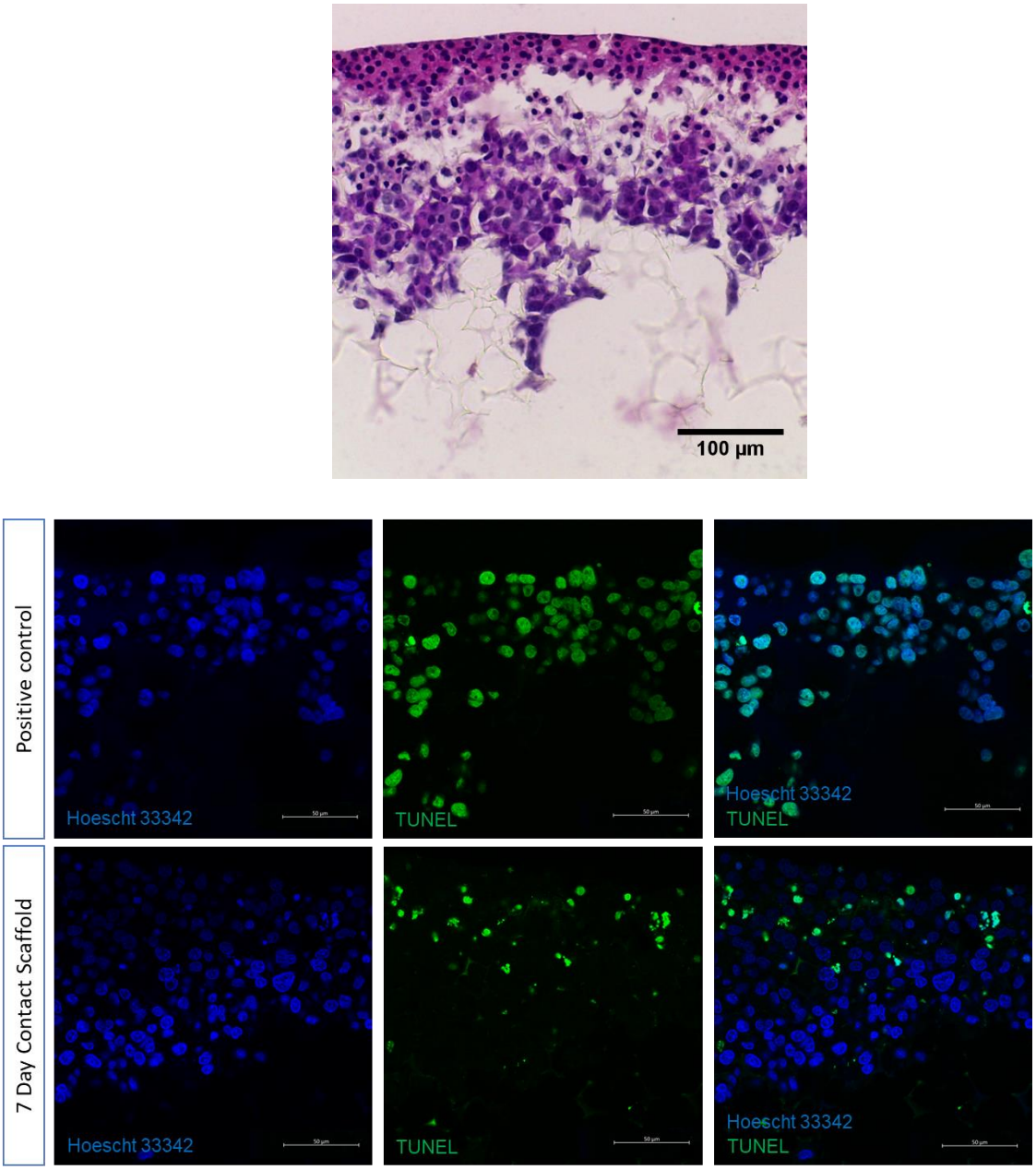

Figure 3.9: Alvetex® Scaffold exhibits cell death due to thick cell layers present.

(Top panel) Image taken of paraffin embedded H&E stained HepG2 cells seeded at 5 x 10^5 cells onto Alvetex® Scaffold using the contact media application technique and grown for 7 days. Scale = 100 µm. (Bottom panel) Image taken of HepG2 cells seeded at 5 x 10^5 cells onto Alvetex® Scaffold using the contact media application technique and grown for 7 days and stained for apoptotic cells using the TUNEL detection kit alongside DAPI to stain the nuclei. Scale = 50 µm.

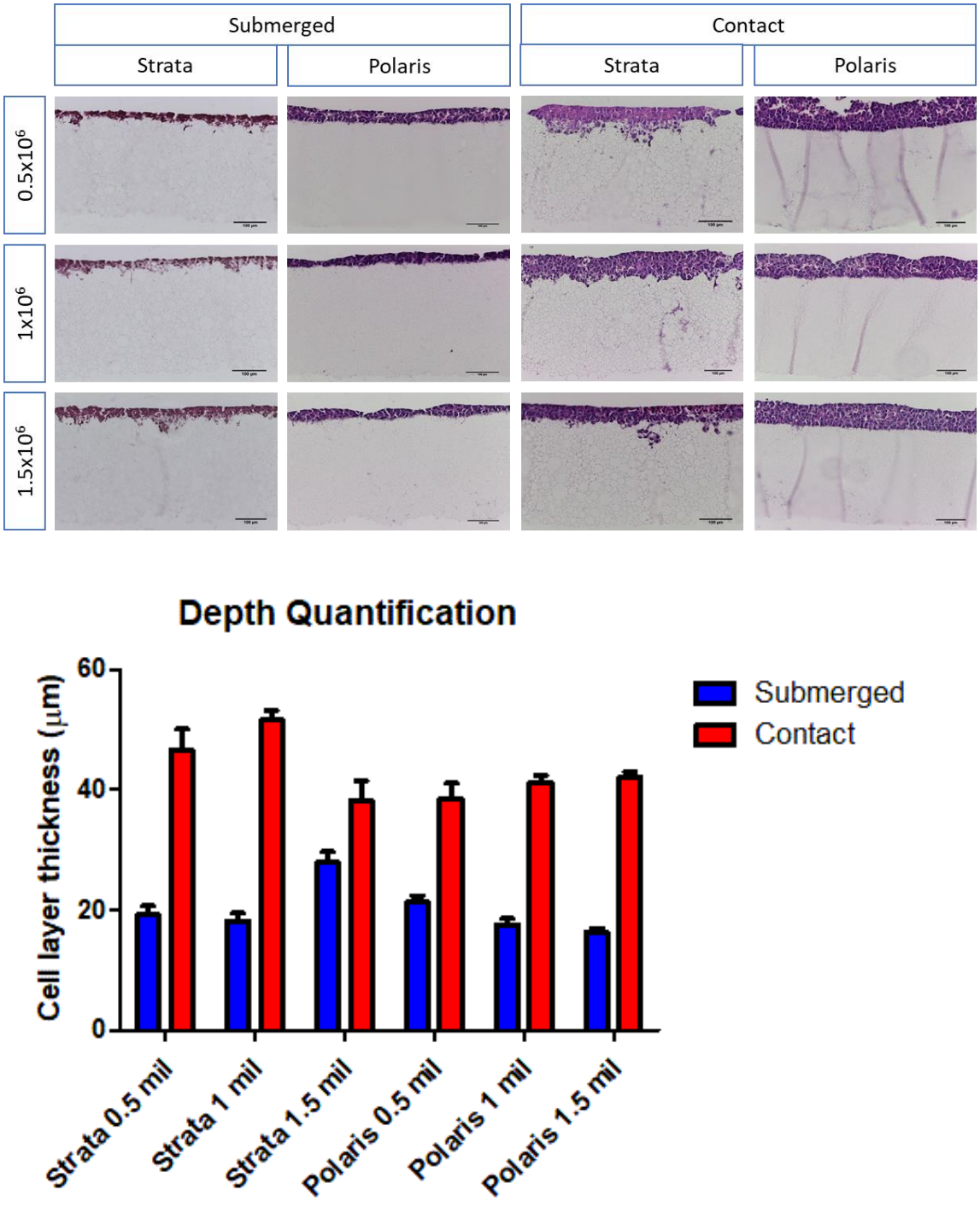

Figure 3.10: Media application but not seeding density significantly affects the thickness of the cell layers.

H&E images taken of paraffin embedded HepG2 cells seeded at three different densities of cells onto the Strata and Polaris formats of Alvetex® using contact and submerged media application after 7 days of growth, fixed in 4 % PFA. Scale bar = 100 µm. Graph showing the subsequent analysis on the cell layer thickness. N= 4, n= 3, Error bars = SEM

3.4.4 Leaving HepG2 cells in 3D culture for longer results in thicker but less viable cultures.

To examine the optimum culture time of the cells, ideally a trypan blue exclusion live/dead cell count would be used, however this relied on having an optimised liberation technique which at this point was not achieved. Therefore, to give an initial idea of how long viability could be maintained in 3D culture, an MTT assay was performed on cells grown for different lengths of time on Alvetex® Strata using the contact media application method (**Figure 3.11**). As the graph demonstrates, the metabolic activity of the cells (as measured by MTT absorbance) decreases after 9 days in culture, with the 10th day and onwards exhibiting notably lower readings. This assay is often used as a measure of cell viability, and this indicated that the health of the cells was impacted over longer culture periods.

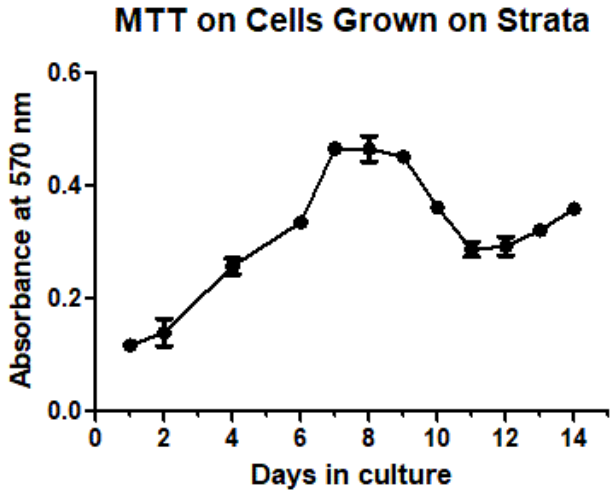

Figure 3.11: MTT assays show that cell metabolic activity notably decreases after 9 days in culture.

Graph created from absorbance readings taken after MTT assays on HepG2 cells grown in Alvetex® Strata for various lengths of time in culture using the contact method of media application and seeded at 1 x 10^6 cells per membrane. N= 3, n= 3, error bars = SEM

In **Figure 3.12,** neutral red staining demonstrates the growth of the total cell populations macroscopically after either 7 or 14 days on the Alvetex® membrane. Allowing for 14 days growth with the contact method resulted in a more homogenous layer that completely covered the membrane, but little difference is observable with the submerged method.

Interestingly, the neutral red stains on Polaris revealed that there was incomplete coverage of the membrane in all conditions. This is likely due to this substrate restricting any form of penetration from the cells, meaning that the layer could easily be disrupted with media changes. The contact method clearly resulted in more intense neutral red staining in both Alvetex® formats, indicating more cells present on the membrane. After 7 days of growth using the contact method, cells on Strata had covered the membrane significantly, but there were some areas with less growth, but still this growth was much less patchy than Polaris. The fact that the membrane was completely covered after 14 days in this condition suggests that the regions of low growth were time related and not due to cells being flushed off.

H&E stains were then performed (**Figure 3.13**) on sections cut from cells grown using the same conditions as in **Figure 3.12**. These H&E stains showed similar patterns to the neutral red stains, with thicker layers consistently present in the contact method over submerged, and with patchy growth on Polaris (particularly evident at 14 days using the contact method). With the submerged method, culture time did not seem to affect thickness, however within the contact method, 14 days of growth results in thicker layers. The quantification of cell layer thickness backed up these observed patterns.

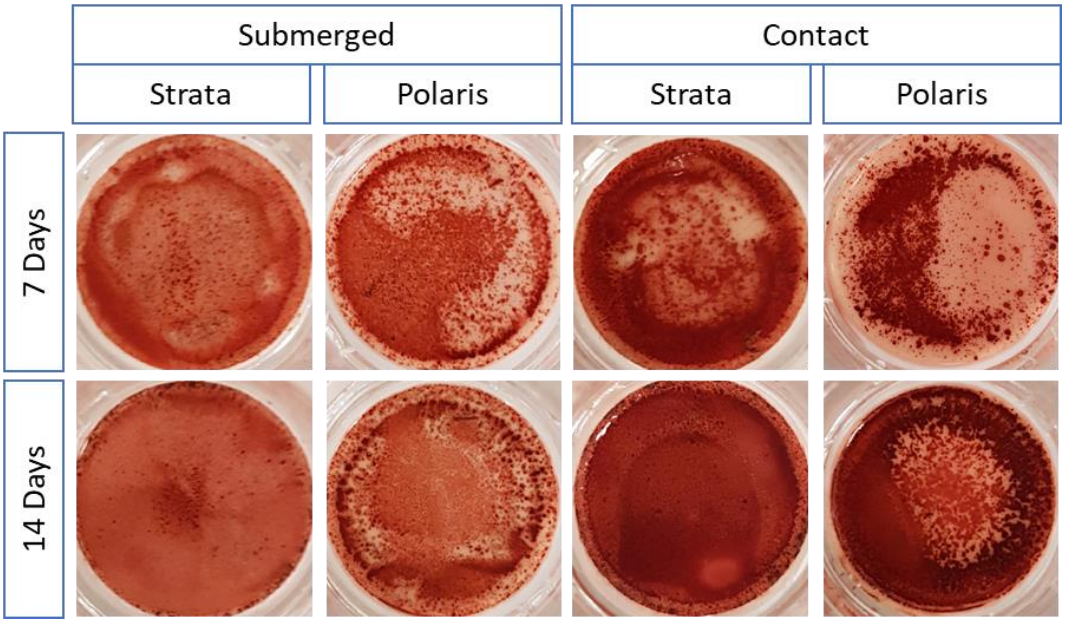

Figure 3.12: Neutral red staining reveals that HepG2 layers grown on Alvetex® Polaris exhibit patchy growth; likely due to low anchorage into the substrate.

Neutral red images taken of HepG2 cells seeded at 1 x 10^6 cells onto the Strata and Polaris format of Alvetex® using contact and submerged media application after 7 and 14 days of growth.

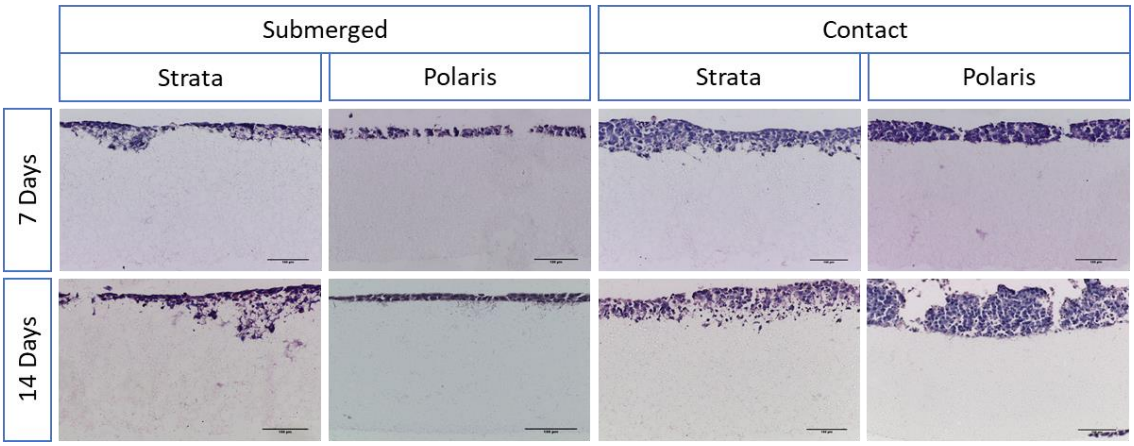

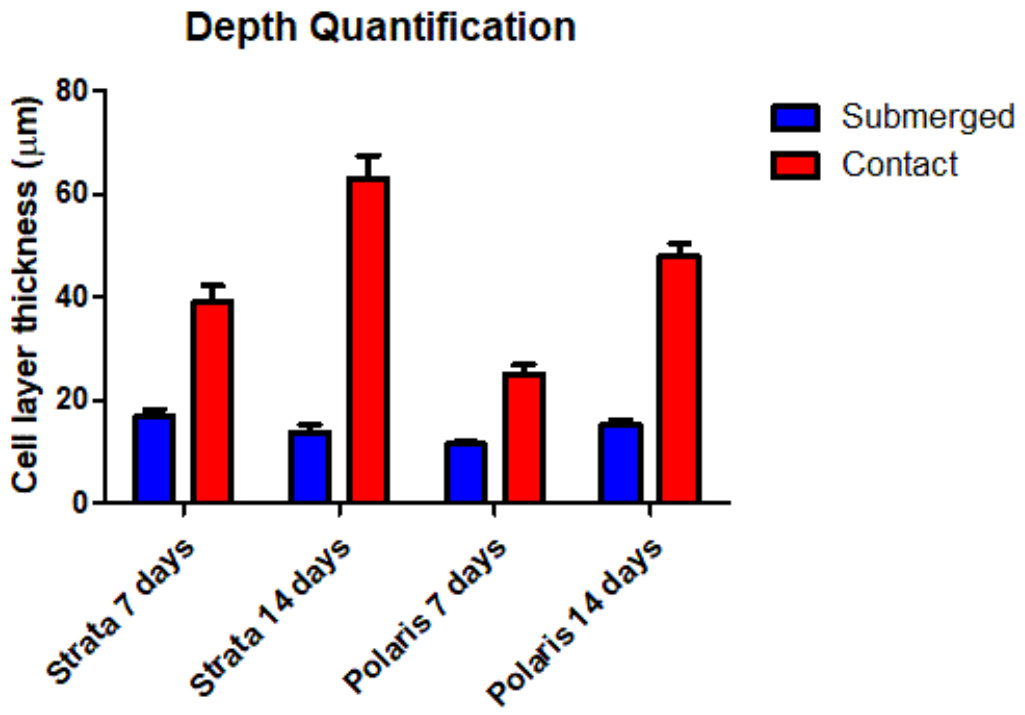

Figure 3.13: Strata is the optimum balance between a thick layer of cells and good adherence to the substrate.

H&E-stained images taken of HepG2 cells seeded at 1 x 10^6 cells onto the Strata and Polaris format of Alvetex® using contact and submerged media application after 7 and 14 days of growth. Scale bar = 100 µm. Graph showing the subsequent analysis on the cell layer thickness. N= 4, n= 3, error bars = SEM

At the 14-day timepoint there is also visual evidence of cell death occurring, with cellular and nuclear shrinkage occurring in the contact cultures, suggesting that the MTT data was indeed indicative of decreasing viability in longer culture periods. Therefore, from the MTT and visual data, it was decided that **8 days of culture time** would be the used going forward.

3.4.5 Mechanically scraping the cell layer after incubation with trypsin proved to be the most suitable method for liberating cells whilst preserving viability.

One key aspect of the priming model was the requirement for easy liberation of the cells whilst maintaining their viability in order to be able to re-seed them into a secondary 3D model. Therefore, multiple potential methods of liberation were tested to determine how best to retrieve the cells. Firstly, a preliminary test of different mechanical methods used in conjunction with a 10-minute incubation of trypsin was carried out on both Polaris and Strata (**Figure 3.14**). The methods employed were either using a soft rubber cell scraper to gently **scrape** the Alvetex® membrane submerged in tryspin, **flushing** the membrane repeatedly with trypsin, or **agitation** via placing the membrane on a shaker whilst incubating with trypsin. H&E images were taken of the Alvetex® membranes fixed either before or after liberation of the cells using the three different methods (top panel, **Figure 3.14**), as well as a trypan blue cell count performed on the liberated cells (bottom panel, **Figure 3.14**). The H&E images highlighted how in Strata, complete liberation was only achievable when the membrane was scraped, with debris and cells still visible after treatment in both the flushing and agitation conditions. In Polaris however, due the lower anchorage of cells, there was less debris in general, and flushing was also able to completely remove the cell layer as well as scraping. Cell counts of the liberated cells were markedly higher in cells removed from Strata when using the scraping technique. Scraping appears to gather the most complete representation of the cell population according to the H&E images, and the cell counts suggest that Strata is able to maintain a higher cell number on the membrane than Polaris.

Now that an initial liberation technique was identified, it was possible to test how the media application affected cell counts and viability (**Figure 3.15**). From the resultant live/dead cell counts, it was clear that using the contact media method allowed for significantly higher numbers of cells to grow, with the liberated live cell count from each membrane sitting at an average of 1.8 million with contact cultures, but only 1.2 million in submerged cultures. Contact cultures were therefore better in growing a suitably high number of cells for reseeding after priming. Viability was decreased in contact cultures, with a mean viable population of 80 % of cells compared to 89 % viability in submerged cultures; given the higher

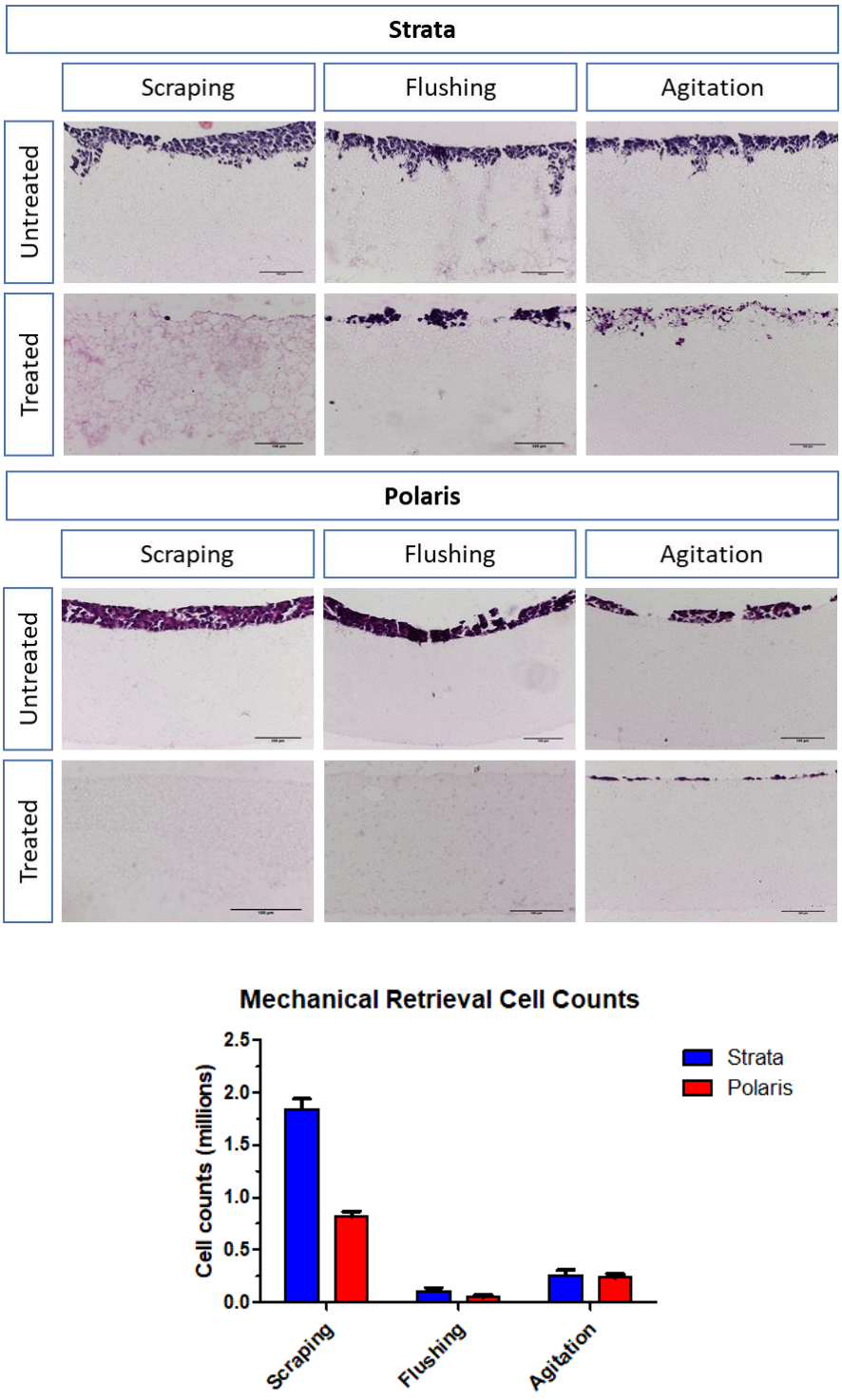

Figure 3.14: Scraping is the optimum retrieval technique to use for cell retrieval

H&E-stained images (top) taken of paraffin embedded HepG2 cells seeded at 1 x 10^6 cells onto the Strata format of Alvetex using contact media application after 7 days of growth, fixed with 4 % PFA. Images taken before and after varying methods of retrieval. Scale: 100 µm. Graph showing the subsequent live cell counts of cells retrieved using each method. N= 1 n= 3 Error bars: SEM.

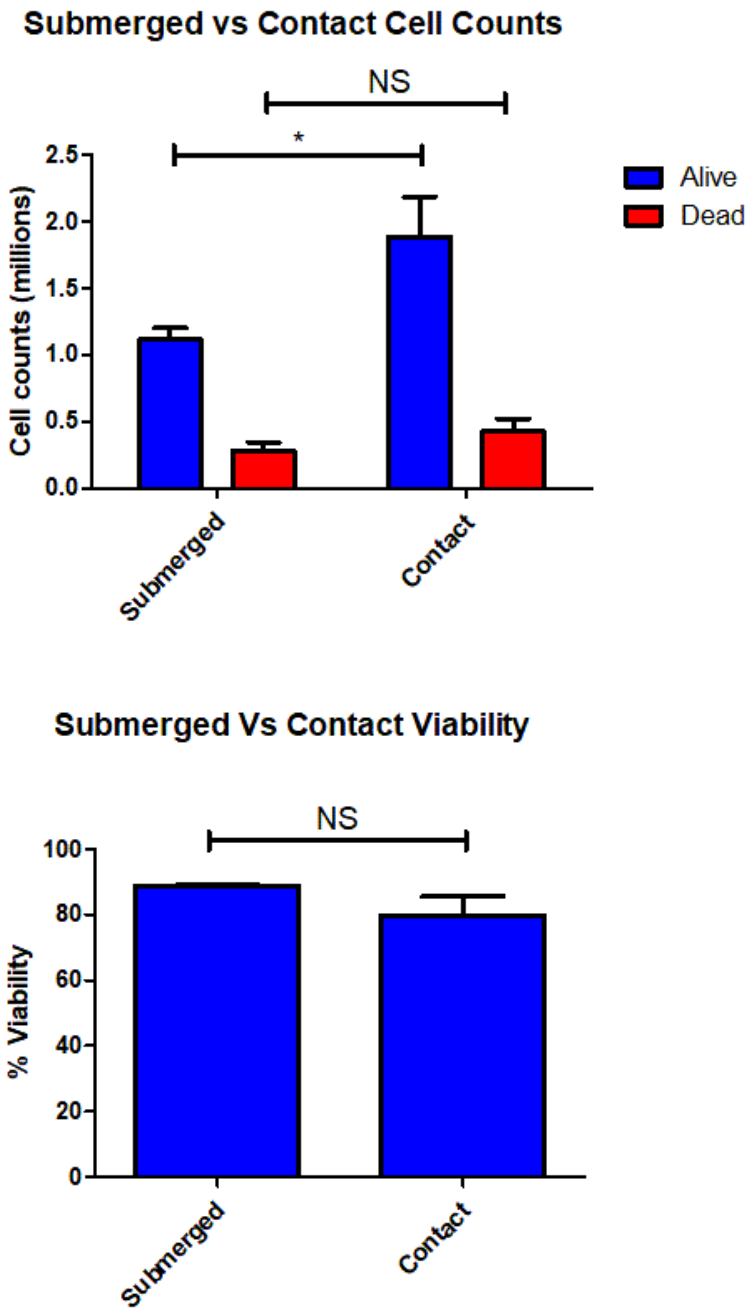

Figure 3.15: Submerged cultures yield much lower cell counts but are more viable than contact cultures.

Graphs displaying live/dead cell counts (top) and percentage viability (bottom) calculated from trypan blue exclusion of HepG2 cells grown on Alvetex® Strata for 8 days at a seeding density of 1 x 10^6 cells per membrane, using either the submerged or contact media application method. Cells were liberated for counting using the scraping method after 10 minutes of trypsinisation. N= 3 n= 3, Error bars = SEM.

cell yields in contact this is expected. Based on this and the previous data, only contact cultures were used going forward.

Trypsin, versene, and a PBS control were compared to see if the liberation agent used would make a difference (**Figure 3.16**). The results from this revealed that trypsin results in the best removal of cells from the membrane due to the much higher viability of liberated cells (78 %) compared to viabilities of under 40 % when using versene or trypsin as liberation agents. In the H&E images, cell debris was observed in all three conditions after liberation, unlike the first experiment, however the cell counts of liberated cells were even higher. The MTT assay showed that after liberation, there was very little metabolic activity present, suggesting that the majority of the cells were removed from the membrane in all conditions.

Each of these liberation agents were considered in greater detail by seeing if the incubation time with trypsin would affect the viability and effectiveness in removing the cells from the substrate. Trypsin appeared effective at removing the cells at all timepoints (**Figure 3.17**), although the overall cell counts of liberated cells did increase slightly in the longer incubations. Viability was not affected though, and the MTT data also indicated complete removal of cells from the membrane. Unlike trypsin, versene (**Figure 3.18**) and PBS (**Figure 3.19**) are not able to produce viable populations of liberated cells at any time points. This is likely due to these agents being much weaker at dissociating cells, resulting in a higher mechanical stress damaging the cells when using a cell scraper. The viability of the liberated cells did not exceed 50 % with versene, and was less than 40 % with PBS, compared to 70 – 80 % viability in trypsin.

The MTT values did however indicate complete removal of cells from Alvetex® Strata in all cases (apart from an outlier after 20 minutes in versene in **Figure 3.18**). This indicates that using a cell scraper is indeed a very effective technique at retrieving complete populations of cells from our chosen substrate. Therefore, the fully optimised liberation technique was to incubate the cells in trypsin for 10 minutes before gently scraping them and counting.

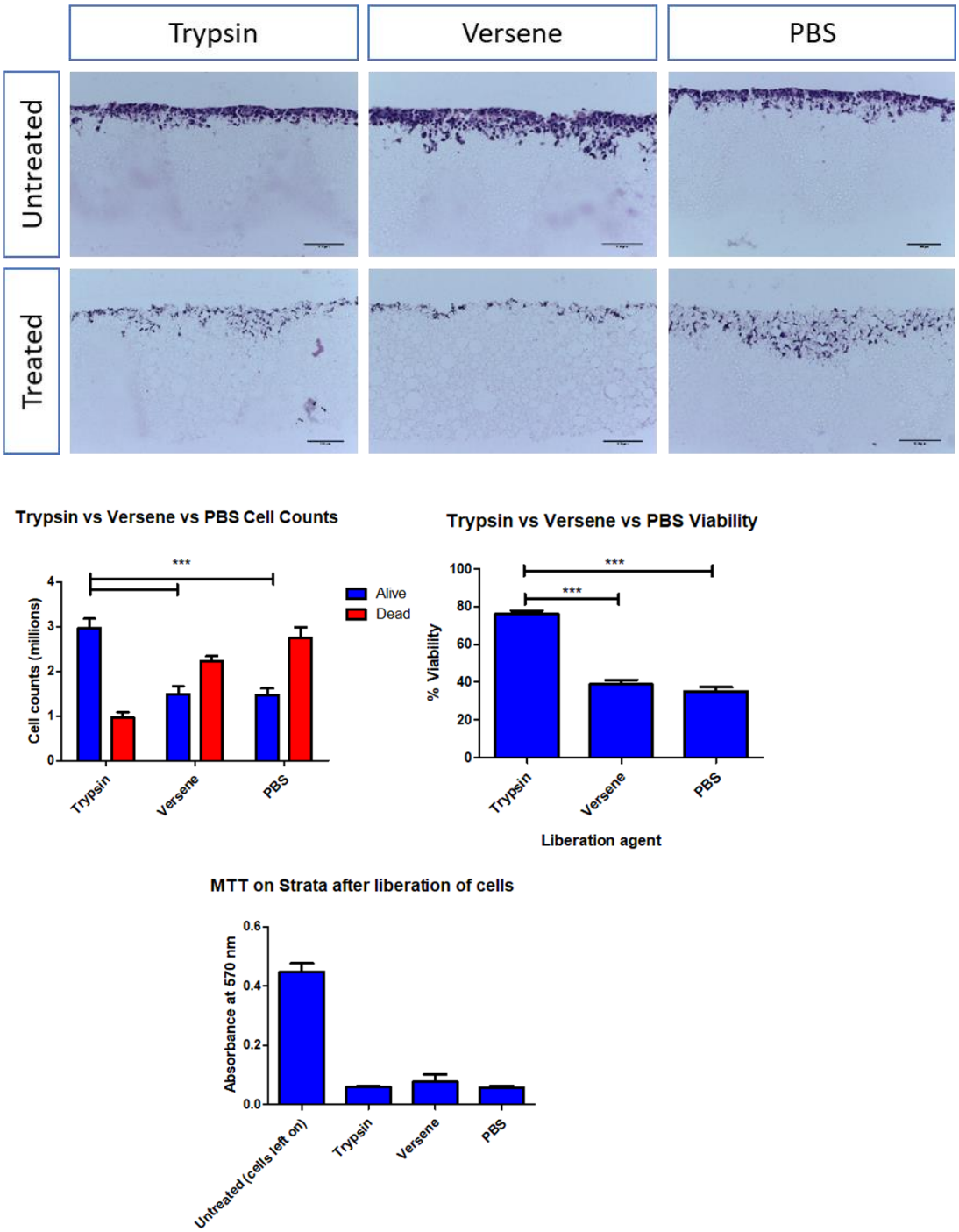

Figure 3.16: Trypsin is the most effective liberation agent for retrieving a viable population of HepG2 cells.

H&E stain of 8 day grown HepG2 cells seeded at 1 x 10^6 cells onto Strata before and after liberation using a cell scraper following 10-minute incubation with different agents (trypsin, versene or PBS). Scale: 100 µm. Bar charts showing quantification of live/dead cell counts and the mean percentage viability for each agent. MTT assays were performed on membranes before and after liberation. N= 3, n= 3, Error bars = SEM.

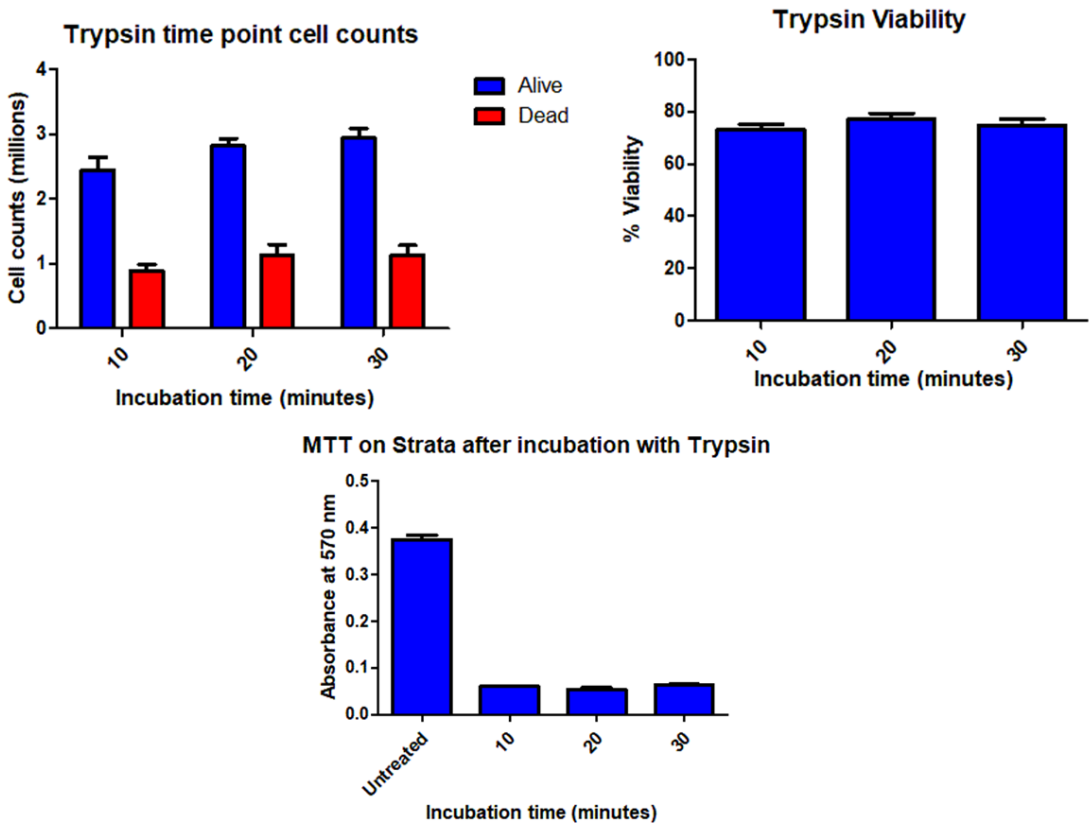

Figure 3.17: Trypsin is effective at removing cells from Alvetex® regardless of how long it is applied for.

Bar charts showing quantification of live/dead cell counts and the mean percentage viability for each agent after liberation using a cell scraper after incubation with trypsin for different time points. MTT assays were performed on membranes before and after liberation. Cells seeded at 1x10^6 per insert and grown for 8 days. Counted on a haemocytometer – images shown above. N= 3, n= 3, Error bars = SEM.

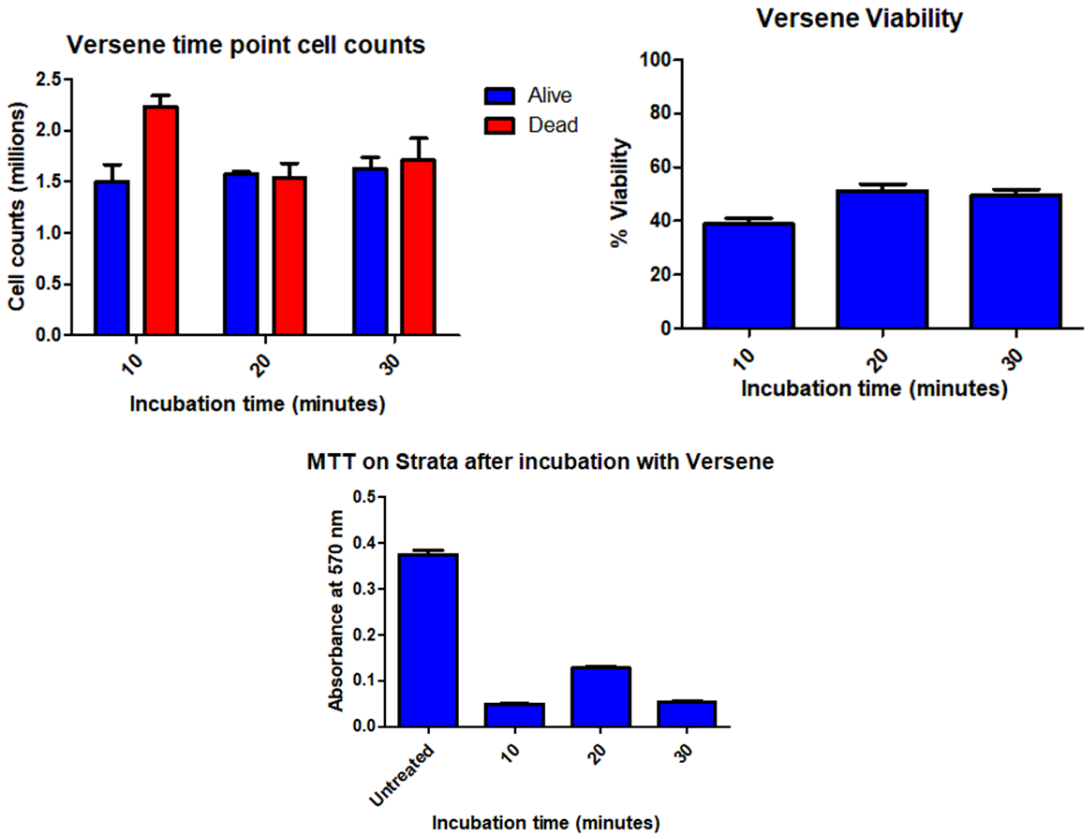

Figure 3.18: Liberation using versene does not produce viable populations.

Bar charts showing quantification of live/dead cell counts and the mean percentage viability for each agent after liberation using a cell scraper after incubation with versene for different time points. MTT assays were performed on membranes before and after liberation. Cells seeded at 1x10^6 per insert and grown for 8 days. Counted on a haemocytometer – images shown above. N= 3, n= 3, Error bars = SEM.

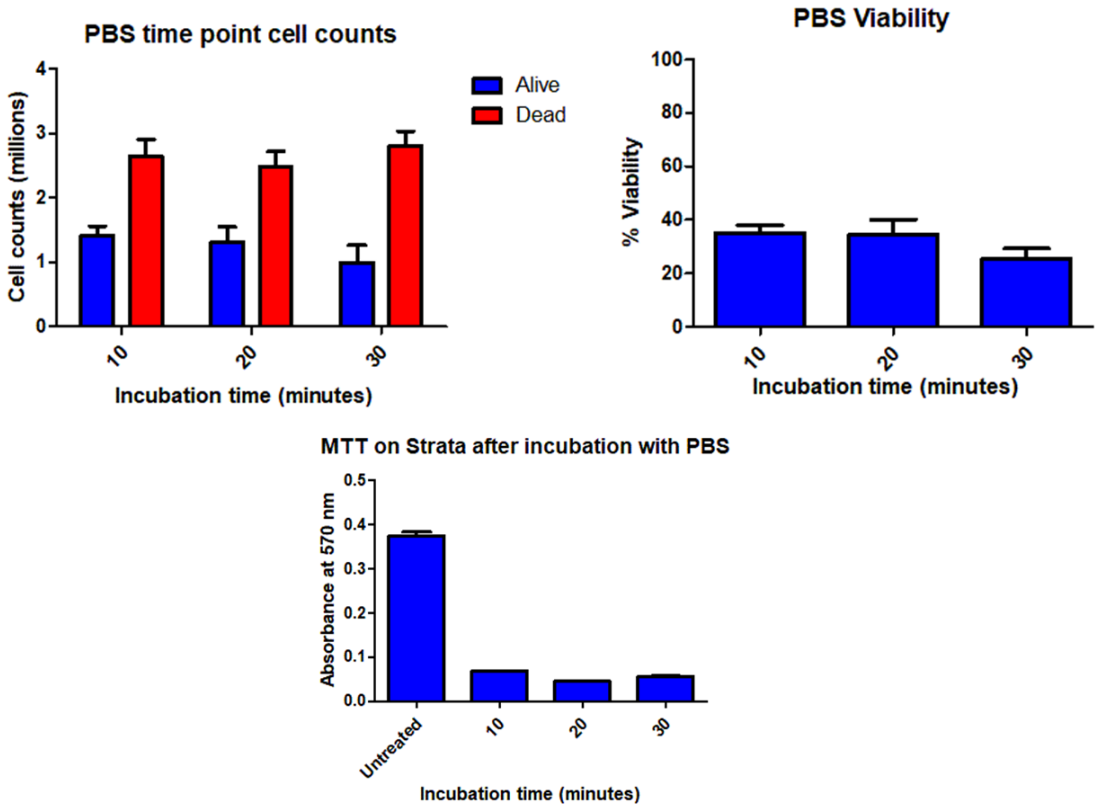

Figure 3.19: Liberation using PBS appears to kill the majority of cells.

Bar charts showing quantification of live/dead cell counts and the mean percentage viability for each agent after liberation using a cell scraper after incubation with PBS for different time points. MTT assays were performed on membranes before and after liberation. Cells seeded at 1x10^6 per insert and grown for 8 days. Counted on a haemocytometer – images shown above. N= 3, n= 3, Error bars = SEM.

These data were able to establish a robust method for liberating cells meaning that trypan blue exclusion live/dead cell counts could be used to further clarify the results seen in **Figure 3.11** regarding optimum growth time of cells. Growth curves were thus created from cells grown using both the contact and submerged media application techniques (**Figure 3.20**). The growth curve from the cells grown using the contact method shows a similar pattern to the MTT growth curve, though it appears that the viability starts dipping here at 10 days in culture rather than after 9 days as indicated by the MTT. Interestingly despite the decrease in viability, there is a spike in total cell numbers occurring at 10 days in submerged and 11 days in contact cultures, though the number of dead cells also increases, resulting in the overall decreasing viability. Cell counts are much higher in contact cultures compared to submerged cultures at all time points, reaching over double the number of cells at the later stages. After 8 days in contact culture there is a healthy cell number present, and viability was high therefore this was kept as the chosen culture time for the priming model.

Finally, the growth of HepG2 cells in the fully optimised 3D priming model was compared to the growth of HepG2 cells in 2D flasks at different time points (**Figure 3.21**). Comparing the H&E images of growth in 3D at 1 and 4 days, there is not much evidence of proliferation with the cell layer looking largely similar in terms of thickness and coverage. However, after 8 days, there is clearly a consistent and thick layer of HepG2 cells growing across the membrane and at this timepoint, the cells have become completely confluent in 2D culture as well. This shows that at 8 days, both 2D culture and 3D culture is comparable due to the cells having formed a confluent layer in both conditions (albeit a monolayer in 2D).

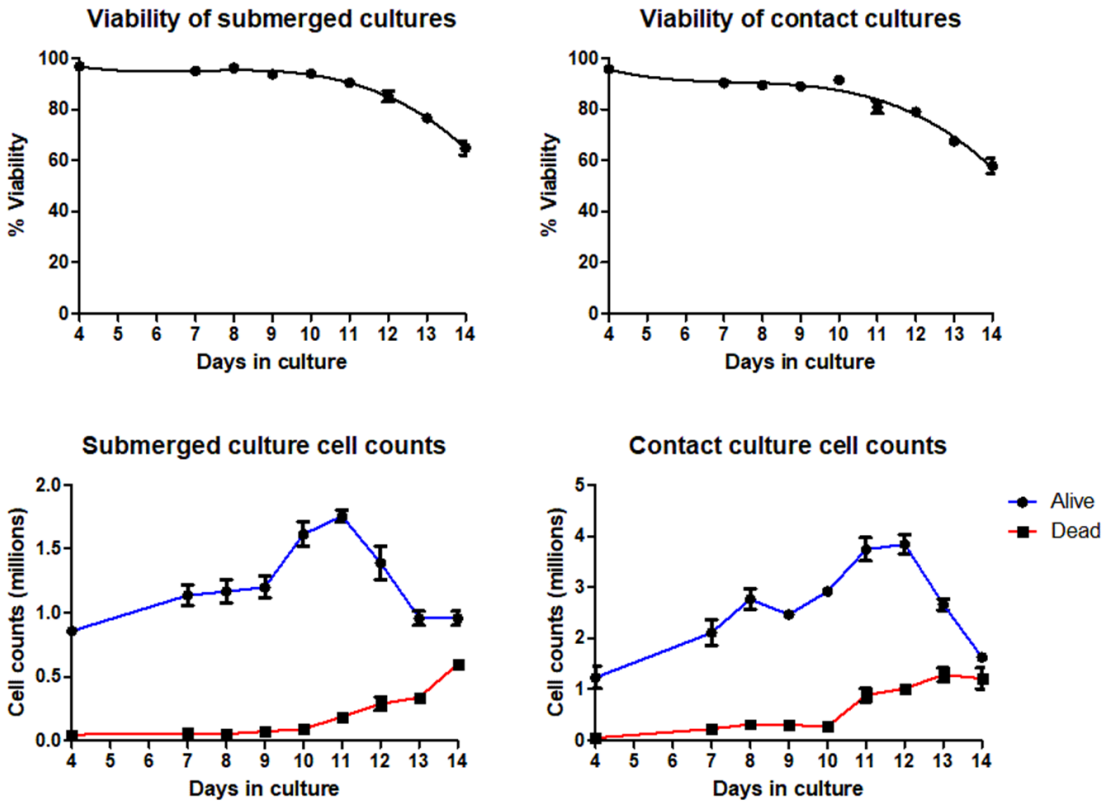

Figure 3.20: Contact cultures have slightly decreased viability than submerged cultures, but contact results in much higher cell counts.

Graphs showing the percentage viability (top) and growth curves (bottom) of both contact and submerged cultures of HepG2 cells seeded at 1x10^6 cells onto the Strata format of Alvetex using contact and submerged media application, counted using the scraping method. N= 3 n= 3 Error bars = SEM.

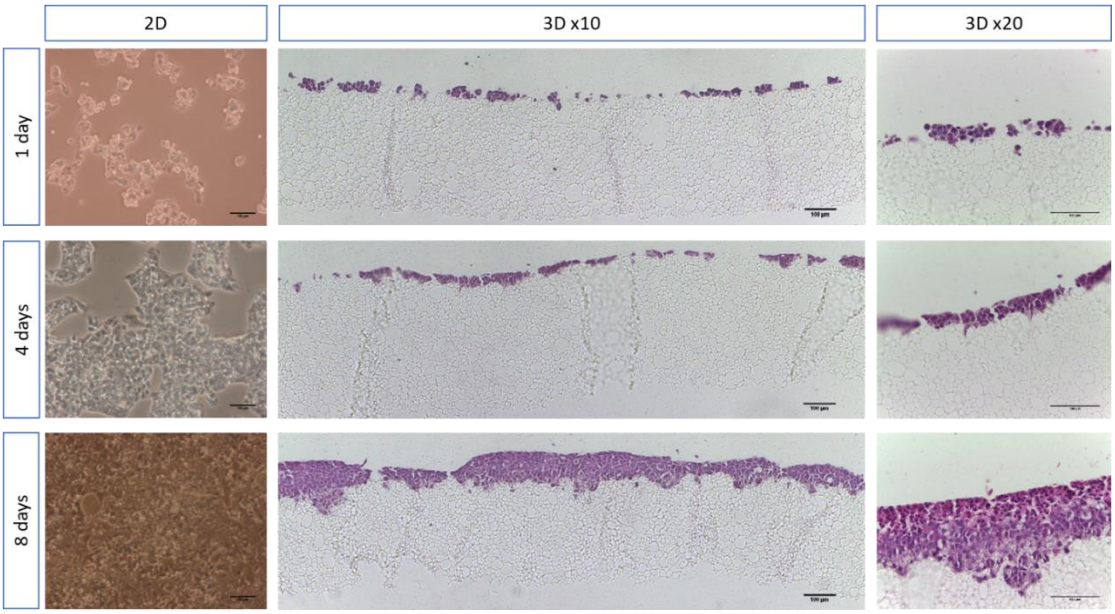

Figure 3.21: Contact cultures have slightly decreased viability than submerged cultures, but contact results in much higher cell counts.

Phase contrast and H&E images of cells grown in a 2D 6 well plate, or in 3D on Alvetex Strata®, seeded at 1x10^6 cells per insert / well, for 1, 4 or 8 days. Scale bar = 100 µm

3.5 Discussion

3.5.1 Optimising a robust and reproducible priming model.

Many variables affecting growth of HepG2 cells were tested in this chapter. The most obvious variable to initially investigate was the format of Alvetex®. With three different options available, and each with different void sizes, the three formats were used in many of the optimisation experiments to fully understand how other variables might impact growth within these different substrates. It became clear through many of the H&E images (e.g. **Figure 3.8**) that while Alvetex® Scaffold was able to facilitate large cell populations, the cells were too embedded within the substrate to make liberation easy. This high level of penetration also meant that many of the cells were not in close contact with each other, and as some preliminary E-cadherin immunofluorescence revealed (**Figure 3.5**), the formation of cell-to-cell contacts was limited to only certain areas of cell growth in Scaffold.

The early test for E-cadherin was also important as it signified the type of analysis that will be carried out later in this project. E-cadherin has important roles in mechanotransduction, including defining the heterogeneity of epithelial cell lines (B. Wang et al., 2016), and modulating cell stiffness through regulating the actomyosin cytoskeleton (Smutny and Yap, 2010). E-cadherin is important in hepatocytes, particularly in the formation of 3D structures such as spheroids (Luebke-Wheeler et al., 2009). Due to the secondary 3D culture step possibly utilising spheroid or aggregate cultures, there is extra significance in looking for E-cadherin expression as expression of it may indicate suitability of this as a priming model for reseeding.

The other two formats of Alvetex®, Strata and Polaris, showed more promise in fulfilling the aims of this chapter, with both membranes able to support a multi-layered cell sheet, which while on top of the substrate, was still maintained on a 3D topography. These cells presented more consistent E-cadherin staining and were more accessible for liberation. Throughout the various experiments, it became apparent that Polaris had a reproducible issue with cells washing off the membrane due to a lower anchorage within the substrate – particularly evident through the neutral red stains **Figure 3.12**. Therefore, ultimately Strata was chosen for its ability to allow consistently thick cell layers to grow on top of it, allowing for easy liberation while providing enough anchorage to the cells to stop excessive cell loss through media changes.

Alongside testing the different Alvetex® formats, many other variables were investigated simultaneously. The cells were able to proliferate much more when the Alvetex was used as an insert over simply placing the membrane at the bottom of a well where the nutrient availability was restricted to only being above the membrane. Another significant variable was how media was applied, with completely submerged Alvetex® inserts resulting in significantly thinner cell layers forming compared to inserts where just a small film of media was applied on top of the membrane (the 'contact' method). This trend has been noticed in previous work in this lab, and is most likely due to increased surface tension, less turbulence between media changes, and a potentially stronger oxygen gradient for the cells which is an important physiological aspect of the liver.

Culture time was a key consideration due to the concept behind this being that we want to provide cells with *time* to adapt structurally and functionally to a 3D microenvironment before reseeding them in a subsequent secondary model to reap the benefits of their enhanced characteristics. Through H&E histology, MTT growth curves and live/dead count growth curves, it was evident that at the 14-day time point, cells were dying. According to the growth curves (**Figure 3.11**, **Figure 3.20**), cell viability was dropping at around 9-10 days in culture, and therefore 8 days was chosen as the optimum culture time due to it striking a balance between duration and viability. The three cell seeding densities tested did not appear to affect the growth significantly, and therefore $1x10^6$ cells per membrane was chosen for ease.

3.5.2 Challenges of cell retrieval.

The other main facet of optimisation was focussed on how to retrieve the cells from the membrane after 8 days of growth. This was an important area to focus on as it is known that mechanical forces for dissociation or disaggregation can be damaging to the cells (Failli et al., 2009). A paper looking at mechanical and enzymatic detachment showed that both these methods were detrimental to cell morphology and the ECM in comparison to a smart polymer used for cell sheet detachment (Canavan et al., 2005).

Inevitably, retrieval of the cells would include some form of disruption to the cell layer, but it was hypothesised that structural and functional changes from priming would be retained due to altered gene expression. Evidence has pointed to this being the case before, with mechanically triggered activation of YAP/TAZ providing a mechanism through which cells can store information from prior physical environments (C. Yang et al., 2014). Compellingly it has

recently been proposed that substrate stiffness results in altered transcriptional responses that then give rise to mechanical memory within the cells (Mathur et al., 2020). Therefore it is reasonable to believe that whilst certain aspects may be disrupted within the cells during liberation (active cell-cell contacts for example) that there will still be a structural and functional advantage to cells that have a history in a 3D environment over cells taken from 2D, due to cells having been pre-conditioned to adopt a three-dimensional structure.

The difference between trypsin-EDTA and EDTA (versene) was investigated due to the importance of wanting to preserve morphology and viability. Trypsin is a serine protease (Rawlings and Barrett, 1994) that is used in cell culture to detach adherent cells from the substrate surfaces by cleaving the adherent proteins. Trypsin has been shown to remove glycoproteins and glycosaminoglycans from the cell surface (Vogel, 1978), and has a more potent effect on detachment compared to just EDTA on its own. EDTA is a Ca^{2+} chelating agent that binds divalent cations and prevent the joining of calcium mediated adhesions (Freshney, 2010). Papers have previously and successfully used EDTA alone for enzyme free cell detachment (Beers et al., 2012; Heng et al., 2009), as it stops the potential batch to batch variability of enzymes, as well as avoiding the proteolytic effect of trypsin and preserving the membrane surface proteins. Therefore, the use of EDTA (versene) alone was compared to trypsin EDTA, along with a PBS control showing just the mechanical effect of scraping the cells.

The data on cell liberation presented a strong case for combining mechanical and chemical dissociation techniques, through using a cell scraper alongside trypsin. A cell scraper clearly removed significantly more cells than flushing or agitating the Alvetex® could yield (**Figure 3.14**). Whilst utilising this method did completely disrupt the cell layer (**Figure 3.16**), the populations retrieved using trypsin and scraping were much more viable (74 %) than using the gentler versene (37 %), or PBS (34 %). This was likely due to less mechanical stress occurring when cell dissociation was aided through the enzymatic action of trypsin. Interestingly, the typical viability range of human hepatocytes is between 70 – 90 % (Bayliss and Somers, 2005), and only through using trypsin and scraping did the HepG2 cells fall within this range. The length of time that cells were incubated with the liberation agent did not impact the viability, therefore 10 minutes was chosen as the optimum time to incubate with trypsin, to avoid overly stressing the cells. It is important to note that in future chapters, when comparing cells with either a 2D or 3D primed history; the cells will have been liberated using the same techniques from both 2D and 3D by disruption through trypsin and scraping,

therefore they will be directly comparable when assessing how they form secondary cultures.

Subsequent chapters will focus on characterisation of these cells in 2D, in the 3D priming model, and after liberation and subsequent reseeding from either origin. With this in mind, an initial comparison between 2D and 3D cells was drawn in this chapter in **Figure 3.21** which shows that when cells are seeded at the same density, cells in 2D proliferate more than cells in 3D, reaching a fully confluent monolayer at 8 days. Cells in 3D proliferate at a slower rate but can form a thick layer at the 8-day time point. Repeatedly, cell counts were higher when liberated from 2D than 3D, and the difference between the two conditions will be explored further in subsequent chapters. The current data corroborates with the known effect of stiffer substrates (2D in this case) favouring cell cycle (Martino et al., 2018b), due to mechanically triggered pathways such as Hippo altering proliferation.

3.6 Conclusions

This chapter has presented data obtained during the optimisation process of a 3D priming model, and this information was used to direct and inform the final conditions used. The initial aim was to create a model through which HepG2 cells could be grown and maintained in a 3D microenvironment, where their growth will reflect in part the tight packing and organisation of hepatocytes in the human liver, and where the total population of cells could be easily liberated to be reseeded into a secondary 3D model. Upon assessment of these data, that aim was clearly achieved. Through methodically selecting different variables and testing growth whilst these were altered, a refined and fully optimised model was developed where $1x10^6$ HepG2 cells could be seeded onto a 6 well Alvetex® Strata insert, grown for 8 days using a specific media volume, and the resultant thick layer could easily be retrieved as a viable population with a 10-minute incubation in trypsin followed by scraping with a soft cell scraper.

This shows that it is possible to support easily accessible growth of cells on a non-planar physical substrate, preserving three-dimensional architecture that resembles the structure of *in vivo* liver tissue. Supporting growth of cells in 3D and ensuring that these cells were accessible was a key aim of this project, as this formed the primary culture step where cells are primed or preconditioned to adopt an enhanced structural and functional phenotype as a result of the 3D microenvironment. Now that this has been achieved, and that liberating the cells was possible whilst preserving viability, these altered characteristics can be thoroughly investigated in the subsequent chapters.

Chapter 4 – 3D priming gives rise to altered structural properties within HepG2 cells

4.1 Introduction

The literature review in Chapter 1 highlighted how structure is a significant factor in determining the functional properties of cells. Stem cell fate for example is determined in part by the physical interactions of cells with the ECM, through alterations in cell geometry and transmitting of mechanical factors (Guilak et al., 2009). The concept of structure determining cell function through mechanotransduction started becoming clearer in the 1980s with Mina Bissell's studies on the effect of the ECM on cell biology (Mina J. Bissell and Barcellos-Hoff, 1987). Now it is widely accepted that in addition to chemical signalling, mechanical forces play a critical role in cell function (Burridge et al., 2019).

It is well documented that 3D culture can be utilised to create more physiologically relevant *in vitro* models, and in biologically inert substrates, this is largely due to the structural changes to the cells exerted through altered substrate topography. Many reviews have been written with the aim of summarising advantages or differences of 3D cultures over the traditional 2D counterparts, and whilst there is a constant stream of novel models being produced, the underlying concept of 3D culture producing more physiologically accurate models is not necessarily new. As a 2007 Nature review points out, utilising the third dimension in research helps to bridge the gap between cell culture and live tissue (Pampaloni et al., 2007), highlighting how aspects such as adhesion, migration and polarisation are more physiologically aligned when cells are cultured in 3D. In many 3D *in* vitro models, cells exhibit more histotypic morphologies (depending on the dimensionality of the tissue in question), which often correlates with altered and usually enhanced or more *in vivo* like biological behaviour, particularly when mimicking tissues with highly specialised cell types such as the intestine (Altay et al., 2020).

Morphology of cells is important due to both the effects of mechanotransduction from altered cytoskeletal dynamics, and the importance of being able to form cell-cell and cell-substrate interactions which are vital factors influencing cell biology. The physical effects of adding a third dimension to *in vitro* cell culture alters signal transduction within and between cells, which influences gene expression and cellular behaviour (Edmondson et al., 2014b), and this will be explored in later chapters in this thesis that analyse how structural changes lead to functional differences. The formation of junctional complexes is both dependant on the morphology of the cells, and the architecture of the total cell populations within the model. Therefore, to fully characterise the structural properties of a novel *in vitro* model, this chapter will assess three areas of interest:

1. Microscopic morphology and cytoskeletal structure of cells within the model.
2. Structure and growth of the total cell population.
3. Presence of structural biomarkers of interest.

4.1.1 Microscopic morphology and cytoskeletal structure indicates underlying mechanical changes.

An important area that is often overlooked in characterisation of 3D models is investigating the micro-structure of cells grown in the model when compared to 2D monolayers of the same cell type. While studies have indicated that the unnatural structure of cells grown in 2D affects the cellular processes and gene expression (Edmondson et al., 2014b; Tibbitt and Anseth, 2009b), the characterisation and comparison of individual cell morphology between 2D and 3D is often skipped in favour of more global characterisation during model development. Part of this is due to the practical difficulties of imaging single cells within 3D multicellular models (Tasnadi et al., 2020), and while certain software can help aid this process, it is a limiting factor in increasing our understanding of the mechanistic changes that cells undergo when cultured in 3D. As outlined in **Chapter 1**, the pathways through which mechanical changes can affect the cell are numerous and complex and much work is still needed to fully uncover the exact links between structure and function (Wang, 2017).

It is therefore arguably important when analysing 3D models to investigate cells on a more individual level due to the profound effect morphology has on the biology of the cell. The historical understanding of how morphology is affected by different substrates – for example the observation that cells grown on softer matrices exhibit differential cytoskeletal structures as single cells (Tony et al., 2005) – may often prove sufficient for researchers to circumvent the need for deep investigation into single cell morphology when producing 3D models. Studies often focus on investigating the holistic effects of altering substrate topography (Kim et al., 2017; Zhu et al., 2019) on function in isolation. However, with increasingly advanced imaging options available, highly detailed pictures of cells residing in 3D cultures are becoming more common (Lucumi Moreno et al., 2015) which can help unpick the more detailed changes occurring. It is still rare to examine the specific mechanisms underlying cellular changes in tandem with testing the functional capabilities of 3D models. This project aims to fulfil both of these aspects by examining the morphological effects of priming cells to further increase our understanding of mechanotransduction as

well as globally assessing the suitability of using a priming model to enhance the overall structure and function of hepatic cultures.

A particular focus of this chapter will revolve around whether 3D primed cells retain structural changes after liberation and reseeding as single cells when compared to single cells from 2D. There is limited evidence suggesting that cells retain a mechanical memory of their prior environment, with epithelial cells for example exhibiting faster migration, higher actomyosin expression and larger focal adhesions when primed on stiffer substrates (Nasrollahi et al., 2017). This concept of priming has been utilised to improve functional properties as well; preconditioning human mesenchymal stem cells (MSCs) on three dimensional ECM based microgel platforms of different stiffnesses enables tuning of the pro-angiogenic qualities before *in vivo* implantation into rats (Thomas et al., 2020). Both studies also revealed increased YAP/TAZ nuclear localisation after priming in stiffer matrices, which is particularly significant due to YAP/TAZ having significant roles in mechanotransduction, affecting migration and proliferation (Dupont et al., 2011). This project takes a similar approach through priming/preconditioning cells in a 3D matrix before moving into a model for functional testing, and therefore a key aspect of analysis is focussed on the altered structure of primed cells, whether individually or as a population.

4.1.2 Structure and growth of the global cell population enables comparison with *in vivo* tissues, and assessment of overall model quality.

In characterisation of 3D models, assessing the overall histology of the model is essential, as this gives an overview of the macroscopic arrangement of cells within the model, and can immediately be used to draw comparisons to *in vivo* tissues. This is often performed through histological stains and through SEM before more detailed analysis is carried out through probing for specific markers or using TEM to investigate ultrastructural elements.

Simple stains such as Haematoxylin and Eosin are commonly used in liver research to inspect the overall morphology of models and the health of cells (Eilenberger et al., 2019; Moscato et al., 2015; Ren et al., 2011). Histological stains can even reveal functional properties, such as with the Periodic Acid Schiff (PAS) stain, which is commonly used in liver research to investigate the glycogen storage capacity of hepatic cells (Ramaiahgari et al., 2014a), with glycogen storage being a key function of hepatocytes. It is commonly seen that 3D models show more *in vivo* like morphology (Ramaiahgari et al., 2014a) and therefore it is expected that this will be the case within the priming and final models in this project. Overall structure

is an important determinant of the ability for cells within models to form key junctions (Edmondson et al., 2014b) and indeed, tissue architecture is a key determinant of responses of *in vitro* models to toxicity (Lelièvre et al., 2017). In this project, histological stains and global morphometric analysis will also help reveal whether priming has any prolonged effect on reseeded cells that are cultured over a significant length of time, particularly on their ability to form subsequent three-dimensional structures.

After priming cells in this project, they could be seeded into a final model, or as single cells onto coverslips for the aforementioned single cell analysis. 2D cells would undergo the same process, but without the need for scraping to release the cells from the first stage. **Figure 4.1** illustrates this process for 3D cells, and it was decided that the final model was going to use aggregates as the 3D method of choice. This is primarily because of the popularity of using aggregate models in liver research, the ability to create homogenous spheroids for high throughput testing, and the inexpensive nature of aggregate technologies when using non specialised equipment (Breslin and O'Driscoll, 2013b). Depending on the method used however, the size can be highly variable, and this can lead to problems with hypoxic cores in larger aggregates due to restricted nutrient availability (Edmondson et al., 2014b). This is something that histological stains such as H&E can pick up with initial screening (Elmore et al., 2016) through detecting cell death, but that can be further probed for using stains such as propidium iodide that cannot enter viable cells with intact plasma membranes (Crowley et al., 2016). Different methods of aggregate formation were explored to ensure that the final model would consist of consistently sized, comparable aggregates that were also similar in properties between both 2D primed and 3D primed cells when seeded into the models.

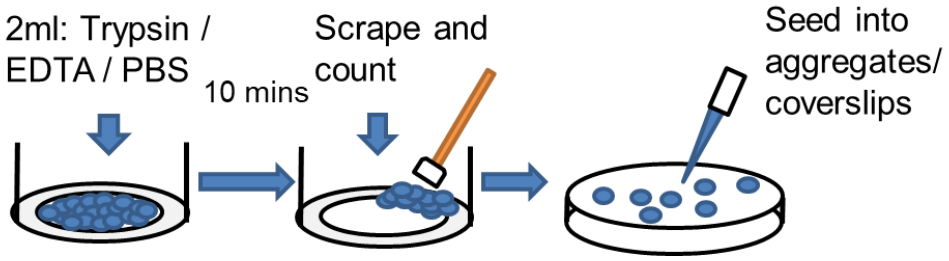

Figure 4.1: Process for liberation and reseeding of primed cells.

4.1.3 Presence of key structural markers can be indicative of model quality.

An important facet of structural characterisation is gaining insight into the presence and localisation of specific structural markers. This can help reveal the maturity of the model through probing for markers whose expression is linked to specific tissue types for example. In the liver, the presence of polarity markers and cell to cell contact proteins are often investigated due to the function of hepatocytes being highly dependent on polarity (Jia et al., 2020). Bile canaliculi are an essential structural feature of the liver, with the organisation of a functional three-dimensional intrahepatic biliary system network being crucial for proper liver function (Si-Tayeb et al., 2010). Tight junctions are essential for bile canaliculi formation, and mutations in these proteins leads to disorders in liver structure, aberrant bile canaliculi network formation and disaggregation of epithelial cells (Cheung et al., 2012). Drug transporters such as multi-drug resistance protein 2 (MRP2) are also critical for detoxification and chemoprotection by transporting products of phase II detoxification of xenobiotic compounds (Jedlitschky et al., 2006). Such structural markers are often seen to have higher expression or better organisation in 3D cultures over 2D counterparts (Jia et al., 2020; Ramaiahgari et al., 2014a).

Regarding tight junctions, claudins are a particular protein group of interest as they are found in tight junctions of all epithelia and endothelia and play a role in modulating the permeability of tight junctions (Günzel and Yu, 2013). Certain claudins such as claudin-1, claudin-2 and claudin-3 are expressed in hepatocytes (with claudin-2 exhibiting an increasing gradient of expression from periportal to perivenous hepatocytes) (Günzel and Yu, 2013; Rahner et al., 2001). RNA expression of Claudin 1 is also particularly elevated in the liver compared to other tissues ("Tissue expression of CLDN1 - Summary - The Human Protein Atlas,"). Elevated claudin-1 and claudin-7 protein expression is significantly elevated in cirrhotic livers (Holczbauer et al., 2014), but the baseline expression is still very high in normal liver.

The establishment of a biliary lumen is also dependent on integrins and cadherins (particularly E-cadherin) which act as transducers of mechanical signals from the ECM to RhoA GEFs and GAPs to induce changes in the cytoskeleton to facilitate bile canaliculi (Cohen et al., 2007; Gissen and Arias, 2015; Gkretsi et al., 2008). The wider importance of cadherins, tight junctions and cell structure in terms of defining cell function has also been outlined in the introduction. The balance between N-cadherin and E-cadherin can also point towards functional implications with epithelial cells typically expressing E-cadherin and mesenchymal cells expressing N-cadherin. Some cancerous cell lines derived from epithelia do express N-

cadherin inappropriately however (Wheelock et al., 2008), and this is a trend seen in hepatocellular carcinoma cells (HCC) such as HepG2. Loss of N-cadherin function in hepatocellular carcinoma cells through using a dominant-negative N-cadherin construct interestingly makes the cells more susceptible to bile acid induced apoptosis indicating that N-cadherin signalling contributes to HCC progression through its anti-apoptotic effects (Gwak et al., 2006). The loss of E-cadherin does also promote tumorigenesis through epithelial-mesenchymal transition (Nakagawa et al., 2014), so for non-cancerous cells, E-cadherin is a key junctional molecule. N-cadherin is found in healthy liver cells too however, with zonal expression of cadherins being seen in mouse liver; E-cadherin was expressed in periportal hepatocytes, and N-cadherin was expressed in perivenous hepatocytes (Hempel et al., 2015).

This project focusses in part on the concept of mechanotransduction, and therefore it is an area that is substantially investigated in this and subsequent chapters through both cytoskeletal analysis and through presence/expression of markers associated with mechanotransduction. As discussed in the introduction, the Sun proteins (Sun-1 and Sun-2) are integral components of the inner nuclear membrane (Starr, 2011) and higher expression of these proteins may be an indicator of increased nuclear stiffness – with depletion of Sun-1 compromising nuclear stiffness in bone-marrow-derived mesenchymal stem cells (BMSCs) (Liu et al., 2019). This study also indicated the important role of the F-actin cytoskeleton in determining the nuclear properties and morphology of the nucleus (Liu et al., 2019). The importance of β-catenin in Wnt signalling and controlling cell function and fate has also been highlighted in the introduction, and interestingly, Sun-1 and Sun-2 co-depletion decreases nuclear β-catenin levels due to interfering with the nucleoskeleton association and nuclear entry of β-catenin (Bouzid et al., 2019). Sun proteins were therefore chosen as key mechanotransduction marker due to the ease with which they can be visualised compared to other mechanotransduction related proteins, and they are able to provide insights into the nuclear structure and how that changes in different culture conditions.

4.2 Hypothesis and aims

We hypothesise that through priming cells on a 3D non-planar substrate will lead to a mechanical memory whereby the cells exhibit altered structural (and subsequently functional) characteristics when moved onto a secondary substrate/culture system. We expect the altered structure to be evident through both cytoskeletal changes, reflecting the altered actin machinery, and through changes in the global population growth. We also

hypothesise that key structural markers will be differentially expressed in the priming model compared to 2D cells, which will play a determining role in the formation of secondary cultures.

4.3 Objectives

The objectives of this chapter were:

- To comprehensively characterise the structural qualities of HepG2 cells at all stages (2D culture, 3D priming model, and secondary models),
- To investigate the retained structural changes that cells inherit after being primed in 3D compared to 2D.
- To investigate how the cytoskeleton changes as a result of altered substrate geometry.
- To visualise structural markers and population growth.

4.4 Results

3.41 Priming HepG2 cells in 3D alters how they grow as populations.

In probing for retained structural differences from priming cells in 3D compared to 2D, using simple methods such as neutral red stains on reseeded cells still provided great insight into the changes taking place within the HepG2 cells. **Figure 4.2** shows the results from performing a neutral red stain on cells that were liberated from either 2D or 3D priming after 8 days of growth, that were reseeded onto coverslips and grown for 7 days. Importantly here, cells were seeded onto the centre of the coverslip in a concentrated droplet, with media then being applied afterwards. These results show stark visual differences between 2D cells and 3D primed cells, with the 3D primed cells clearly forming much denser colonies that are more localised to a specific region on the coverslip. The 2D cells however form a more typical 2D monolayer on the coverslip, spreading to cover the complete surface (albeit with the occasional sparser area of growth). This change in population growth was somewhat unexpected in terms of how pronounced it was after 7 days. It was expected that changes would be evident earlier during growth, but it was initially thought that after 7 days this effect might equalise. This demonstrates the powerful effects on structure that 3D priming has; through providing the cells with a 3D microenvironment in the priming model, the cells have retained a more three-dimensional phenotype when growing on the coverslips, creating multi-layered colonies rather than a monolayer.

To provide further evidence to this effect, this reseeding experiment was performed with cells grown on coverslips for 4 days with a fully dispersed re-seeding of the cells being specifically focussed on, compared to the concentrated seeding in the prior experiment. The results (**Figure 4.3**) still show differences between the cells from 2D compared to 3D, but they are less pronounced here. Macroscopically, the differences are more evident at the edges of the coverslips, with the 2D primed cells forming confluent populations compared to the more punctate colonies from 3D primed HepG2 cells. Structural changes are more obvious in the microscopic images, with the 3D primed cells forming smaller more individual colonies compared to the 2D cells creating more interconnected populations. The milder differences are likely due to the lower confluency of the cells due to the shorter experiment time, and the dispersed seeding resulting in smaller colonies from 3D priming that are not as visually obvious.

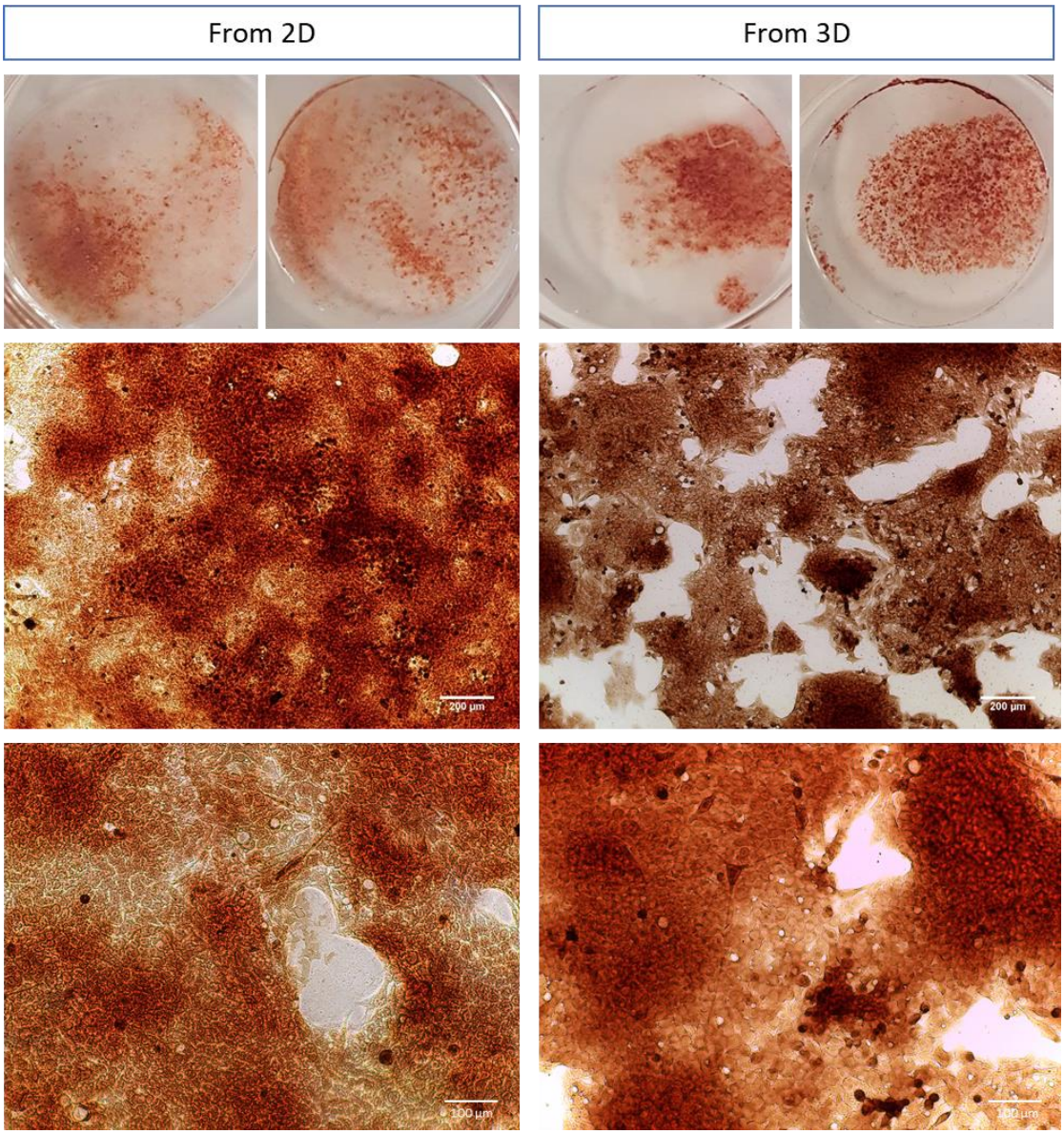

Figure 4.2: 3D primed cells behave differently as a population compared to 2D primed cells when reseeded on coverslips.

Neutral red images taken both macroscopically (top panels) and microscopically (bottom panels) of HepG2 cells grown for 7 days on coverslips at a density of 1 x 10^5 cells per coverslip. Cells were placed on coverslips after liberation from 2D and 3D. Scale = 200 µm

After seeing such differences when reseeding cells back onto 2D coverslips, the same experiment as **Figure 4.2** was repeated but with the cells being reseeded onto Alvetex® Scaffold and grown for 7 days instead of coverslips. Similar to the first experiment, the HepG2 cells reseeded onto Scaffold still exhibited significant differences in how they grew as populations (**Figure 4.4**), with the 3D primed cells clearly forming more distinctive, aggregate like colonies within the scaffold, whereas the 2D grown cells spread out and formed a more confluent layer within the scaffold. This is evident both macroscopically and microscopically through the neutral red stains, and further H&E imaging revealed the same pattern from cross sections (**Figure 4.5**), with multi-layered colonies observable in the 3D primed cells, but a much more consistent thin layer present in 2D grown cells.

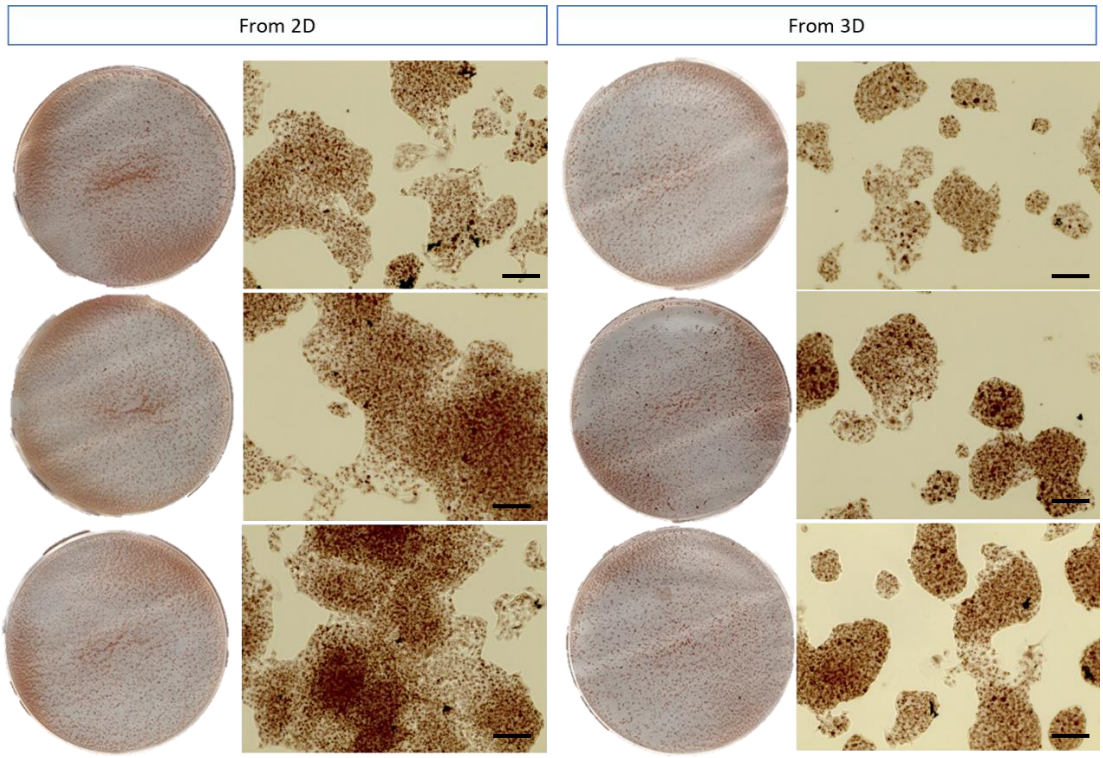

Figure 4.3: Dispersed re-seeding of cells into 2D maintains changes in 3D primed HepG2 cells.

Neutral red images taken both macroscopically (left panels) and microscopically (right panels) of HepG2 cells grown for 4 days on coverslips at a density of 1 x 10^5 cells per coverslip with the cells being seeded in drops around the well. Cells were seeded after liberation from 2D and 3D. Scale = 200 µm

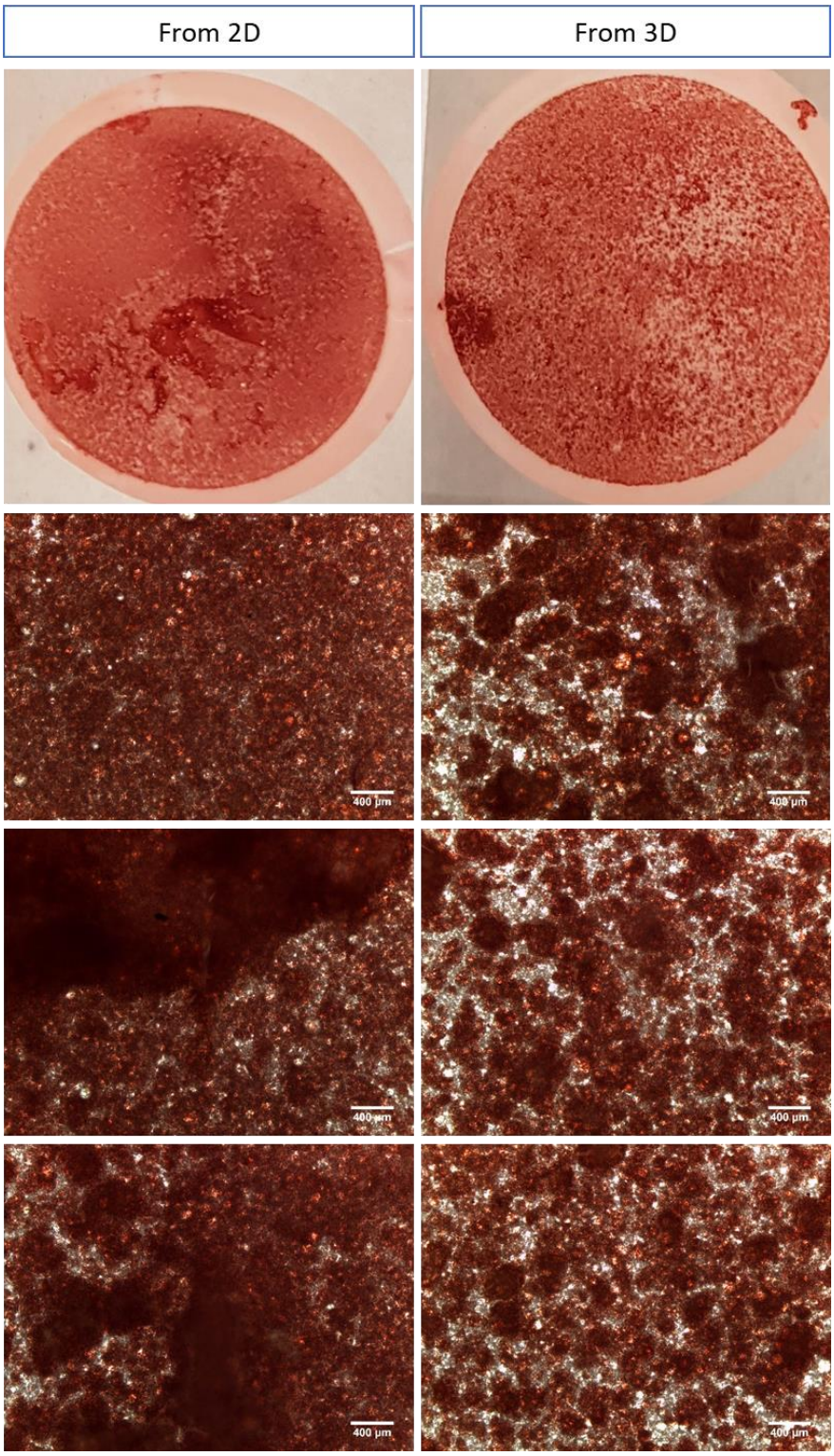

Figure 4.4: When reseeded onto Alvetex® Scaffold, 3D primed cells grow differently to 2D grown cells.

Neutral red stained images of HepG2 cells on Alvetex® Scaffold created from cells liberated from 2D flasks or Alvetex® Strata. Cells seeded at 1 x 10^6 cells per insert and imaged at after 7 days growth. Scale = 400 µm

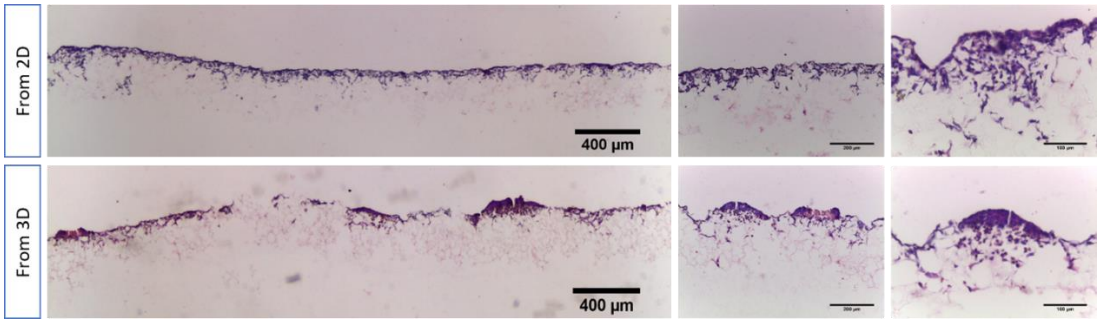

Figure 4.5: H&E stain of reseeded HepG2 cells on Alvetex® Scaffold reveals more 'colony' like appearance of 3D primed cells.

H&E stained images of HepG2 cells on Alvetex® Scaffold created from cells liberated from 2D flasks or Alvetex® Strata. Cells seeded at 1 x 10^6 cells per insert and imaged at after 7 days growth. Images at 4x, 20x and 40x magnification. Scale = 400 µm, 200 µm and 100 µm

4.42 3D primed HepG2 cells retain cytoskeletal changes after reseeding.

It was hypothesised that the differences seen in population growth were due to multiple factors imbuing the cells with a mechanical memory of the 3D priming model, including reorganisation of the cytoskeleton, altered transcription and gene expression, and altered presence of important structural proteins. Cytoskeletal reorganisation is a particularly strong driver of mechanotransduction (Harris et al., 2018; Ohashi et al., 2017) and therefore a significant level of investigation was needed into the cell shape and cytoskeletal changes retained in the cells after priming. The optimum way to do this was through single cell analysis after reseeding. A preliminary experiment was thus performed using phase contrast microscopy to compare the surface areas of cells after 1 hour or 3 hours of reseeding (**Figure 4.6**). With the phase contrast microscopy, the cells appear to have more significant visual differences 3 hours after reseeding, likely due to the cells having had more time to attach to the new substrate. Certain cells reseeded from 2D exhibited notable projections of the cell body, with the appearance of cell spreading, whereas 3D primed cells generally appeared more spherical and less 'spread out'. Quantification of the cell areas and circularity further proves this assessment, with cells from 2D showing significantly larger areas than their 3D primed counterparts at both time points, but with the difference being more pronounced after 3 hours. After 3 hours, cells from 2D averaged an area of nearly 300 µm whereas 3D primed cells were closer to 100 µm in area. Circularity of the cells was also significantly

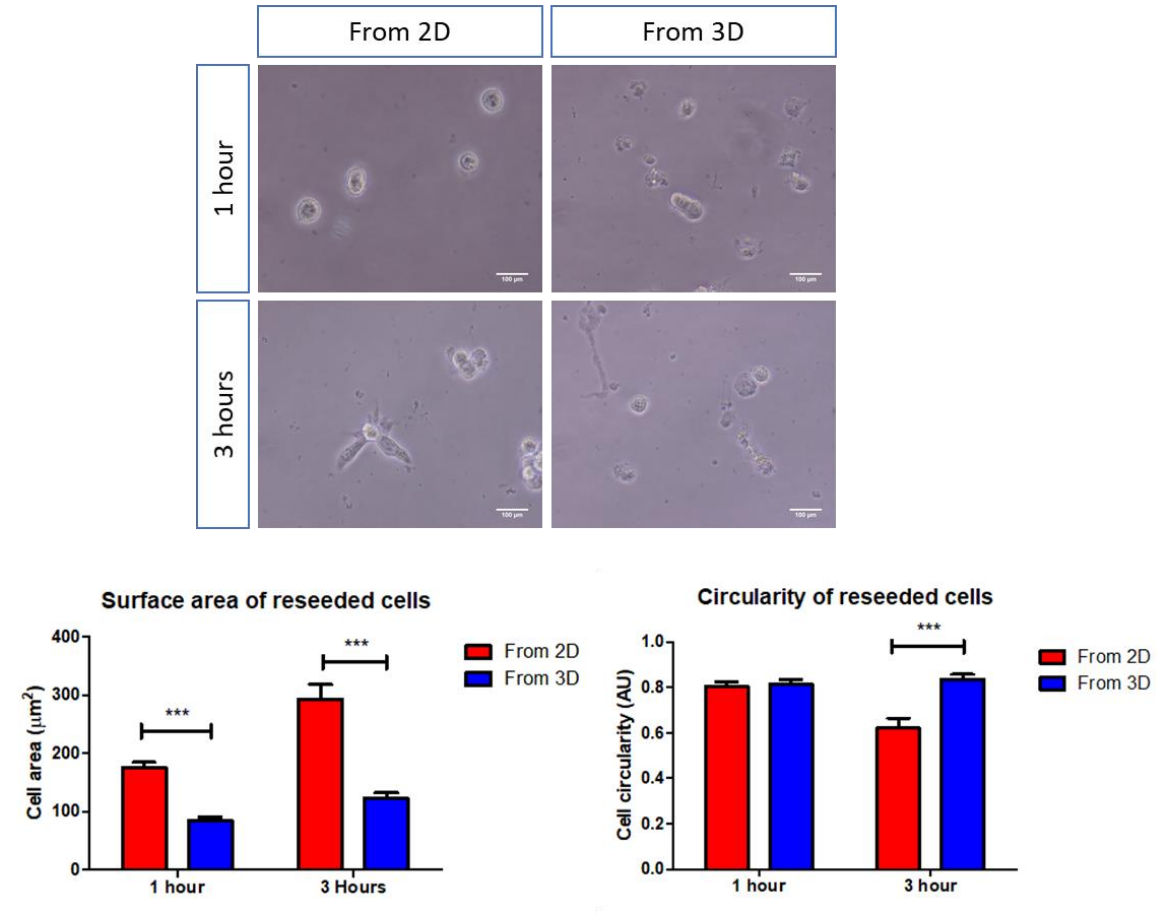

Figure 4.6: Preliminary phase contrast images of reseeded cells suggested that morphological changes were retained in HepG2 cells primed in 3D.

Phase contrast images of HepG2 cells grown on coverslips after being liberated from 2D flasks or Alvetex® Strata (3D). Cells seeded at 5 x 10^4 cells per well and grown for 1 or 3 hours before fixing with 4 % PFA. Scale: 100 µm. Quantification performed using ImageJ after tracing 30 separate cells in each condition. N= 3 n= 3, error bars = SEM

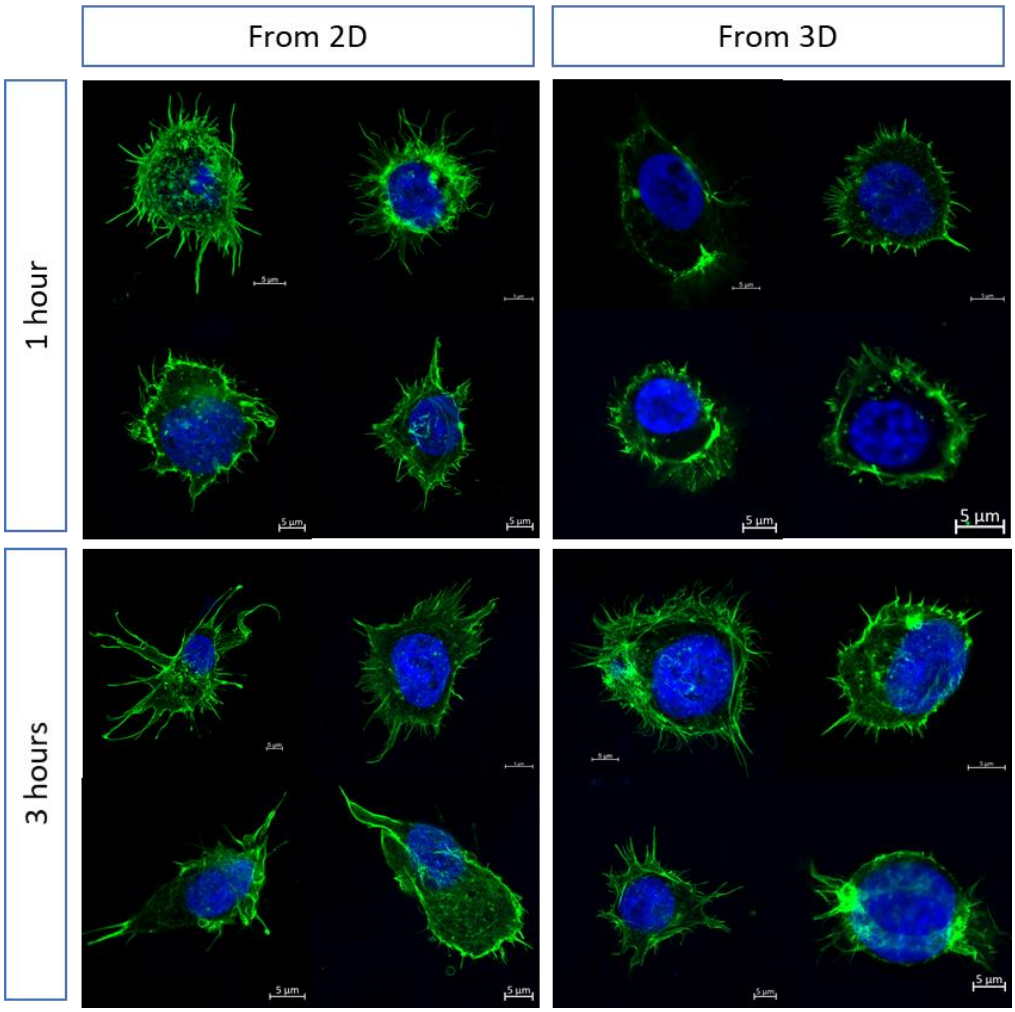

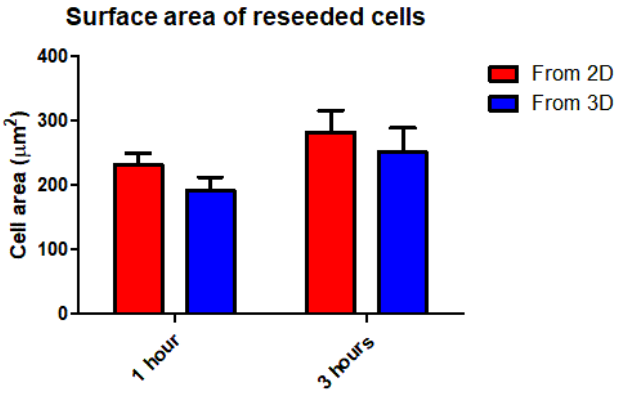

Figure 4.7: 2D grown cells appear to start spreading out earlier than 3D primed cells.

Fluorescent images of phalloidin stained HepG2 cells grown on coverslips after being liberated from 2D or Alvetex® Strata (3D). Cells seeded at 5 x 10^4 cells per well and grown for 1 or 3 hours before fixing with 4 % PFA. Scale: 5 µm. 15 cells were counted in each condition. Area quantification carried out using Zen Blue. N= 3 n= 3, Error bars = SEM

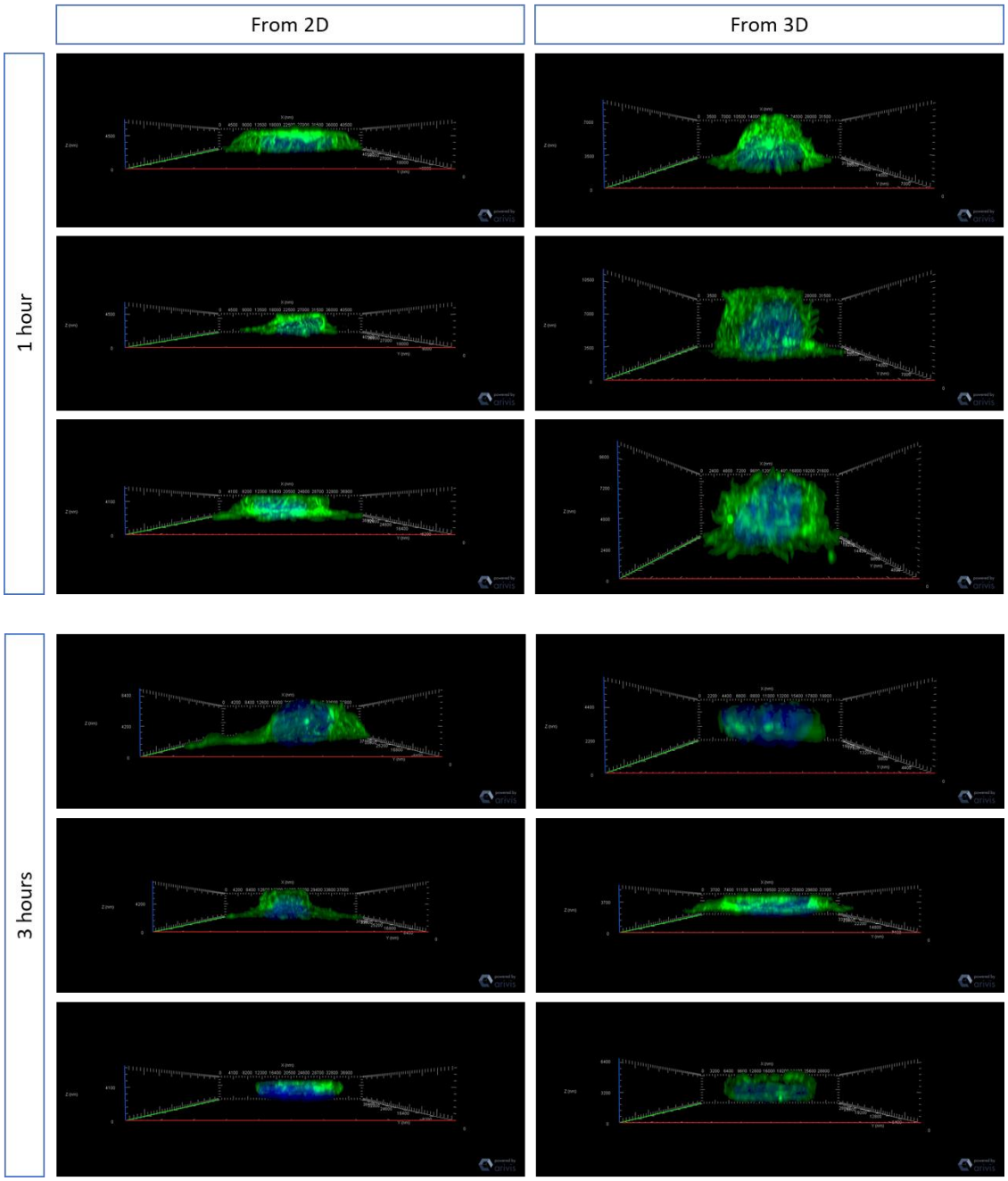

Figure 4.8: 3D primed cells appear taller and more spherical than 2D grown cells one hour after seeding.

Fluorescent Z-stack images of phalloidin stained HepG2 cells grown on coverslips after being liberated from 2D or Alvetex® Strata (3D). Cells seeded at 5 x 10^4 cells per well and grown for 1 or 3 hours before fixing with 4 % PFA. Scale: 5 µm.

decreased in 2D cells 3 hours after reseeding, due to the aforementioned projections creating much more irregular cell shapes in 2D grown HepG2 cells.

Based on the promising data from this preliminary experiment, the conditions were repeated but a phalloidin stain was used to fluorescently visualise filamentous actin in high detail (**Figures 4.7, 4.8, 4.9**), providing a greater insight into what structural changes were occurring. **Figure 4.7** provides representative images of the top-down views taken on a confocal microscope, with the quantification of cell surface area based on the phalloidin stains. In these highly detailed images, the difference between 2D and 3D primed cells is very clear in the images taken of cells fixed 3 hours after reseeding onto the coverslips. The cells from 2D are much more spread out, with noticeable extensions of the cytoplasm and cytoskeleton indicating an attached migratory cell phenotype. The 3D primed cells however have a large number of small protrusions present, but in general are smaller, more spherical and do not have the large cytoskeletal processes extending the cell body. This is reflected in the area quantification which shows a very similar pattern to the phase contrast images, albeit without a statistically significant trend. The lack of significance can be explained by the lower number of measured cells here due to the high magnification images taking a lot longer to process, and the detailed nature of these images means that the stress fibres increase the measured surface areas of the 3D primed cells, decreasing the difference in area previously seen.

Interestingly, despite the slightly reduced magnitude of surface area difference, measuring the heights of the cells revealed a distinctive contrast between 3D primed and 2D cells. **Figure 4.8** highlights a very noticeable change in the side profile of the cells at the 1-hour timepoint, with the 3D primed cells being significantly taller than their 2D counterparts as shown in the quantification in **Figure 4.9.** This difference disappears after 3 hours, with the cells seemingly equilibrating to the surface of the coverslips. From this data, it is evident that the cytoskeleton is altered in single cells during 3D priming and that the cells possess a mechanical memory through which structural changes are retained when reseeding onto a secondary substrate.

The changes seen so far have been relatively short term, with cells fixed up to 3 hours after reseeding. To see if these structural differences were retained over a longer period, cells were fixed after 1 day (24 hours) of reseeding onto coverslips and the areas measured from phalloidin images (**Figure 4.10**). A greater number of cells were able to be analysed here due to using a lower magnification, and a collection of representative images are shown. As

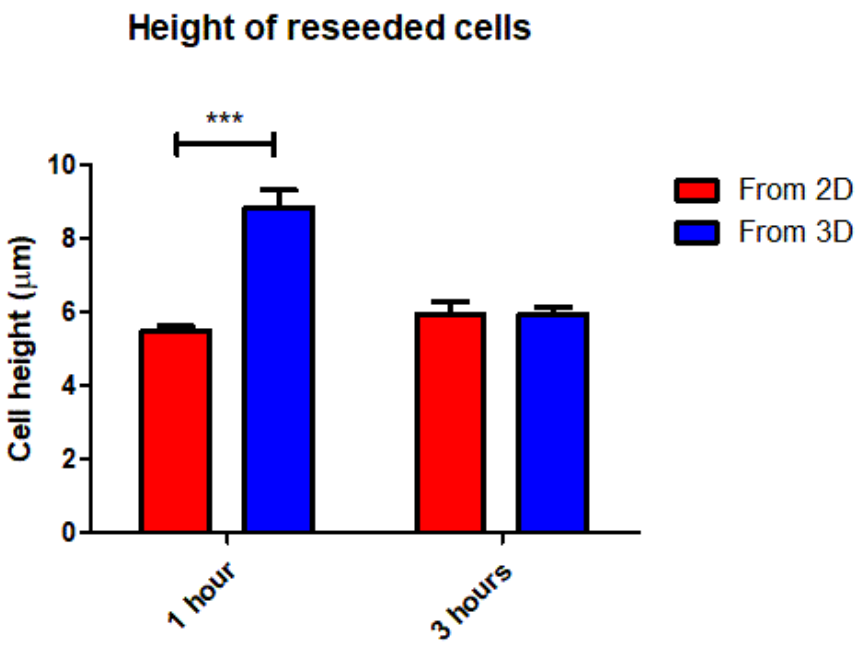

Figure 4.9: 3D primed cells are significantly taller than 2D grown cells 1 hour after seeding, though they equalise after 3 hours.

Bar chart showing the quantification of cell height carried out using Zen Blue software by measuring the total thickness of Z-stacks. 15 cells were measured N= 3 n= 3. Error bars = SEM.

expected, while there is heterogeneity within the populations, there is a general and clear trend of 2D cells exhibiting a more spread-out phenotype. This is reflected in the significantly smaller quantified areas of the 3D primed cells.

To further explore the altered actin machinery, different compounds that interfered with the polymerisation or nucleation activity of actin were applied to the cells at the point of reseeding to ascertain how this may alter the structural phenotype. The three compounds used were picked based on previous work in the lab and are as follows:

CK-666 – inhibits Arp2/3 activity (nucleation inhibitor),

SMIFH2 – inhibits FH2 activity (nucleation inhibitor),

Y-27632 – inhibits ROCK1, inhibiting the activation of myosin-II, destabilising actin filaments (polymerisation inhibitor).

Based on previous results in the lab, it was expected that inhibiting actin nucleation in 2D cells would have a stronger effect on morphology and would bring them closer to a 3D primed phenotype (resulting in smaller, more spherical cells). It was expected that all actin interfering agents would have an effect on the morphology in some way, with the rationale being that if impairing actin nucleation or polymerisation brings the morphologies of 2D cells closer to that of the 3D primed cells, then it may highlight which specific components of the actin machinery are altered in 3D primed cells. **Figure 4.11** shows representative images of coverslips with each agent applied, and a control coverslip with a DMSO vehicle also included. From these images, it is hard to draw concrete conclusions other than the general trend followed of control 2D cells exhibiting more spreading out than the 3D cells. It is noticeable that the cells incubated with SMIFH2 appeared slightly larger from both 2D and 3D compared to the control, but only when looking at the quantification in **Figure 4.12** could this be confirmed. This quantification displays significance levels just calculated between 2D and 3D comparisons within each treatment condition through a T-test, but one-way ANOVA was also performed with Dunnett's post-test (**Table 4.1**) comparing each condition to the 3D primed control as that was the phenotype we wanted to see if the agents could reproduce.

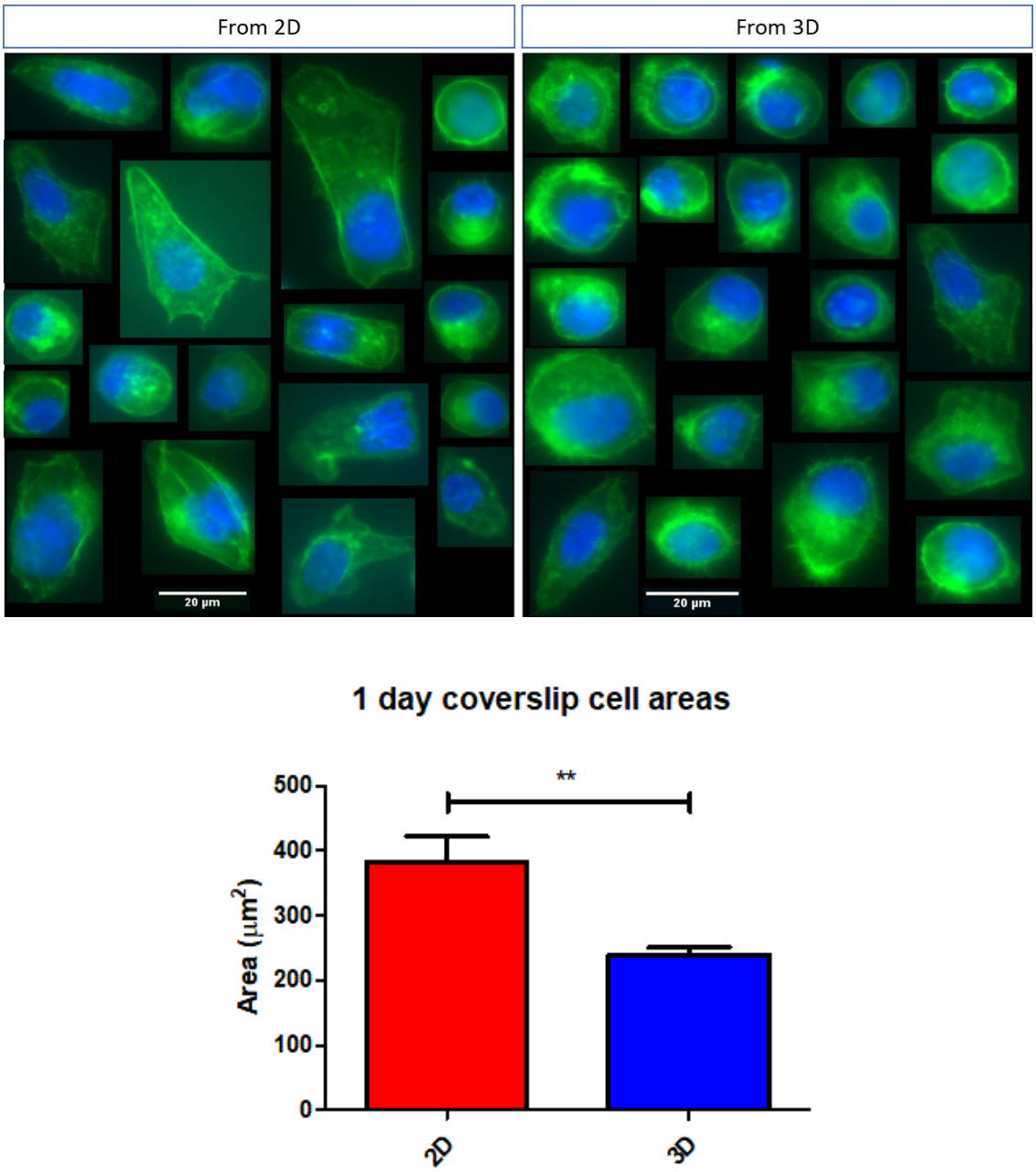

Figure 4.10: After 1 day of growth from reseeding onto coverslips, 2D grown cells spread out significantly more than 3D primed cells.

Fluorescence of phalloidin stained HepG2 cells grown on coverslips after being liberated from 2D or Alvetex® Strata (3D). Cells seeded at 5 x 10^4 cells per well and grown for 1 day. Scale: 20 µm. Bar chart showing quantification of cell areas from image J. Quantification performed on over 40 cells in each condition. N= 3 n= 3. Error bars = SEM.

Nucleus areas and circularities were also quantified to see how/if these related to the overall cell areas and circularities as the cytoskeleton and nucleus are interacting structural aspects of the cell. The quantification highlights some interesting trends, with a very similar surface area pattern of 2D vs 3D primed cells in the control condition as seen before. Out of the 3 actin interfering agents, CK-666 and Y-27632 both seem to bring the 2D cells closer to a 3D phenotype in terms of equalising the surface areas, however CK-666 treated 2D cells are still significantly less circular than the 3D primed cells treated with CK-666 (**Figure 4.12**), though the circularities are not significantly different to the 3D control. This suggests that other actin altering mechanisms are preventing complete morphological changes in 2D cells compared to 3D cells even when Arp2/3 activity is inhibited with CK-666. Y-27632 also alters the structure of 2D cells to appear similar to a 3D primed phenotype, with the cell areas and circularity being comparable to the 3D control. Unexpectedly, with Y-27632 treatment, the nuclear areas are significantly decreased compared to the control, despite there being no significant change in cell area, suggesting that Y-27632 may alter the interactions between the cytoskeleton and nucleus.

SMIFH2 has the most profound effect on the cells from both 2D and 3D when compared to the control, with the cell and nucleus areas being significantly larger than the 3D primed control cells as well as the cell circularity (but not nuclear) being significantly decreased (**Table 4.1**). The effect of SMIFH2 is in the opposite direction than expected, by bringing the cells further away from the comparative control condition. Interestingly, this was also contrasting to previous data in the lab gathered on stem cells that suggested SMIFH2 could bring 2D cells to a 3D primed phenotype. This data indicates that through altering the actin machinery in 2D cells, a more 3D-like phenotype can be achieved, but it is not possible to *completely* recapitulate the 3D phenotype with these agents being used in isolation. Therefore, it is likely that multiple elements of the actin machinery are considerably altered in 2D cells, including ROCK1 and Arp2/3 activity. In **Chapter 5**, this will be explored further through examining gene expression data from RNA sequencing.

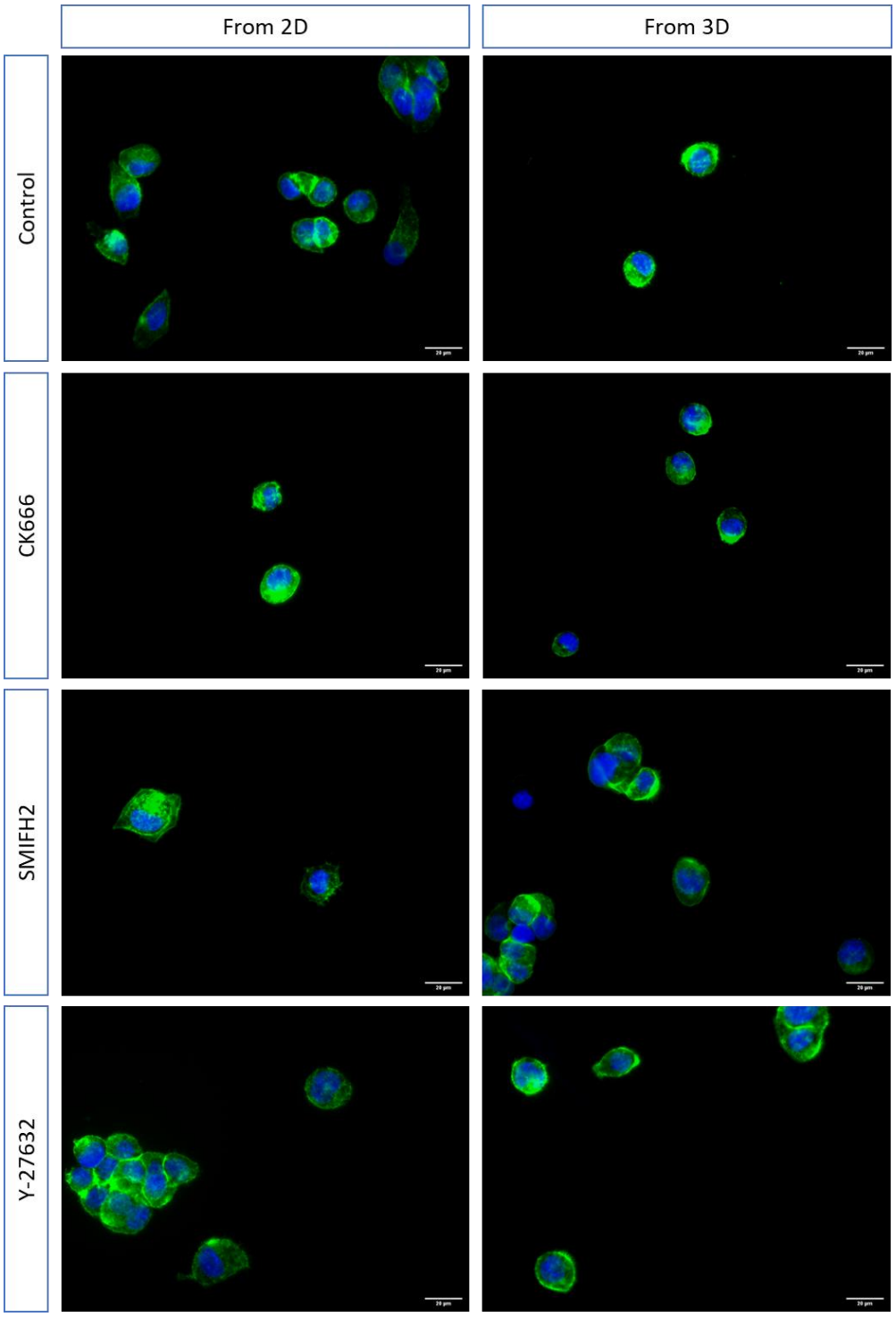

Figure 4.11: Interfering with actin dynamics in 2D cells is able to bring them closer to a 3D morphology.

Fluorescence of phalloidin and Hoechst 33342 stained HepG2 cells grown on coverslips after being liberated from 2D or Alvetex® Strata (3D). Cells seeded at 5 x 10^4 cells per well and grown for 1 day in either control medium or medium containing one of the following actin inhibitors: CK666, SMIFH2 and Y-27632. Scale: 20 µm

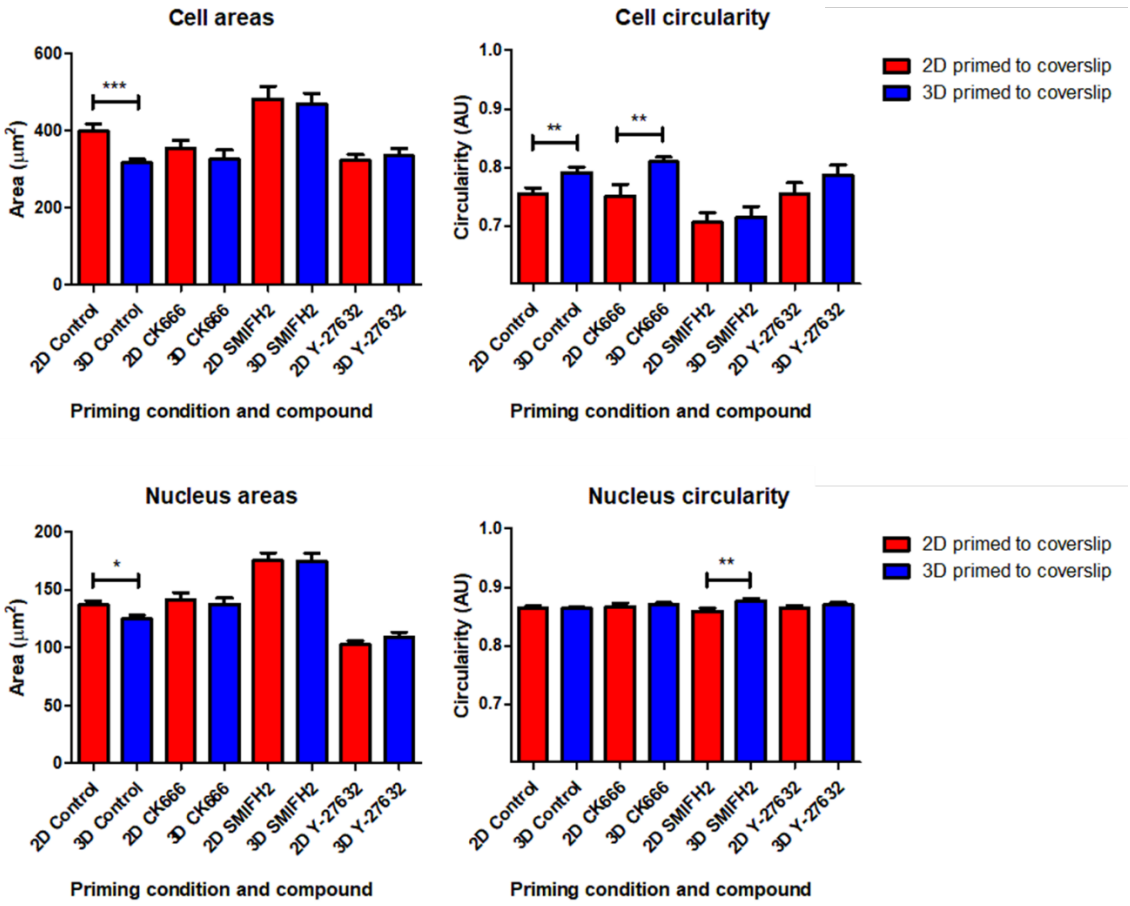

Figure 4.12: Quantification of the cell area and circularity after actin interference highlights how CK666 particularly brings the 2D cells to a 3D phenotype.

Quantification of areas and circularity of both the cells and nuclei performed using image J with significance calculated through an unpaired T-test between 2D and 3D within each condition. Over 50 individual cells measured in each condition. N= 3, n= 3. Error Bars = SEM.

Table 4.1: One way ANOVA, Dunnett's multiple comparison test on actin interference data.

Cell area

Dunnett's Multiple Comparison Test	Mean Diff.	Significant? P < 0.05?	Summary
3D Control vs 2D Control	-80.39	Yes	***
3D Control vs 2D CK666	-35.18	No	ns
3D Control vs 3D CK666	-8.721	No	ns
3D Control vs 2D SMIFH2	-164.2	Yes	***
3D Control vs 3D SMIFH2	-150.9	Yes	***
3D Control vs 2D Y-27632	-4.499	No	ns
3D Control vs 3D Y-27632	-16.65	No	ns

Cell circularity

Dunnett's Multiple Comparison Test	Mean Diff.	Significant? P < 0.05?	Summary
3D Control vs 2D Control	0.03677	Yes	*
3D Control vs 2D CK666	0.04000	No	Ns
3D Control vs 3D CK666	-0.01830	No	Ns
3D Control vs 2D SMIFH2	0.08550	Yes	***
3D Control vs 3D SMIFH2	0.07648	Yes	***
3D Control vs 2D Y-27632	0.03688	No	ns
3D Control vs 3D Y-27632	0.003858	No	ns

Nucleus area

Dunnett's Multiple Comparison Test	Mean Diff.	Significant? P < 0.05?	Summary
2D Control vs 3D Control	11.64	No	ns
2D Control vs 2D CK666	-4.354	No	ns
2D Control vs 3D CK666	-0.8861	No	ns
2D Control vs 2D SMIFH2	-38.55	Yes	***
2D Control vs 3D SMIFH2	-38.25	Yes	***
2D Control vs 2D Y-27632	34.02	Yes	***
2D Control vs 3D Y-27632	27.72	Yes	***

Nucleus Circularity

Dunnett's Multiple Comparison Test	Mean Diff.	Significant? P < 0.05?	Summary
2D Control vs 3D Control	0.001217	No	ns
2D Control vs 2D CK666	-0.002033	No	ns
2D Control vs 3D CK666	-0.005757	No	ns
2D Control vs 2D SMIFH2	0.005822	No	ns
2D Control vs 3D SMIFH2	-0.01232	No	ns
2D Control vs 2D Y-27632	0.0005730	No	ns
2D Control vs 3D Y-27632	-0.005349	No	ns

To get a highly detailed picture of how the structure of cells changes from priming, scanning electron micrograph images were taken of HepG2 cells 1 day after reseeding from either 2D or 3D priming. The results of the single cell images (**Figure 4.13**) showed an astounding difference between 2D and 3D primed cells, with the 3D primed cells appearing much more spherical and less spread out than their 2D counterparts, and the presence of microvilli/extrusions from the cell body appeared to be increased in 3D primed cells too. It is important to note that there was variation, with some more spread-out 3D primed cells, and some more spherical 2D cells, but the images shown are representative of the trends observed, with a very clear general trend towards the morphological patterns previously seen. SEM images were also taken of cells reseeded at a higher confluency (**Figure 4.14**) to visualise how interactions between 3D primed cells might differ on a coverslip. Again, there are distinctive differences here, with the 3D primed cells forming taller, more multi-layered populations, compared to the typical monolayer appearance of the 2D grown cells. This data clearly reinforces what has been previously observed and indicates that there are significant structural changes taking place in primed 3D cells that are retained in subsequent secondary cultures, with short- and long-term secondary culture highlighting cytoskeletal and population-based changes respectively.

4.43 Optimisation of a secondary 3D culture model revealed further retained structural differences from 3D priming.

The central concept behind this project was to prime cells in a 3D microenvironment (in this case on Alvetex® Strata) before liberating and moving them into a secondary 3D culture. That secondary culture step in this case was creating cellular aggregates/spheroids. There are multiple ways to aggregate cells, but to keep in line with the ideals of creating a simple, cost effective culture method, simple aggregation methods were employed. The first attempt used low adherence Petri dishes which prevents cells from adhering to the base of the dish, encouraging spontaneous aggregation. **Figure 4.15** displays the growth of these aggregates over 7 days from either liberated 3D primed cells or 2D cells, and interestingly, similar to the neutral red stains in **Figure 4.2**, the cell populations here grow in different ways depending on the culture origin. 3D primed cell aggregates seem to clump together to form larger ‘multi-aggregates’ whereas the 2D cells form smaller more individual aggregate clusters.

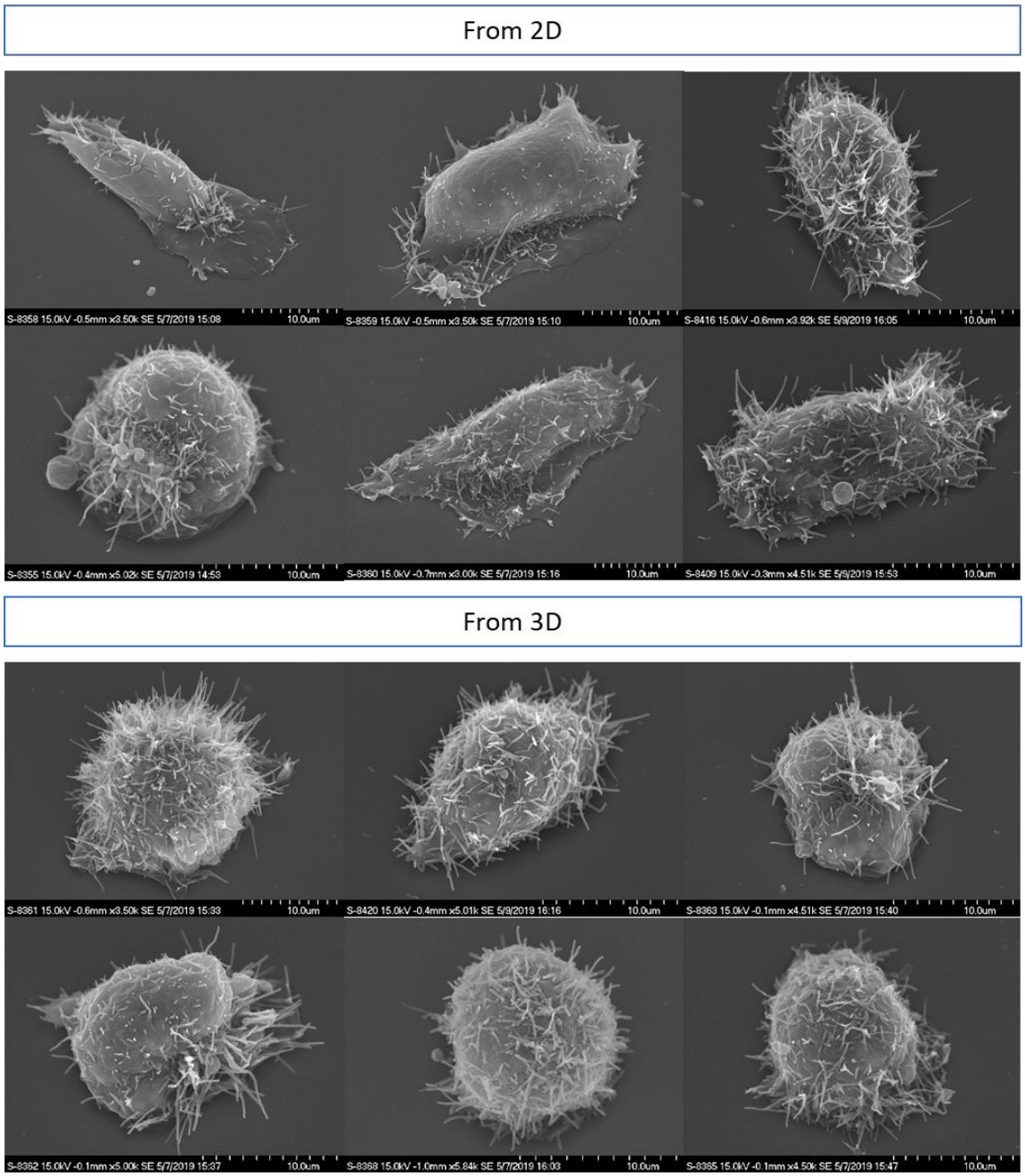

Figure 4.13: SEM images reveal distinct morphological changes in 3D primed cells after 1 day of growth from reseeding onto coverslips.

Scanning electron microscope images of HepG2 cells seeded at 1 x 10^3 cells per silicon coverslip after liberation from 2D or Alvetex® Strata (3D) and grown for 1 day.

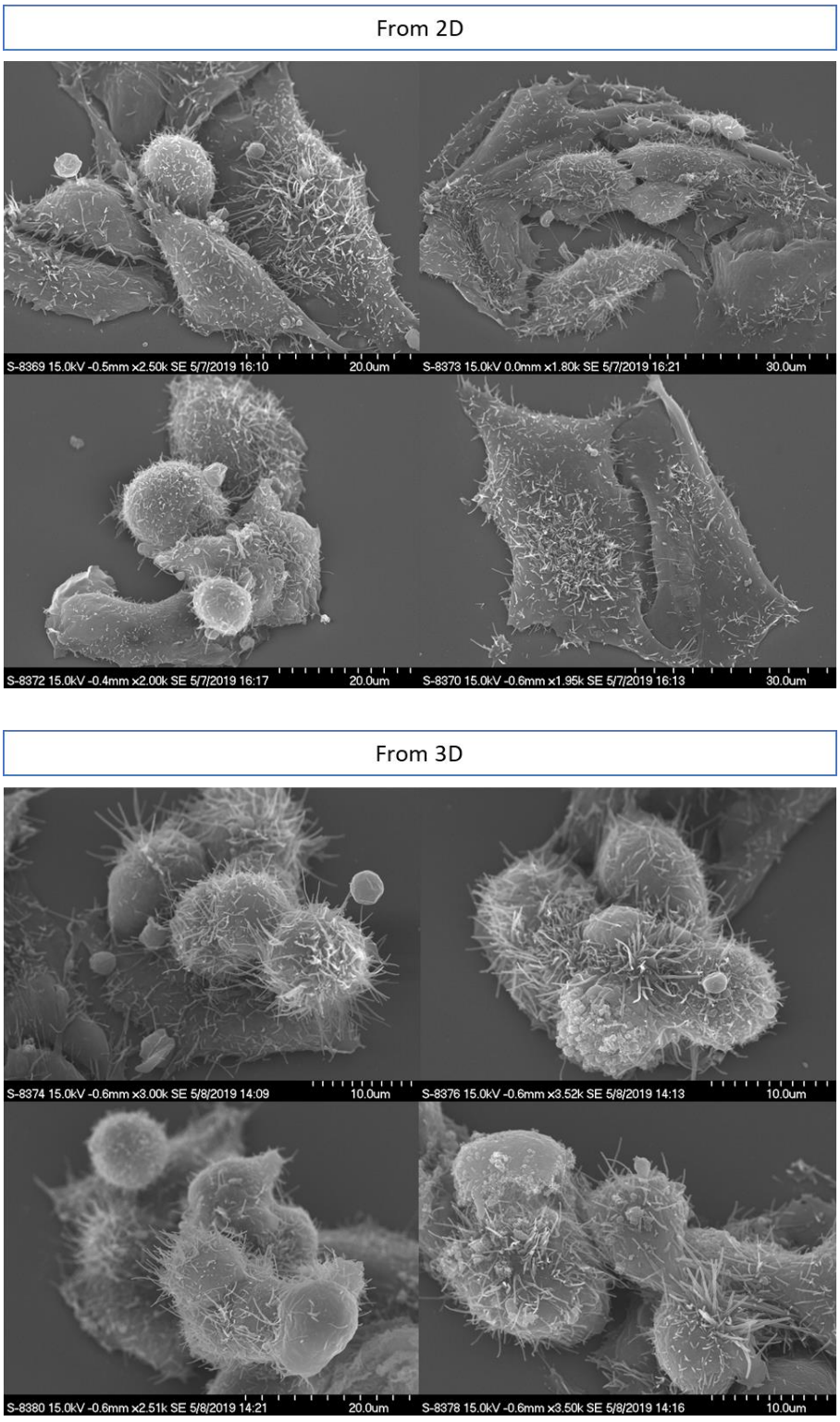

Figure 4.14: SEM images reveal that 3D primed cells grow in a more 3D orientation after reseeding.

Scanning electron microscope images of HepG2 cells seeded at 5 x 10^4 cells per silicon coverslip after liberation from 2D or Alvetex® Strata (3D) and grown for 1 day.

This difference between 3D primed and 2D cells was reproducible as shown in **figure 4.16** where the experiment was repeated (this time with excessive homogenisation) with the same phenomenon seen. Images of the cell suspension are provided here too on the far left, to indicate that the cells were properly lysed and homogenised before reseeding. Phalloidin stains were performed on whole mount aggregates (**Figure 4.17**) to visualise the overall structure, and these images revealed a unique insight into the structural differences, with the larger 3D primed aggregates appearing to be formed from multiple smaller aggregates clumping together. The phalloidin staining appears more intense at the edges of these smaller aggregates due to the cells wrapping round at those locations making for denser cell populations at the periphery of the aggregates when imaging them.

H&E images were also taken of aggregate sections (**Figure 4.18**), and what becomes clear here is that in the larger low adherence aggregates, there is significant cell death occurring with large voids in the centres of the aggregates, with the cells present displaying nuclear shrinkage and hypereosinophilic cytoplasms. To confirm this, aggregates were incubated with propidium iodide (PI) before fixing. PI provides a simple test for cell death, as in-tact membranes exclude the stain, but compromised membranes of dying/dead cells do not, meaning that dead cells stain positive. **Figure 4.19** displays images of Hoechst 33342 and propidium iodide-stained aggregates as well as an example with a co-stain of phalloidin. In the aggregates just stained with Hoechst 33342 and PI, there is a large region in the centres of low adherence aggregates both from 2D and 3D primed cells of PI positive staining, indicating a necrotic core. The Hoescht staining was often unable to penetrate the centres of the fixed aggregates, but the in the combined stains with phalloidin it is made very clear that the dead cells do lie within the centre of the three-dimensional aggregate structure. An additional observation from the phalloidin stains is that the aggregates from 2D cells appear less dense than the 3D primed aggregates, which seem to have tighter packing of the HepG2 cells within the structure. This could be a structural artefact from the priming stage, with the cells retaining a more individually three-dimensional structure (as seen in the single cell analyses) within the 3D structure of the aggregate. This denser appearance is also seen in the phase contrast images of the aggregates, with the 3D primed aggregates appearing significantly darker than the 2D counterparts, suggesting increased cell numbers and tighter packing after 3D priming.

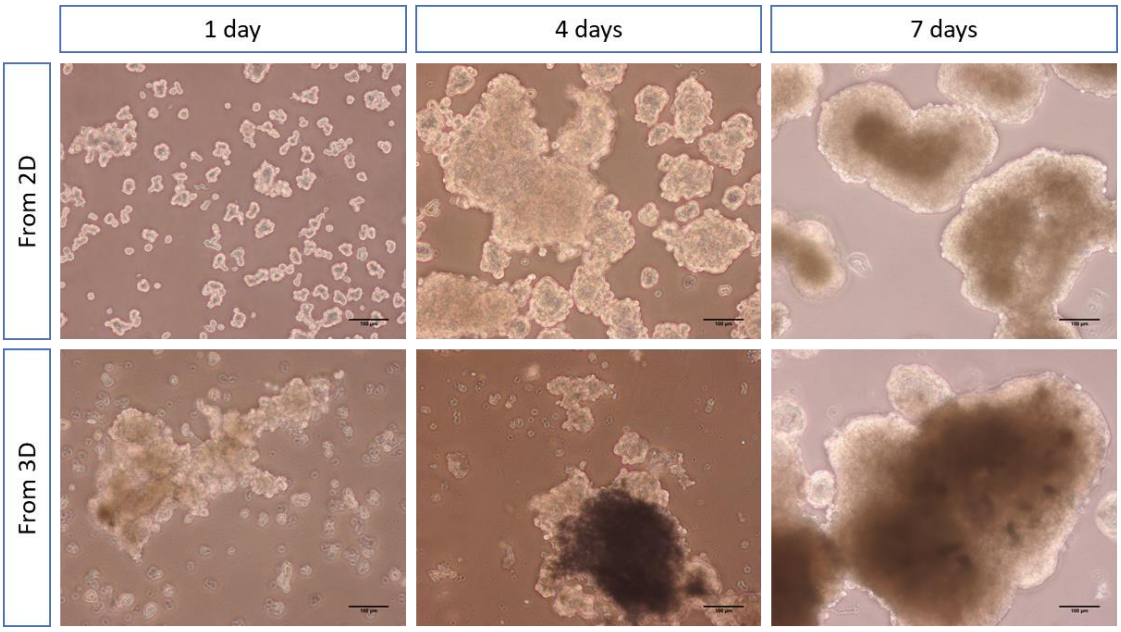

Figure 4.15: After 7 days of growth as low adherence aggregates, 3D primed cells form denser and larger aggregates compared to cells grown in 2D.

Phase contrast images of aggregates created from cells liberated from 2D flasks or Alvetex® Strata. Cells seeded at 1 x 10^6 cells per Petri dish. The 3D cells rapidly formed large, dense aggregates whereas the 2D cells more slowly formed smaller more numerous aggregates. Scale: 100 µm.

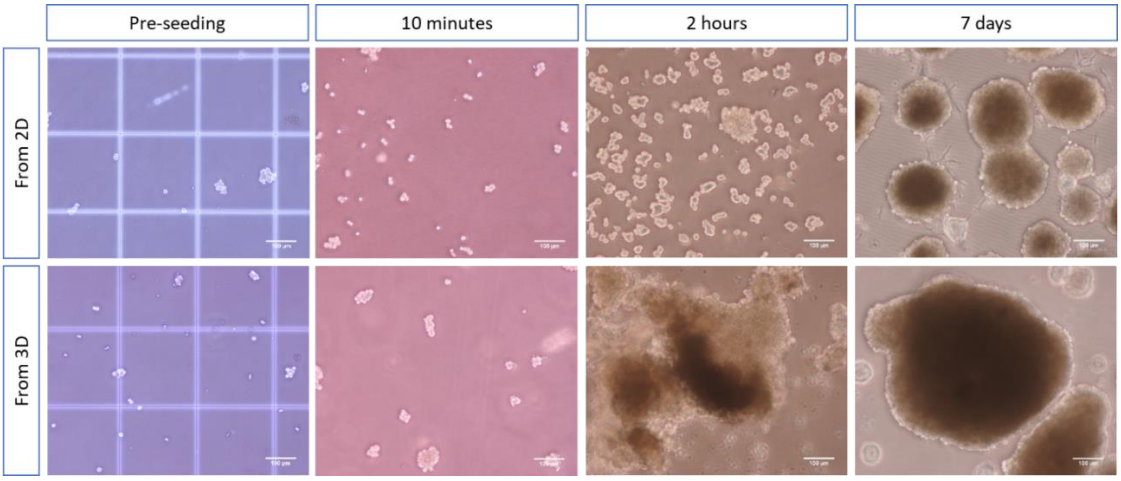

Figure 4.16: Excessive homogenisation of the cells upon liberation still resulted in larger 3D primed aggregates.

Phase contrast images of aggregates created from cells liberated from 2D flasks or Alvetex® Strata. Cells seeded at 1x10^6 cells per petri Scale: 100 µm.

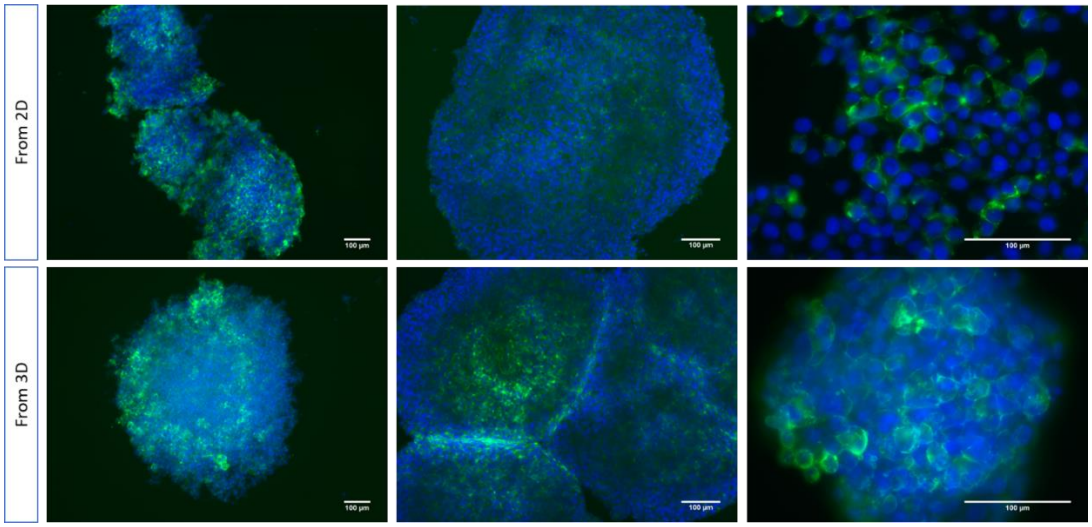

Figure 4.17: 3D primed aggregates tend to conglomerate to form larger masses.

Fluorescence images of cells stained with the F-actin cytoskeletal stain Phalloidin (green) and with Hoechst 33342 to highlight the cell nuclei (blue). Cells grown for 10 days as aggregates after liberation from either 2D or 3D, and seeded at 1 x 10^6 cells per Petri dish. Scale = 100 µm

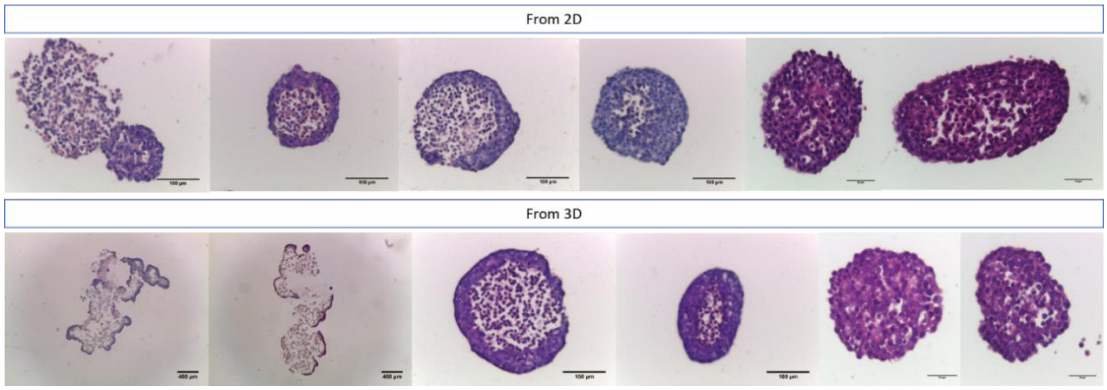

Figure 4.18: Aggregates from both 2D growth and 3D priming are highly heterogenous in shape and size.

H&E-stained images of aggregates created from cells liberated from 2D flasks or Alvetex® Strata. Cells seeded at 1 x 10^6 cells per petri dish and imaged at after 10 days growth. Scale = 100 µm and 400 µm

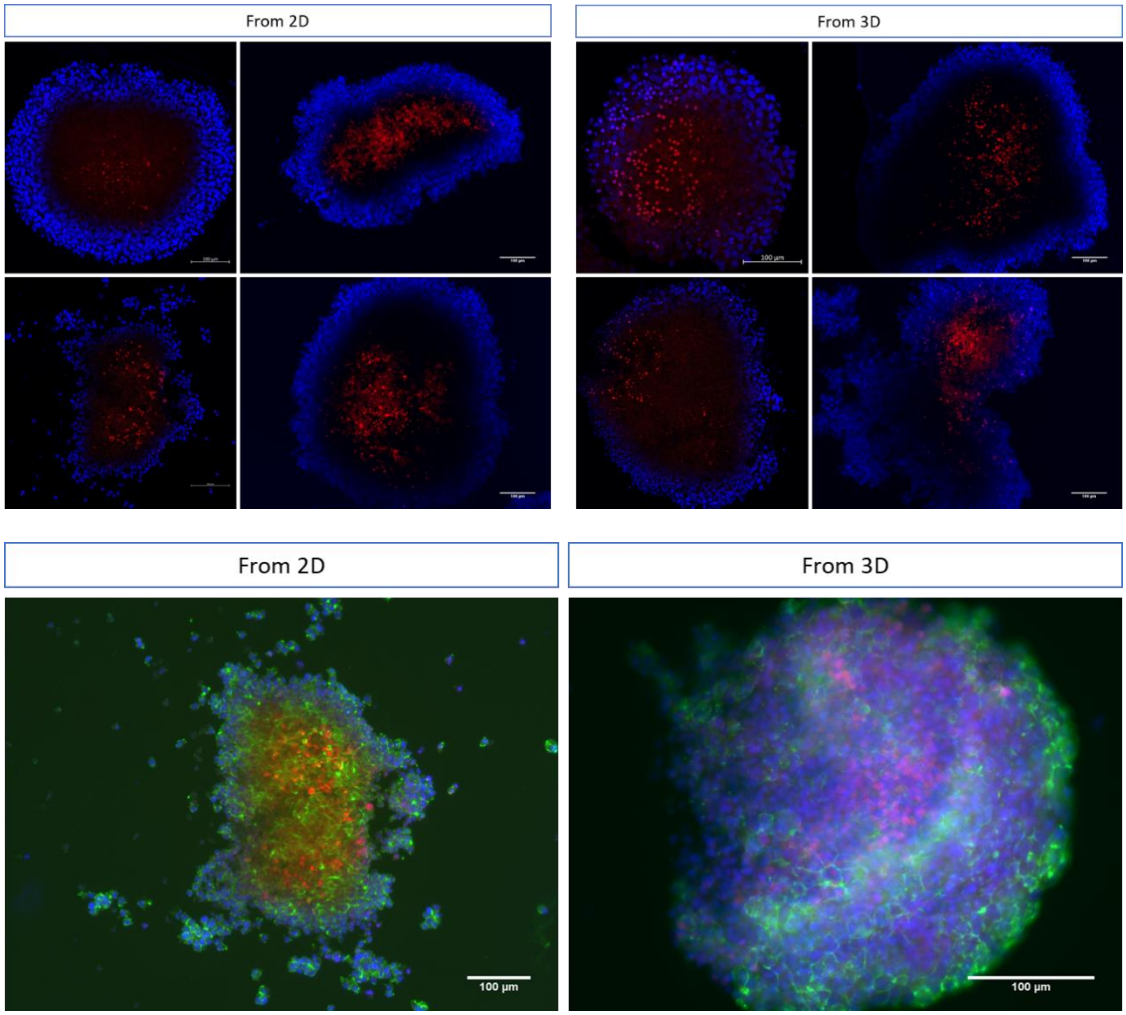

Figure 4.19: Due to the large aggregate size, significant cell death is occurring in the central regions.

Fluorescence images of cells incubated with propidium iodide, an indicator of cell death (red) and stained with Hoechst 33342 to highlight the cell nuclei (blue), with added F-actin stain phalloidin (green) in bottom panels. Cells grown for 10 days as aggregates after liberation from either 2D or 3D, and seeded at 1 x 10^6 cells per Petri dish. Scale = 100 µm

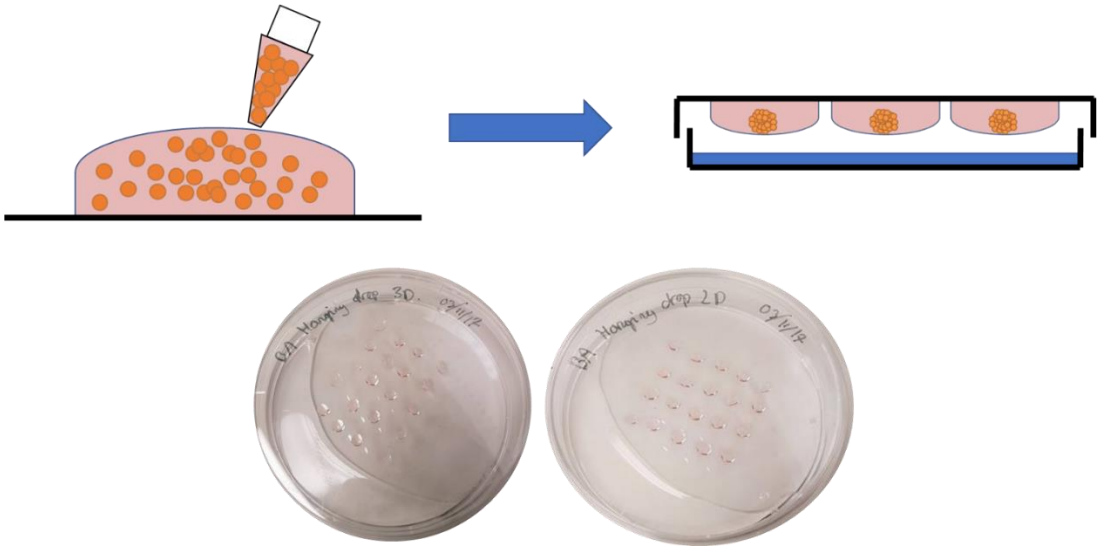

Figure 4.20: Hanging drop spheroids formed using Petri dish lids may allow for more controlled aggregate size due to constraints of the droplet.

Cells were seeded in 20 µL droplets of media onto the inside surface of the lids of petri dishes which were then inverted and placed onto the dish which contains 5 mL of PBS to maintain humidity. Fresh media was added to the hanging drops after 4 days of culture.

The propidium iodide staining of low adherence aggregates revealed high levels of cell death in the centres of the aggregates regardless of their origin, indicating that this was a suboptimal technique to use as a simple liver model, and would be more suited to purely cancer models where hypoxia and nutrient starvation help mimic the heterogeneity of *in vivo* tumours (Zanoni et al., 2016). For the purposes of this model however, a more consistent size of spheroid was desired that was small enough to avoid a significant necrotic core as seen prior. Therefore, the use of a simple hanging drop methodology (**Figure 4.20**) adapted from Shah et al., 2018 was utilised. This involved seeding the desired number of cells suspended in 20 µL droplets onto the inside surface of a Petri dish lid which was then placed back onto a dish humidified with PBS.

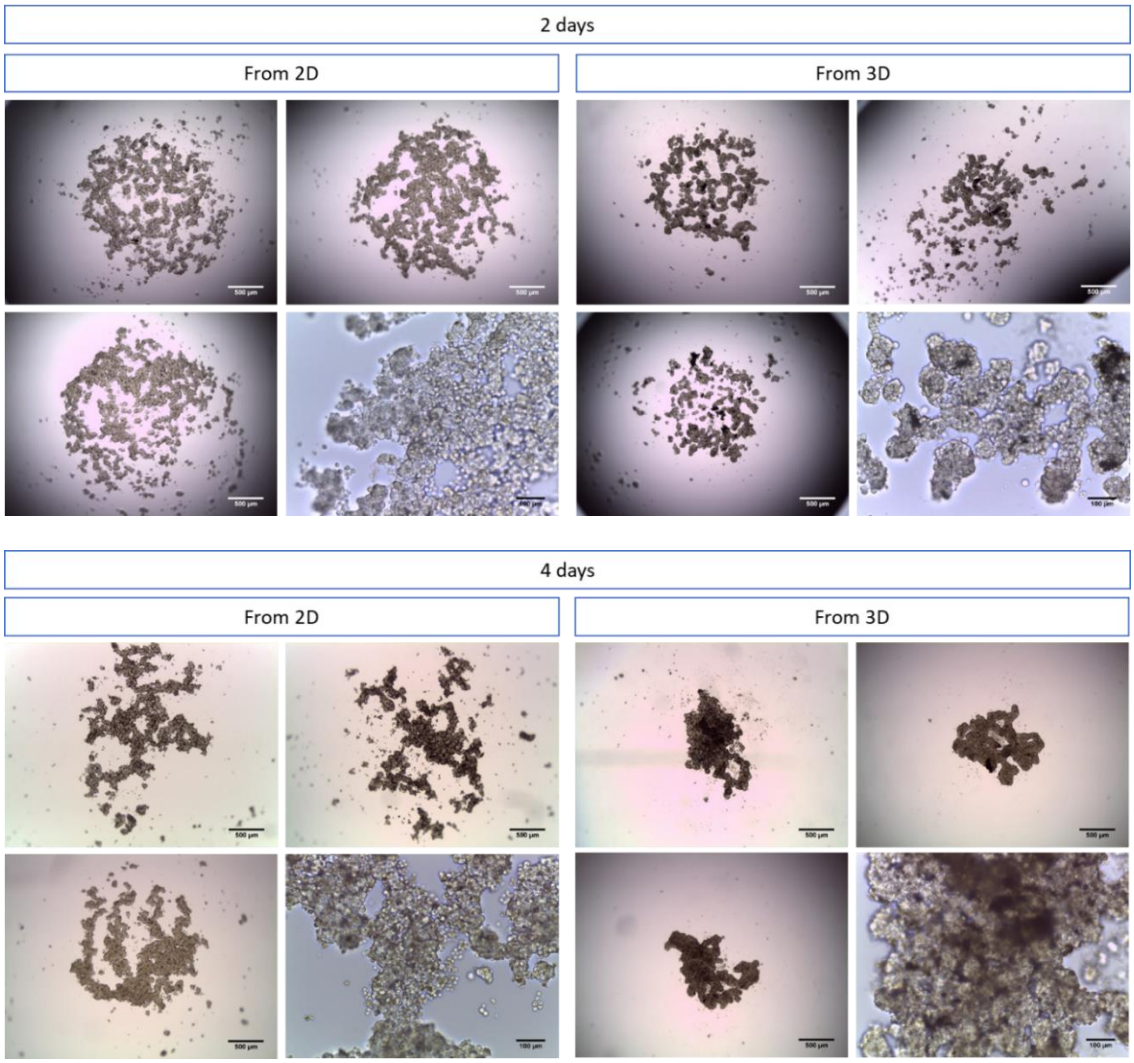

Figure 4.21: Initial experiments indicate that hanging drops seem to compact over time and that there may still be some macrostructural differences in 3D primed spheroids.

Light microscopy images of hanging drop aggregates created from cells liberated from 2D flasks or Alvetex® Strata. Cells seeded at 2.5 x 10^4 cells per drop and imaged at 2 and 4 days growth. Scale: 500 µm and 100 µm (bottom right panels).

The drops then allowed spheroids to naturally form under the influence of gravity. An initial experiment using a large seeding density of 2.5 x 10^4 was run to observe how the cells aggregated over time. It was clear from the light microscopy images of these aggregates (**Figure 4.21**) that the seeding density was excessively high as the aggregates often filled up a large area of the droplet. At the 4-day time point there were already noticeable differences in the way the 3D primed aggregates were forming compared to the 2D aggregates, with 3D primed cells forming larger inter-connected webs of small aggregates, compared to the 2D cells forming just one large, aggregate at the bottom of the droplet. The cells appeared to aggregate and compact over the culture time suggesting that gravity was influencing the formation of aggregate structures.

Moving on from this pilot study, it appeared that droplets were able to support the growth of aggregates, but the seeding density needed optimisation. Therefore, an experiment was run using three different seeding densities: 1 x 10^2, 1 x 10^3 and 1 x 10^4 (**Figure 4.22**), with images taken over a period of 10 days to gauge when mature spheroids could be achieved. From these images, it was evident that the lowest seeding density (1 x 10^2) was able to produce spheroids, however they were too small to be practical for imaging applications. The largest seeding density revealed significant differences between 2D and 3D primed cells in how the aggregates formed over time, with the 2D grown HepG2 cells forming a wide 'lawn' of cells at the bottom of the droplet in the earlier time points, which gradually folded in on itself and compacted to form a more spheroid-like structure at 10 days of culture. The 3D primed cells, like before, formed smaller aggregates that gradually clumped together to form a larger 'multi-aggregate' composed of smaller ones. The macro-structure of the aggregates in this higher seeding density resembles the origin of where the cells came from, with the 2D cells starting with an almost monolayer-like appearance, whereas the 3D cells clumped together more and formed three dimensional structures. Finally, the middle seeding density (1 x 10^3) was able to produce mature, consistent spheroids by the 7-day timepoint consistently.

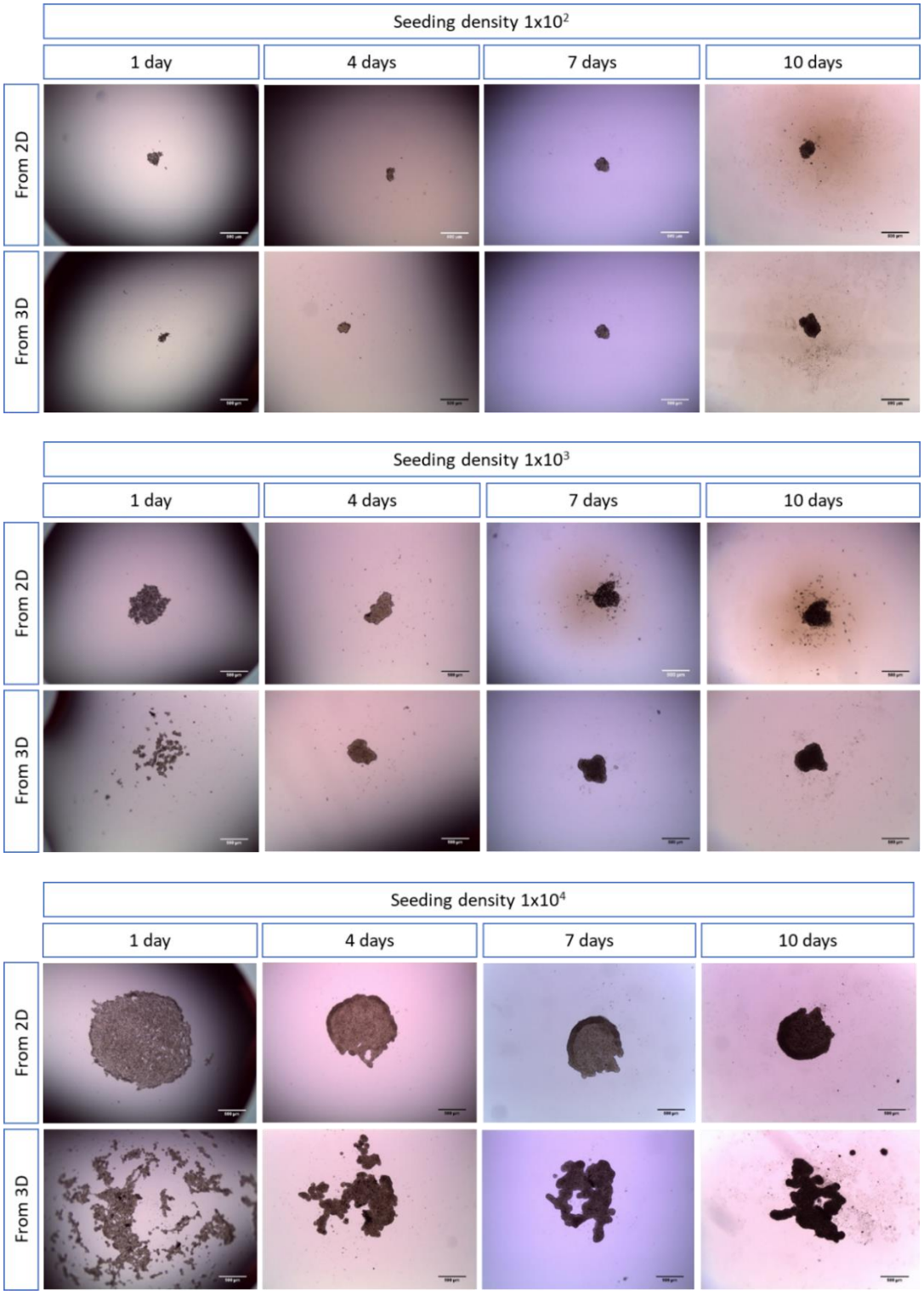

Figure 4.22: A seeding density of 1x10^3 and 7 days of growth is optimal for spheroid formation.

Light microscopy images of hanging drop aggregates created from cells liberated from 2D flasks or Alvetex® Strata. Cells seeded at either 1 x 10^2, 1 x 10^3 or 1 x 10^4 cells per drop and imaged at 1, 4, 7 and 10 days of growth. Scale = 500 µm.

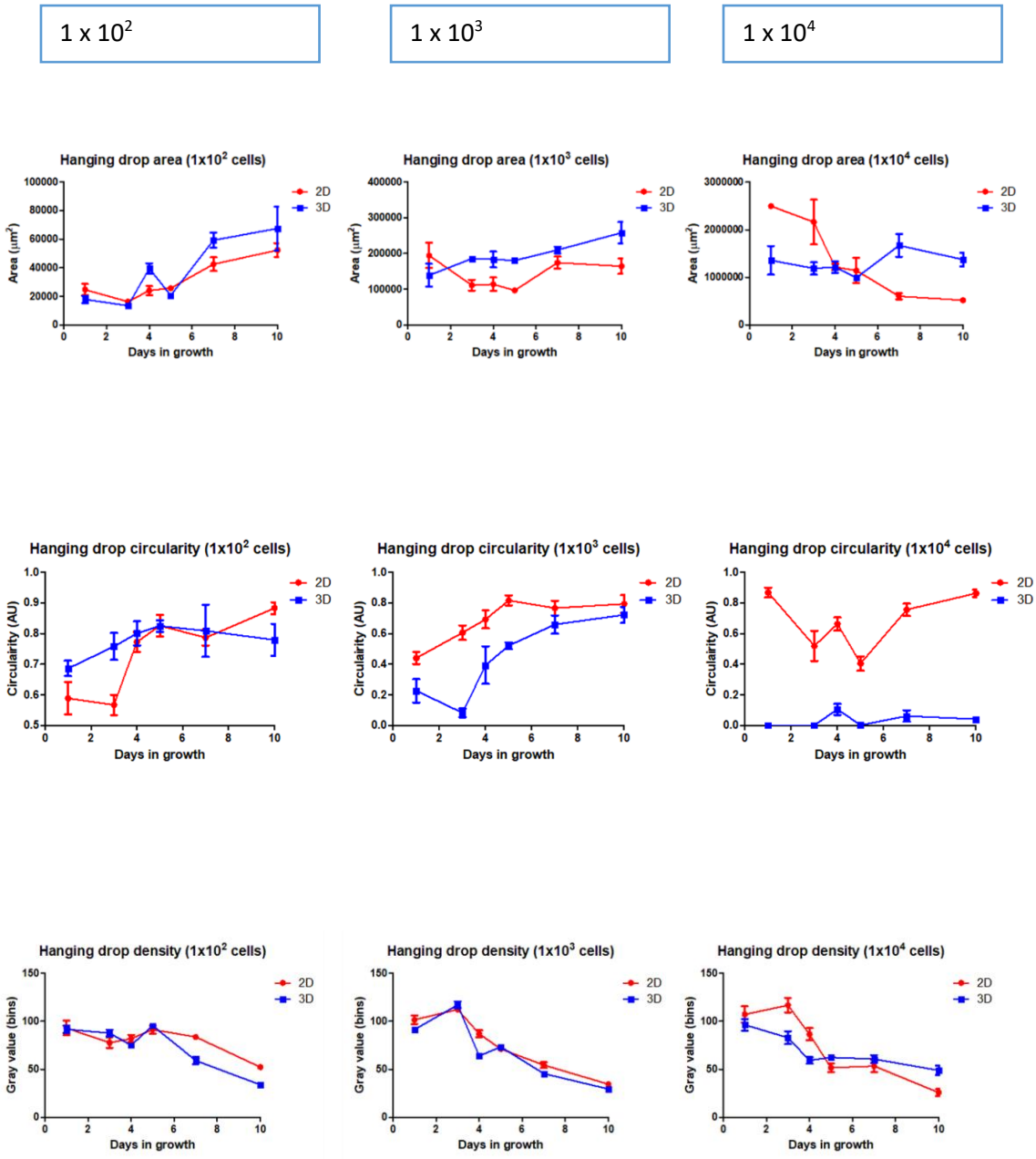

Figure 4.23: Quantification of spheroid formation.

Quantification through ImageJ of the area, circularity and density of spheroids formed from HepG2 cells suspended in hanging drops over multiple time-points. All quantification performed in image J (see methods). Cells seeded at either 1 x 10^2, 1 x 10^3 or 1 x 10^4 cells per drop. N=3 n=20

Quantification of the structural qualities of these aggregates (**Figure 4.23**) revealed that interestingly, only the aggregates from 2D cells in the highest seeding density compacted over time. The 3D primed aggregates in the higher density compacted at first, but area measurements increased in the later stages, possibly because of the more complex shape of these aggregates compared to the aggregates from 2D. In the other two seeding densities, the aggregates grew slightly bigger as the culture time increased. Circularity measurements were not reliable in the 3D primed aggregates in the higher seeding density due to the complex nature of these shapes. In the lower two seeding densities, the areas of the 3D primed aggregates were slightly larger than the aggregates grown from 2D. An increase in circularity is seen in the two lower seeding densities, showing that as time increased, mature spheroids were created, with the circularity measurements stabilising at 7 days. In the seeding density of $1x10^3$ cells, the 3D primed aggregates clearly have a lower circularity than the 2D aggregates initially, though this equalises more as culture time increases. Density of the spheroids was measured through the average grey value in ImageJ, and lower values indicate darker images suggesting a denser aggregate. In all cases, density of the hanging drops increased as time passed, with 3D primed aggregates only presenting as marginally denser than 2D aggregates.

Propidium iodide and phalloidin stained spheroids were also imaged in the seeding densities of 1×10^3 and 1×10^4, with the spheroids of a density of 1×10^2 being too difficult to retain through the processing. **Figure 4.24** shows these images, and there is little difference in the cell death between aggregates formed from 2D or 3D primed cells, however there is a clear increase in dead cells in the centre of the aggregates of 1×10^4 cells compared to aggregates formed from 1×10^3 cells. The lower density of the two shows evidence of a small amount of cell death occurring in the centre, with red propidium iodide staining being present, but this is much less than experiment with the low adherence aggregates and the higher seeding density condition in this experiment. In the lower density, the aggregates have formed very clear spheroids with a defined edge, and therefore a density of $1x10^3$ cells per drop was chosen, and aggregates would be grown for 7 days. **Figure 4.25** shows a repeat experiment using the final chosen seeding density and demonstrates that a consistent spheroid size could be achieved using these conditions and the hanging drop technique.

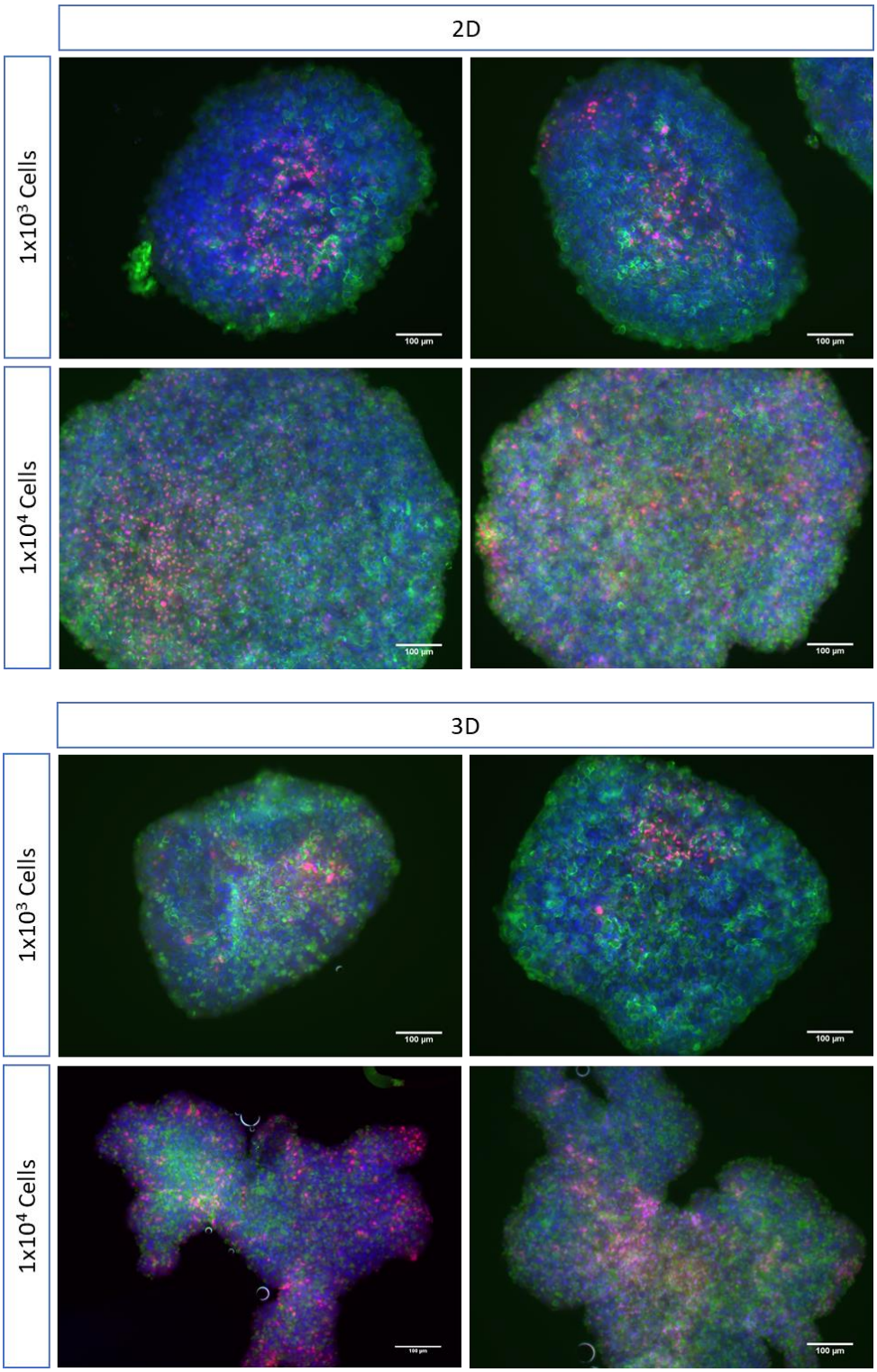

Figure 4.24 Cell death is reduced significantly by using lower seeding densities in spheroids.

Fluorescent images of hanging drop spheroids formed from 2D and 3D primed cells, stained with phalloidin (green), Hoechst 33342 (blue) and propidium iodide (red). Scale = 100 µm

The quantifiable qualities of the optimised hanging drops (spheroid area, circularity, and density) at 7 days were compared to those qualities in the low adherence aggregates in **Figure 4.26.** This clearly demonstrates how the hanging drops were much more comparable in terms of their origin (2D or 3D) than the low adherence aggregates, as both density and area were significantly different in 3D primed low adherence aggregates, but no significant difference is seen in the hanging drop quality. Consistency in the secondary models regardless of their origin is desirable, as any differences in function can be more finely attributed to the changes in cellular function. Inconsistently sized/shaped aggregates and may result in restricted nutrient/drug access which would result in altered function, but that would be hard to deconvolute from the effects of the priming on the cells themselves and the altered biological properties within single cells. This data therefore indicates that hanging drops are an ideal technique for forming a secondary model, by being cheap, simple to use, and possessing high throughput potential after 3D priming (one priming model could easily seed over 100 hanging drops). The low adherence aggregates, while ruled out, did reveal some unique insights into how priming was able to alter how aggregates formed when cells were left to spontaneously assemble.

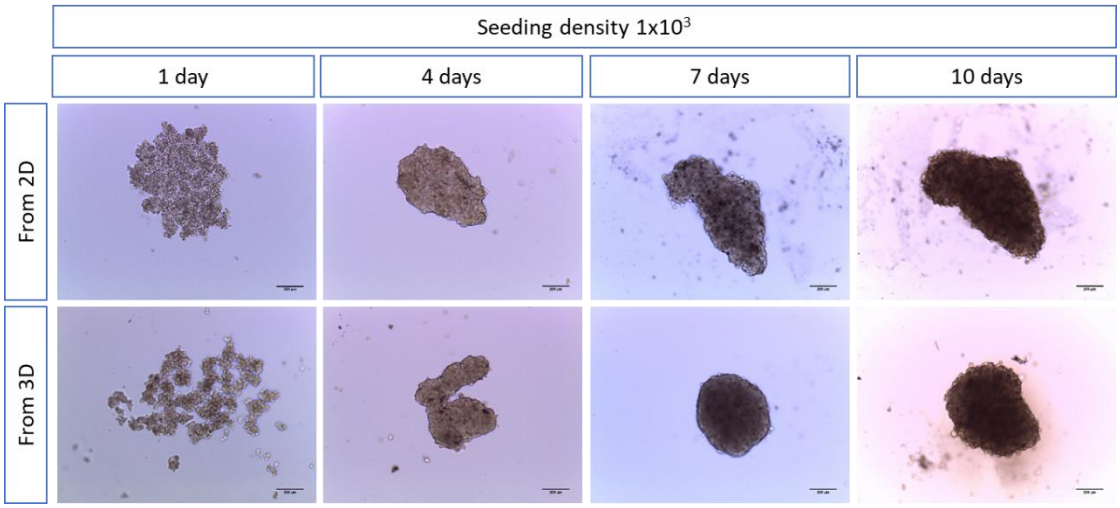

Figure 4.25: Optimised hanging drops were able to form tight spheroids after 7 days in culture.

Light microscopy images of hanging drop aggregates created from cells liberated from 2D flasks or Alvetex® Strata. Cells seeded at 1 x 10^3 cells per drop and imaged at 1, 4, 7, and 10 day's growth. Scale = 200 µm

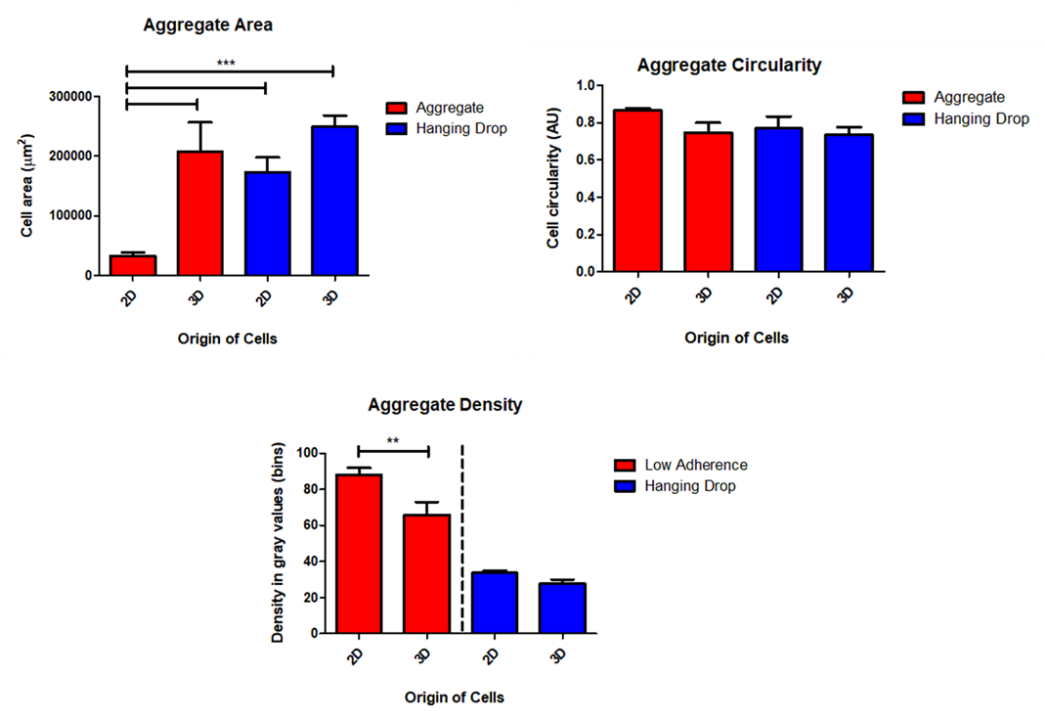

Figure 4.26 Aggregates formed as hanging drops have more consistent characteristics than aggregates formed in low adhesion plates.

Top left: Quantification of aggregate area (µm) performed on ImageJ. Top right: Quantification of aggregate circularity (AU) performed on ImageJ. There are no significant differences in circularity. Bottom: Quantification of density (bins) performed on ImageJ. Density represents grey values and lower numbers indicate denser aggregates. Density is incomparable between phase contrast and light microscopy, however there is no longer a significant difference between 2D and 3D primed cells in the hanging drop cultures compared to the low adherence Petri dish. N= 3, n= 5. Error bars = SEM.

With a secondary model now optimised, the next step was to begin more in-depth characterisation of the HepG2 cells, both during the priming stage and after priming to see how certain structural markers were differentially expressed. Firstly, the priming model was probed with anti-Ki67, a proliferative marker to test for whether cells were still proliferating on the end-stage model, or whether they were all terminally differentiated. As **Figure 4.27** shows, proliferation was occurring in mainly localised areas, specifically towards the top layers of the model. As seen in Chapter 3, when the models were left for longer, cells started dying in the upper layers, and this fits with where the proliferation is seen – the cells are proliferating upwards.

4.44 Structural markers are differentially localised in 3D primed HepG2 cells.

Imaging following on from the Ki67 stain was primarily conducted using three conditions for comparison; 2D cells, 3D primed cells reseeded onto 2D coverslips, and the 3D priming model. Aggregates proved more difficult to image due to the inability of confocal microscopes to adequately capture a full image of the aggregate, with the middle regions often preventing full penetration of light. It was surmised from previous data in this chapter that the retained effects of 3D priming would still be evident in cells reseeded on a 2D substrate. The first structural probe was for N-cadherin (**Figure 4.28**), which is a cell-cell junctional protein, similar in function to E-cadherin, but closely associated with mesenchymal cell populations as opposed to E-cadherin being present in epithelial tissues. As can be seen in this figure, N-cadherin is clearly present at the junctions between HepG2 cells in 2D, 3D and in reseeded 3D primed cells on 2D. The presence of n-cadherin is highly organised in the 2D cells, but there is a slight increase in staining intensity in the 3D primed cells on 2D (middle column) and in this condition, the more island-like structures that arise from 3D priming is also evident. N-cadherin was also present between cells in the 3D priming model, with intense staining, though a slightly more heterogenous appearance, with staining being stronger in certain areas, compared to fairly consistent expression in 2D. This could be an artefact of processing or uneven staining, but it does indicate that the mesenchymal marker is present in all conditions, showing that HepG2 cells are still retaining their cancerous phenotype to an extent.

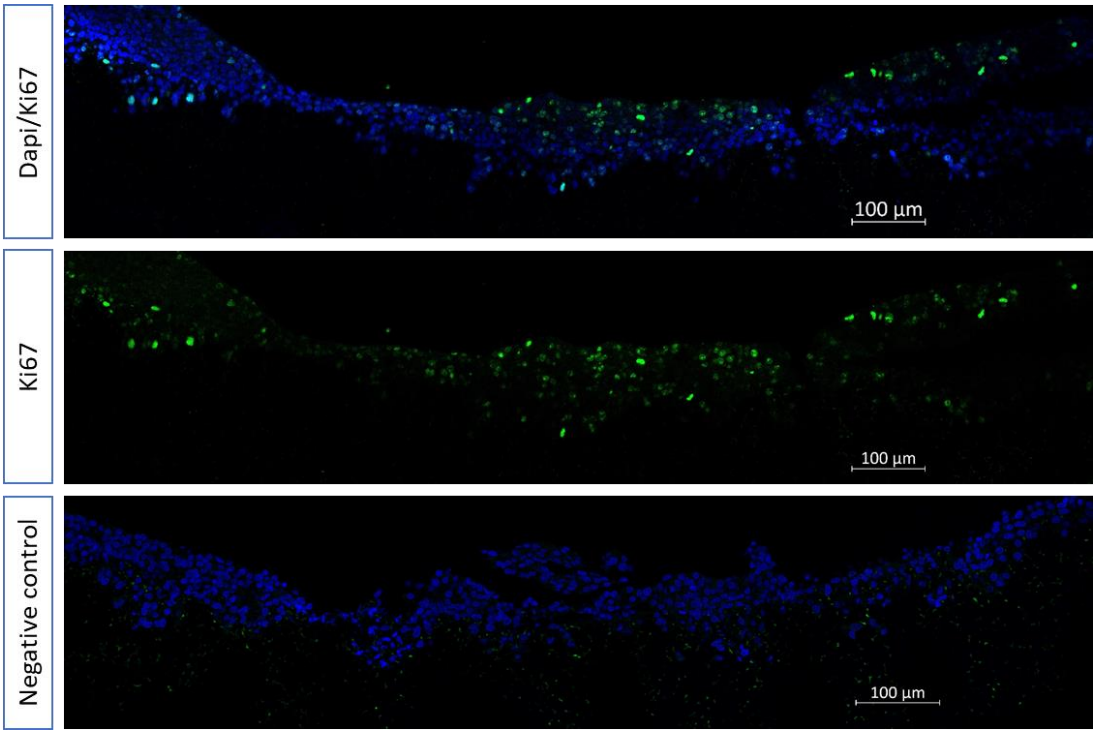

Figure 4.27: Ki67 stains reveal that proliferating cells reside mainly at the top of the cell sheet on the priming model.

Immunofluorescence images from the 880 microscope of cells probed for Ki67 (green) and stained with DAPI (blue). Cells grown for 10 days on Strata using the contact seeding method at a density of 1 x 10^6 cells per insert. Scale bar = 100 µm

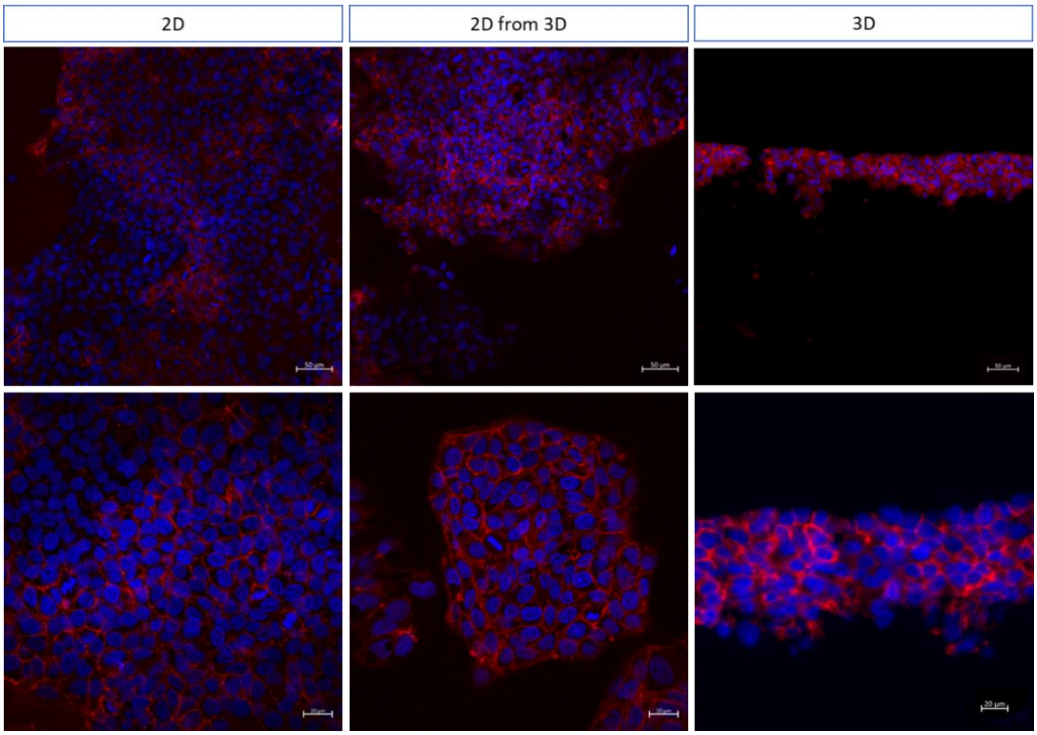

Figure 4.28: N-cadherin appears to form more consistently on 2D substrates.

N-cadherin probed (red) and Hoechst 33342 stained (blue) immunofluorescence images of HepG2 cells grown for 7 days on coverslips after liberation from 2D or 3D priming, or on Alvetex® Strata for 8 days. Cells seeded at a density of 2.5 x 10^5 cells per coverslip and 1 x 10^6 cells per membrane of Alvetex®. Scale bar = 50 µm and 20 µm respectively.

E-cadherin was of interest because this would indicate an epithelial phenotype within the cells, and the presence of this could indicate how similar the model was to *in vivo* hepatocytes, where E-cadherin is known to be expressed. It was expected that this stain would be co-present with N-cadherin due to the previously mentioned presence of both markers in the liver and based on the literature on HepG2 cells. Indeed, E-cadherin expression was observable (**Figure 4.29**), but at a significantly weaker level than N-cadherin. Expression was very heterogenous, with E-cadherin only being present in very specific areas, and there was also a significant level of background, especially in the 2D cultures. Interestingly, the 3D primed cells on 2D seemed to exhibit more intense E-cadherin staining than the 2D cells. The 3D priming cultures expressed stronger E-cadherin staining than the 2D cultures, though it was even more localised in this condition. This could be indicative of some form of metabolic zonation occurring, and perhaps could be linked to alterations in the oxygen concentration across the Alvetex® Strata.

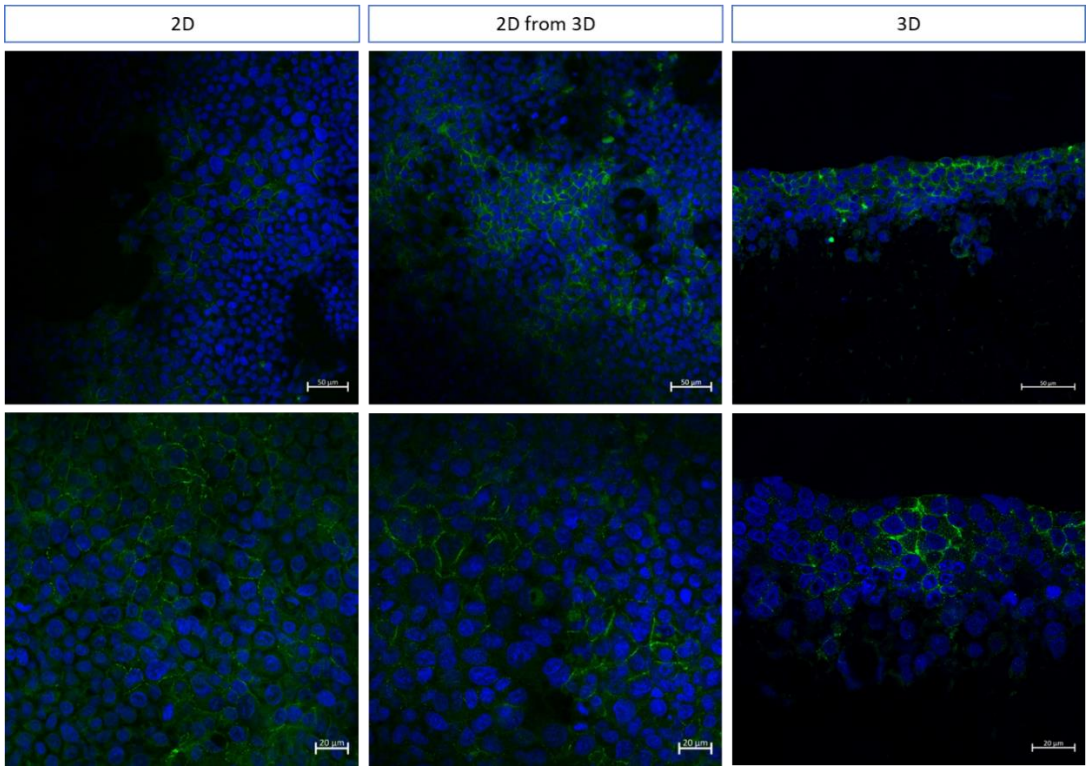

Figure 4.29: E-cadherin weakly stains in HepG2 cells, but appears to be more intense but less ubiquitous in cells grown on a 3D substrate.

E-cadherin probed (green) and Hoechst 33342 stained (blue) immunofluorescence images of HepG2 cells grown for 7 days on coverslips after liberation from 2D or 3D priming, or on Alvetex® Strata for 8 days. Cells seeded at a density of 2.5 x 10^5 cells per coverslip and 1 x 10^6 cells per membrane of Alvetex®. Scale bar = 50 µm and 20 µm respectively.

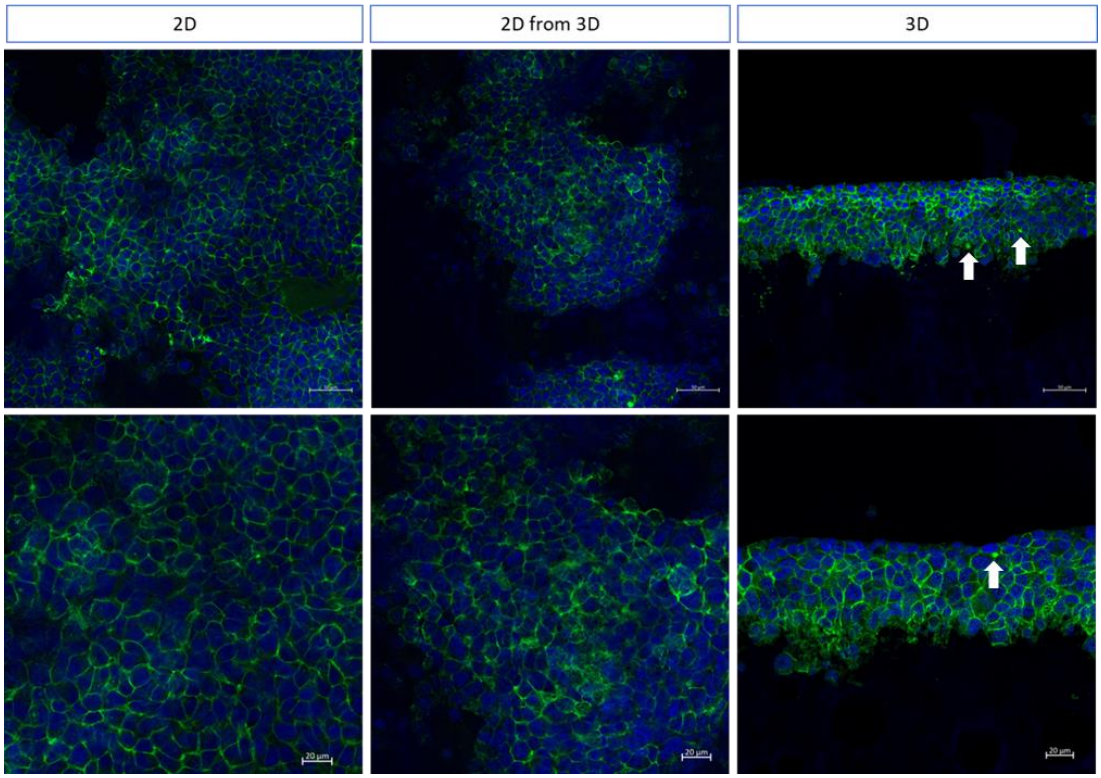

Figure 4.30: Claudin 1 staining is more intense in cells growing on Alvetex® Strata.

Claudin 1 probed (green) and Hoechst 33342 stained (blue) immunofluorescence images of HepG2 cells grown for 7 days on coverslips after liberation from 2D or 3D priming, or on Alvetex® Strata for 8 days. Arrows indicate intense staining 'pools' that could indicate bile canaliculi. Cells seeded at a density of 2.5 x 10^5 cells per coverslip and 1 x 10^6 cells per membrane of Alvetex®. Scale bar = 50 µm and 20 µm respectively.

Claudin 1 is a tight junction protein that is known to be strongly expressed in the liver, and expression in the HepG2 cells was also considerably high, with very clear localisation to the cell edges. With claudin 1 staining in **Figure 4.30** there is no noticeable difference in expression between the two 2D conditions, however, the 3D primed cells on 2D do again exhibit the more three dimensional colony appearance. There is a very clear increase in Claudin 1 staining intensity in the 3D priming model, with the staining lining the edges of all imaged cells, and also unique spots of intense staining seen (white arrows on **Figure 4.30**). Claudin 1 and tight junctions are essential for the highly polarised phenotype of *in vivo* hepatocytes, with claudin 1 particularly being noticeably different in appearance in polarised HepG2 cells – with distinctive pools being seen (Mee et al., 2009). It is possible that the pools of more intense staining seen in the priming model are indicative of bile canaliculi formation and of a more polarised cell phenotype.

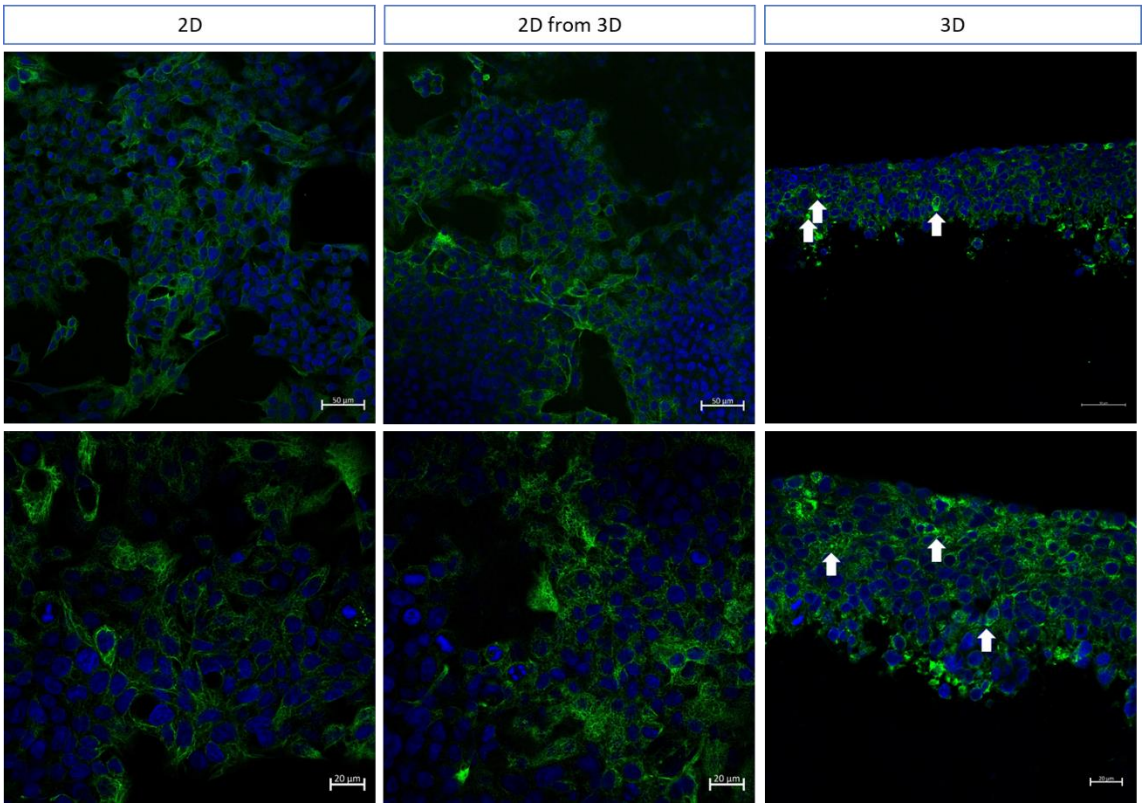

Figure 4.31: Mdr1 stains more intensely in HepG2 cells grown on Alvetex® compared to 2D cells.

Mdr1 probed (green) and Hoechst 33342 stained (blue) immunofluorescence images of HepG2 cells grown for 7 days on coverslips after liberation from 2D or 3D priming, or on Alvetex® Strata for 8 days. Arrows indicate intense staining 'pools' Cells seeded at a density of 2.5 x 10^5 cells per coverslip and 1 x 10^6 cells per membrane of Alvetex®. Scale bar = 50 µm and 20 µm respectively.

Multidrug resistance protein 1 (MDR1) or P-Glycoprotein 1 is a drug transporter protein that is commonly associated with the canalicular membrane in hepatocytes (Cízková et al., 2005). The staining pattern in HepG2 cells of MDR1 tends to be less membrane specific than the prior stains (claudin 1, N-cadherin) but is known to have more intense spots (arrows) where bile canaliculi formation occurs (Wojtal et al., 2006). In both conditions of the 2D HepG2 cells (**Figure 4.31**), the MDR1 staining is diffuse across the cell, showing little specificity for the cell edges, and exhibiting cytoplasmic expression. In the priming model, the stain is still diffuse, but is more intense and more noticeable at the cell edges (see arrows). There are also evidence of more more intense staining noticeable across the HepG2 cells in the priming model, and this – similar to claudin 1 – could be indicative of rudimentary bile canaliculi formation.

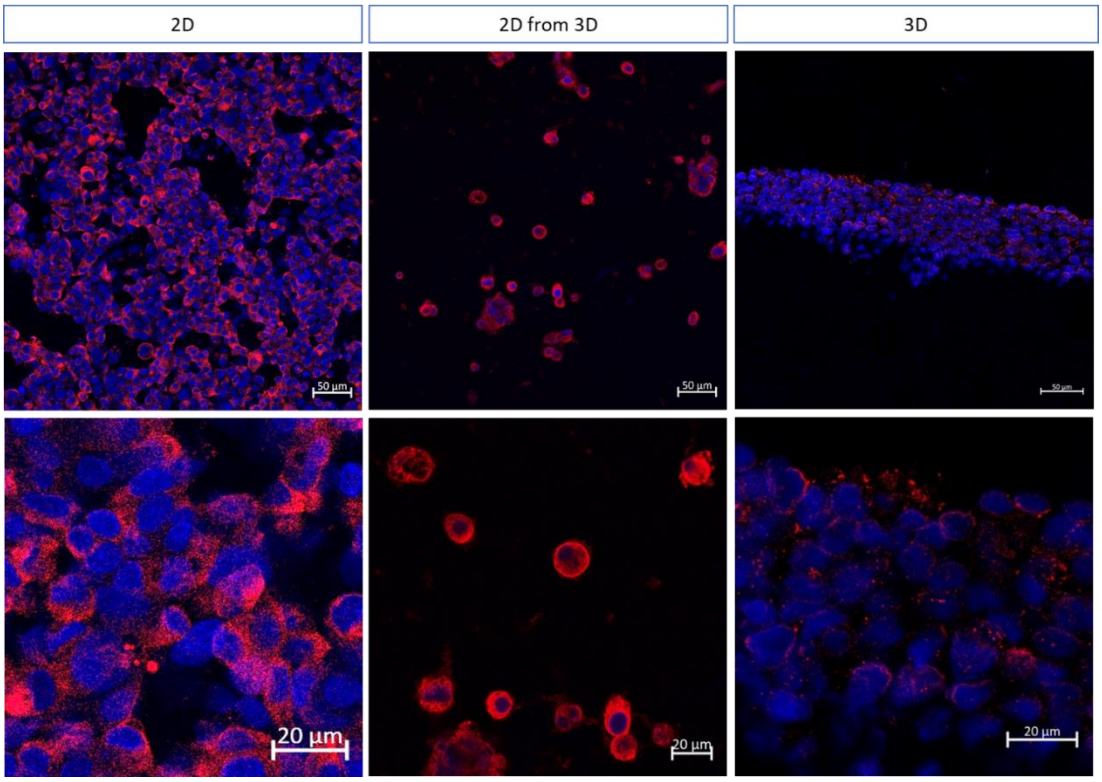

Figure 4.32: Sun1 staining is more intense in 2D cells yet less nuclear specific.

Sun1 probed (red) and Hoechst 33342 stained (blue) immunofluorescence images of HepG2 cells grown for 7 days on coverslips after liberation from 2D or 3D priming, or on Alvetex® Strata for 8 days. Cells seeded at a density of 2.5x10^5 cells per coverslip and 1x10^6 cells per membrane of Alvetex®. Scale bar 50 µm and 20 µm respectively.

The presence of the nuclear laminar proteins sun1 and sun2 was investigated to see whether the altered mechanical properties of the 3D priming model would change the expression or localisation of these important proteins involved in mechanotransduction. Sun1 expression was drastically different between 2D cells and the 3D priming model (**Figure 4.32**) with the appearance of more intense staining in the 2D cells both primed and not than the cells on the 3D priming model. Sun1 did however seem more localised to the nucleus in the 3D priming model whereas the staining was more diffuse and present in the cytoplasm for the 2D cells. This may be indicative that saturation was occuring at the binding sites for Sun1 at the nuclear envelope (Haque et al., 2006).

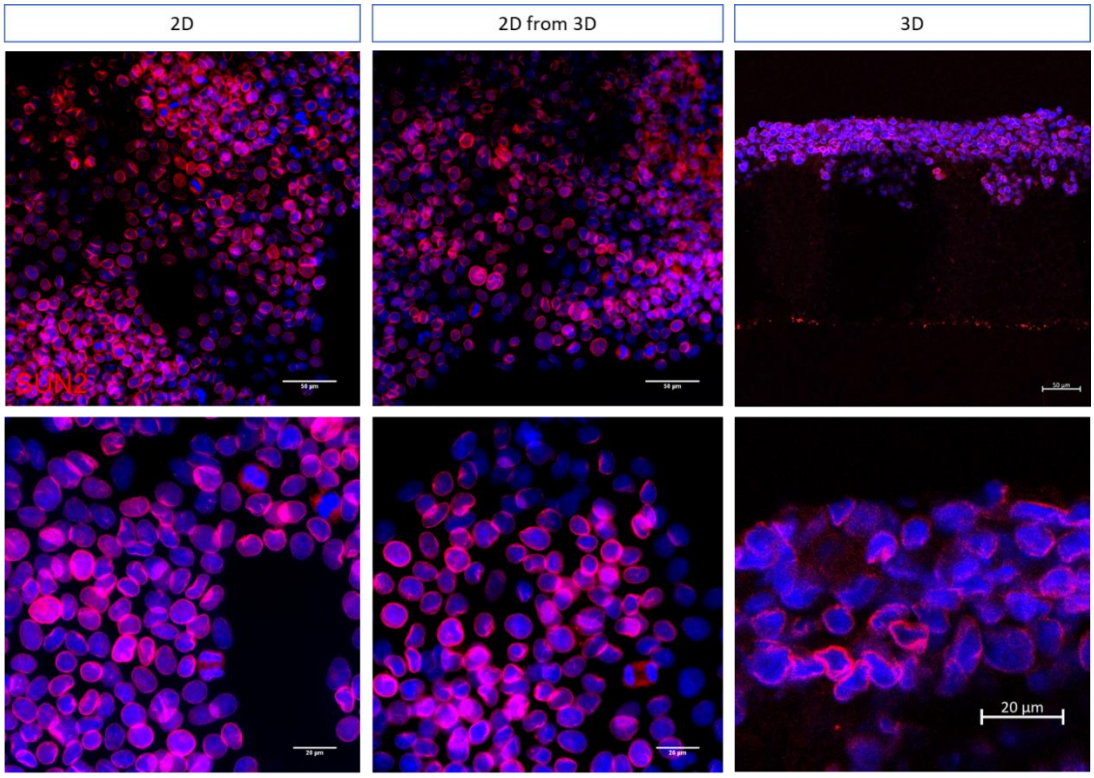

Figure 4.33: Sun2 expression is increased in 2D cells indicating stiffer nuclei.

Sun2 probed (red) and Hoechst 33342 stained (blue) immunofluorescence images of HepG2 cells grown for 7 days on coverslips after liberation from 2D or 3D priming, or on Alvetex® Strata for 8 days. Cells seeded at a density of 2.5x10^5 cells per coverslip and 1x10^6 cells per membrane of Alvetex®. Scale bar 50 µm and 20 µm respectively.

Sun2 (**Figure 4.33**) expression was also significantly different between 2D cells and the 3D priming model. The 3D primed cells on 2D showed little difference to the 2D cells, but both of these conditions had very intense specific staining of sun2 around the nuclei. In the 3D priming model, the staining was a lot less intense but still very localised to the nucleus. It is evident from the sun2 staining on the 3D priming model how different the nuclei are in appearance to the 2D nuclei, with a more deformed shape. The weaker staining of the sun proteins in 3D and the different nuclear shapes suggest that 3D cells have softer nuclei than the 2D cells, and that mechanical forces have indeed resulted in significant internal changes in cell architecture.

When looking at the spheroids themselves, the difference of 3D priming follows a similar pattern as before (**Figure 4.34**). N-cadherin staining appears more localised to the junctions between cells and is slightly more intense in the 3D primed aggregates. MDR1 shows a

heterogenous expression pattern, but the stain appeared more intense in the 3D primed aggregates, and appears to be more specific to the cell edges compared to the faint diffuse staining in the aggregates from 2D. No significant difference was seen in intial Claudin 1 staining, however when using a z stack to fully analyse all focal planes in the spheroids, there was a noticeable increase in the presence of the intense claudin 1 'pools' in 3D primed aggregates (**Figure 4.35 - arrows**) as seen previously in the 3D priming model. To validate this, further quantification through comparative ultra-structural analysis would be required, but it suggests at least that the 3D primed cells are capable of forming important functional structures. This immunofluorescence data indicates that structural differences are occuring as a result of 3D priming, and while the magnitude of these changes equilibrates to an extent in a secondary culture, there are still noteable artefacts of priming. The structural changes may indicate that the primed cells are moving to a more hepatic phenotype in one sense, with an increase in the tight junction markers and bile canaliculi associated markers claudin 1 and MDR1, however the fact that N-cadherin also appears more intense in 3D primed cells suggests that the cells are retaining mesenchymal characteristics.

To assess whether the structure of the HepG2 cells in the priming model resembled hepatic structure *in vivo,* H&E stains of the priming model and human liver were compared (**Figure 4.36**). Despite the presence of other cell types in the human liver, the HepG2 cell morphology in the priming model closely resembled the hepatocytes in the liver, with dense packing, multiple contacts and similar cell shapes/sizes observable. This is further evidence to suggest that priming brings the cells towards a more physiologically relavant phenotype, which will be further investigated through the subsequent transcriptomic and functional analysis. The arrangement of the cells within the model is important as tight junctions for example play a role in the paracellular delivery of hydrophilic drugs (Salama et al., 2006), and the distribution of tight junctions are likely to be modulated (and increased according to the claudin 1 expression) in 3D cell culture. Therefore this has implications for the drug toxicity as well as the intracellular changes occuring due to mechanotransduction.

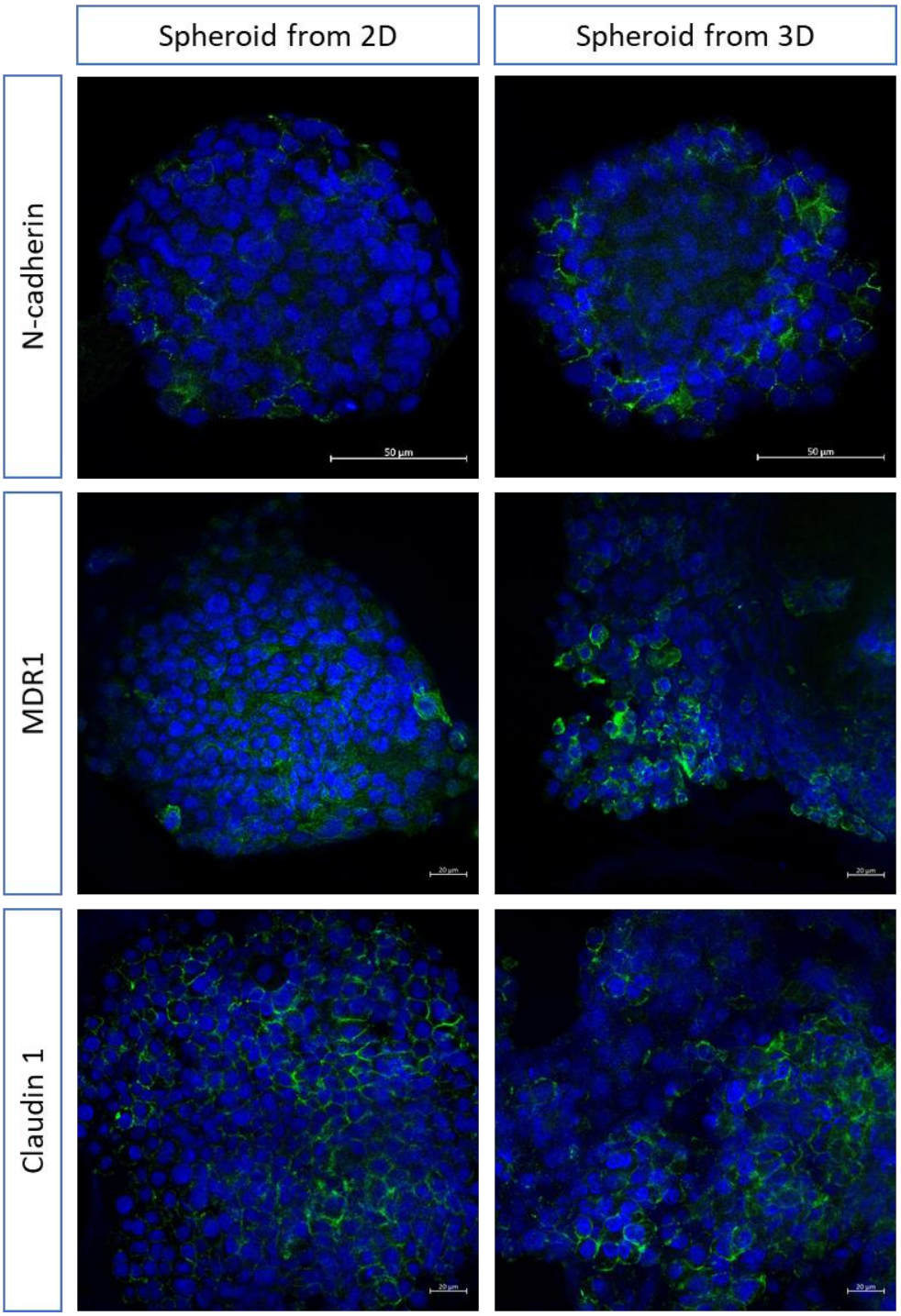

Figure 4.34: N-cadherin and Mdr1 appear to be upregulated in 7 day mature spheroids formed from 3D primed cells compared to spheroids formed from 2D cells.

Immunofluorescence images of HepG2 cells probed for N-cadherin, Mdr1 and Claudin-1 (green) and Hoechst 33342 (blue), grown for 7 days on as hanging drops after liberation from 2D or 3D priming, seeded at a density of 2 x 10^4 cells per aggregate. Scale bar = 50 µm and 20 µm respectively.

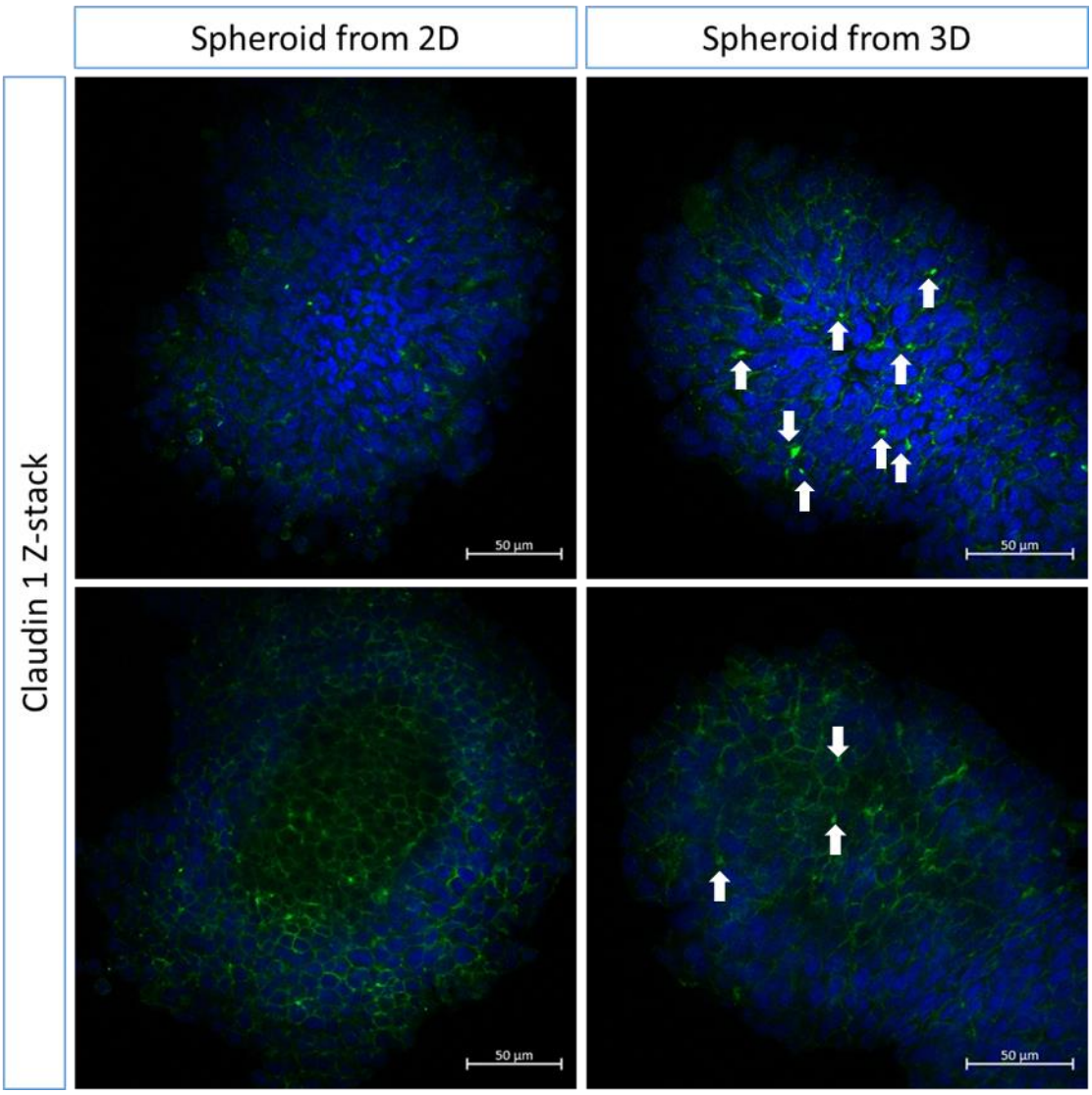

Figure 4.35: There appears to be increased punctate staining of Claudin 1 in 3D primed spheroids, possibly indicating bile canaliculi-like structures.

Immunofluorescence Z-stack images of HepG2 cells probed for Claudin-1 (green) and Hoechst 33342 (blue), grown for 7 days on as hanging drops after liberation from 2D or 3D priming, seeded at a density of 2 x 10^4 cells per aggregate. Arrows show intense staining 'pools' that may be indicative of bile canaliculi. Slices taken from near the top and bottom of the spheroids and are representative of staining patterns observed. Scale bar = 50 µm and 20 µm respectively.

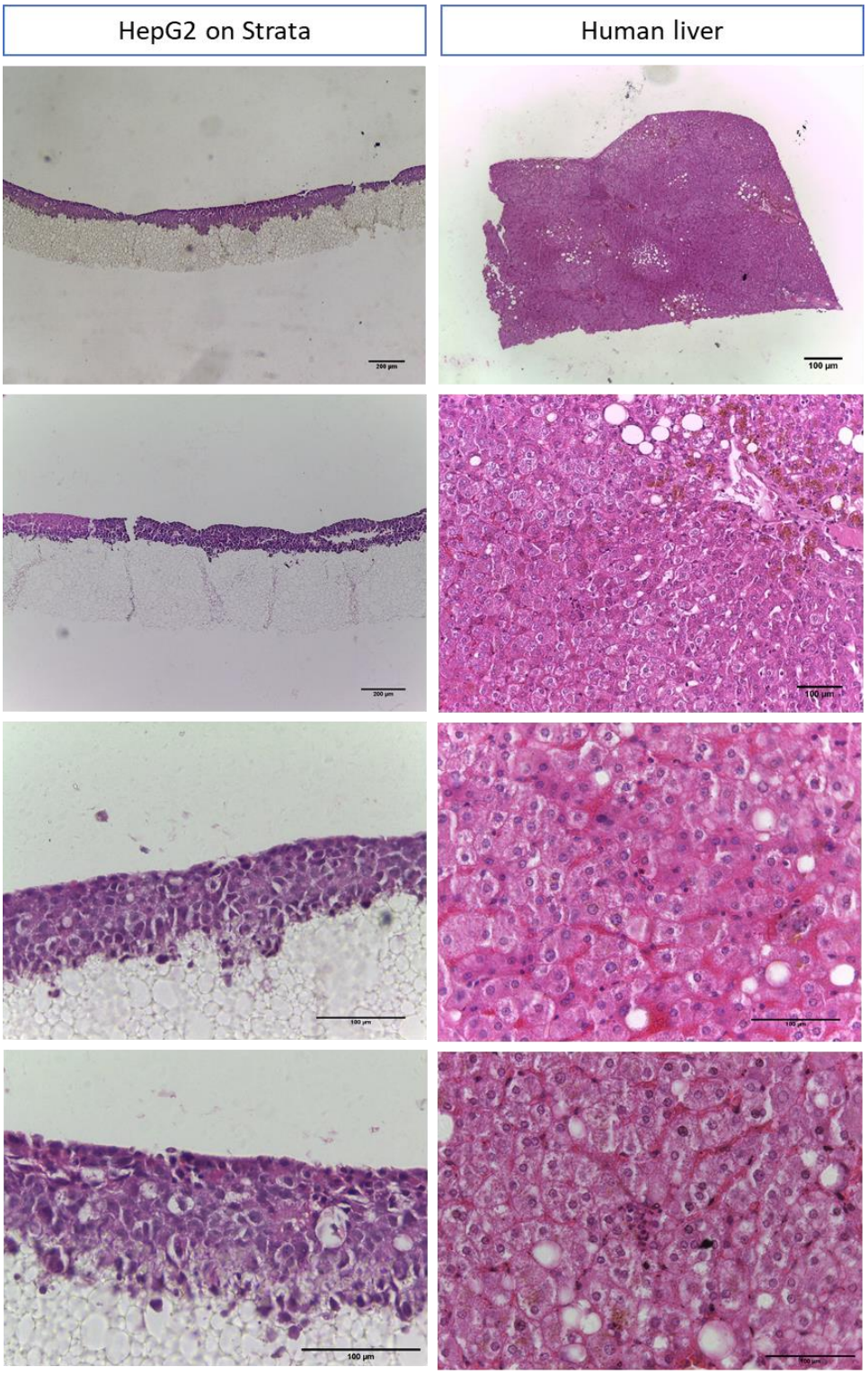

Figure 4.36: HepG2 cells grown on Alvetex resemble the structure of hepatocytes in the human liver.

H&E images of HepG2 cells grown for 8 days on Alvetex® Strata at a seeding density of 1 x 10^6 cells (left) and human liver sections (right). Scale = 200 µm and 100 µm.

4.45 The duration of priming affects the magnitude of the retained morphological changes.

Consideration was given as to when priming starts to have a significant effect on cell structure. Therefore a time-course experiment was set up to investigate this (**Figure 4.37**). This experiment compared cells grown in 2D or in the priming model for either 1, 4 or 8 days before liberation, and then compared the hanging drops formed from these cells, as well as investigating the single cell structure when reseeded onto 2D coverslips.

Looking at the spheroids formed from these cells (**Figure 4.38**), it was clear that cells grown for 8 days in both 2D and 3D were able to create healthier aggregates than the earlier time points, indicating that cells require sufficient time in culture to ensure mature models. This is potentially due to longer culture times permitting the formation of cell-cell contacts and fully confluent layers where the cell structure is fully decided. Spheroids formed from 1 day primed/grown cells often failed to properly form, with evidence of cell death and high debris appearing at the later time points of aggregate formation. There were exceptions, but this indicated that cells were under significant stress having been reseeded after only 1 day of growth in prior culture, having had too little time to properly adhere and settle. Similarly, after 4 days of priming/growth, some spheroids failed to form, though there were more successful aggregates in this instance. Little difference was observable between 2D and 3D primed cells though in aggregate formation however, indicating that this was not enough time for the structures of the cells to settle and mature in the prior culture conditions. Finally, with the 8 days of growth, the differences between 2D and 3D primed cells were not particularly evident in this experiment, but at 4 days of aggregate growth, the 3D primed spheroids possibly exhibited slight differences in structure to the spheroids from 2D cells. While this did not highlight the differences in priming length, it did confirm that allowing cells to grow for longer periods before reseeding is beneficial to the cell population.

The increasing effect of priming with time was more clearly seen in the single cell analysis (**Figure 4.39**), with the differences between 3D primed and 2D cells becoming noticeable at the 4-day time point, and the most visually prominent at 8 days. This follows the same pattern as seen prior in this chapter (**Figures 4.7 to 4.11**), with the 2D cells becoming more spread out and voluminous and the 3D primed cells remaining tight and spherical. Quantification of the cell and nuclear areas in **Figure 4.40** reflects this trend, though interestingly the areas of both 2D and 3D primed cells are slightly smaller on average after 8 days of priming than 4 days.

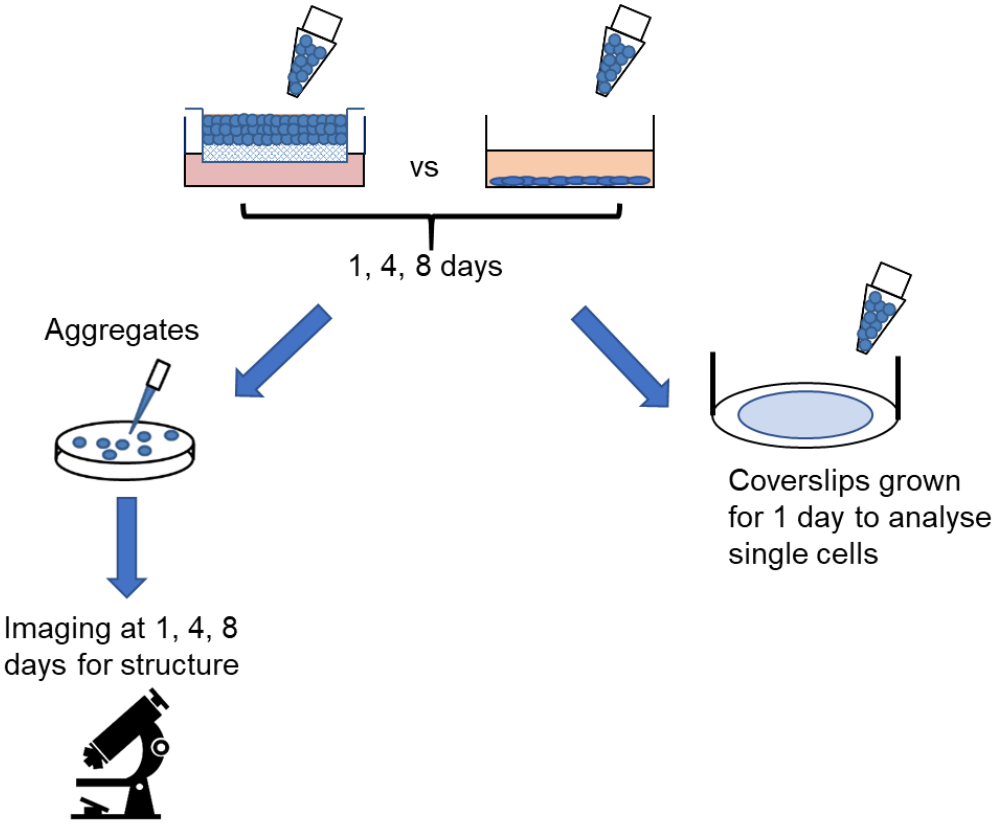

Figure 4.37: Schematic for the time course experiment.

HepG2 cells were grown in 2D or primed in 3D for either 1, 4, or 8 days before either imaging, or liberation for reseeding into hanging drops or onto coverslips. Media was stored at these time points for analysis.

The differences in area between 2D and 3D primed cells only become significant at 4 days onwards though, indicating that priming does require a minimum amount of time to take effect and elicit morphological changes that are retained in subsequent cultures. Interestingly, the nuclear to cell area ratio average decreases as culture time increases, again suggesting that longer time in culture provides chance for the cell to equilibrate to its surroundings, which includes spreading of the cell onto the surface, and alterations in the cyotskeleton and nuclear shapes.

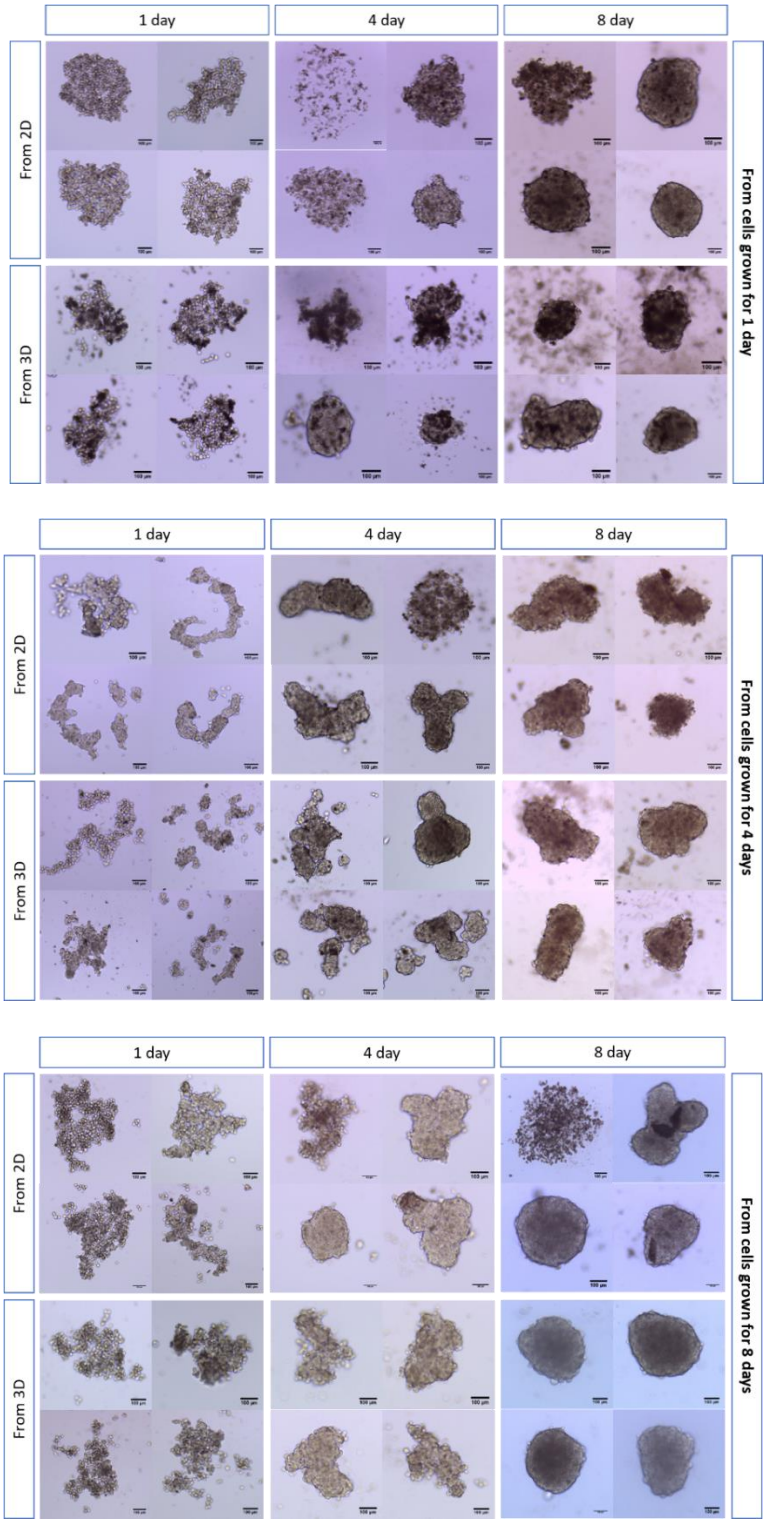

Figure 4.38: Cells in prior cultures for longer were able to form more mature hanging drops.

HepG2 cells seeded as hanging drops at a density of 1 x 10^3 cells per drop and imaged at either 1, 4 or 8 days of growth using brightfield microscopy. Cells were either primed in 3D or 2D for 1, 4 or 8 days of culture before liberation and seeding as hanging drops. Scale bars = 100 µm

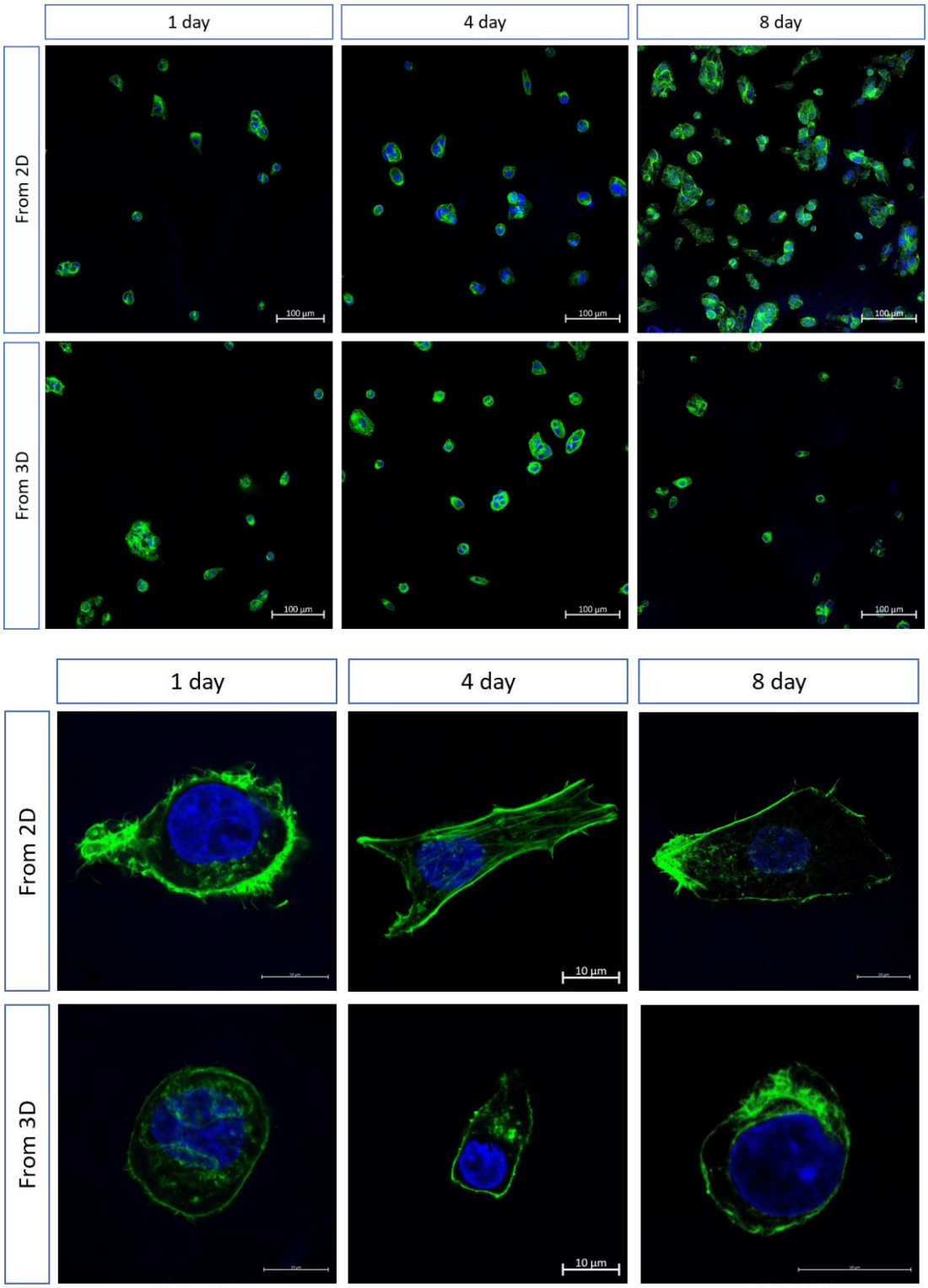

Figure 4.39: Cells primed for 8 days show the biggest difference in cytoskeletal structure between 2D and 3D.

Phalloidin images of HepG2 cells after being plated onto coverslips at a density of $2x10^4$ cells per well and grown for 1 day after 1, 4 or 8 days of priming in either 2D or 3D. Scale bar = 100 µm).

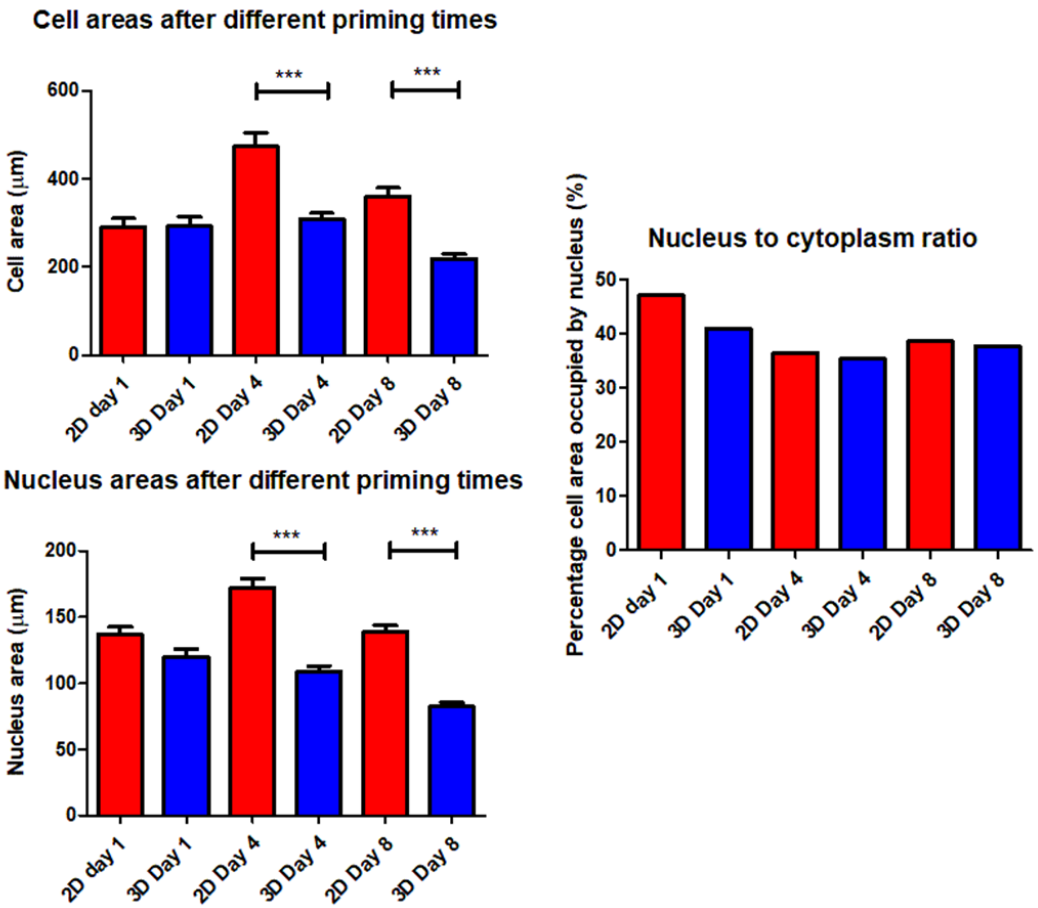

Figure 4.40: Quantification of cell and nucleus areas reveal that both the cells and nuclei of the 2D cells signficantly spread out after 4 or more days of growth compared to 3D primed cells.

Quantification of cell and nucleus areas performed in ImageJ, with the percentage area of the cell that the nucleus occupies displayed in the right hand graph. Over 30 cells measured in each condition. N=3 n= 3, Error bars = SEM

While SEM images had been taken of single, reseeded HepG2 cells, highly detailed images of the cells on the priming model revealed further insights into the growth of HepG2 cells on the Alvetex® substrate, as well as their structures both as a total cell population and as individual cells. The SEM images (**Figures 4.41**) reveal the tight packing of the HepG2 cells on top of the 3D substrate, and highlight how intertwined the cells are with each other in terms of structutre, with projections of the cell body linking the cells together, creating an almost smooth layer of HepG2 cells at the very top (top right and bottom three panels).

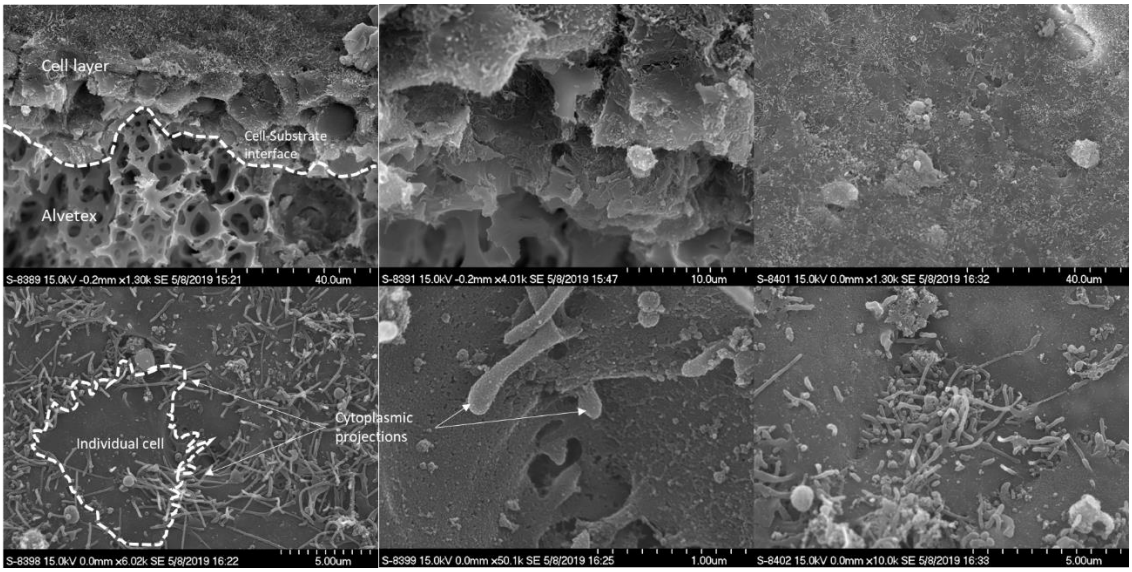

Figure 4.41: SEM images of HepG2 cells grown on Alvetex® highlight the tight packing and close contact of the cells on the substrate.

Scanning electron microscopy (SEM) images taken of HepG2 cells seeded onto Alvetex® at a density of 1x10^6 cells and grown for 8 days.

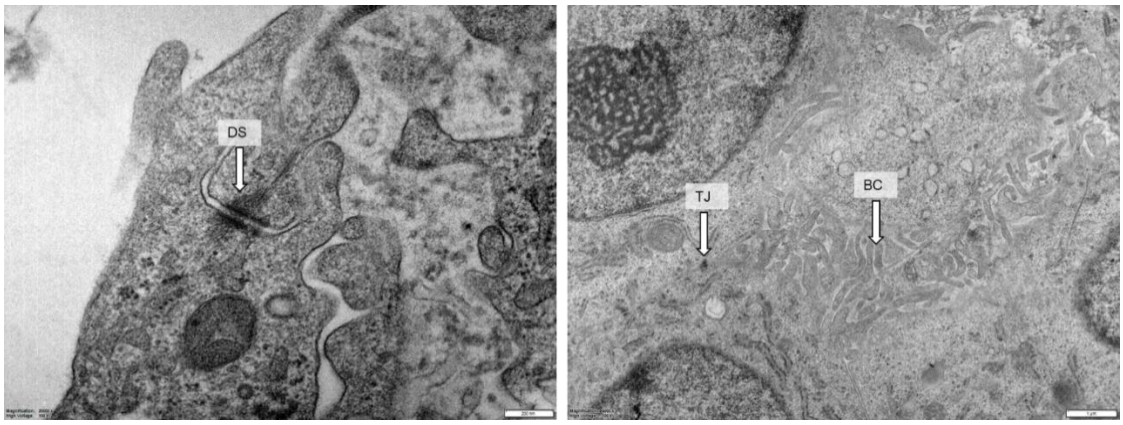

Figure 4.42: TEM images of HepG2 cells grown on Alvetex® highlights the presence of desmosomes, bile canaliculi and tight junction formation.

Transmission electron microscopy (SEM) images taken of HepG2 cells seeded onto Alvetex® at a density of 1x10^6 cells and grown for 8 days. DS = desmosome, TJ = tight junction, BC = bile canaliculi. Scale: 200 nm and 1 µm

It is not surprising that with this extraordinarily close arrangement of cells that the structure is considerably altered. Transmission electron microscopy (TEM) images of the HepG2 cells in the 3D priming model (**Figure 4.42**) further highlight how the cell morphology in 3D is able to form complex structures that help to interlink the cells on the model. These images were also able to detect potential evidence of bile canaliculi, as well as the presence of desmosomes and tight junctions, indicating that these cells are polarising during priming and producing important structures that are key determinants of hepatic function.

4.5 Discussion

4.51 Priming cells in 3D creates a memory of the three-dimensional structure that is preserved after liberation.

There is a growing body of evidence that points towards the benefits of priming in specific applications (Barthes et al., 2015; Lech et al., 2020; Sart et al., 2014), however there is still a lack of research into the specific effect of the bio-physical properties alone of these priming conditions on the structure and functionality of the cells. Therefore, this chapter focussed on the structural implications of using a biologically inert substrate to provide an altered surface topography for cell culture.

Throughout this chapter, evidence has been provided to indicate that through growing HepG2 cells on a three-dimensional topography, they adopt a more three-dimensional phenotype. Alterations in the macro-structure of the cell populations were observable even 7 days after reseeding 3D primed cells (**Figures 4.2 – 4.5**), suggesting that internal changes have taken place to fundamentally alter the biology of the cells. These changes were suspected to be related to the cytoskeletal machinery, expression of junctional and other structural genes, and mechanosensitive elements of the cell. This chapter was able to assess the two former areas, by thorough morphometric analysis on the cell shape, and the cytoskeletal organisation in individual cells, as well as the presence and localisation of certain structural markers with immunofluorescence.

The actin cytoskeleton was focussed on particularly here due to its mechanosensitive nature as discussed in the introduction, and its association with mechanotransduction. Through primarily phalloidin staining, in depth analysis was carried out on single cells that had been reseeded onto coverslips after either priming in 3D or growing in 2D. The differences between the two culture origins were clear to see on the coverslips, with 3D primed cells presenting a highly reproducible phenotype of being smaller in cell area and more spherical, whereas 2D grown cells were spread out, flatter and presented significantly larger areas. This repeated observation pointed towards a mechanical memory in the HepG2 cells that depended on historical substrate geometries. **Figures 4.11** and **4.12** indicated the involvement of the actin cytoskeletal machinery in this, through the observation that interfering with Arp2/3 and ROCK1 particularly appeared to partially restore 2D cells to a 3D phenotype. SEM images (**Figures 4.13, 4.14**) provided highly detailed images of the cell shapes after reseeding from 3D or 2D, and the difference was very substantial, with the 2D

cells clearly exhibiting a more 'traditional' two-dimensional phenotype, with a mesenchymal appearance. The 3D primed cells however in general showed an ability to preserve a spherical shape with much less evidence of cell spreading onto the substrate, providing further proof that these have adopted a memory of their culture origin and are more adapted to a complex microenvironment.

Papers have suggested that over longer periods (>3 days), altered localisation and activation of key mechanotransducers such as YAP/TAZ (C. Yang et al., 2014) and altered transcriptional states are responsible for creating a 'memory' response in cells (Mathur et al., 2020). These could be underlying mechanisms responsible for the 'memory' observed in the HepG2 cells here, and that is investigated through analysis expression of key mechanotransduction genes in **Chapter 5**. What has been made clear throughout this chapter however is that growing cells in a 3D environment – in this case Alvetex® – is sufficient to produce a three-dimensional phenotype in the HepG2 cells that is preserved after liberation, and that prepares the cells for a secondary 3D culture.

4.5.2 Priming cells in 3D prepares them structurally for subsequent 3D models by producing a retained three-dimensional phenotype within the cells.

The secondary 3D culture used in this case was an aggregate model, with spheroids proving a useful model for cytotoxicity studies in hepatocytes (Shri et al., 2017). This model was challenging to optimise at first, due to the inconsistent aggregate sizes, shapes and densities of cells in the first iteration of the technique which used a low adherence Petri dish to allow spontaneous self-assembly of aggregates (**Figures 4.14** to **4.18**). This stage of optimisation was still useful to further indicate that priming cells in 3D before-hand improves the aggregating capacity of the cells, and better prepares them for assembly into 3D structures. Interestingly, the low adherence aggregates formed from 3D primed cells were denser and formed large 'multi-aggregates' as confirmed by phalloidin staining, whereas the 2D grown cells displayed a lower tendency to aggregate in this large-scale manner (**Figure 4.16**). The low adherence aggregates also displayed signs of significant cell death occurring in the hypoxic core of the aggregates, which further indicated the unsuitability of the low adherence technique as a secondary model.

Through optimising the second iteration of the aggregate model – the hanging drop technique – the 3D primed cells still displayed a propensity to form more three-dimensional structures, whereas at higher seeding densities, 2D grown cells created more lawn-like cell

layers that lay at the bottom of the droplet (**Figure 4.21**). Through morphometric analysis of the hanging drops over a time course of 10 days, it was revealed that seeding density was a significant driver of spheroid structural integrity, with the higher seeding density of $1x10^4$ cells resulting in a completely compromised circularity of the 3D primed cell aggregates, as these cells had a propensity to form networks of smaller aggregates rather than one uniform spheroid. The differences between 2D and 3D primed cells in forming aggregates implicates differential expression of junctional proteins on the cell surface, especially when the patterns of larger 3D primed aggregates seen in the low adherence aggregates are also considered.

E-cadherin for example is particularly important in mediating the formation of multicellular epithelial spheroids, and the actin cytoskeleton is closely associated with adherens junctions, with E-cadherin also being essential in epithelial sheet formation (Stadler et al., 2018). It is logical then, that the changes in the cytoskeleton, and the altered aggregate formation suggest altered expression of junctional proteins such as adherens junctions. Differential E-cadherin has been demonstrated to affect spheroid formation in a number of cell lines, including hepatocellular carcinoma cell lines where highly variable E-cadherin expression depending on the mutations present in the HCC lines was reflected in variable spheroid morphology (Pomo et al., 2016). E-cadherin was shown to be directly involved in the transition from loose cell aggregates to compact spheroids (Lin et al., 2006), and this may explain the 'looser' phenotype observed after shorter priming periods in **Figure 4.36** where E-cadherin expression potentially did not have time to stabilise. Conversely, studies have indicated that N-cadherin is not an essential molecule for spheroid formation when other complex cadherins are expressed (Lin et al., 2006; Shimazui et al., 2004).

In the morphometrics of the hanging drops, it was also revealed that the structures had a tendency to both slightly increase in area and in density at the lower seeding numbers ($1x10^2$, $1x10^3$), indicating that cells are still proliferating within the model, as the properties of the spheroids are changing as time progresses. The statistics in general indicate a much more consistent set of structural properties between hanging drop spheroids from 2D and 3D priming, compared to the low adherence aggregates (**Figure 4.25**). Cell death was also drastically decreased in the hanging drops due to the smaller size than in the low adherence aggregates, though it was still detectable to a small extent in the centre, indicating a slightly hypoxic environment present (**Figure 4.23**).

Ultimately, an optimised secondary model was produced, through seeding 3D primed or 2D HepG2 cells at a density of 1×10^3 cells per droplet and culturing them for 7 days. This

produced mature, tight spheroids that were much more consistent regardless of culture origin, meaning that functional qualities could be better assessed and compared in later chapters.

4.5.3 Key structural markers appear more intense in the 3D priming model, indicating a polarised phenotype with better suitability as a liver model.

Based on the differences seen in the aggregates and on the reseeded cells on coverslips, it was hypothesised that differences were present in important structural proteins such as junctional markers like Claudin-1 and E-cadherin, and that this in combination with the internal mechanical alterations would result in the altered behaviour of 3D primed cells after re-seeding. Histologically, the cells in the priming model closely resemble *in vivo* hepatocytes (**Figure 4.35**) which gives reason to hypothesise that the priming model will produce more physiologically relevant characteristics in the HepG2 cells.

This section presented a significant body of evidence to point towards this hypothesis, with the junctional markers E-cadherin, N-cadherin staining noticeably more intensely in the HepG2 cells in the 3D priming model. The staining revealed a tighter organisation of cells in the priming model (**Figures 4.27, 4.28**), but was distinctively heterogenous in nature with E-cadherin specifically, whereas N-cadherin was more present across the whole cell layer. E-cadherin is known to be poorly expressed in HepG2 cells (Yano et al., 2001), but it is not known why in 3D here the expression is so clearly localised to specific areas. It is possible that localisation of the E-cadherin is stronger at the lateral junctions of the HepG2 cells in the 3D priming model which is similar to the expression pattern of β-catenin in polarised HepG2 spheroid models (Ramaiahgari et al., 2014a). It is also possible that some basic form of metabolic zonation is occurring in these cells when in 3D, but this would require further study due to the more homogenous expression of n-cadherin raising questions. In the 3D primed cells reseeded onto 2D, the difference in expression of E-cadherin and N-cadherin was less noticeably altered, however as seen in the neutral red stains, the 3D primed cells had formed more noticeable individual colonies. It is possible that by the 7-day time point at which these were imaged, the expression of many bio-markers had equilibrated between the 2D cells and 3D primed reseeded cells, however it is likely there were significant differences in the expression of these junctional markers during the early stages of growth on the coverslips. This would suggest that a time course imaging experiment would be an interesting future direction, to see how junctional expression might normalise as the secondary culture progresses. When imaging the spheroids themselves (**Figure 4.33**), E-

cadherin expression unfortunately was hard to detect on the whole mount spheroids, however N-cadherin was observable and there was also a possible slight upregulation in the outer edges of the 3D primed spheroids, indicating a knock-on effect from priming.

Claudin-1 particularly appeared significantly upregulated in the 3D priming model (**Figure 4.29**), suggesting a higher presence of tight junctions between the cells, and a more polarised phenotype present in 3D, and distinctive spots of intense staining were present in 3D, which could be indicative of bile canaliculi structures forming. There was little difference between 2D cells and 3D primed cells on 2D, other than marginally more intense staining in the 3D primed cells in specific areas. In the spheroids, while there was little difference in staining intensity, there was a possible increase in the intense spots present in the 3D primed spheroids, indicating an improved tendency to form bile canaliculi-like structures (**Figure 4.34**).

MDR-1 stained unusually in HepG2 cells, with the expected pattern being localised to the cell edges (**Figure 4.30**), however the observed staining pattern was diffuse across the cytoplasm. This has been seen in literature, (Wojtal et al., 2006), and could be indicative of impaired trafficking of MDR1 to the bile canaliculi membranes by the golgi apparatus. In the 3D priming model though, the MDR-1 did appear to be more intense at the cell edges, potentially implying a partially restored trafficking of the protein, and in turn, improved drug trafficking. In the spheroids (**Figure 4.33**), MDR-1 appeared more intensely in 3D primed spheroids, again indicating that the 3D microenvironment had pre-conditioned the cells for a three-dimensional system.

Sun1 and sun2 exhibited the most intense differences between 2D and 3D cells, with the expression of both of these markers being very much increased in the cells on the 2D coverslips (**Figures 4.31, 4.32**). Sun proteins are essential linker proteins that connects the cytoskeleton to the nucleus and are therefore heavily implicated in mechanotransduction. Sun2 particularly is heavily localised to the edge of the nucleus in the 2D cells, whereas in 3D, there is still nuclear localisation, however the stain is much less intense. Sun1 is less specific to the nucleus, appearing diffuse in the cytoplasm of many 2D cells, but is barely detectable in 3D, again pointing to the same pattern. The cytoplasmic presence could indicate saturation of Sun1 proteins at the nuclear membrane (Haque et al., 2006), which would suggest a high level of Sun1 already present around the nucleus, but on the other-hand it may be an indicator of aberrant trafficking similar to what is suggested with MDR1. These staining profiles suggest that the cells in 2D have a much more rigid nucleus with a

more structured connection to the actin cytoskeleton, whereas the 3D cells have a malleable deformable structure, and this is consistent with existing papers (Alisafaei et al., 2019; Lovett et al., 2013). These papers also indicate that altered substrate geometries induce actomyosin dependent shuttling of epigenetic factors that alter the nuclear morphology, nuclear stiffness and the gene expression, with smaller spherical cells exhibiting softer nuclei, disrupted actomyosin contractility and increased nuclear chromatin condensation. This correlates with the cytoskeleton experiments earlier in the chapter, and backs up the hypothesis that 3D culture induces an altered mechanical state, which results in epigenetic changes that persevere after liberation.

4.5.4 Priming cells for longer periods creates a more pronounced three-dimensional phenotype.

As prior evidence suggests (Mathur et al., 2020), this chapter found that longer periods of pre-conditioning cells on a particular substrate stiffness result in a stronger effect on the structural properties after reseeding. While the hanging drop time-point experiment (**Figure 4.37**) did not unveil a particularly noticeable difference between 2D and 3D primed cells, it did reveal the importance of culture time in allowing cells to settle and adapt to their environment before liberation and reseeding. Reseeding cells from 2D or 3D into hanging drops after less than 8 days culture time resulted in a significant number of failed spheroids where the cells did not aggregate properly, and there was a high amount of debris. The debris was particularly noticeable in the 1-day 3D primed spheroids, and this is likely due to the very low cell yields at this early stage meaning that scraping of the substrate had to be more vigorous to retrieve a sufficient cell number. This debris may therefore be an artefact of mechanical damage to the polystyrene substrate, rather than a biological factor, however the nearly complete lack of mature aggregates after 1 day of prior culture does indicate that there is a minimum amount of culture time required before liberation. Longer time in a culture system will allow the cells to form sufficient junctional complexes and will grant time for the expression of these and other structural genes to normalise.

The length of priming time had a more prominent effect however on the structure of the individual cell, with the single cell morphometric analysis on the cytoskeleton (**Figures 4.38, 4.39**) showing that growing cells on the three-dimensional surface of Alvetex® for longer resulted in a progressively smaller nucleus priming time increased, however cell area only decreased significantly after 8 days of priming. With 2D cells, interestingly the areas of reseeded cells and nuclei was greatest after 4 days of 2D growth, with increased areas over

1-day culture time still shown after 8 days, but at a smaller magnitude. It is likely that this was due to cells reaching higher confluency after longer culture times, and therefore compacting slightly to accommodate the higher cell number. The difference in area between 2D and 3D cells was significant and similar in value between 4 day grown 2D vs 3D cells and 8 day grown cells, and interestingly, the nucleus to cell area ratio was very similar across the 4- and 8-day conditions, displaying how the nucleus changes structure in accordance with the cell shape and cytoskeleton. Interestingly, the nucleus to cell area ratio is slightly higher in the 1 day grown cells from both 3D or 2D, indicating that at earlier stages of culture, the nucleus takes up more area in the cell, and the cytoskeleton and therefore cytoplasm expands to accommodate this over time.

Finally, TEM images (**Figure 4.41**) of the 3D priming model reveal how after 8 days of priming, there is evidence of multiple junctions forming, and potential bile canaliculi structures, suggesting polarisation and functionalisation of the HepG2 cells. The SEM images of the cells on top of Alvetex® highlight how closely packed the cells are, with multiple indicators that the cells in 3D are forming close bonds with their neighbouring cells, forming a three-dimensional network of interactions. It is clear how the cellular structure is highly differential when comparing a 2D monolayer to this tight layer of cells on 3D, and these differences are evidently carried over, even after mechanical and enzymatic liberation. This therefore suggests that changes are not just superficial but are occurring on a potentially transcriptomic level. This will be investigated in the next chapter.

4.6 Conclusions

This chapter presents a large body of evidence that characterises the structural changes occurring in the HepG2 cells both during and after being primed in 3D, compared to 2D cells. The reproducible and consistent data here presents a picture that depicts how the structure of HepG2 cells is significantly transformed through priming in a 3D model, showing that the cells have adapted to their surrounding microenvironment and are more 'ready' to move into a secondary culture. While the appearance of certain structural markers is significantly affected during priming, they seem to equilibrate between 2D and 3D primed cells in subsequent cultures after 7 days, but the differences during priming may play a large role in the observations that 3D primed cells exhibit a greater tendency to form three dimensional structures. The individual cells display changed morphological characteristics that hint at preserved differential gene expression, and this gives reason to believe that due to mechanotransduction, transcriptomic changes will also be observable in the next chapter.

Chapter 5 – The gene expression of 3D primed liver cells is significantly altered and shows enriched hepatic function.

5.1 Introduction

5.1.1 Measuring gene expression provides a deep insight into biological mechanisms

Gene expression analysis has long been a method used to determine changes in the transcriptome that occur in *in vitro* models as the result of a test stimulus. Changes in the expression of genes of interest can reveal upstream alterations in the biology of a cell that may be undetectable through broader, less specific assays, and this can provide greater detail into the mechanisms working behind more widespread biological changes. For over 25 years, quantitative PCR has proven to be a robust and invaluable technique for measuring alterations in selected genes (VanGuilder et al., 2008). Quantitative PCR is commonly employed in many in vitro functional tests that when combined with other assays and orthogonal techniques can create a clear picture of a model's biological profile from the level of the gene up to the end stage biological processes.

While quantitative PCR is of great use in determining expression changes in a small number of genes, microarray sequencing technologies provided a new medium through which a much wider set of gene expression changes could be captured via profiling the transcriptome of a cell population (Srivastava et al., 2019). Microarrays can provide a thorough comparison between 2 conditions in terms of how gene expression may differ, however they are limited by the fact that they only profile predefined transcripts/genes through hybridisation (Rao et al., 2019). Another drawback of microarrays is that there is signal saturation at high levels of gene expression and background hybridisation may interfere with low level expression levels, meaning the dynamic range is limited (Srivastava et al., 2019).

While still suitable for many applications, microarrays have been succeeded somewhat with the emergence of next generation RNA sequencing (RNAseq). RNAseq has been shown to be more sensitive than microarray data when validating results with qPCR (Li et al., 2016; Wang et al., 2014), and has a wider dynamic range, with no signal saturation or background hybridization. This process is able to sequence the transcriptome in full and determine the exact cDNA sequences in a sample. There exists a plethora of sequencing technologies, but Illumina next generation sequencing is a well-established technology that utilises a specific approach to sequence by synthesis. Firstly, a library of cDNA fragments is made from a sample's RNA, with adaptors attached to both ends of the fragments, and these fragments are isothermally amplified on a glass flow cell resulting massively parallel clonal amplification

of all fragments generated from the samples. Fluorescently tagged nucleotides then compete for addition to each the immobilised fragments in parallel, and the complementary chain grows one nucleotide at a time, releasing a fluorescent signal with each incorporation ("Next-Generation Sequencing (NGS) | Explore the technology," n.d.). This is done from both ends of the sequence resulting in a paired end read, and a typical sequence length is usually between 30-400 bp (Wang et al., 2009). Ultimately, this produces raw data for each sequence read, which are then mapped to genes in the organisation of interest. From this, a count for each gene is generated and once normalised to the total gene counts from a sample, this number represents the gene expression levels within the chosen samples. Comparisons can then be made between conditions to analyse differential expression. RNAseq is not without disadvantages however, with it requiring a much more extensive and complex analytical pipeline than microarrays – though this also means that there is a high degree of flexibility and depth available in the bioinformatic analysis.

5.1.2 Global gene expression analysis permits deep insight into the effect of an altered microenvironment.

While many transcriptomic studies focus on the effect of a compound or test condition on the gene expression of models, there are only a handful of studies extending the applications of sequencing to investigate how the physical microenvironment affects the transcriptome of *in vitro* models. Ultimately these studies could present a critical shift towards more thorough analysis of how mechanical changes affect the baseline biology of cells, as many prior studies have only focussed on observing changes in set behaviours that they expect the models to show. Transcriptomic analysis provides a much broader and deeper pool of data that can reveal wider effects on the biology which may also indicate how mechanotransduction is involved in the altered functional profile of the models.

Within the studies that have investigated global gene expression changes in 3D culture, structural genes such as those involved in ECM organisation and binding and adhesion related genes are often differentially expressed between 2D and 3D cells, for example in mouse embryonic stem cells, under dynamic culture conditions in a 3D-spinner, certain ECM related genes are over-expressed to a large degree along with growth factor genes, however adhesion related genes were largely downregulated in 3D cells (Liu et al., 2006). When investigating cells from both lung and squamous cell carcinomas, enrichment analysis of genes differentially expressed between the two conditions shows revealed that the ECM was one of the most highly enriched cellular components when comparing monolayer and 3D

matrigel cell cultures (Zschenker et al., 2012). Curiously, transcriptomic profiling of stem-cell derived neurons cultured in 2D and in 3D hydrogels reveals a different expression pattern, with ECM related genes not showing any enrichment within the top 14 enriched biological processes in either the 2D or 3D cells (Tekin et al., 2018). Further to that, a transcriptomic analysis of cardiac differentiation in 3D aggregates showed that ECM genes including different collagens such as COL1A1, COL4A1, COL5A1 and COL9A1 were upregulated in the 2D monolayers, which had been reported previously too (Branco et al., 2019). This was explained due to a higher presence of fibroblast like cells in the monolayer cultures as indicated by the RNAseq and the presence of fibroblast markers. It is highly likely therefore that the cell type is a central factor in determining just what structural related genes are differentially regulated when cultured in 3D. Investigating the global transcriptome is even more crucial when looking at pluripotent stem cells compared to terminally differentiated cell lines such as HepG2, as the microenvironment is a powerful source of cues for differentiation (Edmondson et al., 2014b). In differentiated cell lines however, the transcriptome may provide an indication of the phenotypic or epigenetic plasticity within the cells, and this plasticity can be quite significant even through just mechanical alterations.

As discussed in previous chapters, enhanced functional properties are often an observable trait of 3D *in vitro* models over 2D counterparts, and in transcriptomic studies, and this is a commonly picked up through changes in gene expression patterns alongside the alterations in structural genes. For example, the stem cell derived neurons showed increased expression of astrocytic markers as well as a closer expression profile to that of human brain and human brain organoids (Tekin et al., 2018). 3D cultured human stem cell derived cardiomyocytes also revealed upregulation of genes involved in cardiac cell communication that are preferentially expressed in atrial, nodal and conduction system cardiomyocytes (Branco et al., 2019). The transcriptomic analysis revealed that 3D culture contributed to earlier structural and functional maturation of cardiomyocytes when compared to 2D cells. With mouse stem cells, 3D culture resulted in enhanced expression of genes that promote cell differentiation (Liu et al., 2006), which backed up previous observations of enhanced differentiation efficiency measured through flow cytometry and microscopy (Liu and Roy, 2005). The use of sequencing here provided a more granular insight into why the differentiation states were altered in 3D and revealed unique changes in the transcriptional machinery and regulation of cytokine activity. These findings highlight the strong analytical power of sequencing in providing a simultaneously extraordinarily broad and highly sensitive overview of how 3D culture widely alters cell biology.

5.1.3 Transcriptomic analysis of liver models shows that 3D culture enhances metabolism.

A large number of *in vitro* liver studies have included qPCR analysis to show that 3D cultured liver models induce changes in gene expression. Primarily these have looked at the expression of genes encoding for cytochrome P450 enzymes and selected phase II metabolising enzymes, with a number of liver specific biomarkers often explored. As discussed previously, despite changes in gene expression; HepG2 cells often lack expression of certain CYP450 genes altogether (Takahashi et al., 2015) but when changes in CYP gene levels are observed, the data is often displayed as mRNA/gene expression relative to the 2D sample (Ramaiahgari et al., 2014a; Shah et al., 2018; Štampar et al., 2019), which while useful, does not indicate the *absolute* expression of those genes which could indeed still be very low. Indeed, absolute expression is an important consideration with gene expression analysis, as genes that have very low transcript levels will show higher fold changes with smaller absolute increases in mRNA expression; for example, going from 10 raw counts to 100 is a fold change of x10, however this *may* be less biologically significant that a gene that goes from a count of 1,000 to 1,500 with only a fold change of x1.5. Aside from this certain caveat, the low expression of the cytochrome enzymes in HepG2 cells can be alleviated to some extent through using certain chemical inducers, increasing expression of hepatic enzymes in HepG2 cells (Westerink and Schoonen, 2007a, 2007b). This suggests that to create a fully functionally competent model, the solution may be a combination of 3D culture and chemical inducers.

This thesis, however, was focussed on purely the effects of altering the physical substrate on which cells grow. Despite the many small scale gene expression experiments that have been performed in similar circumstances, there is very little data about global gene expression changes that occur from culturing liver cells, let alone HepG2 cells, in a 3D microenvironment. In one of the only studies performing transcriptomic analysis on HepG2 cells, a microarray was used to compare gene expression changes between monolayer and spheroid rotating wall vessel cultures grown for 3 days in their respective culture format (Chang and Hughes-Fulford, 2009). This experiment grouped genes that were over 2-fold differentially expressed into categories of biological function based on known annotations. The monolayer HepG2 cultures showed upregulation in cytoskeletal, cell adhesion and extracellular matrix related genes amongst others, and the spheroids showed upregulation of genes involved in xenobiotic metabolism and lipid metabolism. The analysis of this study

was somewhat limited in depth, with no further statistical assessment to indicate how strongly enriched those biological functions were. However, qPCR results on selected genes showed a similar pattern indicating reproducible results, and functional assays (CYP1A1 activity and albumin production) showed enhanced liver specific function in the spheroids further backing up the sequencing data. Interestingly, the data showed that continuous culture in the rotating wall vessel was necessary to maintain elevated function, as moving the spheroids to a tissue culture dish drastically decreased CYP1A1 activity and albumin production. This indicates the potent effect that maintaining a 3D microenvironment has on cell biology and provides a rationale as to why priming could be beneficial.

One useful study used a microarray to compare global gene expression between HepG2 cells, HepaRG cells and primary human hepatocytes (Hart et al., 2010). Both HepG2 cells and HepaRG cells had a highly reproducible phenotype between replicates, whereas primary hepatocytes had a lot more variation. This highlights the homogeneous nature of cultured cell lines in comparison to the donor-to-donor variation inherently present in primary hepatocytes. HepaRG cells were shown to have more similar expression profiles to the primary hepatocytes and human tissue, notably in the expression of phase I and phase II enzymes. Another study comparing gene expression with microarray analysis in HepG2 and HepaRG cells before and after exposure to genotoxic and carcinogenic compounds showed similar results to the previous study with non-exposed cells with HepaRG cells more closely resembling liver and primary human hepatocytes in terms of gene expression (Jennen et al., 2010, p. 2). Interestingly though, this study revealed unique strengths and weaknesses within both HepG2 and HepaRG cells; HepaRG cells demonstrated a larger common response to the carcinogens, demonstrating the use of these cells in models for biologically interpreting chemical exposure effects. However, HepG2 cells were better at discriminating between carcinogens, indicating potential in toxicogenomic based classification studies.

In addition to the transcriptomic data, a small number of studies have also shown proteomic responses of liver cells to 3D culture conditions. The proteomic expression of HepG2 cells for example was found to be strongly associated to a cancer cell signature with 3D spheroid cultures unable to substantially alter the expression of key metabolic proteins (Hurrell et al., 2018). Despite the lack of metabolic change, the 3D culture of HepG2 cells did however significantly decrease the number of differentially expressed proteins when compared to primary hepatocytes, indicating that the 3D environment does bring cells closer to a more *in vivo*-like phenotype (Hurrell et al., 2018). The comparison in this study focussed primarily on

the HepG2 cells vs primary hepatocytes however and it did not directly compare monolayer HepG2 cultures to spheroid HepG2 cultures. A different study performed by the same group did directly compare HepG2 monolayers vs spheroids, and showed that protein expression was altered to suggest a more mature hepatic phenotype in spheroid cultures, but the changes were not reproducible between different replicates (Hurrell et al., 2019). Monolayers on the other hand showed more phenotypic stability, and it was hypothesised that longer culture times with the spheroids may be a factor that could reduce the heterogeneity. Proteomic analysis on primary hepatocytes showed a clear trend towards greater metabolic capabilities in 3D spheroid models compared to 2D sandwich models, with proteins involved in drug absorption, distribution, metabolism and excretion being upregulated in the 3D primary hepatocyte spheroids (Catherine C Bell et al., 2018).

It is imperative to clarify, however, that gene expression does not necessarily have a linear relationship with protein expression, as gene expression is a step removed upstream (through post-transcriptional modifications) from protein expression. With a known poor correlation existing between mRNA levels and protein expression, a number of recent studies have focussed on investigating exactly how gene expression can be used as a predictor of protein levels. One such study revealed that transcript and protein levels actually do correlate closely when using a gene-specific RNA-to-protein conversion factor that is independent of tissue type (Edfors et al., 2016). This shows that there *is* a measurable and predictable link between gene and protein expression. Additionally differentially expressed genes between two conditions have been shown to more closely predict protein expression changes across the two conditions too (Koussounadis et al., 2015). Therefore, changes in gene expression do have a significant impact on protein levels, and this provides further confidence when drawing functional inferences from transcriptomic data.

5.1.4 The appropriate analytical techniques to assess gene expression changes are dependent on experimental design and the goal of the study.

Transcriptomic data can provide a wealth of biological information, but this also provides challenges in the fact that there is a lack of a standardised data analysis approach, and the process for transforming the raw data into something meaningful is also a time intensive progress where consideration needs to be given to the methodology. The most basic level of gene expression analysis would consist looking at individual genes and examining the changes in normalised expression between two conditions such as through RTqPCR. That does indeed reveal a limited amount of information, through probing whether the gene of

interest has changed, and the magnitude by which expression has differed. This may provide insight into whether a key hepatic or metabolic gene (such as CYP1A1 or albumin) has increased in expression, though this is of course a very isolated approach by looking at the individual gene and not considering interactions with other genes and how that gene fits into wider biological processes and functions. Context is a critical factor that is lacking in analysis focussing on genes as individual entities (such as qPCR).

A useful way to give genes biological meaningful context is through the Gene Ontology (GO) which provides a uniform vocabulary that is able to describe the function and role of genes across species (Ashburner et al., 2000). The GO does this by annotating genes products with a GO term within the three distinctive ontologies; molecular function, biological processes and cellular components (Gaudet et al., 2017). These GO terms are linked to other terms to form a hierarchical vocabulary where terms may have multiple relationships to 'parent' terms and multiple 'children' terms stemming off it. The main benefit of using GO when looking at transcriptomic data is that it allows more confident conclusions to be drawn through strong statistical power provided with enrichment analysis.

Enrichment analysis is a way of testing whether certain gene annotations (for example biological processes or cellular components) are enriched in one's own data. This can include GO based enrichment analysis which provides a standardised approach that is well accepted in the community (Gaudet et al., 2017), but may alternatively involve analysis based on pathway databases or other ontologies. Enrichment analysis can be performed using different techniques – one common method is through over representation analysis (ORA); this uses a predefined list selected by the user, such as all genes over 2-fold upregulated in 3D, which is fed into one of many possible programmes that work out whether there is an over representation of genes related to a certain process within the user's samples when compared to a reference gene set. In this study, over representation analysis was performed using the online EnrichR software (Kuleshov et al., 2016) which enables GO enrichment analysis as well as enrichment in many other annotated ontologies such as human tissue types and disease phenotypes. This methodology is highly useful if the user knows what parameters they want to use to define their list, however selecting an arbitrary cut-off may exclude meaningful and significant changes in genes outside of that value, and this technique also does not take into account the magnitude of change in any of the genes submitted; it is solely a list of the selected genes that you provide, with no associated expression/fold change values.

An alternative methodology that takes expression data into account is Gene Set Enrichment Analysis (GSEA); a form of functional class scoring (Subramanian et al., 2005). GSEA is different to ORA in that it uses a ranked list of genes – for example ranking the genes in order of fold change or significance, or in the case of many modern tools a list of genes with associated values in a second column. This means that no prior cut off is needed for the list as the analysis takes into account the desired expression metric, though in cases where fold change is supplied as a second column, it is often useful to include a baseline P value to cut out any non-significant changes. GSEA works by 'walking' through the user's gene list, referencing it against known functional groupings, GO terms or pathways and calculating an enrichment score based on the extent of over representation of gene groupings at either extreme of the ranked list; the top of the list being upregulated genes, or the bottom being downregulated. The enrichment score which is weighted by expression levels is then given to the gene set to indicate the extent of over-representation, along with statistical significance being calculated and multiple hypothesis testing (FDR value) (Subramanian et al., 2005). The primary tool used in this study to conduct GSEA was WebGestalt, a web based gene set analysis toolkit (Liao et al., 2019) that provides GSEA in many well established functional databases including GO and pathways from KEGG (Kanehisa and Goto, 2000), Reactome (Fabregat et al., 2017) and WikiPathways (Slenter et al., 2018). Additional pathway based enrichment analysis was carried out on the Reactome web based tool itself, which used a modified GSEA methodology called CAMERA that accounts for inter-gene correlation, something that gene set tests can be sensitive to (Wu and Smyth, 2012).

Ontology based analysis is a valuable technique through which one can infer biologically meaningful conclusions from their data by putting it into context. For both this and individual gene-based analysis to be valuable though, one needs to ensure the data is reliable in the first place. This is aided through a slightly different form of analysis; comparative statistics which provide significant value in transcriptomic studies. A volcano plot for example provides an overview of all differentially expressed genes between two conditions and can show which genes are upregulated, downregulated with applied significance and fold change cut-offs highlighting areas of highly differentially expressed genes. Clustering analysis is a common technique through which to compare similarity of two chosen conditions by calculating a distance measure (often the pairwise distance between all data points). In hierarchical agglomerative cluster analysis (Johnson, 1967), data that is the least distant apart is joined up, followed by the next most similar data point, and this continues until a 'tree' is formed, which can be seen in this study on the heatmaps and cluster analysis graphs.

Similarly, principal component analysis (PCA) can highlight similarities or variation between samples in gene expression analysis by providing "fully unsupervised information on the dominant directions of the highest variability" (Lenz et al., 2016; Ringnér, 2008). This provides understanding of how variable replicates were and how different conditions relate to each other.

5.2 Hypothesis and aims

It is hypothesised that through deep transcriptomic analysis, distinctive enhanced functional gene sets will be enriched in the 3D HepG2 models. These enriched functional genes are expected to be liver specific mainly, with predicted upregulation in metabolism and biosynthesis based on data in the previous chapters and the literature. In contrast, it is expected that the 2D models will demonstrate enrichment in structural and mechanotransduction related genes such as adhesion and cytoskeletal arrangement. In addition, it is expected that enrichment will occur in areas previously not considered which will provide an interesting view of the wider biological ramifications of changing the mechanical properties of the culture format.

It is predicted that through comparison with primary hepatocytes and human liver that the 3D primed HepG2 cells will be closer in gene expression profiles to both the hepatocytes and the human liver. It is likely that the difference between HepG2 cells and the liver/primary hepatocytes will be large though, particularly in the comparison to the human liver due to different cells being present other than just hepatocytes.

5.3 Objectives

- To fully characterise the gene expression profiles of HepG2 cells grown in 2D or in 3D on Alvetex® Strata, and to compare these expression profiles to human liver and primary hepatocytes.
- To investigate differential expression in genes of interest, both functional and structurally related.
- To investigate areas of enrichment in the 2D and 3D HepG2 cells, through using over representation analysis and gene set enrichment analysis with Gene Ontology and known pathways.

5.4 Results

5.4.1 Quality control of the RNA confirmed its suitability for sequencing.

Preparing the RNA for sequencing was a critical process that needed to be tightly controlled and correctly carried out to ensure maximum RNA quality with no contamination or degradation. A preliminary way to check for this was through running RNA samples obtained from 2D HepG2 cells, 3D primed HepG2 cells (both grown for 8 days as described in **Chapter 2 and 3**) and human liver through an agarose gel with ethidium bromide and visualising them with ultra-violet light (**Figure 5.1**). Degraded RNA appears as an indistinct smear, whereas good quality RNA appears with two distinct bands, the 28S RNA (the top band) and 18S (bottom band) and a 2:1 ratio of these respective bands indicates intact RNA ("Agarose Gel Electrophoresis of RNA - UK," n.d.). Human liver was a lot more difficult to isolate RNA from than the HepG2 cells due to the high level of RNAses in the liver, yet aside from some slight smearing in the first human liver sample, all samples looked in-tact with no noticeable degradation.

For a more accurate quality control exercise, these samples were loaded into an Agilent TapeStation system which provides automated electrophoresis and data processing to determine a numerical integrity value of RNA samples based on the ratio of bands (Schroeder et al., 2006). The integrity number, termed RIN is scored out of 10, and anything over an 8 is considered excellent quality. The 4 best scoring replicates were selected from each sample and are shown in **Figure 5.2**, and the scores were very high across the board, with the lowest being a human liver sample scoring 7.5. These data indicated that these samples were of high enough quality to submit for sequencing.

5.4.2 Comparative analysis of samples reveals high similarity between 2D and 3D HepG2 cells, with a large difference to human liver and primary hepatocytes.

These samples were sent to the sequencing department at Durham University Department of Biosciences, who prepared a library and sequenced them, providing the raw data back. After processing the raw data (see methods), differential expression data was generated where any gene with a count higher than 10 in one of the compared samples was listed. Principal components analysis of the three conditions (**Figure 5.3**) highlighted how the HepG2 cells from 2D and 3D were a lot closer to each other in terms of expression profiles than they were to human liver which was highly separate from the HepG2 samples. This is

especially evident in the log transformed PCA data. One key observation is the lack of variability between the replicates in each of the three conditions. This indicates that the *in vitro* models are highly reproducible in terms of the phenotype, though this was more expected with the human liver, which was isolated from one donor, therefore it was likely that variability would be low. Including online data from primary human hepatocytes (PHH) cultured for 1 day on a 2D substrate (**Figure 5.4**) revealed that these cells were highly distinct in terms of expression profile to both the human liver and HepG2 samples but possibly indicated a mid-way point of sorts in terms of expression between human liver and HepG2 cells.

Clustering analysis (**Figure 5.5**) was also used to provide detail on how similar each sample was to every other sample. Darker coloured squares indicate a high degree of similarity, whereas the light squares show that the samples are highly dissimilar to each other. Using log transformed and untransformed data showed the same patterns of similarity between the samples. Each sample was most similar to the replicates within its own condition, and between conditions, 2D HepG2 cells were most similar to 3D HepG2 cells, and PHHs were most similar to human liver, but as seen in the cluster trees, the distance between these two conditions was still considerably high. The HepG2 cells also have a slightly closer similarity to PHHs than human liver as indicated by the very slightly darker squares between the HepG2 and PHH samples.

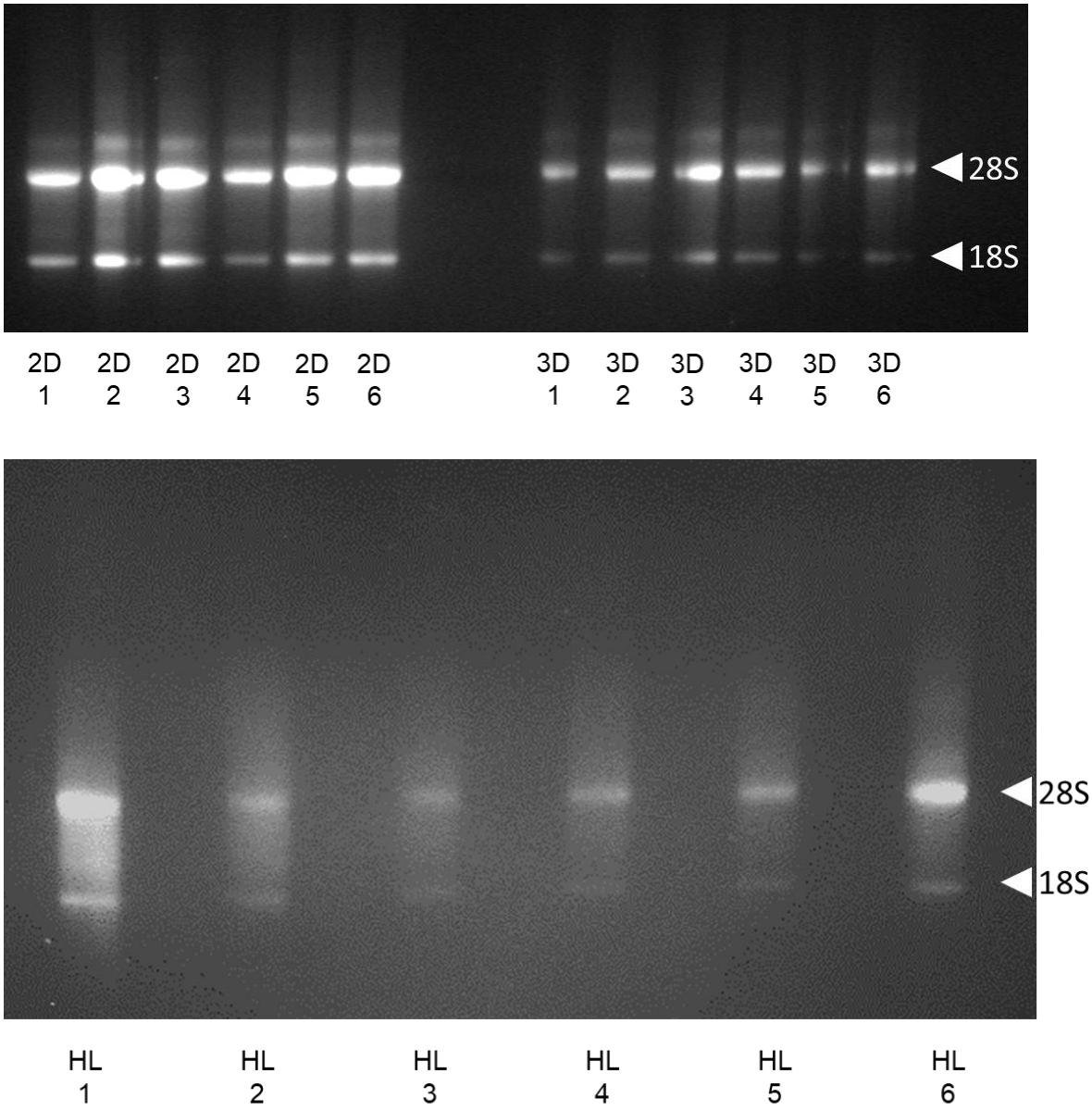

Figure 5.1: Initial quality control on agarose gels showed minimal degradation in the samples.

Fluorescently visualised samples on agarose gels. 6 replicates of either HepG2 cells from 2D (2D) grown for 8 days at a seeding density of $5x10^5$, HepG2 cells in 3D (3D) grown for 8 days on Alvetex® Strata at a seeding density of $1x10^6$, or human liver (HL) were processed to extract RNA. RNA samples were then electrophoresed on a 10 % TAE agarose gel, 100V for 1.5 hours with ethidium bromide. Imaged on a Gel dock using ultraviolet light. Gels were run twice, samples represent N= 6

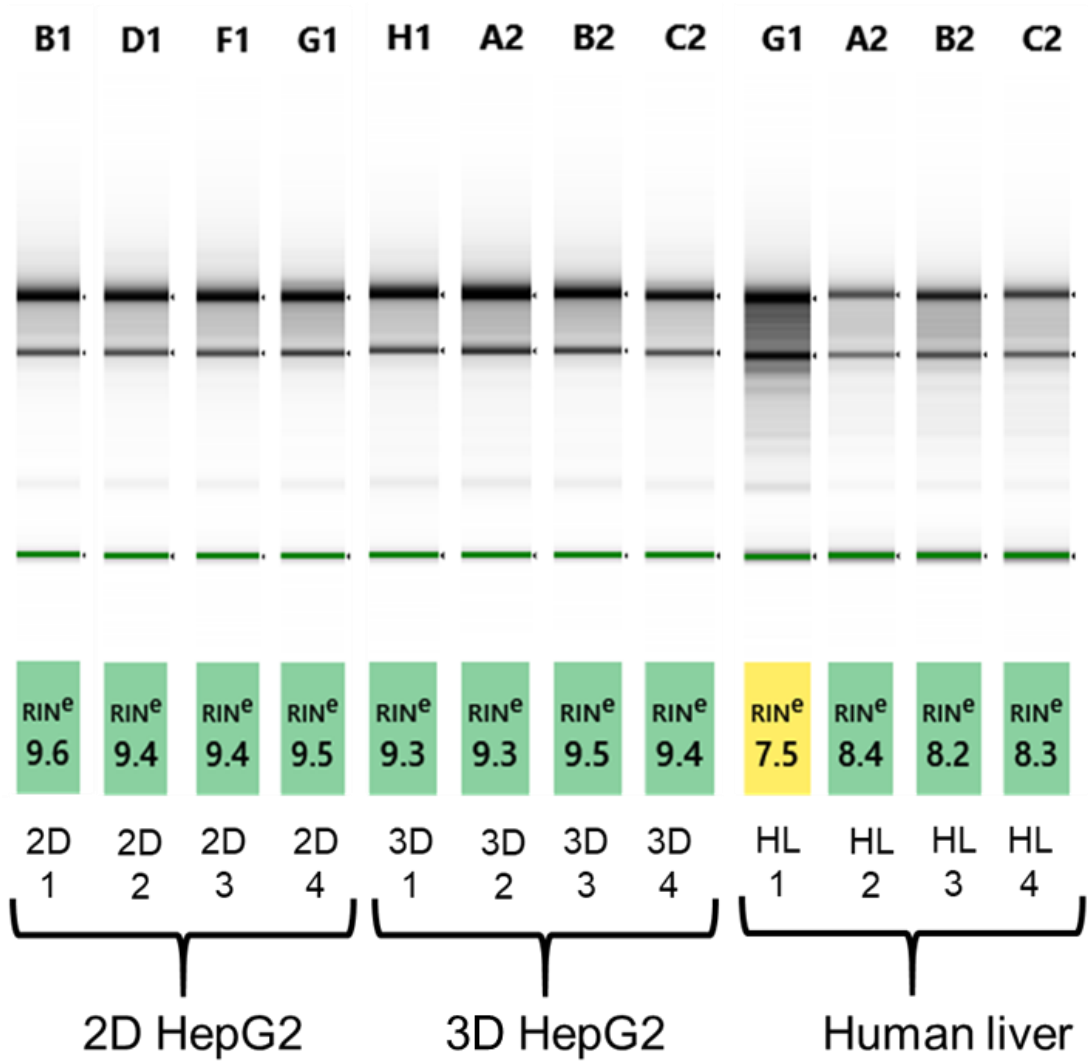

Figure 5.2: RNA samples were high quality when ran on the tape station.

Agilent Tapestation results showing the RNA integrity score (RIN) for the four best scoring biological replicates across the three conditions; 2D HepG2, 3D HepG2 cells and human liver. A score of 10 indicates the highest possible RNA quality. Gels were run twice, samples represent N= 4

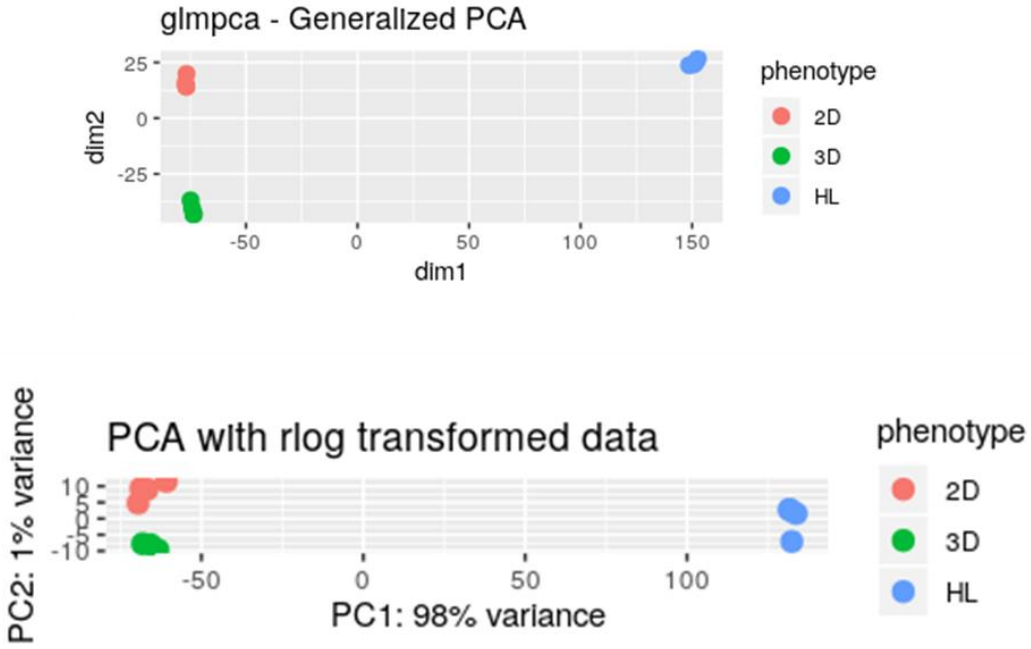

Figure 5.3: Principal component analysis shows that biological repeats are consistent, but human liver is very dissimilar to HepG2 models.

Principle component analysis conducted on gene count data of 2D and 3D primed HepG2 cells compared to human liver, using generalised PCA glmpca and rlog transformed data. Gene data from samples represents N= 4

Figure 5.4: Principal component analysis including data from primary hepatocytes shows that these are also highly distinct from HepG2 cells and human liver in gene expression.

Principle component analysis conducted on gene count data of 2D and 3D primed HepG2 cells compared to human liver, including primary hepatocyte data sourced from EMBL-EBI Expression Atlas, using generalised PCA glmpc and rlog transformed data. Gene data from samples represents N= 4

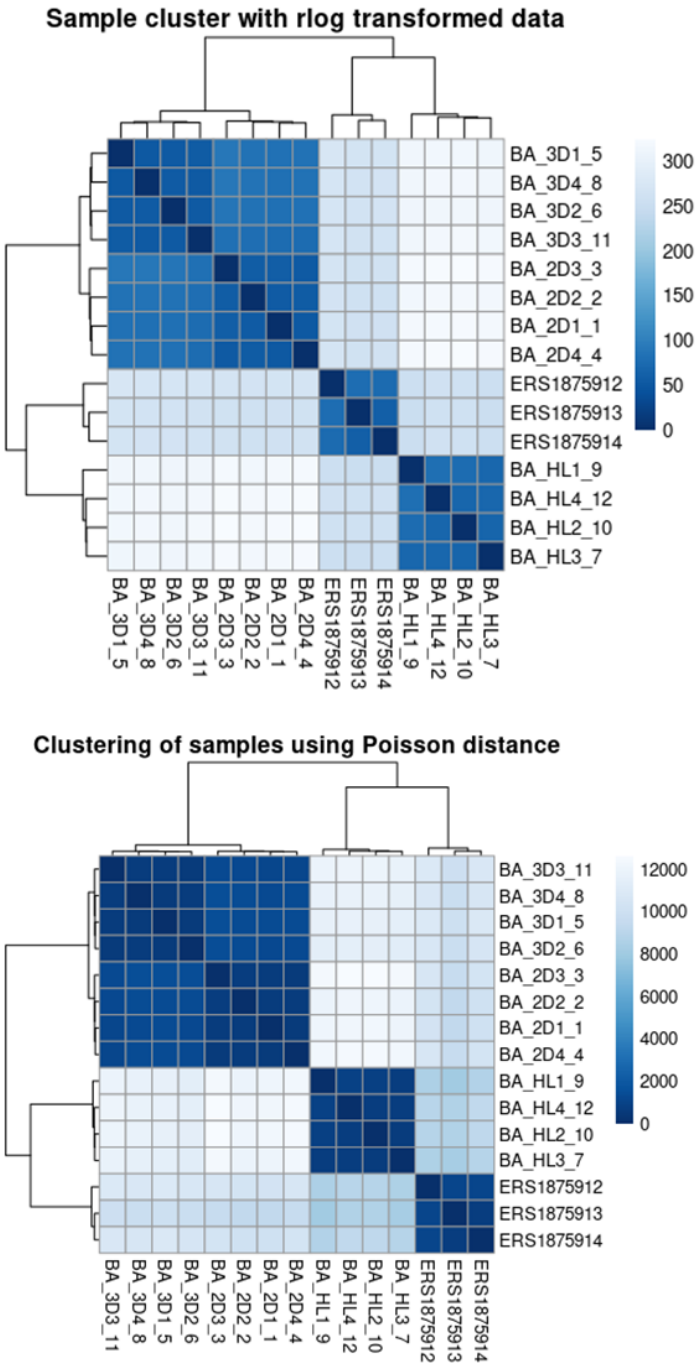

Figure 5.5: Sample clustering shows the highest similarity is between 2D and 3D HepG2 cells.

*Clustering analysis on 2D and 3D HepG2 compared to human liver (HL) and primary hepatocytes (ERS18759__) was performed using rlog transformed data and using untransformed data with Poisson Distance. The number after the condition (e.g. 2D**X**) indicates the repeat number (1 to 4 on each) and the end number (e.g. 2D1_**X**) indicates the order in which the samples were originally numbered. Darker colours indicate a higher measure of similarity (AU). Gene data from samples represents N= 4*

Table 5.1: Significant gene counts vary between comparisons.

Table constructed using total gene counts in each compared condition (genes with a read count of over 10 in either condition). Significant genes filtered by any genes that had differential expression with a P adjusted value of ≤0.05.

	3D vs 2D	HL vs 2D	HL vs 3D	2D vs PHH	3D vs PHH	PHH vs HL
Total genes	13,938	15,724	15,694	15,701	15703	16,061
Significant genes	7,852	13,073	12,800	12,395	12,487	11,876
Upregulated genes	3,846	7,030	6,903	5,749	5,789	5,929
Downregulated genes	4,006	6,043	5,897	6,646	6,698	5,947

Table 5.1 provides a summary of the number of significantly differentially expressed genes between each condition. There is clearly a large number of differentially expressed genes between the HepG2 cells compared to human liver and primary hepatocytes, though despite the relative similarity on the PCA and clustering analysis of the 2D and 3D HepG2 cells, there were still over 7,000 significantly differentially expressed genes between these 2D and 3D conditions. Interestingly, there were less differentially expressed genes between 3D HepG2 cells and human liver than 2D HepG2 cells versus human liver, and although this was marginal, it suggests that the 3D HepG2 cells have a slightly closer gene expression profile to human liver.

Using a volcano plot enabled with a fold change cut-off of ≥2 and an adjusted P value cut-off of ≤0.000001 (**Figure 5.6**) on the 2D vs 3D HepG2 samples further visualised the more extreme differences in gene expression between 2D and 3D HepG2 cells. Interestingly some of the most significant changes in expression were not at the high ends of the differential expression, such as MTHFD2 and TPM4 which were 2.85 and -2.88-fold expressed in in 3D compared to 2D. Some of the largest fold changes were not even statistically significant, often because of low absolute counts combined with high variability. However, this clearly demonstrates that there is a wealth of genes that are significantly differentially expressed

between the two conditions and indicates that further analysis could reveal some interesting patterns. It is useful to clarify that phrasing genes as upregulated in 3D can equally mean genes that were downregulated in 2D, and vice-versa, but the direction of change between the two chosen conditions is what is important for analysis.

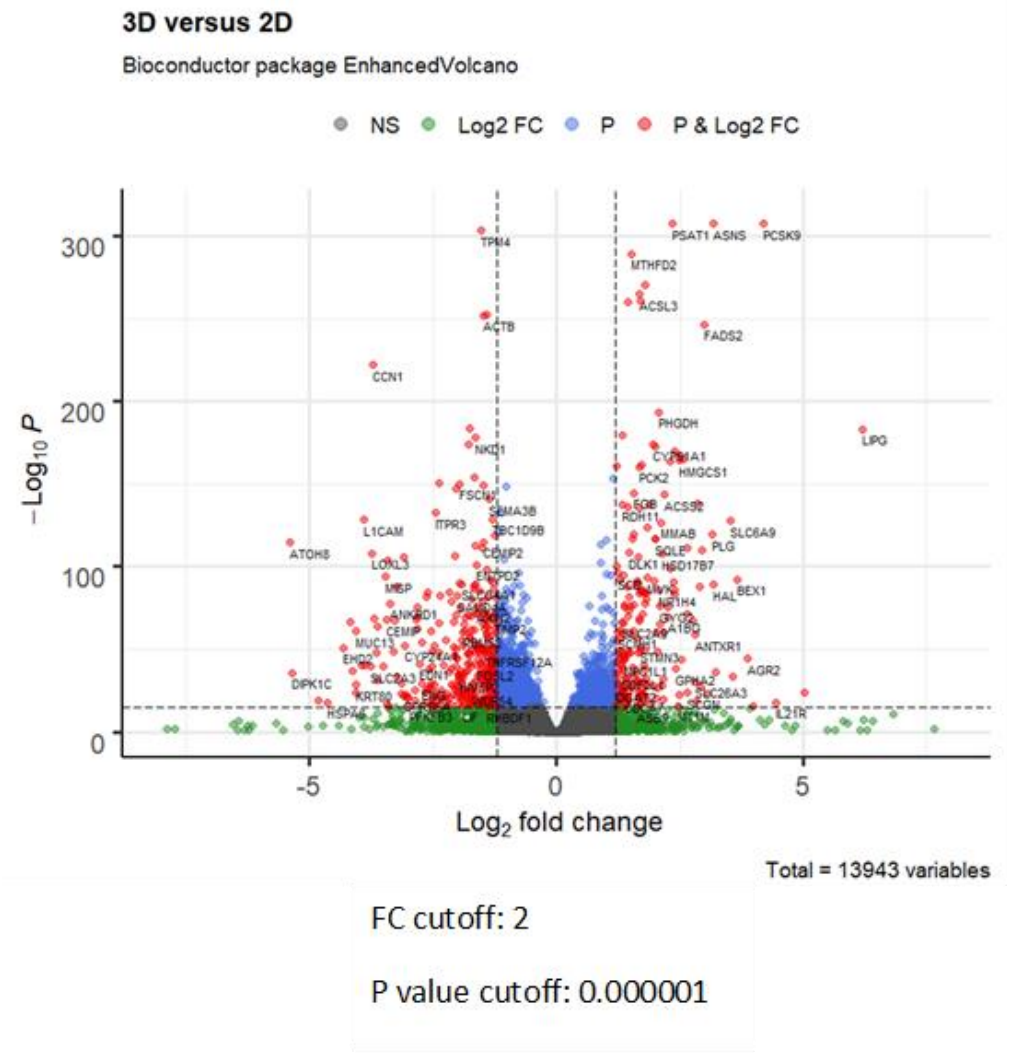

Figure 5.6: Volcano plot performed on 2D vs 3D HepG2 samples shows a similar spread of genes upregulated in 2D and 3D.

Volcano plot created using the Bioconductor package EnhancedVolcano in R. P adjusted value cut off set to ≤1x10^{-6} and fold change cut off set to ≥2 (or 1 when log transformed). Therefore, genes in the top left and right segments (coloured in red) are significantly differentially expressed with over a 2-fold change between the two conditions and are highly statistically significant (≤1x10^{-6}). Gene data from samples represents N= 4

5.4.3 Metabolic genes are upregulated in 3D HepG2 cells though absolute expression is often low.

To investigate differential expression of selected genes of interest, heatmaps were generated. The first heatmap was created using the search term 'cytochrome P450' in R to pull out any gene that had that term in its name from the differential expression data. Two heatmaps were generated; the first heatmap made from all of the genes matching this search term from the average normalised expression values across all expressed genes in 2D HepG2, 3D HepG2, PHH and HL, whether significant or not (**Figure 5.7**). The second heatmap was generated from all significant genes (P adjusted value of ≤0.05) matching the search term that were over 2-fold differentially expressed in either direction between just 2D and 3D HepG2 cells (**Figure 5.8**) including each replicate to provide a more detailed insight. This pattern was used for all heatmaps where a search term was applied (**Figures 5.7 to 5.15**). From the full gene heatmap for cytochrome P450 gene expression, it is immediately evident that the human liver has strong expression in many of the key CYP genes, notably CYP3A4, CYP1A2, CYP2C9, CYP2D6 and CYP2E1 which are critical for xenobiotic metabolism. These enzymes have higher average expression in the human liver over all the other conditions, are weaker in PHHs and have very low absolute expression in HepG2 cells in comparison. Many of the CYP genes are slightly increased in 3D HepG2 cells compared to 2D, however the absolute expression is low for most of the CYPs in the HepG2 cells compared to the primary hepatocytes and human liver. There are exceptions where the HepG2 expression is closer to PHH and human liver such as CYP51A1 and CYP27A1 involved in lanosterol conversion and bile acid synthesis respectively (Pikuleva et al., 1998; Strushkevich et al., 2010) which have distinctively high expression in both HepG2 models (higher in 3D) and human liver but not PHHs. There are also unusual cases such as CYP2W1 and CYP19A1 where expression is higher in HepG2 cells than either PHH or human liver. The differences in expression within many of these key enzymes between the primary cell sources and the HepG2 cells indicate how far removed from *in vivo* physiology the HepG2 cells are.

The ≥2-fold significant genes between 2D and 3D HepG2 cells (**Figure 5.8**) shows that only one of the *key* drug metabolising cytochromes; CYP1A2 is differentially upregulated in 3D culture. Out of the remaining ≥2-fold differentially expressed CYP genes, most of them are upregulated in the 3D HepG2 cells, other than CYP2S1, CYP24A1, and CYP4F22. This indicates that 3D culture does enhance the Phase I metabolism in general, though there is still a low level of absolute expression when compared to the primary cells and human liver. For the

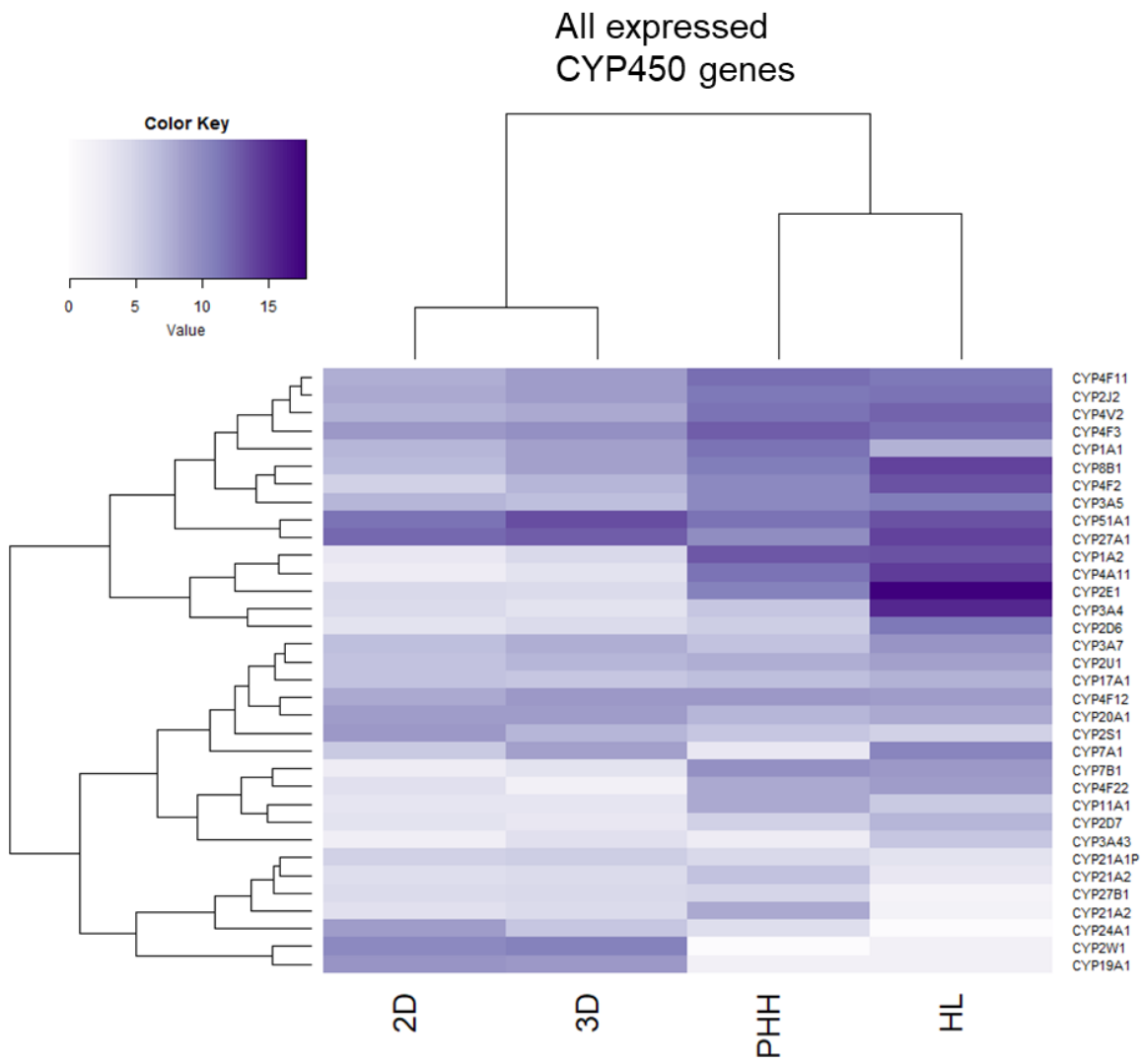

Figure 5.7: Heatmap of all cytochrome P450 genes expressed across the four conditions shows 3D HepG2 cells are more comparable to human liver than 2D HepG2 cells.

Heatmap made using the Heatmap.2 package in R. Heatmap made from the average normalised expression values in each condition, with the search term 'cytochrome P450' used to pull out all the CYP genes. Colour key equates to log10 of the expression value; darker colours mean higher absolute expression. Euclidian clustering performed on the rows and columns to show distance between samples. Gene data from samples represents N= 4

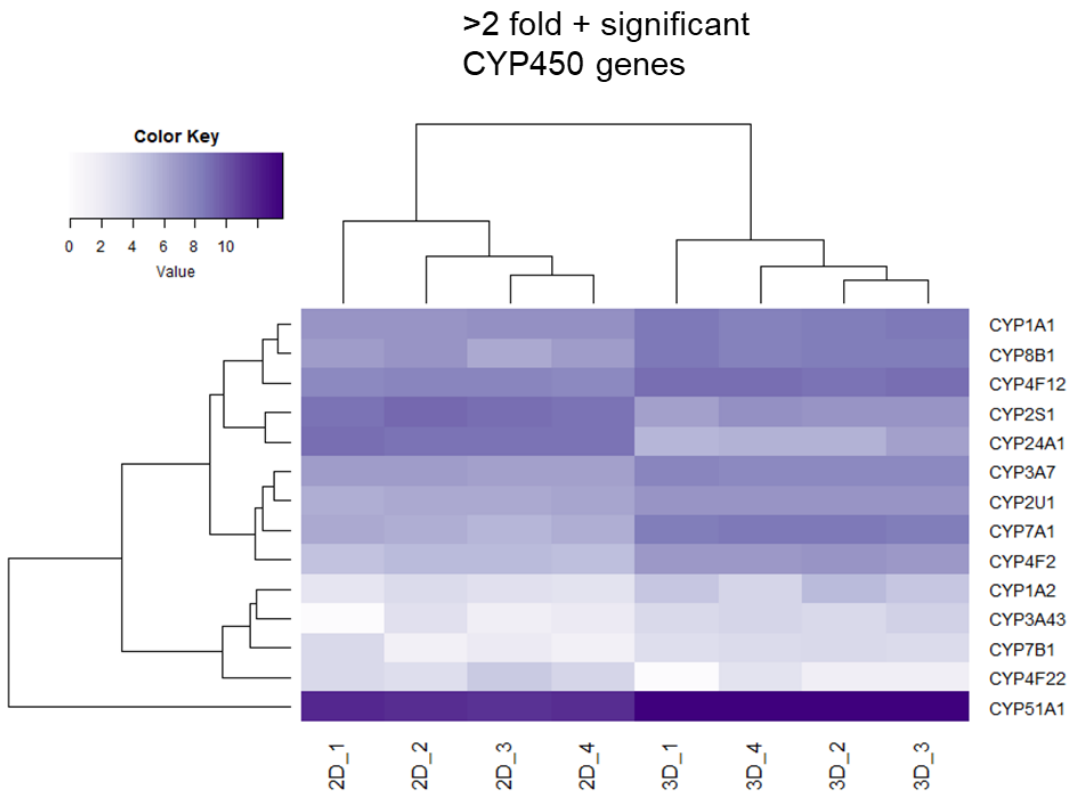

Figure 5.8: A smaller set of CYP450 genes are over 2-fold differentially expressed between 2D and 3D HepG2 cells.

Heatmap made using the Heatmap.2 package in R. Heatmap made from the normalised expression values in each repeat from 2D and 3D HepG2 cells, using P adjusted ≤0.05 and log2FC>1 change, with the search term 'cytochrome P450' used to pull out all the CYP genes. Colour key equates to log10 of the expression value; darker colours mean higher absolute expression. Euclidian clustering performed on the rows and columns to show distance between samples. Gene data from samples represents N= 4

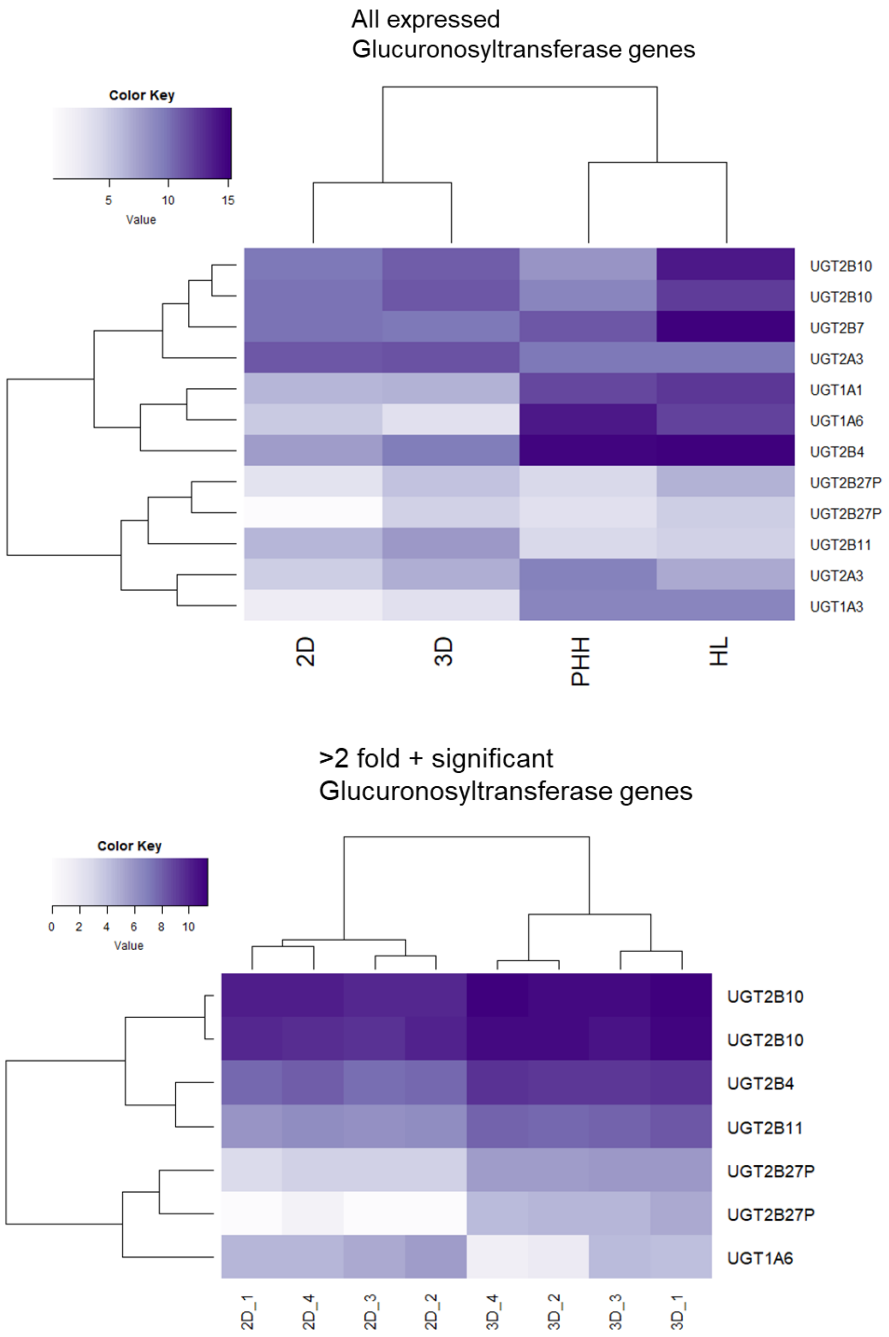

Figure 5.9: Glucuronosyltransferase genes are upregulated in 3D HepG2 cells.

Heatmap made using the Heatmap.2 package in R. Heatmap made from average normalised expression values in each condition (top) and the normalised expression values in each repeat from 2D and 3D HepG2 cells, using P adjusted value ≤0.05 and log2FC>1 change (bottom), with the search term 'Glucuronosyltransferase' used to pull out all the glucuronosyltransferase genes. Colour key equates to log10 of the expression value; darker colours mean higher absolute expression. Euclidian clustering performed on the rows and columns to show distance between samples. Gene data from samples represents N= 4

sake of concision, instead of focussing on the function of the individual genes, the heatmaps will serve to provide an overall view of how expression in certain gene groupings change, but further context will be given to the changes in the enrichment analysis.

Each set of Phase II metabolising genes were then analysed, with glucuronosyltransferase (UGT) genes being investigated first (**Figure 5.9**). Absolute expression of the UGT genes is generally higher than the CYPs in the HepG2 cells, though relative expression is still low compared to human liver and primary hepatocytes. Interestingly though, when looking at the significant ≥2-fold genes, there is a very clear pattern of the 3D HepG2 cells having a higher expression apart from UGT1A6, and the expression in 3D HepG2 cells is closer to human liver in most cases than 2D HepG2 cells indicating a more physiological expression profile. The sulfotransferase (SULT) genes show a very similar pattern of increased expression in 3D HepG2 cells (**Figure 5.10**) when compared to 2D, with the 3D expression levels being closer to those of human liver. Only three of the SULT genes were more than 2-fold differentially expressed between the HepG2 models, though in each case these were higher in the 3D priming models. Primary hepatocytes interestingly seem further removed from human liver expression than 3D HepG2 cells with SULT2A1 and SULT1E1. This could be an artefact of the fact the PHH samples were cultured in 2D (albeit for only 1 day) perhaps already starting de-differentiation in some areas, though it could also be due to donor-donor variation and the fact that human liver has cells other than hepatocytes too which may interfere with expression levels.

The N-acetyltransferase (NAT) genes were strongly expressed across the board in HepG2 cells (**Figure 5.11**), even more so than in human liver and PHH in some examples such as NAT9, NAT14 and NAT8L. Similar to the SULT and UGT genes, the NAT genes are upregulated in 3D primed HepG2 cells in general over 2D HepG2 cells, and in general this brings the 3D cells closer to human liver and PHHs but in some cases it actually brings the expression in HepG2 cells over that of the human liver and PHHs indicating over-expression beyond *in vivo* physiological levels in the HepG2 cells. Again, only 3 of the NAT genes were over 2-fold expressed between the HepG2 cells, but these were each in 3D HepG2 cells. The glutathione S-transferase (GST) followed the same pattern as the other phase II enzymes with a general increase in expression in 3D primed HepG2 cells over 2D, but there is more of a shortfall here when compared to PHH and human liver (**Figure 5.12**) as expression is mostly low across the HepG2 cells. Four of the GST genes are upregulated in 3D by over 2-fold further pointing towards 3D culture enhancing phase II metabolism in a uniform manner.

5.4.4 Integrins are upregulated in 2D HepG2 cells, however cadherins and claudins show a more mixed expression pattern.

Structural adhesion related genes were also specifically selected for analysis due to their importance in mechanical processes and that they are known to be modulated with substrate stiffness. Cadherins did not present a noticeably uniform pattern of expression in either direction between 2D or 3D HepG2 cells, instead showing upregulation in some genes in 2D and some in 3D (**Figure 5.13**). E-cadherin and N-cadherin (CDH1 and CDH2 respectively) are key genes for adhesion as discussed in prior chapters; CDH1 showed almost no difference in expression between 2D and 3D HepG2 cells and showed lower overall expression in HepG2 cells than N-cadherin which was only slightly upregulated in 2D cells. It is also of note that CDH1 was much more highly expressed in PHH and human liver, with human liver expressing more CHD1 than CDH2 whereas PHHs showed very similar expression levels of both cadherins. Compared to the low expression in HepG2 cells, this potentially indicates that the HepG2 cells have moved towards a more mesenchymal phenotype than observed in healthy *in vivo* cells – unsurprising considering they are a cancer cell line. Four of the cadherins were over 2-fold differentially expressed, though these were VE cadherin (CDH5) and cadherin related family member 5 (CDHR5). CHD5 is essential for vascular development (Carmeliet et al., 1999), which is also expressed reasonably highly in the liver, though this is likely due to the presence liver sinusoidal endothelial cells which express VE cadherin, not from the hepatocytes (Géraud et al., 2012). Due to the mixed expression patterns, it is therefore difficult to draw any further conclusions from the cadherin data without using more advanced enrichment analysis.

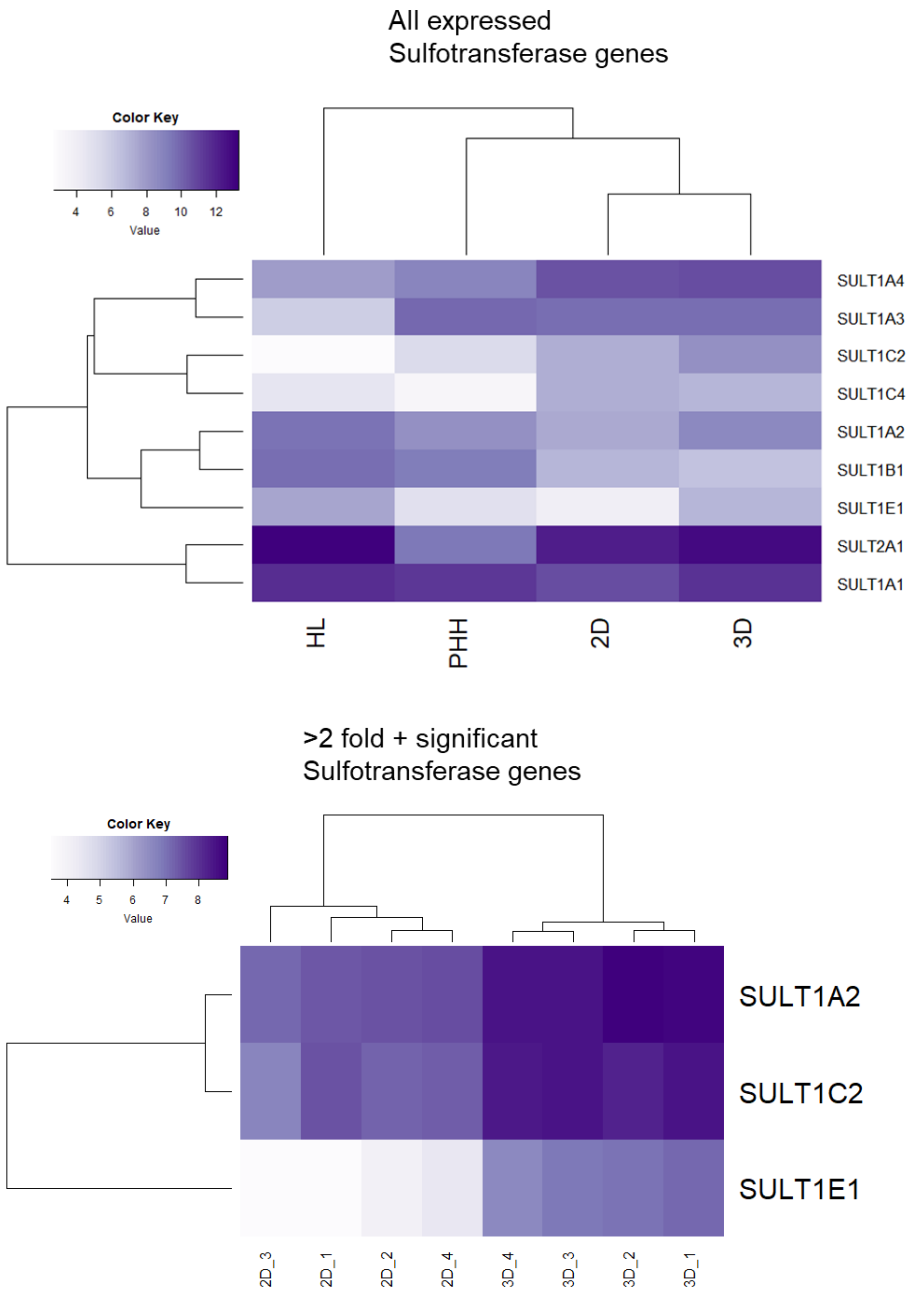

Figure 5.10: Sulfotransferase genes are upregulated in 3D primed HepG2 cells over 2D HepG2 cells.

Heatmap made using the Heatmap.2 package in R. Heatmap made from average normalised expression values in each condition (top) and the normalised expression values in each repeat from 2D and 3D HepG2 cells, using P adjusted value ≤0.05 and log2FC>1 change (bottom), with the search term 'SULT' used to pull out all the sulfotransferase genes. Colour key equates to log10 of the expression value; darker colours mean higher absolute expression. Euclidian clustering performed on the rows and columns to show distance between samples. Gene data from samples represents N= 4

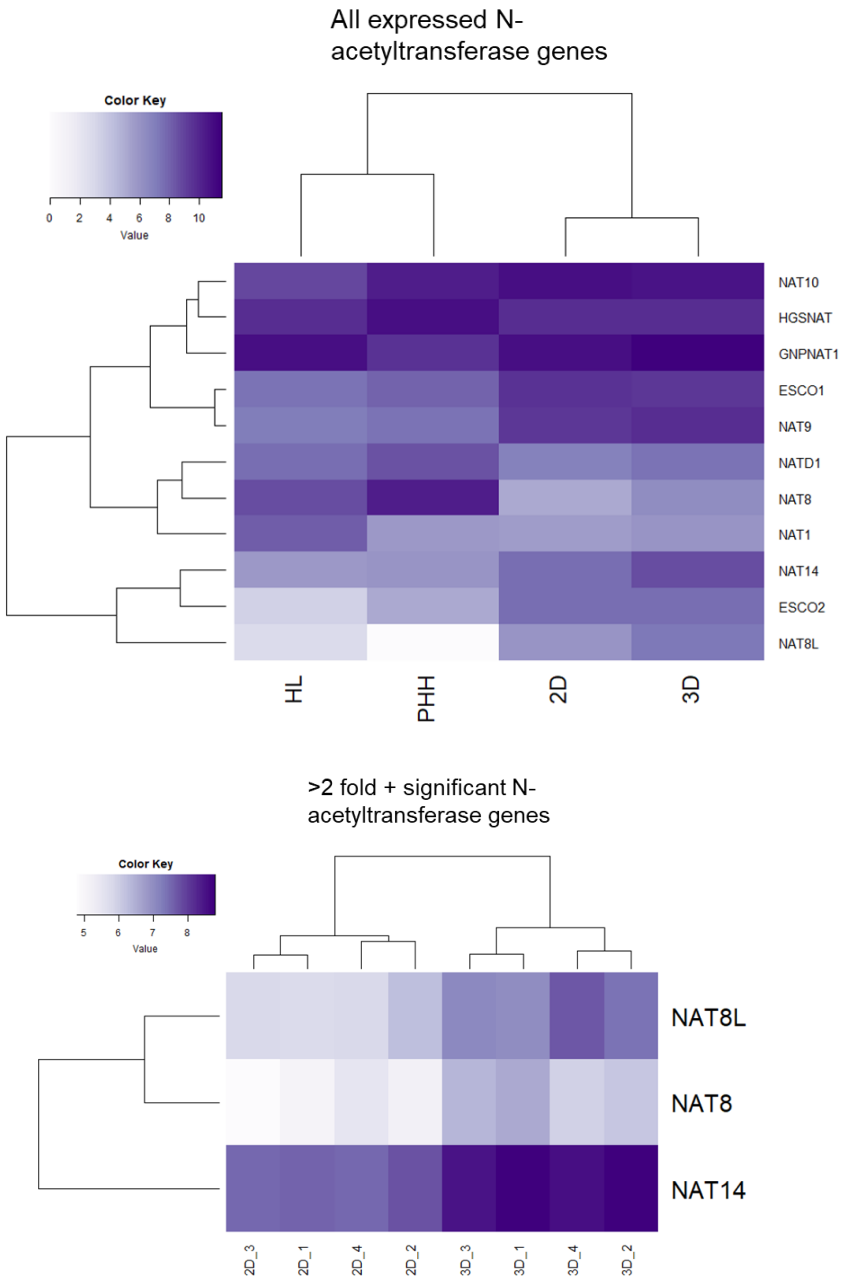

Figure 5.11: N-acetyltransferase genes are upregulated in 3D primed HepG2 cells over 2D HepG2 cells.

Heatmap made using the Heatmap.2 package in R. Heatmap made from average normalised expression values in each condition (top) and the normalised expression values in each repeat from 2D and 3D HepG2 cells, using P adjusted value ≤0.05 and log2FC>1 change (bottom), with the search term 'N-acetyltransferase' used to pull out all the relevant genes. Colour key equates to log10 of the expression value; darker colours mean higher absolute expression. Euclidian clustering performed on the rows and columns to show distance between samples. Gene data from samples represents N= 4

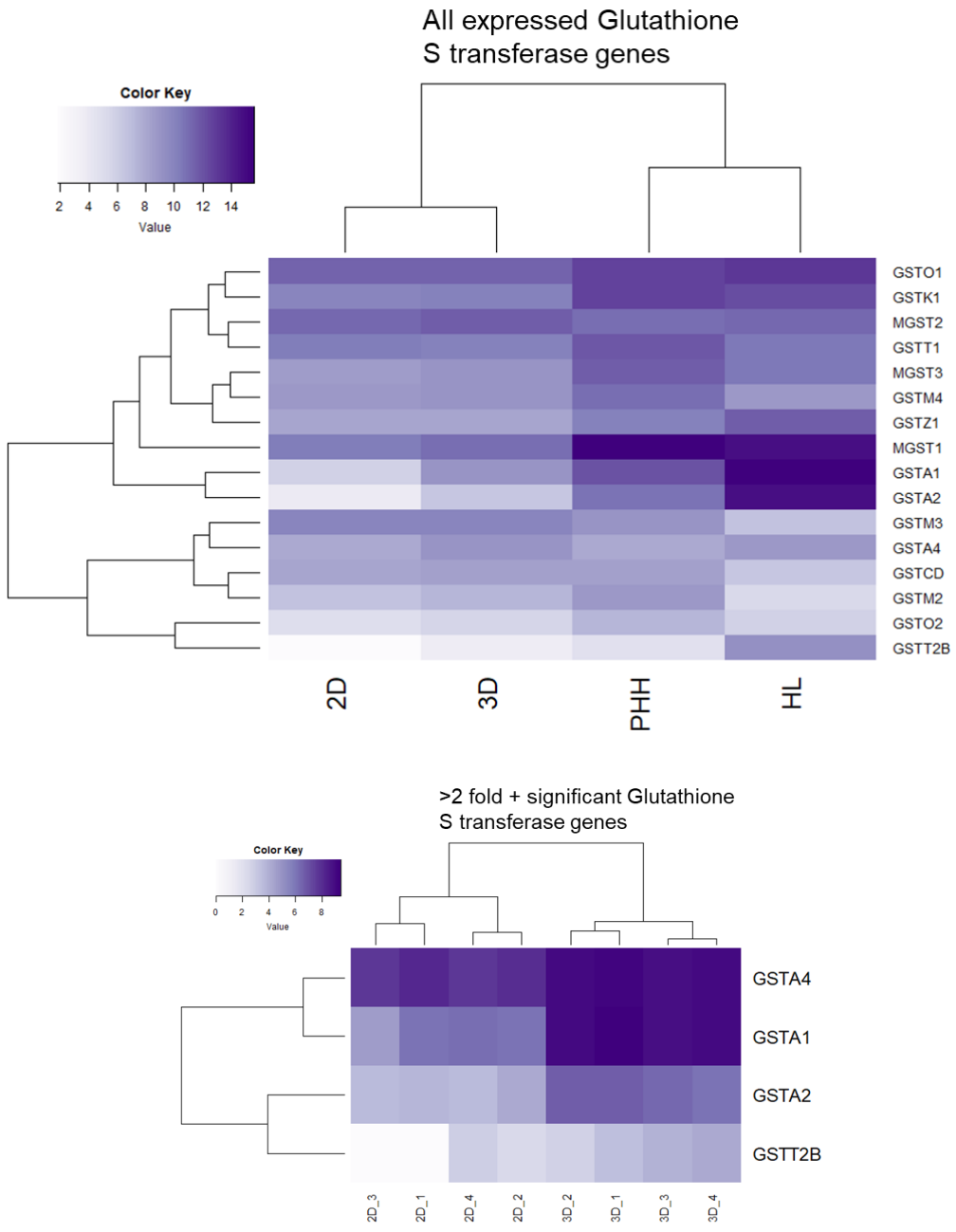

Figure 5.12: Genes associated with Glutathione S transferase are upregulated in 3D primed HepG2 cells.

Heatmap made using the Heatmap.2 package in R. Heatmap made from average normalised expression values in each condition (top) and the normalised expression values in each repeat from 2D and 3D HepG2 cells, using P adjusted value ≤0.05 and log2FC>1 change (bottom), with the search term 'GST' used to pull out all the relevant genes. Colour key equates to log10 of the expression value; darker colours mean higher absolute expression. Euclidian clustering performed on the rows and columns to show distance between samples. Gene data from samples represents N= 4

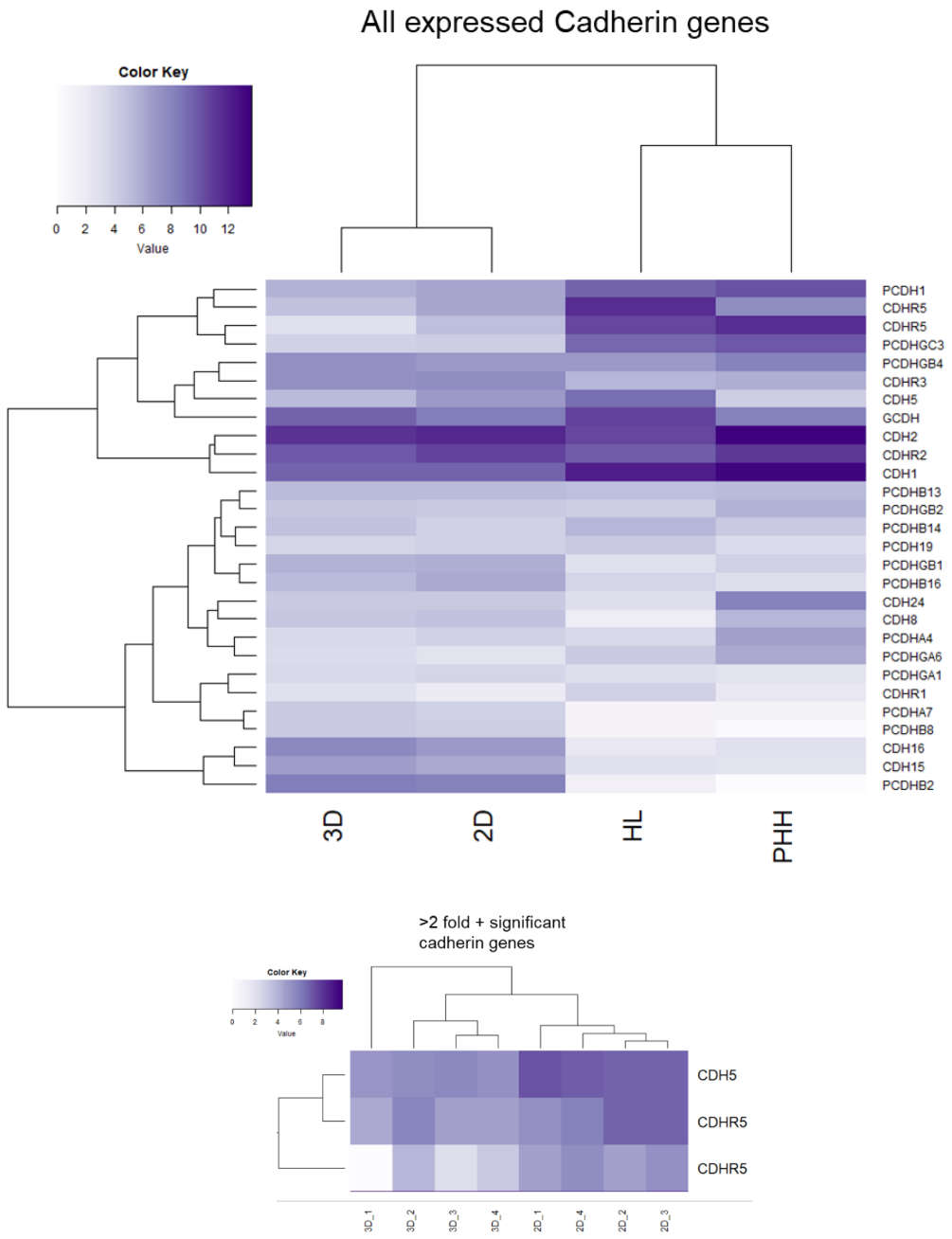

Figure 5.13: Cadherin genes show mixed expression patterns between 2D HepG2 cells and 3D primed HepG2 cells.

Heatmap made using the Heatmap.2 package in R. Heatmap made from average normalised expression values in each condition (top) and the normalised expression values in each repeat from 2D and 3D HepG2 cells, using P adjusted value ≤0.05 and log2FC>1 change (bottom), with the search term 'cadherin' used to pull out all the relevant genes. Colour key equates to log10 of the expression value; darker colours mean higher absolute expression. Euclidian clustering performed on the rows and columns to show distance between samples. Gene data from samples represents N= 4

One of the key gene sets for cell-substrate adhesion is the integrins, and there was a clear pattern of increased expression of these genes in 2D HepG2 cells over 3D (**Figure 5.14**). The expression in human liver is lower than the 2D HepG2 cells in a lot of the integrin genes with a closer expression profile to the 3D HepG2 cells suggesting that the *in vivo* ECM binding properties are more closely mimicked when cells are grown in a 3D scaffold than on a stiff 2D substrate. As the integrin genes encode for various subtypes that group together in different pairings to form focal adhesions it is perhaps unsurprising that the expression is consistently upregulated in the 2D HepG2 cells. The PHH cells show strong upregulation in ITGA5, ITGAV and ITGB1 particularly, significantly overexpressed compared to human liver and the 3D HepG2 cells. This is likely an artefact of the 2D culture in PHH as levels of ITGAV and ITGB1 integrin genes are close to the expression in 2D HepG2 cells. The cluster analysis does still show that the PHH and human liver are more similar to each-other than to HepG2 cells, though the distance measure is high between the two. Only four of the integrin genes were over 2-fold differentially expressed, and these were all upregulated in 2D HepG2 cells compared to 3D HepG2 cells. This upregulation of integrin genes in 2D is likely due to bigger focal adhesions forming as a result of significantly higher contact surface area with the growth substrate compared to cells on a scaffold. Focal adhesions are known to decrease in size as substrate stiffness reduces which is the case in 3D cell culture (Cao et al., 2017; Yeh et al., 2017).

The claudin genes are weakly expressed in both the HepG2 models compared to the human liver and PHH cells, especially in the claudin gene most closely associated with hepatocytes; claudin 1 which is very strongly expressed in human liver and PHH. Claudin 1 is significantly upregulated in the 3D HepG2 cells by 1.3-fold, though this is a highly significant change with a P-adjusted value of 5.8×10^{-8}. Unlike integrin, there is no distinct uniform upregulation in one HepG2 model over the other, with claudin 6 and claudin 9 being over 2-fold upregulated in 2D HepG2 cells, and claudin 19, claudin 14 and claudin 23 being increased in 3D models. The more variable expression patterns in the claudins may be a result of tissue specificity of claudins and suggests that not all tight junctions are inherently increased in a culture format with significantly higher cell-cell contact. These data show that structurally, 2D cells do appear to be enriched in terms of cell-surface adhesions, however with cell-cell contacts, both in tight junctions and cadherins, there is less noticeable enrichment when looking at individual genes. When analysing the full gene set through enrichment analysis, it is expected that expression changes in wider genes also involved in adhesion may reveal a more directed change in the structural genes.

5.4.5 The differential responses of the HepG2 models to xenobiotics may be attributed to wider biological alterations than just the key metabolic genes.

A set of xenobiotic compounds were selected for functional testing in **Chapter 6**. To help predict what the toxicity responses of the HepG2 cells in the primary stage models might be, the expression levels of the genes encoding enzymes and transporters known to interact with each drug (according to go.drugbank.com) were analysed (**Figures 5.16 to 5.21**). based on the already observed differences in metabolic gene levels, it was expected that there would be a noticeable pattern of increased expression in the key metabolic and transporter genes associated with each respective drug. In the genes associated with amiodarone, gemfibrozil, ibuprofen and isoniazid there was very little discernible change in expression in either direction overall (**Figures 5.16 to 5.19**), though interestingly, the genes that *were* upregulated in 3D were either the phase I or II enzymes, yet any significant increase in expression of the ABC transporters was in the 2D HepG2 cells which was unexpected.

The lack of any noticeable pattern with these drugs was largely due to only a small number of known interactors being known, meaning the heatmaps were very limited, and it is of course possible that other genes involved in metabolic and transporter pathways are involved that are not shown in these heatmaps. This places even more importance on using enrichment analysis (particularly pathway analysis) as that takes into account interacting genes that contribute to known biological functions. CYP1A1 which is involved in amiodarone metabolism interestingly exhibited lower expression in human liver compared to the 3D HepG2 cells and was more comparable to the lower expression in the 2D HepG2 cells, though PHH cells showed higher expression of this gene. In most other cases, the human liver had very high expression counts of the phase I and phase II enzymes involved in metabolism of these drugs, with the PHH cells tending to show values in between those of human liver and HepG2.

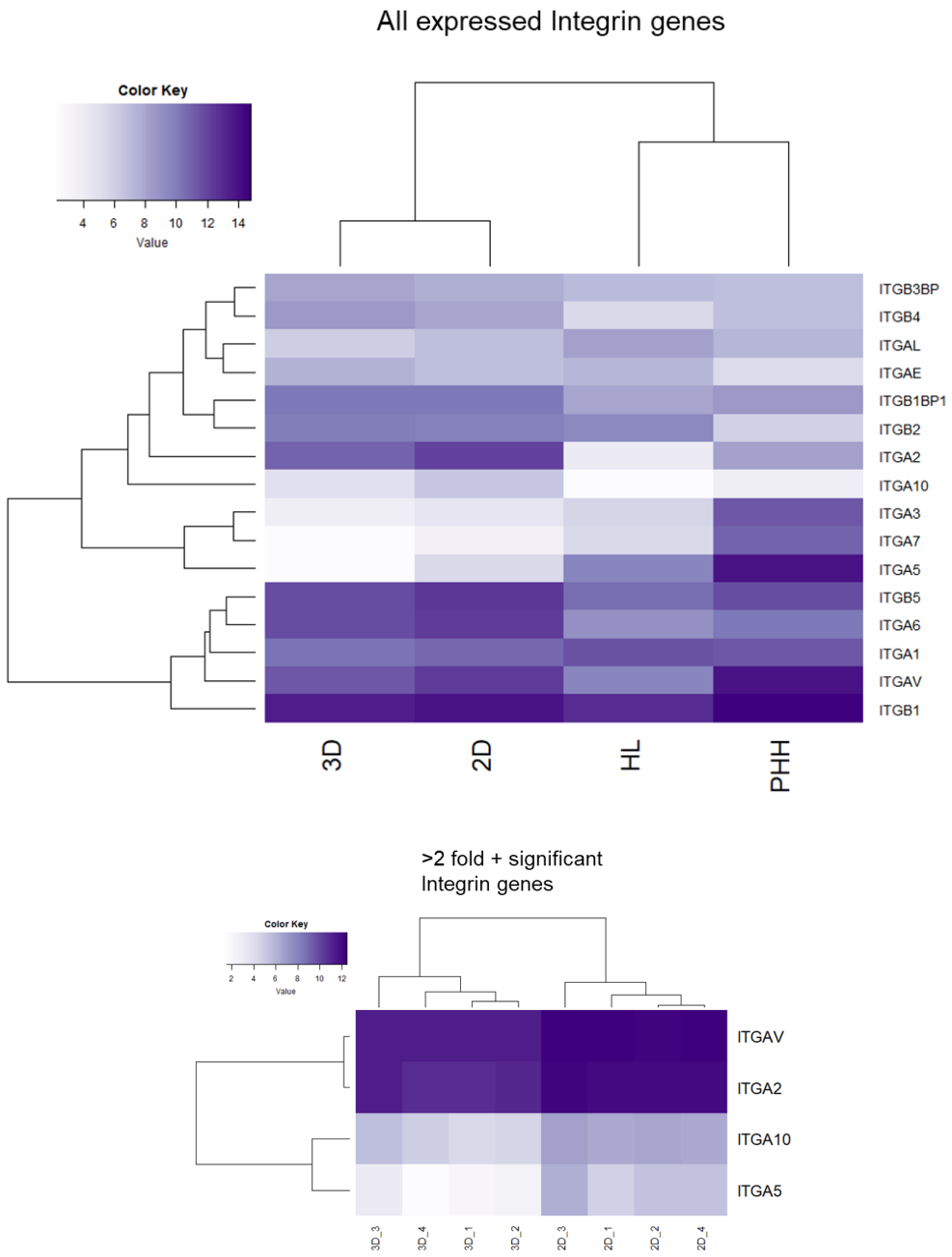

Figure 5.14: Integrin genes, including ITGAV and ITGB1 are upregulated in 2D HepG2 cells compared to 3D primed HepG2 cells.

Heatmap made using the Heatmap.2 package in R. Heatmap made from average normalised expression values in each condition (top) and the normalised expression values in each repeat from 2D and 3D HepG2 cells, using P adjusted value ≤0.05 and log2FC>1 change (bottom), with the search term 'integrin' used to pull out all the relevant genes. Colour key equates to log10 of the expression value; darker colours mean higher absolute expression. Euclidian clustering performed on the rows and columns to show distance between samples. Gene data from samples represents N= 4

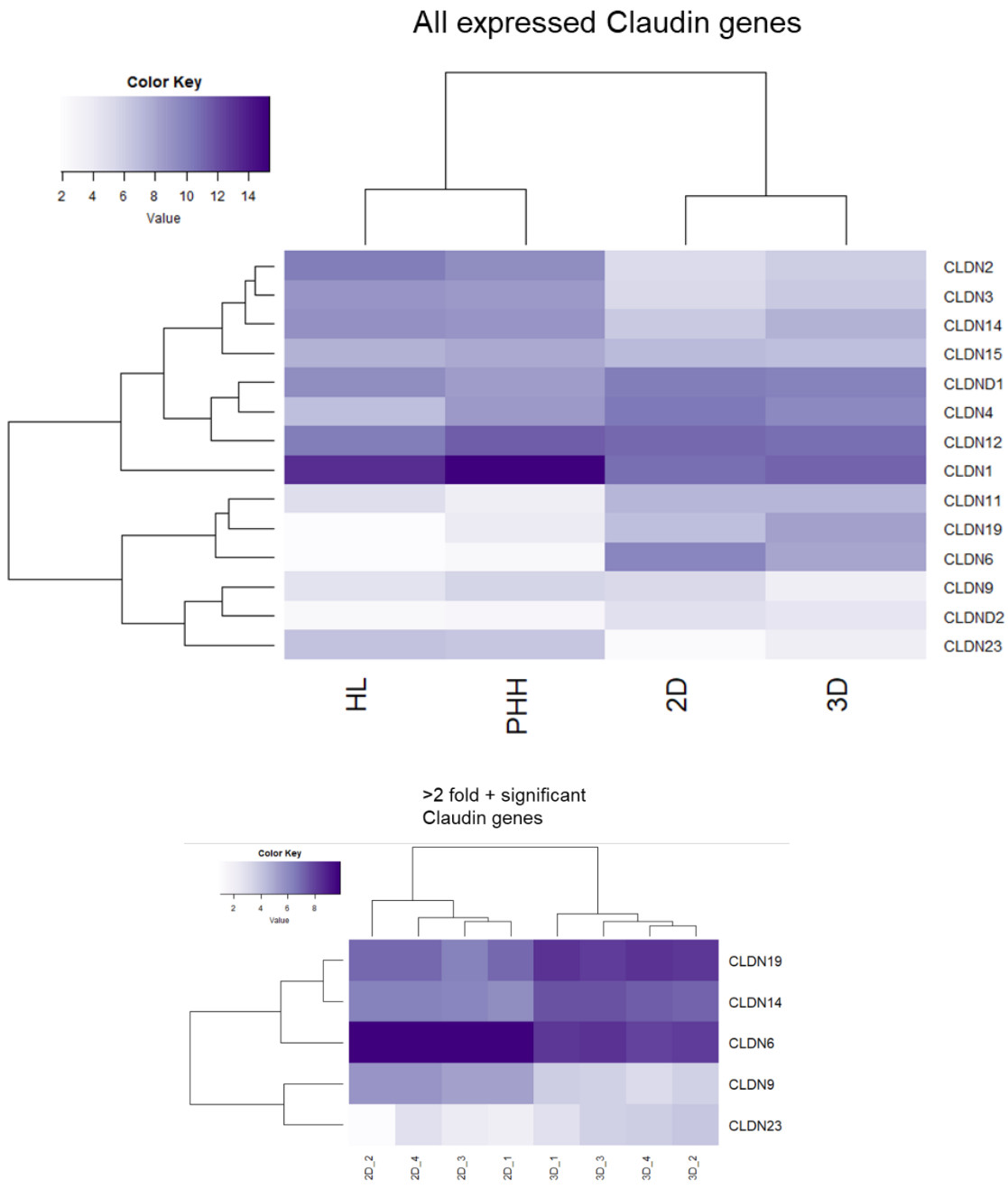

Figure 5.15: Claudin 1 is upregulated in 3D primed HepG2 cells over 2D HepG2 cells, however there is no clear expression pattern.

Heatmap made using the Heatmap.2 package in R. Heatmap made from average normalised expression values in each condition (top) and the normalised expression values in each repeat from 2D and 3D HepG2 cells, using P adjusted value ≤0.05 and log2FC>1 change (bottom), with the search term 'claudin' used to pull out all the relevant genes. Colour key equates to log10 of the expression value; darker colours mean higher absolute expression. Euclidian clustering performed on the rows and columns to show distance between samples. Gene data from samples represents N= 4

With methotrexate and tamoxifen (**Figures 5.20 and 5.21**) there was a lot more information available about known interacting enzymes and transporters, allowing more of an understanding of which areas were enriched in which conditions. Three of the enzymes involved in methotrexate metabolism were upregulated in 3D HepG2 cells (DHFR, AOX1, MTHFR1) but two were upregulated in 2D (TYMS, GGH). Particularly striking however was the split between the ATP-binding case (ABC) family of transporters being upregulated in the 2D HepG2 cells and the solute carrier (SLC) family of transporters showing upregulation in the 3D primed HepG2 cells. Both of these transporter families are majorly implicated in the transport and clearance of drugs in hepatocytes (Giacomini et al., 2010), with expression either based at the sinusoidal pole where they act as influx transporters for uptake of drugs from the blood, or at the canalicular pole where they act as efflux transporters, secreting metabolites into the bile (Funk, 2008; Le Vee et al., 2015). In all cases, the key / rate limiting enzymes in each reaction showed no significant differences between 2D or 3D (**Table 5.2**), however the wider differences in gene expression may still lead to changes in metabolic capacity which will be explored in the next chapter.

Two of the upregulated ABC genes in 2D HepG2 cells are indeed key canalicular efflux transporters; ABCB1 and ABCC2, which were 1.24 and 1.41-fold upregulated in 2D. SLCO1B3 is a sinusoidal influx transporter which is upregulated in 3D, however absolute expression was so low (the maximum raw count was 27 in one of the 3D replicates) that any biological effect of this change may still be small. It is an interesting distinction between expression of the two families of transporters, but when comparing expression of transporters to the known polar location (data not shown) (Sissung et al., 2012), there does not appear to be a distinct correlation with increased expression in either the canalicular or sinusoidal localised transporters. With tamoxifen, there is a distinctive upregulation in 3D HepG2 cells of the genes coding for the enzymes involved in its metabolism (**Figure 5.21**), yet again, the associated ABC transporters are mostly upregulated in 2D. One notable observation is that the expression of some of the significantly upregulated ABC transporters in 2D HepG2 cells is often lower in the human liver, suggesting that despite the increased potential transport capacity, the 2D HepG2 cells are further removed from the *in vivo* expression levels of these transporters than in 3D.

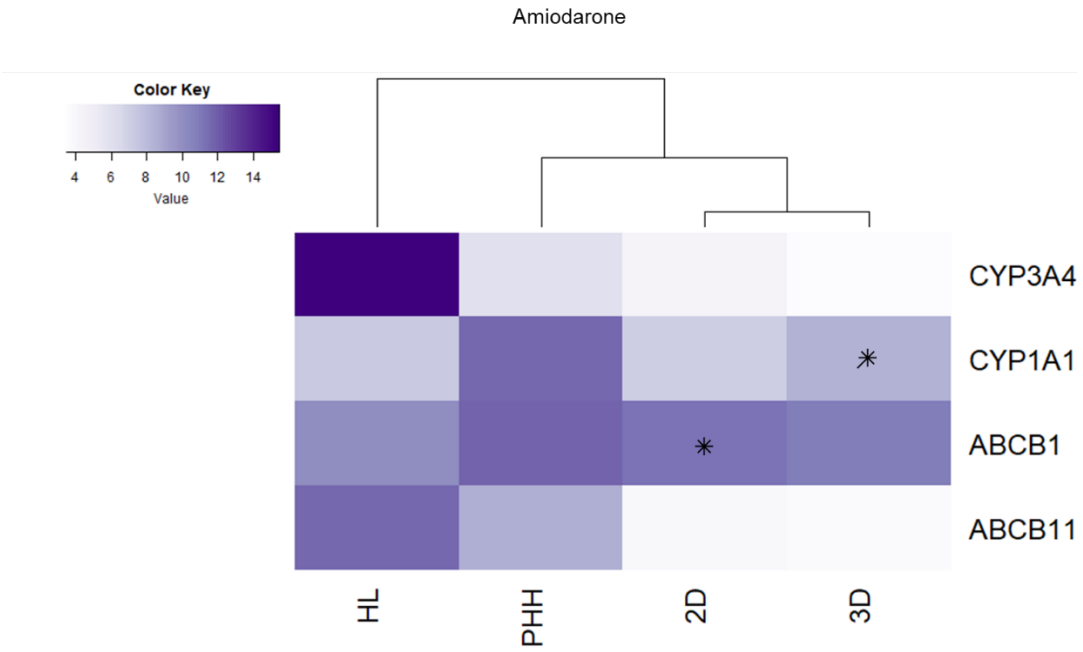

Figure 5.16: Expression patterns of key enzymes and transporters for amiodarone is differential for CYP1A1 and ABCB1 between the HepG2 models.

Heatmap made using the Heatmap.2 package in R. Heatmap made from average normalised expression values in each condition using a list of known amiodarone interactors pulled from Drugbank. Colour key equates to log10 of the expression value; darker colours mean higher absolute expression. Euclidian clustering performed on the columns to show distance between samples. Stars in 2D or 3D columns indicate a significant increase (P adjusted value ≤0.05) in expression in that condition when 2D and 3D HepG2 cells are compared. Gene data from samples represents N= 4

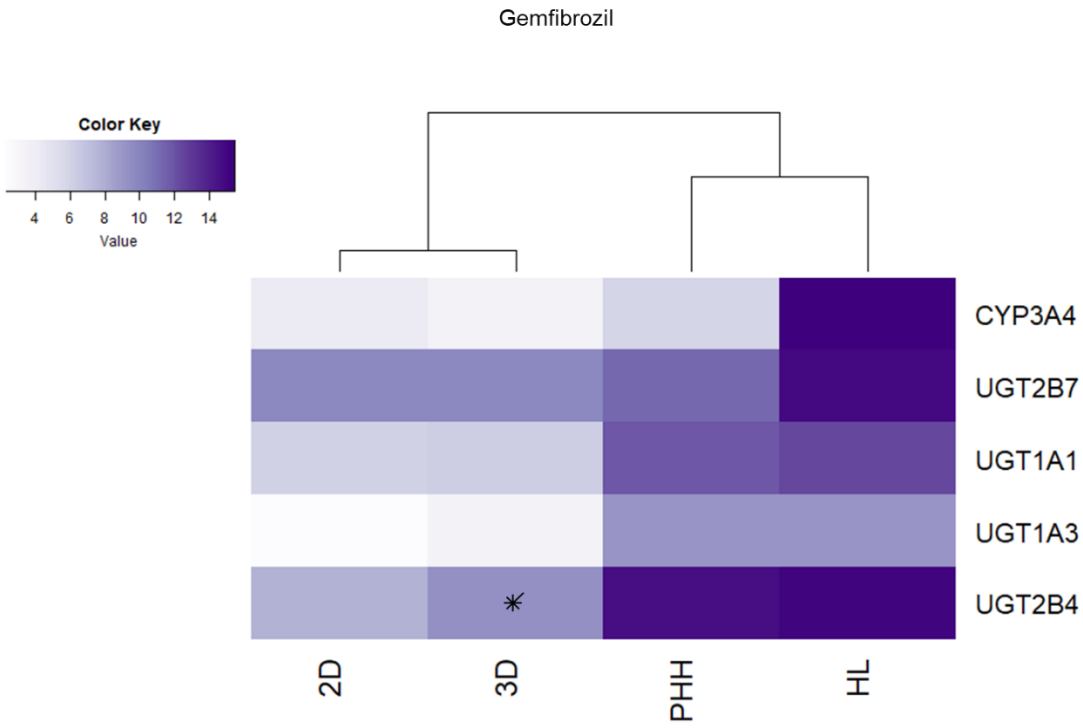

Figure 5.17: Within the phase II enzymes involved in gemfibrozil metabolism, only UGT2B4 shows a significant increase in 3D primed HepG2 cells over 2D HepG2 cells.

Heatmap made using the Heatmap.2 package in R. Heatmap made from average normalised expression values in each condition using a list of known gemfibrozil interactors pulled from Drugbank. Colour key equates to log10 of the expression value; darker colours mean higher absolute expression. Euclidian clustering performed on the columns to show distance between samples. Stars in 2D or 3D columns indicate a significant increase (P adjusted value ≤0.05) in expression in that condition when 2D and 3D HepG2 cells are compared. Gene data from samples represents N= 4

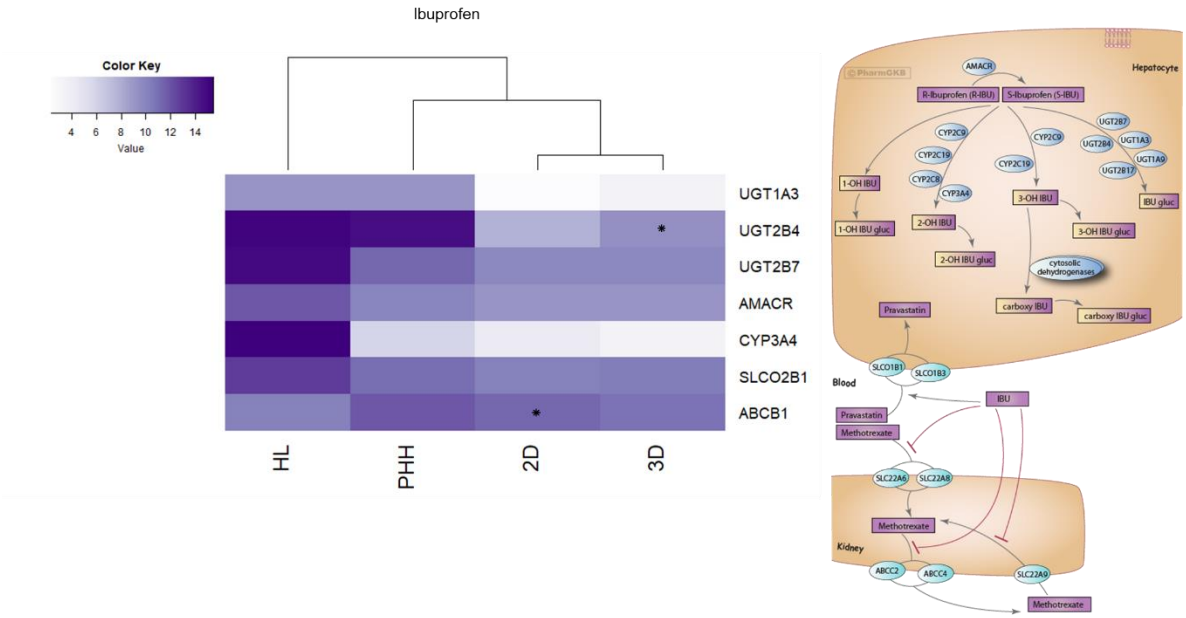

Figure 5.18: With ibuprofen metabolism, UGT2B4 is significantly upregulated in 3D primed HepG2 cells, and the transporter ABCB1 is significantly upregulated in 2D HepG2 cells.

Heatmap made using the Heatmap.2 package in R. Heatmap made from average normalised expression values in each condition using a list of known ibuprofen interactors pulled from Drugbank. Colour key equates to log10 of the expression value; darker colours mean higher absolute expression. Euclidian clustering performed on the columns to show distance between samples. Stars in 2D or 3D columns indicate a significant increase (P adjusted value ≤0.05) in expression in that condition when 2D and 3D HepG2 cells are compared. Gene data from samples represents N= 4 Metabolic pathway provided from PharmaGKB under their Creative Commons Attribution-ShareAlike 4.0 International License available at https://www.pharmgkb.org/page/dataUsagePolicy. (Mazaleuskaya et al., 2015; Whirl-Carrillo et al., 2021)

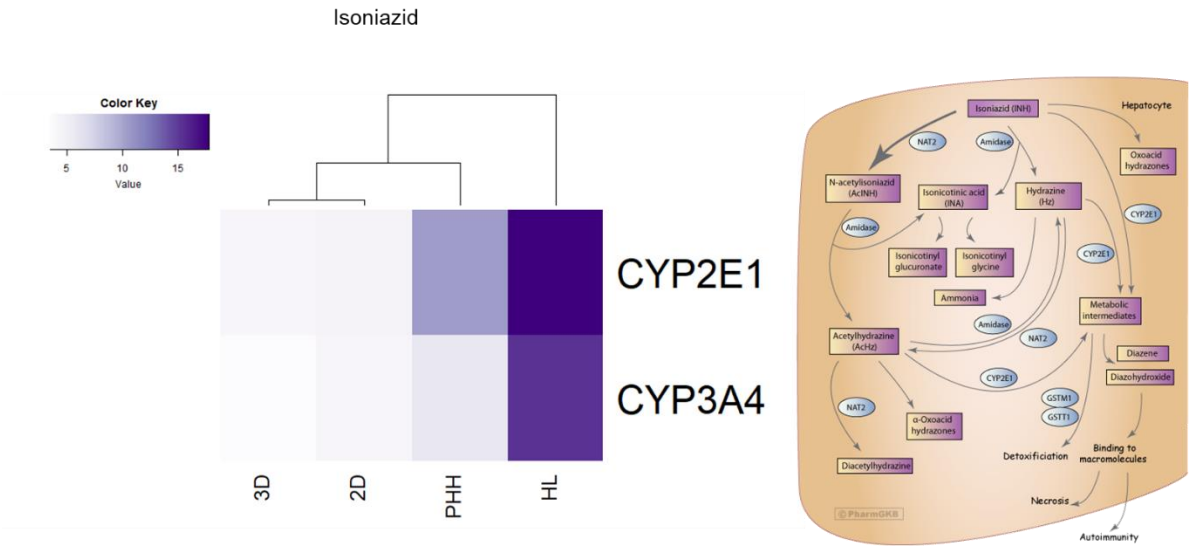

Figure 5.19: Isoniazid metabolism is not well explored, and the only known interacting enzymes are not differentially expressed between 2D and 3D primed HepG2 cells.

Heatmap made using the Heatmap.2 package in R. Heatmap made from average normalised expression values in each condition using a list of known isoniazid interactors pulled from Drugbank. Colour key equates to log10 of the expression value; darker colours mean higher absolute expression. Euclidian clustering performed on the columns to show distance between samples. Stars in 2D or 3D columns indicate a significant increase (P adjusted value ≤0.05) in expression in that condition when 2D and 3D HepG2 cells are compared. Gene data from samples represents N= 4 Metabolic pathway provided from PharmaGKB under their Creative Commons Attribution-ShareAlike 4.0 International License available at https://www.pharmgkb.org/page/dataUsagePolicy. (Klein et al., 2016; Whirl-Carrillo et al., 2021)

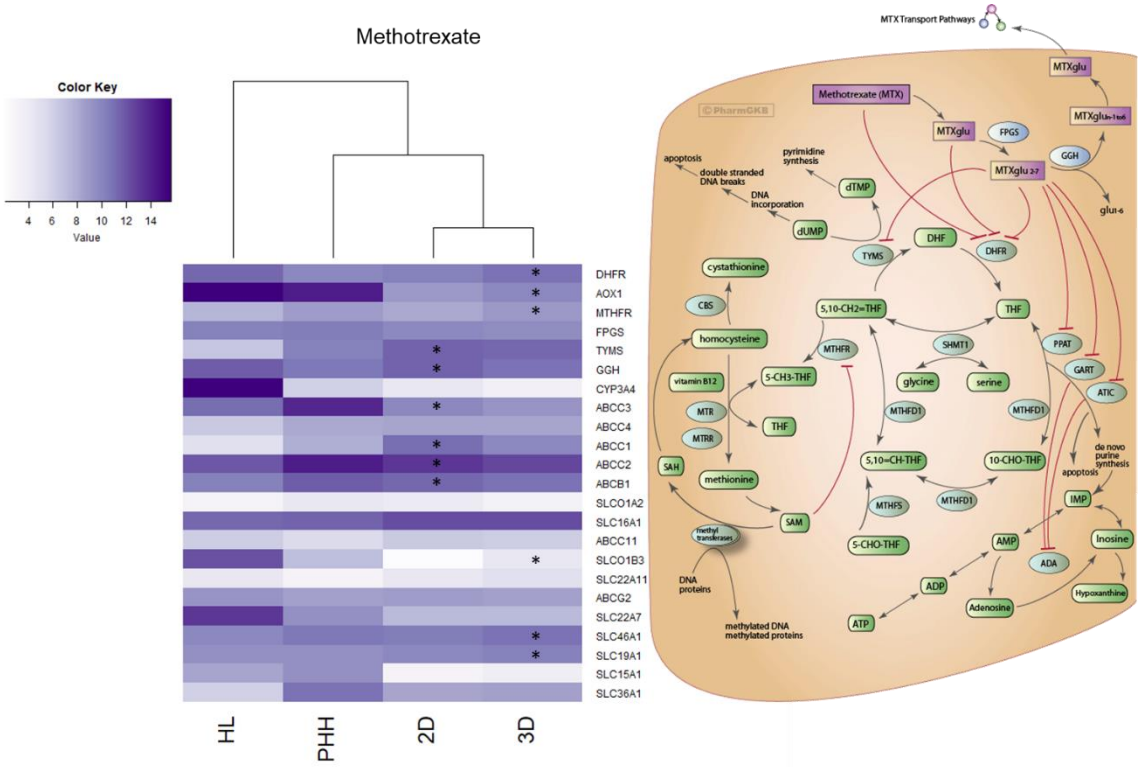

Figure 5.20: Gene expression of enzymes and transporters involved in methotrexate metabolism indicates a general trend towards enhanced metabolism and SLC transporters in 3D primed HepG2 cells, and increased ABC transporters in 2D HepG2 cells.

Heatmap made using the Heatmap.2 package in R. Heatmap made from average normalised expression values in each condition using a list of known methotrexate interactors pulled from Drugbank. Colour key equates to log10 of the expression value; darker colours mean higher absolute expression. Euclidian clustering performed on the columns to show distance between samples. Stars in 2D or 3D columns indicate a significant increase (P adjusted value ≤0.05) in expression in that condition when 2D and 3D HepG2 cells are compared. Gene data from samples represents N= 4 Metabolic pathway provided from PharmaGKB under their Creative Commons Attribution-ShareAlike 4.0 International License available at https://www.pharmgkb.org/page/dataUsagePolicy. (Mikkelsen et al., 2011; Whirl-Carrillo et al., 2021)

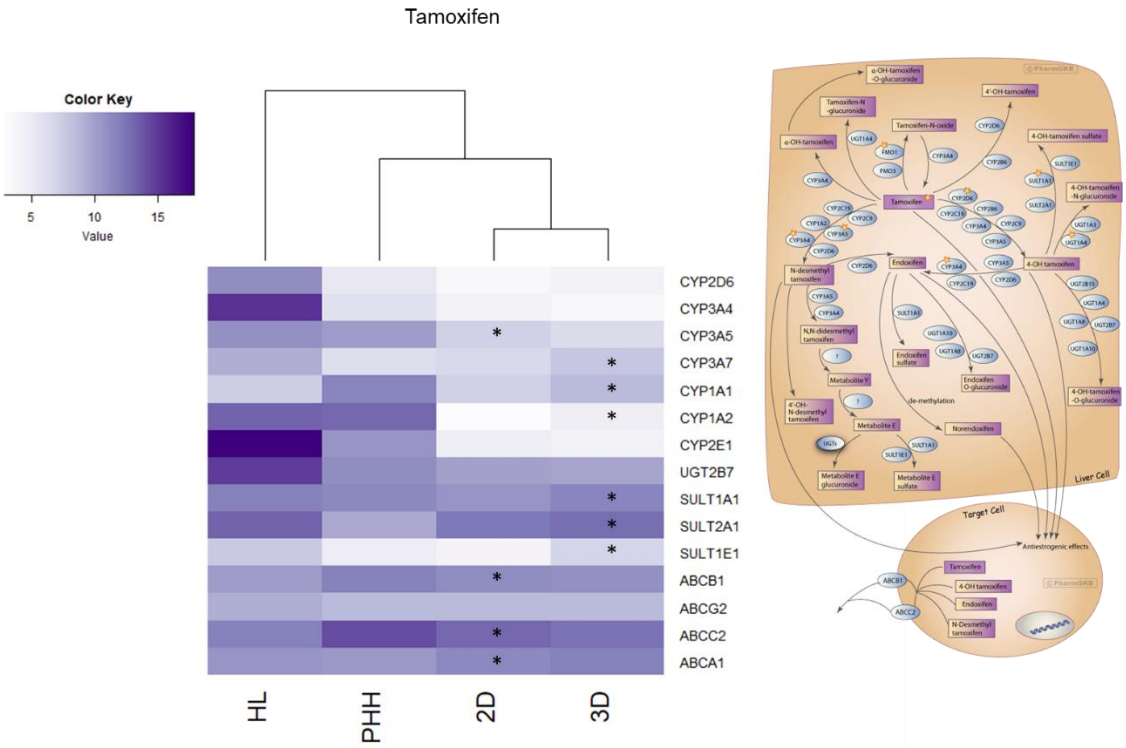

Figure 5.21: Genes involved in Tamoxifen metabolism indicates a similar trend towards enhanced metabolism in 3D primed HepG2 cells, and increased ABC transporters in 2D HepG2 cells.

Heatmap made using the Heatmap.2 package in R. Heatmap made from average normalised expression values in each condition using a list of known tamoxifen interactors pulled from Drugbank. Colour key equates to log10 of the expression value; darker colours mean higher absolute expression. Euclidian clustering performed on the columns to show distance between samples. Stars in 2D or 3D columns indicate a significant increase (P adjusted value ≤0.05) in expression in that condition when 2D and 3D HepG2 cells are compared. Gene data from samples represents N= 4 Metabolic pathway provided from PharmaGKB under their Creative Commons Attribution-ShareAlike 4.0 International License available at https://www.pharmgkb.org/page/dataUsagePolicy. (Klein et al., 2013; Whirl-Carrillo et al., 2021)

Table 5.2: Rate limiting or key enzymes involved in metabolism of each xenobiotic agent.

Drug	Rate limiting / key enzyme	Reference	2D vs 3D Significant change?
Amiodarone	CYP3A4 and CYP2C8 (key enzymes metabolising amiodarone to main metabolite desethylamiodarone).	(Latini et al., 1984)	No
Gemfibrozil	Unknown	N/A	N/A
Ibuprofen	CYP2C9 (key enzyme responsible for ibuprofen clearance, catalyses formation of 3-hydroxy-ibuprofen)	(Kepp et al., 1997)	No
Isoniazid	NAT-2 (rate-limiting acetylating isoniazid to acetylisoniazid)	(Desta and Flockhart, 2017)	No
Methotrexate	FPGS (key enzyme converting methotrexate to active methotrexate polyglutamates)	(Barredo et al., 1994)	No
Tamoxifen	CYP2D6 (rate-limiting metabolising tamoxifen to endoxifen)	(Dean, 2012)	No

5.4.6 Hepatic genes are upregulated in 3D HepG2 cells, and mechanotransduction related genes are upregulated in 2D HepG2 cells.

A selected set of liver related genes, with the addition of the proliferative markers Ki67 and PCNA were analysed and compared to human liver and PHH cells (**Figure 5.22**). Most of these genes were selected because they are known to be expressed in hepatocytes, with many of them being essential functional products of this cell type. With these functionally important genes, there is a very distinctive trend of upregulation in the 3D HepG2 cells. Notably, albumin (ALB) expression is increased significantly (1.69-fold upregulated) in 3D HepG2 cells. This is one of the most common liver biomarkers used to test general metabolic competency in hepatic models, so it is a positive sign of a more hepatic phenotype induced in 3D culture, though albumin expression is massively upregulated in human liver compared to even the 3D HepG2 cells. Interestingly, expression of albumin is significantly higher in the 3D HepG2 cells than the PHHs (2.37-fold change) which was an unexpected direction of change, potentially an effect of the 2D culture dedifferentiating and making the PHHs 'less physiological'.

Expression of the fibrinogen genes (FGA, FGB, FGG) is also higher in the 3D HepG2 cells bringing them closer to the expression levels in the human liver, though interestingly again moving them further from the lower expression in PHHs. Antithrombin (SERPINC1), an important liver synthesised enzyme involved in regulating coagulation (Flood and Scott, 2018) is also upregulated in the 3D primed HepG2 cells, as are SERPINA6, thrombopoietin (THPO) and transthyretin (TTR) and protein S (PROS1) all being brought closer to the expression levels in human liver, often above the expression in PHH cells too. Hepatocyte nuclear factor 4 alpha and gamma (HNF4A, HNF4G) are also upregulated in 3D, though expression of these is quite weak in human liver. These genes encode the two isoforms of hepatocyte nuclear factor 4 with the alpha isoform particularly implicated in regulating liver differentiation, with evidence that it is also involved in transcriptional regulation of CYP3A4 by pregnane X receptor (PXR) and constitutive androstane receptor (CAR) (Tirona et al., 2003; Walesky and Apte, 2015). It is possible that the lower expression in the liver is due to a more terminally differentiated state of the cells, whereas in the HepG2 cells, the higher epigenetic plasticity may still require expression of this nuclear receptor.

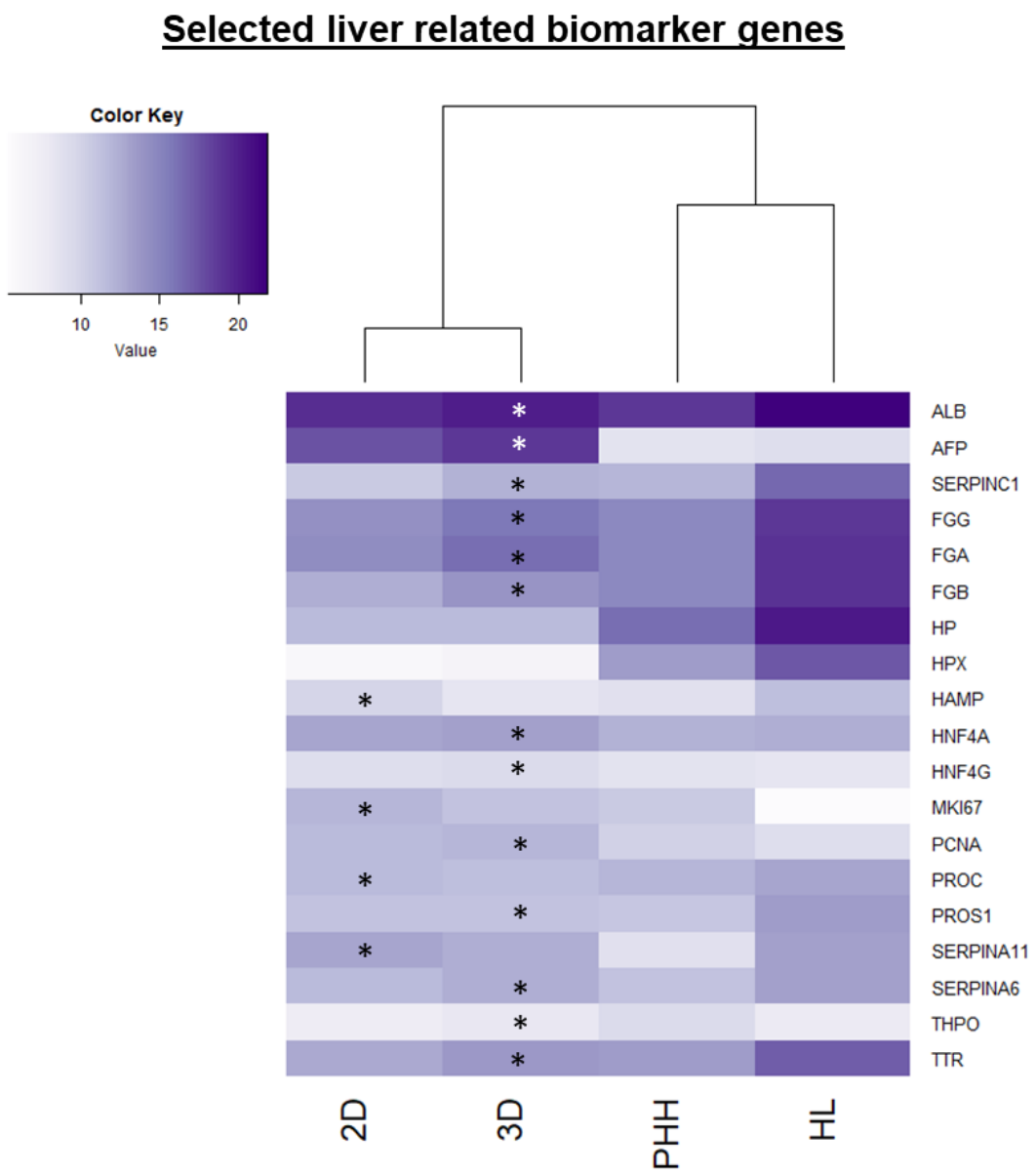

Figure 5.22: Functional genes involved in hepatic processes are mostly enhanced in expression in 3D primed HepG2 cells compared to 2D HepG2 cells.

Heatmap made using the Heatmap.2 package in R. Heatmap made from average normalised expression values in each condition using a list containing genes of interest. Colour key equates to log10 of the expression value; darker colours mean higher absolute expression. Euclidian clustering performed on the columns to show distance between samples. Stars in 2D or 3D columns indicate a significant increase (P adjusted value ≤0.05) in expression in that condition when 2D and 3D HepG2 cells are compared. Gene data from samples represents N= 4

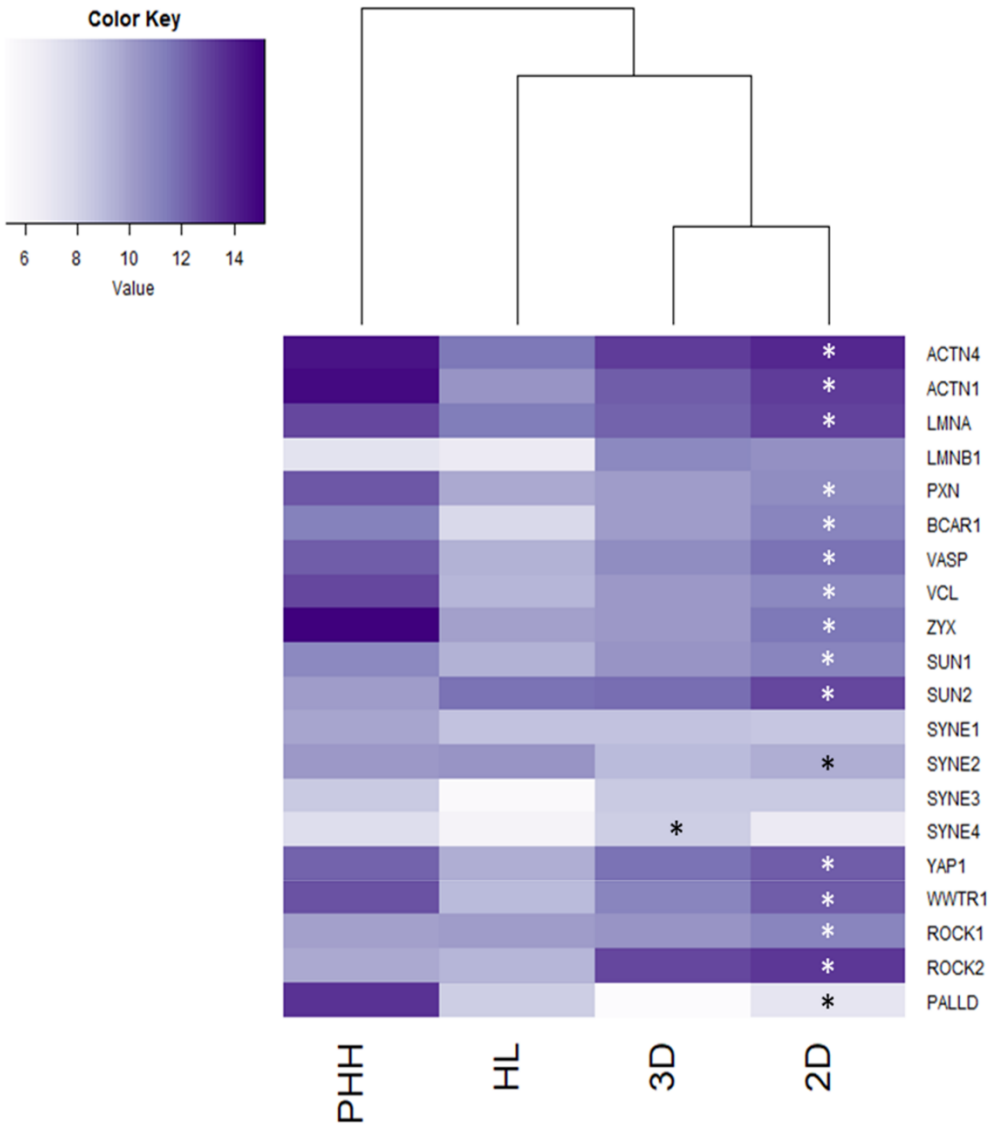

Figure 5.23: Genes involved in mechanotransduction processes are almost unanimously upregulated in 2D HepG2 cells compared to 3D primed HepG2 cells.

Heatmap made using the Heatmap.2 package in R. Heatmap made from average normalised expression values in each condition using a list containing genes of interest. Colour key equates to log10 of the expression value; darker colours mean higher absolute expression. Euclidian clustering performed on the columns to show distance between samples. Stars in 2D or 3D columns indicate a significant increase (P adjusted value ≤0.05) in expression in that condition when 2D and 3D HepG2 cells are compared. Gene data from samples represents N= 4

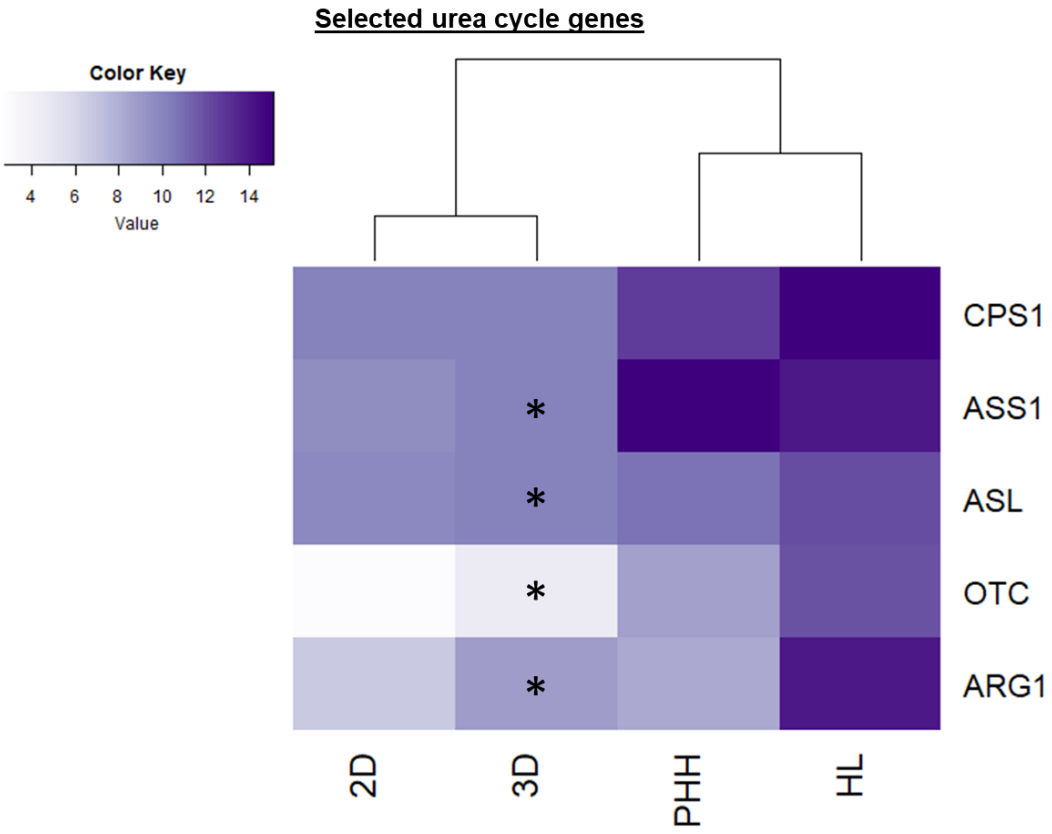

Figure 5.24: Genes involved in the urea cycle are upregulated in 3D primed HepG2 cells compared to 2D HepG2 cells.

Heatmap made using the Heatmap.2 package in R. Heatmap made from average normalised expression values in each condition using a list containing genes of interest. Colour key equates to log10 of the expression value; darker colours mean higher absolute expression. Euclidian clustering performed on the columns to show distance between samples. Stars in 2D or 3D columns indicate a significant increase (P adjusted value ≤0.05) in expression in that condition when 2D and 3D HepG2 cells are compared. Gene data from samples represents N= 4

A curious exception is hepcidin antimicrobial peptide (HAMP), encoding for hepcidin which is synthesised primarily in the liver (Strnad et al., 2011). This gene is upregulated in the 2D HepG2 cells, where it is expressed at a similar level to human liver, albeit with a reasonably low absolute expression. The other two liver related genes upregulated in 2D are for protein C, inactivator of coagulation factors Va and VIIIa (PROC) and SERPINA11, which are both closer to the human liver expression levels in 2D HepG2 cells. These show that despite a very clear overall pattern, of hepatic upregulation in 3D cells, there are certain exceptions to this rule. Ki67, a proliferative marker is upregulated in 2D HepG2 cells too, however this is expected based on the higher rates of proliferation observed in prior chapters; and this is almost completely absent in the human liver indicating the terminally differentiated state of *in vivo* hepatocytes with low proliferation. Having said that, a second proliferation marker, PCNA was also present at low levels in the liver, but was upregulated in 3D unexpectedly, though Ki67 has been shown to be more sensitive for detecting proliferation levels in tumours (Mateoiu et al., 2011; Oka et al., 2011) so Ki67 is potentially more accurate here.

In addition to the specific hepatic genes, the expression levels of a curated set of genes central to mechanotransduction processes was analysed (**Figure 5.23**). There is an instantly recognisable pattern of significant upregulation of all of these genes in the 2D HepG2 cells apart from lamin B4 (LMNB4), nesprin-1 and -3 (SYNE1, SYNE3) which are not significantly differentially expressed, and nesprin-4 (SYNE 4) which is upregulated in 3D. The genes were selected based on their known involvement with mechanotransduction and the function of many of these were discussed in depth in the literature review (**Chapter 1**), such as genes involved in regulating actin dynamics; actinin-1 (ACTN1), actinin-4 (ACTN4), vinculin (VCL), VASP, zyxin (ZYX), ROCK1, ROCK2, palladin (PALLD). These genes involved in actin organisation, polymerisation and dynamics were all upregulated in 2D HepG2 cells and in most cases had elevated expression when also compared to the human liver which was closer to the expression levels in the 3D HepG2 cells. The 2D HepG2 cells had a closer expression profile of the mechanotransduction genes to the PHH cells which also showed stronger expression in many of these genes, suggesting that the transcription of these genes is indeed a result of the culture on a two-dimensional substrate as the cells are adapting to a non-physiological microenvironment.

Additionally, the nuclear related lamins (LMNA, LMN4B1) and sun (SUN1, SUN2) genes were upregulated in 2D HepG2 cells, with 3D HepG2 cells and human liver showing more

comparable expression, though PHH cells did not show elevated levels of these genes, with LMNB1 even being nearly completely absent in both the human liver and PHHs. The transcription regulators YAP1 (YAP), WWTR1 (TAZ) are implicated in signal transduction of mechanical cues and these were both upregulated in 2D HepG2 cells as well. YAP and TAZ were upregulated by about 1.5 and 2.2-fold respectively in the 2D cells, with very similar expression levels to the PHHs, whereas the 3D primed HepG2 cells were closer to the expression levels in human liver. Paxillin and BCAR1, both involved in focal adhesions show very similar expression patterns as the rest of the genes. These data reveal that the mechanical stress of 2D culture is inducing expression of genes involved in cell morphology and mechanical signal transduction, which is differential to the expression profiles *in vivo*. The fact that changes are occurring here at a transcriptional level shows that the dimensionality of the cell culture substrate is creating more than just a superficial alteration in cell shape; it is causing changes in gene expression that – as previous chapters have shown – results in a retained phenotype after liberation and reseeding.

5.4.7 Over-representation analysis reveals over-representation of metabolic and biosynthetic processes in 3D primed HepG2 cells.

Over-representation analysis was performed on genes significantly upregulated by ≥1.2-fold in 2D or 3D using EnrichR online software (Chen et al., 2013). Two sets of GO annotations were analysed using this method: biological processes and cellular component (**Figure 5.25**). This data shows the most over-represented biological processes and cellular components within the user's data set as the longest and lightest bars on the bar chart. With the biological processes, the genes upregulated in 2D HepG2 cells are over-represented in multiple transcriptional regulatory processes, in addition to cell migration, apoptotic processes, signal transduction, cell cycle regulation, and apoptosis. Conversely, in 3D HepG2 cells, three of the most over-represented biological processes are biosynthetic processes for sterol, cholesterol and secondary alcohol. Cholesterol metabolism and amino acid catabolism are also strongly enriched in 3D primed HepG2 cells alongside mitochondrial translational processes. The upregulation in biosynthetic and metabolic processes are key indicators of enhanced hepatic function in 3D primed cells; alcohol, and cholesterol metabolism/biosynthesis are all primarily functions localised to the liver (Berg et al., 2002; Cederbaum, 2012), and the fact that genes with these annotations are overrepresented in the genes upregulated in 3D primed HepG2 cells shows that the 3D microenvironment is significantly enhancing hepatic function and increasing the metabolic and biosynthetic capacity of these cells.

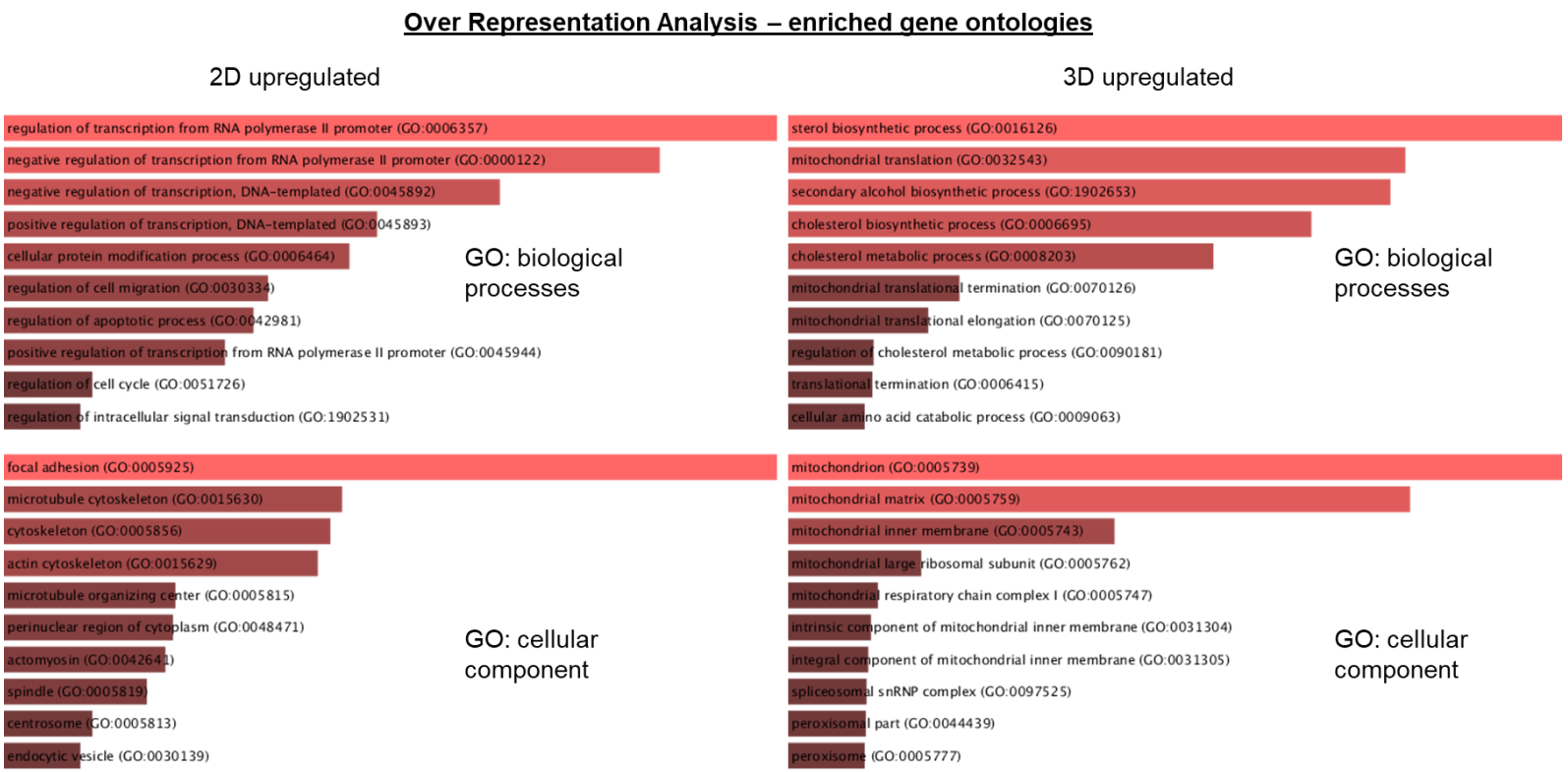

Figure 5.25: Over representation analysis using gene ontology shows that the upregulated genes in 3D primed HepG2 cells exhibit a hepatic phenotype.

Over representation analysis using a set of genes significantly (P adjusted value ≤0.05) upregulated by over 1.2-fold in either 2D HepG2 cells (left) or 3D primed HepG2 cells (right) in the EnrichR online software to calculate enriched biological processes (top) and cellular components (bottom). GO 2018 terms used for analysis. Length and lightness in colour of the bars indicates significance of that selected category (grey would indicate no significance, FDR ≥0.05). Gene data from samples represents N= 4

Additionally, the over-represented processes in 2D show that transcription is altered and that genes involved in transcriptional regulation are over-represented. This in combination with the over-representation of signal transduction suggests the role of mechanotransduction in altering transcriptional machinery due to growth in a 2D microenvironment. This evidently results in mechanical changes towards a non-physiological phenotype where fundamental biological processes are changed. Alongside this, there is an indication that the 2D HepG2 cells are exhibiting a more cancerous phenotype, with regulation of apoptosis, regulation of migration and regulation of cell cycle being significantly altered. Further to this, the bottom bar charts showing cellular components are very revealing through showing which specific areas of the cell are over-represented. In the 2D HepG2 cells, there is marked over-representation in many components closely linked to mechanotransduction responses – focal adhesions, microtubules, actin cytoskeleton and actomyosin to name a few. The fact that focal adhesions are the most enriched is predictable considering the integrin expression patterns, but this confirms the mechanical alterations are bringing the cells away from a physiological phenotype in 2D and explains the altered transcriptional machinery and signal transduction. In the 3D primed HepG2 cells, genes associated with various regions within the mitochondria are overrepresented which fits with the enhanced metabolism and biosynthesis – mitochondria densely populate hepatic cells and are the location for hepatic metabolism of carbohydrates, lipids and proteins (Degli Esposti et al., 2012).

In addition to the GO ontologies, over-representation analysis was also carried out by making a comparison with known gene expression in human tissues as provided by the human gene atlas (**Figure 5.26**). From these bar charts it is clear that the genes upregulated in 3D are highly liver specific due to the most significant over-representation in 3D HepG2 cells being in the human liver, with lymphoblasts and foetal liver being the next best matches (though the significance drops markedly after human liver). The 2D HepG2 cells however show a wide range of tissues in the significantly over-represented genes, with CD33+ myeloid tissue being the most significant, followed closely by colorectal adenocarcinoma and smooth muscle. This serves to demonstrate the wide-ranging enrichment occurring in 2D culture compared to the very liver specific enriched genes in 3D priming cultures and further reinforces the hypothesis that 3D cell culture is inherently more physiological.

Over Representation Analysis – tissue comparison

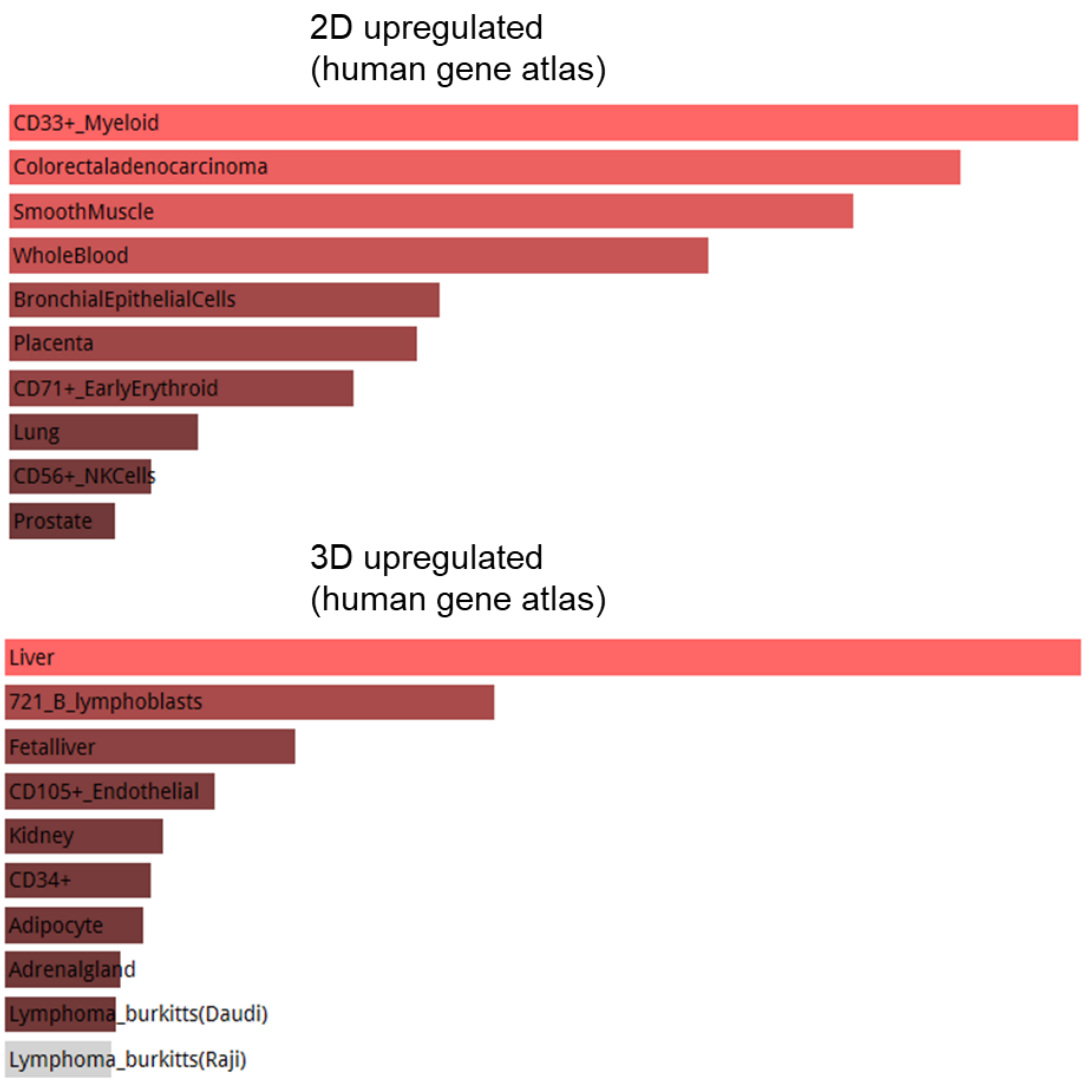

Figure 5.26: Upregulated genes in 3D primed cells match gene expression in liver tissue.

Over representation analysis using a set of genes significantly (P adjusted value ≤0.05) upregulated by over 1.2-fold in either 2D HepG2 cells (top) or 3D primed HepG2 cells (bottom) in the EnrichR online software to calculate similarity to known expression in human tissue as provided by human gene atlas. Length and lightness in colour of the bars indicates significance of that selected category (grey would indicate no significance, FDR ≥0.05). Gene data from samples represents N= 4

5.4.8 Gene set enrichment analysis shows significant enrichment in metabolic and biosynthetic processes in 3D primed HepG2 cells.

Moving on from ORA, gene set enrichment was used to create an un-biased analysis of the sequencing data due to no user selected fold change cut-off level in the data, with only a significance cut-off applied of P adjusted ≤0.05. This was able to take into account all the genes that were significantly differentially expressed between 2D and 3D grown HepG2 cells and revealed which ontologies were enriched in either culture model. Firstly, the GO enriched biological processes were analysed (**Figure 5.27**). This data showed an astounding pattern of metabolic enrichment in the 3D primed HepG2 cells, with many of the top 20 enriched GO terms being metabolic processes often specific to the liver, including steroid metabolism, fatty acid metabolism, amino acid metabolism, antibiotic metabolism. In addition to the vast and broad metabolic enrichment, mitochondrial gene expression is enriched, further demonstrating enhanced hepatic capacity as this is metabolic centre within the hepatocytes. Organic acid transport and extracellular regulation of signal transduction are also enriched in 3D primed HepG2 cells interestingly, contrasting to the over-representation of 'regulation of signal transduction' in the 2D HepG2 cells in the ORA. With terms describing enriched regulation there is sometimes a degree of ambiguity as to which direction the regulation is in, so it is possible that 3D and 2D cultures are regulated in opposite manners regarding signal transduction regulation.

The enriched processes in 2D HepG2 cells reveal a broad range of functions that are altered in monolayer cultures. There is however a repeating theme of enrichment in mechanotransduction-linked processes; response to mechanical stimulus, positive regulation of cell motility, cell-cell fusion, tissue migration cell junction organisation, actomyosin structure organisation are all enriched in 2D which is incredibly revealing about the mechanical changes taking place. The enrichment in these very structural and mechanical processes and the complete absence of any hepatic related enrichment in 2D shows how a non-physiological form of mechanotransduction is occurring. The inference here is that cells cultured in 3D are in their natural structural state where hepatic function is at peak activity, whereas in 2D, the cells are significantly structurally altered, with these mechanical changes negatively affecting hepatic function. Additionally, a number of the enriched terms in 2D suggest a more proliferative and potentially mesenchymal phenotype in these cells too, with angiogenesis being the most enriched term, alongside motility related terms, hinting at this mesenchymal phenotype that is less differentiated than the 3D equivalent. The other

enriched terms in 2D highlight how wide ranging the transcriptomic changes are, with epidermis development, muscle system processes and photoreceptor cell differentiation being some unusual terms of enrichment. These point to the wider picture however of unpredictable and non-physiological changes occurring in 2D which could also further indicate a more cancerous and less differentiated phenotype, whereas the changes in 3D are a lot more specific and focussed on hepatic function. The normalised enrichment scores here also indicate that this enrichment is considerably strong in either direction, meaning that these changes should have a significant impact on the biology of the cells.

Enrichment was also analysed using the GO molecular function category, which provides a more biochemical overview of the changes occurring (**Figure 5.28**). Again, in 3D primed HepG2 cells, the significant enrichment was primarily in metabolic functions, with oxidoreductase activity, transferase activity and steroid dehydrogenase activity being amongst the most enriched terms. In 2D HepG2 cells, a significant number of the enriched terms were in reactions involved in adhesion or actin binding, which further provides evidence as to the altered mechanical state of 2D cells.

Pathway based GSEA was then carried out to provide an even more contextual analytical approach. Through connecting to online pathway databases with known gene associations such as Reactome, GSEA can highlight which cellular pathways are enriched based on the gene expression within the user's sample. The first round of pathway analysis (**Figure 5.29**) was performed using the KEGG pathway database (Kanehisa and Goto, 2000) which contains a large list of metabolic pathways in addition to cellular processes, genetic information processing and more. The results from this pathway analysis show that – similar to the biological process enrichment – a large number of metabolic pathways are enriched in the 3D primed HepG2 cells, alongside a number of biosynthetic pathways. Many of these enriched pathways in 3D are integral to hepatic function; steroid hormone biosynthesis, fatty acid metabolism, drug metabolism, primary bile acid biosynthesis, metabolism of xenobiotics by cytochrome P450 are some of these crucial pathways. The strong specificity of the metabolic enrichment in 3D makes it clear that the unique substrate geometry is promoting a more hepatic phenotype, with 3D primed HepG2 cells being significantly more functionally competent than the 2D HepG2 cells.

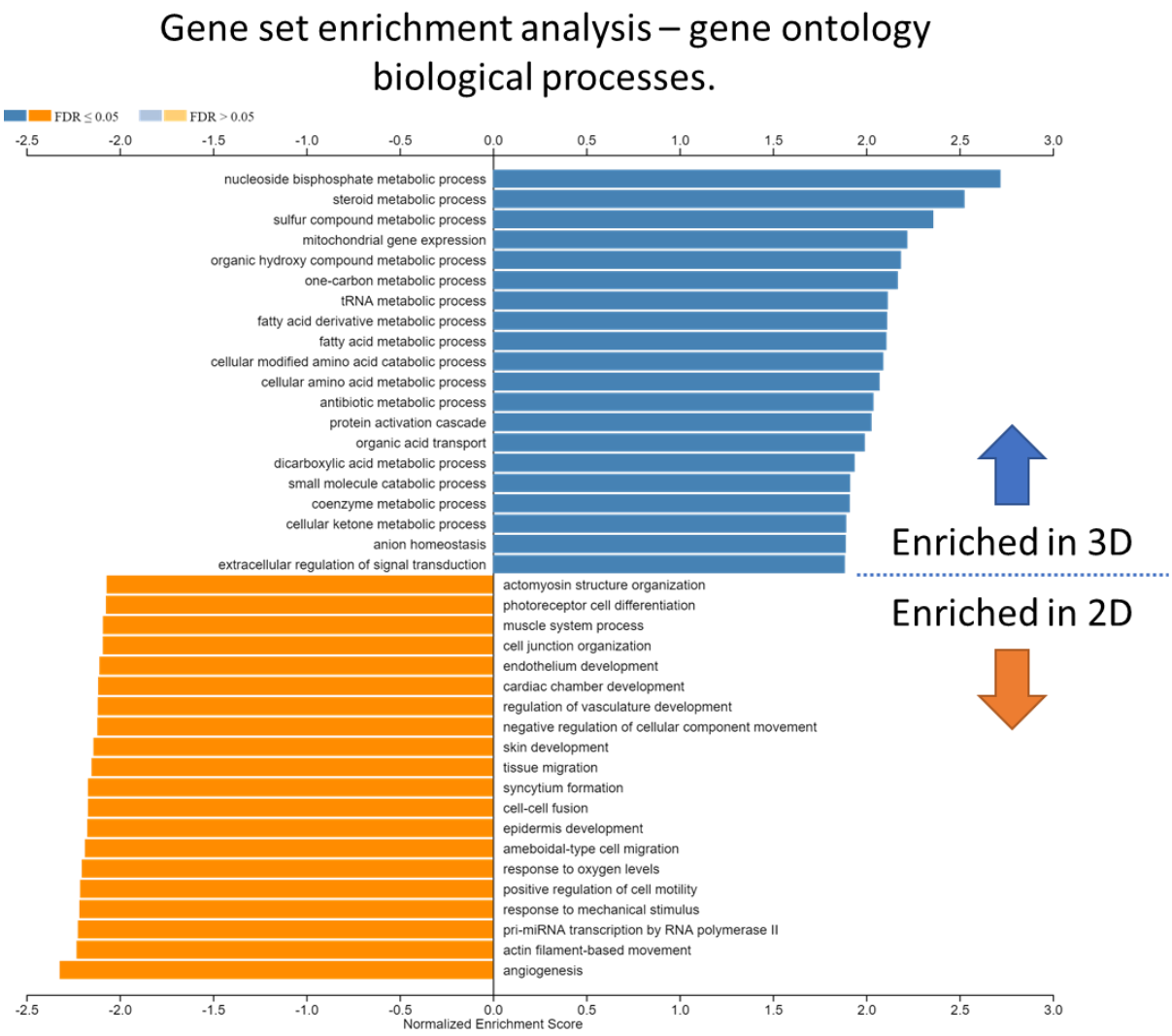

Figure 5.27: Gene set enrichment analysis shows enhanced metabolism and biosynthesis in 3D primed HepG2 cells and enhanced mechanical processes in 2D HepG2 cells.

Gene set enrichment analysis using a full set of significantly (P adjusted value ≤0.05) differentially expressed genes between 2D and 3D primed HepG2 cells, with log 2-fold change values provided. WebGestalt online software was used to calculate non-redundant enriched biological processes using gene ontology annotation downloaded from www.geneontology.org. Length of bars indicates normalised enrichment score, less intense colour would indicate non-significant results with an FDR value of less than 0.05. Gene data from samples represents N= 4

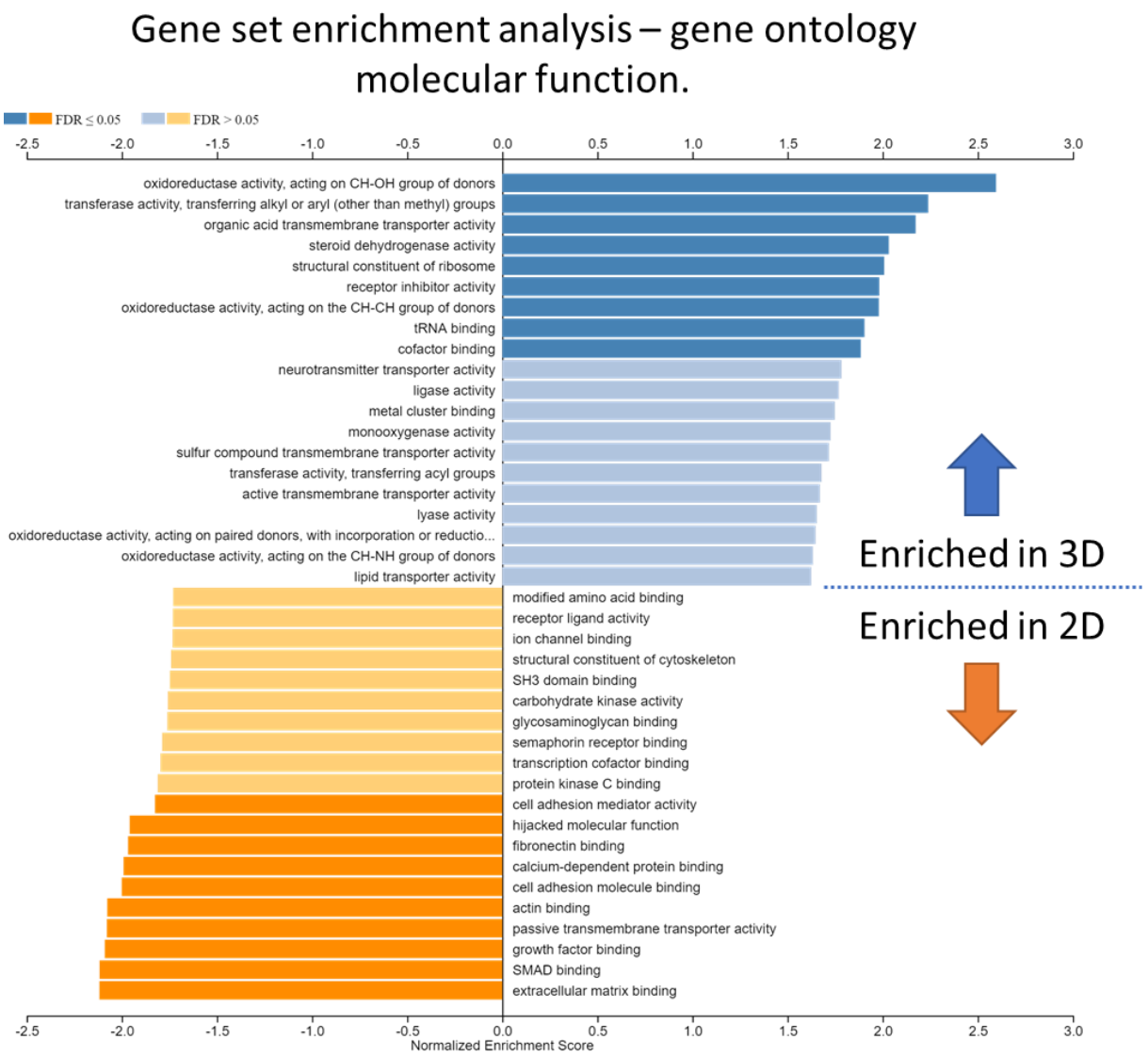

Figure 5.28: Gene set enrichment analysis shows that 2D HepG2 cells exhibit enriched structural properites in molecular function.

Gene set enrichment analysis using a full set of significantly (P adjusted value ≤0.05) differentially expressed genes between 2D and 3D primed HepG2 cells, with log 2-fold change values provided. WebGestalt online software was used to calculate non-redundant enriched molecular function using gene ontology annotation downloaded from www.geneontology.org. Length of bars indicates normalised enrichment score, less intense colour would indicate non-significant results with an FDR value of less than 0.05. Gene data from samples represents N= 4

In contrast to the focussed enrichment of metabolic pathways in 3D, a smaller number of pathways are enriched in 2D. Some of these pathways are expected areas of enrichment, such as focal adhesion and ECM-receptor interaction, being related to the structural differences in 2D. However, the enriched pathways in 2D are seemingly a lot more random than those in 3D, with malaria, cardiac muscle contraction and legionellosis being some particularly wide-ranging areas of enrichment. MAPK signalling pathway and the HIF-1 signalling pathway are upregulated too, and these are both implicated in tumour progression and cell proliferation (Goda et al., 2003, p. 1; Zhang and Liu, 2002b). Alongside the enrichment in microRNAs in cancer, this suggests a more cancerous phenotype in 2D, which fits with previous observations of higher proliferation rates and less epithelial like morphology in monolayer culture. The lower number, and less focussed set of enriched pathways in 2D HepG2 cells compared to the clear functional enrichment in 3D HepG2 cells is testament to the power of mechanotransduction in universally enhancing the tissue specific function of a cell line that is grown in conditions that more closely resemble the *in vivo* microenvironment.

The second round of pathway analysis was performed using Wikipathways (Slenter et al., 2018) (**Figure 5.30**). With the gene expression data compared to the pathways, there is yet again a very similar range of pathways upregulated in 3D primed HepG2 cells, with the focus resting heavily on metabolism and biosynthesis. Cholesterol metabolism and biosynthesis are strongly enriched (normalised enrichment scores of between 2.5 and 3.0) in 3D primed HepG2 cells; a key function of hepatocytes. These are followed by strong enrichment in a variety of metabolic pathways including phase I and II biotransformation, fatty acid biosynthesis and sulfation biotransformation reaction. PPAR signalling is also enriched, a pathway involved in lipid metabolism, glucose metabolism and metabolic homeostasis (Ahmadian et al., 2013), functions that are important to hepatic cells. The blood clotting cascade is also enriched, and coagulation factors are a key product of hepatocyte synthesis. Liver X receptors are also enriched in 3D primed HepG2 cells and these are key receptors involved in liver specific function such as lipid metabolism. These enriched pathways in 3D show a strong selective enrichment in functions that are specific to or at least play a major role in the function of hepatocytes, and importantly, this corroborates with the general trend of enriched pathways as detected with the KEGG database.

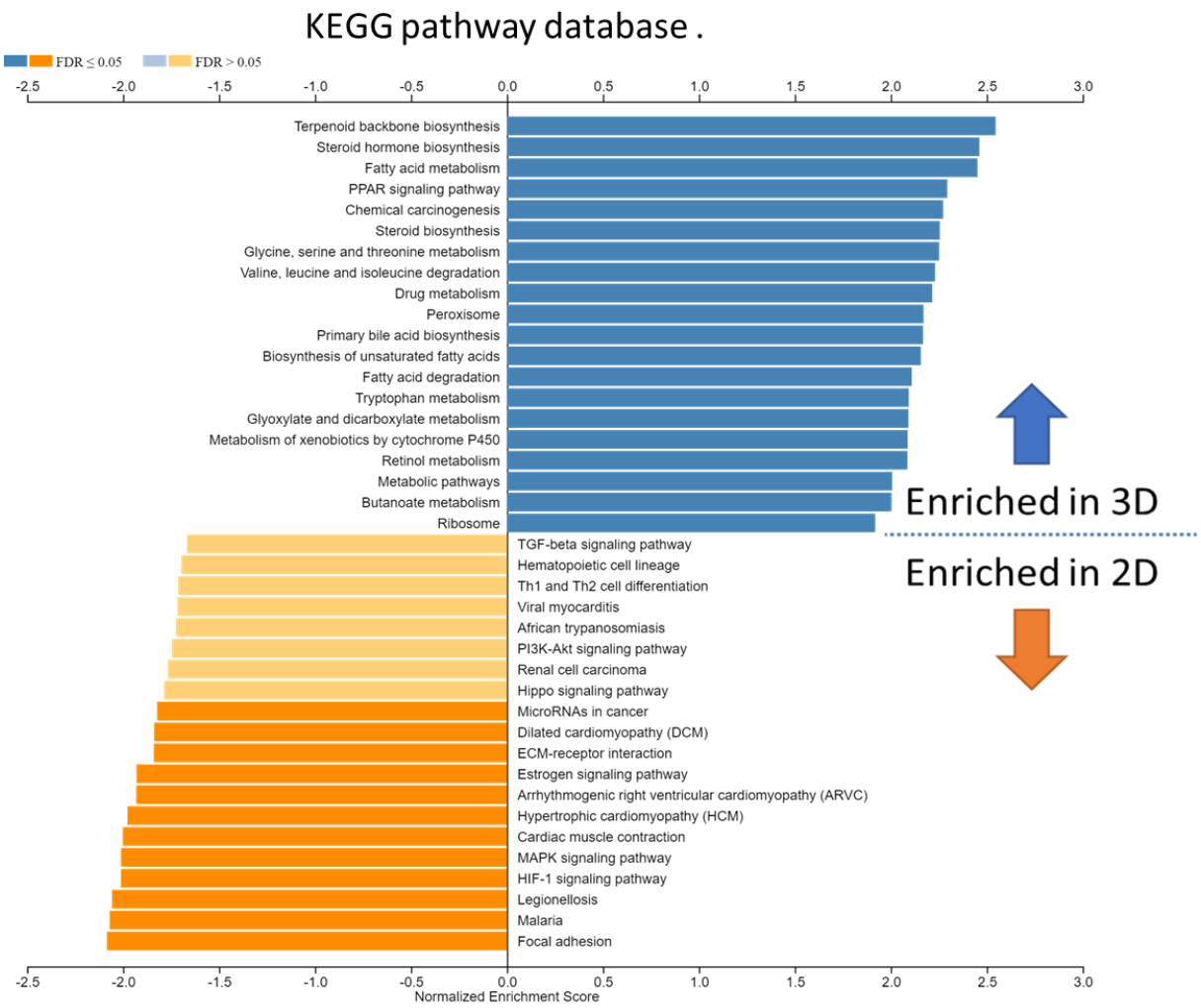

Figure 5.29: GSEA KEGG pathway analysis further demonstrates enrichment in metabolic and biosynthetic pathways in 3D primed HepG2 cells and enhanced adhesive and mechanical related pathways in 2D HepG2 cells.

Gene set enrichment pathway analysis using a full set of significantly (P adjusted value ≤0.05) differentially expressed genes between 2D and 3D primed HepG2 cells, with log 2-fold change values provided. WebGestalt online software was used to calculate enriched pathways within the KEGG pathway database (www.kegg.jp). Length of bars indicates normalised enrichment score, less intense colour indicates non-significant results with an FDR value of less than 0.05. Gene data from samples represents N= 4

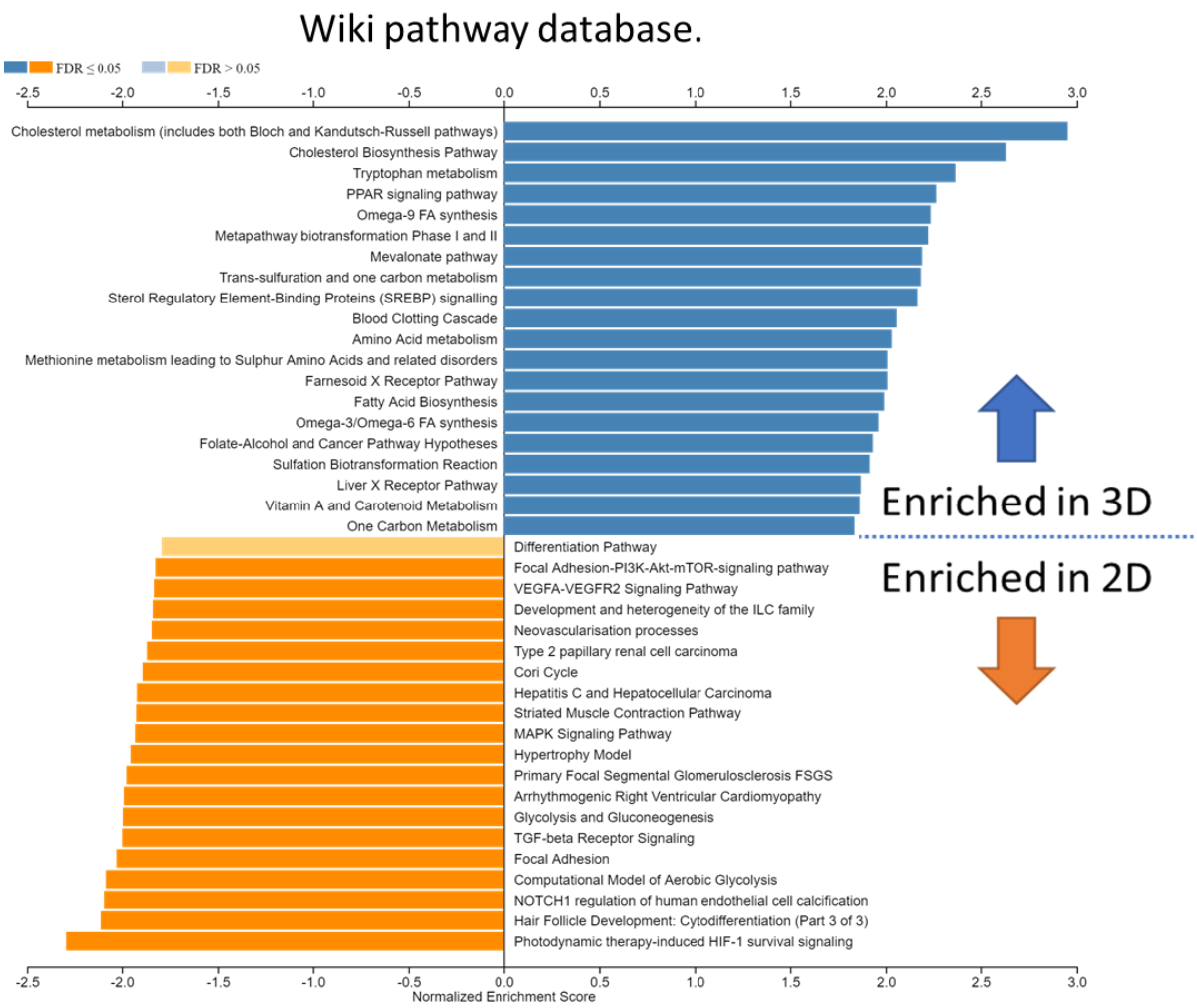

Figure 5.30: GSEA Wiki pathway analysis confirms that 3D primed cells have enriched biosynthetic and metabolic properties.

Gene set enrichment pathway analysis using a full set of significantly (P adjusted value ≤0.05) differentially expressed genes between 2D and 3D primed HepG2 cells, with log 2-fold change values provided. WebGestalt online software was used to calculate enriched pathways within the Wiki pathway database (www.wikipathway.org). Length of bars indicates normalised enrichment score, less intense colour indicates non-significant results with an FDR value of less than 0.05. Gene data from samples represents N= 4

In the 2D HepG2 cells, the enriched pathways as detected by Wikipathways were incredibly diverse, affecting a wide range of cellular functions. No discernible theme of the enriched functions was evident in these cells, and similar to the KEGG analysis, there were a lower number of enriched pathways in 2D with lower normalised enrichment scores. A particularly notable area of enrichment in the 2D cells was the term 'hepatitis C and hepatocellular carcinoma' which indicates that genes with higher expression in the 2D HepG2 cells were genes associated with a disease and cancerous phenotype. Focal adhesions are also enriched, again indicating the structural alterations and larger focal adhesions that are known to form on stiffer substrates. MAPK signalling is also enriched according to Wikipathways, with TGF-β receptor signalling too. Under normal conditions, TGF-β can act as either an inhibitor of proliferation or a promotor of proliferation and tumorigenesis depending on the cell type and tumour stage. In hepatocellular carcinoma however TGF-β levels have been found to be elevated, and correlates with poor prognosis (Kubiczkova et al., 2012, p.; Teicher, 2001) indicating the role it may play in the HepG2 cells in promoting proliferation (which also fits with the higher proliferation seen in prior chapters). An unexpected pathway that is enriched in 2D HepG2 cells is glycolysis and gluconeogenesis which is a function that hepatocytes perform, presenting a possible exception to the overall trend of enhanced hepatic function in 3D, with a case of enriched function in 2D HepG2 cells instead. It is to be expected that there are cases that do not fit the overall trend, and there is still a considerably strong case here pointing towards functional enrichment in 3D.

The final pathway database analysed was the Reactome database (Fabregat et al., 2017), which provides a wide range of cellular pathways including classical intermediary metabolism, signalling, transcriptional regulation and apoptosis (**Figure 5.31**). Here, there is high concordance with the previous two pathway databases in that 3D primed HepG2 cells show enrichment in a range of liver specific metabolic and biosynthetic processes. The enriched pathways in 3D include cholesterol biosynthesis, metabolism of steroids, phase II-conjugation of compounds and synthesis of bile acids and bile salts. It appears that Reactome has picked up enrichment particularly in Phase II metabolic pathways, with glutathione conjugation also enriched, and as seen in the individual gene expression data, phase II enzymes were clearly upregulated in 3D primed HepG2 cells as a general trend. The focus still remains on enhanced hepatic function with the Reactome enrichment in the 3D HepG2 cells, whereas the 2D cells show enrichment in pathways that are non-specific to hepatocytes. As with the other two pathway databases, the 2D cells have a lower number of significantly enriched pathways indicating a more disparate cohort of genes being

upregulated in 2D that affect a wider range of functions with less of a biologically meaningful basis. Of the pathways that are enriched, keratinization, collagen formation and muscle contraction are some of the more surprising areas, with this large spread of functions pointing towards the less differentiated phenotype of HepG2 cells in 2D. RAF-independent MAPK1/3 activation is enriched, showing a similar pattern with the other pathway databases, and enriched extracellular matrix organisation points towards the increased cell-substrate interactions occurring on a 2D planar substrate. As with Wikipathways, glycolysis is detected as an enriched pathway in the 2D cells with Reactome, further consolidating that this particular metabolic function is increased in monolayers.

Considering the data from the three combined pathway databases, there is a very high consistency in which pathways are enriched in the 3D primed HepG2 cells, all being metabolic and biosynthetic functions that are pertinent to the physiological functioning of hepatocytes. In 2D HepG2 cells however, there is a broader range of pathways that are enriched, with a number of these being involved in proliferation and ECM interactions. The disparity between the enrichment in 2D and 3D reveals the nature of mechanotransduction driving the 2D cells further away from a physiological phenotype and creating a more proliferative and potentially less differentiated cell population. In 3D cells, the mechanical microenvironment is closer to that of *in vivo* hepatocytes, which therefore results in a functional profile closer to that of the hepatocytes.

To demonstrate the wide-ranging enrichment in 2D HepG2 cells and the much more focussed enrichment in 3D primed HepG2 cells, a Voronoi diagram was created from the Reactome website (**Figure 5.32**). This diagram was created through using a specific form of GSEA available in Reactome called CAMERA which accounts for inter-gene correlation (Wu and Smyth, 2012). After running this analysis, all enriched pathways according to Reactome were listed, with significant enrichment in 3D (FDR value of ≤0.05) overlaid as bright yellow colouring, and significant enrichment in 2D (FDR value of ≤0.05) as dark blue. Less intense colouring indicated enrichment with an FDR value of over 0.05. The Voronoi tessellation provides a high-level overview of biological pathways by providing visual representation of all pathway groupings in the database, with overlaid enrichment data. As is very clear from the diagram creating with this data, there is a smaller range of upregulated pathways in 3D primed HepG2 cells, with most areas of significant enrichment lying within the parent

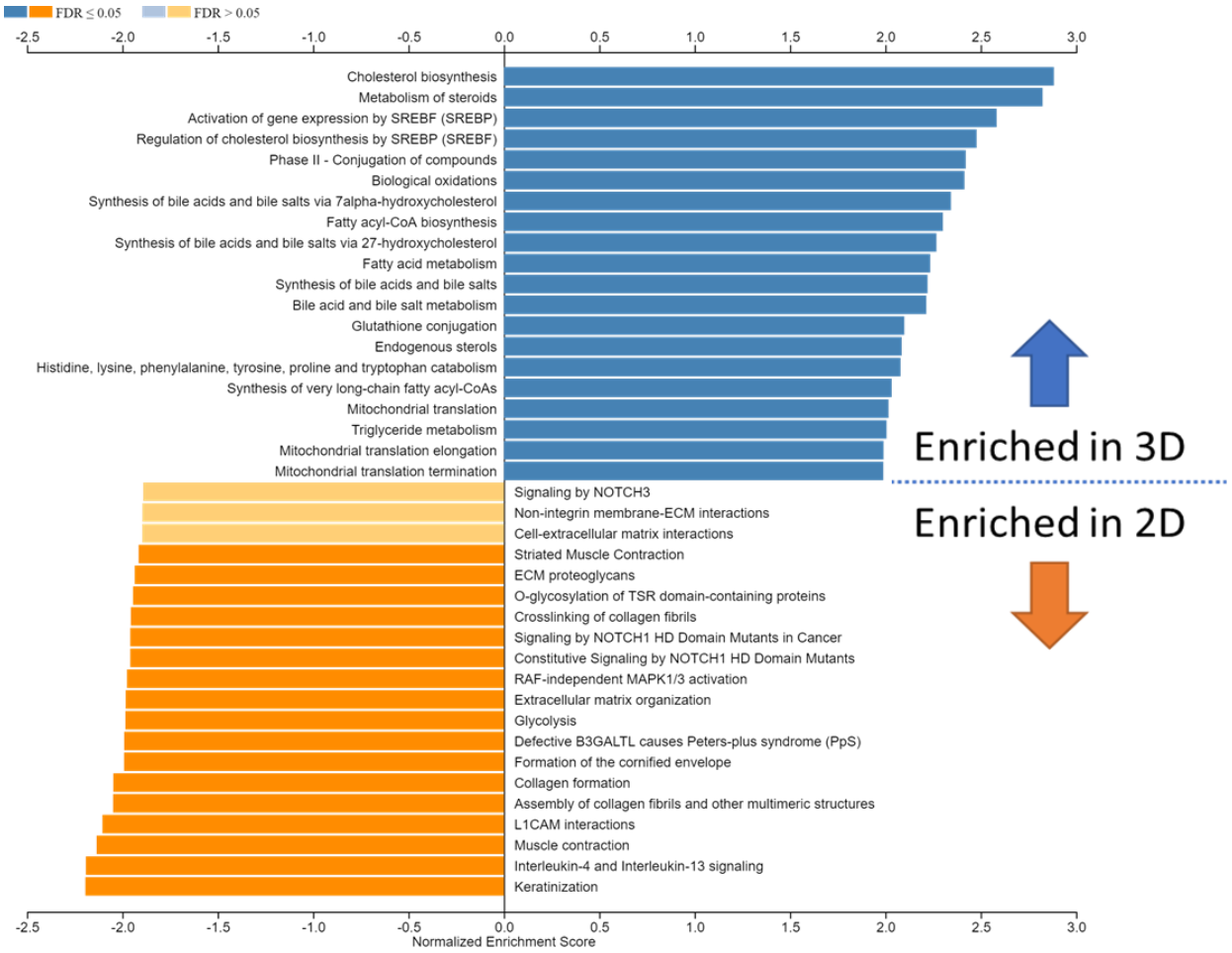

Figure 5.31: GSEA Reactome pathway analysis highlights wide ranging enriched processes in 2D HepG2 cells, but still shows enrichment in metabolic and biosynthetic pathways in 3D primed HepG2 cells.

Gene set enrichment pathway analysis using a full set of significantly (P adjusted value ≤0.05) differentially expressed genes between 2D and 3D primed HepG2 cells, with log 2-fold change values provided. WebGestalt online software was used to calculate enriched pathways within the Reactome pathway database (www.reactome.org). Length of bars indicates normalised enrichment score, less intense colour indicates non-significant results with an FDR value of less than 0.05. Gene data from samples represents N= 4

category of metabolism. Some wider enrichment occurs in protein localisation and DNA regulation, as well as some significantly enriched pathways in areas under metabolism of RNA and metabolism of proteins, but the categorical grouping of enrichment clearly lies within metabolic functions with 3D primed HepG2 cells.

Conversely, the 2D grown HepG2 cells show evidence of significant enrichment in 'parent' categories of ECM organisation, cell-cell communication and circadian clock. The former two of these highlights the upregulation occurring in many structurally related genes in 2D culture. Elsewhere, however, the 2D HepG2 cells have wide-spread enrichment in many specific pathways across the Voronoi tessellation, with no particular theme that is identifiable. Signal transduction does have a high number of enriched pathways in for 2D, though a lot of these are non-significant according to the FDR value. A particularly high number of enriched pathways in 2D appears to be present in signal transduction, and when combined with the specific enrichment in 3D, this shows that while signal transduction increases as a result of monolayer culture, this is not functionally beneficial to the cells and in fact may play a role in facilitating the less differentiated phenotype seen in the 2D HepG2 cells. This also provides a comprehensive overview of the depth and breadth available to researchers when using transcriptomic techniques. Without using an approach that analysed global gene expression, many of these patterns would not have been picked up, and user bias (through selecting only genes that one wants to investigate) is much more of a risk. The CAMERA method is even less prone to bias than the GSEA approach used on WebGestalt, as for CAMERA, the user inputs the whole gene list with normalised expression values for each without even filtering for significance, meaning no user cut-off is supplied at all. This means a completely unbiased data set is submitted to the software, so all results in the Voronoi tessellation are a complete and whole depiction of what changes are occurring in the HepG2 cells between 2D and 3D culture substrates.

To further demonstrate the merit of pathway analysis and the close association of upregulated genes with the most enriched categories, the most enriched pathway in 2D and 3D primed HepG2 cells as calculated by CAMERA on Reactome were visualised with the gene expression data overlayed. In 2D HepG2 cells, the most enriched pathway was that of cell-junction organisation (**Figure 5.33**). The diagram here shows the complete pathways feeding into cell-cell junction organisation (which is highlighted with a blue box), and the associated genes or gene groups in boxes with colour coding indicating either significant (FDR value of ≤0.05) upregulation in 3D (dark orange/red), significant (FDR value of ≤0.05) upregulation in

2D (dark green) or non-significant (FDR value of >0.05) upregulation with the lighter colours. It is very evident that the vast majority of genes involved in cell-cell junction organisation are upregulated in 2D HepG2 cells, with a large proportion of those being significant. This provides a visual demonstration of how significantly enriched pathways are detected, through correlating a known set of interacting genes with an almost unanimous upregulation in one of the compared conditions. This upregulation in junction organisation may be because the contact points are more localised in 2D, meaning that there is a distinctive upregulation of structural genes to concentrate junctions at those points. It may also be due to outside in signalling, with increased stress on actin networks meaning a recruitment of more junctional complexes between cells (Ladoux et al., 2010). Regardless, this indicates a significant structural alteration occurring in the 2D cells that will evidently influence the signal transduction through altered cytoskeleton mechanics and is leading to a less physiologically relevant culture model than in 3D.

In the 3D primed HepG2 cells, the most enriched pathway according to CAMERA on Reactome was cholesterol biosynthesis (**Figure 5.34**). It is very apparent that the genes implicated in this pathway – and those that feed into the pathway – are strongly upregulated in 3D culture of HepG2 cells, with all gene groupings within the cholesterol biosynthesis section having a dark orange colouring showing significant upregulation. This consistent pattern indicates that 3D culture is a strong driver in enhancing hepatic function, and while some pathways may have a less united upregulation of genes, the fact that in this hepatic pathway, nearly all genes involved in the liver specific function of cholesterol biosynthesis are upregulated shows the directed and targeted functional changes that can occur simply from changing the mechanical properties of the cell culture substrate.

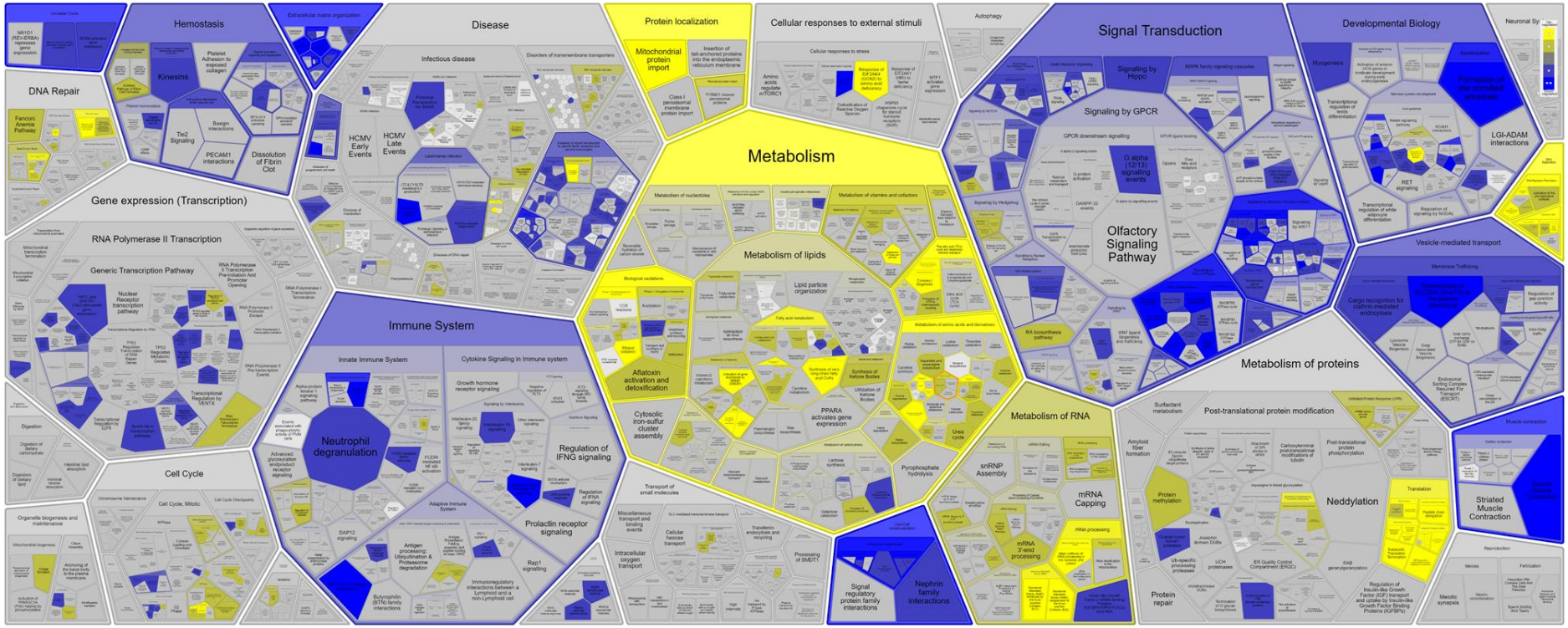

Figure 5.32: The range of enrichment in 2D HepG2 cells is much wider ranging than the enrichment in 3D primed HepG2 cells.

Voronoi treemap generated from Correlation Adjusted Mean Rank gene set test (CAMERA) analysis using Reactome online software. Complete normalised expression data from each repeat of 2D and 3D primed HepG2 cells were put into the analysis, with the returned data showing areas of significant enrichment. Bright yellow and dark blue indicates significant enrichment in 3D primed and 2D HepG2 cells respectively, whereas less intense colouring indicates less significant enrichment that has an FDR value of ≥0.05. Gene data from samples represents N= 4

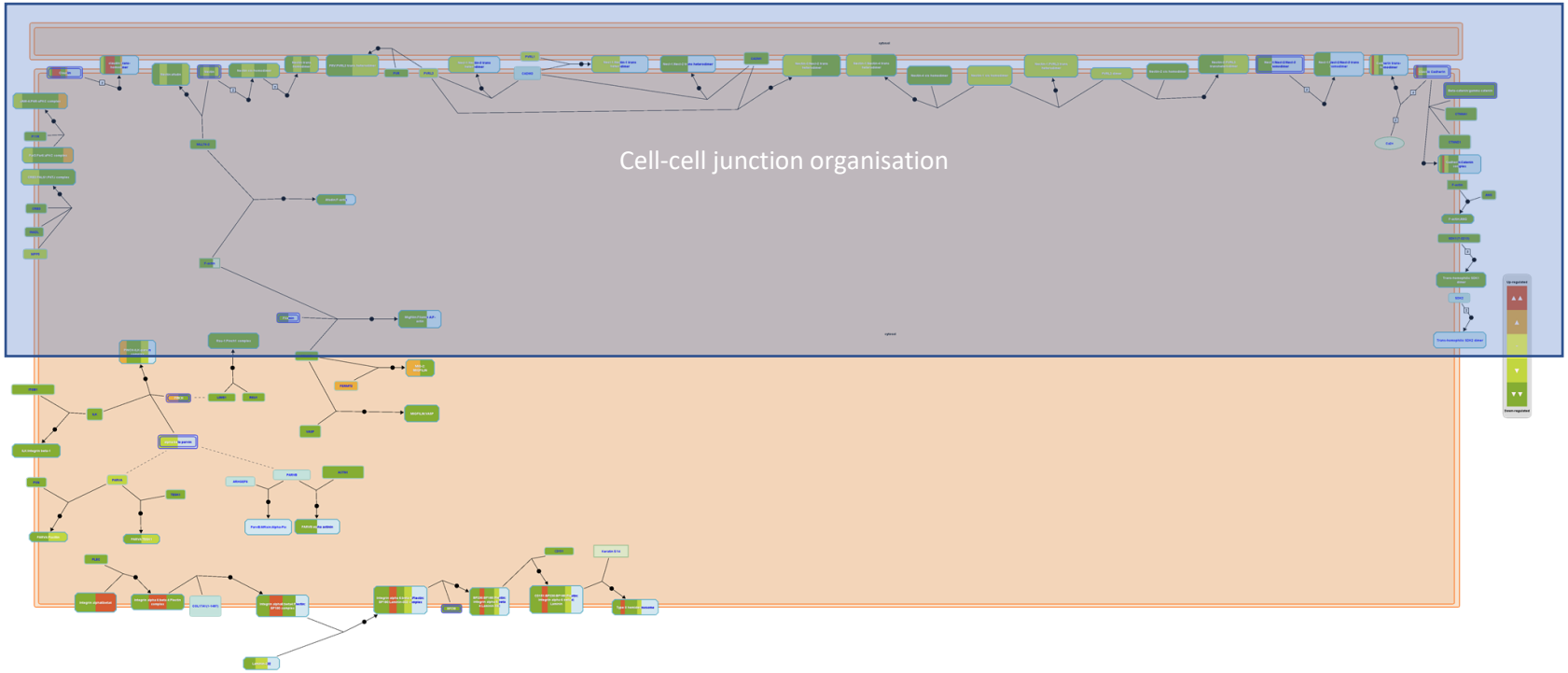

Figure 5.33: Cell junction organisation is the most significantly enriched pathway in 2D HepG2 cells on reactome.

Reactome pathway showing cell junction organisation (blue box) and interacting genes overlayed with expression data generated from Correlation Adjusted Mean Rank gene set test (CAMERA) analysis using Reactome online software. Complete normalised expression data from each repeat of 2D and 3D primed HepG2 cells were put into the analysis, with the returned data showing areas of significant enrichment. Dark red and dark green indicates significant enrichment in the selected gene groups (boxes on pathway) in 3D primed and 2D HepG2 cells respectively, whereas less intense colouring indicates less significant enrichment that has an FDR value of over 0.05. Gene data from samples represents N= 4

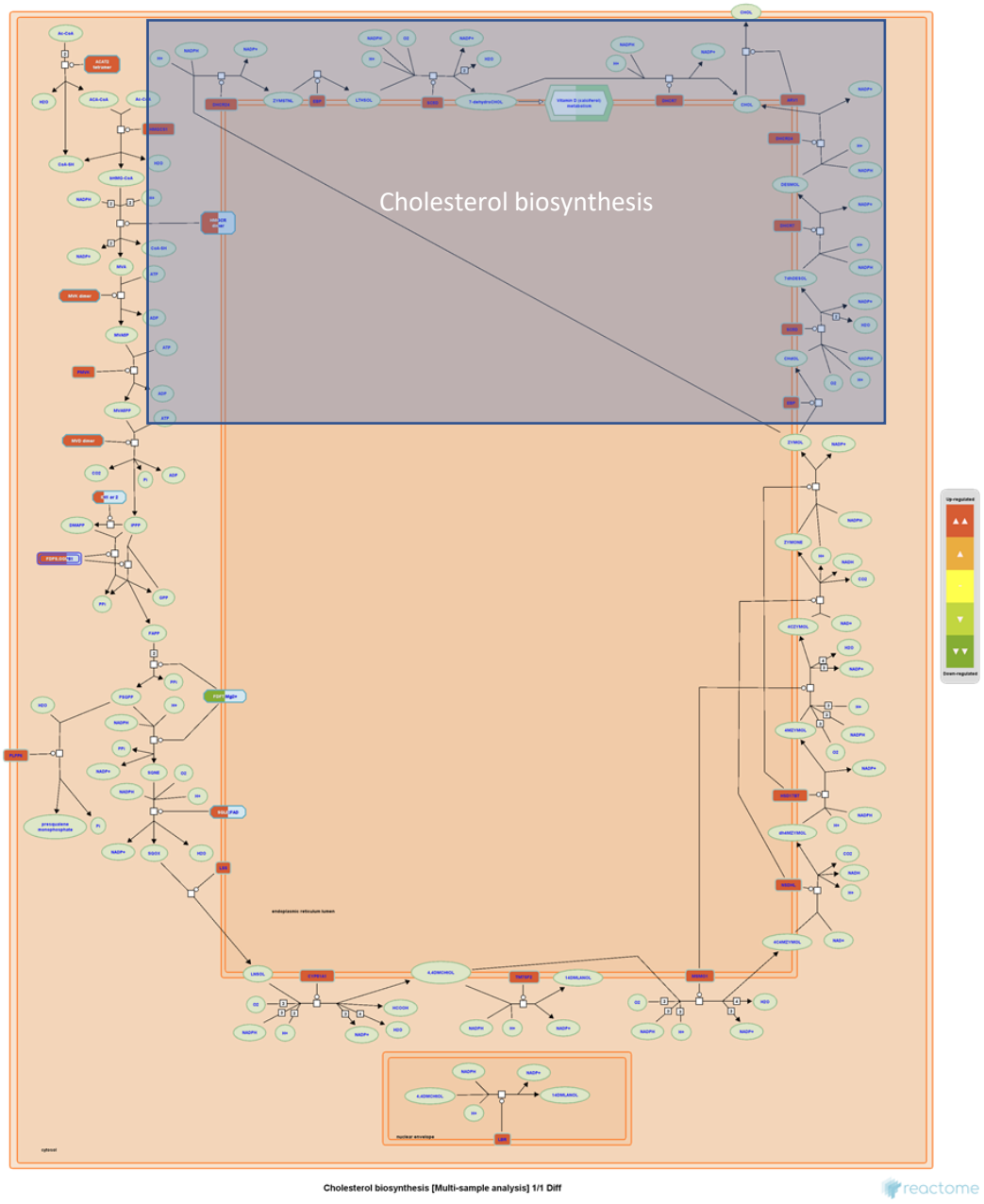

Figure 5.34: Cholesterol biosynthesis is the most significantly enriched pathway in 3D primed HepG2 cells on reactome.

Reactome pathway showing cholesterol biosynthesis (blue box) and interacting genes overlayed with expression data generated from Correlation Adjusted Mean Rank gene set test (CAMERA) analysis using Reactome online software. Complete normalised expression data from each repeat of 2D and 3D primed HepG2 cells were put into the analysis, with the returned data showing areas of significant enrichment. Dark red and dark green indicates significant enrichment in the selected gene groups (boxes on pathway) in 3D primed and 2D HepG2 cells respectively, whereas less intense colouring indicates less significant enrichment that has an FDR value of over 0.05. Gene data from samples represents N= 4

5.4.9 RT qPCR validation proves that the results are accurate and reproducible.

To validate the RNAseq data, RTqPCR was performed on a selected set of 13 genes. The genes were chosen based on both their specific functions and the significant differential expression that they exhibited in RNAseq between 2D and 3D primed HepG2 cells. The genes chosen either fell under structural/mechanotransduction related function= SUN1, SUN2, VASP, ZYX, TGB1, CDH2; or liver specific function= HAMP, SERPINC1, FGG, CLDN1, ALB, SULT1A1, GSTA1. After running the qPCR on pre-optimised primers (KiCqStart® SYBR® Green Primers) for these genes, results were analysed using the ΔΔCt method and relative fold changes of 3D vs 2D were generated. Statistical significance was then calculated and the results compared to those from the RNAseq experiments.

The results of the RTqPCR (**Figure 5.35**) show a strong correlation with the sequencing data in terms of directional fold change. All of the RTqPCR results were significant apart from that of CDH2, and they all changed expression levels in the same direction as the genes in the RNAseq did. The exact magnitudes of fold change did sometimes vary between the two techniques, however a number of the changes were very similar in the fold-changes such as SUN1, HAMP, FGG and ALB. In general, the genes that exhibited a large fold-change in RNAseq also showed a similarly large difference in the RTqPCR, and likewise, those that changed only a small amount in sequencing were also less differential in the RTqPCR. Importantly, the close correlation between the two orthogonal techniques is indicative of two key things; firstly, this provides a strong case that the RNAseq results were accurate and valid, justifying the conclusions drawn from the changes in gene expression, the ORA and the GSEA. The second point is that this indicates a fundamentally robust and reproducible quality within the priming model; with completely distinct experimental techniques performed on completely separately prepared samples still able to show similar changes in genes of interest. Therefore, the sequencing data can be considered reliable, showing that the priming model is able to produce consistent and reproducible changes in the gene expression within the HepG2 cells which have a significant effect on hepatic functions.

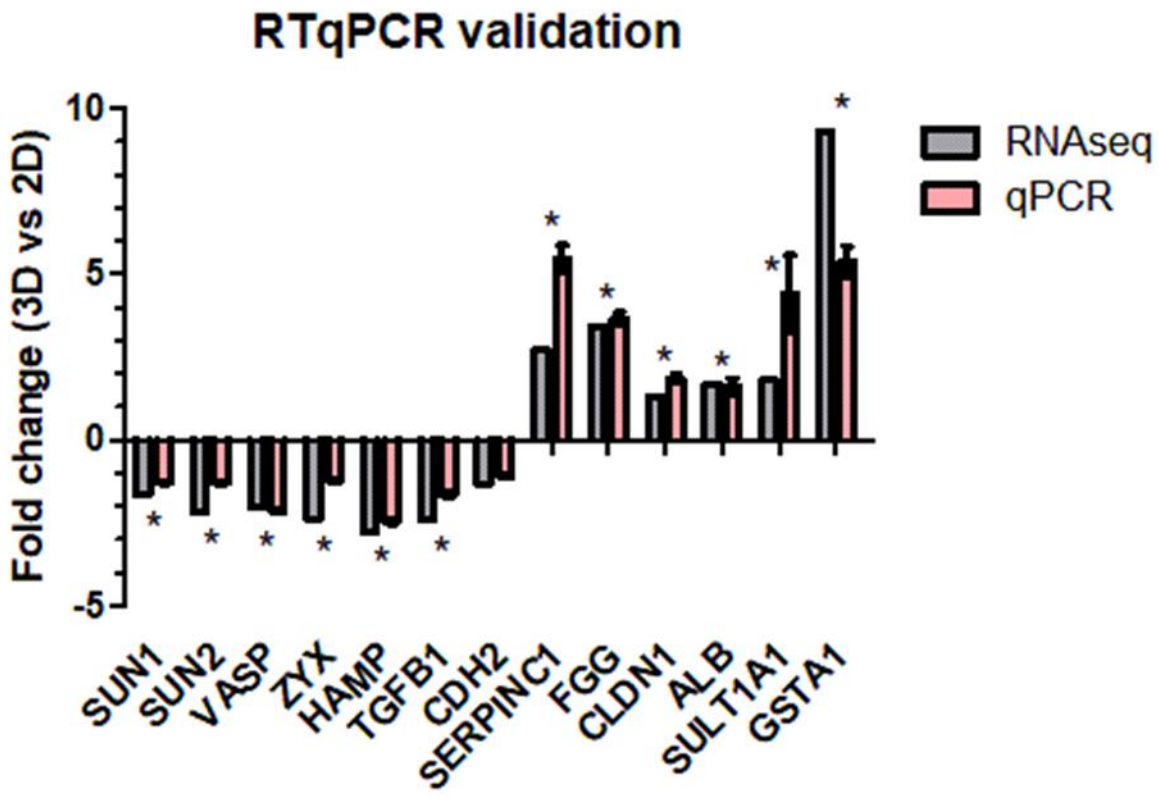

Figure 5.35: RT-qPCR analysis shows a high degree of reproducibility in the RNAseq results, and demonstrates that 3D priming is a robust technique.

RT-qPCR analysis conducted using KiCqStart® SYBR® Green Primers for selected genes chosen from the RNAseq data. All genes were chosen based on showing significant (P adjusted value ≤0.05) differential expression from the RNAseq data. Cells for the RT-qPCR were grown completely separately to the models used in the RNAseq but grown in the same conditions; 8 days 3D priming on Alvetex® Strata, or 8 days in a 2D well. Two tailed T-test used to calculate significance of fold-change in RTqPCR data (shown by stars above bars). Error bars on PCR results (red bars) = SEM, N = 4, n = 2.

5.5 Discussion

5.5.1 HepG2 cells, primary human hepatocytes and human liver formed three very distinctive populations with their gene expression profiles.

This chapter has provided a thorough investigation of the biological changes occurring at a transcriptional level as a result of changing culture conditions from 2D to 3D for HepG2 cells. HepG2 cells were grown in monolayers (2D) or in the priming model using Alvetex® Strata (3D) for 8 days with both conditions, and these were compared to a healthy human liver biopsy taken from a middle-aged female and primary human hepatocytes (PHH) cultured for 1 day in a monolayer (data from online). Adding the two comparisons of primary human hepatocytes and human liver allowed for a deeper investigation into how individual genes of interest that were differentially expressed between 2D and 3D compared to *in vivo* tissue and primary cells.

As was expected, the HepG2 cells from both 2D and 3D were drastically different in their expression profiles compared to the human liver and primary human hepatocytes. These differences were evident even before comparative analysis; in the Deseq2 data, there were just under 8,000 differentially expressed genes between 2D and 3D, but over 12,000 between either HepG2 model compared to the human liver/PHHs. 3D primed HepG2 cells did have a slightly lower count of significantly differentially expressed cells compared to human liver than the 2D HepG2 cells, but the 2D cells had a marginally lower count when compared to the PHHs; this could suggest a slender increase in similarity between 3D HepG2 cells and human liver which were more three-dimensional in nature, and 2D HepG2 cells and primary human hepatocytes which were both grown as a monolayer. **Figure 5.36** shows a Venn diagram highlighting that over 4,500 genes were commonly differentially expressed between 2D, 3D and human liver whereas actually only a small set of genes (around 300) were uniquely differentially expressed in each condition. Despite the numbers, it is the *functions* of those genes that makes the differences and similarities meaningful, and to investigate this more closely, specific gene sets were selected to compare between 2D, 3D, human liver and PHH. Human liver and primary hepatocytes were also rather dissimilar to each other, highlighted through comparative measures such as PCA and clustering analysis, though the within each respective condition, the replicates had a high degree of similarity which was beneficial in ensuring statistical strength of the differential expression analysis.

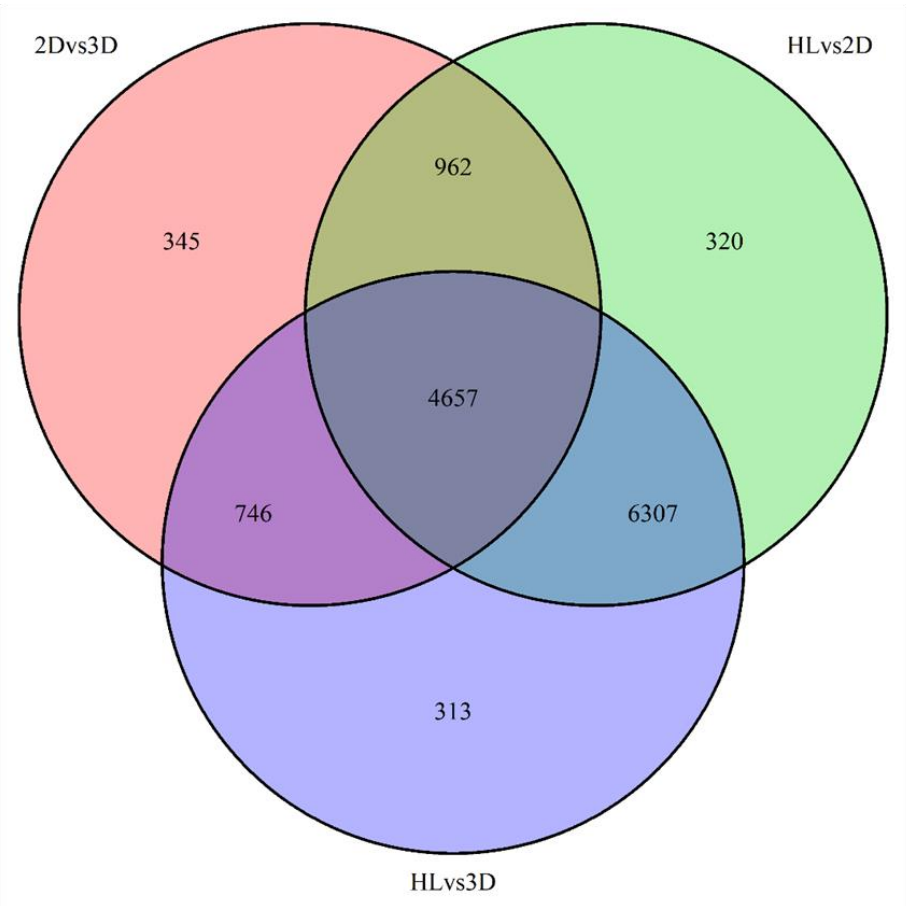

Figure 5.36: Venn diagram of differential expression shows a large number of genes are commonly differentially expressed between 2D and 3D primed HepG2 cells and human liver.

Made using venndiagram in R; diagram shows differentially expressed genes with a P value of ≤0.05 and a fold change of 1.2 or greater. Gene data from samples represents N= 4

The difference between HepG2 cells and human liver / primary hepatocytes in this data demonstrates the distinctly non-physiological phenotype inherent tof the cell line and draws attention to the fact these are a cancer cell, and will never truly replicate the biological profile of primary cells. Despite the vast differences, the data here is still valuable in demonstrating that the transcriptome can be modulated to present more similarly to human liver when placed in an environment that more closely mimics *in vivo*. However, it does serve as a reminder that other cell lines may be more appropriate to use when a 'true' physiological response is needed for research.

5.5.2 Metabolic gene expression increased in 3D primed HepG2 cells, though expression of certain key enzyme genes did not change.

In comparing the expression of important metabolic genes involved in both phase I and phase II metabolism of xenobiotics, a clear trend emerged with human liver having the strongest expression (in general) of the particularly key enzymes, with primary hepatocytes often displaying a medium level of expression somewhere between human liver and HepG2 cells. With all the genes encoding for enzymes, a search term using either the name or part of the gene symbol for those enzymes was used to pull out all relevant genes from the differential expression data for comparison via a heatmap. This means that some of the selected genes were slightly less involved in key hepatic processes but still fell under the 'cytochrome P450' category for example. When looking specifically at many of the key cytochrome P450 genes primarily responsible for bioactivation and metabolism of many xenobiotics, there was a notably low level of expression of these in HepG2 cells, both in 2D and 3D. Human liver expressed these at higher (and of course physiological) levels, and interestingly, the PHHs also fell short of the expression levels in human liver in a few of the cases – CYP3A4 and CYP2E1 for example. When inspecting the individual cytochromes however, it did appear that 3D HepG2 cells exhibited a generally increased expression across these genes, though statistical power was somewhat impeded due to the very low expression numbers in some cases.

A collection of different phase II enzyme sets was also analysed, with a generally similar trend to the CYP450 enzymes, with a lower overall expression in the HepG2 cells compared to PHHs and human liver – at least in most of the cases. Despite this, the absolute expression of the phase II enzymes was usually higher than a lot of the phase I enzymes, indicating a balance towards phase II detoxification in HepG2 cells, similar to what the literature has previously identified (Westerink and Schoonen, 2007a). The expression data also highlighted the difficulty in inducing phase I enzyme expression in HepG2 cells (Westerink and Schoonen, 2007b). There were some more prominent exceptions with the phase II enzymes however, with the HepG2 cells in some cases actually having higher expression than the human liver/PHHs for example in some of the less hepatically related SULT and NAT genes. When expression of these enzymes *was* significantly altered between 2D and 3D, it was again usually higher in 3D primed HepG2 cells.

Despite the general trend of upregulation in 3D primed HepG2 cells; isolating the expression levels of individual metabolic genes proved difficult in determining any concrete conclusions

about how this would functionally affect the cell lines. A selection of drug toxicity tests was planned (and was underway during the sequencing experiment) and therefore, to enable a more specific and tailored approach; the expression levels of transporter and metabolic genes that were known to be interactors with the planned drugs were analysed and compared between the 2D and 3D HepG2 cells. In four of the drugs (amiodarone, gemfibrozil, ibuprofen and isoniazid), there are only a limited number of interacting genes known, therefore usually one or two of the small number of known metabolic genes were upregulated in 3D primed HepG2 cells.

For the drugs methotrexate and tamoxifen however, there was a large known set of interactors, and these revealed a distinctive pattern of increased metabolic gene expression and solute carrier transporters (SLC) in the 3D HepG2 cells, but a very specific increase in the ABC transporters in 2D HepG2 cells. This suggests that while the metabolism may be enhanced in 3D cells – possibly due to the effects of mechanotransduction – the altered structure of the HepG2 cells in monolayers is facilitating faster formation of ABC transporters. Despite this, there did not seem to be a specific correlation with either sinusoidal or canalicular transporters, so it does not necessarily contrast with the immunofluorescence data from **Chapter 4** that indicated an increase in canalicular-like structures in the 3D priming model with MDR1 (ABCB1). It is certainly possible that while expression of the ABC transporters was higher in 2D, 3D cells were still more capable of developing mature canaliculi-like structures as the immunofluorescence data indicates. Interestingly, other than ABCC2, expression levels in human liver were lower than the 2D HepG2 cells, so the 2D culture may indeed be forcing 'unnatural' formation of these transporters past a physiological level. Previous studies have shown enhanced transporter function in 3D cells (Oshikata et al., 2011; Schyschka et al., 2013), and despite the increased expression in the monolayers, the transporters may still be *functionally* more adept in 3D. Considering these expression patterns, it is still predicted that in the drug toxicity tests, the 3D primed HepG2 cells will show a higher capacity for detoxification than 2D, primarily due to the enhanced expression of metabolic genes and inherent differences in the global structure and cell organisation of 3D culture models.

5.5.3 Monolayer culture on a stiff substrate results in higher expression of focal adhesion related genes.

2D HepG2 cells have a substantially higher surface area in contact with the culture substrate than cells grown on a porous scaffold such as in the priming model. It is known that culturing

cells on stiffer substrates increases the size of focal adhesions (Yeh et al., 2017), and that phosphorylation of key proteins involved in focal adhesion regulation (FAK, paxillin) increases on stiffer substrates (Bae et al., 2014), so with all of this considered, it was expected that expression of integrins would be upregulated in 2D to reflect this, which would further confirm the mechanically sensitive nature of focal adhesions. Indeed, this was the case, with most integrins showing increased expression in 2D HepG2 cells. This increased expression in 2D was further removed from the relatively low expression levels of most integrin subtypes in human liver, though was interestingly closer to the expression levels in the 2D PHH cells.

This helped clarify the nature of integrins *in vivo*, through the revelation that expression is relatively low. This is possibly due to the unique ECM properties in the liver, with no basement membrane present in the liver lobules and an attenuated ECM consisting mainly fibronectin and only limited collagen (Martinez-Hernandez and Amenta, 1993). Therefore, it is likely that the differences in expression between 2D and 3D HepG2 cells are likely a representation of the more physiological microenvironment in the 3D priming model, where there is less of a substrate to adhere to and form focal adhesions with. Furthermore, increased integrin expression in the 2D HepG2 cells may be indicative of a more fibrotic phenotype, with increased expression of certain integrin subtypes being observable in various *in vivo* liver injury studies – $\alpha_v\beta_6$ for example is upregulated markedly in mouse models of biliary atresia (Nadler et al., 2009; Patsenker and Stickel, 2011). The increase in expression of integrin chains β_1, α_1, α_5, and α_6 was found in patients with chronic hepatitis C, and were correlated with inflammation and fibrosis progression (Nejjari et al., 2001; Patsenker and Stickel, 2011), and the genes for these four chains were all upregulated in 2D HepG2 cells. This suggests not only a less physiological, but a less 'healthy' phenotype present too in 2D, with 3D culture able to rescue cells from this phenotype to an extent.

When investigating the junctional genes, both the cadherins and claudins, representing adherens junctions and tight junctions respectively, showed a mixed pattern of differential expression between the 2D and 3D primed HepG2 cells. One of the key cadherins in the liver – E-cadherin (CDH1) did not change in expression levels, whereas N-cadherin (CDH2) was slightly upregulated in 2D. Additionally, the balance is tipped towards stronger N-cadherin expression over E-cadherin in both HepG2 models, whereas in human liver, the balance is very clearly in the other direction. This does suggest that the HepG2 cells, and perhaps the 2D HepG2 cells in particular are adopting a more mesenchymal phenotype, with N-cadherin expression typically associated with cells that have undergone EMT (Fontana et al., 2019).

Although human liver and PHHs exhibited stronger expression of E-cadherin, with many of the proto-cadherins (PCDH), expression levels were elevated in the HepG2 cells when compared to the primary cell sources. Protocadherins are typically associated with a developing verterbrate nervous system (Weiner and Jontes, 2013), and the fact these are expressed at a higher level in HepG2 cells highlights their physiologically aberrant phenotype. In addition to the cadherin genes, the genes encoding for the claudin proteins associated with tight junctions were also upregulated in 2D in some cases and 3D in others. Importantly though, claudin 1 which is very highly expressed in human liver was higher in expression in 3D primed HepG2 cells, though still at a far lower level than in human liver and PHHs. This does fit with the expression patterns of claudin 1 seen in the immunofluorescence data in chapter 4, where there was clear upregulation and better organisation in 3D primed HepG2 cells.

Considering the overall structures of these models, it may be expected that 3D primed cells would be able to form more cell-to-cell junctions based on the higher number of physical contacts occurring in the 3D primed HepG2 models. As the SEM images in chapter 4 showed, the HepG2 cells were very densely packed on 3D culture, whereas on 2D culture, even if fully confluent there is only a limited number of connections the cells can make. There are a few considerations to make here; firstly, when looking at the immunofluorescence data in chapter 2, N-cadherin appeared more intense in 3D primed HepG2 cells over 2D cells, as did E-cadherin (albeit with seemingly lower expression than N-cadherin); while this potentially indicates the inverse of what was seen in the gene expression data, it is not necessarily the case. Firstly, as discussed in the introduction, gene expression does not necessarily have a linear relationship with protein expression, and secondly, while the genes for N-cadherin may be upregulated in 2D, it may be that the junctions are not correctly forming in the 2D cells and are more *functional* in the 3D primed HepG2 cells. Furthermore, the 3D cells may have stained more intensely as there is more potential overlap of cells in the sections made from the 3D models, whereas only one plane of view for the monolayer images. Based on the literature though, cadherin based junctions appear to more readily form on rigid surfaces where cells are more spread out (Ladoux et al., 2010), so the increase in N-cadherin does fit with this observation. In addition, while immunofluorescence staining of these two junctional markers was more intense in 3D HepG2 cells, the junctional organisation did appear high in 2D with less heterogenous staining – possibly due to the rigid structure of the 2D cultures where there are very defined points of contact between the cells. This high organisation does not equate to physiological structure however, as the 3D primed HepG2

cells were a lot closer to *in vivo* hepatocytes in morphology. This does explain another reason behind the increased expression of N-cadherin in 2D, fitting too with the more mesenchymal phenotype. It is possible that there is a more consistent junction formation in 2D, however in 3D, junctions are more strongly localised to certain points, which could explain both the immunofluorescence data and the sequencing results.

5.5.4 Grouping genes by involvement in wider hepatic function and in mechanotransduction reveals structural enrichment in 2D which pulls cells away from a functional hepatic model phenotype.

So far, both the structural and functional gene data has revealed the inherent weakness of looking at gene expression in isolation; despite many papers doing so, it limits the validity of drawing larger conclusions about the biological changes occurring in the cell – especially when not coupled with orthologous techniques. It is fine to keep conclusions constrained to the genes in question – for example saying that expression (and therefore likely activity) of certain CYP450 enzymes is increased, but from looking at an increase in a small number of the metabolic genes as individual entities, it would be a large and possibly erroneous assumption to conclude that 'hepatic-metabolism' as a whole has increased. Therefore, to start more a more holistic analytical view, more bespoke groupings of genes were made. With this, a heatmap was created of genes heavily implicated in mechanical responses and mechanotransduction and a separate one made of genes known to be particularly associated with the liver with the hope of seeing clearer patterns of expression emerging.

This was certainly the case, with the hepatic genes very clearly showing a general trend of upregulation in 3D primed HepG2 cells, and genes involved in mechanotransduction showing a very distinctive upregulation in 2D HepG2 cells. The patterns seen here were a lot clearer than using a general search term for a specific gene category as performed prior, and in this user curated list of genes, the analytical power was significantly higher, as it provided a very key insight into how 2D and 3D culture is able to direct the biological behaviour of the cells. A particularly exciting insight was that nearly all of the upregulated hepatic genes in 3D primed HepG2 cells brought the expression levels closer to that of the functional human liver, whereas the increase in expression of the mechanotransduction genes in the 2D HepG2 cells was often further away from the expression of those genes in human liver. This importantly indicated that 3D cells had both a more similar expression of the functional and mechanotransduction genes to the liver, highlighting the correlation between making the

mechanical microenvironment more closely reflect the native tissue, and the subsequently more physiological functional properties that arise as a result.

The hepatic genes are important to consider as this was a distinctive collection of genes that are known to be produced majorly in hepatocytes that were upregulated in 3D primed cells. Additionally, a heatmap was also made from a distinctive set of genes involved in the urea cycle, and these were also upregulated in 3D primed HepG2 cells. The fact that these genes pertaining to the physiological functioning of hepatocytes are upregulated in 3D, yet the mechanical genes are upregulated in 2D really points to the two directions that the cells can be pulled towards as a result of altering the culture substrate – a mechanically stressed and less functional 2D state, and a mechanically settled and more functional state in 3D. Albumin for example is one of the most common biomarkers used in literature to mark liver function, and the fact that it is increased significantly in the 3D primed cells is a strong indicator that hepatic function is enhanced – though as discussed, only a fully contextual analysis of the genes through ORA and GSEA could provide true validity to that statement. One notable gene that was very highly upregulated in HepG2 cells over both human liver and primary hepatocytes was alpha fetoprotein (AFP); a glycoprotein that is produced in early stages of development but that disappears in normal cells after birth (K. I. Kim et al., 2013). In hepatocarcinoma cells however, AFP is expressed in around 80 % of cases (Tangkijvanich et al., 2000), and is now thought to be significantly involved in regulating proliferation and apoptosis, with AFP knockdown inhibiting cell growth and promoting apoptosis (X. Yang et al., 2018). Therefore, this is more closely associated with a cancer phenotype than liver function, and interestingly it shows upregulation in 3D primed HepG2 cells, suggesting a more apoptosis resistant cell line in 3D. Outside of AFP, all other genes in the hepatic heatmap point towards liver specific functional enrichment in 3D.

The mechanotransduction genes were selected based on key genes that have a role in responding to mechanical stimuli, through reorganising cellular junctions, altering the actin cytoskeleton machinery and changing the structural integrity of the nucleus. The fact that nearly all of these genes were upregulated in 2D, shows the mechanical stress exerted upon the cells with the stiffer substrate. The increase in expression of the SUN1 and SUN2 genes for example may be indicative of a stiffer nuclei (Liu et al., 2019), which is known to be a result of culturing on stiffer substrates (Alisafaei et al., 2019; Lovett et al., 2013). This backs up the results seen with the immunofluorescence of sun1 and sun2 in **Chapter 4**, which very clearly showed increased intensity in staining for these proteins in 2D HepG2 cells. It is known

that actin networks increase in organisation and in density under tension (Ladoux et al., 2010; Mueller et al., 2017), and VASP and zyxin recruitment increased at adherens junctions when under thrombin induced tension (Oldenburg et al., 2015), so the enhanced transcription of these and similar actin linked genes is very fitting in the 2D HepG2 cells. In **Chapter 4,** data showed that inhibiting the nucleation activity of ARP2/3 through use of the compound CK-666, and inhibiting ROCK1 through Y-27632 could both partially rescue the 2D cell phenotype to more closely resemble the 3D primed cell shape. As disrupting this machinery restores the 3D phenotype, this suggests that in 2D cells there is an increase in activity within this actin cytoskeleton machinery. This too is made clear here with the increased expression observed in many of the genes responsible for organisation of the actin cytoskeleton.

The uniform increase of many of these genes involved in various mechanotransduction related functions may possibly be a direct result of the increased YAP/TAZ expression. YAP/TAZ is a transcription factor that is very closely implicated in mechanotransduction; YAP/TAZ is shown to be responsible for promoting transcription of genes involved in ECM composition, cell-matrix interaction and cytoskeleton integrity (Calvo et al., 2013; Martino et al., 2018c; Morikawa et al., 2015; Nardone et al., 2017). This correlates strongly with the upregulation of YAP/TAZ in the 2D cells. Combined with the increased expression of genes within all of these YAP/TAZ affected categories (ECM composition, cell-matrix interaction and cytoskeleton integrity), there is a very strong case here that points towards YAP/TAZ based mechanotransduction occurring. Further to this, the YAP-mTOR axis has also been closely implicated in the downstream effectors of 3D cellular mechanotransduction. Hepatic tumour cells grown on cellular scaffolds were compared to monolayers, and in the scaffolds, there was a downregulation of YAP and pmTOR leading to a slower proliferation rate and altered cell size and morphology (Frtús et al., 2020). YAP/TAZ is inhibited through contact inhibition and considering the dense packing of the cells in 3D, this could be one of the mechanisms leading to the lower levels of YAP/TAZ in 3D primed cells, with increased YAP/TAZ activity possibly providing one of the mechanisms through which the HepG2 cells growing in 2D are more proliferative. Further bolstering the data is the fact that 2D cells exhibited altered cytoskeletal and nuclear shape even after liberation (**Chapter 4**). Nuclear stretching due to stiff substrates has been demonstrated as a mechanism through which increased YAP nuclear translocation can occur due to reduced mechanical resistance in the nuclear pores (Elosegui-Artola et al., 2017), which elegantly fits with the overall observations

of increased expression of YAP/TAZ in the 2D HepG2 cells alongside the other mechanotransduction genes.

5.5.5 Enrichment analysis further consolidates the hepatic functional enrichment observed in 3D primed HepG2 cells.

While the examination of expression levels of genes within a common functional category (hepatic function or mechanotransduction) yielded a very clear change in the biological properties of the HepG2 cells, it still did not provide a statistical measure to indicate the strength of that change. For this reason, enrichment analysis either through over-representation analysis or gene set enrichment analysis filled a key gap in the data by calculating the significance of over-represented or enriched ontologies. This analytical method was very important due to its use of a standardised and unbiased annotation of genes when using GO or pathway databases, meaning that it was not just looking for upregulation of genes in a list of known hepatic genes (for example) that the user had picked out.

The over representation analysis used a list of genes significantly upregulated by over 1.2-fold in either 2D or 3D HepG2 cells, and the results were very revealing as to the overrepresentation of biological processes related to hepatic function in 3D primed HepG2 cells. These over-represented categories in 3D lay primarily in biosynthesis and metabolism of cholesterol, sterols and secondary alcohols as well as in mitochondrial activity. These categories – particularly cholesterol metabolism and biosynthesis – are essential to hepatic function, with cholesterol being produced in the endoplasmic reticulum of hepatic cells in the liver. Initial steps of cholesterol biosynthesis start with Acetyl-CoA which is primarily produced through an oxidation reaction in the mitochondria (an enriched cellular component in 3D), with the rate of formation being highly sensitive on changes in activity and levels of 3-hydroxy-3-methylglutaryl CoA reductase (HMG CoA reductase) (Berg et al., 2002; “Cholesterol Biosynthesis,” n.d.). Through showing over-representation in a category such as this, the EnrichR software has determined that a higher number of genes than expected within this functional category are present in the 3D primed upregulated gene list, and that this is not down to random chance, providing a strong case that these expression changes are the result of genuine biological alterations.

Conversely, in 2D, the top over-represented categories were primarily involved in transcriptional regulation which is interesting when considering the upregulation of the

mechano-sensitive genes, particularly YAP/TAZ which have a profound impact on transcription. As also discussed in the literature review, changes in the structural conformations in the chromosomes result in restriction or easing of access of the transcriptional machinery to the genes, with increased mechanical stress (such as on a 2D stiff substrate) resulting in open chromatin conformations with increased transcription (Heo et al., 2016b). This altered transcriptional response is consistent with both the literature and the known sustained morphological effects of culturing the HepG2 cells on 2D as opposed to 3D. When considering the increased hepatic function in 3D, this over-representation in transcriptional regulation in 2D suggests that this is promoting the transcription of genes involved associated in mechanical responses and/or suppressing the transcription of hepatic genes when HepG2 cells. Either way, it reveals the profound effect that simply altering mechanical substrate properties holds over the biology of *in vitro* models. Another noteworthy observation is that when looking at over-representation of genes associated with specific cellular components, the 3D upregulated genes are very significantly over-represented in the mitochondria – the metabolic powerhouses of the cell, and in 2D HepG2 cells, it is in focal adhesions and the cytoskeleton providing a very clear indication that these are primarily mechanically associated genes upregulated in 2D.

Gene set enrichment analysis was also performed using a full set of significant genes with no fold-change cut-off, and this indicated that very similar biological processes were enriched in the 3D HepG2 cells as was found in the ORA. When looking at the GO biological processes, and the three pathway databases (KEGG, WikiPathways, Reactome), a very consistent pattern of enrichment in metabolic and biosynthetic pathways in 3D was evident. These enriched categories covered a set of pathways/processes which were nearly all closely associated with the functional processes of hepatocytes, including cholesterol biosynthesis, fatty acid metabolism, steroid metabolism and many more. One could dissect these categories and associated genes to a very detailed level, however for the purposes of this project, the results are astoundingly clear; across all forms of analysis, 3D priming HepG2 cells enhances hepatic function through significantly upregulated gene expression in many relevant pathways. Normalised enrichment scores were considerably high across the top enriched categories in 3D primed HepG2 cells which indicates that the biological effects of this enrichment should be reasonably potent. A particularly key set of categories that were enriched according to the KEGG, WikiPathway and Reactome databases respectively were ‘drug metabolism’, ‘metapathway biostransformation phase I and phase II’, and ‘phase II metabolism’. These categories are all closely linked to detoxification, biotransformation and

metabolism of xenobiotics, and due to the importance of drug toxicity tests in liver research, it is especially encouraging to see enrichment in these and other similar categories, indicating a significantly more metabolically competent *in vitro* model when cells are primed in 3D. The strength of enrichment and clear patterns of 3D functional enhancement make a clear rationale for using functional testing and validation to fully demonstrate how the core biology of the cells is changing, and this will be pursued in the subsequent chapter.

Another very clear pattern that emerged through the GSEA was the incredibly diverse array of processes and categories enriched in the 2D HepG2 cells, which while much broader in functional groupings, were actually less numerous in terms of the categories detected as significant. The categories enriched in 2D ranged from understandable enrichment in processes and pathways such as proliferation, focal adhesions and ECM-receptor interaction, to surprising categories such as hair follicle development, muscle contraction and even malaria. It is likely that the enrichment in these unusual areas is primarily a result of the absence of the focussed phenotypical development that occurs with 3D priming. In 3D, enrichment is clearly focussed on hepatic function which leaves a more diverse set of non-tissue specific genes upregulated in 2D that apply to a range of non-hepatic processes and may be more an artefact of the 2D culture than the cell type itself. One of the pathways identified as enriched in 2D by Wikipathways was 'hepatitis C and hepatocellular carcinoma', which aligns with the observed upregulation of many integrin subtypes which are upregulated in hepatitis C (Nejjari et al., 2001). This also indicates the more carcinogenic and fibrotic phenotype present in 2D HepG2 cells. Another enriched pathway in 2D that was commonly identified in multiple databases was MAPK signalling which is implicated closely in cancer and proliferation, and this is consistent with the higher proliferation rates seen with the 2D HepG2 cells in prior chapters. TGF-beta receptor signalling is also enriched in 2D HepG2 cells, and interestingly both MAPK and TGF-beta signalling have a synergistic effect in promoting epithelial-mesenchymal transition (EMT) (Gui et al., 2012). Therefore, with prior observations on growth and behaviour in conjunction with the pathways upregulated in 2D alongside the enhanced function in 3D, it points towards 2D cells possessing a more mesenchymal and less differentiated phenotype in 2D.

One more pathway of interest that was enriched in the 2D cells was glycolysis and gluconeogenesis. While this may appear to indicate some form of enhanced hepatic function in 2D, it may in-fact be very much due to the change in the global organisation of cells. Increased glycolysis is a known phenomenon in 2D cells when compared to 3D spheroids,

with strong downregulation in 3D potentially being due to the slower proliferation and more hypoxic environment in spheroids, causing a shift away from aerobic glycolysis (Lagies et al., 2020, p. 0).

Further to the in-depth pathway and GO based GSEA, using the CAMERA GSEA method within Reactome also very elegantly highlighted the overall situation with these cells. The Voronoi tessellation demonstrates nicely the highly focussed enrichment in the 3D primed HepG2 cells, with categories primarily residing in metabolism. In the 2D cells, however, the enrichment was spread across a wide variety of areas; including categories involved with mechanotransduction processes such as cell-cell communication, signal transduction and ECM organisation. When overlaying gene expression data on the top enriched Reactome pathways in 2D and 3D – cell junction organisation and cholesterol biosynthesis respectively – there is a very clear, nearly uniform upregulation of all genes involved in those pathways. This shows how strong the biological effects of mechanotransduction are, and highlights how broad the epigenetic plasticity is of HepG2 cells just from altering external mechanical properties.

Without appropriate validation, sequencing data loses a degree of impact due to the potential for technical errors, and processing issues that could lead to systemic changes in the results applied across the full set of involved samples. Therefore, using a separate, orthogonal technique such as RTqPCR provides a method through which one can test for the same changes, and the same end results, but using a different methodology to get there. The genes selected for RTqPCR were carefully selected to represent key areas of upregulation in 2D and 3D, with a focus primarily on mechanical/structural genes that were overexpressed in 2D and hepatic/functional genes that were overexpressed in 3D primed cells. The results showed a very distinctive correlation with the sequencing data, and while the exact fold-change may have varied across certain genes, the direction of change was always in the right direction, with the general magnitude usually being similar too. This was really key to demonstrate, as it proved that the fundamental and wide-ranging biological effects of priming as demonstrated by RNAseq were robust and reproducible, with important genes of interest showing the same patterns. This indicated that the sequencing data was valid and powerful in pointing towards meaningful biological change. While important in of itself, the conclusions revealed here could further be strengthened by functional validation through drug tests to test for metabolic changes, western blotting to test for protein level changes and assays to detect the presence of important liver-specific biomarkers such as albumin.

Therefore, the next chapter focusses on functionally characterising the *in vitro* models study the end stage biological consequences of 3D priming. A further indication that the results of this study are valid comes from the similar expression profiles as found in the paper comparing monolayer vs spheroid gene expression in HepG2 cells by microarray analysis (Chang and Hughes-Fulford, 2009). This study found that genes relating to liver specific function were upregulated in the rotating wall vessel spheroids over monolayers, with ECM and cytoskeletal related genes upregulated in the monolayers, which is closely consistent with this project. The advantages of this thesis are that it provides a significantly more in-depth look at the functional and structural changes than any previous paper.

5.5.6 The significance of the altered transcriptome in 3D primed cells further validates the priming approach as a beneficial technique to prepare cells for a final 3D model.

A small number of papers have demonstrated that through priming cells on mechanically altered substrate, a mechanical memory is imbued that results in retained historical characteristics after liberation. A particular focus of these studies is the role that YAP/TAZ has in controlling this storage of mechanical information. In human mesenchymal stem cells (hMSCs) for example, it was hypothesised that YAP/TAZ acts as a mechanical sensor of sorts that, after a threshold of mechanical dosing is passed, is constitutively activated even after the mechanical dose is removed (C. Yang et al., 2014). Through persistent activation in the nucleus, YAP was able to influence stem cell fate, with mechanically dosed hMSCs favouring osteogenesis when placed on soft matrices, which usually favours adipogenesis. The primary message here was that persistent and prolonged exposure to YAP activating culture conditions (stiffer substrates) switches on the irreversible activation of YAP.

A different study showed similar effects with epithelial cells, demonstrating memory-dependent and stiffness-sensitive migration through retained nuclear YAP after priming on a stiff matrix, even when moved onto softer secondary matrices (Nasrollahi et al., 2017). Stiffer priming predicted a higher nuclear YAP localisation, and depletion of YAP drastically reduced the 'mechanical memory' ability, meaning that cell migration was no longer dependent on historic mechanical matrix properties. The same patterns of mechanical memory were also seen in this study when priming in the opposite order; cells grown on softer matrices and moved on to a stiffer substrate showed significantly reduced nuclear YAP localisation in addition to slower migration. Again, in this study, the strength of the 'priming' effect was temporally dependent, with less than 2 days of priming cells resulting in reduced

stiffness-dependent migratory behaviour, indicating that 2-3 days may be appropriate for these mammary epithelial MCF10A cells to respond to matrix stiffness and localise YAP. Further to this, the YAP activation continued to rise as time points increased showing that priming for longer continues to yield increasing effects.

The temporal responses to priming may well be tissue/cell type dependent, as mathematical models of mechano-activation predict that 7-10 days is sufficient to store a significant mechanical memory in epithelial cells, though experimental observations have shown that these calculations do not match experimental observations on stem cells for example as they were calibrated for epithelial cells (Mathur et al., 2020). This mathematical model of mechanical memory predicted that 7 days of priming would yield nearly 3 days of mechanical memory in the cells. Additionally, this paper theorised that mechanical memory is influenced by three factors; firstly, stiff matrix priming induces transcriptional reinforcement of cytoskeletal signalling; secondly, over longer periods on stiff substrates, more memory regulating factors are produced and epigenetic plasticity is reduced; and finally, the reduced epigenetic plasticity results in stalled transcription of genes that allow adaption to a softer matrix (Mathur et al., 2020). All evidence in this study so far fits in with that hypothesis.

This small but important collection of studies nicely demonstrate similar concepts of priming to that used in this project, though these studies primarily focussed very much on the mechanical effects of priming cells on a particular mechanically defined substrate. This project more broadly focussed on both the structural and functional effects of maintenance of cells in a soft/3D environment, and the effects of moving these back to a stiffer matrix. Other studies have shown a similar pattern in this effect but have been less focussed on the mechanisms involved; Wharton's Jelly derived MSCs showed improved physiological characteristics after preconditioning in 3D scaffolds (Lech et al., 2020), and altering the stiffness of hydrogels encapsulating stem cells allowed tuning of the angiogenic phenotype (Thomas et al., 2020). **Chapter 4** of this project produced clear data showing that priming cells on a 3D scaffold also yields a mechanical memory that is evident when cells are liberated and reseeded onto a stiffer substrate, with cytoskeletal changes occurring in single cells, and altered aggregation properties after priming in 3D. When considering upregulated mechanical genes and the increased YAP/TAZ in the 2D cells demonstrated in this chapter, the fundamental mechanisms behind priming become more lucid, with evident involvement of the global transcriptome in altering mechanical properties of 2D cells. Compared against the enhanced physiological function in 3D primed HepG2 cells, it presents a very compelling

case for priming due to the deep biological changes occurring in the cell which can then be carried over to subsequent cultures to utilise and further enhance these functional properties. Functional validation in the next chapter will be key in revealing the downstream biological effects of these transcriptomic changes.

5.6 Conclusions

This chapter has demonstrated the immense value that utilising global transcriptome analysis can provide. Through using cutting edge RNAseq technologies, a broad but thorough insight into the effects of the mechanical microenvironment on cell biology has been elucidated. The key compared conditions in this data were 2D and 3D primed HepG2 cells, with the each being grown in their respective cultures for 8 days. The rationale behind these time points was that one would be able to observe the greatest difference between any effect of 3D priming and 2D cells at the end point of the initial priming stage model where both models are the most phenotypically different to each other. Both of these conditions had four biological repeats which showed low variation and were validated through RTqPCR highlighting close adherence to the RNAseq data. Further value has been gained from these samples through comparison with human liver tissue and primary human hepatocyte gene expression data.

This chapter has explored different methodologies through which transcriptomic data can be analysed, each providing value, but ultimately culminating in powerful gene set enrichment analysis. The individual gene heatmap based analysis provided unique insights into specific genes of interest and how these change between the four conditions of 2D and 3D primed HepG2 cells alongside human liver and the primary human hepatocytes. The primary patterns observed in the heatmaps were that expression of metabolic genes including certain phase I and phase II metabolic genes was increased as a result of 3D priming, however there was often still a shortfall in expression levels compared to the primary cell sources. Other wider hepatic genes were also significantly increased in the 3D primed HepG2 cells. In the 2D HepG2 cells, distinctive upregulation was detected in mechanical genes involved in the actin cytoskeleton, ECM adhesion and specifically YAP/TAZ which are heavily implicated in mechanotransduction and mechanical memory of cells.

Further gene expression analysis placed these gene expression changes into context, considering the wider interactions and processes that each gene is involved in and using this to demonstrate statistically powerful data of which cellular pathways are enriched in the two key conditions: 2D and 3D primed HepG2 cells. Running this analysis across different pathway databases repeatedly detected focussed enrichment in a number of hepatically specific metabolic and biosynthetic pathways in 3D primed cells compared to a broad and sometimes unpredictable range of pathways enriched in 2D. Enriched pathways in 2D did include mechanical processes however the broad focus and lower number of significantly

enriched pathways showed less contextual grouping of upregulated genes in 2D HepG2 cells. This chapter has clearly and reliably demonstrated that priming cells on Alvetex® Strata for 8 days significantly enriches liver specific functions over 2D grown HepG2 cells, and indicates the potential for priming as a method to increase the biological value of *in vitro* models.

Chapter 6 – Priming HepG2 cells in a three-dimensional microenvironment enhances biosynthesis and metabolism.

6.1 Introduction

6.1.1 Functional analysis of hepatic models

Functional analysis of the HepG2 cells in various three-dimensional models is an essential process that can help clarify the potential benefits of utilising a three-dimensional substrate to grow and prime cells. As most in vitro models are intended to mimic biological functions, assessing the functional and biological properties of in vitro culture is nearly always in most studies on various liver models. Usually, the purpose of liver models is to provide physiologically relevant analogues to the in vivo liver for disease modelling and drug discovery (Collins et al., 2019). Possessing a significant degree of hepatic function is critical for these models to provide a relevant in vitro analogue, and in many cases using a three-dimensional culture substrate for liver cells may help enhance these qualities. Functional tests can also provide downstream validation of more molecular tests such as the transcriptomic analysis performed in the previous chapter.

6.1.2 Common hepatic functional tests

Hepatic function can be examined through a broad number of experimental methods, though there are some common tests to probe for physiologically relevant activity. Important areas to consider in terms of liver specific function include synthesis of important proteins, regulation of amino acids, carbohydrates and fatty acids, biotransformation and metabolism of xenobiotics and resilience to senescence (with early senescence being a common issue in primary cells) (Collins et al., 2019). Albumin production for example is a function highly specific to the liver, with albumin in humans being synthesised by hepatocytes and rapidly excreted into the blood stream to modulate plasma oncotic pressure and to transport drugs (Moman et al., 2020). Albumin synthesis is therefore often used in functional tests as it is an indicator of metabolic activity and function (X. Yang et al., 2014). Urea is also an important liver product for ammonia detoxification, and is often tested for, despite a known deficiency of certain urea cycle genes (arginase I and Ornithine Transcarbamylase) in HepG2 cells (Mavri-Damelin et al., 2007). Histological stains such as Periodic Acid Schiff can be used to indicate glycogen storage capacity too which is another important function of hepatocytes, where it accumulates to function as a reserve of glucose and is mobilised in accordance with blood glucose levels (Rocha Leão, 2003). In addition to the enhanced structure often seen in 3D liver models, many studies have demonstrated enhanced liver function using these markers in 3D HepG2 models through displaying

elevated albumin synthesis, urea production, drug transport, drug metabolism, glycogen storage, indicating a functional advantage of 3D models (Bokhari et al., 2007; Chang and Hughes-Fulford, 2009; Mueller et al., 2011; Ramaiahgari et al., 2014a; Shah et al., 2018; Štampar et al., 2019).

6.1.3 Existing hepatic models often exhibit low physiological relevance.

One use for liver models is to investigate non-alcoholic fatty liver disease (NAFLD), which is a significant health problem across the world. Models for NAFLD require stable, long-term cultures to mimic the chronic nature of the condition, and 2D cultures often prove inadequate due to their typically short-term nature (Lauschke et al., 2019). Spheroids made from primary hepatocytes are more appropriate, showing an ability to induce a reversible accumulation of lipid droplets when exposed to a mixture of free fatty acids, insulin and carbohydrates (Lauschke et al., 2019). More common with HepG2 cells however are models focussing on drug discovery. Absorption, distribution, metabolism and excretion and toxicity (ADMET) screening is now proving to be a crucial method for determining suitable drug candidates and ruling out weak compounds that would go on to fail in clinical trials (Tsaioun and Jacewicz, 2009). There is a fundamental requirement for accurate screening models to help identify suitable drugs before moving on to clinical trials which are both highly expensive and take a long time to progress.

Both animal and *in vitro* models are used to help drug discovery, but both have issues in terms of validity. When investigating drug safety, animal systems have additional problems in regard to the ethical concerns of animal use in research, and it was reported that only approximately half of known hepatotoxic pharmaceutical compounds were detected as true positive for hepatotoxicity in rodent models for toxicity (Olson et al., 2000). Combined tests in rodent and non-rodent species did raise the concordance with human toxicity to 71 %, but of course this requires more animal use which may be less desirable. *In vitro* models present a cheaper and often easier to use alternative to animals, but again, predictive power is poor, for example with the simple 2D HepG2 models that are routinely used in research, there is a reported insensitive to predicting hepatotoxicity in known pharmaceutical agents (Xu et al., 2004). This is partly due to impaired expression of phase I and certain phase II drug metabolising enzymes (Wilkening et al., 2003), with physiological levels of expression and activity of these enzymes proving one of the most important and desirable features in organotypic liver models (Zhou et al., 2019).

Due to the complicated and diverse mechanisms of drug toxicity, it is unlikely that there is a single solution to facilitate prediction of toxic compounds, and it is more plausible that a panel of assays should be employed in parallel, combining data from multiple experimental methods to create a more consistent and robust criteria for eliminating drugs (Xu et al., 2004). It has also been suggested that traditional endpoint predictive methods of hepatotoxicity such as measuring cytotoxicity are inappropriate, and that more intricate methods such as investigating mitochondrial impairment, biliary transport, CYP450 inhibition and metabolite-mediated toxicity are potentially better predictors (Gerets et al., 2012; Greer et al., 2010). It is important to note that *in vitro* models do not just suffer from false negative results; false positive results are also a problem (Kenna and Uetrecht, 2018) and this may be down to the toxicity mechanisms of the drugs being tested. *In vitro* studies often use concentrations of 100 times the clinical C_{max} of a drug to test for toxicity (used as an approximate guideline in this study as well). This was found to represent *in vivo* drug responses and accounts for the higher concentration of drugs in the liver compared to plasma as well as all the many levels of uncertainty that may influence how drugs are metabolised between different individuals (Kenna and Uetrecht, 2018; Xu et al., 2008). Due to the extraordinarily complex nature of drug metabolism and transport, using a clinically relevant *dose* for *in vitro* studies is a significant challenge, so a set concentration measured in Moles is mostly used instead. An important difference may also lie with acute versus chronic toxicity testing, and this is therefore a consideration one must make when using *in vitro* models.

6.1.4 Hepatic metabolism is impaired in HepG2 cells.

The presence of phase I and phase II metabolising enzymes is particularly important due to the different potential safety profiles of intermediate metabolites compared to parent molecules (Zhou et al., 2019). The diversity of mechanisms through which drugs can damage the liver is broad, with drug reactions ranging from hepatocellular - from production of drug-enzyme adducts, to autoimmune reactions and even oncogenesis (Lee, 2003). The phase I enzymes primarily consist of cytochrome P450s, and the enzymes in this group responsible for catalysing the oxidation of almost 90 % of human drugs are: CYP3A4, CYP1A2, CYP2C9, CYP2C19, CYP2D6 and CYP2E1 (Rendic and Di Carlo, 1997; P. Wang et al., 2016). Other enzymes are sometimes involved however, and not all drugs are metabolised through CYP450 enzymes – methotrexate for example is metabolised by folylpolyglutamate synthase in the liver (Mikkelsen et al., 2011). Phase I metabolism reactions involve oxidation,

reduction or hydrolysis of the drug, whereas phase II metabolism involves conjugation of the drug or its metabolites to other molecules (Lu and Xue, 2019). In addition to the enzymes, the expression of nuclear xenobiotic receptors such as aryl hydrocarbon receptor (AhR), pregnane X receptor (PXR) and constitutive androstane receptor (CAR) play a key role in metabolism through regulating transcriptional expression of phase I and phase II metabolising enzymes (Gerets et al., 2012; Naspinski et al., 2008).

Table 6.1: Drugs used in this project, and their mechanisms of hepatotoxicity.

Drug name	Mechanism of injury	Drug reaction type	Main metabolising enzymes
Amiodarone	Direct damage to lipid bilayers and disturbance of lysosomal or mitochondrial function. ("Amiodarone," 2012)	Hepatocellular, mixed or cholestatic (Jersey, 2016)	Phase I: CYP3A4, CYP2C8, CYP2C19, CYP1A1. Phase II: UDP-glucuronosyltransferases (specifics unknown). ("Amiodarone DrugBank," n.d.; Deng et al., 2011)
Tamoxifen	Direct estrogenic effects, and idiosyncratic reaction to toxic metabolites. ("Tamoxifen," 2012)	Steatohepatitis (Lee, 2003)	Phase I: CYP2D6, CYP3A4, CYP3A5, CYP3A7, CYP2C9, CYP2C19, CYP2B6, CYP1A1, CYP1B1, CYP2C8, CYP19A1, CYP2A6, CYP2E1, CYP1A2. Phase II: UGT1A10, UGT2B7, UGT2B17, UGT1A3, UGT1A4, SULT1A1, SULT2A1, SULT1E1. ("Tamoxifen DrugBank," n.d.; "Tamoxifen Pathway, Pharmacokinetics Overview," n.d.)

Ibuprofen	Response to toxic metabolic intermediate. (“Ibuprofen,” 2012)	Mixed, cholestatic (“Ibuprofen,” 2012)	Phase I: CYP2C9, CYP2C19, CYP2C8, CYP3A4. Phase II: UGT2B7, UGT2B4, UGT1A3, UGT1A9, UGT2B17. (“Ibuprofen DrugBank,” n.d.; Mazaleuskaya et al., 2015)
Gemfibrozil	Likely an immunologic response to toxic intermediate of metabolism. (“Gemfibrozil,” 2012)	Hepatocellular, mixed, cholestatic (“Gemfibrozil,” 2012)	Phase I: CYP3A4. Phase II: UGT1A1, UGT1A3, UGT1A9, UGT2B4, UGT2B17. (“Gemfibrozil DrugBank,” n.d.)
Isoniazid	Toxic metabolites produced by bioactivation of isoniazid through amidases. NAT2 thought to play a role too. (P. Wang et al., 2016)	Acute hepatocellular (Jersey, 2016)	Phase I: CYP2E1, possibly CYP2C19, CYP3A4. Phase II: NAT2, possibly GSTM1 and GSTT1. (P. Wang et al., 2016)
Methotrexate	Direct toxicity through inhibition of RNA and DNA synthesis. (“Methotrexate,” 2012)	Fatty liver, fibrosis (Jersey, 2016)	Phase I: CYP3A4. Other: DHFR, AOX1, MTHFR, PGD, FPGS, TYMS, ATIC, GGH. (“Methotrexate DrugBank,” n.d.; Mikkelsen et al., 2011)

As seen in the transcriptomic data in **Chapter 5**, a panel of 6 drugs was chosen for testing on the primary and secondary stage models, and the gene expression of the known interacting enzymes and transporters was analysed. **Table 6.1** displays the toxicity mechanisms through which these selected drugs work as well as the phase I and phase II enzymes associated with their metabolism. The drugs in this project were chosen due to their appearance either in liver research literature (Bokhari et al., 2007; Ramaiahgari et al., 2014a) for example, or due to previously being tested on in the lab. All these drugs are known to exert hepatotoxicity, and effort was made to collect drugs that had different mecahinisms of action and a range of associated enzymes. While toxicity is being tested in this chapter, it is not just being used to predict hepatotoxicity, but to highlight metabolic differences in the drugs that may also indicate whether the HepG2 models are better for drug efficacy screening. As mentioned, the literature on HepG2 cells describes how the expression of CYP450 enzymes is particularly impaired, however expression of phase II enzymes apart from UDP glucuronosyl transferases is known to be at a more physiological level. In the data from **Chapter 5**, the gene expression echoed this, with CYP450 genes being generally poorly expressed in HepG2 cells, though they were increased through 3D priming. This creates a potential imbalance in these cells towards phase II detoxification, due to the bias towards phase II metabolism which, in the case of many drugs, is an essential step in removing the toxic metabolic intermediates created after phase I metabolism (Westerink and Schoonen, 2007a). HepG2 cells also exhibit low expression of the nuclear receptors PXR and CAR which may contribute in part to the often poor predictivity of hepatotoxicity that the cells exhibit (Kanno and Inouye, 2010; Naspinski et al., 2008). Phase II enzymes may also contribute to toxicity too, for example with the formation of reactive nitrenium ions and cabocations due to the modification of aryl hydroxylamines and benzylic alcohols by sulfonylation (Miller and Surh, 1994).

The issue of low CYP450 expression can be circumvented to an extent in certain model systems. For example, one study showed that CYP1A1, CYP1A2, CYP2B6 and CYP3A4 expression and activity could be induced to similar levels of primary hepatocytes when agonists to the xenobiotic receptors (AhR, PXR and CAR) were applied to HepG2 cells (Westerink and Schoonen, 2007b). Other studies however have reported poor chemical inducibility of metabolism related genes in HepG2 cells compared to HepaRG cells and primary human hepatocytes (Gerets et al., 2012). This study by Gerets only compared the inducers when used in isolation, but the paper from Westerink and Schoonen used a combination of known xenobiotic receptor inducers for each respective receptor, possibly explaining the more potent induction. Promising results have also been observable through

the use of lentiviral expression systems that were able to produce HepG2 cells that individually expressed 14 of the key CYP450 enzymes stably (Xuan et al., 2016). This study showed a significantly increased cytotoxic response to amiodarone exposure in HepG2 cells overexpressing CYP1A1 and CYP3A4, whereas other CYP isoforms markedly decreased the cytotoxicity of amiodarone, indicating the different role that CYP450 enzymes have in metabolism and detoxification of drugs. HepG2 cells have also demonstrated markedly increased CYP450 enzyme expression through epigenetic modification of the cell line by treatment with the cytidine analogue 5-Azacytidine (5-AZA) and Vitamin C (Ruoß et al., 2019). Treatment with these two compounds increased the expression of epithelial markers too, showing a reduction of the tumorigenic phenotype of the HepG2 cells and a partial reversal of EMT. These studies indicate that it is possible to induce CYP450 expression and activation in HepG2 cells, showing that they are still a potentially valuable cell line for *in vitro* drug testing as well as cancer modelling, especially considering their robustness and ease of use compared to the expensive primary human hepatocytes that so quickly lose their hepatic function.

6.1.5 The microenvironment significantly influences the response of *in vitro* models to drugs.

In addition to the expression of important phase I and phase II enzymes, the cellular microenvironment is particularly important in determining phenotype and therefore the drug-dose response of models. The lack of *in vivo*-like cell-cell, cell-matrix interactions and tissue architecture in many *in vitro* models is a contributing factor to the disconnect seen in the biological behaviour of cell cultures on plastic substrates (particularly in 2D) (Astashkina et al., 2012). Drug toxicity often compromises intercellular connections in tissue injury, and downstream results of this include loss of function, apoptosis and necrosis. Cell-cell contacts such as E- and N-cadherins are known to be damaged in drug toxicity events (Prozialeck et al., 2003), with cadherin related damage in the livers being attributed to oxidative stress (Parrish et al., 1999). Alterations in the cadherins induce pathological cellular changes, and this implicates these junctional molecules in drug toxicity events and points towards the importance of physiological expression of these when using *in vitro* models.

The cell-matrix interactions are important for detection of signalling changes associated with toxicity (Astashkina et al., 2012), due to the bi-directional transmission of mechanical, stress induced and soluble signals between the ECM and the cells. Integrins for example are a key molecule in the creation of focal adhesions which are largely implicated in

mechanotransduction, and control aspects such as survival, proliferation, and cytoskeletal reorganisation (Legate et al., 2009) and integrin disruption is commonly involved in tissue injury mechanisms (Astashkina et al., 2012). With the nature of integrin adhesions being dependent in part on the mechanical properties (Katz et al., 2000), it is important to consider expression and distribution of cell-matrix adhesions in cytotoxicity sensing. Polarity and organisation of hepatocytes in the liver is indelibly linked with the function of drug and toxin metabolism, with the apically based bile canaliculi and the basal contact with the sinusoids enabling the endocytosis and transport of molecules that is so crucial for hepatic function (Schroeder and McNiven, 2014; Schulze et al., 2019).

The arrangement of cells within *in vitro* models, or the tissue architecture can also have a profound effect on cell biology (Lelièvre et al., 2017), and may play a significant role in determining the cytotoxic responses of cells. 2D cell cultures may provide a suitable analogue for acute toxicity testing in certain cases, but the unnatural nature of the substrate results in rapid dedifferentiation of primary cells, and in the case of cell lines such as HepG2, considerably increased proliferation (Ramaiahgari et al., 2014a) resulting in a phenotype far removed from their *in vivo* counterparts. This presents a particular issue with chronic toxicity testing, where a stably differentiated, non-proliferative model is required (Lelièvre et al., 2017). This is due to the more subtle effects on that chronic toxicity has on gene expression (Kulkarni et al., 2008), compared to the more immediately measurable effects of acute toxicity. 2D models will respond differently to drugs due in part to the inherent differences in cell behaviour, but equally the position of cells and ease of access of drugs to cells in a 2D monolayer culture will clearly be different compared to 3D cultures where cells are arranged in more complex, multi-layered structures.

The structure of the nucleus is a particularly important determinant of cell behaviour, and 3D culture can significantly alter the morphology and organisation of the nucleus, as already shown in **Chapter 4**. This was also demonstrated decades ago through the re-localisation of the nuclear proteins such as the nuclear matrix protein NuMA observed in cells cultured on a reconstituted basement membrane (Lelièvre et al., 1998). Furthermore, expression of p53, a regulator of cell death, was shown to be correlated with nucleus circularity (Mijovic et al., 2013). Changes in the shape and size of the nucleus are an observable part of the early cellular response to toxins and long term toxicity can also have an impact on nuclear organisation due to sustained gene modifications (Lelièvre et al., 2017). It is probable

therefore that the structure of the nucleus as defined in part by the cellular microenvironment plays a role in the response of cells to toxins.

6.1.6 3D hepatic models demonstrate altered sensitivity to xenobiotic compounds.

Further credence is given to the role of the microenvironment in toxicity responses through the well explored differences in the metabolic profiles and toxicity responses between 2D and 3D liver models. 3D hepatic models often demonstrate a somewhat elevated expression of particular CYP450 enzymes over 2D models, though absolute expression values are often not revealed and when they are, they still tend to fall dramatically short of expression levels in primary hepatocytes and human liver – as seen in **Chapter 5**. Results of drug toxicity tests are often variable between different studies, with 3D HepG2 models sometimes demonstrating increased or decreased sensitivity that seems to be both dependent on the model and the drugs tested (Fey and Wrzesinski, 2012). On one hand, 3D cultured HepG2 cells exhibit many enhanced features such as improved hepatocyte-like morphology (Kelm et al., 2003) and increased MRP2 activity – shown through the export of CMFDA dye into the bile canaliculi of HepG2 spheroids (Mueller et al., 2011). Indeed, the expression of important drug metabolising enzymes often show a trend of increasing in 3D cultures; microarray results of monolayer HepG2 cultures compared to spheroids showed that metabolic and synthetic genes were upregulated in the spheroids, but adhesion and ECM related genes were upregulated in the monolayers (Chang and Hughes-Fulford, 2009). One study compared their spheroid models made from C3A HepG2 cells (a clonal derivative of HepG2 cells) and compared toxicity responses to combined data from a number of prior studies. This experiment used assumptions to adjust the median lethal concentration (LC50) to normalise for cell number differences by creating a median lethal dose (LD50) (Fey and Wrzesinski, 2012). Adjusting for cell number did alter the toxicity profiles considerably, though results across studies were still rather variable. In some cases, the 3D spheroids were more sensitive to toxicity, and in other instances, the 2D cells were more sensitive.

In many cases, spheroid cultures exhibit a surprisingly decreased sensitivity to hepatotoxicants. Studies testing the effect of methotrexate on HepG2 cells grown in 3D scaffolds (Bokhari et al., 2007) and rat hepatocyte spheroids (Walker et al., 2000) showed significantly less sensitivity than cells in monolayers. Studies seem to be inconsistent in their conclusions as to whether this is an advantage or not. It is possible that this differential sensitivity makes 3D HepG2 models a better model cancer system; HepG2 spheroids had higher LC50s of chemotherapeutic drugs doxorubicin and epirubicin compared to monolayer

cultures, and this decreased reaction to the drugs supposedly better reflected the *in vivo* response of cancer cells to the same compounds (though physiological responses were not shown for comparison) (Oshikata et al., 2011). Other studies have also purported that 2D cell culture systems may be overly sensitive to toxicity in some cases, due to the lack of three dimensional structures present (Battle et al., 1999). Interestingly, HepG2 spheroids were drastically more sensitive to anti-proliferative agents that do not rely on hepatic metabolism when compared to spheroids grown from induced pluripotent stem cells (iPSC) derived liver spheroids (O et al., 2016). HepG2 cells cultured in spheroids showed a diminished response to the cytotoxic effects of colchicine, chlorpromazine hydrochloride and methyl methanesulfonate (Elje et al., 2019), with the different responses attributed to metabolic changes and decreased drug availability in spheroids. HepG2 spheroids also showed a decreased sensitivity to tamoxifen toxicity in another study (Mueller et al., 2011) which was explained through the increased expression of the drug transporter MRP2, but it is likely also due to a combination of altered expression patterns and epigenetic factors in reality.

Decreased sensitivity to drugs in 3D models is largely attributed to both a change in the metabolic profile of the cells and the structural changes inherent with 3D culture that may limit access of the drug (aspects such as diffusion distance, and tighter cell-cell contacts). What is not clear is whether this is particularly beneficial, especially considering the fact that many *in vitro* models are poor predictors of toxicity. The matter of whether this altered sensitivity makes a better model or not may well depend on what one is testing for; for example, if solely looking at whether a drug is hepatotoxic, then decreased sensitivity in 3D cultures may obscure this, however in situations where the efficacy of a drug is under examination (such as anti-cancer drugs), then this may be the opposite case. For example, it may well appear that drugs were successful in treatment due to the poor metabolism in 2D, however a more accurate representation of the drug's effects may be present in 3D models (Jensen and Teng, 2020). This picture is somewhat complicated through the fact that traditional toxicity measures may not be appropriate for accurately reflecting what would happen *in vivo* (Gerets et al., 2012; Xu et al., 2008). In addition, the differences in cell number and organisation makes matters more difficult, especially when trying to find an appropriate test dosage. Chronic/acute toxicity also work through different mechanisms and the drugs themselves can work through different pathways, depending on their purpose and the mechanism of toxicity. One paper eloquently suggests that 3D HepG2 models present an ideal model for repeated drug exposures to simulate chronic toxicity (Ramaiahgari et al., 2014a). This paper suggested that due to the high proliferation and turnover of cells in 2D, it

is impossible to accurately measure long-term toxicity, whereas HepG2 cells grown in 3D present a more differentiated phenotype, with enhanced hepatic function, and importantly are low in proliferation. It is evident though that drug tests require consideration of many factors *in vitro* and there is not a 'one size fits all' solution and that metabolic and functional competencies of *in vitro* models are a key facet to assess. In this study however, the drug tests serve an additional purpose in functionally validating the global gene expression analysis that clearly showed enrichment in both phase I and phase II metabolism.

6.2 Hypothesis and aims

Through probing for protein expression of structural markers, we expect to further evidence what was seen in the previous chapter, with 2D grown HepG2 cells displaying elevated expression of nuclear structural proteins compared to 3D primed HepG2 cells. We hypothesise that through priming HepG2 cells on Alvetex® for 8 days, the metabolic and synthetic profiles of the cells will be enhanced in line with the significant gene expression enrichment in these categories. We expect to see a significant increase in expression of liver specific proteins as well as albumin and urea synthesis when testing the cells both at the priming stage compared to monolayers, and when testing the secondary stage hanging drop spheroids formed from 3D primed HepG2 cells compared to hanging drops formed from 2D grown cells. Based on the literature and the hypothesis that 3D grown HepG2 cells will be more metabolically competent, we expect there to be a significant differential response to drug toxicity too with 3D primed cells tending towards an improved capacity for detoxification of xenobiotics. We anticipated that the magnitude of this difference in response will be decreased in the spheroids due to the prior 2D cells equilibrating to the 3D microenvironment after 7 days, being drawn closer in phenotype to the 3D primed cells in the secondary model.

6.3 Objectives

- To functionally characterise the priming model and subsequent hanging drop 3D model, validating the RNAseq data.
- To investigate differences in how the models respond to toxicological challenges.
- To probe for selected structural markers in western blotting to show that protein expression backs up the immunofluorescence data and gene expression.
- To probe for specific hepatic markers in western blots to investigate the hepatic phenotype of the cells in the priming model compared to 2D grown HepG2 cells.

- To investigate how urea and albumin synthesis differs between cells coming from 2D or 3D priming, both in the primary and secondary stage of the models.

6.4 Results

6.4.1 Functional and structural protein expression is different between 2D and 3D primed HepG2 cells.

To further validate the structural data from the previous chapter, western blots were carried out on the nuclear structural markers SUN1 and SUN2 as well as the E-cadherin associated protein, β-catenin (**Figure 6.1**). β -actin and GAPDH were used as loading controls, and both of these appeared stable across the three biological repeats and between the two conditions (2D vs 3D). These westerns were performed on lysates made from cells at the end point of the priming model (8 days on Alvetex® Strata) and after 8 days in 2D. The expression of SUN2 clearly reflects the immunofluorescence and gene expression data in the previous chapters, showing a notable and significant increase in expression in the 2D models. Sun1 also shows an increase in the 2D models, though the presence of this band was slightly harder to detect, and the semi-quantitation did not present it as a significant change. β -catenin stained very strongly and showed no significant change between the two conditions, but gene expression data showed only a small change in expression of 1.2-fold towards 2D HepG2 cells, so a large difference was not expected. These data further strengthen the hypothesis that the 2D cells have stiffer nuclei due to increased sun expression creating more linkage with the actin cytoskeleton.

To assess the biosynthetic capabilities, protein expression of albumin and fibrinogen gamma chain were also investigated, alongside another mechanotransduction marker; vinculin, using PCNA and β-actin as loading controls (**Figure 6.2**). Both fibrinogen alpha chain and albumin had a substantial and significant increase in expression in the 3D priming models, with fibrinogen alpha chain not even being detectable in the 2D HepG2 cells. This large increase in fibrinogen echoes the more than 3-fold upregulation of fibrinogen alpha gene expression in the 3D primed HepG2 cells, though baseline gene expression was still high in 2D, so the lack of any 2D band is curious here, though may be due to short incubation times for the photographic film. It was expected that vinculin would be higher in 2D due to the less natural state of the substrate putting mechanical stress on the cells, and a 1.5-fold upregulation of vinculin gene expression in 2D HepG2 cells, however the difference in vinculin was very slender with only a slight and insignificant increase in the 2D cells. The

expression of albumin was also probed for in hanging drops using a western blot, with β-actin as a loading control (**Figure 6.3**). In the hanging drops, the albumin expression was strong in both conditions, but there was still a slight increase in albumin expression in

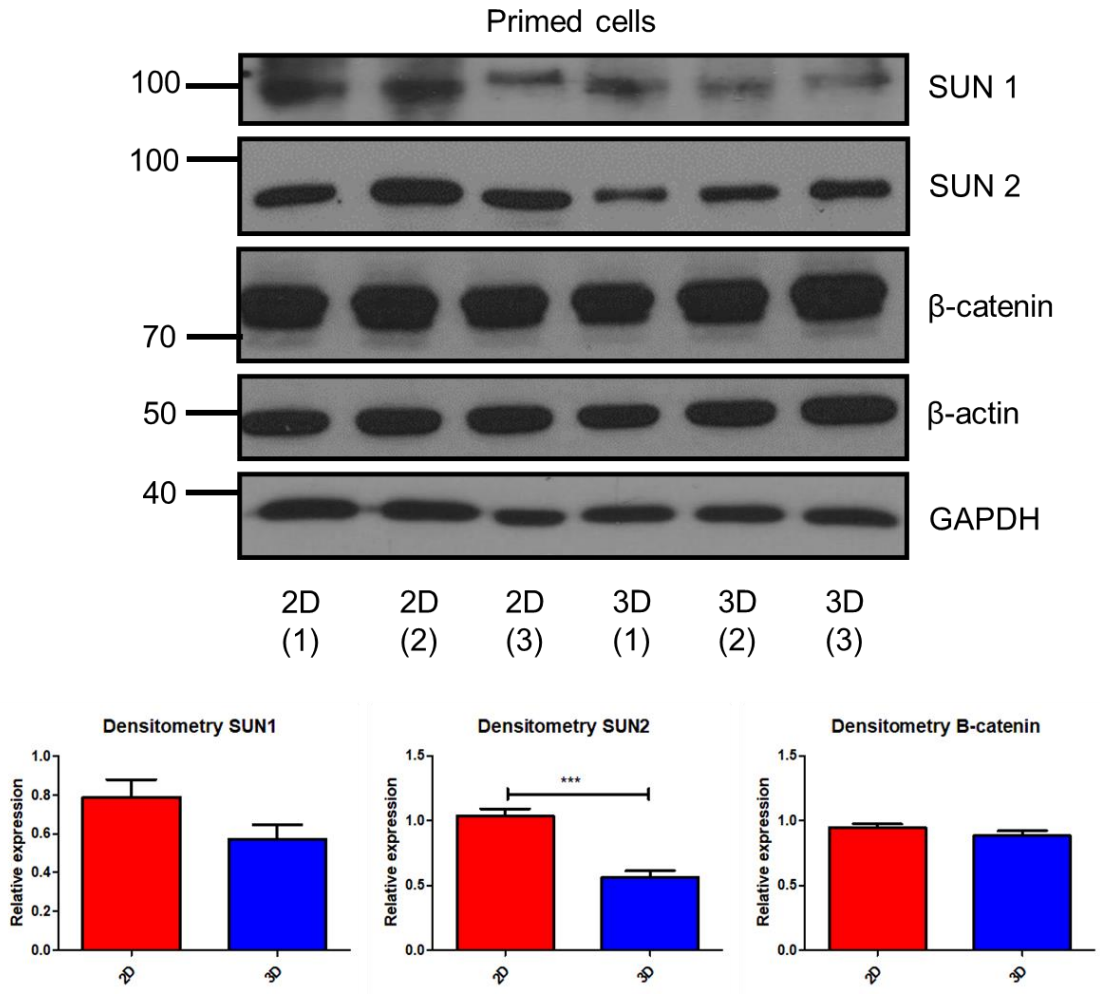

Figure 6.1: Nuclear lamina proteins are upregulated in 2D cells indicating stiffer nuclei.

Western blots of lysates taken from 3 biological replicates of 8-day grown HepG2 cells in 2D or in the priming model. Cells seeded at 5 x 10^5 cells per 2D well and 1 x 10^6 cells per Alvetex® membrane. Semi-quantitation performed using densitometry measurements in image J. Graphs display relative expression of antibodies between 2D and 3D with values normalised to the loading controls GAPDH and β-actin. Error bars = SEM. Gels were run twice, data represents N= 3.

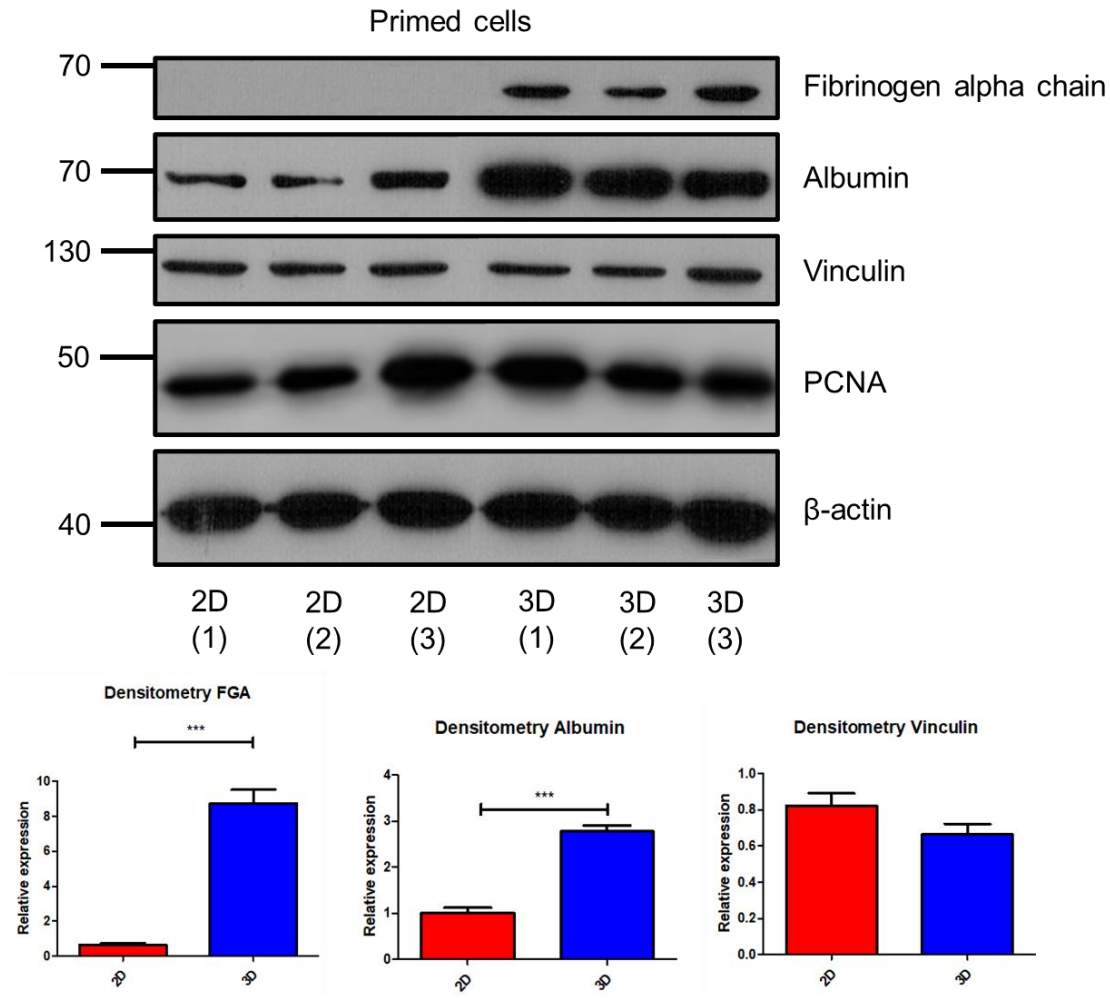

Figure 6.2: Hepatic functional proteins are upregulated in 3D primed cells.

Western blots of lysates taken from 3 biological replicates of 8-day grown HepG2 cells in 2D or in the priming model. Cells seeded at 5 x 10^5 cells per 2D well and 1 x 10^6 cells per Alvetex® membrane. Semi-quantitation performed using densitometry measurements in image J. Graphs display relative expression of antibodies between 2D and 3D with values normalised to the loading controls PCNA and β-actin. Error bars = SEM. Gels were run twice, data represents N= 3.

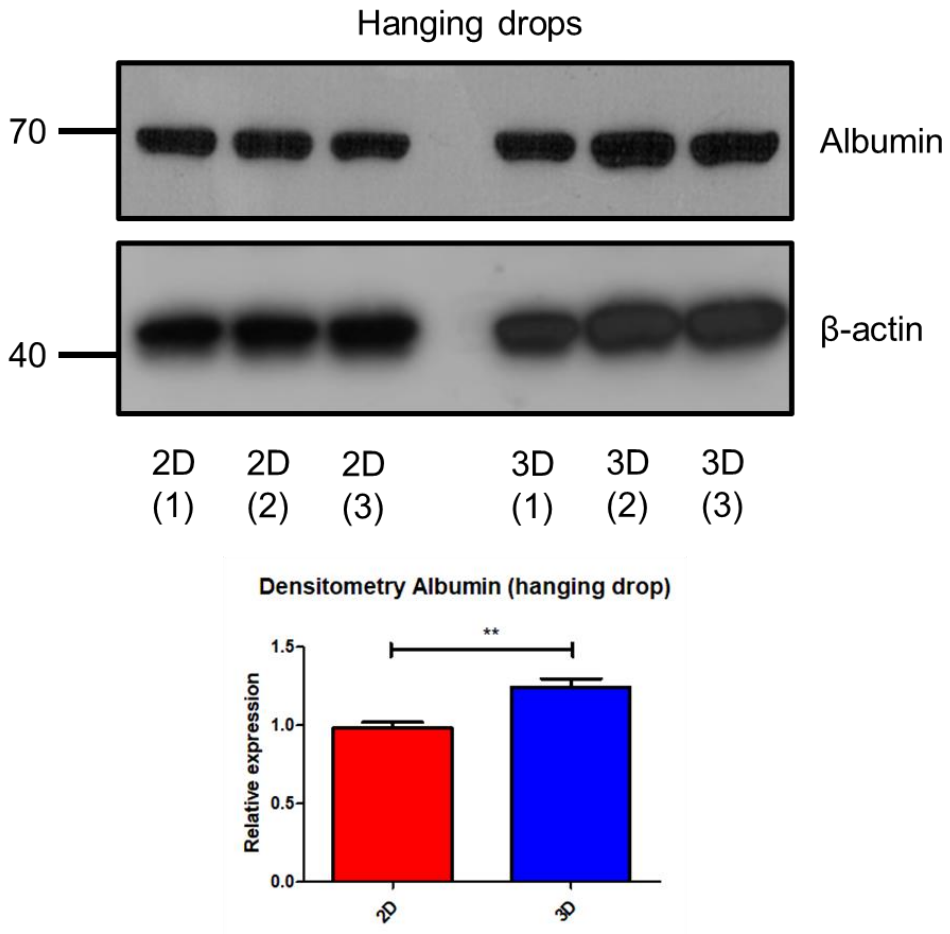

Figure 6.3: After seven days of hanging drop growth, albumin is still slightly elevated in 3D primed aggregates.

Western blots of lysates taken from 3 biological replicates of 7-day grown HepG2 cells reseeded in hanging drops after growing in 2D or in the priming model. Cells seeded at 1 x 10^3 cells per drop. Semi-quantitation performed using densitometry measurements in image J. Graphs display relative expression of antibodies between 2D and 3D with values normalised to the loading controls β-actin. Error bars = SEM. Gels were run twice, data represents N= 3.

aggregates made from 3D primed HepG2 cells. Interestingly, this presented as significant in the semi-quantitation which provides limited evidence that albumin production remains elevated even after liberation and reseeding. However, this was a smaller increase than seen in the westerns of the priming stage models.

6.4.2 Albumin and urea synthesis is increased in 3D primed cells both during the primary and secondary culture stages.

To further explore albumin production both in the priming stage and secondary stage, both albumin synthesis (**Figure 6.4**) and urea production (**Figure 6.5**) were investigated. Albumin synthesis was measured through an ELISA assay, and urea through a simple colorimetric assay, both measuring the presence of the products in the cell culture media supernatant, and the results normalised to total protein. It is important to note that media was changed on these models every 2 days, so the values here represent cumulative production over the 2 days prior to the noted timepoints. In the priming stage, levels of albumin were measured after 8 days of culture and there was a significant increase in albumin production in 3D primed cells. To note, a pilot experiment was done on 4 day grown cells from 2D and 3D, and interestingly, there was no significant difference between 2D and 3D cultures at that timepoint, but this data is not shown due to an insufficient number of repeats. At 8 days, the 3D primed HepG2 cells showed an increase of albumin production by a magnitude of nearly 1.5 x compared to the 2D HepG2 cells. This increase in albumin synthesis in 3D cells follows the gene expression (1.7-fold upregulation in 3D), the western blots and patterns commonly seen in the literature, with only one known study providing an exception where the albumin actually decreased in 3D culture (Elje et al., 2019).

Interestingly though, there was also a significant increase in albumin synthesis in the 3D primed spheroid models compared to the spheroids formed from 2D grown cells (**Figure 6.4 bottom panel**). The overall albumin levels in hanging drops are higher than those in the priming stage, however this is likely due to the lack of media changes, meaning a larger build-up of albumin in the media likely occurs. This increase in 3D primed spheroids is much more drastic than the pattern seen in the western blot (**Figure 6.3**), which provides further credibility to the hypothesis that priming the cells in 3D better prepares them for the secondary model stage, allowing them to more readily form three-dimensional structures, and providing them with an already enhanced hepatic function. This means that the albumin levels in the media will build up more in the 3D primed secondary models (as seen in **Figure 6.4**) due to the already enhanced production. The actual direct albumin synthesis between 2D and 3D primed cells in the secondary model mostly equalises after 7 days due to adaption of the 2D cells to the 3D environment, reflected in the western blots (**Figure 6.3**) which measures the presence of the cellular protein, not the build-up in the media.

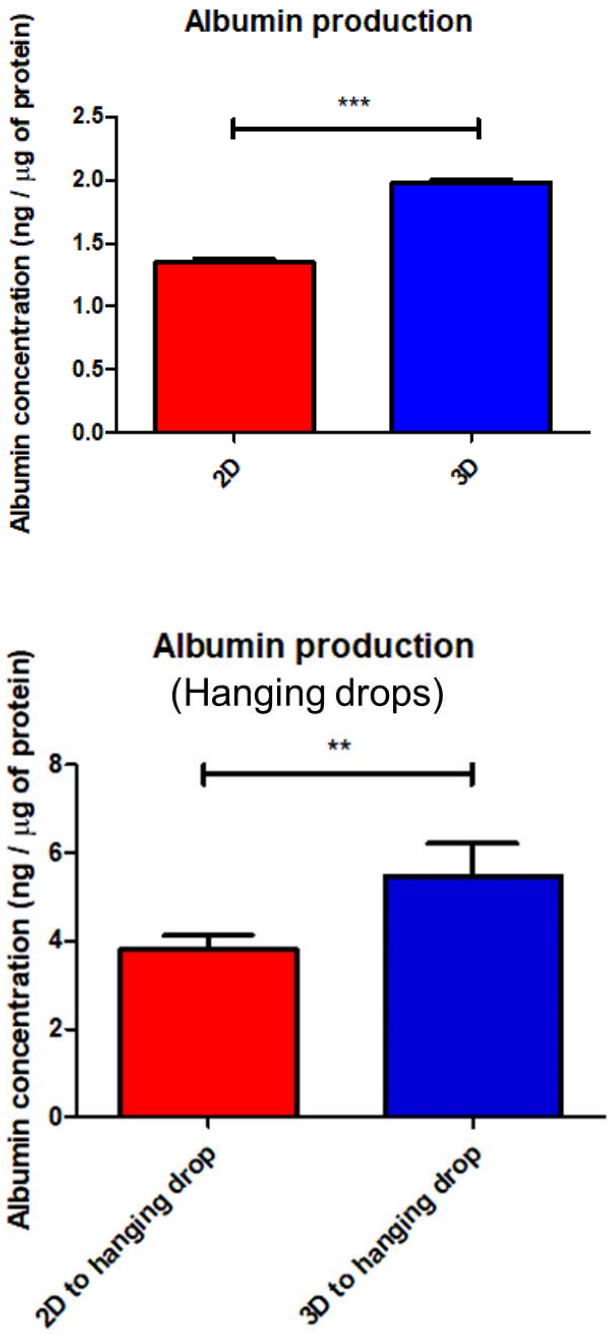

Figure 6.4: Albumin secretion increases during 3D priming and stays elevated in hanging drops.

Graphs showing the albumin production as quantified by the Human Albumin AssayMax ELISA kit. ELISA performed on media taken from 2D or 3D priming HepG2 cultures, seeded at $5x10^5$ cells per 2D well and $1x10^6$ cells per Alvetex® membrane after either 4 or 8 days of culture (top graph). ELISA performed on media taken from hanging drops formed from 2D or 3D primed HepG2 cells, seeded at $1x10^3$ cells per drop, after 7 days of culture (bottom graph). Results normalised to total protein. N= 6, n= 4.

Urea production follows a similar trend, with a statistically significant increase in the 3D primed cells over 2D cells in the priming stage (**Figure 6.5 top panel**), though the magnitude of increase is slightly less than that with albumin, being an increase of around 1.4 x. Again, an increase in urea production is noted in the 3D primed secondary spheroid models too compared to the 2D grown spheroid models, and this time there is nearly an increase of 1.9-fold in the 3D primed spheroids. This validates the increased gene expression seen amongst the urea cycle genes in the 3D primed cells. Both the albumin and urea data suggest that priming cells in 3D is functionally beneficial for the cells before placing them into a secondary model.

6.4.3 HepG2 cells primed in 3D exhibit a differential response to drug toxicity.

For drug toxicity tests, cells in either the priming stage models or in hanging drop models were exposed to varying concentrations of the test drug dissolved in media using a vehicle (see methods) 24 hours before testing viability with an MTT assay (priming stage only) and measuring LDH release (priming and secondary stage models). MTT is often used to indirectly measure viability, as it is a sensitive measure of cellular metabolic activity. However, due to metabolic activity also being intrinsically linked to the cellular response to toxicological challenge, an orthologous technique in the form of measuring LDH release was used. The LDH assay measures the release of lactate dehydrogenase into the medium which occurs upon damage to the plasma membrane, providing an indicator of cellular damage and therefore toxicity (Kumar et al., 2018). In the priming stage models then, the LDH and MTT assays should largely provide a reflected image of each other, with MTT measuring viability, and LDH measuring cell death.

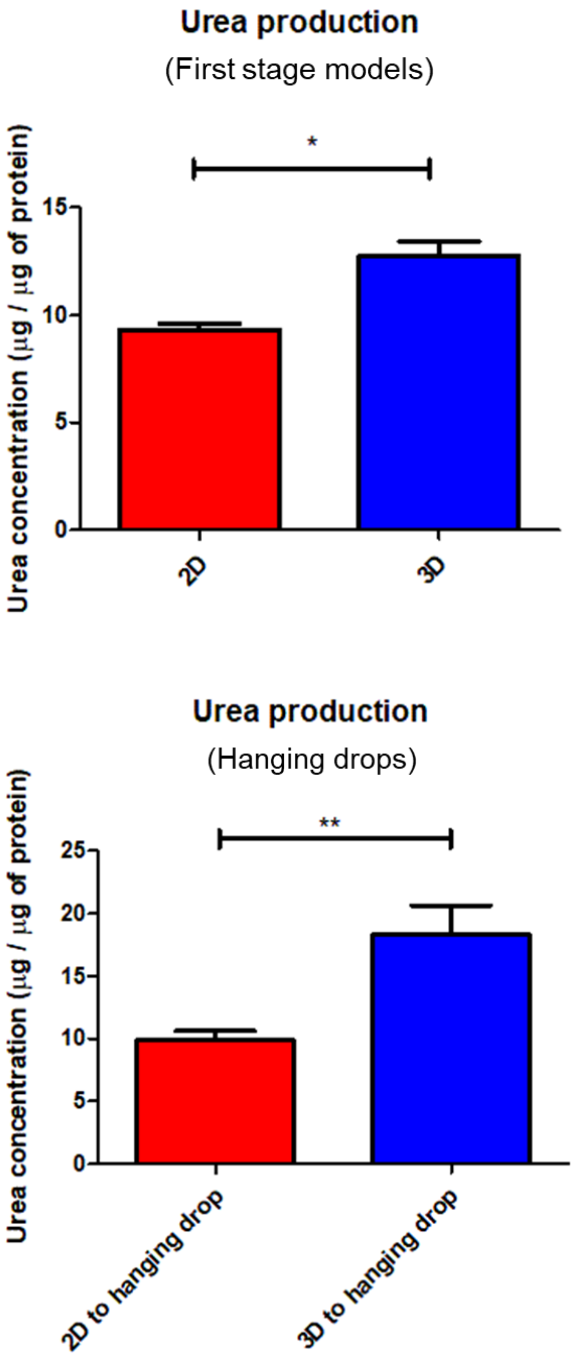

Figure 6.5: Urea production increases during 3D priming and stays elevated in hanging drops.

Graphs showing the urea production as quantified by the QuantiChrom™ Urea Assay Kit. Assay performed on media taken from 2D or 3D priming HepG2 cultures, seeded at 5x10^5 cells per 2D well and 1x10^6 cells per Alvetex® membrane after 8 days of culture (top graph). Assay performed on media taken from hanging drops formed from 2D or 3D primed HepG2 cells, seeded at 1x10^3 cells per drop, after 7 days of culture (bottom graph). Normalised to total protein. N= 6, n= 4.

The first drug to be tested was amiodarone; an arrhythmia suppressing agent with known hepatotoxic effects *in vivo,* of both an acute and a chronic nature ("Amiodarone," 2012). In the priming stage models (**Figure 6.6**). The LDH and MTT assays both indicated that the 2D grown HepG2 cells were distinctively more sensitive to the toxic effects of amiodarone compared to the 3D primed HepG2 cells, although at the top concentration of 300 µM, there was a detectable level of cell death occurring in the 3D primed HepG2 cells seen through the LDH assay, though curiously, the MTT assay does not reflect this pattern. Nonetheless, there is clearly a difference between the behaviour of the two models. Due to the purported direct toxic effect of amiodarone, the difference in response here may well be due to an increase in the key CYP450 enzymes involved in phase I metabolism of the substance (**Table 6.1**), as an increase of phase I metabolism would biotransform the drug and help remove the direct toxicity risk. Toxicity was measured in the secondary spheroid models too (**Figure 6.7**), and here there was almost no difference between the 2D and 3D primed spheroids, suggesting that the enzymes involved in amiodarone metabolism had somewhat levelled out after the 7-day period of spheroid growth. The spheroids showed a response to toxicity that was almost directly in-between the profiles of the 2D and 3D primed cells in the priming stage. This suggests that the hanging drop spheroids retain a sensitivity to the drugs, perhaps due to the smaller surface area and cell number compared to the 3D priming model, but also suggests altered enzyme levels over that of the 2D HepG2 cells.

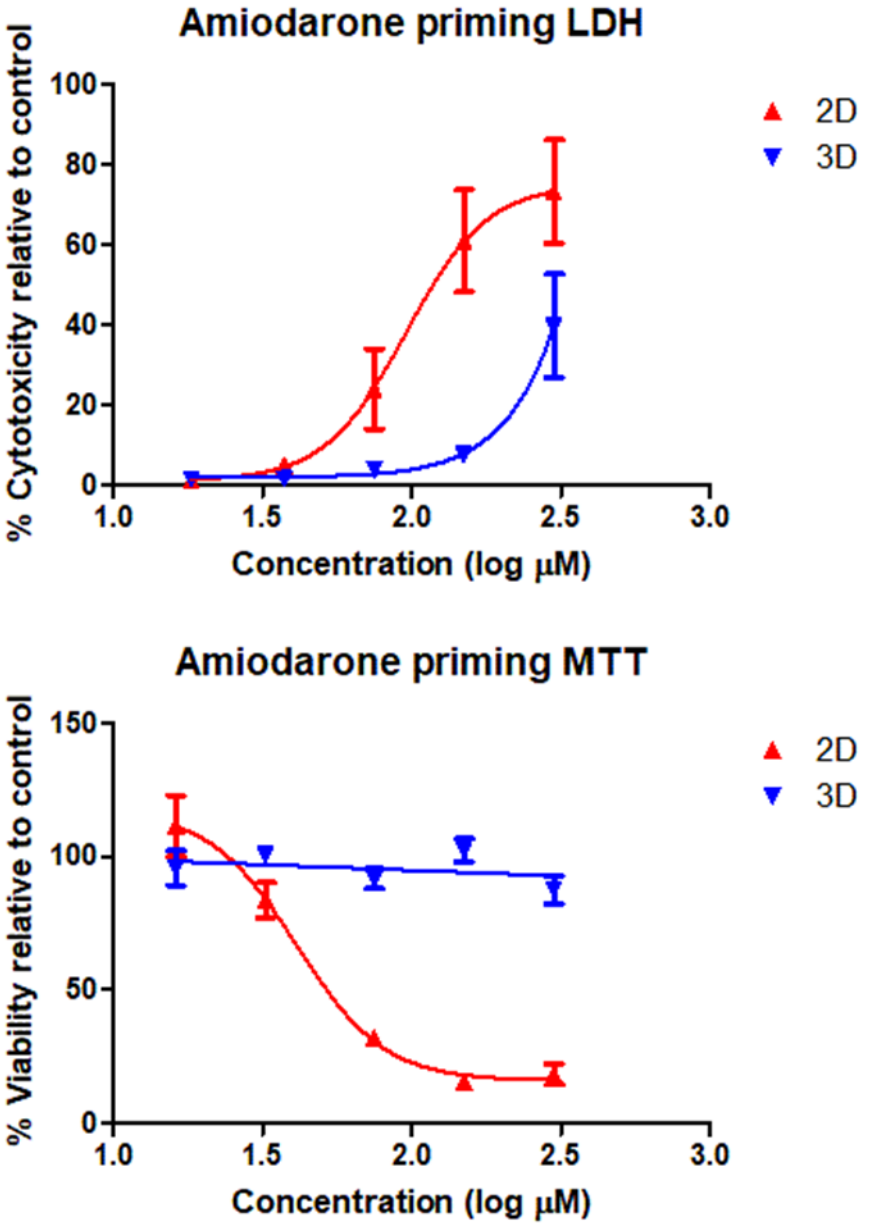

Figure 6.6: 3D cells in the priming model are less sensitive to amiodarone toxicity than 2D cells.

Graphs showing the drug toxicity curves from LDH and MTT assays of HepG2 cells in 2D and 3D priming models exposed to increasing concentrations of amiodarone applied on day 7 of culture. LDH assay performed on media taken from 2D or 3D priming HepG2 cultures, and MTT assay performed directly on cultures, seeded at 2.5 x 10^5 cells per 2D well (12 well plate) and 5 x 10^5 cells per Alvetex® 12 well membrane after 8 days of culture. N= 4, n= 2. Error bars = SEM

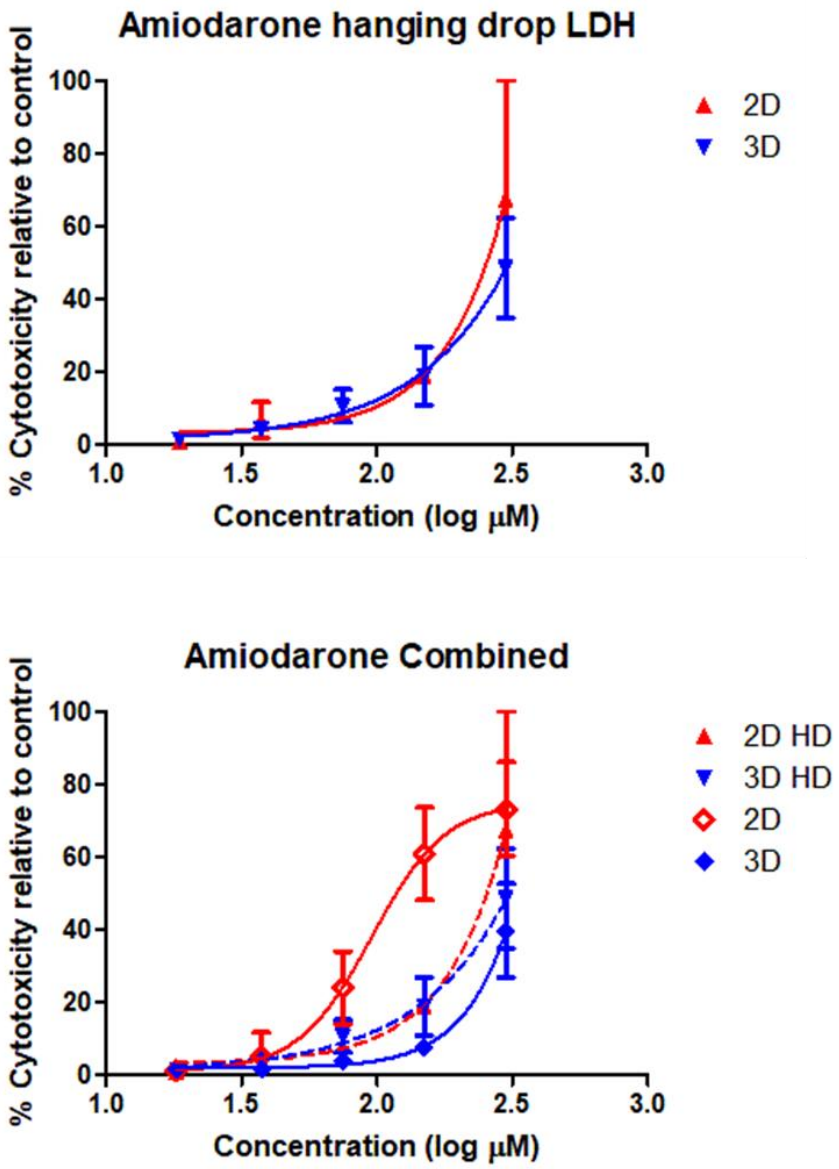

Figure 6.7: Differences in drug toxicity responses to amiodarone equalise in the secondary hanging drop model.

Top: Graphs showing the drug toxicity curves from LDH assays of 2D and 3D primed HepG2 cells reseeded into hanging drop models, exposed to increasing concentrations of amiodarone applied on day 6 of culture. LDH assay performed on media taken from hanging drops, seeded at 1 x 10^3 cells per drop, after 7 days of culture (bottom graph). N= 4, n= 2. Bottom: graph combining the LDH response from both the hanging drop data (dashed line – 2D/3D HD) with the priming stage data (solid line – 2D/3D). Error bars = SEM

Tamoxifen toxicity was tested for in the same manner; tamoxifen is a nonsteroidal antiestrogen that is often used to treat breast cancer, and in rare instances can cause acute liver injury *in vivo* ("Tamoxifen," 2012). In the priming stage models (**Figure 6.8**), tamoxifen has a more potent effect on the viability of 2D grown HepG2 cells, with a notable increase in cell death at 18.75 µM of the drug, whereas in 3D primed cells, an increase in death was only apparent at 75 µM. With this drug, the MTT and LDH results resembled a close mirror image of each other that provided a clear picture of what is occurring. Similar to amiodarone, the mechanism of tamoxifen hepatotoxicity is thought to be through direct estrogenic effects of the drug, and therefore the difference in the toxicity response seen here may point towards a difference in phase I enzyme expression, mirroring the increase in CYP3A7, CYP1A1 and CYP1A2 seen in the gene expression. Additionally, the toxicity profiles do appear very similar to those of the models with amiodarone exposure. Again, similar to amiodarone, the hanging drop spheroid models (**Figure 6.9**) have almost no difference between the 2D and 3D primed cells, aside from higher variability in 2D. This provides further suggestion that the CYP450 enzyme expression has equalised in the spheroids. The response of the spheroid models shows slightly lower sensitivity than the primary 2D model, but increased sensitivity over the 3D priming model, indicating that spheroids possess a medium-level sensitivity to drugs.

Ibuprofen is a common nonsteroidal anti-inflammatory (NSAID) drug used as a pain killer, that can in rare cases lead to chronic or acute liver failure ("Ibuprofen," 2012). The differential response of the priming models to ibuprofen (**Figure 6.10**) is less pronounced than with amiodarone and tamoxifen, though there is still a difference. The LDH assay shows that at the highest concentration of 5000 µM, both the 2D and 3D primed HepG2 cells reach nearly 100 % cytotoxicity, but the 3D primed cells have a more delayed response, reacting less to the lower concentrations. The MTT results however suggest that viability of the 2D HepG2 cells drops off significantly at 5000 µM (albeit not to 0 %), but the 3D primed HepG2 cells remain viable throughout. This emphasises the importance of using two techniques, especially when one relies on metabolism, as sometimes an inappropriate test may conceal what is really happening. Judging by the LDH assay, it appears that ibuprofen is toxic to both models, and ibuprofen is toxic through a metabolite, not directly, and therefore both phase I and phase II enzymes are implicated. The slightly less sensitive response in 3D may indicate a tip towards phase II detoxification, with a possible greater increase in the glucuronosyltransferase enzymes (UGT2B4 was the only detected increase in the enzyme gene expression) involved in removing the toxic intermediate, outweighing any increase in CYP450 enzymes.

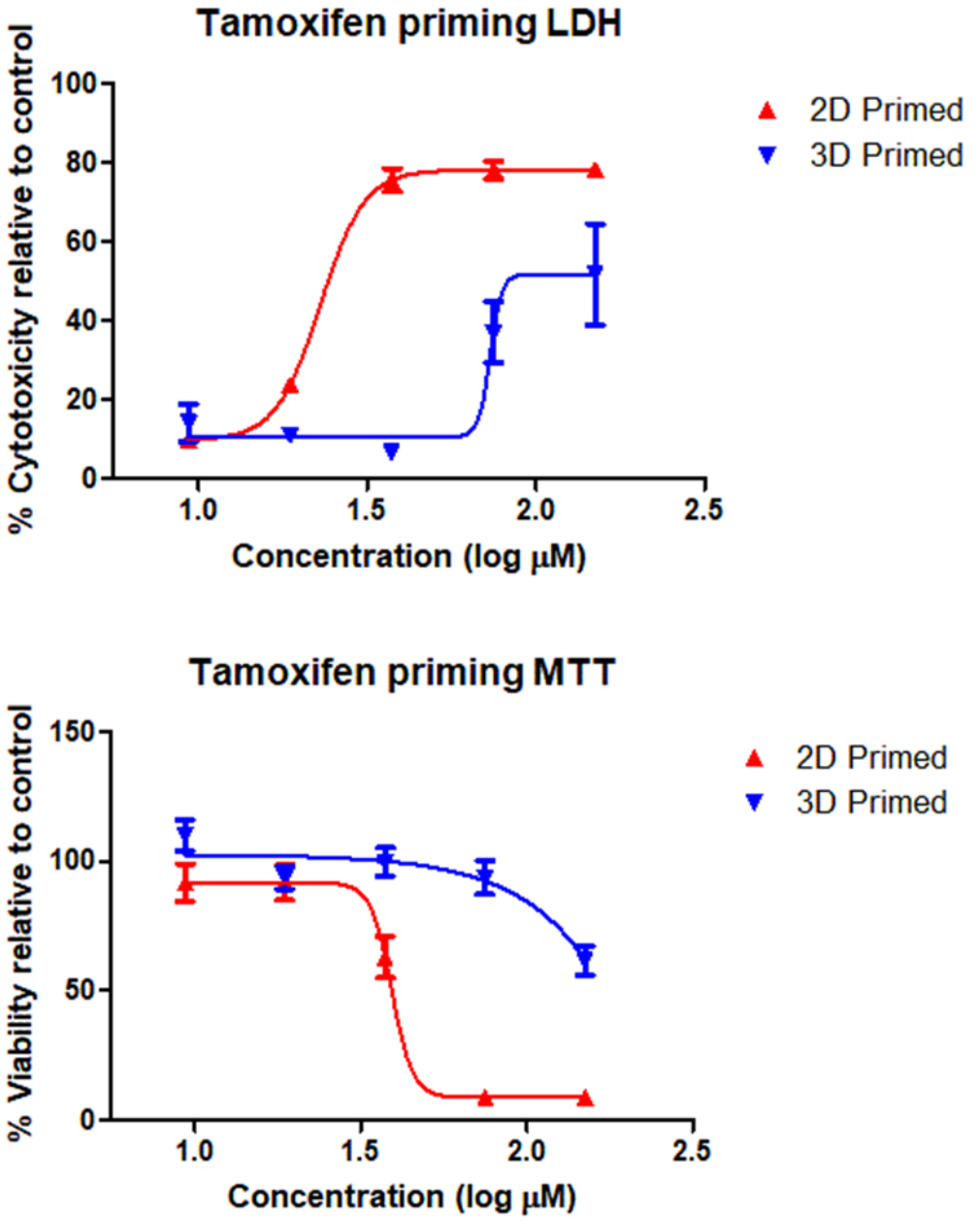

Figure 6.8: 3D cells in the priming model are less sensitive to tamoxifen toxicity than 2D cells.

Graphs showing the drug toxicity curves from LDH and MTT assays of HepG2 cells in 2D and 3D priming models exposed to increasing concentrations of tamoxifen applied on day 7 of culture. LDH assay performed on media taken from 2D or 3D priming HepG2 cultures, and MTT assay performed directly on cultures, seeded at 2.5 x 10^5 cells per 2D well (12 well plate) and 5 x 10^5 cells per Alvetex® 12 well membrane after 8 days of culture. N= 4, n= 2. Error bars = SEM

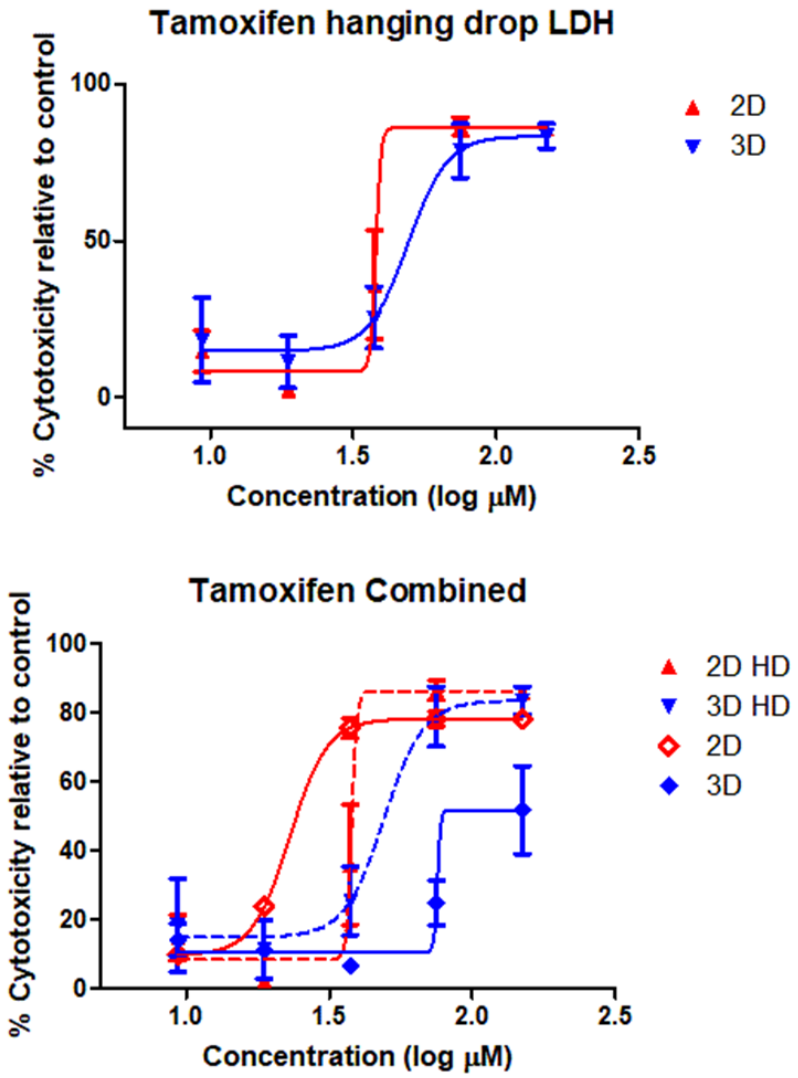

Figure 6.9: Differences in drug toxicity responses to tamoxifen disappear in the secondary hanging drop model.

Top: Graphs showing the drug toxicity curves from LDH assays of 2D and 3D primed HepG2 cells reseeded into hanging drop models, exposed to increasing concentrations of tamoxifen applied on day 6 of culture. LDH assay performed on media taken from hanging drops, seeded at 1x10^3 cells per drop, after 7 days of culture (bottom graph). N= 4, n= 2. Bottom: graph combining the LDH response from both the hanging drop data (dashed line – 2D/3D HD) with the priming stage data (solid line – 2D/3D). Error bars = SEM

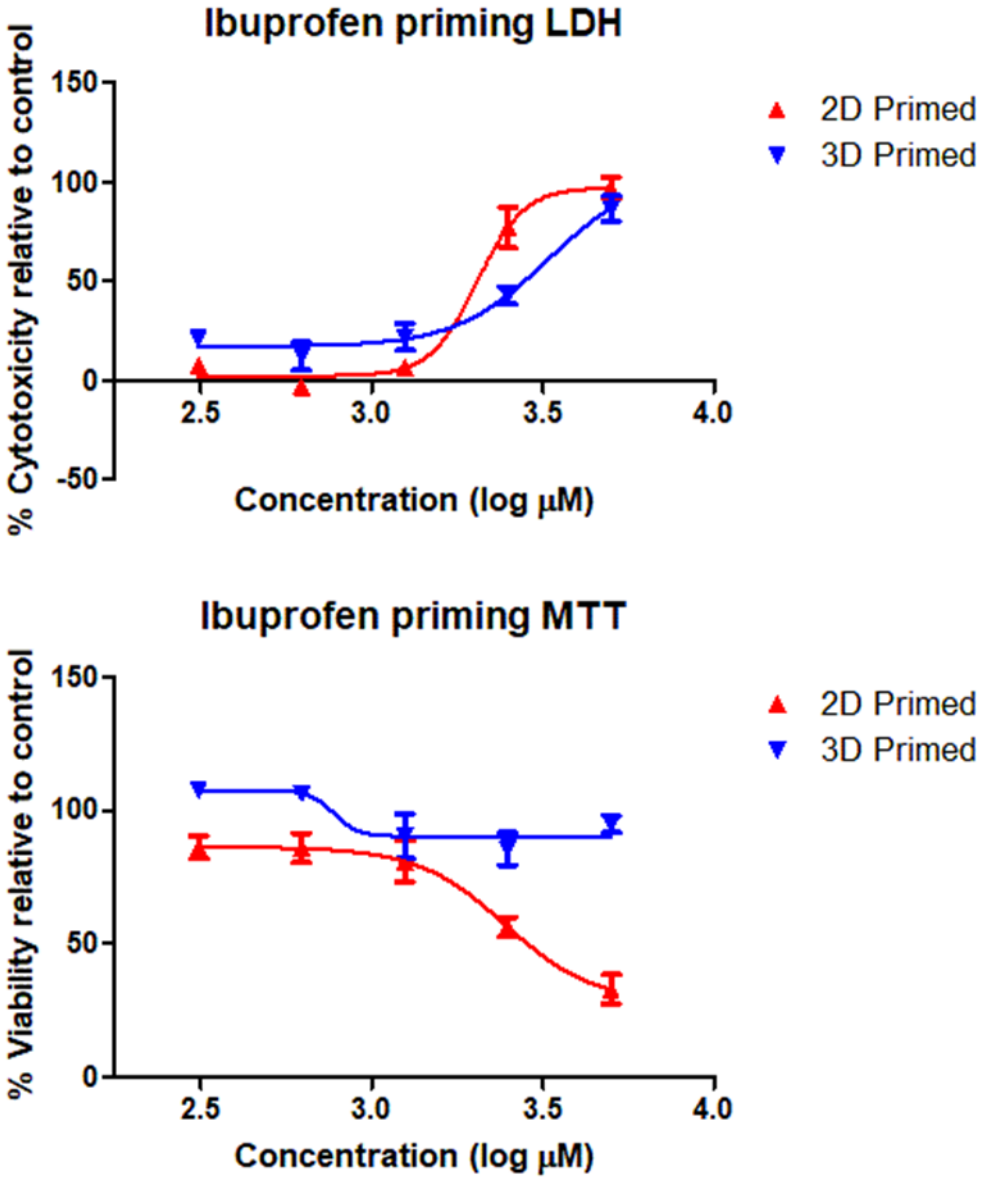

Figure 6.10: 3D cells in the priming model are slightly less sensitive to ibuprofen toxicity than 2D cells.

Graphs showing the drug toxicity curves from LDH and MTT assays of HepG2 cells in 2D and 3D priming models exposed to increasing concentrations of ibuprofen applied on day 7 of culture. LDH assay performed on media taken from 2D or 3D priming HepG2 cultures, and MTT assay performed directly on cultures, seeded at 2.5 x 10^5 cells per 2D well (12 well plate) and 5 x 10^5 cells per Alvetex® 12 well membrane after 8 days of culture. N= 4, n= 2. Error bars = SEM

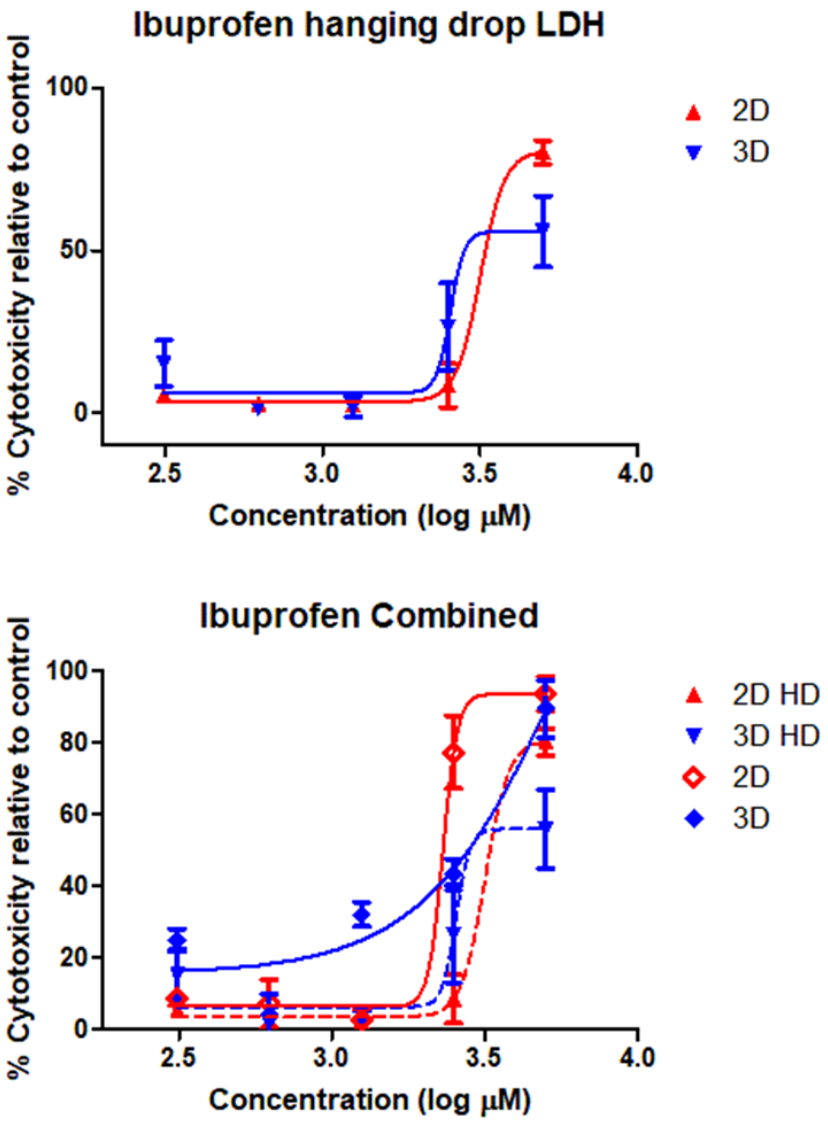

Figure 6.11: Hanging drops from 2D cells remain slightly more sensitive to ibuprofen toxicity in the secondary hanging drop model.

Top: Graphs showing the drug toxicity curves from LDH assays of 2D and 3D primed HepG2 cells reseeded into hanging drop models, exposed to increasing concentrations of ibuprofen applied on day 6 of culture. LDH assay performed on media taken from hanging drops, seeded at 1x10^3 cells per drop, after 7 days of culture (bottom graph). N= 4, n= 2. Bottom: graph combining the LDH response from both the hanging drop data (dashed line – 2D/3D HD) with the priming stage data (solid line – 2D/3D). Error bars = SEM

In the spheroid models (**Figure 6.11**), the 3D primed spheroids show a slightly lower sensitivity to the drugs at the final concentration of 5000 µM, though this was a more variable data point. This could however suggest that some of the changes in metabolism of 3D primed HepG2 cells are potentially retained even after 7 days of secondary culture; and perhaps these retained differences lie in the phase II enzyme expression as they are linked to detoxification of this drug. With this drug however, the priming models seem more sensitive to toxicity overall than the hanging drop models, marking a difference from the previous two drugs.

Gemfibrozil is used to lower triglycerides in the blood and to raise the presence of high-density lipoproteins and can cause acute liver injury in rare instances. It is thought that the hepatotoxicity mechanism is through a toxic intermediate of metabolism ("Gemfibrozil," 2012). The response of the priming stage models to gemfibrozil followed the same trend as before, with 3D primed cells showing an improved ability to cope with the toxicity of the drug, but similar to ibuprofen, the difference between the two models is less pronounced. The gemfibrozil on the 3D primed HepG2 cells does appear to reach maximum cytotoxicity as well as the 2D grown HepG2 cells, at 8000 µM, and but there is a slower curve in reaching this with the 3D primed cells. The LDH assay suggests that both 2D and 3D primed HepG2 cells are nearly all dead at 4000 µM also, though the MTT suggests that metabolism is still at roughly 60 % at this concentration in the 3D primed cells. Aside from this, the MTT and LDH assays create a close mirror image of each other for this drug, indicating that the results are indicative of a true toxic response. Again, this suggests that the 2D cells are perhaps more vulnerable to the toxic intermediate due to a lower ratio of phase II to phase I enzymes. The only metabolising enzyme for Gemfibrozil that showed differential gene expression was UGT2B4 increasing in the 3D primed cells. A curious response is seen in the hanging drops (**Figure 6.13**), with a very similar pattern shown where the 3D primed spheroids appear to be less sensitive to the lower concentrations of gemfibrozil, yet ultimately reaching the same levels of cell death at the top concentration as the spheroids from 2D HepG2 cells. This result signals the possibility of retained changes in the metabolic profile of 3D primed spheroids, and like ibuprofen, it seems that glucuronosyltransferases may be involved as they are the key phase II enzymes involved in detoxification of this drug.

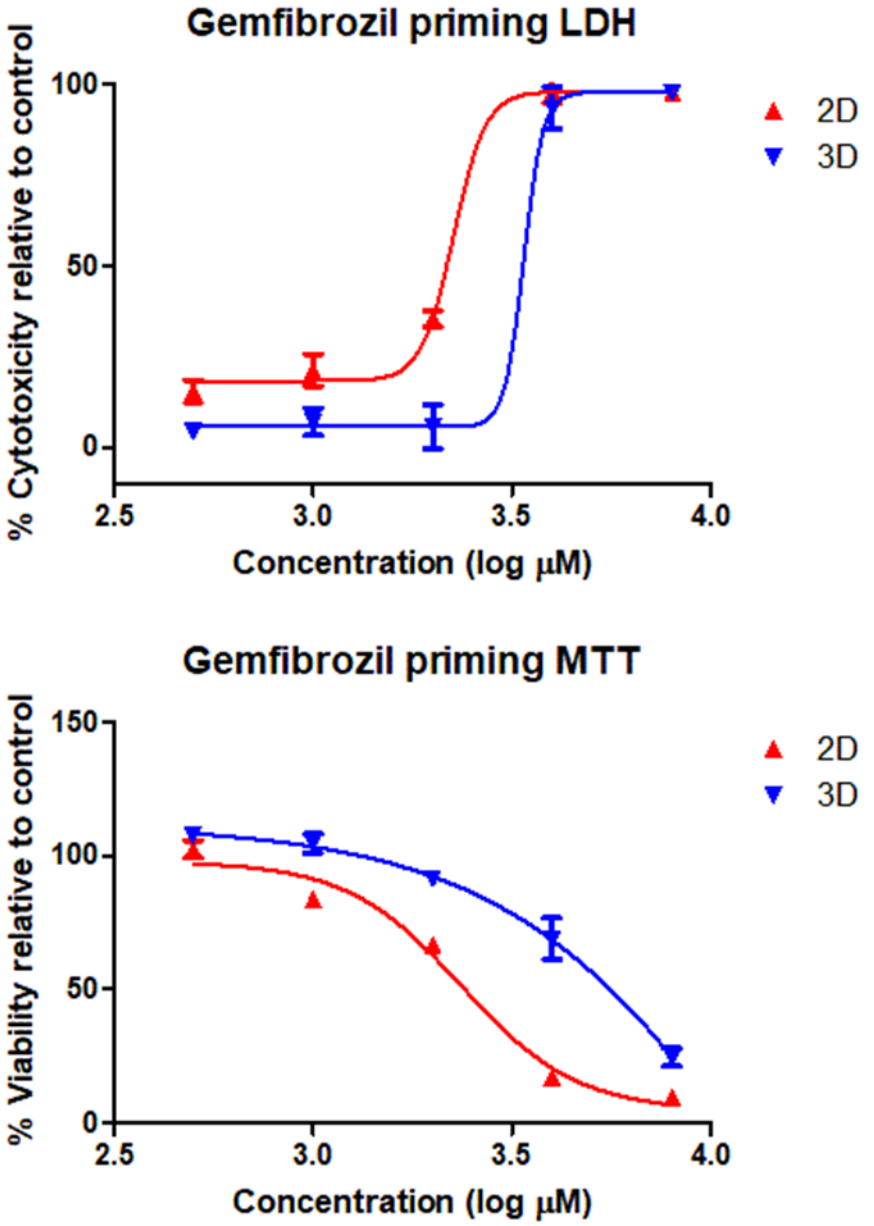

Figure 6.12: 3D primed HepG2 cells are less sensitive to gemfibrozil toxicity than 2D cells.

Graphs showing the drug toxicity curves from LDH and MTT assays of HepG2 cells in 2D and 3D priming models exposed to increasing concentrations of ibuprofen applied on day 7 of culture. LDH assay performed on media taken from 2D or 3D priming HepG2 cultures, and MTT assay performed directly on cultures, seeded at 2.5 x 10^5 cells per 2D well (12 well plate) and 5 x 10^5 cells per Alvetex® 12 well membrane after 8 days of culture. N= 4, n= 2. Error bars = SEM

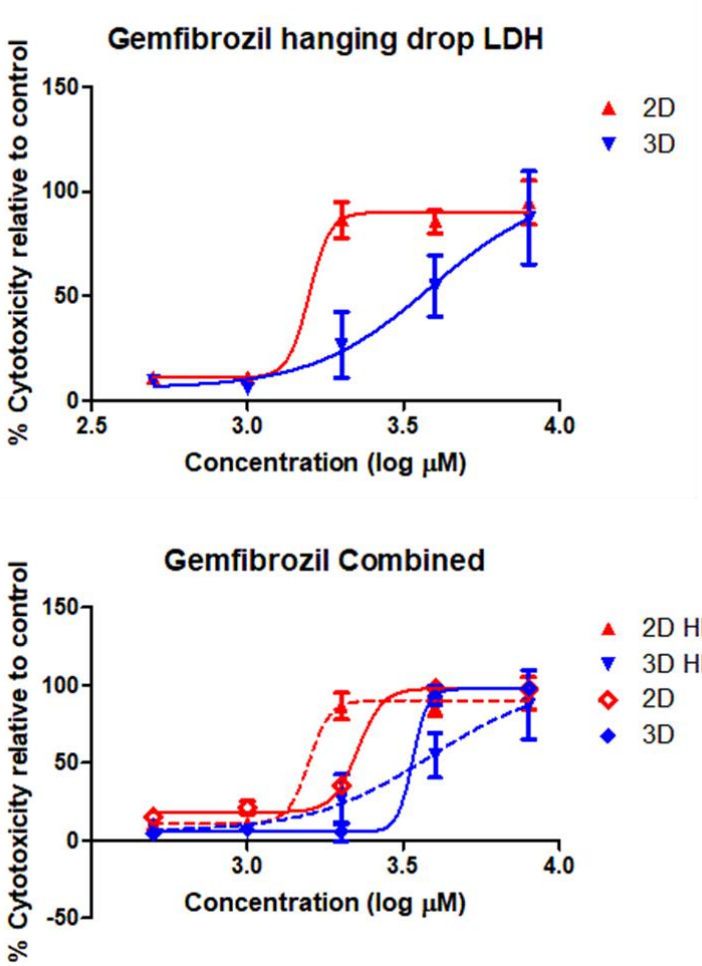

Figure 6.13: Hanging drops made from 2D HepG2 cells remain more sensitive to ibuprofen toxicity in the secondary hanging drop model.

Top: Graphs showing the drug toxicity curves from LDH assays of 2D and 3D primed HepG2 cells reseeded into hanging drop models, exposed to increasing concentrations of ibuprofen applied on day 6 of culture. LDH assay performed on media taken from hanging drops, seeded at 1x10^3 cells per drop, after 7 days of culture (bottom graph). N= 4, n= 2. Bottom: graph combining the LDH response from both the hanging drop data (dashed line – 2D/3D HD) with the priming stage data (solid line – 2D/3D). Error bars = SEM

Isoniazid is a medication commonly used for tuberculosis, which is well known to cause acute liver injury. It is believed that toxicity is exerted through an intermediate of metabolism, and seems to be more pronounced in patients with slow acetylation or abnormalities in CYP2E1 ("Isoniazid," 2012). There is a very distinctive lack of sensitivity to isoniazid in the 3D primed cells during the priming stage (**Figure 6.12**), with almost no change in viability or cytotoxicity as measured by MTT and LDH. However, the 2D cells show a fairly typical curve, reaching maximum LDH release at 10,000 µM. This points towards a significant alteration in the metabolic status of the 3D primed cells, however, out of the only two currently identified interacting enzymes, there was very weak expression in both 2D and 3D HepG2 cells, with no differential expression. The differential response to toxicity may lie in wider biological changes, and based on the underlying hepatotoxicity mechanisms, this may be due to a difference in acetylation status between the two models. Uniquely, the spheroid models show nearly no reaction to isoniazid in the tested concentration range (**Figure 6.13**), with only a slight increase in LDH release at the final concentration of 10,000 µM. This could well indicate that altered acetylation status is very much a product of a 3D environment, with both 2D and 3D primed spheroid models showing almost no sensitivity, similar to the 3D priming model.

Methotrexate is an immunosuppressant that can cause acute liver injury in rare instances where high dose intravenous methotrexate is administered, however in long term methotrexate treatment (commonly after 2 to 10 years of treatment), hepatic fibrosis and cirrhosis occurs in a considerable number of patients (>20 % after 5 years). Methotrexate is thought to exert injury directly, through inhibiting RNA and DNA synthesis ("Methotrexate," 2012). The enzymes involved in methotrexate metabolism differ slightly from the 'typical' enzymes in liver detoxification (see **Table 6.1**). Three out of the seven genes encoding for enzymes that metabolise methotrexate were upregulated in 3D primed HepG2 cells, with two upregulated in 2D, and two showing no significant differential expression. The LDH response of the priming stage models to methotrexate show a very clear difference between 2D and 3D HepG2 cell responses to toxicity, fitting with the consistent pattern that 3D primed HepG2 cells are less sensitive to toxicity. There was only a slight increase in 3D primed HepG2 cell death at the top two concentrations of 75 and 150 µM (**Figure 6.16**). There is however a distinct lack of response in both models when measuring MTT absorbance, with 2D grown HepG2 cells still showing a drop in metabolism but only down to 78 % of it's original value at the maximum concentration of 150 µM. This is in contrast with the LDH which shows nearly 80 % cytotoxicity at 75 and 150 µM. It is unclear as to the reasons for this disparity, but the

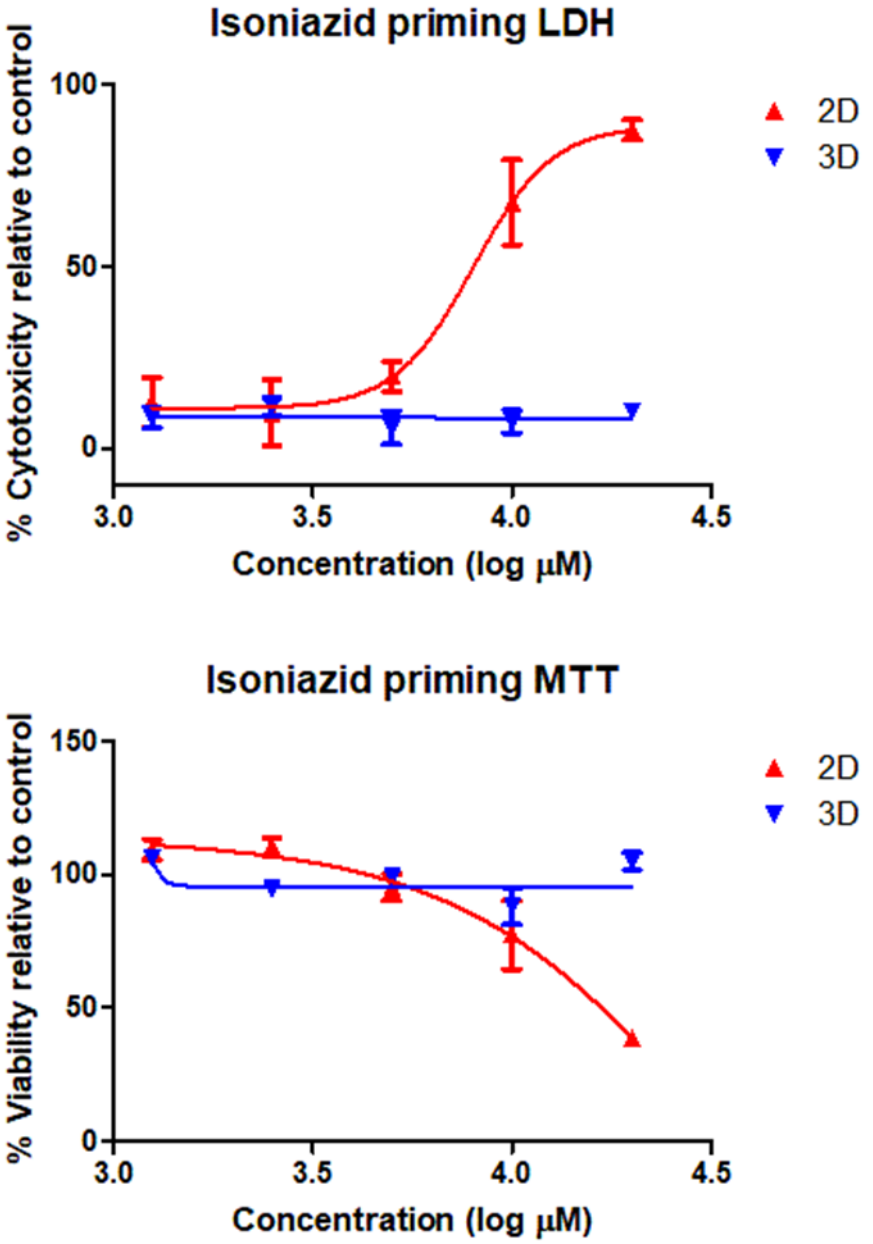

Figure 6.14: 3D cells in the priming model are less sensitive to isoniazid toxicity than 2D cells.

Graphs showing the drug toxicity curves from LDH and MTT assays of HepG2 cells in 2D and 3D priming models exposed to increasing concentrations of isoniazid applied on day 7 of culture. LDH assay performed on media taken from 2D or 3D priming HepG2 cultures, and MTT assay performed directly on cultures, seeded at 2.5 x 10^5 cells per 2D well (12 well plate) and 5 x 10^5 cells per Alvetex® 12 well membrane after 8 days of culture. N= 4, n= 2. Error bars = SEM

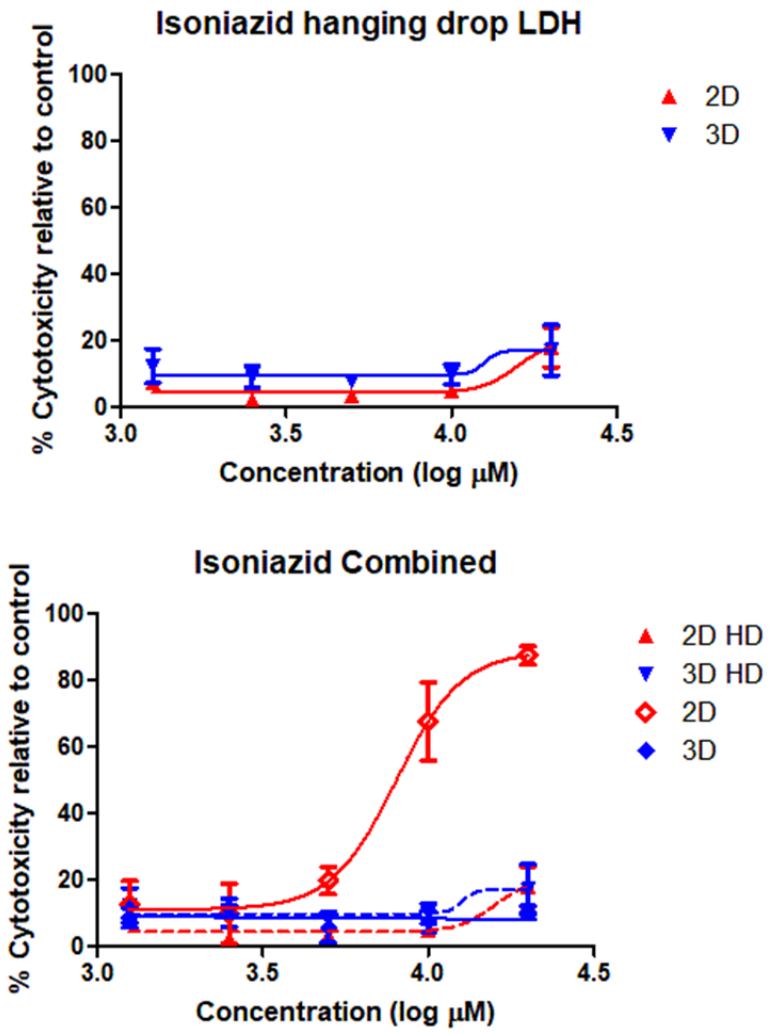

Figure 6.15: Little to no toxicity response was detectable in hanging drops exposed to isoniazid.

Top: Graphs showing the drug toxicity curves from LDH assays of 2D and 3D primed HepG2 cells reseeded into hanging drop models, exposed to increasing concentrations of isoniazid applied on day 6 of culture. LDH assay performed on media taken from hanging drops, seeded at 1x10^3 cells per drop, after 7 days of culture (bottom graph). N= 4, n= 2. Bottom: graph combining the LDH response from both the hanging drop data (dashed line – 2D/3D HD) with the priming stage data (solid line – 2D/3D). Error bars = SEM

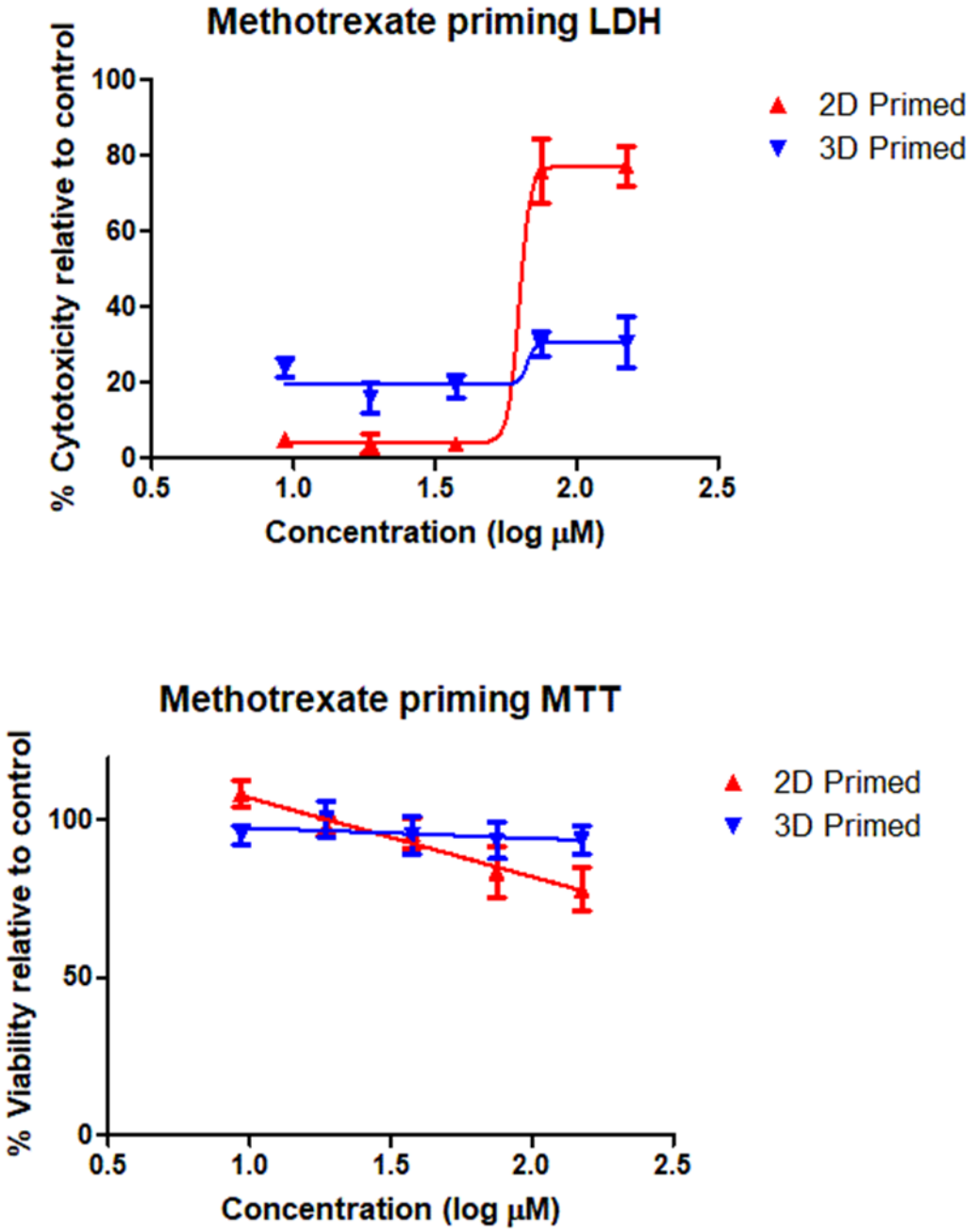

Figure 6.16: 3D cells in the priming model are less sensitive to methotrexate toxicity than 2D cells, though there is a disparity between MTT and LDH values.

Graphs showing the drug toxicity curves from LDH and MTT assays of HepG2 cells in 2D and 3D priming models exposed to increasing concentrations of methotrexate applied on day 7 of culture. LDH assay performed on media taken from 2D or 3D priming HepG2 cultures, and MTT assay performed directly on cultures, seeded at 2.5 x 10^5 cells per 2D well (12 well plate) and 5 x 10^5 cells per Alvetex® 12 well membrane after 8 days of culture. N= 4, n= 2. Error bars = SEM

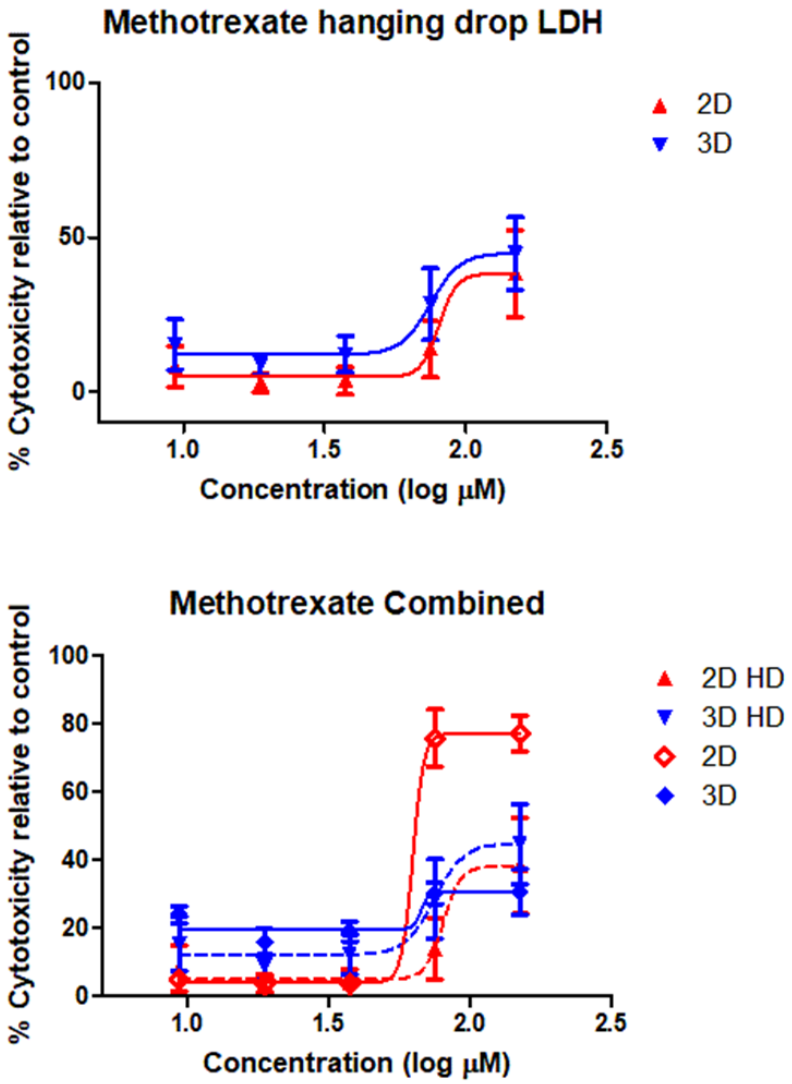

Figure 6.17: A similar toxicity response was observable in hanging drops formed from 2D and 3D primed cells exposed to methotrexate.

Top: Graphs showing the drug toxicity curves from LDH assays of 2D and 3D primed HepG2 cells reseeded into hanging drop models, exposed to increasing concentrations of methotrexate applied on day 6 of culture. LDH assay performed on media taken from hanging drops, seeded at 1x10^3 cells per drop, after 7 days of culture (bottom graph). N= 4, n= 2. Bottom: graph combining the LDH response from both the hanging drop data (dashed line – 2D/3D HD) with the priming stage data (solid line – 2D/3D). Error bars = SEM

LDH assay does seem to indeed confirm that the 2D HepG2 cells are dying at the top concentrations. While the 3D cells in the priming stage have a distinctively higher baseline LDH activity level, the response of the spheroid models (**Figure 6.15**) again shows a trend of being midway between the behaviour of the 2D and 3D priming models. Both 2D and 3D primed spheroids showing a very similar response to methotrexate, which slightly less sensitive than the primary stage 2D HepG2 cells. The methotrexate data indicates that there is indeed a difference in metabolism, even when not involving the CYP450s as directly.

6.5 Discussion

6.5.1 Functional and structural proteins are differentially expressed in 3D primed HepG2 cells.

This chapter has presented a data set that functionally characterises 3D primed HepG2 cells and compares them to HepG2 cells grown in 2D, which also shows that priming cells does carry forward enhanced function into a secondary 3D spheroid model, although the functional differences equalise to an extent after 7 days. Enhanced hepatic function is apparent in the 3D primed models through a very clear upregulation of both albumin and fibrinogen alpha chain proteins. Production of certain proteins is often used to indicate liver function, and albumin is the most abundant serum protein that hepatocytes produce (Nishikawa et al., 2017) that helps maintain oncotic pressure and transport drugs (Buyl et al., 2015; Cameron et al., 2020, p. 10) and is a key marker of liver function. Fibrinogen alpha chain is a protein synthesised in hepatocytes that is a component of fibrinogen, a glycoprotein complex that helps in blood clotting and contributes towards angiogenesis, and has been used previously to indicate synthetic liver function (Khalil et al., 2001). Indeed, the observation that these proteins are both clearly upregulated in 3D, and the structural proteins sun1/2 upregulated in the 2D HepG2 cells indicates that through priming, the HepG2 cells are moving away from the two-dimensional phenotype with a rigid nuclear structure, to a more malleable three-dimensional phenotype where the synthetic function is enhanced. The expression of albumin in the spheroids was more consistent between 2D and 3D primed spheroids, though there was still a slight potential increase in the 3D primed secondary model, however this indicated that synthetic activity levels mostly equalised after 7 days of secondary culture.

6.5.2 Albumin and urea production are enhanced in 3D primed cells and in spheroids formed from 3D primed cells.

The western blots indicated the specific differences in synthesis during the precise timepoint of harvesting the cells, but it was also of interest to measure whether there was an increased build-up of albumin and urea (both key liver specific biomarkers) in the media. The presence of these two markers was measured in the media at the end of the culture period in both the priming stage and secondary stage models. It is important to specify that in the priming models, media was changed every two days, hence the concentrations in the media were

lower compared to the secondary models where media was not changed but was just added to the models at the mid-point of culture. Regardless of that proviso, both albumin and urea levels were significantly enhanced in the 3D priming model and the 3D primed spheroids over the 2D counterparts, and this provided further evidence that the synthetic properties of the HepG2 cells could be enhanced through priming in a three-dimensional microenvironment.

It was particularly encouraging to see enhanced levels of urea and albumin in the 3D primed spheroids as this indicated that the beneficial effects of priming are indeed carried over to the secondary model, even if after 7 days, the direct albumin levels had equalised somewhat. This indicates that priming cells does better prepare HepG2 cells for a 3D environment better, providing them with the advantageous functional properties from the very beginning of the secondary model, and amplifying the overall production of important functional molecules. Despite an increase in urea detected, this data should be caveated with the fact that the urea cycle is known to be diminished in HepG2 cells due to ornithine transcarbamylase (OTC) and arginase 1 (ARG1) deficiency (Mavri-Damelin et al., 2007). An increase in the expression of urea cycle genes (including ARG1 and OTC) was seen in the transcriptomic analysis which could partially explain the increase in urea detection, however the cycle is likely still deficient compared to primary cells. Further analysis such as gas-chromatography mass-spectrometry analysis for ^{15}N-urea production could help more accurately quantify the urea production.

A previous thesis from the our lab corroborated with this, indicating that maintaining cells in Alvetex® over multiple passages enhanced albumin and urea production as well as enhancing metabolism (Chhatwal, 2016). In this instance, time spent in a three-dimensional microenvironment appeared to be the influencing factor on synthetic function, and the model used in this project demonstrates that even through using a simplified one-step priming method, beneficial results can be achieved. Interestingly, the spheroids from 2D cells did not show much of an increase of urea production over monolayer cultured HepG2 cells, though it is harder to compare these conditions due to the drastically different media volumes tested. The data here in combination with the western blot results closely corroborates with the patterns seen in the transcriptomic analysis, where liver specific genes such as albumin, fibrinogens and urea cycle genes were upregulated in 3D, along with enrichment in metabolism and biosynthesis. This serves as an extra validation step to show

that the sequencing data did in fact portray biologically meaningful changes in gene expression that resulted in differential downstream processes as a result of 3D culture.

6.5.3 Challenges in testing for drug toxicity.

Drug toxicity is a very common method for testing functionality as it indirectly indicates the metabolic competency of *in vitro* models through showing direct differences in functional responses. As discussed in the introduction however, *in vitro* toxicity testing is a complex matter with many areas to consider such as the mechanism of action of the drugs, the type of toxicity to test (chronic or acute), appropriate measures of toxicity, the difficulty of applying a relevant dosage and more. It is known that *in vitro* models are often insensitive to hepatotoxic agents (Xu et al., 2004), however other reports suggest that false positives are also an issue when detecting genotoxic agents (Kenna and Uetrecht, 2018). Regardless of which direction the toxicity tests point, *in vitro* models are evidently not a perfect representation of *in vivo* behaviour and work still needs to be done to reach a better understanding of the mechanisms underlying the response to toxic agents and how these are altered in model systems. Work like this is important therefore in helping to reach an understanding of how the microenvironment in which cells are cultured effects the behaviour of the cells and can help aid more informed decision making when selecting the appropriate format in which to culture cells.

In this project, during the priming stage, MTT absorbance and LDH release were used to indicate toxicity through measuring viability and cytotoxicity, respectively. In most cases the MTT and LDH assays mirrored each other fairly closely, however in the case of ibuprofen and methotrexate, the 3D primed HepG2 cells showed only a small drop in viability according to the MTT results, but the LDH values suggested a more noticeable response to the increasing concentrations of the drugs. This emphasises the need for multiple tests for drug toxicity, as using only one test may not provide an accurate reflection of what is occurring. This is especially relevant to MTT tests which, while widely used, are primarily an indicator of cell metabolism and only indirectly point towards viability. Therefore, when testing toxicity of xenobiotic agents which directly affect and are affected by metabolism, measuring MTT absorbance may not be appropriate.

6.5.4 During the priming stage, 3D primed HepG2 cells show reduced sensitivity to xenobiotic toxicity.

Regardless of the sometimes-inconsistent MTT results, the models in the priming stage demonstrated a consistent pattern in these cells. 3D priming models followed the general trend seen in previous studies of showing a decreased sensitivity to xenobiotic compounds. The exact patterns of the dose response curves differed between the drugs, but in all cases during the priming stage models, the 2D grown HepG2 cells showed a tendency to lose viability faster than the 3D primed cells. In two of the drugs; gemfibrozil and ibuprofen (though only in the LDH assay for ibuprofen), the higher concentrations of the drug were similarly toxic for both the 2D and 3D primed cells, however during the lower concentrations, the 2D cells indicated signs of cytotoxicity earlier than the 3D primed cells. Other drugs however had a drastically different effect on cytotoxicity between 2D and 3D primed HepG2 cells. For example with amiodarone and isoniazid, there was little to no toxicity elicited in cells grown in 3D, whereas the 2D cells indicated a very typical response with a gradual increase in cell death and drop in viability as the drug concentration increased.

There are many potential reasons for this difference in response to the drugs, with the primary candidate being that the metabolic profile of the cells is changing. This is a well characterised phenomenon in the literature as discussed in the introduction, with three-dimensional models consistently showing enhanced expression of the CYP450 enzymes responsible for phase I metabolism of drugs, and increased expression of phase II enzymes, which are responsible for biotransformation of the intermediates created by phase I metabolism. Importantly, drugs are not always metabolised by the cytochrome P450 enzymes however, as is the case with methotrexate whose related enzymes include folylpolyglutamate synthase (FPGS) and methylenetetrahydrofolate reductase (MTHFR). **Table 5.1** highlighted the key enzymes involved in metabolism of each of the drugs tested here and the purported mechanisms of toxicity, and through correlating the experimental data with that table, one can observe some interesting patterns. Specifically, in the drugs where the mechanism of toxicity was thought to lie purely in the direct effects of the drug on the liver (amiodarone, methotrexate), the patterns of toxicity tend to show a large difference between 2D and 3D cultures, with the 3D primed cells showing very little response. This data both validates the sequencing data, and reveals more about the possible metabolic mechanisms occurring, as with the drugs that directly damage the liver, the key detoxification occurs through phase I metabolism with a key set of CYP450 enzymes for many of the drugs, and a unique set for methotrexate. The patterns seen indicate therefore that the activity of these phase I enzymes is elevated in the 3D cells due to their greater ability to cope with toxicological challenges, which was a general trend seen in the gene expression.

This is a beneficial change due to the known difficulty in inducing the CYP450 enzymes in HepG2 cells, and it shows that mechanically altering the physical microenvironment can direct the epigenetic plasticity of HepG2 cells towards a more functional phenotype.

In the drugs where intermediates of metabolism exert the toxicity (ibuprofen, gemfibrozil and isoniazid), the response is slightly less clear cut. Ibuprofen and gemfibrozil results show similar behaviour in that the 3D primed cells appear slightly less sensitive during the earlier concentrations, but ultimately reach the same levels of cytotoxicity as the 2D grown HepG2 cells. The responses with these drugs imply two things; firstly, it suggests that phase I metabolism *is* occurring in both the 3D primed *and* the 2D cells due to the fact that the toxic intermediates have to be produced to exert toxicity, meaning the drug must have been biotransformed by the cytochrome P450 enzymes initially. Secondly, this indicates that due to the slightly lessened sensitivity in the 3D primed cells, there is a balance in 3D towards phase II metabolism which is more capably removing the active metabolites produced by the CYP450 enzymes than the 2D cells. An unusual result was apparent with isoniazid, however; isoniazid has one of the most radical differences between the models, with the 3D primed HepG2 cells showing a complete absence of cytotoxicity in response to the drug, whereas the 2D cells remain highly sensitive. This may be related to the fact that toxicity is thought to be pronounced in patients with slow acetylation, suggesting that perhaps in 2D there is potent drop in acetylation activity. This data also suggests that the potential increase in phase I metabolism (as hinted at by the models' responses to the directly toxic drugs) is increased disproportionately by a smaller magnitude compared to the increase in phase II acetylation activity, and perhaps it is this imbalance that is creating the differential response in 3D primed cultures.

Finally, tamoxifen is an interesting candidate due to the reports that it can exert toxicity both through direct estrogenic effects and through a toxic intermediate ("Tamoxifen," 2012), and therefore the results are interesting due to the implications of both direct phase I and phase II involvement in detoxification. Interestingly, this drug shows a very similar pattern to amiodarone in the response of the priming stage models, with the 3D primed HepG2 cells showing very little sensitivity until a final increase in cytotoxicity / drop in viability at the final concentrations. Due to the multiple mechanisms of toxicity with tamoxifen, it is difficult to make any assumptions about which enzymes are changing in their activity/expression but, as with all other drug responses, the 3D priming cells are more metabolically competent, showing a greater ability to cope with toxicity.

This data followed the general patterns seen in the sequencing data (**Chapter 5**) which revealed upregulation in certain phase I enzymes and a large number of phase II enzymes in 3D primed HepG2 cells, in addition with significant enrichment in drug metabolising pathways. When looking at the genes encoding for enzymes that metabolise these specific drugs, there was less of a distinctive pattern, particularly in the less characterised drugs (as the number of identified interactors was considerably low). Interestingly too, the toxicity curves here show very clear patterns despite the lack of significant gene expression changes in the key / rate limiting enzymes for each drug, suggesting it is wider metabolic changes, and differences in model architecture that are driving the different biological response. Despite this, the drug test data does validate the gene expression data, and the fact that drug metabolism was an enriched category in 3D suggests that wider genes are interacting to make the 3D cells more metabolically competent.

6.5.5 3D primed spheroids are slightly less sensitive than spheroids from 2D, but the responses largely equilibrate between spheroids from 2D and 3D.

When looking at the response of the secondary models – the spheroids – to xenobiotic compounds, the results are different than the priming stage models. Primarily, in the hanging drop spheroids, there is much less of a difference in response of the spheroids from 2D and 3D HepG2 cells to the drugs. Amiodarone, tamoxifen, ibuprofen, isoniazid and methotrexate all elicit dose response curves that generally follow a similar trend in spheroids formed from 2D and 3D cells, with only minor differences in sensitivity. This could mean two things; firstly the metabolic profiles of the cells may have levelled out somewhat due to both the 2D and 3D primed cells having spent 7 days in the same spheroid culture format. Secondly, as the overall architecture of the model is much more comparable between the two spheroid conditions than between the priming stage models, a big reason for the differences observed in the primary stage models could indeed be the architecture of the models and arrangement of the cells. With these possibilities in mind, this does not however mean that 3D primed cells behave exactly the same as 2D cells in spheroids; observable changes in the spheroid formation and structure were noted in the previous chapter, and even after 7 days in the spheroids, there were still small differences noticeable in structure.

The 3D primed spheroids produce more overall albumin and urea, and with the drug toxicity, the curves are not all the same. Gemfibrozil reveals a difference in how the 3D primed spheroids respond to the drugs, with both models ultimately reaching the same levels of cytotoxicity at the final concentration, but with a delayed response to cytotoxicity at the

lower drug concentrations the 3D primed spheroids. Gemfibrozil's toxicity is suspected to be due to a metabolic intermediate, and this suggests that the 3D primed cells may retain increased metabolic activity of the phase II enzymes. Additionally, in the final concentration of ibuprofen there is a diminished (though more variable) cytotoxicity in the 3D cells, which provides further indication that there are still some retained differences in drug response of the spheroid models from priming even after 7 days. Isoniazid is a particularly unusual example of a drug response in that in the priming stage it had a normal reaction on the 2D HepG2 cells but no reaction on the 3D priming model. Based on all other secondary model patterns showing an intermediate level of sensitivity, one would expect that spheroids exposed to isoniazid would also replicate this pattern, but with isoniazid there is almost no response at all from either spheroid model. This suggests that for some unknown reason, the changes in structure from a 2D monolayer to any form of three-dimensional layout (spheroid or scaffold) are sufficient to render the cells completely insensitive to the toxicity of this range of isoniazid concentrations. The spheroid models were also more variable in the response to drugs than the priming stage models highlighting the slightly less controlled nature of this 3D culture method.

6.5.6 Many considerations are required with *in vitro* toxicity testing.

Certain assumptions have been made in this chapter regarding the enzymes involved and potential mechanistic explanations behind the differential responses to drug toxicity. For example, the suggestion that only certain named phase I and phase II enzymes were implicated was made for the sake of simplicity, but it is crucial to pay heed to the many other factors that could influence the responses of the models in this chapter. This is a similar comparison to looking at isolated gene expression in the previous chapter, against the more holistic and contextual enrichment analysis which took into account a wider set of interacting genes. Firstly, as discussed in the introduction, the structure and arrangement of cells in *in vitro* models may itself exert a strong influence on the responses to toxic compounds (Astashkina et al., 2012). In chapters 3 and 4 the structures of the priming models and secondary models were well characterised, and from the SEM and H&E images, it was very clear how the cells on Alvetex® are very tightly packed and closely arranged, forming a *thick* epithelial like layer on top of the substrate. Compared to the mesenchymal monolayer morphology of the 2D grown HepG2 cells, this creates an essential difference between the two models that will influence how drugs may act on the cells. In the 3D priming models, media is available above and below the cell layer, however the tighter packing in 3D means

that access of drugs to the cells in the middle may be significantly restricted which contrasts with the monolayers in 2D where all cells are instantly available and exposed to the substance.

A revealing aspect of the spheroid models is that the dose response curves mostly fit into the middle of the two extremes of the 2D and 3D primed HepG2 cells, which provides a unique insight into how there is almost a 'sliding scale' of structural effects on the biological behaviour of *in vitro* models. From this data it would seem that 2D cells are the most sensitive to drugs, spheroids exhibit medium sensitivity and scaffold models are the least sensitive. When comparing the different structure of spheroids which are relatively small with lower cell numbers to the dense layers of HepG2 cells on Alvetex®, these differences make sense. It is possible that the high level of cell contact on a scaffold induces a different magnitude of mechanotransduction, but the different architecture is also likely a large factor itself in influencing the biological properties when responding to drugs.

In addition to the changes in global structure, the previous chapters have highlighted how the cytoskeleton and nucleus of cells in 3D culture are altered significantly, even when moved into a secondary culture format. This alteration in cellular morphology is also likely to contribute to the differential response to various drugs. The cytoskeleton and nucleus are closely linked, and with the heavy involvement of nuclear architecture in determining cellular responses to toxicological challenge (Lelièvre et al., 2017), it is likely that on top of metabolic alterations, structural changes and the influence of mechanotransduction on the nucleus have a more direct effect on the hepatic behaviour.

Besides the metabolism, there are other biological factors that can influence the processing of drugs too, particularly the presence and activity of transporters and polarisation of the cells. Polarisation is an essential feature of *in vitro* models in order to achieve presentation of exogenous agents in a physiologically relevant manner (Astashkina and Grainger, 2014). Cells grown in 3D produce differential polarisation as well as overall architecture, with HepG2 cells grown on Alvetex® having previously demonstrated an increased presence of bile canaliculi-like structures in ultrastructural analysis (Bokhari et al., 2007, p. 2). Data from the **Chapter 4** also indicates enhanced polarity in the HepG2 cells through a more organised presentation of claudin-1 and Mdr1 with structures also resembling bile canaliculi. Bile canaliculi are a key functional element of hepatocytes, excreting bile composed of sequestered materials that are transported out of hepatocytes, including drugs and their metabolites (Gallin, 1997). In addition to the canaliculi, drug transporter proteins such as

MRP2, MDR1, BCRP and others also play an essential role in absorption, distribution, metabolism and elimination of exogenous substances, working through a variety of mechanisms such as ATP hydrolysis for efflux with the ABC transporters, and uptake of small molecules with the SLC transporters (Nigam, 2015). Across the different forms of drug transporters, a wide range of drugs and toxins are handled, and there is a growing body of evidence suggesting that they have a role beyond that of pharmacology and toxicology, extending to wider physiology too. It is believed that as well as transporting drugs, these transporters can regulate the trafficking of nutrients, anti-oxidants, bile salts, hormones and more (Nigam, 2015). This shows that it is important to consider the role of transporters in both the mediation of toxicity and wider endogenous function. The decreased sensitivity of the 3D models to drugs therefore points towards not only alterations in drug metabolism, but also in drug transport due to altered expression of transporters in 3D which is a known occurrence (Mueller et al., 2011). This is further complicated through the upregulation of certain ABC transporter genes in 2D HepG2 cells, and upregulation of SLC transporter genes in 3D HepG2 cells (**Chapter 5**). The fact that the 3D primed transporter levels were often closer to those seen in the human liver does suggest that the transporters may be functioning more physiologically in the 3D primed cells, but exactly how this is affecting the drug response is unclear.

Another point of interest is that the increased proliferation observed in 2D cultures makes them inappropriate for testing over repeated drug exposures due to the high turnover of cells (Ramaiahgari et al., 2014a), and the decreased sensitivity in the 3D primed cells here may indicate more suitability for long-term drug studies. Additionally, the potential differences in cell number makes it nearly impossible to apply a consistent *dosage* per cell of drug across the 2D and 3D models, and therefore a consistent concentration was used instead. There was a degree of normalisation through the toxicity measurements which are taken as a percentage of a maximal response within that respective model, but this makes comparing the different culture formats more challenging as the amount of drug delivered per cell might be significantly different. These considerations show how complex drug toxicity can be, and that simple conclusions are often hard to make, as there are many factors working in combination to determine how an *in vitro* model may respond to xenobiotics.

As discussed in the introduction, the benefit of this model in drug responses may very well depend on what the biological question is, but there is no doubt that the 3D culture has increased the metabolic capacity for drug detoxification and therefore may be a better

model for predicting effective cancer drug treatments. The higher cell death in 2D also means that chronic drug testing would pose a challenge, and the more robust response of the 3D priming, and spheroid models would suit this purpose better. There is also the consideration that the 3D primed spheroid models provide a very simple yet effective high throughput model where each hanging drop could be tested for a different dosage/type of drug. It is important to recognise that HepG2 cells are a cancer cell line, and while the liver specific properties are clearly enhanced in 3D cultures, it may be that priming also creates a better model of *in vivo* liver cancer. While certain cancer related pathways in the gene expression analysis were upregulated in 2D (MAPK for example), this does not discount the 3D cells in providing a more physiologically relevant cancer model for drug testing, with the increased drug resistance posing a distinctive advantage in drug discovery and testing for chemotherapeutic agents (Jensen and Teng, 2020). It is possible therefore that the 3D priming model itself would be best suited to genotoxicity experiments or liver pathology, rather than necessarily providing an accurate of DILI. Having said this, primed cells in the secondary model seem to present a more sensitive model to hepatotoxicity, and therefore may be suitable to predict DILI. This study does also show that both individual cell morphology and overall tissue architecture play large roles in determining the biological properties of *in vitro* models. 3D culture should not be considered a blanket technique that has a singular effect on cells, as the spheroids had notably different properties to even the 3D priming model. With these observed properties though, 3D primed spheroids possess significant potential for both cancer models and DILI predictive models. These models could be further developed and improved through using a transfected or chemically altered HepG2 cell line to better induce the CYP450 enzymes.

With all of this in mind, it is difficult to draw a conclusion on whether the priming is beneficial in terms of providing a more physiologically accurate response to drug toxicity, however this data does follow the expected patterns of decreased sensitivity enhanced metabolism in 3D cultures. More broadly though, 3D priming does appear to create a more *in vivo*-like behaviour in the HepG2 cells, and there are certainly enhanced synthetic properties in the 3D models – a very important aspect of hepatocytes. There is also clearly evidence of enhanced metabolic activity, demonstrating that the 3D models are more metabolically competent. In a practical sense, as discussed, a more refined and bespoke drug testing model that uses CYP450 inducers to specifically upregulate desired enzymes may be required to fully realise the potential of 3D primed HepG2 cells as a predictive tool. Again, it is likely a case that there is not a one-size-fits-all solution, and that different models/cell types might

have to be used depending on the properties of a drug and the suspected metabolic pathways. The ease of using HepG2 cells though does make them a very compelling cell line to utilise in research, and this chapter has indicated that the functional properties of HepG2 cells can be considerably altered by 3D culture, and maintained even after moving them into a secondary form of 3D culture. From a more conceptual viewpoint, this data provides further evidence that the effects of mechanotransduction can be carried over passages, with the 3D primed HepG2 cells showing increased production of biomarkers over 2D grown HepG2 cells when placed into a secondary model. **Chapter 4** showed that HepG2 cells seem to base their structure in-part on their mechanical history and that cells grown in 3D more readily form three-dimensional structures after liberation and possess a more spherical morphology. The key advantages of priming cells lie in both the enhanced morphology, and liver function.

Additionally, this chapter validates the sequencing data, showing that the predicted biological changes from differential gene expression and enrichment analysis are indeed occurring. The 3D primed cells are changed at a transcriptomic level, and do exhibit increased biosynthetic and metabolic capacity purely as a result of altered substrate geometry, and these altered properties are carried over to subsequent cultures. Considering all the data in this and previous chapters, **Figure 6.15** presents a hypothesis of how priming in a 3D environment can amplify the temporal enhancement of function in *in vitro* cell culture. After reseeding into a secondary 3D culture, the effects of priming result in cells gain functional competence more rapidly than cells grown in 2D as they can equilibrate to the 3D culture condition more readily. While towards the end stage of the secondary model, the measured functional enrichment in this study has normalised to an extent, there is still the possibility of wider enhanced functional properties in 3D primed cells that could be further explored in future work. For *in vitro* research, this could be beneficial in studying longer term drug responses due to priming creating models that are functionally competent at an earlier stage, which could also be advantageous in high throughput research. It also offers potential for improved pathology research due to providing a more physiologically relevant final 3D model from the outset. This also raises the possibility that 3D priming could be theoretically used to promote faster acceptance of cell-based therapies *in vivo*. It is reasonable to believe that as a wider principle, priming could apply to many other cell types to better prepare them for 3D *in vitro* models.

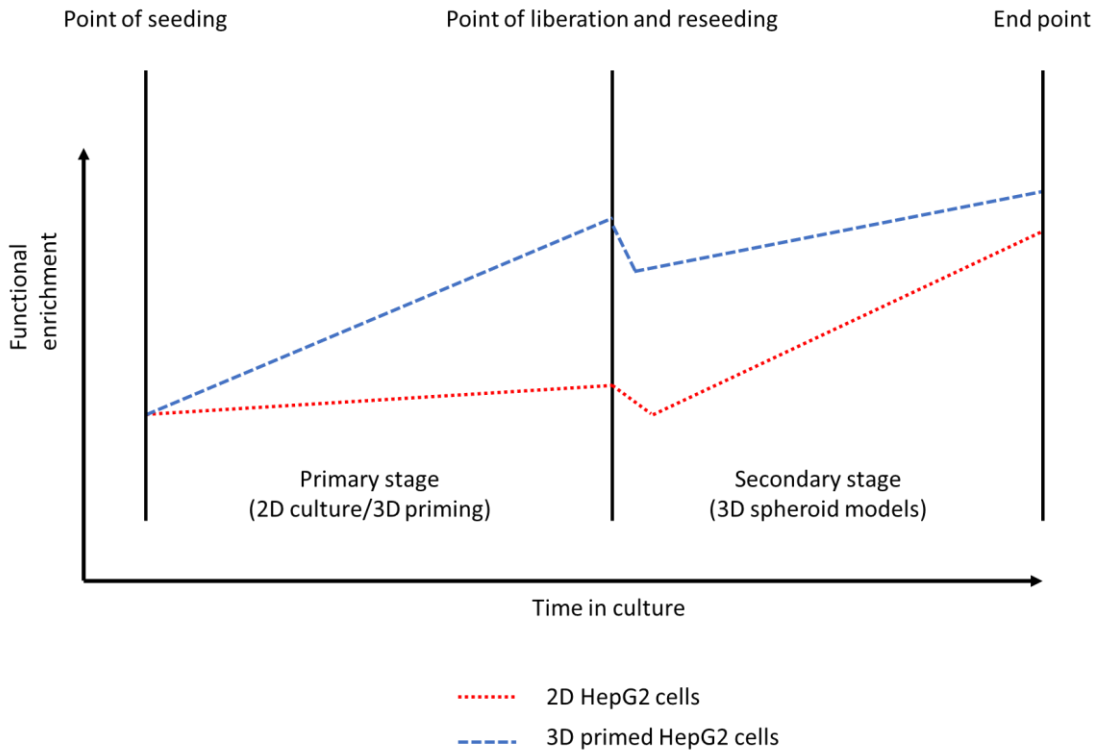

Figure 6.15: Priming cells in 3D enhances their functional properties.

Schematic showing the hypothesised effect on function that 3D priming has over a prolonged period of cell culture. Blue dashed line indicates 3D primed cells, that when seeded onto a 3D substrate, immediately start improving their structural and functional properties, which are then preconditioned to a higher baseline level upon reseeding in a secondary spheroid culture. Red dotted line indicates 2D grown cells only show limited functional enrichment over a culture period, meaning they start off the secondary culture in a functionally inferior position.

6.6 Conclusions

This chapter has provided deep insight into the functional profiles of HepG2 cells in four formats; 2D, 3D priming, spheroids from 2D, and spheroids from 3D. There is a definitively clear pattern of enhanced biosynthetic function in the 3D primed HepG2 cells in both the priming model and the secondary spheroid model over the 2D equivalents. It appears that the functional properties in the secondary models partially balance out after 7 days, however there is still evidence of differential function through the elevated albumin and urea levels in the media of the 3D primed spheroids. The overall conclusion can be made that 3D priming HepG2 cells makes them more functionally active and provides them with a more hepatic phenotype, better preparing them for a secondary 3D model where those enhanced characteristics are preserved.

The response of the HepG2 cells to an array of drugs in the various models reveals a consistently decreased sensitivity to toxicity in the 3D priming model. The 3D primed spheroid models retain a slightly decreased sensitivity over the spheroids from 2D HepG2 cells, however the responses are more comparable in these models. The large differential response to toxicity in the priming stage models clearly shows that the biggest difference in response is between monolayers and 3D scaffold-based models, and it is likely that this is due to a combination of factors at play, including enhanced metabolism and drug transport in 3D as well as altered model architecture limiting drug access.

The enhanced metabolic and synthetic biology of 3D primed cells shows that priming is a beneficial technique to prepare cells for an *in vitro* liver model, although this chapter has also highlighted the many elements that require thought when specifically using *in vitro* models as predictors for liver toxicity. Further mechanistic investigation would help elucidate the specific circumstances in which priming could offer a biological advantage. From a wider perspective, this chapter has helped identify the aspects of cell biology that are altered through changes purely in the mechanical properties of the cell culture substrate. This validates the deep global gene expression data in the previous chapter. It also adds value to the growing body of evidence that 3D culture promotes a more hepatic phenotype and demonstrates that mechanical ‘memory’ in cells is intrinsically linked with functional properties.

Chapter 7 – General Discussion and Future Directions.

7.1 Introduction

This project has taken a two-tiered approach to answering the biological question of whether the properties of an *in vitro* model can be altered in a sustained manner through exploiting the mechanisms of mechanotransduction after priming in an initial three-dimensional culture format. The first part of this approach was investigating the structural and mechanical effects of culturing cells in a 3D microenvironment before liberating and reseeding them onto a secondary substrate. This part of the analysis was carried out with the intention of clarifying firstly whether 3D priming does fundamentally affect the biology of the cells beyond the initial culture format, and secondly to clarify some of the possible mechanisms behind those retained changes. The second part of the approach was the more focussed analysis on how priming as a concept could be used to tune the functional properties of HepG2 cells to create a secondary 3D model with more desirable biological characteristics that better resembles the behaviour of *in vivo* hepatocytes. While this project looked at these two areas; the broad effects of mechanotransduction and the specific focus on *in vitro* liver models, these two areas often fed seamlessly into each other, and in the end helped to elucidate how priming could be used to improve HepG2 based liver models, whilst further clarifying the underpinning mechanisms involved in this process too.

As discussed in the introduction, mechanotransduction is a highly complex process with still much characterisation needed to elucidate the pathways involved and exactly how it can influence the behaviour of cells. Some of the outstanding questions on this matter include the temporal effects of mechanotransduction – how long does it take for the various pathways to trigger and how quickly would these reverse on a different substrate? Additionally, there is still a significant amount of work needed to understand how it plays a role in different tissue types. Mechanotransduction has perhaps been the most thoroughly characterised in stem cells due to the very clear role it has in directing stem cell differentiation and fate; (Liu et al., 2018; Tekin et al., 2018). These studies and many more highlighted the clear impact that altered mechanical properties of a substrate have on stem cell differentiation, though the role of mechanotransduction has not been as thoroughly considered across different cell types, despite the effects of mechanotransduction seemingly being cell specific. Integrins for example are made up of different combinations of subtypes which are tissue specific, changing the affinity for various ECM compositions and altering the cellular adaption to substrate rigidity (Seetharaman and Etienne-Manneville, 2018). Further to this, YAP/TAZ – transcriptional co-activators heavily involved in the cellular response to

mechanical stimuli – activate cell specific transcription factors upon mechanical stimuli to induce pre-determined transcriptional responses (Martino et al., 2018b). Transcriptomic responses do indeed seem to differ in terms of which specific genes are upregulated as a result of 3D culture between different cell types (Tekin et al., 2018; Zschenker et al., 2012). A key question that arises from this then, is *why* do cells possess a tissue specific mechanical response? This reveals the need for more in-depth investigation of mechanotransduction across different cell types, and this study goes some way to facilitating this, clarifying the role it has in directing the biological response of a hepatocellular carcinoma cell line, something that has not been fully investigated up to this point. There is a common disconnect between mechanotransduction research as a separate entity to research looking into the end stage functional results of an altered microenvironment. There is a wealth of papers showing that 3D culture can enhance functional properties in specific cell lines, and a large number of papers also discussing the molecular pathways involved in mechanotransduction but there is often a significant gap in marrying these two areas of research together. Functional research often uses 3D culture to grow improved *in vitro* models, but rarely considers just *how* these models are improving other than basing it on the knowledge that 3D culture is often just 'better'. Therefore, this project presents a unique and novel perspective through investigating and connecting these two key areas of research.

Liver models were chosen for this project due to the breadth of research available on HepG2 cells used in *in vitro* models, making them an extraordinarily well-characterised cell line in terms of their functional properties. These cells are very commonly used in creating functional models that can be used to test drugs, model disease and predict physiological liver responses, however it is known that they have poor expression of CYP450 enzymes (Westerink and Schoonen, 2007b), urea cycle genes (Mavri-Damelin et al., 2007), and often do not represent the responses of *in vivo* hepatocytes when testing for hepatotoxic xenobiotic compounds (Gerets et al., 2012). These shortfalls could be rescued to some extent through either 3D culture (Ramaiahgari et al., 2014a) or chemically induced epigenetic modifications (Ruoß et al., 2019), however results were often inconsistent in terms of which functional properties were enriched (Luckert et al., 2017) and poor CYP450 inducibility often remained. The robust and workable properties of HepG2 cells cannot be ignored and make them highly suitable to high throughput analysis, especially when compared to primary human hepatocytes which are difficult to isolate and tend to dedifferentiate in longer culture periods (Heslop et al., 2017). A key alternative to HepG2 cells based models would be models using HepaRG cells that are differentiated using DMSO treatment, but these may also

dedifferentiate in subcultures and low density cultures (Adam et al., 2020; Malinen et al., 2014). A newly developed HepaRG-CAR cell line does circumvent these limitations somewhat through overexpressing constitutive androstane receptor, a regulator of detoxification and energy metabolism (Adam et al., 2020). Nonetheless, HepG2 cells are inexpensive, easy to culture and well characterised, therefore there was a strong rationale behind trying to harness mechanotransduction to further improve the biological qualities of a HepG2 based model.

7.2 A robust and reproducible cell priming model showed enhanced structural properties analogous to the human liver and created a mechanical memory within the cells.

The first data chapter (**Chapter 3**) of this thesis was primarily focussed on the optimisation of a robust and reproducible model for priming the HepG2 cells. The 3D technology used was Alvetex® Strata, a specific format of a biologically inert porous polystyrene scaffold, as this maximised comparability with the polystyrene 2D culture format whilst minimising any extraneous biological variables that formats such as Matrigel would contain. This meant that any biological effects seen were purely attributable to the physical properties of the microenvironment changing. Through experimenting with a series of variables including media delivery, growth time, and positioning of the Alvetex® insert, an optimum model was created that used 1 x 10^6 HepG2 cells on a 6 well Strata format (or 5 x 10^5 cells on a 12 well format for drug tests) and grew them for 8 days. Using this format, a consistent, thick and viable layer of HepG2 cells was formed on top of the substrate, with a 3D arrangement and tight packing of the cells that resembled the morphology and architecture of hepatocytes in the human liver. These cells were easy to liberate using a combination of trypsin and gentle mechanical scraping, whereupon the largely viable population could be reseeded onto a secondary substrate for further testing.

It is difficult to isolate the effects of an altered physical microenvironment on just cell morphology and function due to the fact that altering the substrate properties changes the global organisation of cells within the model. This in itself can have a significant role in altering cell biology (Lelièvre et al., 2017), through aspects such as altered availability to drugs and nutrient restriction. Therefore, in some ways, it is difficult to deconvolute the more direct biological effects of the mechanical environment on cells from secondary effects that arise from an altered global structure. Nonetheless, any biological changes occurring *will* be

a result of altered mechanical properties, it just may be difficult in some cases to tell whether these are direct or indirect consequences, though experiments such as global gene expression analysis did help in making this clearer. With this in mind, an interesting finding of the first chapter was that using a form of media application termed 'contact feeding', where media was supplied underneath the substrate in combination with only a thin layer on top, managed to provide a significantly thicker layer of cells than when the substrate was more completely submerged. This was likely due to a higher surface tension and lower turbulence in media changes helping to encourage a thick cell layer due to less disruption. More importantly though, this environment potentially more closely mimicked the conditions of the liver, where hepatocytes are exposed to significant oxygen gradients in the lobules. This oxygen gradient is a strong driver of metabolic function *in vivo* (Kietzmann, 2017), and therefore this may also have played a role in the improved metabolic properties detected in the transcriptomic and functional characterisation of this 3D model.

The final model created after optimisation in **Chapter 3** was able to hold a significant population of HepG2 cells in a 3D environment for a sustained period of time of 8 days – a time frame that according to the literature should be long enough to elicit a significant mechanical memory in the 2D and 3D cells (Mathur et al., 2020; Nasrollahi et al., 2017). This initial model was therefore named the priming model as it primed cells to a three-dimensional microenvironment before liberation. Based on the limited literature knowledge, and previous work by Rebecca Quelch and Alisha Chhatwal in Professor Stefan Przyborski's research group, there was a significant body of evidence to suggest that this priming stage would alter the structure (and consequently the function) of the HepG2 cells. Based on the organisation of cells on top of the Alvetex® membrane, it was expected that 3D primed cells would be smaller and more spherical than cells from a monolayer after liberation, and that the 3D primed cells would more readily form a subsequent three-dimensional structure in secondary cultures. **Chapter 4** consisted of extensive structural characterisation of the model to determine whether this was the case, and indeed it proved to be. A key set of experiments involved reseeding HepG2 cells at low confluency onto a 2D stiff substrate and analysing the structure of single cells after varying times of adaption to this substrate. These HepG2 cells were reseeded onto the stiff substrate from either prior growth in 2D or from the 3D priming model, and the results were very clear in indicating that cells grown in 2D more readily spread out and increased their surface area on the secondary substrate, whereas 3D cells kept more spherical with a lower surface area. This was shown to be a highly reproducible phenomenon, and interestingly, the altered structural qualities appeared to differ as time in

the secondary substrate elapsed. Within 1 hour of reseeding, the cell height was significantly altered, with 2D cells being significantly flatter, but this evened out after 3 hours. This switched to a significant difference in cell area after 1 day in the secondary substrate, with the surface areas of 3D primed cells being significantly smaller, but heights having equalled out. This indicated that the 2D grown HepG2 cells had altered cytoskeletal machinery which permitted a faster spreading and perhaps an increased migratory phenotype – though the latter aspect was not thoroughly tested for. Perhaps the most revealing data set was the scanning electron microscopy images which showed the single cells in incredibly high detail. These images highlighted very clear differences in structure with the 2D cells showing a flatter, more spread-out phenotype, whereas 3D primed cells were generally spherical and had a high presence of protrusions. This altered phenotype also extended to higher confluency cell populations, with SEM images showing that 3D primed HepG2 cells formed a more three-dimensional islands consisting of spherical cells compared to the more monolayer-like formation of the 2D grown cells. The nuclear areas appeared to change very much in line with the cell areas, decreasing significantly in 3D primed cells, which displayed the close links between the cytoskeleton and nuclear architecture.

Further to the single cell experiments, when allowing 3D primed cells to grow for longer and in higher densities on a 2D substrate, they exhibited a more colony-like growth pattern, demonstrating that it was not just single cell structure that was altered – the global organisation of cells was shifted due to 3D priming. Additionally, when cells were reseeded into a 3D Alvetex® scaffold, the 3D primed cells formed more island-like structures and tended to clump together as opposed to a more consistent layer from 2D cells. These data indicated that cellular aspects controlling structure and tissue architecture were significantly altered in the 3D primed cells. Disrupting various components of the actin cytoskeleton machinery also was able to restore 2D cells to a phenotype closer to 3D primed cells, further implicating cytoskeletal mechanisms in determining mechanical memory. Finally, when optimising the secondary aggregate models, it was clear that there were differences in how 3D primed cells assembled themselves compared to 2D cells, especially in higher density hanging drops where 2D grown cells often formed an almost two-dimensional layer of cells on the meniscus of the droplet compared to the more three-dimensional network organisation of the 3D primed cells. The final optimised secondary model used a lower cell count however to facilitate consistent hanging drop spheroids after 7 days of growth regardless of whether the cells were 3D primed or not.

These data hinted at transcriptional changes occurring in the cell, leading to prolonged effects of 3D priming. This fits with the mathematical modelling of mechanotransduction suggesting that altered YAP/TAZ activation leads to increased reinforcement of cytoskeletal signalling on stiff matrices (Mathur et al., 2020). The data in this thesis suggested that the opposite effect also occurs when priming on softer matrices, potentially hinting at some form of constitutive on/off switch regarding YAP/TAZ and mechano-activation. Another experiment in this project showed that priming in 2D or 3D for longer exerted a stronger sustained effect on the cells with significant differences in cell areas only occurring after 4 days or longer after priming, and this is consistent with other studies that indicate a minimum of 2-3 days of priming is needed for epithelial cells to adapt to matrix stiffness and alter YAP activity (Nasrollahi et al., 2017).

Structural markers were probed for in the priming model compared to 2D cells, and reseeded cells on 2D after priming in 3D. These revealed that N-cadherin expression was high in both 2D and 3D priming models, though expression was more consistent in the 2D models, yet more intense in the 3D priming models. E-cadherin was expressed at a lower level in both 2D and 3D models, with only faint staining, however a similar pattern was seen of more ubiquitous staining in the 2D models, but more intense localised regions of staining in the 3D models, and interestingly, the intensity of staining appeared higher in 3D primed cells reseeded on a 2D substrate, indicating a potential artefact of the 3D priming. The more heterogenous patterns of these two markers in the 3D priming model may be an indicator that some form of metabolic zonation was occurring in the priming model, as different regions of E-cadherin and N-cadherin staining signals this *in vivo* (Hempel et al., 2015). This possibly links to the increased oxygen gradient that may be present with the 'contact' media method and the thick cell layers, though more testing would be needed to determine this.

Claudin 1, a highly liver specific tight junction marker was – unlike the cadherins – very clearly more intense and more organised in the 3D priming model, and along with MDR1, showed distinctive intense staining spots in the 3D models that may be indicative of canaliculi-like structures forming. Additionally, more of these intense staining spots appeared to form in spheroids formed from 3D primed cells, alongside increased MDR1 staining intensity. The nuclear lamina associated sun1 and sun2 proteins were also very distinctively more intense in the 2D cells over cells in the priming model indicating stiffer nuclei in the 2D cells, which is a known occurence in cells on stiffer substrates with higher actomyosin contractility (Alisafaei et al., 2019). This further fits with the hypothesis that the changes in primed cells

could be occurring due to altered transcriptional machinery, with stiffer and flatter nuclei resulting in less condensed nuclear chromatin (Alisafaei et al., 2019) allowing increased access to transcriptional machinery (Heo et al., 2016a), and less mechanical resistance in nuclear pores to transcription factors such as YAP/TAZ (Elosegui-Artola et al., 2017). Importantly, in probing for these structural markers, the reseeded cells had been growing for 7 days, and therefore it was expected that differences between 2D and 3D primed cells would have normalised to an extent, and while this was true, subtle differences were still present in the increased intensity of the cadherins in 3D primed cells reseeded on 2D for example, and the more island-like structure of reseeded 3D cells was still present.

Through using transcriptomic analysis comparing 2D HepG2 cells to the 3D priming model, many of the observations in the structural characterisation sections were backed up with high quality gene expression data. Through comparing to human liver and 2D primary human hepatocytes, further value was provided as it showed that gene expression levels in HepG2 cells were considerably lower in many of the key hepatic genes when compared to these primary cell sources. Despite this, in expression of structural genes, 3D HepG2 cells were often closer to the expression profile of the human liver, and 2D HepG2 cells were in some cases closer to the 2D primary hepatocytes, particularly in expression of integrins and mechanotransduction markers. This indicated that the structural state of cells in the human liver was more closely mimicked by the 3D culture conditions in the priming model, and that 2D culture has a distinctive effect in making expression of these genes less physiological. In this data, there was a very clear upregulation of genes linked to mechanotransduction processes in 2D HepG2 cells, and a number of the enriched processes/pathways in 2D cells related to the cytoskeleton, cell junction organisation or actin cytoskeleton organisation. This was clearly consistent with the data obtained in the structural characterisation chapter, where the 2D cells showed differential morphology, were more spread out on substrates, had a higher consistency of junctional organisation with the cadherins and showed an altered cytoskeleton.

There were some interesting highlights in expression of the structural markers. N cadherin showed increased gene expression in 2D cells, and the balance in both HepG2 models was very much in favour of N-cadherin expression over E-cadherin expression. This backed up the immunofluorescence data to an extent, with the N-cadherin having stained much more intensely in 2D and 3D than the E-cadherin. While the integrins showed a clear pattern of upregulation in 2D, the cadherins and claudins were more mixed, though claudin 1 was

upregulated in the 3D cells, consistent with the immunofluorescence data. The less physiological expression of many of these genes in the 2D HepG2 cells compared to 3D primed cells indicated that the physical microenvironment is a strong regulator of transcription. The SUN genes were also significantly upregulated in the 2D HepG2 cells which closely aligned with the observed staining in the characterisation chapter, and further pointed towards stiffer nuclei in 2D cells. The increased expression of the sun proteins was also backed up through western blots which showed a very similar pattern of increased expression across three biological repeats of 2D HepG2 cells compared to 3D primed HepG2 cells.

There was also a significant upregulation of YAP/TAZ in 2D cells, meaning it is likely that this was at least one of the mechanisms through which the upregulation of many of the mechanical genes was achieved. With enrichment in processes and pathways such as ECM organisation, focal adhesions and actomyosin structure organisation in this data, all of which are key target functions of YAP/TAZ promoted transcription (Calvo et al., 2013; Martino et al., 2018c; Morikawa et al., 2015; Nardone et al., 2017), it seems to heavily implicate these transcription factors in the differential structural response of HepG2 cells to a 2D and 3D microenvironment. This further backs up the purported involvement of YAP/TAZ in mechanical memory too, with increased activity of these being a primary driver behind sustained mechanical characteristics (Mathur et al., 2020), which were also seen in these experiments. The key pattern that the transcriptomics revealed was that the structural enrichment was always in the 2D HepG2 cells. This indicated that genes pertaining to these mechanical functions were specifically upregulated in 2D over 3D HepG2 cells, and revealed that the stiffer substrate creates a more mechanically stressed cell (as Alisafaei et al. described (Alisafaei et al., 2019)), which in turn increases epigenetic factors and transcription of many genes involved in the mechanically responsive machinery, pushing the cell towards a phenotype more focussed on coping with the high tension microenvironment.

7.3 Priming HepG2 cells in 3D significantly enhanced a broad range of hepatic functions.

While the transcriptomic data was important in investigating mechanisms behind mechanotransduction, it was perhaps even more useful in unveiling what functional properties were enriched in the 3D primed cells. A selected group of genes closely related to liver function such as albumin, fibrinogen, antithrombin and more had a clear trend of

upregulation in the 3D primed cells. This upregulation was also highly significant in many cases, for example with the 1.7-fold increase in albumin production, the adjusted P value was $7.94003x10^{-31}$. Albumin production is a very common test employed in liver research to provide an index of liver function (Nishikawa et al., 2017), with higher levels often indicating a more functionally competent model. Indeed the higher production here brought the 3D primed HepG2 cells close to the physiological levels in the human liver, although *in vivo* expression was still very much higher than the expression levels in either model of the HepG2 cells. As albumin is such a critical test for liver function, this was further tested for in the functional characterisation chapter (**Chapter 6**), where albumin secretion was measured in the supernatant from HepG2 cells both in the primary stage models (2D and 3D priming) and the secondary spheroid models (cells reseeded from either 2D or 3D priming). After normalising to protein levels, this showed a very clear trend of increased albumin production in both the 3D priming model, and the 3D primed spheroid models over the 2D counterparts. This measured the build-up or secretion of albumin in media, so western blots were also used to detect direct albumin protein production *within* the cells, and there was a strong upregulation of the protein in the 3D priming model over monolayers. This increase was not as pronounced when comparing the 3D primed spheroid model over spheroids from 2D. This indicated that albumin production had partly evened out after 7 days of spheroid culture, however the fact that overall albumin in media was still increased in the 3D primed spheroids showed that those cells had indeed been primed to a 3D phenotype where they were more functionally competent from the offset in the secondary model.

The transcriptomic data also showed a specific pattern of upregulation in genes involved in the urea cycle (ASS1, ASL, OTC, ARG1) in 3D primed cells, and this too was validated through a colorimetric assay measuring urea levels in the media for both the primary and secondary stage models. Similar to albumin, urea levels were increased in both the 3D priming model and the 3D primed spheroids and this showed that the transcriptomic upregulation was having a biological effect, which was maintained after liberation and reseeding, exhibiting the potential use of priming in preparing the HepG2 cells for a functionally enhanced end-stage model. Despite this, the known dysfunction of the urea cycle in HepG2 cells (Mavri-Damelin et al., 2007) means that the urea results should be interpreted with a degree of scepticism. The increase in production and gene expression is a positive sign, however the cells still likely have a significant shortfall in production compared to primary samples. The increase in fibrinogen genes was also validated through a very clear upregulation of fibrinogen alpha chain protein in 3D primed cells detected through western blotting,

indicating increased biosynthesis capacity in the 3D HepG2 cells and further validating the sequencing data which also picked up enrichment in many biosynthetic categories for the 3D cells.

The transcriptomic data revealed a slightly more mixed picture of expression of metabolic genes, particularly with the cytochrome P450 which were key for phase I metabolism of xenobiotic compounds. The expression of these genes tended towards increased expression in the 3D primed HepG2 cells, though in some of the cytochrome P450 genes less linked to drug metabolism, there was an increase in 2D HepG2 cells, such as CYP2S1 and CYP24A1. On the whole, 3D primed cells had a closer expression profile to human liver, though human liver had particularly strong expression in the key drug metabolising CYP450 genes such as CYP1A2, CYP2E1, CYP3A4 which were much higher than expression levels in HepG2 cells. Expression of many of these particularly key genes was *very* low in the HepG2 models, though was still usually increased in the 3D primed cells. This further indicated the poor inducibility of cytochrome P450 enzymes in HepG2 cells, and while 3D culture does go some way to increase this, it is still far below the levels of human liver. A potential solution to this could be through combining the beneficial effects of 3D culture with epigenetic modification through chemical treatment with inducers such as 5-Azacytidine (Ruoß et al., 2019) to create a stronger induction of the phase I enzymes.

In the various sets of phase II enzymes, expression patterns were more consistent in showing a generally increased expression in the 3D primed HepG2 cells, with expression levels also tending to be closer to physiological levels with less of a shortfall than with the phase I enzymes. The clearest functional patterns were revealed through the various forms of enrichment analysis which picked up a very consistent trend of enrichment in metabolic and biosynthetic pathways that were often closely associated with hepatic function. These included enrichment in cholesterol metabolism and biosynthesis, steroid metabolism, drug metabolism (both phase I and phase II) and bile acid biosynthesis. This revealed the importance of putting genes into context of their interactions and wider functions as it highlighted incredibly specific, significant and strong enrichment in hepatic pathways for the 3D primed HepG2 cells.

The fact that enrichment was detected in phase I and phase II metabolism provided a clear validation route for this data through a series of drug tests in the functional validation chapter. These drug tests were carried out on the primary and secondary stage models, using six selected xenobiotic compounds whose toxicity was measured. There was a marked

difference in how the HepG2 cells in the 3D priming model reacted, with a significantly increased capacity to cope with toxicological challenges, whereas HepG2 cells in monolayers showed increased sensitivity to cytotoxicity at lower dosages of the drugs. The responses to all drugs followed this trend, and no *particularly* strong correlation was noticeable in whether differences in sensitivity were stronger in drugs that are directly toxic compared to drugs that are toxic through a metabolite. In two of the cases where toxicity is exerted through a metabolite (ibuprofen and gemfibrozil), the difference in cytotoxicity seemed less pronounced between the 2D and 3D HepG2 cells, which may be an indicator that either the bioactivation by phase I enzymes or the detoxification by phase II enzymes was rebalancing the difference to an extent. Ultimately though, the 3D primed cells were still less sensitive to toxicity, and this indicates a significant difference in metabolic activity as shown in the gene expression data. The interplay between phase I and phase II enzyme expression was clarified further through the gene expression data, with the drug toxicity results showing high consistency with the enriched terms of the transcriptomic data such as 'drug metabolism'. The increased phase I and phase II metabolic capacity evidently had a functional effect of more efficient detoxification in the 3D cells. Looking at the specific gene expression, and particularly the low absolute expression levels of the CYP450 genes compared to the higher general presence of phase II enzymes, it is likely that while 3D culture increased activity in both stages of drug metabolism, the balance was further tipped towards phase II metabolism in the priming model.

In the spheroid models, it was clear that after 7 days of culture, the toxicity responses had normalised partially between spheroids from 2D and 3D primed cells. The spheroids commonly showed a response to drug toxicity that was somewhere in between that of the 2D HepG2 cells and the 3D priming model. This helped clarify the role that the overall cell organisation had in contributing to the response to xenobiotics, with the medium response of spheroids suggesting that there was a higher drug availability in the spheroids compared to the tightly packed 3D priming models, yet lower availability when compared to the monolayer cultures where all cells could be exposed to the compounds. Generally, in the secondary models, the responses of 2D and 3D primed spheroid models were closer to each other. There was a potentially small decrease in sensitivity still evident in the 3D primed cells, shown in the responses to gemfibrozil and ibuprofen, though these differences had largely normalised. This data suggests that the priming effect had somewhat diminished after 7 days, with the increased transcription of the metabolic genes in the 3D primed cells possibly re-adjusting to the microenvironment of spheroid cultures, and the decreased transcription

in the monolayer HepG2 cells likely increasing to adapt to the new 3D environment. In addition, the decreased sensitivity to toxic compounds seen in spheroids compared to monolayer responses does still point towards increased expression and activity of key phase I and phase II metabolic genes.

Expression of transporters further complicates things however, as 2D cells tended towards a higher expression of genes for ABC transporters, yet 3D cultures exhibited increased expression of genes for SLC transporters, and both of these transporter families are involved in drug transport and clearance (Li et al., 2012). It is hard to deconvolute how the differential expression of these affects the drug responses of the models, and why these expression patterns are there in the first place. Of course, expression data does not necessarily equate to protein levels and correct functioning of said transporters, so this is also a consideration with this data. A similar pattern to this was seen in primary mouse hepatocytes where at the 3 day growth time-point there was a significantly higher induction of ABC transporter mRNA in monolayer cultures as opposed to sandwich cultures (Noel et al., 2013), whereas induction of SLC transporter mRNA was low in general, though slightly higher in the sandwich cultures for Oatp1a4 and Ntcp. The expression levels appeared very dependent on culture time however, and it was suggested that the sandwich culture may 'transiently limit the culture-associated over-expression of some ABC transporters' (Noel et al., 2013). This may be the same situation in this study, with certain ABC transporter mRNA levels in the 2D HepG2 cells actually appearing higher than human liver in some cases suggesting a non-physiological overexpression. Further to this, the bile canaliculi-like structures observed in the immunofluorescence staining and TEM of the 3D primed HepG2 cells does suggest that functional transporters are forming, and this may play a role in the increased detoxification seen with priming.

It is hard to conclude whether 3D culture made a 'better' model for drug testing due to the inherent complexity of *in vitro* drug tests, with false-positives and false-negatives both being an issue in *in vitro* liver research. However, it is clear that 3D culture significantly enhances a broad range of metabolic and biosynthetic processes that are key to liver function. The 3D priming model may be beneficial for drug efficacy screening, liver pathology, and even providing a physiologically relevant cancer model. With the enhanced metabolic expression, it may present an improved model for metabolomics studies too. With this focussed functional enrichment of the primed cells from simply altering the mechanical properties of the microenvironment, it brings to mind the potential for further developing and

functionalising these models through combining 3D culture with epigenetic modifications. Perhaps with a combination of methods, a truly competent functional model could be produced that is even closer to replicating *in vivo* physiology.

In addition to thoroughly demonstrating the immediate functional impact that culturing cells on a 3D scaffold has, this project has also demonstrated that through culturing cells in 3D, the altered structure and function can be carried over into subsequent cultures. There is a significant body of evidence here that demonstrates how as both single cells and as a population, the mechanical 'history' of a cell is of fundamental importance in determining its behaviour in subsequent cultures. The altered growth patterns of populations reseeded onto coverslips demonstrates the key role that the mechanical status of a cell has in forming confluent populations, and differences in how 2D vs 3D primed cells formed aggregates were also very clear especially at higher seeding densities. The exact mechanisms that allow 3D primed cells to more readily form 3D structures after reseeding are unknown, but more clarity has been provided here regarding the significant downregulation of mechanically related genes that occurs in 3D. This helps correlate how mechanical cellular dynamics are intrinsically linked with the functional properties.

Alterations in the cell biology at a transcriptional level is evidently a key driving force behind mechanical memory, and it makes sense therefore that the increased transcription of functional genes in 3D culture is a key driver of the *functional* memory. This functional memory was apparent through the markedly increased cumulative albumin and urea production in the supernatant of the 3D primed spheroids. This provides a causative link between the mechanical memory that has been described in literature, and an accompanying functional memory that arises as a direct consequence. Despite this increased albumin and urea secretion, it appeared that the direct production of albumin may have converged to a state of equilibrium between the spheroids formed from 2D HepG2 cells after 7 days in culture. This agrees with the literature that suggests that cells primed on a stiff matrix for between 7-10 days are imbued with around 3 days mechanical memory, with mechano-activation degrading between 12-24 hours after this period (Mathur et al., 2020). Therefore, the benefit of 3D priming here has been proven to lie in the **early stages** of secondary culture, where the 3D primed cells more readily form 3D structures and exhibit enhanced function from the start compared to the 2D cells which must adapt to the 3D microenvironment and accordingly decrease the transcription of the mechanical genes and increase transcription of the cell specific functional genes. This means that 3D priming

permits earlier formation of a functionally mature end stage model that may prove especially beneficial for long term or high throughput studies such as chronic toxicity testing. **Figure 7.1** is a simplified graphical representation of what this study has shown, through culturing cells in 2D and 3D before reseeding them onto either 2D to scrutinize structural changes, or into a secondary 3D model to show global alterations in organisation and functional enhancement in 3D primed cells.

Another area in which priming may have a particular benefit is the fact it can facilitate a significantly large cell number; using this priming model on 6 lots of 6 well inserts for example would yield a number of liberated cells usually in excess of 1.2×10^7. This makes the technique highly suitable for creating subsequent high-throughput models. The simplicity of the priming technique for easy-to-use cell lines such as HepG2 makes it a very desirable technique to give cells a functional advantage in preparation for the secondary model.

The priming concept could also be rephrased to put the emphasis on 2D culture, by describing that monolayer culture of HepG2 cells leads to a stiff-priming response with mechano-activation that pulls the cells away from a physiological phenotype. While this unnatural phenotype is eventually rescued when cells are moved to a 3D end stage model, by adding an extra step of 3D culture, cells are given an extra time-period to restore their natural phenotype before being placed in a final secondary model to make use of the enhanced qualities. It could also be argued that just maintaining cells in a 3D environment for longer would have the same effect, however in a cancerous cell line such as HepG2 cells, this would be less than ideal, as longer culture periods resulted in over-confluency and large patches of cell death, likely due to nutrient starvation. This has demonstrated that even after mechanical and enzymatic liberation of cells, the previous culture format has a lasting impression on the cell biology. Therefore, on a fundamental level, this project has demonstrated that cells mechanically and functionally adapt to the mechanical properties of the substrate they reside in and this creates a lasting impact on the biology of the cell, imbuing them with a 'memory', both structurally and functionally of their mechanical history.

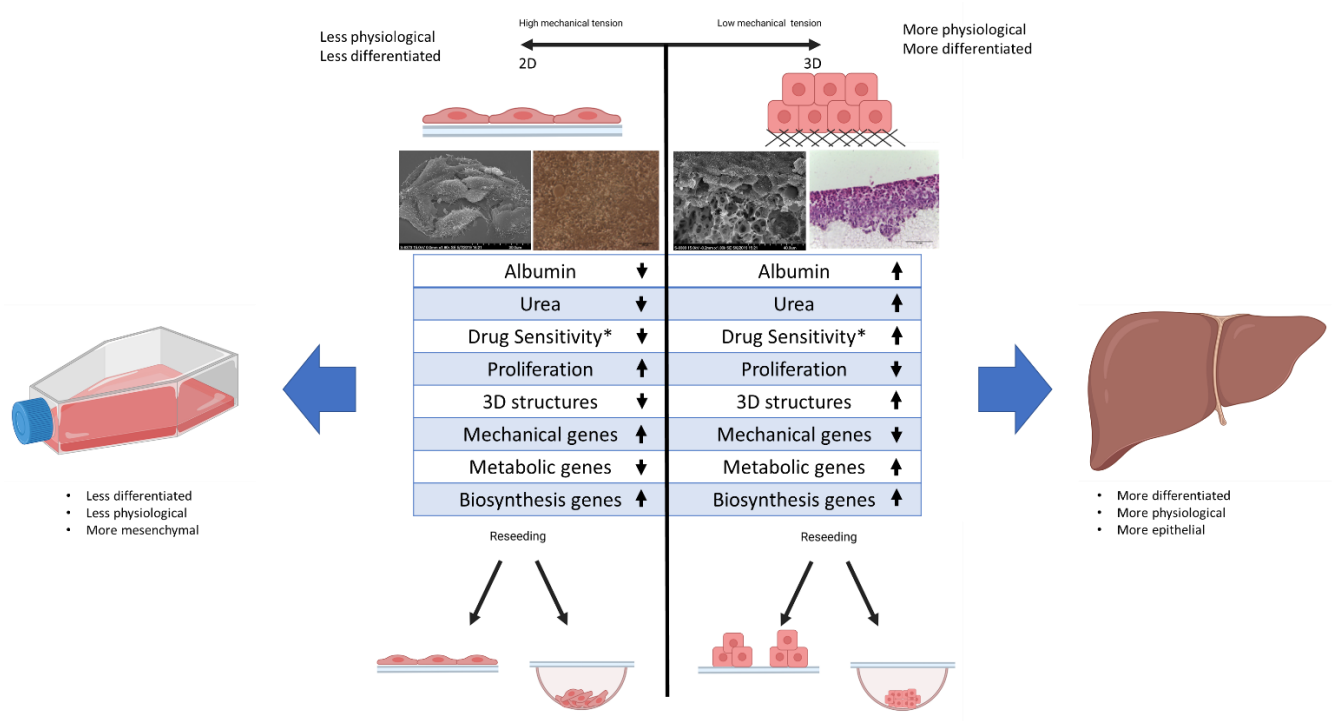

Figure 7.1 Priming cells in a 3D microenvironment leads to significantly altered structure and function that is carried over to subsequent cultures.

3D primed cells exhibit a phenotype closer to in vivo hepatocytes. Cells grown in 2D retain structural properties after reseeding, with cells replated on to 2D substrates being flatter and growing in more consistent monolayers than the more three-dimensional colony like structures formed by 3D primed cells. 3D primed cells have instantly enhanced function when moved to a secondary model whereas 2D grown cells have to adapt first to the 3D environment of a secondary model. Created using Biorender.com

7.4 Future directions and wider applications.

While functional and enrichment has been shown to carry over as an artefact of priming in different microenvironments, there is still a lot that could be done to unpick exactly what functional qualities are enhanced in the secondary model and for how long. It would be particularly interesting to investigate how long it takes for the priming effect to wear off – is it three days as literature would suggest, or does this depend on cell type and the exact mechanical qualities of the priming environment? It was evident that the length of time spent in priming had an impact on the magnitude of the sustained impact, though does this also affect the time it takes for the primed qualities to re-adapt? It is also clear that time is a key variable in driving the priming process, but just *how* does time effect the process? Investigating this would be an incredibly complex affair, and as more studies are undertaken and more details are revealed about factors involved in mechanotransduction, inevitably more questions will surface. Ultimately though, gaining a thorough understanding of mechanotransduction will be incredibly beneficial in the world of *in vitro* research, allowing much greater control over cell culture-based models where properties may be tuneable to a very precise degree. To make *in vitro* models accurate to *in vivo* equivalent tissue is a key aim of many research studies, and this project is a step towards that direction, further solidifying the evidence that structure is a critical driver of function.

Figure 7.2 shows the proposed simplified mechanisms through which transcription of mechanical genes may be altered in 2D compared to 3D cells. This is not exhaustive and there will be many factors not included that are involved in the altered response. However, altered transcription will likely be in part due to the changing cytoskeletal dynamics, nuclear architecture and altered internal mechanical properties. While this purports that mechanical transcription factors such as YAP/TAZ may be increased due to these factors, it is still unknown precisely why hepatic genes in particular are upregulated in the 3D culture. Mechanisms behind this are clearly exerted in part through mechanical means as the physical microenvironment is the most significant variable changing in between the two culture conditions. It would therefore be of great interest to investigate in further detail the exact molecular pathways that are triggered or suppressed as a result of 3D mechanotransduction and how these directly relate to the functional changes seen. This study, alongside a large body of literature, helps in providing a strong correlation between using a three-dimensional topography and more physiological qualities in cells. Understanding is increasing with each study performed in this field, however it is clear that there is still a long way to go to uncover

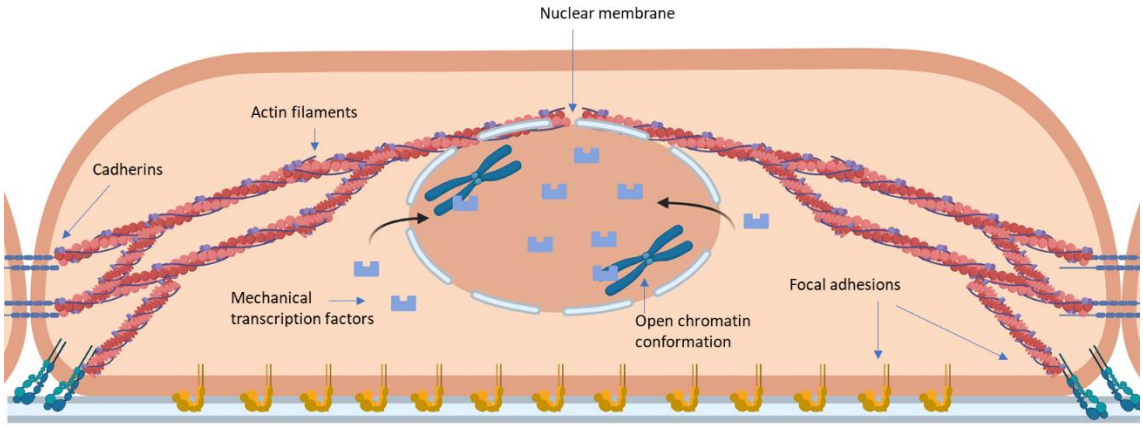

- Under high tension 2D culture, there is a higher presence of focal adhesions leading to denser actin networks. Nuclear architecture is affected, with a stiffer nuclear lamina leading to open chromatin conformations and less mechanical resistance in nuclear pores. This allows greater access of YAP/TAZ and other mechanically linked transcription factors into the nucleus. This results in increased transcription of mechanical genes and supressed (or lower) hepatic transcription.

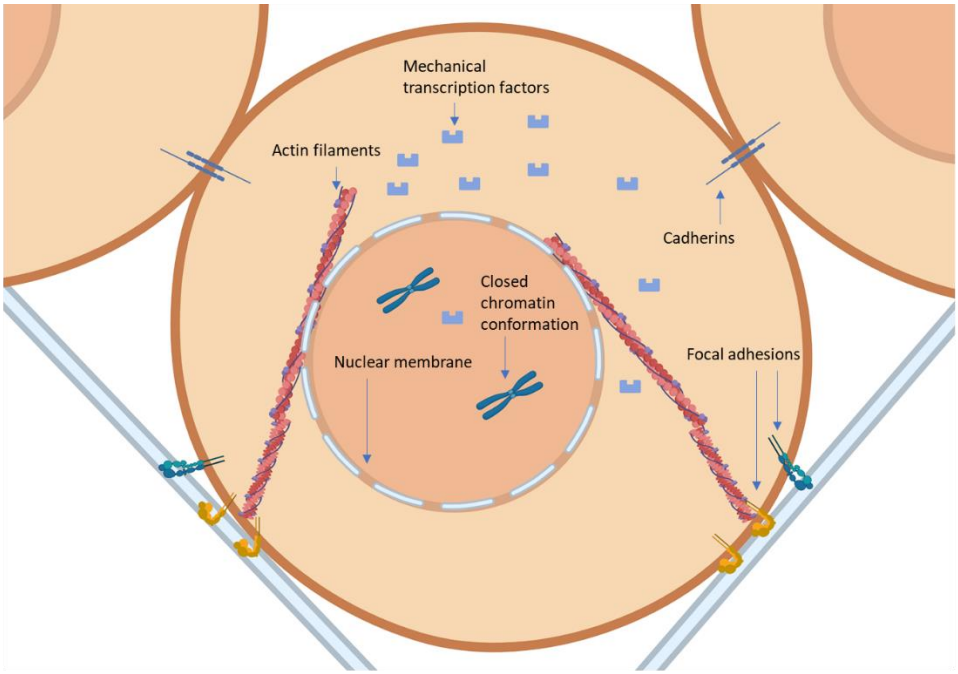

- Under low tension 3D culture, there is a lower presence of focal adhesions leading to less dense actin networks and a lower tension cell state. Nuclear architecture is affected, with a softer nuclear lamina leading to closed chromatin conformations and more mechanical resistance in nuclear pores. This restricts access of YAP/TAZ and other mechanically linked transcription factors into the nucleus. This results in increased transcription of mechanical genes and through an unknown mechanism linked to mechanotransduction leads to increased hepatic transcription.

Figure 7.2 Mechanical differences between 2D and 3D culture lead to altered transcriptional states.

Top panel adapted from (Alisafaei et al., 2019). Created using biorender.com.

the full extent of the processes involved in mechanotransduction.

A step towards understanding this more greatly would also be to dissect whether there are functional properties that remain enhanced in primed cells that continue to increase towards more physiological levels. It is possible that priming and reseeding into a secondary culture continues to amplify certain biological processes, but currently the data so far points towards the benefit of priming lying in better preparing cultures for a 3D environment. It would be of great interest then to have a more thorough investigation of the secondary spheroid model over the time period of 7 days, perhaps with a time point at day 1, day 4 and day 7, and to run similar transcriptomic analysis and functional analysis on the models at these stages. It would be expected that expression of a number of the differentially expressed genes would normalise over the secondary culture period, however it is certainly possible that some genes already upregulated in the 3D primed cells would continue to rise. This would provide further clarity as to how mechanical memory directly relates to functional memory.

A major consideration would be whether adding in additional cell types can further enhance functional properties either during priming or in the secondary model. Fibroblasts for example have been co-cultured previously with HepG2 cells which demonstrated increased albumin secretion over monocultures (Lee et al., 2014), and with primary hepatocytes, co-culturing with endothelial cells resulted in increased albumin and urea secretion along with increased expression of ALB, CYP3A4 and HNF4α (Wang et al., 2018). Endothelial cells in combination with hepatocytes make up 80-90 % of the cell populations in the liver (Wang et al., 2018), with liver sinusoidal endothelial cells providing an essential role in vascular function as well as maintain hepatic stellate cell quiescence, inhibiting fibrosis development and preventing vasoconstriction (Poisson et al., 2017). One paper has shown that co-culture with primary hepatocytes and liver sinusoidal endothelial cells results in both cell lines simultaneously supporting maintenance of the differentiated phenotypes of each other, with enhanced heterotypic cell-cell interactions being observed alongside increased albumin production and CYP1A1, CYP1A2 and CYP3A4 activity (Kim and Rajagopalan, 2010). Similar functional enhancement was seen with primary rat hepatocytes co-cultured with human umbilical vein endothelial cells (HUVECs) (Unal et al., 2018) and even in HepG2 cells, increased albumin and urea production was observed in co-cultures with HUVECs (Guzzardi et al., 2009).

Based on this body of evidence, some preliminary experiments were run as part of this study using the Sk-Hep1 cell line; a human liver adenocarcinoma cell line which are endothelial in

origin. Initial experiments using HepG2 and Sk-Hep1 cell lines showed potential promise in creating an even more functional model. When cultured individually in 3D, HepG2 and Sk-Hep1 cells populated the substrate very differently (**Figure 7.3**). When co-cultured, HepG2 cells and Sk-Hep1 cells seemed to compartmentalise within the Alvetex® Strata substrate, and interestingly, when Sk-Hep1 cells were grown on the bottom of the well to condition the media with paracrine signalling, the HepG2 cells on top of the substrate seemed to grow significantly slower. It was thought that this may be down to paracrine signalling making HepG2 cells less proliferative and supporting quiescence, so a live-cell imaging migration assay was performed to test whether this was the case. **Figure 7.4** shows the results of that assay, and after using TrackMate software on ImageJ, it was clear that Sk-Hep1 pre-conditioned media significantly slowed down the speed of migration in HepG2 cells as well as decreasing the migration distance. This was also the case for Sk-Hep1 cells grown in media pre-conditioned from HepG2 growth, with significantly lower migration distances and speeds. This indicated that both cell lines were having a significant paracrine effect on the other cell line's growth and could indeed be an indication that co-culture helps maintain phenotype and reduce proliferation.

To check for any altered function, both a urea and albumin and urea assay were performed on the paracrine and co-cultures in the 3D priming model alongside 2D HepG2 cells and 3D primed HepG2 cells grown for 8 days, with results normalised to total protein (**Figure 7.5**). Both albumin and urea production were increased in 3D HepG2 cells over 2D as seen in the functional characterisation chapter. For urea assay, both paracrine and co-cultured conditions exhibited significantly enhanced urea secretion over both 2D and 3D HepG2 cells. With albumin however, the secretion did not significantly increase over 3D cells in either paracrine or culture conditions which was an interesting contrast to the urea secretion. This increase in urea secretion does suggest that Sk-Hep1 cells are able to enhance functional properties over a standard monoculture 3D priming model. As no enhanced albumin secretion was observable, it suggests that using an immortalised endothelial cell line seems to result in less enhancement when compared with primary endothelial cells which were used in other co-culture studies where albumin production was significantly raised. It was interesting to note that the paracrine condition seemed to have a stronger effect on the albumin and urea secretion than the co-culture, which actually appeared to decrease albumin secretion over the 3D monoculture of HepG2 cells. It is important to clarify that this

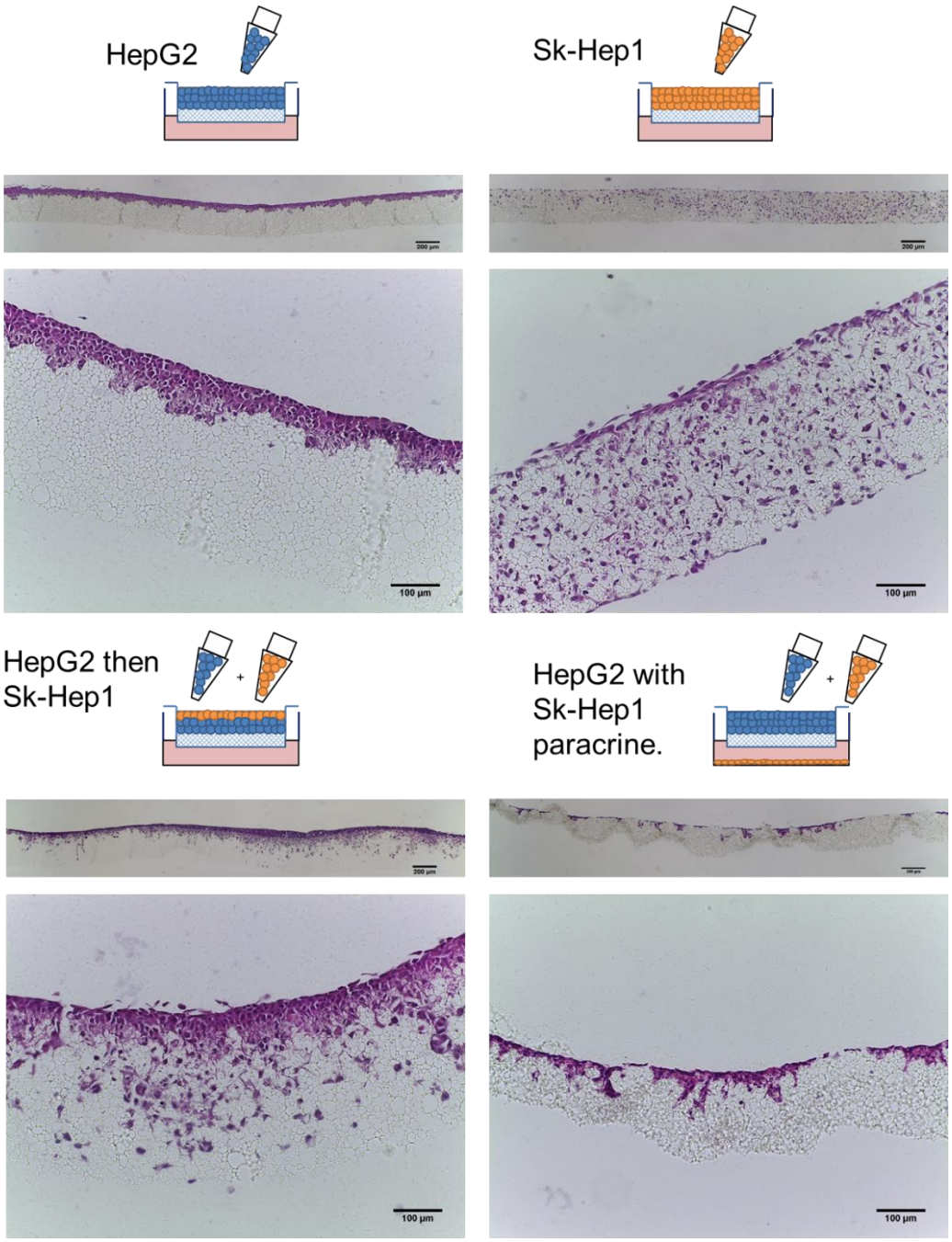

Figure 7.3 Alvetex® Strata is able to support co-culture of HepG2 and Sk-Hep1 cells.

H&E stains of HepG2 cells (top left) or Sk-Hep-1 cells (top right) seeded at 1 x 10^6 cells onto Alvetex® strata and grown for 8 days. Co-culture conditions are the bottom panel, with HepG2 cells seeded simultaneously with Sk-Hep-1 cells at densities of 7.5 x 10^5 and 2.5 x 10^5 cells per insert respectively (co-culture, bottom left) or HepG2 cells seeded at 1 x 10^6 cells onto Alvetex® strata, with SK-Hep-1 cells seeded onto the bottom of each well at 1 x 10^6 cells per well (paracrine, bottom right) and grown for 8 days; Scale bars = 200 and 100 µm respectively.

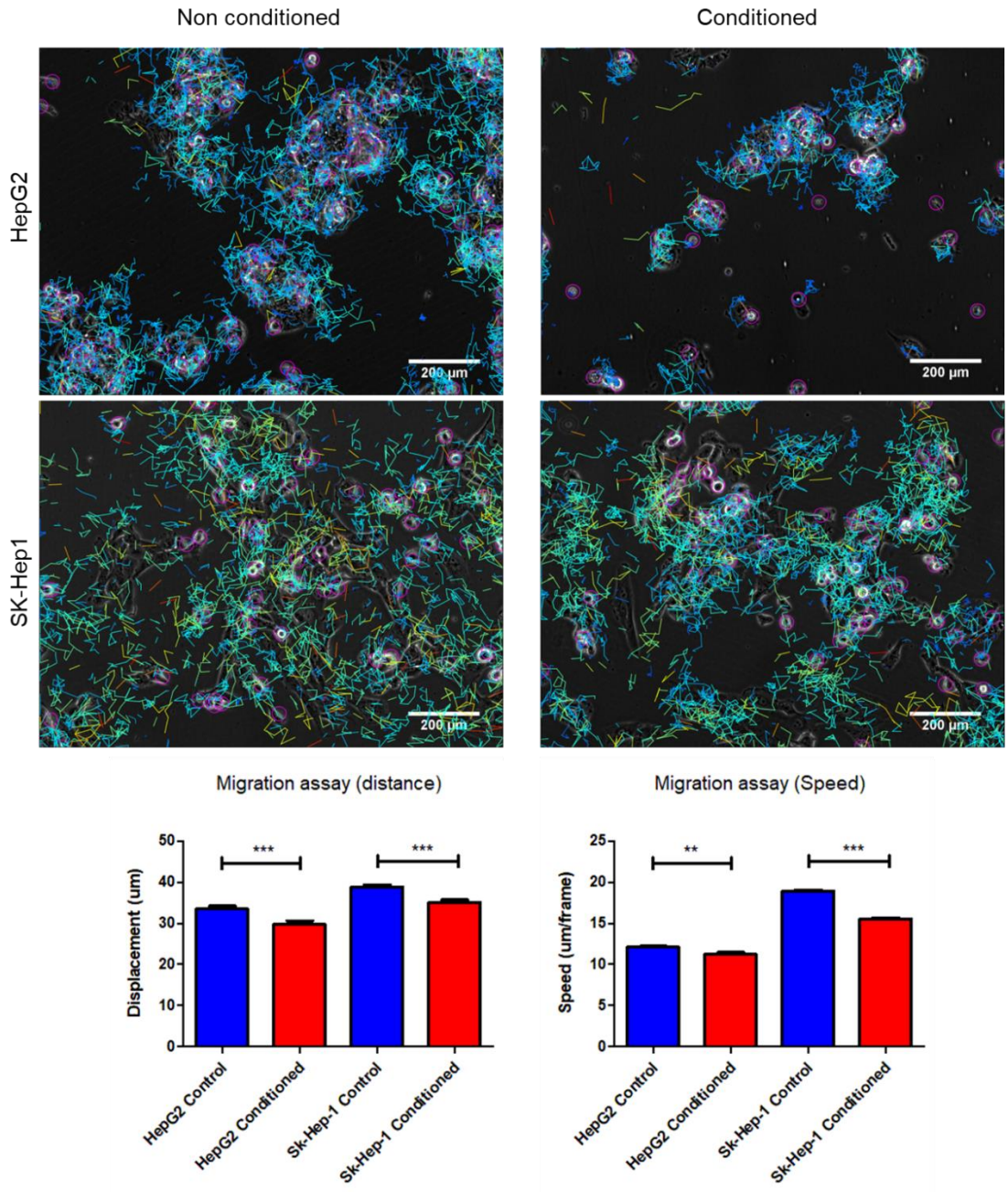

Figure 7.4 Media conditioned with either HepG2 or Sk-Hep1 cells reduces migration of the other cell line when cultured in the conditioned media.

Phase contrast images of HepG2 cells and Sk-Hep1 cells with a tracking overlay. Cell lines were seeded at a density of 1 x 10^5 cells per coverslip, and either grown in untreated MEM cell culture media (non-conditioned), or in MEM filtered from 4-day conditioned media from the opposing cell line (conditioned – see methods). Tracking of cells over 3 days was performed using TrackMate plugin on ImageJ. Colour of tracking lines from Blue to Red indicates increasing mean velocity. Scale bar = 200 µm. N= 3.

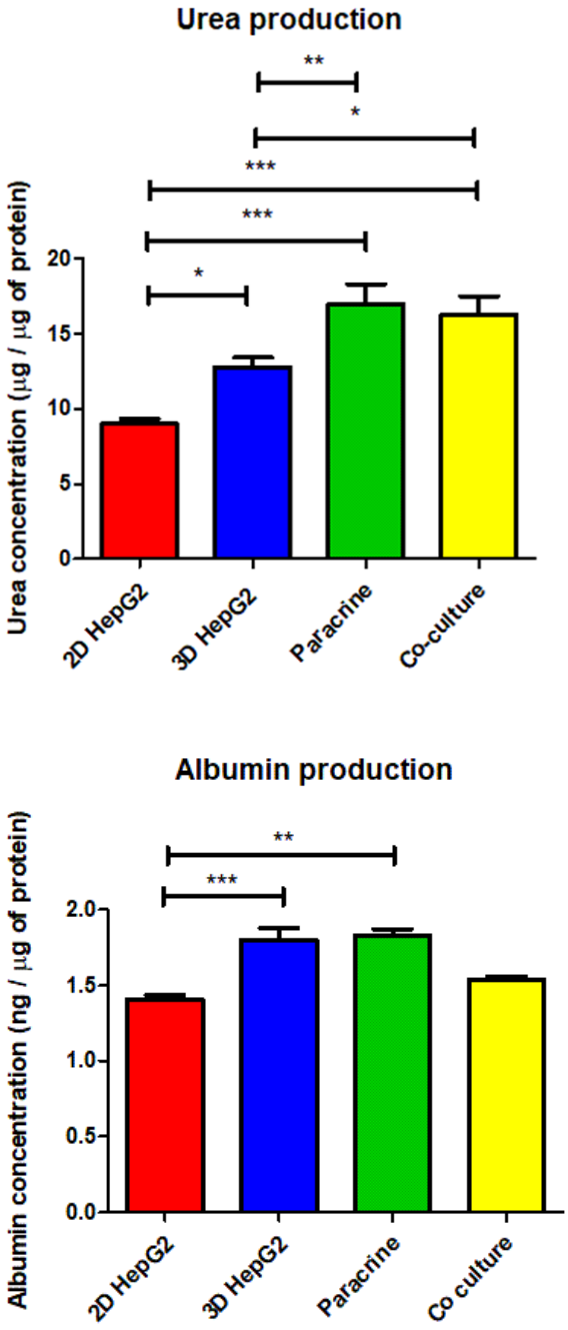

Figure 7.5 Paracrine 3D cultures with Sk-Hep1 cells increase urea secretion but not albumin over monocultures.

Urea assay performed on media supernatants taken from HepG2 cells alone or in co-culture with Sk-Hep-1 cells in either 2D or grown in Strata for 8 days. Normalised to protein concentration, N= 2 n= 2, error bars = SEM Albumin assay performed on media supernatants taken from HepG2 cells alone or in co-culture with Sk-Hep-1 cells in either 2D or grown in Strata for 8 days. Normalised to protein concentration, N= 1 n= 3, error bars = SEM

was a pilot experiment however and there were not sufficient repeats to draw full conclusions based on this data alone.

Finally, to see if Sk-Hep1 cells could form hanging drops by themselves and as a co-culture, 2D grown Sk-Hep1 cells were cultured as hanging drops both as a monoculture and co-culture with HepG2 cells, and these spheroids were compared with HepG2 spheroids formed from 2D cells (**Figure 7.6**). The H&E images of these showed that Sk-Hep1 cells by themselves are able to form spheroids, however the organisation of these spheroids was looser than those formed from HepG2 cells, with clear space between the cells. In co-culture, the spheroids with HepG2 and Sk-Hep1 cells failed to properly aggregate in many cases, and when spheroids were formed, it was clear that they were poorly organised with evidence of cell death occurring too. This suggested that co-culture with this specific cell-line would perhaps be better suited to the priming stage rather than the secondary model, and that it might be more beneficial to culture Sk-Hep1 cells on the bottom of the well for a paracrine effect rather than in direct co-culture with the HepG2 cells.

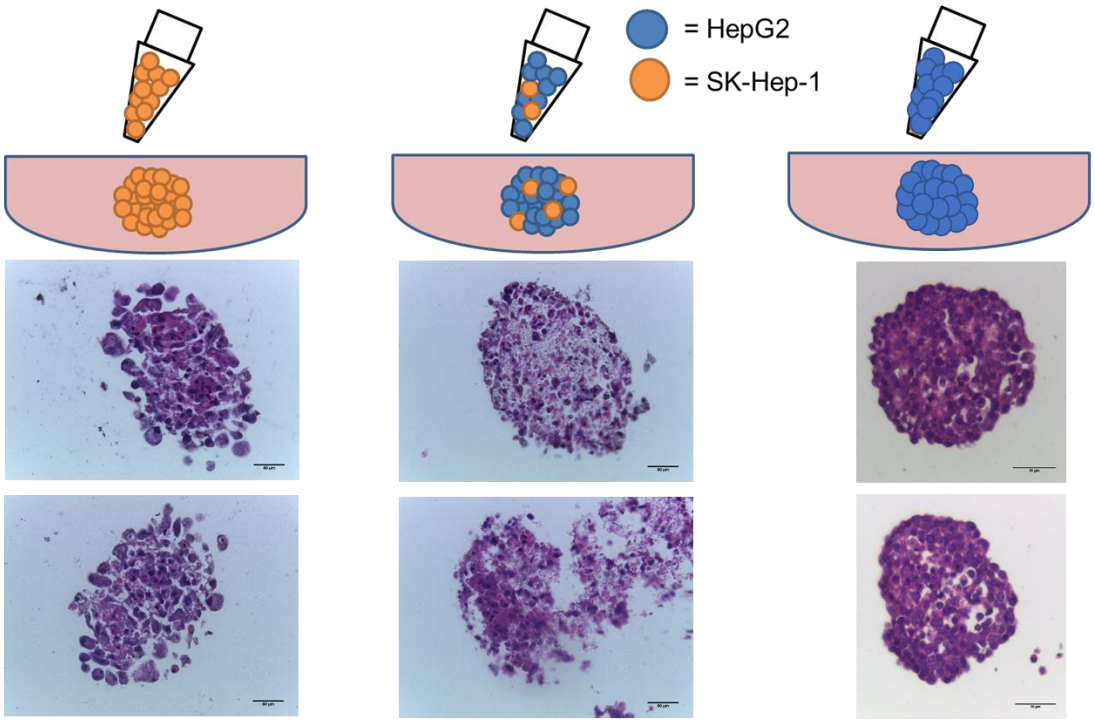

Figure 7.6 HepG2 and Sk-Hep1 cells failed to make mature spheroids in co-culture.

H&E of SK-Hep-1 (left), co culture (middle) and HepG2 hanging drops (right). SK-Hep-1 and HepG2 cells alone were seeded at 1x10^3 cells per drop, and in co-culture, Sk-Hep-1 cells were seeded at 2.5x10^2 and HepG2 cells seeded at 7.5x10^2 cells per drop, and all grown for 10 days. Scale bars: 50 µm

These results were interesting, however there is a large amount of further research that could be done to clarify how Sk-Hep1 cells effect the HepG2 cells. Do the enhanced functional benefits of paracrine culture priming have a further enhanced function in the secondary model, and how are wider functions such as drug metabolism affected? Would Sk-hep1 conditioned media work in further enhancing the functionality of 3D primed cells in the secondary model? Would these results be amplified using HUVECs or liver sinusoidal endothelial cells? It would also be interesting to see whether adding a third cell type such as fibroblasts would make conditions even closer to the liver *in vivo*. These are all questions that are still being explored in research without the added complication of additional techniques such as priming cells, but making connections between techniques such as co-culture and 3D priming could be essential in realising the full potential of *in vitro* models.

Thinking more widely than HepG2 cells, a particularly key aspect to explore is how can priming be utilised beneficially in wider cell lines and wider applications. Primary hepatocytes would be a key cell line to test this concept on, due to the known issues with dedifferentiation in 2D culture (Kiamehr et al., 2019). 3D culture circumvents this to an extent, enriching a range of functional processes (Lauschke et al., 2019), thus it is possible that through the 3D priming technique, these qualities may be further enhanced. As mentioned, there is evidence that priming can help tune the functional properties of stem cells and epithelial cells but does this extend to other cell types that are strongly reliant on mechanical cues *in vivo*? Some particularly interesting cells to test this question on would be mammary epithelial cells, osteocytes, cardiomyocytes and many more cells that reside in very distinctive mechanical niches. On the inverse of this, there is also the question of whether 3D priming would adversely affect certain cell lines where *in vivo* conditions are more two-dimensional in nature such as endothelial cells or simple squamous epithelial cells, where their physiological state is more akin to a monolayer. Would priming these cells in *2D* benefit them more than priming in 3D, or would priming them be detrimental to physiological function? Cell culture is certainly not a one size fits all solution, and one should always choose the substrate with the mechanical dynamics of the original tissue in mind (and this project has only gone to further prove the importance of that consideration), so it would make sense for priming in 3D to make cells less physiological in certain cases too.

Another area to investigate would be making the models dynamic. The liver is an environment under constant blood flow due to the high vascularisation present in the lobules. Shear stress, a force exerted through fluids flowing over cells, is absent in static

cultures, yet is an essential mechanical force that drives organogenesis (Freund et al., 2012; Rashidi et al., 2016). One study has shown that by adding fluid dynamics to liver models, they are able to significantly improve the metabolic capacity of the liver through increased CYP1A2 activity (Rashidi et al., 2016). In addition, CYP2D6 appeared to increase in activity, as there was a nine-fold increase in sensitivity when a drug known to interact with this enzyme was applied to the perfused models. This demonstrates the role of the phase I enzymes in increasing the drug sensitivity of models, and points towards the decreased sensitivity in the 3D primed models in this thesis being attributable to a higher ratio of phase II to phase I enzymes. Other studies have also shown increased expression of key liver enzymes in perfused models (Shvartsman et al., 2009; Vinci et al., 2011). There is a clear rationale for using bioreactors, with improvements over static models, and it would be particularly fascinating to explore whether 3D priming can better prepare cells for input into a dynamic model. Additionally, further research should be performed on the mechanical changes occurring in the cell, through techniques such as atomic force microscopy for example to measure the stiffness of the cells in different conditions. Migratory assays may also indicate cytoskeletal changes that have taken place in the cells, resulting in altered motility. This would add clarity to the underpinning structural changes that drive the resultant functional alterations.

Finally, thinking beyond *in vitro* research, the benefits of priming may have a clear role in cell-based therapies. Cell therapies involve implantation/grafting of viable cells into a patient for therapeutic purposes. Based on the evidence from this study and from previous priming studies, there is high potential for priming in preparing cells for such therapeutic uses. If one can adapt cells to a three-dimensional physiological phenotype, then it is possible that therapies such as these may benefit from these primed cells, with a faster uptake and better acceptance in the patient. Priming may be even more beneficial in stem cell-based therapies where cell differentiation could be tuned and directed to an extent before implanting in a patient. It is clear that the concept of priming is an area of tissue engineering that is still in its infancy, but this project demonstrates that there is potential to harness this technique for a wide range of applications.

7.5 Final conclusions

This project has presented a novel technique through which to culture cells on a 3D scaffold, whereby their structural and functional properties are enhanced. These cells are 'primed' to a 3D microenvironment and can be easily liberated from the priming substrate for reseeding into a secondary culture. In this secondary culture, this study has shown significant structural alterations are carried over from 3D priming in contrast to cells grown in 2D beforehand. These structural differences are evident in both single cells, with altered cytoskeletal properties, and in cell populations, with different growth patterns observed. These structural changes in 3D primed cells are coupled with significantly enhanced functional profile too, with very focussed enrichment in hepatic metabolic and biosynthetic processes. These changes were detected through genome wide gene expression analysis and were functionally validated proving a high level of reproducibility and robustness within the models. The enriched functional processes were carried over to the secondary models after the 3D priming period, however seemed to equilibrate with secondary models made from 2D cells after 7 days of growth as both conditions adapted to the new mechanical environment.

This project was intended in part to develop a functional liver model, and it has demonstrated enhanced function from 3D priming, but another key aspect was to demonstrate a proof of concept that mechanically pre-conditioning cells exerts a sustained effect on the cell biology even when moved to a different substrate. Both questions have been addressed through a broad range of analytical and experimental techniques, ranging from in-depth structural characterisation, transcriptomic analysis and functional validation.

It is possible that to create the most optimum *in vitro* model for the liver, one could combine the concepts of mechanical priming, co-culture, chemical treatment and perfusion. The 3D priming HepG2 model alone is not a perfect solution to liver research, with potential challenges still present in reflecting *in vivo* responses to drug toxicity. However, ideal physiological qualities are yet to be shown in *any in vitro* model, partly due to the inherently non-physiological nature of culturing cells outside of the body. Regardless, this data has

shown that priming in a unique substrate geometry does bring the cells *closer* to their *in vivo* counterparts in morphology, global structure, gene expression and in biosynthetic and metabolic processes. Priming as a concept appears to help in creating a better final stage 3D model due to pre-conditioning cells with a more physiological and three-dimensional phenotype ready for functional testing. In addition, this has provided a broad range of further questions that can be explored in future mechano-biology research, with many aspects of mechanical priming to be explored. This study presents an effective, practical and simple method through which one can improve *in vitro* models.

Chapter 8 – Bibliography.

Adam, A.A.A., Jongejan, A., Moerland, P.D., van der Mark, V.A., Oude Elferink, R.P., Chamuleau, R.A.F.M., Hoekstra, R., 2020. Genome-wide expression profiling reveals increased stability and mitochondrial energy metabolism of the human liver cell line HepaRG-CAR. Cytotechnology 72, 377–395. https://doi.org/10.1007/s10616-020-00384-w

Adeola, F., 2018. Normalization of Gene Expression by Quantitative RT-PCR in Human Cell Line: comparison of 12 Endogenous Reference Genes. Ethiop. J. Health Sci. 28, 741–748. https://doi.org/10.4314/ejhs.v28i6.9

Adkison, J.B., Miller, G.T., Weber, D.S., Miyahara, T., Ballard, S.T., Frost, J.R., Parker, J.C., 2006. Differential responses of pulmonary endothelial phenotypes to cyclical stretch. Microvasc. Res. 71, 175–184. https://doi.org/10.1016/j.mvr.2006.02.007

Agarose Gel Electrophoresis of RNA - UK [WWW Document], n.d. URL //www.thermofisher.com/uk/en/home/references/protocols/nucleic-acid-purification-and-analysis/rna-protocol/agarose-gel-electrophoresis-of-rna.html (accessed 2.11.21).

Ahmadian, M., Suh, J.M., Hah, N., Liddle, C., Atkins, A.R., Downes, M., Evans, R.M., 2013. PPARγ signaling and metabolism: the good, the bad and the future. Nat. Med. 19. https://doi.org/10.1038/nm.3159

Alberts, B., Johnson, A., Lewis, J., Raff, M., Roberts, K., Walter, P., 2002a. Cell Junctions. Mol. Biol. Cell 4th Ed.

Alberts, B., Johnson, A., Lewis, J., Raff, M., Roberts, K., Walter, P., 2002b. Integrins. Mol. Biol. Cell 4th Ed.

Alisafaei, F., Jokhun, D.S., Shivashankar, G.V., Shenoy, V.B., 2019. Regulation of nuclear architecture, mechanics, and nucleocytoplasmic shuttling of epigenetic factors by cell geometric constraints. Proc. Natl. Acad. Sci. 116, 13200–13209. https://doi.org/10.1073/pnas.1902035116

Altay, G., Tosi, S., García-Díaz, M., Martínez, E., 2020. Imaging the Cell Morphological Response to 3D Topography and Curvature in Engineered Intestinal Tissues. Front. Bioeng. Biotechnol. 8. https://doi.org/10.3389/fbioe.2020.00294

Amano, M., Nakayama, M., Kaibuchi, K., 2010. Rho-Kinase/ROCK: A Key Regulator of the Cytoskeleton and Cell Polarity. Cytoskelet. Hoboken Nj 67, 545–554. https://doi.org/10.1002/cm.20472

Amiodarone, 2012. , in= LiverTox: Clinical and Research Information on Drug-Induced Liver Injury. National Institute of Diabetes and Digestive and Kidney Diseases, Bethesda (MD).

Amiodarone DrugBank [WWW Document], n.d. URL https://go.drugbank.com/drugs/DB01118 (accessed 1.4.21).

Anderson, J.M., Van Itallie, C.M., 2009. Physiology and Function of the Tight Junction. Cold Spring Harb. Perspect. Biol. 1. https://doi.org/10.1101/cshperspect.a002584

Aragona, M., Panciera, T., Manfrin, A., Giulitti, S., Michielin, F., Elvassore, N., Dupont, S., Piccolo, S., 2013. A mechanical checkpoint controls multicellular growth through YAP/TAZ regulation by actin-processing factors. Cell 154, 1047–1059. https://doi.org/10.1016/j.cell.2013.07.042

Arrowsmith, J., Miller, P., 2013. Phase II and Phase III attrition rates 2011–2012. Nat. Rev. Drug Discov. 12, 569–569. https://doi.org/10.1038/nrd4090

Arsenovic, P.T., Ramachandran, I., Bathula, K., Zhu, R., Narang, J.D., Noll, N.A., Lemmon, C.A., Gundersen, G.G., Conway, D.E., 2016. Nesprin-2G, a Component of the Nuclear LINC Complex, Is Subject to Myosin-Dependent Tension. Biophys. J. 110, 34–43. https://doi.org/10.1016/j.bpj.2015.11.014

Ashburner, M., Ball, C.A., Blake, J.A., Botstein, D., Butler, H., Cherry, J.M., Davis, A.P., Dolinski, K., Dwight, S.S., Eppig, J.T., Harris, M.A., Hill, D.P., Issel-Tarver, L., Kasarskis, A., Lewis,

S., Matese, J.C., Richardson, J.E., Ringwald, M., Rubin, G.M., Sherlock, G., 2000. Gene Ontology: tool for the unification of biology. Nat. Genet. 25, 25–29. https://doi.org/10.1038/75556

Astashkina, A., Grainger, D.W., 2014. Critical analysis of 3-D organoid in vitro cell culture models for high-throughput drug candidate toxicity assessments. Innov. Tissue Models Drug Discov. Dev. 69–70, 1–18. https://doi.org/10.1016/j.addr.2014.02.008

Astashkina, A., Mann, B., Grainger, D.W., 2012. A critical evaluation of in vitro cell culture models for high-throughput drug screening and toxicity. Pharmacol. Ther. 134, 82–106. https://doi.org/10.1016/j.pharmthera.2012.01.001

Auernheimer, V., Lautscham, L.A., Leidenberger, M., Friedrich, O., Kappes, B., Fabry, B., Goldmann, W.H., 2015. Vinculin phosphorylation at residues Y100 and Y1065 is required for cellular force transmission. J. Cell Sci. 128, 3435–3443. https://doi.org/10.1242/jcs.172031

Austen, K., Ringer, P., Mehlich, A., Chrostek-Grashoff, A., Kluger, C., Klingner, C., Sabass, B., Zent, R., Rief, M., Grashoff, C., 2015. Extracellular rigidity sensing by talin isoform-specific mechanical linkages. Nat. Cell Biol. 17, 1597–1606. https://doi.org/10.1038/ncb3268

Ayollo, D.V., Zhitnyak, I.Y., Vasiliev, J.M., Gloushankova, N.A., 2009. Rearrangements of the Actin Cytoskeleton and E-Cadherin–Based Adherens Junctions Caused by Neoplasic Transformation Change Cell–Cell Interactions. PLOS ONE 4, e8027. https://doi.org/10.1371/journal.pone.0008027

Bae, Y.H., Mui, K.L., Hsu, B.Y., Liu, S.-L., Cretu, A., Razinia, Z., Xu, T., Puré, E., Assoian, R.K., 2014. A FAK-Cas-Rac-Lamellipodin Signaling Module Transduces Extracellular Matrix Stiffness into Mechanosensitive Cell Cycling. Sci. Signal. 7, ra57. https://doi.org/10.1126/scisignal.2004838

Baker, B.M., Chen, C.S., 2012. Deconstructing the third dimension – how 3D culture microenvironments alter cellular cues. J. Cell Sci. 125, 3015–3024. https://doi.org/10.1242/jcs.079509

Balda, M.S., Matter, K., 2000. The tight junction protein ZO-1 and an interacting transcription factor regulate ErbB-2 expression. EMBO J. 19, 2024–2033. https://doi.org/10.1093/emboj/19.9.2024

Barredo, J.C., Synold, T.W., Laver, J., Relling, M.V., Pui, C.H., Priest, D.G., Evans, W.E., 1994. Differences in constitutive and post-methotrexate folylpolyglutamate synthetase activity in B-lineage and T-lineage leukemia. Blood 84, 564–569.

Barthes, J., Vrana, N.E., Özçelik, H., Gahoual, R., François, Y.N., Bacharouche, J., Francius, G., Hemmerlé, J., Metz-Boutigue, M.-H., Schaaf, P., Lavalle, P., 2015. Priming cells for their final destination= microenvironment controlled cell culture by a modular ECM-mimicking feeder film. Biomater. Sci. 3, 1302–1311. https://doi.org/10.1039/C5BM00172B

Barzik, M., Kotova, T.I., Higgs, H.N., Hazelwood, L., Hanein, D., Gertler, F.B., Schafer, D.A., 2005. Ena/vasp proteins enhance actin polymerization in the presence of barbed end capping proteins. J. Biol. Chem. 280, 28653–28662. https://doi.org/10.1074/jbc.M503957200

Battle, T., Maguire, T., Moulsdale, H., Doyle, A., 1999. Progressive maturation resistance to microcystin-LR cytotoxicity in two different hepatospheroidal models. Cell Biol. Toxicol. 15, 3–12. https://doi.org/10.1023/A:1007587304619

Bayliss, M., Somers, G., 2005. Isolation and Culture of Human Hepatocytes, in= Picot, J. (Ed.), Human Cell Culture Protocols, Methods in Molecular Medicine™. Humana Press, pp. 249–267. https://doi.org/10.1385/1-59259-861-7:249

Bazellières, E., Conte, V., Elosegui-Artola, A., Serra-Picamal, X., Bintanel-Morcillo, M., Roca-Cusachs, P., Muñoz, J.J., Sales-Pardo, M., Guimerà, R., Trepat, X., 2015. Control of

cell-cell forces and collective cell dynamics by the intercellular adhesome. Nat. Cell Biol. 17, 409–420. https://doi.org/10.1038/ncb3135

Beers, J., Gulbranson, D.R., George, N., Siniscalchi, L.I., Jones, J., Thomson, J.A., Chen, G., 2012. Passaging and colony expansion of human pluripotent stem cells by enzyme-free dissociation in chemically defined culture conditions. Nat. Protoc. 7, 2029–2040. https://doi.org/10.1038/nprot.2012.130

Belin, B.J., Cimini, B.A., Blackburn, E.H., Mullins, R.D., 2013. Visualization of actin filaments and monomers in somatic cell nuclei. Mol. Biol. Cell 24, 982–994. https://doi.org/10.1091/mbc.e12-09-0685

Bell, Catherine C., Dankers, A.C.A., Lauschke, V.M., Sison-Young, R., Jenkins, R., Rowe, C., Goldring, C.E., Park, K., Regan, S.L., Walker, T., Schofield, C., Baze, A., Foster, A.J., Williams, D.P., van de Ven, A.W.M., Jacobs, F., Houdt, J. van, Lähteenmäki, T., Snoeys, J., Juhila, S., Richert, L., Ingelman-Sundberg, M., 2018. Comparison of Hepatic 2D Sandwich Cultures and 3D Spheroids for Long-term Toxicity Applications: A Multicenter Study. Toxicol. Sci. 162, 655–666. https://doi.org/10.1093/toxsci/kfx289

Bell, Catherine C, Dankers, A.C.A., Lauschke, V.M., Sison-Young, R., Jenkins, R., Rowe, C., Goldring, C.E., Park, K., Regan, S.L., Walker, T., Schofield, C., Baze, A., Foster, A.J., Williams, D.P., van de Ven, A.W.M., Jacobs, F., van Houdt, J., Lähteenmäki, T., Snoeys, J., Juhila, S., Richert, L., Ingelman-Sundberg, M., 2018. Comparison of Hepatic 2D Sandwich Cultures and 3D Spheroids for Long-term Toxicity Applications: A Multicenter Study. Toxicol. Sci. 162, 655–666. https://doi.org/10.1093/toxsci/kfx289

Berg, J.M., Tymoczko, J.L., Stryer, L., 2002. The Complex Regulation of Cholesterol Biosynthesis Takes Place at Several Levels. Biochem. 5th Ed.

Bieling, P., Li, T.-D., Weichsel, J., McGorty, R., Jreij, P., Huang, B., Fletcher, D.A., Mullins, R.D., 2016. Force feedback controls motor activity and mechanical properties of self-assembling branched actin networks. Cell 164, 115. https://doi.org/10.1016/j.cell.2015.11.057

Birgersdotter, A., Sandberg, R., Ernberg, I., 2005. Gene expression perturbation in vitro--a growing case for three-dimensional (3D) culture systems. Semin. Cancer Biol. 15, 405–412. https://doi.org/10.1016/j.semcancer.2005.06.009

Bissell, M. J., Barcellos-Hoff, M.H., 1987. The influence of extracellular matrix on gene expression= is structure the message? J. Cell Sci. Suppl. 8, 327–343.

Bissell, Mina J., Barcellos-Hoff, M.H., 1987. The Influence of Extracellular Matrix on Gene Expression= Is Structure the Message? J. Cell Sci. 1987, 327–343. https://doi.org/10.1242/jcs.1987.Supplement_8.18

Bokhari, M., Carnachan, R.J., Cameron, N.R., Przyborski, S.A., 2007. Culture of HepG2 liver cells on three dimensional polystyrene scaffolds enhances cell structure and function during toxicological challenge. J. Anat. 211, 567–576. https://doi.org/10.1111/j.1469-7580.2007.00778.x

Bonnans, C., Chou, J., Werb, Z., 2014. Remodelling the extracellular matrix in development and disease. Nat. Rev. Mol. Cell Biol. 15, 786–801. https://doi.org/10.1038/nrm3904

Booth-Gauthier, E.A., Alcoser, T.A., Yang, G., Dahl, K.N., 2012. Force-Induced Changes in Subnuclear Movement and Rheology. Biophys. J. 103, 2423–2431. https://doi.org/10.1016/j.bpj.2012.10.039

Bouck, D.C., Bloom, K., 2007. Pericentric Chromatin Is an Elastic Component of the Mitotic Spindle. Curr. Biol. 17, 741–748. https://doi.org/10.1016/j.cub.2007.03.033

Bouzid, T., Kim, E., Riehl, B.D., Esfahani, A.M., Rosenbohm, J., Yang, R., Duan, B., Lim, J.Y., 2019. The LINC complex, mechanotransduction, and mesenchymal stem cell function and fate. J. Biol. Eng. 13, 68. https://doi.org/10.1186/s13036-019-0197-9

Boyer, J.L., 2013. Bile Formation and Secretion. Compr. Physiol. 3, 1035–1078. https://doi.org/10.1002/cphy.c120027

Branco, M.A., Cotovio, J.P., Rodrigues, C.A.V., Vaz, S.H., Fernandes, T.G., Moreira, L.M., Cabral, J.M.S., Diogo, M.M., 2019. Transcriptomic analysis of 3D Cardiac Differentiation of Human Induced Pluripotent Stem Cells Reveals Faster Cardiomyocyte Maturation Compared to 2D Culture. Sci. Rep. 9, 1–13. https://doi.org/10.1038/s41598-019-45047-9

Breslin, S., O'Driscoll, L., 2013a. Three-dimensional cell culture: the missing link in drug discovery. Drug Discov. Today 18, 240–249. https://doi.org/10.1016/j.drudis.2012.10.003

Breslin, S., O'Driscoll, L., 2013b. Three-dimensional cell culture: the missing link in drug discovery [WWW Document]. Drug Discov. Today. https://doi.org/10.1016/j.drudis.2012.10.003

Brückner, B.R., Janshoff, A., 2018. Importance of integrity of cell-cell junctions for the mechanics of confluent MDCK II cells. Sci. Rep. 8, 14117. https://doi.org/10.1038/s41598-018-32421-2

Bryant, D., Clemens, L., Allard, J., 2017. Computational simulation of formin-mediated actin polymerization predicts homologue-dependent mechanosensitivity. Cytoskelet. Hoboken NJ 74, 29–39. https://doi.org/10.1002/cm.21344

Burke, B., Stewart, C.L., 2013. The nuclear lamins: flexibility in function. Nat. Rev. Mol. Cell Biol. 14, 13–24. https://doi.org/10.1038/nrm3488

Burridge, K., Monaghan-Benson, E., Graham, D.M., 2019. Mechanotransduction= from the cell surface to the nucleus via RhoA. Philos. Trans. R. Soc. B Biol. Sci. 374, 20180229. https://doi.org/10.1098/rstb.2018.0229

Butin-Israeli, V., Adam, S.A., Goldman, A.E., Goldman, R.D., 2012. Nuclear lamin functions and disease. Trends Genet. TIG 28, 464–471. https://doi.org/10.1016/j.tig.2012.06.001

Buyl, K., De Kock, J., Bolleyn, J., Rogiers, V., Vanhaecke, T., 2015. Measurement of Albumin Secretion as Functionality Test in Primary Hepatocyte Cultures. Methods Mol. Biol. Clifton NJ 1250, 303–308. https://doi.org/10.1007/978-1-4939-2074-7_22

Cailliez, F., Lavery, R., 2005. Cadherin Mechanics and Complexation= The Importance of Calcium Binding. Biophys. J. 89, 3895–3903. https://doi.org/10.1529/biophysj.105.067322

Cain, N.E., Starr, D.A., 2014. SUN proteins and nuclear envelope spacing. Nucleus 6, 2–7. https://doi.org/10.4161/19491034.2014.990857

Caliari, S.R., Burdick, J.A., 2016. A practical guide to hydrogels for cell culture. Nat. Methods 13, 405–414. https://doi.org/10.1038/nmeth.3839

Calvo, F., Ege, N., Grande-Garcia, A., Hooper, S., Jenkins, R.P., Chaudhry, S.I., Harrington, K., Williamson, P., Moeendarbary, E., Charras, G., Sahai, E., 2013. Mechanotransduction and YAP-dependent matrix remodelling is required for the generation and maintenance of cancer-associated fibroblasts. Nat. Cell Biol. 15, 637–646. https://doi.org/10.1038/ncb2756

Cameron, J.M., Bruno, C., Parachalil, D.R., Baker, M.J., Bonnier, F., Butler, H.J., Byrne, H.J., 2020. Chapter 10 - Vibrational spectroscopic analysis and quantification of proteins in human blood plasma and serum, in= Ozaki, Y., Baranska, M., Lednev, I.K., Wood, B.R. (Eds.), Vibrational Spectroscopy in Protein Research. Academic Press, pp. 269–314. https://doi.org/10.1016/B978-0-12-818610-7.00010-4

Cao, X., Ban, E., Baker, B.M., Lin, Y., Burdick, J.A., Chen, C.S., Shenoy, V.B., 2017. Multiscale model predicts increasing focal adhesion size with decreasing stiffness in fibrous matrices. Proc. Natl. Acad. Sci. U. S. A. 114, E4549–E4555. https://doi.org/10.1073/pnas.1620486114

Cao, X., Moeendarbary, E., Isermann, P., Davidson, P.M., Wang, X., Chen, M.B., Burkart, A.K., Lammerding, J., Kamm, R.D., Shenoy, V.B., 2016. A Chemomechanical Model for

Nuclear Morphology and Stresses during Cell Transendothelial Migration. Biophys. J. 111, 1541–1552. https://doi.org/10.1016/j.bpj.2016.08.011

Carletti, E., Motta, A., Migliaresi, C., 2011. Scaffolds for tissue engineering and 3D cell culture. Methods Mol. Biol. Clifton NJ 695, 17–39. https://doi.org/10.1007/978-1-60761-984-0_2

Carmeliet, P., Lampugnani, M.-G., Moons, L., Breviario, F., Compernolle, V., Bono, F., Balconi, G., Spagnuolo, R., Oosthuyse, B., Dewerchin, M., Zanetti, A., Angellilo, A., Mattot, V., Nuyens, D., Lutgens, E., Clotman, F., Ruiter, M.C. de, Groot, A.G., Poelmann, R., Lupu, F., Herbert, J.-M., Collen, D., Dejana, E., 1999. Targeted Deficiency or Cytosolic Truncation of the VE-cadherin Gene in Mice Impairs VEGF-Mediated Endothelial Survival and Angiogenesis. Cell 98, 147–157. https://doi.org/10.1016/S0092-8674(00)81010-7

Castella, L.F., Buscemi, L., Godbout, C., Meister, J.-J., Hinz, B., 2010. A new lock-step mechanism of matrix remodelling based on subcellular contractile events. J. Cell Sci. 123, 1751–1760. https://doi.org/10.1242/jcs.066795

Cederbaum, A.I., 2012. ALCOHOL METABOLISM. Clin. Liver Dis. 16, 667–685. https://doi.org/10.1016/j.cld.2012.08.002

Cha, B., Geng, X., Mahamud, M.R., Fu, J., Mukherjee, A., Kim, Y., Jho, E.-H., Kim, T.H., Kahn, M.L., Xia, L., Dixon, J.B., Chen, H., Srinivasan, R.S., 2016. Mechanotransduction activates canonical Wnt/β-catenin signaling to promote lymphatic vascular patterning and the development of lymphatic and lymphovenous valves. Genes Dev. 30, 1454–1469. https://doi.org/10.1101/gad.282400.116

Chaicharoenaudomrung, N., Kunhorm, P., Noisa, P., 2019. Three-dimensional cell culture systems as an in vitro platform for cancer and stem cell modeling. World J. Stem Cells 11, 1065–1083. https://doi.org/10.4252/wjsc.v11.i12.1065

Chang, T.T., Hughes-Fulford, M., 2009. Monolayer and spheroid culture of human liver hepatocellular carcinoma cell line cells demonstrate distinct global gene expression patterns and functional phenotypes. Tissue Eng. Part A 15, 559–567. https://doi.org/10.1089/ten.tea.2007.0434

Chang, Y.-C., Wu, J.-W., Wang, C.-W., Jang, A.C.-C., 2020. Hippo Signaling-Mediated Mechanotransduction in Cell Movement and Cancer Metastasis. Front. Mol. Biosci. 6. https://doi.org/10.3389/fmolb.2019.00157

Chen, E.Y., Tan, C.M., Kou, Y., Duan, Q., Wang, Z., Meirelles, G.V., Clark, N.R., Ma'ayan, A., 2013. Enrichr: interactive and collaborative HTML5 gene list enrichment analysis tool. BMC Bioinformatics 14, 128. https://doi.org/10.1186/1471-2105-14-128

Chen, W., Lou, J., Evans, E.A., Zhu, C., 2012. Observing force-regulated conformational changes and ligand dissociation from a single integrin on cells. J. Cell Biol. 199, 497–512. https://doi.org/10.1083/jcb.201201091

Chesarone, M.A., Goode, B.L., 2009. Actin Nucleation and Elongation Factors: Mechanisms and Interplay. Curr. Opin. Cell Biol. 21, 28–37. https://doi.org/10.1016/j.ceb.2008.12.001

Cheung, I.D., Bagnat, M., Ma, T.P., Datta, A., Evason, K., Moore, J.C., Lawson, N., Mostov, K.E., Moens, C.B., Stainier, D.Y.R., 2012. Regulation of intrahepatic biliary duct morphogenesis by Claudin 15-like b. Dev. Biol. 361, 68–78. https://doi.org/10.1016/j.ydbio.2011.10.004

CHHATWAL, A., 2016. Investigating the effect of a 3D physical microenvironment on hepatocyte structure, function, and adhesion signalling (Doctoral). Durham University.

Cho, S., Irianto, J., Discher, D.E., 2017. Mechanosensing by the nucleus: From pathways to scaling relationships. J. Cell Biol. 216, 305–315. https://doi.org/10.1083/jcb.201610042

Choi, W., Acharya, B.R., Peyret, G., Fardin, M.-A., Mège, R.-M., Ladoux, B., Yap, A.S., Fanning, A.S., Peifer, M., 2016. Remodeling the zonula adherens in response to tension and the role of afadin in this response. J. Cell Biol. 213, 243–260. https://doi.org/10.1083/jcb.201506115

Cholesterol Biosynthesis [WWW Document], n.d. . Sigma-Aldrich. URL https://www.sigmaaldrich.com/technical-documents/articles/biofiles/cholesterol-biosynthesis.html (accessed 2.25.21).

Chrzanowska-Wodnicka, M., Burridge, K., 1996. Rho-stimulated contractility drives the formation of stress fibers and focal adhesions. J. Cell Biol. 133, 1403–1415. https://doi.org/10.1083/jcb.133.6.1403

Citi, S., 2019. The mechanobiology of tight junctions. Biophys. Rev. 11, 783–793. https://doi.org/10.1007/s12551-019-00582-7

Cízková, D., Morký, J., Micuda, S., Osterreicher, J., Martínková, J., 2005. Expression of MRP2 and MDR1 transporters and other hepatic markers in rat and human liver and in WRL 68 cell line. Physiol. Res. 54, 419–428.

Cohen, D., Tian, Y., Müsch, A., 2007. Par1b Promotes Hepatic-type Lumen Polarity in Madin Darby Canine Kidney Cells via Myosin II- and E-Cadherin–dependent Signaling. Mol. Biol. Cell 18, 2203–2215. https://doi.org/10.1091/mbc.E07-02-0095

Collins, S.D., Yuen, G., Tu, T., Budzinska, M.A., Spring, K., Bryant, K., Shackel, N.A., 2019. In Vitro Models of the Liver: Disease Modeling, Drug Discovery and Clinical Applications, in= Tirnitz-Parker, J.E.E. (Ed.), Hepatocellular Carcinoma. Codon Publications, Brisbane (AU).

Coon, B.G., Baeyens, N., Han, J., Budatha, M., Ross, T.D., Fang, J.S., Yun, S., Thomas, J.-L., Schwartz, M.A., 2015. Intramembrane binding of VE-cadherin to VEGFR2 and VEGFR3 assembles the endothelial mechanosensory complex. J. Cell Biol. 208, 975–986. https://doi.org/10.1083/jcb.201408103

Cooper, G.M., 2000. Microtubules. Cell Mol. Approach 2nd Ed.

Cooper, J.A., Sept, D., 2008. New Insights into Mechanism and Regulation of Actin Capping Protein. Int. Rev. Cell Mol. Biol. 267, 183–206. https://doi.org/10.1016/S1937-6448(08)00604-7

Courtemanche, N., 2018. Mechanisms of formin-mediated actin assembly and dynamics. Biophys. Rev. 10, 1553–1569. https://doi.org/10.1007/s12551-018-0468-6

Crawford, A.W., Michelsen, J.W., Beckerle, M.C., 1992. An interaction between zyxin and alpha-actinin. J. Cell Biol. 116, 1381–1393. https://doi.org/10.1083/jcb.116.6.1381

Crowley, L.C., Scott, A.P., Marfell, B.J., Boughaba, J.A., Chojnowski, G., Waterhouse, N.J., 2016. Measuring Cell Death by Propidium Iodide Uptake and Flow Cytometry. Cold Spring Harb. Protoc. 2016, pdb.prot087163. https://doi.org/10.1101/pdb.prot087163

Cunniffe, G.M., Díaz-Payno, P.J., Sheehy, E.J., Critchley, S.E., Almeida, H.V., Pitacco, P., Carroll, S.F., Mahon, O.R., Dunne, A., Levingstone, T.J., Moran, C.J., Brady, R.T., O'Brien, F.J., Brama, P.A.J., Kelly, D.J., 2019. Tissue-specific extracellular matrix scaffolds for the regeneration of spatially complex musculoskeletal tissues. Biomaterials 188, 63–73. https://doi.org/10.1016/j.biomaterials.2018.09.044

Dahl, K.N., Kalinowski, A., 2011. Nucleoskeleton mechanics at a glance. J. Cell Sci. 124, 675–678. https://doi.org/10.1242/jcs.069096

Dahl, K.N., Ribeiro, A.J.S., Lammerding, J., 2008. Nuclear shape, mechanics, and mechanotransduction. Circ. Res. 102, 1307–1318. https://doi.org/10.1161/CIRCRESAHA.108.173989

Danen, E.H.J., 2013. Integrins: An Overview of Structural and Functional Aspects. Landes Bioscience.

Dean, L., 2012. Tamoxifen Therapy and CYP2D6 Genotype, in= Pratt, V.M., Scott, S.A., Pirmohamed, M., Esquivel, B., Kane, M.S., Kattman, B.L., Malheiro, A.J. (Eds.), Medical Genetics Summaries. National Center for Biotechnology Information (US), Bethesda (MD).

Degli Esposti, D., Hamelin, J., Bosselut, N., Saffroy, R., Sebagh, M., Pommier, A., Martel, C., Lemoine, A., 2012. Mitochondrial Roles and Cytoprotection in Chronic Liver Injury. Biochem. Res. Int. 2012. https://doi.org/10.1155/2012/387626

Dehn, P.F., White, C.M., Conners, D.E., Shipkey, G., Cumbo, T.A., 2004. Characterization of the human hepatocellular carcinoma (HEPG2) cell line as an in vitro model for cadmium toxicity studies. Vitro Cell. Dev. Biol. - Anim. 40, 172–182. https://doi.org/10.1290/1543-706X(2004)40<172:COTHHC>2.0.CO;2

del Rio, A., Perez-Jimenez, R., Liu, R., Roca-Cusachs, P., Fernandez, J.M., Sheetz, M.P., 2009. Stretching single talin rod molecules activates vinculin binding. Science 323, 638–641. https://doi.org/10.1126/science.1162912

Delon, I., Brown, N.H., 2007. Integrins and the actin cytoskeleton. Curr. Opin. Cell Biol., Cell structure and dynamics 19, 43–50. https://doi.org/10.1016/j.ceb.2006.12.013

DeMali, K.A., Barlow, C.A., Burridge, K., 2002. Recruitment of the Arp2/3 complex to vinculin. J. Cell Biol. 159, 881–891. https://doi.org/10.1083/jcb.200206043

DeMali, K.A., Wennerberg, K., Burridge, K., 2003. Integrin signaling to the actin cytoskeleton. Curr. Opin. Cell Biol. 15, 572–582. https://doi.org/10.1016/S0955-0674(03)00109-1

Deng, P., You, T., Chen, X., Yuan, T., Huang, H., Zhong, D., 2011. Identification of Amiodarone Metabolites in Human Bile by Ultraperformance Liquid Chromatography/Quadrupole Time-of-Flight Mass Spectrometry. Drug Metab. Dispos. 39, 1058–1069. https://doi.org/10.1124/dmd.110.037671

Densham, R.M., O'Neill, E., Munro, J., König, I., Anderson, K., Kolch, W., Olson, M.F., 2009. MST Kinases Monitor Actin Cytoskeletal Integrity and Signal via c-Jun N-Terminal Kinase Stress-Activated Kinase To Regulate p21Waf1/Cip1 Stability. Mol. Cell. Biol. 29, 6380–6390. https://doi.org/10.1128/MCB.00116-09

Desai, R., Sarpal, R., Ishiyama, N., Pellikka, M., Ikura, M., Tepass, U., 2013. Monomeric α-catenin links cadherin to the actin cytoskeleton. Nat. Cell Biol. 15, 261–273. https://doi.org/10.1038/ncb2685

Desta, Z., Flockhart, D.A., 2017. Chapter 18 - Pharmacogenetics of Drug Metabolism, in= Robertson, D., Williams, G.H. (Eds.), Clinical and Translational Science (Second Edition). Academic Press, pp. 327–345. https://doi.org/10.1016/B978-0-12-802101-9.00018-1

Disanza, A., Steffen, A., Hertzog, M., Frittoli, E., Rottner, K., Scita, G., 2004. Actin polymerization machinery: the finish line of signaling networks, the starting point of cellular movement. Cell. Mol. Life Sci. CMLS. https://doi.org/10.1007/s00018-004-4472-6

Donato, M.T., Tolosa, L., Gómez-Lechón, M.J., 2015. Culture and Functional Characterization of Human Hepatoma HepG2 Cells. Methods Mol. Biol. Clifton NJ 1250, 77–93. https://doi.org/10.1007/978-1-4939-2074-7_5

Dong, J.-M., Lau, L.-S., Ng, Y.-W., Lim, L., Manser, E., 2009. Paxillin nuclear-cytoplasmic localization is regulated by phosphorylation of the LD4 motif: evidence that nuclear paxillin promotes cell proliferation. Biochem. J. 418, 173–184. https://doi.org/10.1042/BJ20080170

Doyle, A.D., Carvajal, N., Jin, A., Matsumoto, K., Yamada, K.M., 2015. Local 3D matrix microenvironment regulates cell migration through spatiotemporal dynamics of contractility-dependent adhesions. Nat. Commun. 6, 8720. https://doi.org/10.1038/ncomms9720

Doyle, A.D., Yamada, K.M., 2016. Mechanosensing via cell-matrix adhesions in 3D microenvironments. Exp. Cell Res. 343, 60–66. https://doi.org/10.1016/j.yexcr.2015.10.033

Driscoll, T.P., Cosgrove, B.D., Heo, S.-J., Shurden, Z.E., Mauck, R.L., 2015. Cytoskeletal to Nuclear Strain Transfer Regulates YAP Signaling in Mesenchymal Stem Cells. Biophys. J. 108, 2783–2793. https://doi.org/10.1016/j.bpj.2015.05.010

Dupont, S., Morsut, L., Aragona, M., Enzo, E., Giulitti, S., Cordenonsi, M., Zanconato, F., Le Digabel, J., Forcato, M., Bicciato, S., Elvassore, N., Piccolo, S., 2011. Role of YAP/TAZ in mechanotransduction. Nature 474, 179–183. https://doi.org/10.1038/nature10137

Edfors, F., Danielsson, F., Hallström, B.M., Käll, L., Lundberg, E., Pontén, F., Forsström, B., Uhlén, M., 2016. Gene-specific correlation of RNA and protein levels in human cells and tissues. Mol. Syst. Biol. 12. https://doi.org/10.15252/msb.20167144

Edmondson, R., Broglie, J.J., Adcock, A.F., Yang, L., 2014a. Three-Dimensional Cell Culture Systems and Their Applications in Drug Discovery and Cell-Based Biosensors. Assay Drug Dev. Technol. 12, 207–218. https://doi.org/10.1089/adt.2014.573

Edmondson, R., Broglie, J.J., Adcock, A.F., Yang, L., 2014b. Three-Dimensional Cell Culture Systems and Their Applications in Drug Discovery and Cell-Based Biosensors. Assay Drug Dev. Technol. 12, 207–218. https://doi.org/10.1089/adt.2014.573

Eilenberger, C., Rothbauer, M., Ehmoser, E.-K., Ertl, P., Küpcü, S., 2019. Effect of Spheroidal Age on Sorafenib Diffusivity and Toxicity in a 3D HepG2 Spheroid Model. Sci. Rep. 9, 1–11. https://doi.org/10.1038/s41598-019-41273-3

Elje, E., Hesler, M., Rundén-Pran, E., Mann, P., Mariussen, E., Wagner, S., Dusinska, M., Kohl, Y., 2019. The comet assay applied to HepG2 liver spheroids. Comet Assay Vitro 845, 403033. https://doi.org/10.1016/j.mrgentox.2019.03.006

Elmore, S.A., Dixon, D., Hailey, J.R., Harada, T., Herbert, R.A., Maronpot, R.R., Nolte, T., Rehg, J.E., Rittinghausen, S., Rosol, T.J., Satoh, H., Vidal, J.D., Willard-Mack, C.L., Creasy, D.M., 2016. Recommendations from the INHAND Apoptosis/Necrosis Working Group. Toxicol. Pathol. 44, 173–188. https://doi.org/10.1177/0192623315625859

Elosegui-Artola, A., Andreu, I., Beedle, A.E.M., Lezamiz, A., Uroz, M., Kosmalska, A.J., Oria, R., Kechagia, J.Z., Rico-Lastres, P., Roux, A.-L.L., Shanahan, C.M., Trepat, X., Navajas, D., Garcia-Manyes, S., Roca-Cusachs, P., 2017. Force Triggers YAP Nuclear Entry by Regulating Transport across Nuclear Pores. Cell 171, 1397-1410.e14. https://doi.org/10.1016/j.cell.2017.10.008

Engler, A.J., Rehfeldt, F., Sen, S., Discher, D.E., 2007. Microtissue elasticity: measurements by atomic force microscopy and its influence on cell differentiation. Methods Cell Biol. 83, 521–545. https://doi.org/10.1016/S0091-679X(07)83022-6

Fabregat, A., Sidiropoulos, K., Viteri, G., Forner, O., Marin-Garcia, P., Arnau, V., D'Eustachio, P., Stein, L., Hermjakob, H., 2017. Reactome pathway analysis: a high-performance in-memory approach. BMC Bioinformatics 18, 142. https://doi.org/10.1186/s12859-017-1559-2

Fabry, B., Klemm, A.H., Kienle, S., Schäffer, T.E., Goldmann, W.H., 2011. Focal adhesion kinase stabilizes the cytoskeleton. Biophys. J. 101, 2131–2138. https://doi.org/10.1016/j.bpj.2011.09.043

Fanning, A.S., Van Itallie, C.M., Anderson, J.M., 2012. Zonula occludens-1 and -2 regulate apical cell structure and the zonula adherens cytoskeleton in polarized epithelia. Mol. Biol. Cell 23, 577–590. https://doi.org/10.1091/mbc.E11-09-0791

Fernández, B.G., Gaspar, P., Brás-Pereira, C., Jezowska, B., Rebelo, S.R., Janody, F., 2011. Actin-Capping Protein and the Hippo pathway regulate F-actin and tissue growth in Drosophila. Dev. Camb. Engl. 138, 2337–2346. https://doi.org/10.1242/dev.063545

Fernández-Sánchez, M.E., Barbier, S., Whitehead, J., Béalle, G., Michel, A., Latorre-Ossa, H., Rey, C., Fouassier, L., Claperon, A., Brullé, L., Girard, E., Servant, N., Rio-Frio, T., Marie, H., Lesieur, S., Housset, C., Gennisson, J.-L., Tanter, M., Ménager, C., Fre, S., Robine, S., Farge, E., 2015. Mechanical induction of the tumorigenic β-catenin pathway by tumour growth pressure. Nature 523, 92–95. https://doi.org/10.1038/nature14329

Ferron, F., Rebowski, G., Lee, S.H., Dominguez, R., 2007. Structural basis for the recruitment of profilin–actin complexes during filament elongation by Ena/VASP. EMBO J. 26, 4597–4606. https://doi.org/10.1038/sj.emboj.7601874

Fey, S.J., Wrzesinski, K., 2012. Determination of Drug Toxicity Using 3D Spheroids Constructed From an Immortal Human Hepatocyte Cell Line. Toxicol. Sci. 127, 403–411. https://doi.org/10.1093/toxsci/kfs122

Fink, J., Carpi, N., Betz, T., Bétard, A., Chebah, M., Azioune, A., Bornens, M., Sykes, C., Fetler, L., Cuvelier, D., Piel, M., 2011. External forces control mitotic spindle positioning. Nat. Cell Biol. 13, 771–778. https://doi.org/10.1038/ncb2269

Fischer, A.H., Jacobson, K.A., Rose, J., Zeller, R., 2008. Hematoxylin and eosin staining of tissue and cell sections. CSH Protoc. 2008, pdb.prot4986. https://doi.org/10.1101/pdb.prot4986

Flood, V.H., Scott, J.P., 2018. 38 - Bleeding and Thrombosis, in= Kliegman, R.M., Lye, P.S., Bordini, B.J., Toth, H., Basel, D. (Eds.), Nelson Pediatric Symptom-Based Diagnosis. Elsevier, pp. 682-700.e1. https://doi.org/10.1016/B978-0-323-39956-2.00038-8

Fontana, F., Raimondi, M., Marzagalli, M., Sommariva, M., Limonta, P., Gagliano, N., 2019. Epithelial-To-Mesenchymal Transition Markers and CD44 Isoforms Are Differently Expressed in 2D and 3D Cell Cultures of Prostate Cancer Cells. Cells 8. https://doi.org/10.3390/cells8020143

Freshney, R.I., 2010. Subculture and Cell Lines, in= Culture of Animal Cells. John Wiley & Sons, Inc., pp. 187–206. https://doi.org/10.1002/9780470649367.ch12

Freund, J.B., Goetz, J.G., Hill, K.L., Vermot, J., 2012. Fluid flows and forces in development: functions, features and biophysical principles. Dev. Camb. Engl. 139, 1229–1245. https://doi.org/10.1242/dev.073593

Friedrich, J., Seidel, C., Ebner, R., Kunz-Schughart, L.A., 2009. Spheroid-based drug screen= considerations and practical approach. Nat. Protoc. 4, 309–324. https://doi.org/10.1038/nprot.2008.226

Frtús, A., Smolková, B., Uzhytchak, M., Lunova, M., Jirsa, M., Hof, M., Jurkiewicz, P., Lozinsky, V.I., Wolfová, L., Petrenko, Y., Kubinová, Š., Dejneka, A., Lunov, O., 2020. Hepatic Tumor Cell Morphology Plasticity under Physical Constraints in 3D Cultures Driven by YAP–mTOR Axis. Pharmaceuticals 13, 430. https://doi.org/10.3390/ph13120430

Funk, C., 2008. The role of hepatic transporters in drug elimination. Expert Opin. Drug Metab. Toxicol. 4, 363–379. https://doi.org/10.1517/17425255.4.4.363

Gallin, W.J., 1997. Development and maintenance of bile canaliculi in vitro and in vivo. Microsc. Res. Tech. 39, 406–412. https://doi.org/10.1002/(SICI)1097-0029(19971201)39:5<406::AID-JEMT3>3.0.CO;2-E

Gaspar, P., Tapon, N., 2014. Sensing the local environment: actin architecture and Hippo signalling. Curr. Opin. Cell Biol. 31, 74–83. https://doi.org/10.1016/j.ceb.2014.09.003

Gaudet, P., Škunca, N., Hu, J.C., Dessimoz, C., 2017. Primer on the Gene Ontology. Methods Mol. Biol. Clifton NJ 1446, 25–37. https://doi.org/10.1007/978-1-4939-3743-1_3

Gemfibrozil, 2012. , in= LiverTox: Clinical and Research Information on Drug-Induced Liver Injury. National Institute of Diabetes and Digestive and Kidney Diseases, Bethesda (MD).

Gemfibrozil DrugBank [WWW Document], n.d. URL https://go.drugbank.com/drugs/DB01241 (accessed 1.4.21).

Géraud, C., Evdokimov, K., Straub, B.K., Peitsch, W.K., Demory, A., Dörflinger, Y., Schledzewski, K., Schmieder, A., Schemmer, P., Augustin, H.G., Schirmacher, P., Goerdt, S., 2012. Unique Cell Type-Specific Junctional Complexes in Vascular Endothelium of Human and Rat Liver Sinusoids. PLoS ONE 7. https://doi.org/10.1371/journal.pone.0034206

Gerets, H.H.J., Tilmant, K., Gerin, B., Chanteux, H., Depelchin, B.O., Dhalluin, S., Atienzar, F.A., 2012. Characterization of primary human hepatocytes, HepG2 cells, and HepaRG cells at the mRNA level and CYP activity in response to inducers and their predictivity for the detection of human hepatotoxins. Cell Biol. Toxicol. 28, 69–87. https://doi.org/10.1007/s10565-011-9208-4

Giacomini, K.M., Huang, S.-M., Tweedie, D.J., Benet, L.Z., Brouwer, K.L.R., Chu, X., Dahlin, A., Evers, R., Fischer, V., Hillgren, K.M., Hoffmaster, K.A., Ishikawa, T., Keppler, D., Kim, R.B., Lee, C.A., Niemi, M., Polli, J.W., Sugiyama, Y., Swaan, P.W., Ware, J.A., Wright, S.H., Wah Yee, S., Zamek-Gliszczynski, M.J., Zhang, L., The International Transporter Consortium, 2010. Membrane transporters in drug development. Nat. Rev. Drug Discov. 9, 215–236. https://doi.org/10.1038/nrd3028

Giannone, G., 2015. Super-resolution links vinculin localization to function in focal adhesions. Nat. Cell Biol. 17, 845–847. https://doi.org/10.1038/ncb3196

Gieni, R.S., Hendzel, M.J., 2008. Mechanotransduction from the ECM to the genome: are the pieces now in place? J. Cell. Biochem. 104, 1964–1987. https://doi.org/10.1002/jcb.21364

Gingras, A.R., Vogel, K.-P., Steinhoff, H.-J., Ziegler, W.H., Patel, B., Emsley, J., Critchley, D.R., Roberts, G.C.K., Barsukov, I.L., 2006. Structural and dynamic characterization of a vinculin binding site in the talin rod. Biochemistry 45, 1805–1817. https://doi.org/10.1021/bi052136l

Gissen, P., Arias, I.M., 2015. Structural and functional hepatocyte polarity and liver disease. J. Hepatol. 63, 1023–1037. https://doi.org/10.1016/j.jhep.2015.06.015

Gkretsi, V., Apte, U., Mars, W.M., Bowen, W.C., Luo, J.-H., Yang, Y., Yu, Y.P., Orr, A., St.-Arnaud, R., Dedhar, S., Kaestner, K.H., Wu, C., Michalopoulos, G.K., 2008. Liver-Specific Ablation of Integrin-Linked Kinase in Mice Results in Abnormal Histology, Enhanced Cell Proliferation, and Hepatomegaly. Hepatol. Baltim. Md 48, 1932–1941. https://doi.org/10.1002/hep.22537

Goda, N., Dozier, S.J., Johnson, R.S., 2003. HIF-1 in cell cycle regulation, apoptosis, and tumor progression. Antioxid. Redox Signal. 5, 467–473. https://doi.org/10.1089/152308603768295212

Godoy, P., Hewitt, N.J., Albrecht, U., Andersen, M.E., Ansari, N., Bhattacharya, S., Bode, J.G., Bolleyn, J., Borner, C., Böttger, J., Braeuning, A., Budinsky, R.A., Burkhardt, B., Cameron, N.R., Camussi, G., Cho, C.-S., Choi, Y.-J., Craig Rowlands, J., Dahmen, U., Damm, G., Dirsch, O., Donato, M.T., Dong, J., Dooley, S., Drasdo, D., Eakins, R., Ferreira, K.S., Fonsato, V., Fraczek, J., Gebhardt, R., Gibson, A., Glanemann, M., Goldring, C.E.P., Gómez-Lechón, M.J., Groothuis, G.M.M., Gustavsson, L., Guyot, C., Hallifax, D., Hammad, S., Hayward, A., Häussinger, D., Hellerbrand, C., Hewitt, P., Hoehme, S., Holzhütter, H.-G., Houston, J.B., Hrach, J., Ito, K., Jaeschke, H., Keitel, V., Kelm, J.M., Kevin Park, B., Kordes, C., Kullak-Ublick, G.A., LeCluyse, E.L., Lu, P., Luebke-Wheeler, J., Lutz, A., Maltman, D.J., Matz-Soja, M., McMullen, P., Merfort, I., Messner, S., Meyer, C., Mwinyi, J., Naisbitt, D.J., Nussler, A.K., Olinga, P., Pampaloni, F., Pi, J., Pluta, L., Przyborski, S.A., Ramachandran, A., Rogiers, V., Rowe, C., Schelcher, C., Schmich, K., Schwarz, M., Singh, B., Stelzer, E.H.K., Stieger, B., Stöber, R., Sugiyama, Y., Tetta, C., Thasler, W.E., Vanhaecke, T., Vinken, M., Weiss, T.S.,

Widera, A., Woods, C.G., Xu, J.J., Yarborough, K.M., Hengstler, J.G., 2013. Recent advances in 2D and 3D in vitro systems using primary hepatocytes, alternative hepatocyte sources and non-parenchymal liver cells and their use in investigating mechanisms of hepatotoxicity, cell signaling and ADME. Arch. Toxicol. 87, 1315–1530. https://doi.org/10.1007/s00204-013-1078-5

Goffin, J.M., Pittet, P., Csucs, G., Lussi, J.W., Meister, J.-J., Hinz, B., 2006. Focal adhesion size controls tension-dependent recruitment of alpha-smooth muscle actin to stress fibers. J. Cell Biol. 172, 259–268. https://doi.org/10.1083/jcb.200506179

Goldmann, W.H., 2012. Mechanotransduction and focal adhesions. Cell Biol. Int. 36, 649–652. https://doi.org/10.1042/CBI20120184

Graham, D.M., Burridge, K., 2016. Mechanotransduction and nuclear function. Curr. Opin. Cell Biol. 40, 98–105. https://doi.org/10.1016/j.ceb.2016.03.006

Grashoff, C., Hoffman, B.D., Brenner, M.D., Zhou, R., Parsons, M., Yang, M.T., McLean, M.A., Sligar, S.G., Chen, C.S., Ha, T., Schwartz, M.A., 2010. Measuring mechanical tension across vinculin reveals regulation of focal adhesion dynamics. Nature 466, 263–266. https://doi.org/10.1038/nature09198

Greer, M.L., Barber, J., Eakins, J., Kenna, J.G., 2010. Cell based approaches for evaluation of drug-induced liver injury. This Issue Incl. Spec. Issue Sect. Highlights 2009 Annu. Congr. Br. Toxicol. Soc. 268, 125–131. https://doi.org/10.1016/j.tox.2009.08.007

Gruenbaum, Y., Goldman, R.D., Meyuhas, R., Mills, E., Margalit, A., Fridkin, A., Dayani, Y., Prokocimer, M., Enosh, A., 2003. The nuclear lamina and its functions in the nucleus. Int. Rev. Cytol. 226, 1–62. https://doi.org/10.1016/s0074-7696(03)01001-5

Gui, T., Sun, Y., Shimokado, A., Muragaki, Y., 2012. The Roles of Mitogen-Activated Protein Kinase Pathways in TGF-β-Induced Epithelial-Mesenchymal Transition. J. Signal Transduct. 2012. https://doi.org/10.1155/2012/289243

Guilak, F., Cohen, D.M., Estes, B.T., Gimble, J.M., Liedtke, W., Chen, C.S., 2009. Control of stem cell fate by physical interactions with the extracellular matrix. Cell Stem Cell 5, 17. https://doi.org/10.1016/j.stem.2009.06.016

Guilluy, C., Burridge, K., 2015. Nuclear mechanotransduction= Forcing the nucleus to respond. Nucleus 6, 19–22. https://doi.org/10.1080/19491034.2014.1001705

Guilluy, C., Swaminathan, V., Garcia-Mata, R., O'Brien, E.T., Superfine, R., Burridge, K., 2011. The Rho GEFs LARG and GEF-H1 regulate the mechanical response to force on integrins. Nat. Cell Biol. 13, 722–727. https://doi.org/10.1038/ncb2254

Günzel, D., Yu, A.S.L., 2013. Claudins and the Modulation of Tight Junction Permeability. Physiol. Rev. 93, 525–569. https://doi.org/10.1152/physrev.00019.2012

Gurski, L., 2010. 3D Matrices for Anti-Cancer Drug Testing and Development. ResearchGate 20–25.

Guzzardi, M.A., Vozzi, F., Ahluwalia, A.D., 2009. Study of the crosstalk between hepatocytes and endothelial cells using a novel multicompartmental bioreactor: a comparison between connected cultures and cocultures. Tissue Eng. Part A 15, 3635–3644. https://doi.org/10.1089/ten.TEA.2008.0695

Gwak, G.-Y., Yoon, J.-H., Yu, S.J., Park, S.C., Jang, J.J., Lee, K.B., Lee, S.-H., Lee, S.-M., Shin, C.S., Suh, K.-S., Lee, H.-S., 2006. Anti-apoptotic N-cadherin signaling and its prognostic implication in human hepatocellular carcinomas. Oncol. Rep. 15, 1117–1123. https://doi.org/10.3892/or.15.5.1117

Haase, K., Macadangdang, J.K.L., Edrington, C.H., Cuerrier, C.M., Hadjiantoniou, S., Harden, J.L., Skerjanc, I.S., Pelling, A.E., 2016. Extracellular Forces Cause the Nucleus to Deform in a Highly Controlled Anisotropic Manner. Sci. Rep. 6, 21300. https://doi.org/10.1038/srep21300

Haining, A.W.M., von Essen, M., Attwood, S.J., Hytönen, V.P., del Río Hernández, A., 2016. All Subdomains of the Talin Rod Are Mechanically Vulnerable and May Contribute To

Cellular Mechanosensing. ACS Nano 10, 6648–6658. https://doi.org/10.1021/acsnano.6b01658
Hansen, C.G., Moroishi, T., Guan, K.-L., 2015. YAP and TAZ: a nexus for Hippo signaling and beyond. Trends Cell Biol. 25, 499–513. https://doi.org/10.1016/j.tcb.2015.05.002
Hansen, M.D.H., Beckerle, M.C., 2006. Opposing Roles of Zyxin/LPP ACTA Repeats and the LIM Domain Region in Cell-Cell Adhesion. J. Biol. Chem. 281, 16178–16188. https://doi.org/10.1074/jbc.M512771200
Haque, F., Lloyd, D.J., Smallwood, D.T., Dent, C.L., Shanahan, C.M., Fry, A.M., Trembath, R.C., Shackleton, S., 2006. SUN1 Interacts with Nuclear Lamin A and Cytoplasmic Nesprins To Provide a Physical Connection between the Nuclear Lamina and the Cytoskeleton. Mol. Cell. Biol. 26, 3738–3751. https://doi.org/10.1128/MCB.26.10.3738-3751.2006
Harris, A.J., Dial, S.L., Casciano, D.A., 2004. Comparison of basal gene expression profiles and effects of hepatocarcinogens on gene expression in cultured primary human hepatocytes and HepG2 cells. Mutat. Res. 549, 79–99. https://doi.org/10.1016/j.mrfmmm.2003.11.014
Harris, A.R., Jreij, P., Fletcher, D.A., 2018. Mechanotransduction by the Actin Cytoskeleton= Converting Mechanical Stimuli into Biochemical Signals. Annu. Rev. Biophys. 47, 617–631. https://doi.org/10.1146/annurev-biophys-070816-033547
Hart, S.N., Li, Y., Nakamoto, K., Subileau, E., Steen, D., Zhong, X., 2010. A Comparison of Whole Genome Gene Expression Profiles of HepaRG Cells and HepG2 Cells to Primary Human Hepatocytes and Human Liver Tissues. Drug Metab. Dispos. 38, 988–994. https://doi.org/10.1124/dmd.109.031831
Hartsock, A., Nelson, W.J., 2008. Adherens and Tight Junctions: Structure, Function and Connections to the Actin Cytoskeleton. Biochim. Biophys. Acta 1778, 660–669. https://doi.org/10.1016/j.bbamem.2007.07.012
Hatte, G., Prigent, C., Tassan, J.-P., 2018. Tight junctions negatively regulate mechanical forces applied to adherens junctions in vertebrate epithelial tissue. J. Cell Sci. 131. https://doi.org/10.1242/jcs.208736
Hayakawa, K., Tatsumi, H., Sokabe, M., 2011. Actin filaments function as a tension sensor by tension-dependent binding of cofilin to the filament. J. Cell Biol. 195, 721–727. https://doi.org/10.1083/jcb.201102039
Haycock, J.W., 2011. 3D cell culture: a review of current approaches and techniques. Methods Mol. Biol. Clifton NJ 695, 1–15. https://doi.org/10.1007/978-1-60761-984-0_1
Hempel, M., Schmitz, A., Winkler, S., Kucukoglu, O., Brückner, S., Niessen, C., Christ, B., 2015. Pathological implications of cadherin zonation in mouse liver. Cell. Mol. Life Sci. 72, 2599–2612. https://doi.org/10.1007/s00018-015-1861-y
Heng, B.C., Cowan, C.M., Basu, S., 2009. Comparison of Enzymatic and Non-Enzymatic Means of Dissociating Adherent Monolayers of Mesenchymal Stem Cells. Biol. Proced. Online 11, 161–169. https://doi.org/10.1007/s12575-009-9001-4
Heo, S.-J., Driscoll, T.P., Thorpe, S.D., Nerurkar, N.L., Baker, B.M., Yang, M.T., Chen, C.S., Lee, D.A., Mauck, R.L., 2016a. Differentiation alters stem cell nuclear architecture, mechanics, and mechano-sensitivity. eLife 5. https://doi.org/10.7554/eLife.18207
Heo, S.-J., Han, W.M., Szczesny, S.E., Cosgrove, B.D., Elliott, D.M., Lee, D.A., Duncan, R.L., Mauck, R.L., 2016b. Mechanically Induced Chromatin Condensation Requires Cellular Contractility in Mesenchymal Stem Cells. Biophys. J. 111, 864–874. https://doi.org/10.1016/j.bpj.2016.07.006
Hep G2 [HEPG2] ATCC® HB-8065™ [WWW Document], n.d. URL https://www.lgcstandards-atcc.org/products/all/HB-8065.aspx?geo_country=gb (accessed 3.12.21).
Herrema, H., Czajkowska, D., Théard, D., van der Wouden, J.M., Kalicharan, D., Zolghadr, B., Hoekstra, D., van IJzendoorn, S.C.D., 2006. Rho Kinase, Myosin-II, and p42/44 MAPK

Control Extracellular Matrix-mediated Apical Bile Canalicular Lumen Morphogenesis in HepG2 Cells. Mol. Biol. Cell 17, 3291–3303. https://doi.org/10.1091/mbc.E06-01-0067

Heslop, J.A., Rowe, C., Walsh, J., Sison-Young, R., Jenkins, R., Kamalian, L., Kia, R., Hay, D., Jones, R.P., Malik, H.Z., Fenwick, S., Chadwick, A.E., Mills, J., Kitteringham, N.R., Goldring, C.E.P., Park, B.K., 2017. Mechanistic evaluation of primary human hepatocyte culture using global proteomic analysis reveals a selective dedifferentiation profile. Arch. Toxicol. 91, 439–452. https://doi.org/10.1007/s00204-016-1694-y

Hieda, M., 2019. Signal Transduction across the Nuclear Envelope: Role of the LINC Complex in Bidirectional Signaling. Cells 8. https://doi.org/10.3390/cells8020124

Higashi, T., Arnold, T.R., Stephenson, R.E., Dinshaw, K.M., Miller, A.L., 2016. Maintenance of the Epithelial Barrier and Remodeling of Cell-Cell Junctions during Cytokinesis. Curr. Biol. CB 26, 1829–1842. https://doi.org/10.1016/j.cub.2016.05.036

Hirata, H., Tatsumi, H., Sokabe, M., 2008a. Zyxin emerges as a key player in the mechanotransduction at cell adhesive structures. Commun. Integr. Biol. 1, 192–195.

Hirata, H., Tatsumi, H., Sokabe, M., 2008b. Mechanical forces facilitate actin polymerization at focal adhesions in a zyxin-dependent manner. J. Cell Sci. 121, 2795–2804. https://doi.org/10.1242/jcs.030320

Hoffman, L.M., Jensen, C.C., Kloeker, S., Wang, C.-L.A., Yoshigi, M., Beckerle, M.C., 2006. Genetic ablation of zyxin causes Mena/VASP mislocalization, increased motility, and deficits in actin remodeling. J. Cell Biol. 172, 771–782. https://doi.org/10.1083/jcb.200512115

Holczbauer, Á., Gyöngyösi, B., Lotz, G., Törzsök, P., Kaposi-Novák, P., Szijártó, A., Tátrai, P., Kupcsulik, P., Schaff, Z., Kiss, A., 2014. Increased Expression of Claudin-1 and Claudin-7 in Liver Cirrhosis and Hepatocellular Carcinoma. Pathol. Oncol. Res. 20, 493–502. https://doi.org/10.1007/s12253-013-9683-4

Hongisto, V., Jernström, S., Fey, V., Mpindi, J.-P., Kleivi Sahlberg, K., Kallioniemi, O., Perälä, M., 2013. High-Throughput 3D Screening Reveals Differences in Drug Sensitivities between Culture Models of JIMT1 Breast Cancer Cells. PLoS ONE 8. https://doi.org/10.1371/journal.pone.0077232

Hotulainen, P., Lappalainen, P., 2006. Stress fibers are generated by two distinct actin assembly mechanisms in motile cells. J. Cell Biol. 173, 383–394. https://doi.org/10.1083/jcb.200511093

Hu, S., Eberhard, L., Chen, J., Love, J.C., Butler, J.P., Fredberg, J.J., Whitesides, G.M., Wang, N., 2004. Mechanical anisotropy of adherent cells probed by a three-dimensional magnetic twisting device. Am. J. Physiol. Cell Physiol. 287, C1184-1191. https://doi.org/10.1152/ajpcell.00224.2004

Humphrey, J.D., Dufresne, E.R., Schwartz, M.A., 2014. Mechanotransduction and extracellular matrix homeostasis. Nat. Rev. Mol. Cell Biol. 15, 802–812. https://doi.org/10.1038/nrm3896

Humphries, J.D., Byron, A., Humphries, M.J., 2006. Integrin ligands at a glance. J. Cell Sci. 119, 3901–3903. https://doi.org/10.1242/jcs.03098

Humphries, J.D., Wang, P., Streuli, C., Geiger, B., Humphries, M.J., Ballestrem, C., 2007. Vinculin controls focal adhesion formation by direct interactions with talin and actin. J. Cell Biol. 179, 1043–1057. https://doi.org/10.1083/jcb.200703036

Hurrell, T., Lilley, K.S., Cromarty, A.D., 2019. Proteomic responses of HepG2 cell monolayers and 3D spheroids to selected hepatotoxins. Toxicol. Lett. 300, 40–50. https://doi.org/10.1016/j.toxlet.2018.10.030

Hurrell, T., Segeritz, C.-P., Vallier, L., Lilley, K.S., Cromarty, A.D., 2018. Proteomic Comparison of Various Hepatic Cell Cultures for Preclinical Safety Pharmacology. Toxicol. Sci. 164, 229–239. https://doi.org/10.1093/toxsci/kfy084

Huveneers, S., Oldenburg, J., Spanjaard, E., van der Krogt, G., Grigoriev, I., Akhmanova, A., Rehmann, H., de Rooij, J., 2012. Vinculin associates with endothelial VE-cadherin junctions to control force-dependent remodeling. J. Cell Biol. 196, 641–652. https://doi.org/10.1083/jcb.201108120

Hynes, R.O., 2002. Integrins: bidirectional, allosteric signaling machines. Cell 110, 673–687.

Ibuprofen, 2012. , in= LiverTox: Clinical and Research Information on Drug-Induced Liver Injury. National Institute of Diabetes and Digestive and Kidney Diseases, Bethesda (MD).

Ibuprofen DrugBank [WWW Document], n.d. URL https://go.drugbank.com/drugs/DB01050 (accessed 1.4.21).

Imamura, Y., Mukohara, T., Shimono, Y., Funakoshi, Y., Chayahara, N., Toyoda, M., Kiyota, N., Takao, S., Kono, S., Nakatsura, T., Minami, H., 2015. Comparison of 2D- and 3D-culture models as drug-testing platforms in breast cancer. Oncol. Rep. 33, 1837–1843. https://doi.org/10.3892/or.2015.3767

Ingber, D.E., 2006. Cellular mechanotransduction= putting all the pieces together again. FASEB J. Off. Publ. Fed. Am. Soc. Exp. Biol. 20, 811–827. https://doi.org/10.1096/fj.05-5424rev

Ingber, D.E., 2003. Mechanosensation through integrins: Cells act locally but think globally. Proc. Natl. Acad. Sci. 100, 1472–1474. https://doi.org/10.1073/pnas.0530201100

Isoniazid, 2012. , in= LiverTox: Clinical and Research Information on Drug-Induced Liver Injury. National Institute of Diabetes and Digestive and Kidney Diseases, Bethesda (MD).

Jain, R., Chittiboyina, S., Chang, C.-L., Lelièvre, S.A., Savran, C.A., 2020. Deterministic culturing of single cells in 3D. Sci. Rep. 10, 1–13. https://doi.org/10.1038/s41598-020-67674-3

Jedlitschky, G., Hoffmann, U., Kroemer, H.K., 2006. Structure and function of the MRP2 (ABCC2) protein and its role in drug disposition. Expert Opin. Drug Metab. Toxicol. 2, 351–366. https://doi.org/10.1517/17425255.2.3.351

Jennen, D.G.J., Magkoufopoulou, C., Ketelslegers, H.B., van Herwijnen, M.H.M., Kleinjans, J.C.S., van Delft, J.H.M., 2010. Comparison of HepG2 and HepaRG by whole-genome gene expression analysis for the purpose of chemical hazard identification. Toxicol. Sci. Off. J. Soc. Toxicol. 115, 66–79. https://doi.org/10.1093/toxsci/kfq026

Jensen, C., Teng, Y., 2020. Is It Time to Start Transitioning From 2D to 3D Cell Culture? Front. Mol. Biosci. 7. https://doi.org/10.3389/fmolb.2020.00033

Jersey, D.M.L., PharmD, BCPS, BCPP Clinical Pharmacist Somerset, New, 2016. Drug-Induced Liver Injury: An Overview [WWW Document]. URL https://www.uspharmacist.com/article/druginduced-liver-injury-an-overview (accessed 1.4.21).

Jia, Z., Cheng, Y., Jiang, X., Zhang, C., Wang, G., Xu, J., Li, Y., Peng, Q., Gao, Y., 2020. 3D Culture System for Liver Tissue Mimicking Hepatic Plates for Improvement of Human Hepatocyte (C3A) Function and Polarity [WWW Document]. BioMed Res. Int. https://doi.org/10.1155/2020/6354183

Jj, X., Pv, H., Mc, D., Ar, S., Jr, C., D, de G., 2008. Cellular imaging predictions of clinical drug-induced liver injury [WWW Document]. Toxicol. Sci. Off. J. Soc. Toxicol. https://doi.org/10.1093/toxsci/kfn109

Jo, J., Abdi Nansa, S., Kim, D.-H., 2020. Molecular Regulators of Cellular Mechanoadaptation at Cell–Material Interfaces. Front. Bioeng. Biotechnol. 8.

Johnson, S.C., 1967. Hierarchical clustering schemes. Psychometrika 32, 241–254. https://doi.org/10.1007/BF02289588

Kadrmas, J.L., Beckerle, M.C., 2004. The LIM domain= from the cytoskeleton to the nucleus. Nat. Rev. Mol. Cell Biol. 5, 920–931. https://doi.org/10.1038/nrm1499

Kanehisa, M., Goto, S., 2000. KEGG: Kyoto Encyclopedia of Genes and Genomes. Nucleic Acids Res. 28, 27–30.

Kanno, Y., Inouye, Y., 2010. A consecutive three alanine residue insertion mutant of human CAR: a novel CAR ligand screening system in HepG2 cells. J. Toxicol. Sci. 35, 515–525. https://doi.org/10.2131/jts.35.515

Katsumi, A., Naoe, T., Matsushita, T., Kaibuchi, K., Schwartz, M.A., 2005. Integrin Activation and Matrix Binding Mediate Cellular Responses to Mechanical Stretch. J. Biol. Chem. 280, 16546–16549. https://doi.org/10.1074/jbc.C400455200

Katz, B.-Z., Zamir, E., Bershadsky, A., Kam, Z., Yamada, K.M., Geiger, B., 2000. Physical State of the Extracellular Matrix Regulates the Structure and Molecular Composition of Cell-Matrix Adhesions. Mol. Biol. Cell 11, 1047–1060.

Kelm, J.M., Timmins, N.E., Brown, C.J., Fussenegger, M., Nielsen, L.K., 2003. Method for generation of homogeneous multicellular tumor spheroids applicable to a wide variety of cell types. Biotechnol. Bioeng. 83, 173–180. https://doi.org/10.1002/bit.10655

Kenna, J.G., Uetrecht, J., 2018. Do In Vitro Assays Predict Drug Candidate Idiosyncratic Drug-Induced Liver Injury Risk? Drug Metab. Dispos. 46, 1658–1669. https://doi.org/10.1124/dmd.118.082719

Kepp, D.R., Sidelmann, U.G., Hansen, S.H., 1997. Isolation and characterization of major phase I and II metabolites of ibuprofen. Pharm. Res. 14, 676–680. https://doi.org/10.1023/a:1012125700497

Khalil, M., Shariat-Panahi, A., Tootle, R., Ryder, T., McCloskey, P., Roberts, E., Hodgson, H., Selden, C., 2001. Human hepatocyte cell lines proliferating as cohesive spheroid colonies in alginate markedly upregulate both synthetic and detoxificatory liver function. J. Hepatol. 34, 68–77. https://doi.org/10.1016/s0168-8278(00)00080-5

Khatau, S.B., Hale, C.M., Stewart-Hutchinson, P.J., Patel, M.S., Stewart, C.L., Searson, P.C., Hodzic, D., Wirtz, D., 2009. A perinuclear actin cap regulates nuclear shape. Proc. Natl. Acad. Sci. U. S. A. 106, 19017–19022. https://doi.org/10.1073/pnas.0908686106

Kiamehr, M., Heiskanen, L., Laufer, T., Düsterloh, A., Kahraman, M., Käkelä, R., Laaksonen, R., Aalto-Setälä, K., 2019. Dedifferentiation of Primary Hepatocytes is Accompanied with Reorganization of Lipid Metabolism Indicated by Altered Molecular Lipid and miRNA Profiles. Int. J. Mol. Sci. 20. https://doi.org/10.3390/ijms20122910

Kietzmann, T., 2017. Metabolic zonation of the liver: The oxygen gradient revisited. Redox Biol. 11, 622–630. https://doi.org/10.1016/j.redox.2017.01.012

Kim, B.S., Lee, J.-S., Gao, G., Cho, D.-W., 2017. Direct 3D cell-printing of human skin with functional transwell system. Biofabrication 9, 025034. https://doi.org/10.1088/1758-5090/aa71c8

Kim, D.-H., Chambliss, A.B., Wirtz, D., 2013. The multi-faceted role of the actin cap in cellular mechanosensation and mechanotransduction. Soft Matter 9, 5516–5523. https://doi.org/10.1039/C3SM50798J

Kim, J.B., 2005. Three-dimensional tissue culture models in cancer biology. Semin. Cancer Biol., 3D Cultures in Cancer Biology 15, 365–377. https://doi.org/10.1016/j.semcancer.2005.05.002

Kim, J.-G., Islam, R., Cho, J.Y., Jeong, H., Cap, K.-C., Park, Y., Hossain, A.J., Park, J.-B., 2018. Regulation of RhoA GTPase and various transcription factors in the RhoA pathway. J. Cell. Physiol. 233, 6381–6392. https://doi.org/10.1002/jcp.26487

Kim, K.I., Lee, Y.J., Lee, T.S., Song, I., Cheon, G.J., Lim, S.M., Chung, J.-K., Kang, J.H., 2013. In Vitro Radionuclide Therapy and In Vivo Scintigraphic Imaging of Alpha-Fetoprotein-Producing Hepatocellular Carcinoma by Targeted Sodium Iodide Symporter Gene Expression. Nucl. Med. Mol. Imaging 47, 1–8. https://doi.org/10.1007/s13139-012-0166-4

Kim, N.-G., Koh, E., Chen, X., Gumbiner, B.M., 2011. E-cadherin mediates contact inhibition of proliferation through Hippo signaling-pathway components. Proc. Natl. Acad. Sci. U. S. A. 108, 11930–11935. https://doi.org/10.1073/pnas.1103345108

Kim, Y., Rajagopalan, P., 2010. 3D Hepatic Cultures Simultaneously Maintain Primary Hepatocyte and Liver Sinusoidal Endothelial Cell Phenotypes. PLOS ONE 5, e15456. https://doi.org/10.1371/journal.pone.0015456

Kimura, K., Ito, M., Amano, M., Chihara, K., Fukata, Y., Nakafuku, M., Yamamori, B., Feng, J., Nakano, T., Okawa, K., Iwamatsu, A., Kaibuchi, K., 1996. Regulation of myosin phosphatase by Rho and Rho-associated kinase (Rho-kinase). Science 273, 245–248. https://doi.org/10.1126/science.273.5272.245

Klein, D.J., Boukouvala, S., McDonagh, E.M., Shuldiner, S.R., Laurieri, N., Thorn, C.F., Altman, R.B., Klein, T.E., 2016. PharmGKB summary: isoniazid pathway, pharmacokinetics. Pharmacogenet. Genomics 26, 436–444. https://doi.org/10.1097/FPC.0000000000000232

Klein, D.J., Thorn, C.F., Desta, Z., Flockhart, D.A., Altman, R.B., Klein, T.E., 2013. PharmGKB summary: tamoxifen pathway, pharmacokinetics. Pharmacogenet. Genomics 23, 643–647. https://doi.org/10.1097/FPC.0b013e3283656bc1

Komiya, Y., Habas, R., 2008. Wnt signal transduction pathways. Organogenesis 4, 68–75.

Koussounadis, A., Langdon, S.P., Um, I.H., Harrison, D.J., Smith, V.A., 2015. Relationship between differentially expressed mRNA and mRNA-protein correlations in a xenograft model system. Sci. Rep. 5, 1–9. https://doi.org/10.1038/srep10775

Kubiczkova, L., Sedlarikova, L., Hajek, R., Sevcikova, S., 2012. TGF-β – an excellent servant but a bad master. J. Transl. Med. 10, 183. https://doi.org/10.1186/1479-5876-10-183

Kular, J.K., Basu, S., Sharma, R.I., 2014. The extracellular matrix: Structure, composition, age-related differences, tools for analysis and applications for tissue engineering. J. Tissue Eng. 5, 2041731414557112. https://doi.org/10.1177/2041731414557112

Kuleshov, M.V., Jones, M.R., Rouillard, A.D., Fernandez, N.F., Duan, Q., Wang, Z., Koplev, S., Jenkins, S.L., Jagodnik, K.M., Lachmann, A., McDermott, M.G., Monteiro, C.D., Gundersen, G.W., Ma'ayan, A., 2016. Enrichr: a comprehensive gene set enrichment analysis web server 2016 update. Nucleic Acids Res. 44, W90–W97. https://doi.org/10.1093/nar/gkw377

Kulkarni, K., Larsen, P., Linninger, A.A., 2008. Assessing chronic liver toxicity based on relative gene expression data. J. Theor. Biol. 254, 308–318. https://doi.org/10.1016/j.jtbi.2008.05.032

Kumar, A., Mazzanti, M., Mistrik, M., Kosar, M., Beznoussenko, G.V., Mironov, A.A., Garrè, M., Parazzoli, D., Shivashankar, G.V., Scita, G., Bartek, J., Foiani, M., 2014. ATR Mediates a Checkpoint at the Nuclear Envelope in Response to Mechanical Stress. Cell 158, 633–646. https://doi.org/10.1016/j.cell.2014.05.046

Kumar, P., Nagarajan, A., Uchil, P.D., 2018. Analysis of Cell Viability by the Lactate Dehydrogenase Assay. Cold Spring Harb. Protoc. 2018. https://doi.org/10.1101/pdb.prot095497

Lachowski, D., Cortes, E., Robinson, B., Rice, A., Rombouts, K., Del Río Hernández, A.E., 2018. FAK controls the mechanical activation of YAP, a transcriptional regulator required for durotaxis. FASEB J. Off. Publ. Fed. Am. Soc. Exp. Biol. 32, 1099–1107. https://doi.org/10.1096/fj.201700721R

Ladoux, B., Anon, E., Lambert, M., Rabodzey, A., Hersen, P., Buguin, A., Silberzan, P., Mège, R.-M., 2010. Strength dependence of cadherin-mediated adhesions. Biophys. J. 98, 534–542. https://doi.org/10.1016/j.bpj.2009.10.044

Lagies, S., Schlimpert, M., Neumann, S., Wäldin, A., Kammerer, B., Borner, C., Peintner, L., 2020. Cells grown in three-dimensional spheroids mirror in vivo metabolic response of epithelial cells. Commun. Biol. 3, 1–10. https://doi.org/10.1038/s42003-020-0973-6

Langhans, S.A., 2018. Three-Dimensional in Vitro Cell Culture Models in Drug Discovery and Drug Repositioning. Front. Pharmacol. 9. https://doi.org/10.3389/fphar.2018.00006

Latini, R., Tognoni, G., Kates, R.E., 1984. Clinical pharmacokinetics of amiodarone. Clin. Pharmacokinet. 9, 136–156. https://doi.org/10.2165/00003088-198409020-00002

Lauschke, V.M., Shafagh, R.Z., Hendriks, D.F.G., Ingelman-Sundberg, M., 2019. 3D Primary Hepatocyte Culture Systems for Analyses of Liver Diseases, Drug Metabolism, and Toxicity: Emerging Culture Paradigms and Applications. Biotechnol. J. 14, 1800347. https://doi.org/10.1002/biot.201800347

Lauschke, V.M., Vorrink, S.U., Moro, S.M.L., Rezayee, F., Nordling, Å., Hendriks, D.F.G., Bell, C.C., Sison-Young, R., Park, B.K., Goldring, C.E., Ellis, E., Johansson, I., Mkrtchian, S., Andersson, T.B., Ingelman-Sundberg, M., 2016. Massive rearrangements of cellular MicroRNA signatures are key drivers of hepatocyte dedifferentiation. Hepatol. Baltim. Md 64, 1743–1756. https://doi.org/10.1002/hep.28780

Le Beyec, J., Xu, R., Lee, S.-Y., Nelson, C.M., Rizki, A., Alcaraz, J., Bissell, M.J., 2007. Cell shape regulates global histone acetylation in human mammary epithelial cells. Exp. Cell Res. 313, 3066–3075. https://doi.org/10.1016/j.yexcr.2007.04.022

le Duc, Q., Shi, Q., Blonk, I., Sonnenberg, A., Wang, N., Leckband, D., de Rooij, J., 2010. Vinculin potentiates E-cadherin mechanosensing and is recruited to actin-anchored sites within adherens junctions in a myosin II–dependent manner. J. Cell Biol. 189, 1107–1115. https://doi.org/10.1083/jcb.201001149

Le, H.Q., Ghatak, S., Yeung, C.-Y.C., Tellkamp, F., Günschmann, C., Dieterich, C., Yeroslaviz, A., Habermann, B., Pombo, A., Niessen, C.M., Wickström, S.A., 2016. Mechanical regulation of transcription controls Polycomb-mediated gene silencing during lineage commitment. Nat. Cell Biol. 18, 864–875. https://doi.org/10.1038/ncb3387

Le Vee, M., Jouan, E., Noel, G., Stieger, B., Fardel, O., 2015. Polarized location of SLC and ABC drug transporters in monolayer-cultured human hepatocytes. Toxicol. In Vitro 29, 938–946. https://doi.org/10.1016/j.tiv.2015.03.019

Lech, W., Sarnowska, A., Kuczynska, Z., Dabrowski, F., Figiel-Dabrowska, A., Domanska-Janik, K., Buzanska, L., Zychowicz, M., 2020. Biomimetic microenvironmental preconditioning enhance neuroprotective properties of human mesenchymal stem cells derived from Wharton's Jelly (WJ-MSCs). Sci. Rep. 10, 1–15. https://doi.org/10.1038/s41598-020-74066-0

Leckband, D.E., Rooij, J. de, 2014. Cadherin Adhesion and Mechanotransduction. Annu. Rev. Cell Dev. Biol. 30, 291–315. https://doi.org/10.1146/annurev-cellbio-100913-013212

Lee, H.W., Kook, Y.-M., Lee, H.J., Park, H., Koh, W.-G., 2014. A three-dimensional co-culture of HepG2 spheroids and fibroblasts using double-layered fibrous scaffolds incorporated with hydrogel micropatterns. RSC Adv. 4, 61005–61011. https://doi.org/10.1039/C4RA12269K

Lee, W.M., 2003. Drug-induced hepatotoxicity. N. Engl. J. Med. 349, 474–485. https://doi.org/10.1056/NEJMra021844

Legate, K.R., Wickström, S.A., Fässler, R., 2009. Genetic and cell biological analysis of integrin outside-in signaling. Genes Dev. 23, 397–418. https://doi.org/10.1101/gad.1758709

Lelièvre, S.A., Kwok, T., Chittiboyina, S., 2017. Architecture in 3D Cell Culture: An Essential Feature for in vitro Toxicology. Toxicol. Vitro Int. J. Publ. Assoc. BIBRA 45, 287–295. https://doi.org/10.1016/j.tiv.2017.03.012

Lelièvre, S.A., Weaver, V.M., Nickerson, J.A., Larabell, C.A., Bhaumik, A., Petersen, O.W., Bissell, M.J., 1998. Tissue phenotype depends on reciprocal interactions between the extracellular matrix and the structural organization of the nucleus. Proc. Natl. Acad. Sci. U. S. A. 95, 14711–14716.

Lenz, M., Müller, F.-J., Zenke, M., Schuppert, A., 2016. Principal components analysis and the reported low intrinsic dimensionality of gene expression microarray data. Sci. Rep. 6, 1–11. https://doi.org/10.1038/srep25696

Lessey, E.C., Guilluy, C., Burridge, K., 2012. From mechanical force to RhoA activation. Biochemistry 51, 7420–7432. https://doi.org/10.1021/bi300758e

Li, F.-F., Zhang, B., Cui, J.-H., Chen, F.-L., Ding, Y., Feng, X., 2018. Alterations in β-catenin/E-cadherin complex formation during the mechanotransduction of Saos-2 osteoblastic cells. Mol. Med. Rep. 18, 1495–1503. https://doi.org/10.3892/mmr.2018.9146

Li, J., Hou, R., Niu, X., Liu, R., Wang, Q., Wang, C., Li, X., Hao, Z., Yin, G., Zhang, K., 2016. Comparison of microarray and RNA-Seq analysis of mRNA expression in dermal mesenchymal stem cells. Biotechnol. Lett. 38, 33–41. https://doi.org/10.1007/s10529-015-1963-5

Li, Y., Lu, J., Paxton, J.W., 2012. The role of ABC and SLC transporters in the pharmacokinetics of dietary and herbal phytochemicals and their interactions with xenobiotics. Curr. Drug Metab. 13, 624–639. https://doi.org/10.2174/1389200211209050624

Liao, Y., Wang, J., Jaehnig, E.J., Shi, Z., Zhang, B., 2019. WebGestalt 2019: gene set analysis toolkit with revamped UIs and APIs. Nucleic Acids Res. 47, W199–W205. https://doi.org/10.1093/nar/gkz401

Lin, R.-Z., Chou, L.-F., Chien, C.-C.M., Chang, H.-Y., 2006. Dynamic analysis of hepatoma spheroid formation= roles of E-cadherin and β1-integrin. Cell Tissue Res. 324, 411–422. https://doi.org/10.1007/s00441-005-0148-2

Link, J., Jahn, D., Alsheimer, M., 2015. Structural and functional adaptations of the mammalian nuclear envelope to meet the meiotic requirements. Nucleus 6, 93–101. https://doi.org/10.1080/19491034.2015.1004941

Liu, H., Lin, J., Roy, K., 2006. Effect of 3D scaffold and dynamic culture condition on the global gene expression profile of mouse embryonic stem cells. Biomater. Stem Cells 27, 5978–5989. https://doi.org/10.1016/j.biomaterials.2006.05.053

Liu, H., Roy, K., 2005. Biomimetic Three-Dimensional Cultures Significantly Increase Hematopoietic Differentiation Efficacy of Embryonic Stem Cells. Tissue Eng. 11, 319–330. https://doi.org/10.1089/ten.2005.11.319

Liu, J., Lin, A., 2005. Role of JNK activation in apoptosis: A double-edged sword. Cell Res. 15, 36–42. https://doi.org/10.1038/sj.cr.7290262

Liu, L., Luo, Q., Sun, J., Song, G., 2019. Cytoskeletal control of nuclear morphology and stiffness are required for OPN-induced bone-marrow-derived mesenchymal stem cell migration. Biochem. Cell Biol. https://doi.org/10.1139/bcb-2018-0263

Liu, N., Zhou, M., Zhang, Q., Yong, L., Zhang, T., Tian, T., Ma, Q., Lin, S., Zhu, B., Cai, X., 2018. Effect of substrate stiffness on proliferation and differentiation of periodontal ligament stem cells. Cell Prolif. 51, e12478. https://doi.org/10.1111/cpr.12478

Liu, Q., Pante, N., Misteli, T., Elsagga, M., Crisp, M., Hodzic, D., Burke, B., Roux, K.J., 2007. Functional association of Sun1 with nuclear pore complexes. J. Cell Biol. 178, 785–798. https://doi.org/10.1083/jcb.200704108

Liu, Z., Tan, J.L., Cohen, D.M., Yang, M.T., Sniadecki, N.J., Ruiz, S.A., Nelson, C.M., Chen, C.S., 2010. Mechanical tugging force regulates the size of cell-cell junctions. Proc. Natl. Acad. Sci. U. S. A. 107, 9944–9949. https://doi.org/10.1073/pnas.0914547107

Lombardi, M.L., Jaalouk, D.E., Shanahan, C.M., Burke, B., Roux, K.J., Lammerding, J., 2011. The interaction between nesprins and sun proteins at the nuclear envelope is critical for force transmission between the nucleus and cytoskeleton. J. Biol. Chem. 286, 26743–26753. https://doi.org/10.1074/jbc.M111.233700

López-Colomé, A.M., Lee-Rivera, I., Benavides-Hidalgo, R., López, E., 2017. Paxillin= a crossroad in pathological cell migration. J. Hematol. Oncol.J Hematol Oncol 10, 50. https://doi.org/10.1186/s13045-017-0418-y

Lovett, D.B., Shekhar, N., Nickerson, J.A., Roux, K.J., Lele, T.P., 2013. Modulation of Nuclear Shape by Substrate Rigidity. Cell. Mol. Bioeng. 6, 230–238. https://doi.org/10.1007/s12195-013-0270-2

Lu, J.-D., Xue, J., 2019. Chapter 101 - Poisoning: Kinetics to Therapeutics, in= Ronco, C., Bellomo, R., Kellum, J.A., Ricci, Z. (Eds.), Critical Care Nephrology (Third Edition). Elsevier, Philadelphia, pp. 600-629.e7. https://doi.org/10.1016/B978-0-323-44942-7.00101-1

Luckert, C., Schulz, C., Lehmann, N., Thomas, M., Hofmann, U., Hammad, S., Hengstler, J.G., Braeuning, A., Lampen, A., Hessel, S., 2017. Comparative analysis of 3D culture methods on human HepG2 cells. Arch. Toxicol. 91, 393–406. https://doi.org/10.1007/s00204-016-1677-z

Luckert, C., Schulz, C., Lehmann, N., Thomas, M., Hofmann, U., Hammad, S., Hengstler, J.G., Braeuning, A., Lampen, A., Hessel, S., 2016. Comparative analysis of 3D culture methods on human HepG2 cells. Arch. Toxicol. 1–14. https://doi.org/10.1007/s00204-016-1677-z

Lucumi Moreno, E., Hachi, S., Hemmer, K., J. Trietsch, S., S. Baumuratov, A., Hankemeier, T., Vulto, P., C. Schwamborn, J., T. Fleming, R.M., 2015. Differentiation of neuroepithelial stem cells into functional dopaminergic neurons in 3D microfluidic cell culture. Lab. Chip 15, 2419–2428. https://doi.org/10.1039/C5LC00180C

Luebke-Wheeler, J.L., Nedredal, G., Yee, L., Amiot, B.P., Nyberg, S.L., 2009. E-cadherin protects primary hepatocyte spheroids from cell death by a caspase-independent mechanism. Cell Transplant. 18, 1281–1287. https://doi.org/10.3727/096368909X474258

M, T., T, I., O, T., Ma, C., Bc, B., 1997. Mechanotransduction in endothelial cells: temporal signaling events in response to shear stress [WWW Document]. J. Vasc. Res. https://doi.org/10.1159/000159225

Maiuri, A.R., Wassink, B., Turkus, J.D., Breier, A.B., Lansdell, T., Kaur, G., Hession, S.L., Ganey, P.E., Roth, R.A., 2017. Synergistic Cytotoxicity from Drugs and Cytokines In Vitro as an Approach to Classify Drugs According to Their Potential to Cause Idiosyncratic Hepatotoxicity: A Proof-of-Concept Study. J. Pharmacol. Exp. Ther. 362, 459–473. https://doi.org/10.1124/jpet.117.242354

Malinen, M.M., Kanninen, L.K., Corlu, A., Isoniemi, H.M., Lou, Y.-R., Yliperttula, M.L., Urtti, A.O., 2014. Differentiation of liver progenitor cell line to functional organotypic cultures in 3D nanofibrillar cellulose and hyaluronan-gelatin hydrogels. Biomaterials 35, 5110–5121. https://doi.org/10.1016/j.biomaterials.2014.03.020

Mammoto, A., Mammoto, T., Ingber, D.E., 2012. Mechanosensitive mechanisms in transcriptional regulation. J. Cell Sci. 125, 3061–3073. https://doi.org/10.1242/jcs.093005

Manco, R., Leclercq, I.A., Clerbaux, L.-A., 2018. Liver Regeneration= Different Sub-Populations of Parenchymal Cells at Play Choreographed by an Injury-Specific Microenvironment. Int. J. Mol. Sci. 19. https://doi.org/10.3390/ijms19124115

Maronpot, R., 2016. Recommendations from the INHAND Apoptosis/Necrosis Working Group [WWW Document]. Toxicol. Pathol. URL

https://focusontoxpath.com/recommendations-from-the-inhand-apoptosisnecrosis-working-group/ (accessed 10.8.20).
Martinez-Hernandez, A., Amenta, P.S., 1993. The hepatic extracellular matrix. Virchows Arch. A 423, 77–84. https://doi.org/10.1007/BF01606580
Martino, F., Perestrelo, A.R., Vinarský, V., Pagliari, S., Forte, G., 2018a. Cellular Mechanotransduction= From Tension to Function. Front. Physiol. 9. https://doi.org/10.3389/fphys.2018.00824
Martino, F., Perestrelo, A.R., Vinarský, V., Pagliari, S., Forte, G., 2018b. Cellular Mechanotransduction= From Tension to Function. Front. Physiol. 9. https://doi.org/10.3389/fphys.2018.00824
Martino, F., Perestrelo, A.R., Vinarský, V., Pagliari, S., Forte, G., 2018c. Cellular Mechanotransduction= From Tension to Function. Front. Physiol. 9. https://doi.org/10.3389/fphys.2018.00824
Mateoiu, C., Pirici, A., Bogdan, F., 2011. Immunohistochemical nuclear staining for p53, PCNA, Ki-67 and bcl-2 in different histologic variants of basal cell carcinoma. Romanian J. Morphol. Embryol. Rev. Roum. Morphol. Embryol. 52, 315–319.
Mathur, J., Shenoy, V.B., Pathak, A., 2020. Mechanical memory in cells emerges from mechanotransduction with transcriptional feedback and epigenetic plasticity. bioRxiv 2020.03.20.000802. https://doi.org/10.1101/2020.03.20.000802
Mavri-Damelin, D., Eaton, S., Damelin, L.H., Rees, M., Hodgson, H.J.F., Selden, C., 2007. Ornithine transcarbamylase and arginase I deficiency are responsible for diminished urea cycle function in the human hepatoblastoma cell line HepG2. Int. J. Biochem. Cell Biol. 39, 555–564. https://doi.org/10.1016/j.biocel.2006.10.007
May, C.K., Carroll, C.W., 2018. Differential incorporation of SUN-domain proteins into LINC complexes is coupled to gene expression. PLoS ONE 13. https://doi.org/10.1371/journal.pone.0197621
Mayer, U., 2003. Integrins: Redundant or Important Players in Skeletal Muscle? J. Biol. Chem. 278, 14587–14590. https://doi.org/10.1074/jbc.R200022200
Mazaleuskaya, L.L., Theken, K.N., Gong, L., Thorn, C.F., FitzGerald, G.A., Altman, R.B., Klein, T.E., 2015. PharmGKB summary: ibuprofen pathways. Pharmacogenet. Genomics 25, 96–106. https://doi.org/10.1097/FPC.0000000000000113
McKee, T.J., Perlman, G., Morris, M., Komarova, S.V., 2019. Extracellular matrix composition of connective tissues: a systematic review and meta-analysis. Sci. Rep. 9, 1–15. https://doi.org/10.1038/s41598-019-46896-0
Mee, C.J., Harris, H.J., Farquhar, M.J., Wilson, G., Reynolds, G., Davis, C., van IJzendoorn, S.C.D., Balfe, P., McKeating, J.A., 2009. Polarization Restricts Hepatitis C Virus Entry into HepG2 Hepatoma Cells. J. Virol. 83, 6211–6221. https://doi.org/10.1128/JVI.00246-09
Mellad, J.A., Warren, D.T., Shanahan, C.M., 2011. Nesprins LINC the nucleus and cytoskeleton. Curr. Opin. Cell Biol. 23, 47–54. https://doi.org/10.1016/j.ceb.2010.11.006
Methotrexate, 2012. , in= LiverTox: Clinical and Research Information on Drug-Induced Liver Injury. National Institute of Diabetes and Digestive and Kidney Diseases, Bethesda (MD).
Methotrexate DrugBank [WWW Document], n.d. URL https://go.drugbank.com/drugs/DB00563 (accessed 1.4.21).
Michael, K.E., Dumbauld, D.W., Burns, K.L., Hanks, S.K., García, A.J., 2009. Focal Adhesion Kinase Modulates Cell Adhesion Strengthening via Integrin Activation. Mol. Biol. Cell 20, 2508–2519. https://doi.org/10.1091/mbc.E08-01-0076
Mijovic, Z., Kostov, M., Mihailovic, D., Zivkovic, N., Stojanovic, M., Zdravkovic, M., 2013. Correlation of nuclear morphometry of primary melanoma of the skin with

clinicopathological parameters and expression of tumor suppressor proteins (p53 and p16(INK4a)) and bcl-2 oncoprotein. J. BUON Off. J. Balk. Union Oncol. 18, 471–476.

Mikkelsen, T.S., Thorn, C.F., Yang, J.J., Ulrich, C.M., French, D., Zaza, G., Dunnenberger, H.M., Marsh, S., McLeod, H.L., Giacomini, K., Becker, M.L., Gaedigk, R., Leeder, J.S., Kager, L., Relling, M.V., Evans, W., Klein, T.E., Altman, R.B., 2011. PharmGKB summary: methotrexate pathway. Pharmacogenet. Genomics 21, 679–686. https://doi.org/10.1097/FPC.0b013e328343dd93

Miller, J.A., Surh, Y.J., 1994. Historical perspectives on conjugation-dependent bioactivation of foreign compounds. Adv. Pharmacol. San Diego Calif 27, 1–16. https://doi.org/10.1016/s1054-3589(08)61027-3

Milner, E., Ainsworth, M., McDonough, M., Stevens, B., Buehrer, J., Delzell, R., Wilson, C., Barnhill, J., 2020. Emerging Three-Dimensional Hepatic Models in Relation to Traditional Two-Dimensional In Vitro Assays for Evaluating Drug Metabolism and Hepatoxicity. Med. Drug Discov. 8, 100060. https://doi.org/10.1016/j.medidd.2020.100060

Miroshnikova, Y.A., Nava, M.M., Wickström, S.A., 2017. Emerging roles of mechanical forces in chromatin regulation. J. Cell Sci. 130, 2243–2250. https://doi.org/10.1242/jcs.202192

Mizuno, K., 2013. Signaling mechanisms and functional roles of cofilin phosphorylation and dephosphorylation. Cell. Signal. 25, 457–469. https://doi.org/10.1016/j.cellsig.2012.11.001

Moman, R.N., Gupta, N., Varacallo, M., 2020. Physiology, Albumin, in= StatPearls. StatPearls Publishing, Treasure Island (FL).

Morikawa, Y., Zhang, M., Heallen, T., Leach, J., Tao, G., Xiao, Y., Bai, Y., Li, W., Willerson, J.T., Martin, J.F., 2015. Actin cytoskeletal remodeling with protrusion formation is essential for heart regeneration in Hippo-deficient mice. Sci. Signal. 8, ra41–ra41. https://doi.org/10.1126/scisignal.2005781

Morimoto, A., Shibuya, H., Zhu, X., Kim, J., Ishiguro, K., Han, M., Watanabe, Y., 2012. A conserved KASH domain protein associates with telomeres, SUN1, and dynactin during mammalian meiosis. J. Cell Biol. 198, 165–172. https://doi.org/10.1083/jcb.201204085

Moscato, S., Ronca, F., Campani, D., Danti, S., 2015. Poly(vinyl alcohol)/gelatin Hydrogels Cultured with HepG2 Cells as a 3D Model of Hepatocellular Carcinoma: A Morphological Study. J. Funct. Biomater. 6, 16–32. https://doi.org/10.3390/jfb6010016

Mueller, D., Koetemann, A., Noor, F., 2011. Organotypic Cultures of Hepg2 Cells for In Vitro Toxicity Studies. J. Bioeng. Biomed. Sci. https://doi.org/10.4172/2155-9538.S2-002

Mueller, J., Szep, G., Nemethova, M., de Vries, I., Lieber, A.D., Winkler, C., Kruse, K., Small, J.V., Schmeiser, C., Keren, K., Hauschild, R., Sixt, M., 2017. Load Adaptation of Lamellipodial Actin Networks. Cell 171, 188-200.e16. https://doi.org/10.1016/j.cell.2017.07.051

Mylavarapu, S., Kumar, H., Kumari, S., Sravanthi, L.S., Jain, M., Basu, A., Biswas, M., Mylavarapu, S.V.S., Das, A., Roy, M., 2019. Activation of Epithelial-Mesenchymal Transition and Altered β-Catenin Signaling in a Novel Indian Colorectal Carcinoma Cell Line. Front. Oncol. 9. https://doi.org/10.3389/fonc.2019.00054

Nadler, E.P., Patterson, D., Violette, S., Weinreb, P., Lewis, M., Magid, M.S., Greco, M.A., 2009. Integrin αvβ6 and Mediators of Extracellular Matrix Deposition Are Up-Regulated in Experimental Biliary Atresia. J. Surg. Res. 154, 21–29. https://doi.org/10.1016/j.jss.2008.05.023

Nakagawa, H., Hikiba, Y., Hirata, Y., Font-Burgada, J., Sakamoto, K., Hayakawa, Y., Taniguchi, K., Umemura, A., Kinoshita, H., Sakitani, K., Nishikawa, Y., Hirano, K., Ikenoue, T., Ijichi, H., Dhar, D., Shibata, W., Akanuma, M., Koike, K., Karin, M., Maeda, S., 2014. Loss of liver E-cadherin induces sclerosing cholangitis and promotes carcinogenesis. Proc. Natl. Acad. Sci. U. S. A. 111, 1090–1095. https://doi.org/10.1073/pnas.1322731111

Nardone, G., Cruz, J.O.-D.L., Vrbsky, J., Martini, C., Pribyl, J., Skládal, P., Pešl, M., Caluori, G., Pagliari, S., Martino, F., Maceckova, Z., Hajduch, M., Sanz-Garcia, A., Pugno, N.M., Stokin, G.B., Forte, G., 2017. YAP regulates cell mechanics by controlling focal adhesion assembly. Nat. Commun. 8, 1–13. https://doi.org/10.1038/ncomms15321

Naspinski, C., Gu, X., Zhou, G.-D., Mertens-Talcott, S.U., Donnelly, K.C., Tian, Y., 2008. Pregnane X Receptor Protects HepG2 Cells from BaP-Induced DNA Damage. Toxicol. Sci. 104, 67–73. https://doi.org/10.1093/toxsci/kfn058

Nasrollahi, S., Walter, C., Loza, A.J., Schimizzi, G.V., Longmore, G.D., Pathak, A., 2017. Past matrix stiffness primes epithelial cells and regulates their future collective migration through a mechanical memory. Biomaterials 146, 146–155. https://doi.org/10.1016/j.biomaterials.2017.09.012

Naumanen, P., Lappalainen, P., Hotulainen, P., 2008. Mechanisms of actin stress fibre assembly. J. Microsc. 231, 446–454. https://doi.org/10.1111/j.1365-2818.2008.02057.x

Nejjari, M., Couvelard, A., Mosnier, J.-F., Moreau, A., Feldmann, G., Degott, C., Marcellin, P., Scoazec, J.-Y., 2001. Integrin up-regulation in chronic liver disease: relationship with inflammation and fibrosis in chronic hepatitis C. J. Pathol. 195, 473–481. https://doi.org/10.1002/path.964

Next-Generation Sequencing (NGS) | Explore the technology [WWW Document], n.d. URL https://www.illumina.com/science/technology/next-generation-sequencing.html (accessed 2.3.21).

Nieset, J.E., Redfield, A.R., Jin, F., Knudsen, K.A., Johnson, K.R., Wheelock, M.J., 1997. Characterization of the interactions of alpha-catenin with alpha-actinin and beta-catenin/plakoglobin. J. Cell Sci. 110 (Pt 8), 1013–1022.

Nigam, S.K., 2015. What do drug transporters really do? Nat. Rev. Drug Discov. 14, 29–44. https://doi.org/10.1038/nrd4461

Nishikawa, T., Tanaka, Y., Nishikawa, M., Ogino, Y., Kusamori, K., Mizuno, N., Mizukami, Y., Shimizu, K., Konishi, S., Takahashi, Y., Takakura, Y., 2017. Optimization of Albumin Secretion and Metabolic Activity of Cytochrome P450 1A1 of Human Hepatoblastoma HepG2 Cells in Multicellular Spheroids by Controlling Spheroid Size. Biol. Pharm. Bull. 40, 334–338. https://doi.org/10.1248/bpb.b16-00833

Nix, D.A., Beckerle, M.C., 1997. Nuclear-cytoplasmic shuttling of the focal contact protein, zyxin= a potential mechanism for communication between sites of cell adhesion and the nucleus. J. Cell Biol. 138, 1139–1147. https://doi.org/10.1083/jcb.138.5.1139

Nix, D.A., Fradelizi, J., Bockholt, S., Menichi, B., Louvard, D., Friederich, E., Beckerle, M.C., 2001. Targeting of Zyxin to Sites of Actin Membrane Interaction and to the Nucleus. J. Biol. Chem. 276, 34759–34767. https://doi.org/10.1074/jbc.M102820200

Noel, G., Le Vee, M., Moreau, A., Stieger, B., Parmentier, Y., Fardel, O., 2013. Functional expression and regulation of drug transporters in monolayer- and sandwich-cultured mouse hepatocytes. Eur. J. Pharm. Sci. 49, 39–50. https://doi.org/10.1016/j.ejps.2013.01.013

O, S., Mk, H., J, H., D, H., A, C., J, G., Cb, C., Da, M., 2016. Phenotypic Characterization of Toxic Compound Effects on Liver Spheroids Derived from iPSC Using Confocal Imaging and Three-Dimensional Image Analysis [WWW Document]. Assay Drug Dev. Technol. https://doi.org/10.1089/adt.2016.729

O'Brien, F.J., 2011. Biomaterials & scaffolds for tissue engineering. Mater. Today 14, 88–95. https://doi.org/10.1016/S1369-7021(11)70058-X

Odenwald, M.A., Choi, W., Kuo, W.-T., Singh, G., Sailer, A., Wang, Y., Shen, L., Fanning, A.S., Turner, J.R., 2018. The scaffolding protein ZO-1 coordinates actomyosin and epithelial apical specializations in vitro and in vivo. J. Biol. Chem. 293, 17317–17335. https://doi.org/10.1074/jbc.RA118.003908

Ohashi, K., Fujiwara, S., Mizuno, K., 2017. Roles of the cytoskeleton, cell adhesion and rho signalling in mechanosensing and mechanotransduction. J. Biochem. (Tokyo) 161, 245–254. https://doi.org/10.1093/jb/mvw082

Oka, S., Uramoto, H., Shimokawa, H., Iwanami, T., Tanaka, F., 2011. The Expression of Ki-67, but Not Proliferating Cell Nuclear Antigen, Predicts Poor Disease Free Survival in Patients with Adenocarcinoma of the Lung. Anticancer Res. 31, 4277–4282.

Oldenburg, J., Krogt, G. van der, Twiss, F., Bongaarts, A., Habani, Y., Slotman, J.A., Houtsmuller, A., Huveneers, S., Rooij, J. de, 2015. VASP, zyxin and TES are tension-dependent members of Focal Adherens Junctions independent of the α-catenin-vinculin module. Sci. Rep. 5, 1–14. https://doi.org/10.1038/srep17225

Olson, H., Betton, G., Robinson, D., Thomas, K., Monro, A., Kolaja, G., Lilly, P., Sanders, J., Sipes, G., Bracken, W., Dorato, M., Van Deun, K., Smith, P., Berger, B., Heller, A., 2000. Concordance of the toxicity of pharmaceuticals in humans and in animals. Regul. Toxicol. Pharmacol. RTP 32, 56–67. https://doi.org/10.1006/rtph.2000.1399

Oshikata, A., Matsushita, T., Ueoka, R., 2011. Enhancement of drug efflux activity via MDR1 protein by spheroid culture of human hepatic cancer cells. J. Biosci. Bioeng. 111, 590–593. https://doi.org/10.1016/j.jbiosc.2011.01.006

Ow, P., L, R.-J., Ar, H., Mj, B., 1992. Interaction with basement membrane serves to rapidly distinguish growth and differentiation pattern of normal and malignant human breast epithelial cells [WWW Document]. Proc. Natl. Acad. Sci. U. S. A. https://doi.org/10.1073/pnas.89.19.9064

Ozawa, M., Baribault, H., Kemler, R., 1989. The cytoplasmic domain of the cell adhesion molecule uvomorulin associates with three independent proteins structurally related in different species. EMBO J. 8, 1711–1717.

Padrick, S.B., Doolittle, L.K., Brautigam, C.A., King, D.S., Rosen, M.K., 2011. Arp2/3 complex is bound and activated by two WASP proteins. Proc. Natl. Acad. Sci. U. S. A. 108, E472-479. https://doi.org/10.1073/pnas.1100236108

Pal, M., Chen, H., Lee, B.H., Lee, J.Y.H., Yip, Y.S., Tan, N.S., Tan, L.P., 2019. Epithelial-mesenchymal transition of cancer cells using bioengineered hybrid scaffold composed of hydrogel/3D-fibrous framework. Sci. Rep. 9, 1–11. https://doi.org/10.1038/s41598-019-45384-9

Paluch, E.K., Nelson, C.M., Biais, N., Fabry, B., Moeller, J., Pruitt, B.L., Wollnik, C., Kudryasheva, G., Rehfeldt, F., Federle, W., 2015. Mechanotransduction= use the force(s). BMC Biol. 13. https://doi.org/10.1186/s12915-015-0150-4

Pampaloni, F., Reynaud, E.G., Stelzer, E.H.K., 2007. The third dimension bridges the gap between cell culture and live tissue. Nat. Rev. Mol. Cell Biol. 8, 839–845. https://doi.org/10.1038/nrm2236

Parrish, A.R., Catania, J.M., Orozco, J., Gandolfi, A.J., 1999. Chemically induced oxidative stress disrupts the E-cadherin/catenin cell adhesion complex. Toxicol. Sci. Off. J. Soc. Toxicol. 51, 80–86. https://doi.org/10.1093/toxsci/51.1.80

Parsons, J.T., 2003. Focal adhesion kinase: the first ten years. J. Cell Sci. 116, 1409–1416. https://doi.org/10.1242/jcs.00373

Parsons, J.T., Horwitz, A.R., Schwartz, M.A., 2010. Cell adhesion= integrating cytoskeletal dynamics and cellular tension. Nat. Rev. Mol. Cell Biol. 11, 633–643. https://doi.org/10.1038/nrm2957

Patsenker, E., Stickel, F., 2011. Role of integrins in fibrosing liver diseases. Am. J. Physiol.-Gastrointest. Liver Physiol. 301, G425–G434. https://doi.org/10.1152/ajpgi.00050.2011

Pećina-Šlaus, N., 2003. Tumor suppressor gene E-cadherin and its role in normal and malignant cells. Cancer Cell Int. 3, 17. https://doi.org/10.1186/1475-2867-3-17

Petit, M.M.R., Fradelizi, J., Golsteyn, R.M., Ayoubi, T.A.Y., Menichi, B., Louvard, D., Van de Ven, W.J.M., Friederich, E., 2000. LPP, an Actin Cytoskeleton Protein Related to Zyxin, Harbors a Nuclear Export Signal and Transcriptional Activation Capacity. Mol. Biol. Cell 11, 117–129.

Pikuleva, I.A., Babiker, A., Waterman, M.R., Björkhem, I., 1998. Activities of Recombinant Human Cytochrome P450c27 (CYP27) Which Produce Intermediates of Alternative Bile Acid Biosynthetic Pathways *. J. Biol. Chem. 273, 18153–18160. https://doi.org/10.1074/jbc.273.29.18153

Pinheiro, D., Bellaïche, Y., 2018. Mechanical Force-Driven Adherens Junction Remodeling and Epithelial Dynamics. Dev. Cell 47, 3–19. https://doi.org/10.1016/j.devcel.2018.09.014

Poisson, J., Lemoinne, S., Boulanger, C., Durand, F., Moreau, R., Valla, D., Rautou, P.-E., 2017. Liver sinusoidal endothelial cells: Physiology and role in liver diseases. J. Hepatol. 66, 212–227. https://doi.org/10.1016/j.jhep.2016.07.009

Pollard, T.D., 1986. Rate constants for the reactions of ATP- and ADP-actin with the ends of actin filaments. J. Cell Biol. 103, 2747–2754.

Pollard, T.D., Borisy, G.G., 2003. Cellular motility driven by assembly and disassembly of actin filaments. Cell 112, 453–465. https://doi.org/10.1016/s0092-8674(03)00120-x

Pollard, T.D., Cooper, J.A., 1984. Quantitative analysis of the effect of Acanthamoeba profilin on actin filament nucleation and elongation. Biochemistry 23, 6631–6641. https://doi.org/10.1021/bi00321a054

Pomo, J.M., Taylor, R.M., Gullapalli, R.R., 2016. Influence of TP53 and CDH1 genes in hepatocellular cancer spheroid formation and culture: a model system to understand cancer cell growth mechanics. Cancer Cell Int. 16. https://doi.org/10.1186/s12935-016-0318-1

Price, A.J., Cost, A.-L., Ungewiß, H., Waschke, J., Dunn, A.R., Grashoff, C., 2018. Mechanical loading of desmosomes depends on the magnitude and orientation of external stress. Nat. Commun. 9, 1–11. https://doi.org/10.1038/s41467-018-07523-0

Price, K.J., Tsykin, A., Giles, K.M., Sladic, R.T., Epis, M.R., Ganss, R., Goodall, G.J., Leedman, P.J., 2012. Matrigel basement membrane matrix influences expression of microRNAs in cancer cell lines. Biochem. Biophys. Res. Commun. 427, 343–348. https://doi.org/10.1016/j.bbrc.2012.09.059

Prozialeck, W.C., Lamar, P.C., Lynch, S.M., 2003. Cadmium alters the localization of N-cadherin, E-cadherin, and β-catenin in the proximal tubule epithelium. Toxicol. Appl. Pharmacol. 189, 180–195. https://doi.org/10.1016/S0041-008X(03)00130-3

Puklin-Faucher, E., Gao, M., Schulten, K., Vogel, V., 2006. How the headpiece hinge angle is opened: new insights into the dynamics of integrin activation. J. Cell Biol. 175, 349–360. https://doi.org/10.1083/jcb.200602071

Quadrato, G., Nguyen, T., Macosko, E.Z., Sherwood, J.L., Yang, S.M., Berger, D.R., Maria, N., Scholvin, J., Goldman, M., Kinney, J.P., Boyden, E.S., Lichtman, J.W., Williams, Z.M., McCarroll, S.A., Arlotta, P., 2017. Cell diversity and network dynamics in photosensitive human brain organoids. Nature 545, 48–53. https://doi.org/10.1038/nature22047

QUELCH, R., 2018. Dynamic Regulation of the Pluripotent Stem Cell Structure-Function Relationship through Topographical Cues. (Doctoral). Durham University.

R, L., Mm, S., L, S., Y, L., S, B., G, L., Pm, B., Cr, B., S, S., Jj, Y., A, A., Y, Z., 2011. Three-dimensional culture of hepatocytes on porcine liver tissue-derived extracellular matrix [WWW Document]. Biomaterials. https://doi.org/10.1016/j.biomaterials.2011.06.005

Rahner, C., Mitic, L.L., Anderson, J.M., 2001. Heterogeneity in expression and subcellular localization of claudins 2, 3, 4, and 5 in the rat liver, pancreas, and gut. Gastroenterology 120, 411–422. https://doi.org/10.1053/gast.2001.21736

Rajgor, D., Shanahan, C.M., 2013. Nesprins: from the nuclear envelope and beyond. Expert Rev. Mol. Med. 15. https://doi.org/10.1017/erm.2013.6

Ramaiahgari, S.C., Braver, M.W. den, Herpers, B., Terpstra, V., Commandeur, J.N.M., Water, B. van de, Price, L.S., 2014a. A 3D in vitro model of differentiated HepG2 cell spheroids with improved liver-like properties for repeated dose high-throughput toxicity studies. Arch. Toxicol. 88, 1083–1095. https://doi.org/10.1007/s00204-014-1215-9

Ramaiahgari, S.C., Braver, M.W. den, Herpers, B., Terpstra, V., Commandeur, J.N.M., Water, B. van de, Price, L.S., 2014b. A 3D in vitro model of differentiated HepG2 cell spheroids with improved liver-like properties for repeated dose high-throughput toxicity studies. Arch. Toxicol. 88, 1083–1095. https://doi.org/10.1007/s00204-014-1215-9

Rao, M.S., Vleet, V., R, T., Ciurlionis, R., Buck, W.R., Mittelstadt, S.W., Blomme, E.A.G., Liguori, M.J., 2019. Comparison of RNA-Seq and Microarray Gene Expression Platforms for the Toxicogenomic Evaluation of Liver From Short-Term Rat Toxicity Studies. Front. Genet. 9. https://doi.org/10.3389/fgene.2018.00636

Rashidi, H., Alhaque, S., Szkolnicka, D., Flint, O., Hay, D.C., 2016. Fluid shear stress modulation of hepatocyte-like cell function. Arch. Toxicol. 90, 1757–1761. https://doi.org/10.1007/s00204-016-1689-8

Rashmi, R.N., Eckes, B., Glöckner, G., Groth, M., Neumann, S., Gloy, J., Sellin, L., Walz, G., Schneider, M., Karakesisoglou, I., Eichinger, L., Noegel, A.A., 2012. The nuclear envelope protein Nesprin-2 has roles in cell proliferation and differentiation during wound healing. Nucleus 3, 172–186. https://doi.org/10.4161/nucl.19090

Rauh, J., Jacobi, A., Stiehler, M., 2015. Identification of Stable Reference Genes for Gene Expression Analysis of Three-Dimensional Cultivated Human Bone Marrow-Derived Mesenchymal Stromal Cells for Bone Tissue Engineering. Tissue Eng. Part C Methods 21, 192–206. https://doi.org/10.1089/ten.tec.2014.0230

Rawlings, N.D., Barrett, A.J., 1994. Families of serine peptidases. Methods Enzymol. 244, 19–61.

Rendic, S., Di Carlo, F.J., 1997. Human cytochrome P450 enzymes: a status report summarizing their reactions, substrates, inducers, and inhibitors. Drug Metab. Rev. 29, 413–580. https://doi.org/10.3109/03602539709037591

Ringnér, M., 2008. What is principal component analysis? Nat. Biotechnol. 26, 303–304. https://doi.org/10.1038/nbt0308-303

Roa-Espitia, A.L., Hernández-Rendón, E.R., Baltiérrez-Hoyos, R., Muñoz-Gotera, R.J., Cote-Vélez, A., Jiménez, I., González-Márquez, H., Hernández-González, E.O., 2016. Focal adhesion kinase is required for actin polymerization and remodeling of the cytoskeleton during sperm capacitation. Biol. Open 5, 1189–1199. https://doi.org/10.1242/bio.017558

Roca-Cusachs, P., del Rio, A., Puklin-Faucher, E., Gauthier, N.C., Biais, N., Sheetz, M.P., 2013. Integrin-dependent force transmission to the extracellular matrix by α-actinin triggers adhesion maturation. Proc. Natl. Acad. Sci. U. S. A. 110, E1361–E1370. https://doi.org/10.1073/pnas.1220723110

Rocha Leão, M.H.M., 2003. GLYCOGEN, in= Caballero, B. (Ed.), Encyclopedia of Food Sciences and Nutrition (Second Edition). Academic Press, Oxford, pp. 2930–2937. https://doi.org/10.1016/B0-12-227055-X/00563-0

Rogers, A.B., Dintzis, R.Z., 2018. 13 - Hepatobiliary System, in= Treuting, P.M., Dintzis, S.M., Montine, K.S. (Eds.), Comparative Anatomy and Histology (Second Edition). Academic Press, San Diego, pp. 229–239. https://doi.org/10.1016/B978-0-12-802900-8.00013-0

Rouwkema, J., Koopman, B., Blitterswijk, C., Dhert, W., Malda, J., 2010. Supply of nutrients to cells in engineered tissues. Biotechnol. Genet. Eng. Rev. 26, 163–178. https://doi.org/10.5661/bger-26-163

Ruoß, M., Damm, G., Vosough, M., Ehret, L., Grom-Baumgarten, C., Petkov, M., Naddalin, S., Ladurner, R., Seehofer, D., Nussler, A., Sajadian, S., 2019. Epigenetic Modifications of the Liver Tumor Cell Line HepG2 Increase Their Drug Metabolic Capacity. Int. J. Mol. Sci. 20. https://doi.org/10.3390/ijms20020347

Saez, A., Ghibaudo, M., Buguin, A., Silberzan, P., Ladoux, B., 2007. Rigidity-driven growth and migration of epithelial cells on microstructured anisotropic substrates. Proc. Natl. Acad. Sci. U. S. A. 104, 8281–8286. https://doi.org/10.1073/pnas.0702259104

Salama, N.N., Eddington, N.D., Fasano, A., 2006. Tight Junction Modulation and Its Relationship to Drug Delivery, in= Gonzalez-Mariscal, L. (Ed.), Tight Junctions. Springer US, Boston, MA, pp. 206–219. https://doi.org/10.1007/0-387-36673-3_15

Sart, S., Ma, T., Li, Y., 2014. Preconditioning Stem Cells for In Vivo Delivery. BioResearch Open Access 3, 137–149. https://doi.org/10.1089/biores.2014.0012

Sassa, S., Sugita, O., Galbraith, R.A., Kappas, A., 1987. Drug metabolism by the human hepatoma cell, Hep G2. Biochem. Biophys. Res. Commun. 143, 52–57.

Sawada, Y., Sheetz, M.P., 2002. Force transduction by Triton cytoskeletons. J. Cell Biol. 156, 609–615. https://doi.org/10.1083/jcb.200110068

Schreiber, K.H., Kennedy, B.K., 2013. When Lamins Go Bad: Nuclear Structure and Disease. Cell 152, 1365–1375. https://doi.org/10.1016/j.cell.2013.02.015

Schroeder, A., Mueller, O., Stocker, S., Salowsky, R., Leiber, M., Gassmann, M., Lightfoot, S., Menzel, W., Granzow, M., Ragg, T., 2006. The RIN= an RNA integrity number for assigning integrity values to RNA measurements. BMC Mol. Biol. 7, 3. https://doi.org/10.1186/1471-2199-7-3

Schroeder, B., McNiven, M.A., 2014. Importance of Endocytic Pathways in Liver Function and Disease. Compr. Physiol. 4, 1403–1417. https://doi.org/10.1002/cphy.c140001

Schulze, R.J., Schott, M.B., Casey, C.A., Tuma, P.L., McNiven, M.A., 2019. The cell biology of the hepatocyte: A membrane trafficking machine. J. Cell Biol. 218, 2096–2112. https://doi.org/10.1083/jcb.201903090

Schyschka, L., Sánchez, J.J.M., Wang, Z., Burkhardt, B., Müller-Vieira, U., Zeilinger, K., Bachmann, A., Nadalin, S., Damm, G., Nussler, A.K., 2013. Hepatic 3D cultures but not 2D cultures preserve specific transporter activity for acetaminophen-induced hepatotoxicity. Arch. Toxicol. 87, 1581–1593. https://doi.org/10.1007/s00204-013-1080-y

Seetharaman, S., Etienne-Manneville, S., 2018. Integrin diversity brings specificity in mechanotransduction. Biol. Cell 110, 49–64. https://doi.org/10.1111/boc.201700060

Shah, F., Leung, L., Barton, H.A., Will, Y., Rodrigues, A.D., Greene, N., Aleo, M.D., 2015. Setting Clinical Exposure Levels of Concern for Drug-Induced Liver Injury (DILI) Using Mechanistic in vitro Assays. Toxicol. Sci. 147, 500–514. https://doi.org/10.1093/toxsci/kfv152

Shah, U.-K., Mallia, J. de O., Singh, N., Chapman, K.E., Doak, S.H., Jenkins, G.J.S., 2018. A three-dimensional in vitro HepG2 cells liver spheroid model for genotoxicity studies.

Mutat. Res. Toxicol. Environ. Mutagen. 825, 51–58. https://doi.org/10.1016/j.mrgentox.2017.12.005

Shimazui, T., Schalken, J.A., Kawai, K., Kawamoto, R., van Bockhoven, A., Oosterwijk, E., Akaza, H., 2004. Role of complex cadherins in cell-cell adhesion evaluated by spheroid formation in renal cell carcinoma cell lines. Oncol. Rep. 11, 357–360.

Shimi, T., Pfleghaar, K., Kojima, S., Pack, C.-G., Solovei, I., Goldman, A.E., Adam, S.A., Shumaker, D.K., Kinjo, M., Cremer, T., Goldman, R.D., 2008. The A- and B-type nuclear lamin networks: microdomains involved in chromatin organization and transcription. Genes Dev. 22, 3409–3421. https://doi.org/10.1101/gad.1735208

Shin, J.-W., Spinler, K.R., Swift, J., Chasis, J.A., Mohandas, N., Discher, D.E., 2013. Lamins regulate cell trafficking and lineage maturation of adult human hematopoietic cells. Proc. Natl. Acad. Sci. 110, 18892–18897. https://doi.org/10.1073/pnas.1304996110

Shiu, J.-Y., Aires, L., Lin, Z., Vogel, V., 2018. Nanopillar force measurements reveal actin-cap-mediated YAP mechanotransduction. Nat. Cell Biol. 20, 262–271. https://doi.org/10.1038/s41556-017-0030-y

Shri, M., Agrawal, H., Rani, P., Singh, D., Onteru, S.K., 2017. Hanging Drop, A Best Three-Dimensional (3D) Culture Method for Primary Buffalo and Sheep Hepatocytes. Sci. Rep. 7, 1–14. https://doi.org/10.1038/s41598-017-01355-6

Shuaib, A., Motan, D., Bhattacharya, P., McNabb, A., Skerry, T.M., Lacroix, D., 2019. Heterogeneity in The Mechanical Properties of Integrins Determines Mechanotransduction Dynamics in Bone Osteoblasts. Sci. Rep. 9, 1–14. https://doi.org/10.1038/s41598-019-47958-z

Shvartsman, I., Dvir, T., Harel-Adar, T., Cohen, S., 2009. Perfusion cell seeding and cultivation induce the assembly of thick and functional hepatocellular tissue-like construct. Tissue Eng. Part A 15, 751–760. https://doi.org/10.1089/ten.tea.2008.0024

Silverthorn, D.U., 2013. Focus on the Liver, in= Human Physiology: An Integrated Approach. Pearson, p. 709.

Sissung, T.M., Troutman, S.M., Campbell, T.J., Pressler, H.M., Sung, H., Bates, S.E., Figg, W.D., 2012. Transporter polymorphisms affect normal physiology, diseases, and pharmacotherapy. Discov. Med. 13, 19–34.

Si-Tayeb, K., Lemaigre, F., Sa, D., 2010. Organogenesis and development of the liver [WWW Document]. Dev. Cell. https://doi.org/10.1016/j.devcel.2010.01.011

Slenter, D.N., Kutmon, M., Hanspers, K., Riutta, A., Windsor, J., Nunes, N., Mélius, J., Cirillo, E., Coort, S.L., Digles, D., Ehrhart, F., Giesbertz, P., Kalafati, M., Martens, M., Miller, R., Nishida, K., Rieswijk, L., Waagmeester, A., Eijssen, L.M.T., Evelo, C.T., Pico, A.R., Willighagen, E.L., 2018. WikiPathways: a multifaceted pathway database bridging metabolomics to other omics research. Nucleic Acids Res. 46, D661–D667. https://doi.org/10.1093/nar/gkx1064

Sluysmans, S., Vasileva, E., Spadaro, D., Shah, J., Rouaud, F., Citi, S., 2017. The role of apical cell-cell junctions and associated cytoskeleton in mechanotransduction. Biol. Cell 109, 139–161. https://doi.org/10.1111/boc.201600075

Smutny, M., Yap, A.S., 2010. Neighborly relations: cadherins and mechanotransduction. J. Cell Biol. 189, 1075–1077. https://doi.org/10.1083/jcb.201005151

Spadaro, D., Le, S., Laroche, T., Mean, I., Jond, L., Yan, J., Citi, S., 2017. Tension-Dependent Stretching Activates ZO-1 to Control the Junctional Localization of Its Interactors. Curr. Biol. 27, 3783-3795.e8. https://doi.org/10.1016/j.cub.2017.11.014

Spadaro, D., Tapia, R., Jond, L., Sudol, M., Fanning, A.S., Citi, S., 2014. ZO proteins redundantly regulate the transcription factor DbpA/ZONAB. J. Biol. Chem. 289, 22500–22511. https://doi.org/10.1074/jbc.M114.556449

Spagnol, S.T., Dahl, K.N., 2016. Spatially Resolved Quantification of Chromatin Condensation through Differential Local Rheology in Cell Nuclei Fluorescence Lifetime Imaging. PLOS ONE 11, e0146244. https://doi.org/10.1371/journal.pone.0146244

Srivastava, A., George, J., Karuturi, R.K.M., 2019. Transcriptome Analysis, in= Ranganathan, S., Gribskov, M., Nakai, K., Schönbach, C. (Eds.), Encyclopedia of Bioinformatics and Computational Biology. Academic Press, Oxford, pp. 792–805. https://doi.org/10.1016/B978-0-12-809633-8.20161-1

Stadler, M., Scherzer, M., Walter, S., Holzner, S., Pudelko, K., Riedl, A., Unger, C., Kramer, N., Weil, B., Neesen, J., Hengstschläger, M., Dolznig, H., 2018. Exclusion from spheroid formation identifies loss of essential cell-cell adhesion molecules in colon cancer cells. Sci. Rep. 8, 1151. https://doi.org/10.1038/s41598-018-19384-0

Stamos, J.L., Weis, W.I., 2013. The β-catenin destruction complex. Cold Spring Harb. Perspect. Biol. 5, a007898. https://doi.org/10.1101/cshperspect.a007898

Štampar, M., Tomc, J., Filipič, M., Žegura, B., 2019. Development of in vitro 3D cell model from hepatocellular carcinoma (HepG2) cell line and its application for genotoxicity testing. Arch. Toxicol. 93, 3321–3333. https://doi.org/10.1007/s00204-019-02576-6

Starr, D.A., 2011. KASH and SUN proteins. Curr. Biol. CB 21, R414–R415. https://doi.org/10.1016/j.cub.2011.04.022

steve, n.d. What are mature focal adhesions composed of? [WWW Document]. MBInfo. URL https://www.mechanobio.info/what-is-mechanosignaling/what-is-the-extracellular-matrix-and-the-basal-lamina/what-are-focal-adhesions/what-are-mature-focal-adhesions-composed-of/ (accessed 3.8.21).

Strnad, P., Schwarz, P., Rasenack, M.C.D., Kucukoglu, O., Habib, R.I., Heuberger, D., Ehehalt, R., Müller, M.W., Stiehl, A., Adler, G., Kulaksiz, H., 2011. Hepcidin Is an Antibacterial, Stress-Inducible Peptide of the Biliary System. PLOS ONE 6, e16454. https://doi.org/10.1371/journal.pone.0016454

Strushkevich, N., Usanov, S.A., Park, H.-W., 2010. Structural Basis of Human CYP51 Inhibition by Antifungal Azoles. J. Mol. Biol. 397, 1067–1078. https://doi.org/10.1016/j.jmb.2010.01.075

Stutchbury, B., Atherton, P., Tsang, R., Wang, D.-Y., Ballestrem, C., 2017. Distinct focal adhesion protein modules control different aspects of mechanotransduction. J. Cell Sci. 130, 1612–1624. https://doi.org/10.1242/jcs.195362

Subramanian, A., Tamayo, P., Mootha, V.K., Mukherjee, S., Ebert, B.L., Gillette, M.A., Paulovich, A., Pomeroy, S.L., Golub, T.R., Lander, E.S., Mesirov, J.P., 2005. Gene set enrichment analysis: A knowledge-based approach for interpreting genome-wide expression profiles. Proc. Natl. Acad. Sci. U. S. A. 102, 15545–15550. https://doi.org/10.1073/pnas.0506580102

Sun, M., Chi, G., Li, P., Lv, S., Xu, Juanjuan, Xu, Z., Xia, Y., Tan, Y., Xu, Jiayi, Li, L., Li, Y., 2018. Effects of Matrix Stiffness on the Morphology, Adhesion, Proliferation and Osteogenic Differentiation of Mesenchymal Stem Cells. Int. J. Med. Sci. 15, 257–268. https://doi.org/10.7150/ijms.21620

Sun, Z., Huang, S., Li, Z., Meininger, G.A., 2012. Zyxin is involved in regulation of mechanotransduction in arteriole smooth muscle cells. Front. Physiol. 3. https://doi.org/10.3389/fphys.2012.00472

Swift, J., Ivanovska, I.L., Buxboim, A., Harada, T., Dingal, P.C.D.P., Pinter, J., Pajerowski, J.D., Spinler, K.R., Shin, J.-W., Tewari, M., Rehfeldt, F., Speicher, D.W., Discher, D.E., 2013. Nuclear Lamin-A Scales with Tissue Stiffness and Enhances Matrix-Directed Differentiation. Science 341, 1240104. https://doi.org/10.1126/science.1240104

Szot, C.S., Buchanan, C.F., Freeman, J.W., Rylander, M.N., 2011. 3D in vitro bioengineered tumors based on collagen I hydrogels. Biomaterials 32, 7905–7912. https://doi.org/10.1016/j.biomaterials.2011.07.001

T, Y., Pc, G., La, F., B, M., M, O., M, F., N, Z., W, M., V, W., Pa, J., 2005. Effects of substrate stiffness on cell morphology, cytoskeletal structure, and adhesion [WWW Document]. Cell Motil. Cytoskeleton. https://doi.org/10.1002/cm.20041

Takahashi, Y., Hori, Y., Yamamoto, T., Urashima, T., Ohara, Y., Tanaka, H., 2015. 3D spheroid cultures improve the metabolic gene expression profiles of HepaRG cells. Biosci. Rep. 35. https://doi.org/10.1042/BSR20150034

Takeichi, M., 1990. Cadherins: A Molecular Family Important in Selective Cell-Cell Adhesion. Annu. Rev. Biochem. 59, 237–252. https://doi.org/10.1146/annurev.bi.59.070190.001321

Tamoxifen, 2012. , in= LiverTox: Clinical and Research Information on Drug-Induced Liver Injury. National Institute of Diabetes and Digestive and Kidney Diseases, Bethesda (MD).

Tamoxifen DrugBank [WWW Document], n.d. URL https://go.drugbank.com/drugs/DB00675 (accessed 1.4.21).

Tamoxifen Pathway, Pharmacokinetics Overview [WWW Document], n.d. . PharmGKB. URL https://www.pharmgkb.org/pathway/PA145011119 (accessed 1.4.21).

Tan, J.L., Tien, J., Pirone, D.M., Gray, D.S., Bhadriraju, K., Chen, C.S., 2003. Cells lying on a bed of microneedles: An approach to isolate mechanical force. Proc. Natl. Acad. Sci. 100, 1484–1489. https://doi.org/10.1073/pnas.0235407100

Tang, D.D., 2015. Critical role of actin-associated proteins in smooth muscle contraction, cell proliferation, airway hyperresponsiveness and airway remodeling. Respir. Res. 16. https://doi.org/10.1186/s12931-015-0296-1

Tang, V.W., Brieher, W.M., 2012. α-Actinin-4/FSGS1 is required for Arp2/3-dependent actin assembly at the adherens junction. J. Cell Biol. 196, 115–130. https://doi.org/10.1083/jcb.201103116

Tangkijvanich, P., Anukulkarnkusol, N., Suwangool, P., Lertmaharit, S., Hanvivatvong, O., Kullavanijaya, P., Poovorawan, Y., 2000. Clinical Characteristics and Prognosis of Hepatocellular Carcinoma: Analysis Based on Serum Alpha-fetoprotein Levels. J. Clin. Gastroenterol. 31, 302–308.

Taranum, S., Sur, I., Müller, R., Lu, W., Rashmi, R.N., Munck, M., Neumann, S., Karakesisoglou, I., Noegel, A.A., 2012. Cytoskeletal Interactions at the Nuclear Envelope Mediated by Nesprins. Int. J. Cell Biol. 2012. https://doi.org/10.1155/2012/736524

Tasnadi, E.A., Toth, T., Kovacs, M., Diosdi, A., Pampaloni, F., Molnar, J., Piccinini, F., Horvath, P., 2020. 3D-Cell-Annotator: an open-source active surface tool for single-cell segmentation in 3D microscopy images. Bioinformatics 36, 2948–2949. https://doi.org/10.1093/bioinformatics/btaa029

Tee, S.-Y., Bausch, A., Janmey, P.A., 2009. The mechanical cell. Curr. Biol. CB 19, R745–R748. https://doi.org/10.1016/j.cub.2009.06.034

Teicher, B.A., 2001. Malignant cells, directors of the malignant process: role of transforming growth factor-beta. Cancer Metastasis Rev. 20, 133–143. https://doi.org/10.1023/a:1013177011767

Tekin, H., Simmons, S., Cummings, B., Gao, L., Adiconis, X., Hession, C.C., Ghoshal, A., Dionne, D., Choudhury, S.R., Yesilyurt, V., Sanjana, N.E., Shi, X., Lu, C., Heidenreich, M., Pan, J.Q., Levin, J.Z., Zhang, F., 2018. Effects of 3D culturing conditions on the transcriptomic profile of stem-cell-derived neurons. Nat. Biomed. Eng. 2, 540–554. https://doi.org/10.1038/s41551-018-0219-9

Théry, M., 2010. Micropatterning as a tool to decipher cell morphogenesis and functions. J. Cell Sci. 123, 4201–4213. https://doi.org/10.1242/jcs.075150

Thomas, D., Marsico, G., Isa, I.L.M., Thirumaran, A., Chen, X., Lukasz, B., Fontana, G., Rodriguez, B., Marchetti-Deschmann, M., O'Brien, T., Pandit, A., 2020. Temporal changes guided by mesenchymal stem cells on a 3D microgel platform enhance

angiogenesis in vivo at a low-cell dose. Proc. Natl. Acad. Sci. 117, 19033–19044. https://doi.org/10.1073/pnas.2008245117
Tibbitt, M.W., Anseth, K.S., 2009a. Hydrogels as Extracellular Matrix Mimics for 3D Cell Culture. Biotechnol. Bioeng. 103, 655–663. https://doi.org/10.1002/bit.22361
Tibbitt, M.W., Anseth, K.S., 2009b. Hydrogels as Extracellular Matrix Mimics for 3D Cell Culture. Biotechnol. Bioeng. 103, 655–663. https://doi.org/10.1002/bit.22361
Tirona, R.G., Lee, W., Leake, B.F., Lan, L.-B., Cline, C.B., Lamba, V., Parviz, F., Duncan, S.A., Inoue, Y., Gonzalez, F.J., Schuetz, E.G., Kim, R.B., 2003. The orphan nuclear receptor HNF4α determines PXR- and CAR-mediated xenobiotic induction of CYP3A4. Nat. Med. 9, 220–224. https://doi.org/10.1038/nm815
Tissue expression of CLDN1 - Summary - The Human Protein Atlas [WWW Document], n.d. URL https://www.proteinatlas.org/ENSG00000163347-CLDN1/tissue (accessed 11.4.20).
Tojkander, S., Gateva, G., Lappalainen, P., 2012. Actin stress fibers--assembly, dynamics and biological roles. J. Cell Sci. 125, 1855–1864. https://doi.org/10.1242/jcs.098087
Tokuda, S., Higashi, T., Furuse, M., 2014. ZO-1 knockout by TALEN-mediated gene targeting in MDCK cells: involvement of ZO-1 in the regulation of cytoskeleton and cell shape. PloS One 9, e104994. https://doi.org/10.1371/journal.pone.0104994
Trefts, E., Gannon, M., Wasserman, D.H., 2017. The liver. Curr. Biol. 27, R1147–R1151. https://doi.org/10.1016/j.cub.2017.09.019
Treyer, A., Müsch, A., 2013. Hepatocyte Polarity. Compr. Physiol. 3, 243–287. https://doi.org/10.1002/cphy.c120009
Tsaioun, K., Jacewicz, M., 2009. De-risking drug discovery with ADDME -- avoiding drug development mistakes early. Altern. Lab. Anim. ATLA 37 Suppl 1, 47–55. https://doi.org/10.1177/026119290903701S10
Tsimbouri, P.M., 2015. Adult Stem Cell Responses to Nanostimuli. J. Funct. Biomater. 6, 598–622. https://doi.org/10.3390/jfb6030598
Tsompana, M., Buck, M.J., 2014. Chromatin accessibility: a window into the genome. Epigenetics Chromatin 7, 33. https://doi.org/10.1186/1756-8935-7-33
Turgay, Y., Eibauer, M., Goldman, A.E., Shimi, T., Khayat, M., Ben-Harush, K., Dubrovsky-Gaupp, A., Sapra, K.T., Goldman, R.D., Medalia, O., 2017. The molecular architecture of lamins in somatic cells. Nature 543, 261–264. https://doi.org/10.1038/nature21382
Uemura, A., Nguyen, T.-N., Steele, A.N., Yamada, S., 2011. The LIM Domain of Zyxin Is Sufficient for Force-Induced Accumulation of Zyxin During Cell Migration. Biophys. J. 101, 1069–1075. https://doi.org/10.1016/j.bpj.2011.08.001
Uhler, C., Shivashankar, G.V., 2017. Regulation of genome organization and gene expression by nuclear mechanotransduction. Nat. Rev. Mol. Cell Biol. 18, 717–727. https://doi.org/10.1038/nrm.2017.101
Unal, A.Z., Jeffs, S.E., West, J.L., 2018. 3D Co-Culture with Vascular Cells Supports Long-Term Hepatocyte Phenotype and Function In Vitro. Regen. Eng. Transl. Med. 4, 21–34. https://doi.org/10.1007/s40883-018-0046-2
Ungricht, R., Kutay, U., 2017. Mechanisms and functions of nuclear envelope remodelling. Nat. Rev. Mol. Cell Biol. 18, 229–245. https://doi.org/10.1038/nrm.2016.153
Uzer, G., Rubin, C.T., Rubin, J., 2016. Cell Mechanosensitivity is Enabled by the LINC Nuclear Complex. Curr. Mol. Biol. Rep. 2, 36–47. https://doi.org/10.1007/s40610-016-0032-8
Valenta, T., Hausmann, G., Basler, K., 2012. The many faces and functions of β-catenin. EMBO J. 31, 2714–2736. https://doi.org/10.1038/emboj.2012.150
van IJzendoorn, S.C.D., Théard, D., van der Wouden, J.M., Visser, W., Wojtal, K.A., Hoekstra, D., 2004. Oncostatin M-stimulated Apical Plasma Membrane Biogenesis Requires

p27Kip1-Regulated Cell Cycle Dynamics. Mol. Biol. Cell 15, 4105–4114. https://doi.org/10.1091/mbc.E04-03-0201

VanGuilder, H.D., Vrana, K.E., Freeman, W.M., 2008. Twenty-five years of quantitative PCR for gene expression analysis. BioTechniques 44, 619–626. https://doi.org/10.2144/000112776

Varelas, X., Miller, B.W., Sopko, R., Song, S., Gregorieff, A., Fellouse, F.A., Sakuma, R., Pawson, T., Hunziker, W., McNeill, H., Wrana, J.L., Attisano, L., 2010. The Hippo Pathway Regulates Wnt/β-Catenin Signaling. Dev. Cell 18, 579–591. https://doi.org/10.1016/j.devcel.2010.03.007

Vincent, L.G., Choi, Y.S., Alonso-Latorre, B., del Álamo, J.C., Engler, A.J., 2013. Mesenchymal stem cell durotaxis depends on substrate stiffness gradient strength. Biotechnol. J. 8, 472–484. https://doi.org/10.1002/biot.201200205

Vinci, B., Duret, C., Klieber, S., Gerbal-Chaloin, S., Sa-Cunha, A., Laporte, S., Suc, B., Maurel, P., Ahluwalia, A., Daujat-Chavanieu, M., 2011. Modular bioreactor for primary human hepatocyte culture: medium flow stimulates expression and activity of detoxification genes. Biotechnol. J. 6, 554–564. https://doi.org/10.1002/biot.201000326

Virtanen, J.A., Vartiainen, M.K., 2017. Diverse functions for different forms of nuclear actin. Curr. Opin. Cell Biol. 46, 33–38. https://doi.org/10.1016/j.ceb.2016.12.004

Vogel, K.G., 1978. Effects of hyaluronidase, trypsin, and EDTA on surface composition and topography during detachment of cells in culture. Exp. Cell Res. 113, 345–357. https://doi.org/10.1016/0014-4827(78)90375-0

Wada, K.-I., Itoga, K., Okano, T., Yonemura, S., Sasaki, H., 2011. Hippo pathway regulation by cell morphology and stress fibers. Development 138, 3907–3914. https://doi.org/10.1242/dev.070987

Walesky, C., Apte, U., 2015. Role of Hepatocyte Nuclear Factor 4 alpha (HNF4α) in Cell Proliferation and Cancer. Gene Expr. 16, 101–108. https://doi.org/10.3727/105221615X14181438356292

Walker, T.M., Rhodes, P.C., Westmoreland, C., 2000. The differential cytotoxicity of methotrexate in rat hepatocyte monolayer and spheroid cultures. Toxicol. In Vitro 14, 475–485. https://doi.org/10.1016/S0887-2333(00)00036-9

Wang, B., Qin, P., Zhao, H., Xia, T., Wang, J., Liu, L., Zhu, L., Xu, J., Huang, C., Shi, Y., Du, Y., 2016. Substrate stiffness orchestrates epithelial cellular heterogeneity with controlled proliferative pattern via E-cadherin/β-catenin mechanotransduction. Acta Biomater. 41, 169–180. https://doi.org/10.1016/j.actbio.2016.05.025

Wang, C., Gong, B., Bushel, P.R., Thierry-Mieg, J., Thierry-Mieg, D., Xu, J., Fang, H., Hong, H., Shen, J., Su, Z., Meehan, J., Li, X., Yang, L., Li, H., Łabaj, P.P., Kreil, D.P., Megherbi, D., Florian, C., Gaj, S., van Delft, J., Kleinjans, J., Scherer, A., Viswanath, D., Wang, J., Yang, Y., Qian, H.-R., Lancashire, L.J., Bessarabova, M., Nikolsky, Y., Furlanello, C., Chierici, M., Albanese, D., Jurman, G., Riccadonna, S., Filosi, M., Visintainer, R., Zhang, K.K., Li, J., Hsieh, J.-H., Svoboda, D.L., Fuscoe, J.C., Deng, Y., Shi, L., Paules, R.S., Auerbach, S.S., Tong, W., 2014. A comprehensive study design reveals treatment- and transcript abundance–dependent concordance between RNA-seq and microarray data. Nat. Biotechnol. 32, 926–932. https://doi.org/10.1038/nbt.3001

Wang, G., Zheng, Y., Wang, Y., Cai, Z., Liao, N., Liu, J., Zhang, W., 2018. Co-culture system of hepatocytes and endothelial cells: two in vitro approaches for enhancing liver-specific functions of hepatocytes. Cytotechnology 70, 1279–1290. https://doi.org/10.1007/s10616-018-0219-3

Wang, H.B., Dembo, M., Hanks, S.K., Wang, Y., 2001. Focal adhesion kinase is involved in mechanosensing during fibroblast migration. Proc. Natl. Acad. Sci. U. S. A. 98, 11295–11300. https://doi.org/10.1073/pnas.201201198

Wang, N., 2017. Review of Cellular Mechanotransduction. J. Phys. Appl. Phys. 50.

Wang, P., Pradhan, K., Zhong, X., Ma, X., 2016. Isoniazid metabolism and hepatotoxicity. Acta Pharm. Sin. B 6, 384–392. https://doi.org/10.1016/j.apsb.2016.07.014

Wang, Y., Wang, G., Luo, X., Qiu, J., Tang, C., 2012. Substrate stiffness regulates the proliferation, migration, and differentiation of epidermal cells. Burns J. Int. Soc. Burn Inj. 38, 414–420. https://doi.org/10.1016/j.burns.2011.09.002

Wang, Y.-X., Wang, D.-Y., Guo, Y.-C., Guo, J., 2019. Zyxin= a mechanotransductor to regulate gene expression. Eur. Rev. Med. Pharmacol. Sci. 23, 413–425. https://doi.org/10.26355/eurrev_201901_16790

Wang, Z., Gerstein, M., Snyder, M., 2009. RNA-Seq: a revolutionary tool for transcriptomics. Nat. Rev. Genet. 10, 57–63. https://doi.org/10.1038/nrg2484

Washabau, R.J., Day, M.J. (Eds.), 2013. Chapter 61 - Liver, in= Canine and Feline Gastroenterology. W.B. Saunders, Saint Louis, pp. 849–957. https://doi.org/10.1016/B978-1-4160-3661-6.00061-4

Weiner, J.A., Jontes, J., 2013. Protocadherins, not prototypical: a complex tale of their interactions, expression, and functions. Front. Mol. Neurosci. 6. https://doi.org/10.3389/fnmol.2013.00004

Westerink, W.M.A., Schoonen, W.G.E.J., 2007a. Phase II enzyme levels in HepG2 cells and cryopreserved primary human hepatocytes and their induction in HepG2 cells. Toxicol. Vitro Int. J. Publ. Assoc. BIBRA 21, 1592–1602. https://doi.org/10.1016/j.tiv.2007.06.017

Westerink, W.M.A., Schoonen, W.G.E.J., 2007b. Cytochrome P450 enzyme levels in HepG2 cells and cryopreserved primary human hepatocytes and their induction in HepG2 cells. Toxicol. Vitro Int. J. Publ. Assoc. BIBRA 21, 1581–1591. https://doi.org/10.1016/j.tiv.2007.05.014

Wheelock, M.J., Shintani, Y., Maeda, M., Fukumoto, Y., Johnson, K.R., 2008. Cadherin switching. J. Cell Sci. 121, 727–735. https://doi.org/10.1242/jcs.000455

Whirl-Carrillo, M., Huddart, R., Gong, L., Sangkuhl, K., Thorn, C.F., Whaley, R., Klein, T.E., 2021. An Evidence-Based Framework for Evaluating Pharmacogenomics Knowledge for Personalized Medicine. Clin. Pharmacol. Ther. 110, 563–572. https://doi.org/10.1002/cpt.2350

Wieschaus, E., Nüsslein-Volhard, C., Jürgens, G., 1984. Mutations affecting the pattern of the larval cuticle inDrosophila melanogaster : III. Zygotic loci on the X-chromosome and fourth chromosome. Wilhelm Rouxs Arch. Dev. Biol. 193, 296–307. https://doi.org/10.1007/BF00848158

Wilkening, S., Stahl, F., Bader, A., 2003. Comparison of primary human hepatocytes and hepatoma cell line Hepg2 with regard to their biotransformation properties. Drug Metab. Dispos. Biol. Fate Chem. 31, 1035–1042. https://doi.org/10.1124/dmd.31.8.1035

Wojtal, K.A., de Vries, E., Hoekstra, D., van IJzendoorn, S.C.D., 2006. Efficient Trafficking of MDR1/P-Glycoprotein to Apical Canalicular Plasma Membranes in HepG2 Cells Requires PKA-RIIα Anchoring and Glucosylceramide. Mol. Biol. Cell 17, 3638–3650. https://doi.org/10.1091/mbc.E06-03-0230

Wu, D., Smyth, G.K., 2012. Camera: a competitive gene set test accounting for inter-gene correlation. Nucleic Acids Res. 40, e133. https://doi.org/10.1093/nar/gks461

Xu, J.J., Diaz, D., O'Brien, P.J., 2004. Applications of cytotoxicity assays and pre-lethal mechanistic assays for assessment of human hepatotoxicity potential. Chem. Biol. Interact. 150, 115–128. https://doi.org/10.1016/j.cbi.2004.09.011

Xu, J.J., Henstock, P.V., Dunn, M.C., Smith, A.R., Chabot, J.R., de Graaf, D., 2008. Cellular Imaging Predictions of Clinical Drug-Induced Liver Injury. Toxicol. Sci. 105, 97–105. https://doi.org/10.1093/toxsci/kfn109

Xu, P., Davis, R.J., 2010. c-Jun NH2-terminal kinase is required for lineage-specific differentiation but not stem cell self-renewal. Mol. Cell. Biol. 30, 1329–1340. https://doi.org/10.1128/MCB.00795-09

Xuan, J., Chen, S., Ning, B., Tolleson, W.H., Guo, L., 2016. Development of HepG2-derived cells expressing cytochrome P450s for assessing metabolism-associated drug-induced liver toxicity. Chem. Biol. Interact. 255, 63–73. https://doi.org/10.1016/j.cbi.2015.10.009

Yamazaki, Y., Umeda, K., Wada, M., Nada, S., Okada, M., Tsukita, Shoichiro, Tsukita, Sachiko, 2008. ZO-1- and ZO-2-dependent integration of myosin-2 to epithelial zonula adherens. Mol. Biol. Cell 19, 3801–3811. https://doi.org/10.1091/mbc.e08-04-0352

Yang, C., Tibbitt, M.W., Basta, L., Anseth, K.S., 2014. Mechanical memory and dosing influence stem cell fate. Nat. Mater. 13, 645–652. https://doi.org/10.1038/nmat3889

Yang, J., Mani, S.A., Donaher, J.L., Ramaswamy, S., Itzykson, R.A., Come, C., Savagner, P., Gitelman, I., Richardson, A., Weinberg, R.A., 2004. Twist, a master regulator of morphogenesis, plays an essential role in tumor metastasis. Cell 117, 927–939. https://doi.org/10.1016/j.cell.2004.06.006

Yang, X., Chen, L., Liang, Y., Si, R., Jiang, Z., Ma, B., Gao, P., 2018. Knockdown of alpha-fetoprotein expression inhibits HepG2 cell growth and induces apoptosis. J. Cancer Res. Ther. 14, S634–S643. https://doi.org/10.4103/0973-1482.180681

Yang, X., Schnackenberg, L.K., Shi, Q., Salminen, W.F., 2014. Chapter 13 - Hepatic toxicity biomarkers, in= Gupta, R.C. (Ed.), Biomarkers in Toxicology. Academic Press, Boston, pp. 241–259. https://doi.org/10.1016/B978-0-12-404630-6.00013-0

Yang, Y., Qu, R., Fan, T., Zhu, X., Feng, Y., Yang, Yuchao, Deng, T., Peng, Y., Huang, W., Ouyang, J., Dai, J., 2018. Cross-talk between microtubules and the linker of nucleoskeleton complex plays a critical role in the adipogenesis of human adipose-derived stem cells. Stem Cell Res. Ther. 9, 125. https://doi.org/10.1186/s13287-018-0836-y

Yano, T., Hernandez-Blazquez, F.-J., Omori, Y., Yamasaki, H., 2001. Reduction of malignant phenotype of HEPG2 cell is associated with the expression of connexin 26 but not connexin 32. Carcinogenesis 22, 1593–1600. https://doi.org/10.1093/carcin/22.10.1593

Yeh, Y.-C., Ling, J.-Y., Chen, W.-C., Lin, H.-H., Tang, M.-J., 2017. Mechanotransduction of matrix stiffness in regulation of focal adhesion size and number: reciprocal regulation of caveolin-1 and β1 integrin. Sci. Rep. 7, 1–14. https://doi.org/10.1038/s41598-017-14932-6

Yoshigi, M., Hoffman, L.M., Jensen, C.C., Yost, H.J., Beckerle, M.C., 2005. Mechanical force mobilizes zyxin from focal adhesions to actin filaments and regulates cytoskeletal reinforcement. J. Cell Biol. 171, 209–215. https://doi.org/10.1083/jcb.200505018

Zamir, E., Geiger, B., 2001. Molecular complexity and dynamics of cell-matrix adhesions. J. Cell Sci. 114, 3583–3590.

Zanoni, M., Piccinini, F., Arienti, C., Zamagni, A., Santi, S., Polico, R., Bevilacqua, A., Tesei, A., 2016. 3D tumor spheroid models for in vitro therapeutic screening: a systematic approach to enhance the biological relevance of data obtained. Sci. Rep. 6, 1–11. https://doi.org/10.1038/srep19103

Zhang, W., Liu, H.T., 2002a. MAPK signal pathways in the regulation of cell proliferation in mammalian cells. Cell Res. 12, 9–18. https://doi.org/10.1038/sj.cr.7290105

Zhang, W., Liu, H.T., 2002b. MAPK signal pathways in the regulation of cell proliferation in mammalian cells. Cell Res. 12, 9–18. https://doi.org/10.1038/sj.cr.7290105

Zhang, X., Jiang, G., Cai, Y., Monkley, S.J., Critchley, D.R., Sheetz, M.P., 2008. Talin depletion reveals independence of initial cell spreading from integrin activation and traction. Nat. Cell Biol. 10, 1062–1068. https://doi.org/10.1038/ncb1765

Zhang, Y., He, Y., Bharadwaj, S., Hammam, N., Carnagey, K., Myers, R., Atala, A., Van Dyke, M., 2009. Tissue-specific extracellular matrix coatings for the promotion of cell proliferation and maintenance of cell phenotype. Biomaterials 30, 4021–4028. https://doi.org/10.1016/j.biomaterials.2009.04.005

Zhang, Y., Wang, H., 2012. Integrin signalling and function in immune cells. Immunology 135, 268–275. https://doi.org/10.1111/j.1365-2567.2011.03549.x

Zhao, B., Li, L., Guan, K.-L., 2010. Hippo signaling at a glance. J. Cell Sci. 123, 4001–4006. https://doi.org/10.1242/jcs.069070

Zhao, B., Wei, X., Li, W., Udan, R.S., Yang, Q., Kim, J., Xie, J., Ikenoue, T., Yu, J., Li, L., Zheng, P., Ye, K., Chinnaiyan, A., Halder, G., Lai, Z.-C., Guan, K.-L., 2007. Inactivation of YAP oncoprotein by the Hippo pathway is involved in cell contact inhibition and tissue growth control. Genes Dev. 21, 2747–2761. https://doi.org/10.1101/gad.1602907

Zhao, X., Guan, J.-L., 2011. Focal adhesion kinase and its signaling pathways in cell migration and angiogenesis. Adv. Drug Deliv. Rev. 63, 610–615. https://doi.org/10.1016/j.addr.2010.11.001

Zhou, Y., Shen, J.X., Lauschke, V.M., 2019. Comprehensive Evaluation of Organotypic and Microphysiological Liver Models for Prediction of Drug-Induced Liver Injury. Front. Pharmacol. 10. https://doi.org/10.3389/fphar.2019.01093

Zhu, Y., Shi, Q., Peng, Q., Gao, Y., Yang, T., Cheng, Y., Wang, H., Luo, Y., Huang, A., He, T.-C., Fan, J., 2019. A simplified 3D liver microsphere tissue culture model for hepatic cell signaling and drug-induced hepatotoxicity studies. Int. J. Mol. Med. 44, 1653–1666. https://doi.org/10.3892/ijmm.2019.4321

Zschenker, O., Streichert, T., Hehlgans, S., Cordes, N., 2012. Genome-Wide Gene Expression Analysis in Cancer Cells Reveals 3D Growth to Affect ECM and Processes Associated with Cell Adhesion but Not DNA Repair. PLOS ONE 7, e34279. https://doi.org/10.1371/journal.pone.0034279

Appendix 1 – DESEQ2 data explanation.

The Deseq2 data is attached as an Excel file. This file shows the compared gene expression data of genes showing 10 or more raw counts in one or more of the replicates between each comparison of 2D HepG2 cells, 3D primed HepG2 cells, human liver and primary hepatocytes (PHH). Each sheet of this spreadsheet shows a different comparison, with each column outlining a key metric. Full explanations of these metrics can be found here https://bioc.ism.ac.jp/packages/2.14/bioc/vignettes/DESeq2/inst/doc/beginner.pdf, but a brief description will be outlined below.

The column headings are:

ensembl_gene_id	This provides an ID for each gene using the Ensembl nomenclature.
hgnc_symbol	This provides an identifier symbol for each gene using the HUGO Gene Nomenclature Committee
Description	This provides a full gene description
log2FoldChange	This provides the effect size estimate of the fold change reported on a logarithmic scale of base 2
lfcSE	This provides the standard error estimate of the log2FoldChange value
pvalue	p value indicates the probability that a fold change as strong as the observed one, or even stronger, would be seen under the situation described by the null hypothesis.
padj	This uses Benjamini-Hochberg (BH) adjustment of the P value to account for false discover rate (FDR).
Fold Change	This provides the fold change without logarithmic transformation
BA_2DX_, BA_3DX_, BA_HLX_, ERS187591X,	These are the raw counts for the samples 2D HepG2, 3D primed HepG2, human liver, and primary hepatocytes, with X being the repeat number.
BA_2DX_X_norm_count …	These provide the normalised counts that corrects for library size and RNA composition bias (https://chipster.csc.fi/manual/deseq2.html)